# TRANSESTERIFICATION OF *CROTON MEGALOCARPUS* OIL BY HETEROGENEOUS CATALYSIS AND MICROWAVE IRRADIATION – REACTION KINETICS AND PROCESS OPTIMIZATION

**ANIL KUMAR**

**A Thesis submitted in partial fulfilment of the requirements for the award of the degree of Doctor of Philosophy of Moi University**

**2015**

## DECLARATION

This thesis is my original work and has not been submitted for a degree in any other university. No part of this thesis may be reproduced without the prior written permission of the author and/or Moi University.

Anil Kumar
Admission No. TEC/DPHIL/03/10 Date

This thesis has been submitted for examination with our approval as University supervisors.

Prof Henry Kirimi Kiriamiti Signature:
Dept of Chemical & Process Engineering Date:

Prof David K Some Signature:
Dept of Agriculture & Biosystems Engineering`````` Date:

## ABSTRACT

Use of biomass such as vegetable oils in the biodiesel synthesis decreases the need for fossil energy, provides an outlet for utilizing the abundant resources effectively and economically, results in a cleaner fuel that is biodegradable, renewable, and non-toxic. Biodiesel is produced by catalytic transesterification of vegetable oils. Homogeneous catalysts have problems of downstream processing and heterogeneous catalysts are being developed as they are environmentally better option to produce biodiesel. Transesterification of *Croton megalocarpus* oil was studied using homogeneous NaOH and heterogeneous alkaline earth BeO, Nano MgO, MgO, Nano CaO, CaO, Reoxidized CaO, SrO and BaO catalysts. The objective was to study the effect of key process variables on Fatty acid methyl esters (FAME) yield, to study the reaction kinetics, to optimize the reaction process, to compare conventional and microwave heating modes, and to compare batch and continuous reaction processes. Characteristic surface, bulk and chemical properties of the heterogeneous catalysts were obtained which included surface area, pore properties, scanning electron micrography, X-ray diffraction, basic strength and basicity. Transesterification reaction variables were reaction temperature, reaction time, catalyst concentration, methanol to oil ratio and microwave power. Gas chromatography was used for FAME analysis. Polymath 6.1, Matlab R2009b, and Design Expert 9 were used for data analysis. Process variable reaction temperature was 313, 323, 333, 343K; catalyst concentration was 0.5, 1.0, 1.5, 2 mass%; and methanol to triglyceride molar ratio 6, 9, 12, and 15. Highest reaction time for conventional heating was 180 min, and for microwave irradiation 5 min. Highest FAME yield for NaOH catalyst was 98% for conventional heating and 96% for microwave irradiation. For heterogeneous catalysts highest FAME yield for BaO, SrO, Nano CaO, CaO RO, CaO, Nano MgO, MgO and BeO under conventional heating were 83%, 77%, 74%, 42%, 32%, 25%, 20% and 4%; and for microwave irradiation were 78%, 72%, 62%, 24%, 19%, 7%, 6% and 3% respectively. Reaction order, rate constant and activation energy were obtained, for homogenous and heterogeneous catalysts, and for conventional heating and microwave irradiation. FAME yields for continuous transesterification were similar to batch process. Central Composite Design was used to optimize process variables and FAME yield presented in Response Surface Methodology surface and contour plots. FAME was analyzed for properties as a biodiesel fuel and it satisfied the international standards. Study established that *Croton megalocarpus* oil was a suitable feedstock for transesterification reaction, heterogeneous catalysts have a potential to replace conventional homogenous catalyst, and microwave irradiation was superior to conventional heating. Further studies on leaching, recyclability, modification of calcium oxide catalyst and scale-up of microwave irradiation were recommended.

## *Contents*

## LIST OF TABLES

## LIST OF FIGURES

## ACKNOWLEDGEMENTS

First and foremost I acknowledge the trust and support I received from my supervisors, Prof Kirimi Kiriamiti and Prof David Some. They were always available for consultancy and guidance in spite of their extremely busy schedules.

This work could not have been completed without the assistance of Prof Maurice Onyango of TUT. I would always be grateful for his help in various aspects of my work.

My colleagues in the Dept of Chemical and Process Engineering have all supported me during my research work. I am thankful to all of them. The Technical staff Mr Paul Langat, Mr Vincent Bitok and Mr Alex Koech deserve special mention for helping in the laboratory experiments and instrumental analysis. Secretarial assistance by Ms Esther Kessio is also appreciated.

Laboratory facilities of Dept of Chemical Engineering, Tshwane University of Technology; Dept of Food Science and Technology, Jomo Kenyatta University of Agriculture & Technology; Kenya Industrial Research & Development Institute; Kenya Pipeline Company Ltd.; School of Environmental Studies, University of Eldoret and Kipevu Power Station (Kengen) were used during the research. Assistance by the technical staff of those labs is gratefully acknowledged.

I also thank my own family members, Atula, Neha and Prashant for their understanding.

# NOMENCLATURE

## Abbreviations

| | |
|---|---|
| ASTM | American Society for Testing and Materials |
| CCD | Central composite design |
| CSTR | Continuous stirred tank reactor |
| DOE | Design of Experiments |
| FAME | Fatty acid methyl esters |
| FFA | Free fatty acids |
| GC | Gas chromatograph |
| ID | Internal diameter |
| IUPAC | International Union of Pure and Applied Chemistry |
| JAOCS | Journal of American Oil Chemists Society |
| L.H.S | Left hand side |
| MW | Microwave |
| PFR | Plug flow reactor |
| R.H.S | Right hand side |
| RSM | Response surface methodology |
| STP | Standard Temperature and Pressure (273.15K, 100 kPa) |
| WB | Water bath |
| WCO | Waste cooking oil |

## Symbols

| | |
|---|---|
| $\bar{V}$ | molar volume of liquid in Kelvin equation [$L^3$] |
| $a$ | effective cross section area ($m^2$) of one adsorbate molecule ($16.2 \times 10^{-20}$ $m^2$ for $N_2$) |
| $A$ | Pre-exponential factor, Frequency factor in Arrhenius equation |
| $b$ | constant in Langmuir isotherm [$M^{-1}LT^2$] |

$c$ Constant in BET equation (dimensionless)

$d_I$ Impeller diameter [L]

$d_p$ Particle diameter [L]

E Activation energy in Arrhenius equation [$ML^2T^{-2}$]

g Acceleration of gravity [$m^2s^{-1}$]

$G$ Gibbs energy [$ML^2T^{-2}$]

$H$ Enthalpy [$ML^2T^{-2}$]

$k$ Chemical reaction rate constant

$k_o$ frequency factor in Arrhenius equation

m mass [M]

$N$ Avogadro constant ($6.023x10^{23}$)

$N_I$ Impeller speed [$T^{-1}$]

$p$ Partial pressure [$ML^{-1}T^{-2}$]

p pressure [$ML^{-1}T^{-2}$]

$p_o$ saturation pressure [$ML^{-1}T^{-2}$]

$p_{sat}$ Saturation pressure [$ML^{-1}T^{-2}$]

r radius [L]

R Universal gas constant [$L^2T^{-2}\theta^{-1}$]

Re Reynolds number (dimensionless)

$r_p$ average catalyst pore radius, [L]

$S$ Entropy ($ML^2T^{-1}$)

$S_{BET}$ BET Surface area, [$L^2M^{-1}$]

T Absolute temperature [$\theta$]

$v$ Volume of gas adsorbed per unit mass of adsorbent in BET equation[$L^3M^{-1}$]

$v_m$ Volume of gas adsorbed in a monolayer per unit mass of adsorbent in BET

$V_m$ volume of gas ($N_2$) adsorbed at STP for a monolayer adsorption [$L^3$]

$W_a$ adsorbed amount (t-plot analysis) [M]

**Greek letters**

$\gamma$ surface tension [$MT^{-2}$]

$\varepsilon_p$ particle porosity (dimensionless)

$\varepsilon_s$ catalyst fraction in slurry (dimensionless)

$\rho_L$ density of liquid [$M\ L^{-3}$]

$\rho_p$ catalyst density, [$M\ L^{-3}$]

$\rho_{p,wet}$ density of catalyst filled with liquid [$M\ L^{-3}$]

$\sigma_t$ thickness of a single adsorbed layer (t- plot analysis) [L]

# 1 INTRODUCTION

## 1.1 Diesel Engine and petroleum fuel

German engineer Rudolf Diesel patented an internal combustion engine in 1892 which used groundnut oil as fuel (Shay, 1993). Due to widespread availability of cheap petroleum, the petroleum diesel soon replaced vegetable oil in commercial diesel engines. Petroleum fuel are non-renewable. As per International Energy Statistics for the year 2010, the Africa and the World consumed 3.4 and 85.7 million barrels of petroleum fuel respectively. It is speculated that the present rate of consumption of the petroleum fuel is 2.7% of the reserves, and the petroleum stocks may deplete within the next 50 years or so (International Energy Statistics, 2012; Taufiqurrahmi and Bhatia, 2011). Use of petroleum fuel is also considered to have a negative environmental effect. Petroleum is a mixture of a number of organic compounds and many of them are toxic. Combustion of petroleum hydrocarbons leads to a net increase in carbon dioxide, a factor seems to be responsible for global warming and climate change.

## 1.2 Biofuels

Biofuels are fuels from renewable sources and are recognized to be an alternative to petroleum derived fuels. Liquid biofuels consist of biodiesel and bio-gasoline. Unlike petroleum hydrocarbons, these fuels add little to net carbon dioxide; and also do not lead to air pollution, being free of nitrogen and sulphur. Biofuels consist of mainly C, H and O, the oxygen percentage ranging from 10 to 45%, whereas petroleum diesel is mainly C and H with no oxygen. This makes the chemical properties of the two fuels very different (Demirbas, 2008). Bio-gasoline is a blend of ethanol, obtained from renewable plant sources, and petroleum gasoline. According to year end data for 2011, North America leads the production of biofuels by producing above 1 billion barrel/day, followed by Central & South America with a production of 519,000 barrels/day. Similar data for Europe, Asia & Oceania and Africa are: 250,500 barrels/day, 118,000 barrels/ day and 790 barrels/day respectively (International Energy Statistics, 2012).

### 1.2.1 Biodiesel

According to American Society for Testing and Materials (ASTM), a biodiesel is a fuel comprised of mono-alkyl esters of long chain fatty acids derived from vegetable oils or animal fats, designated B100, and meeting the requirements of ASTM D 6751. A

biodiesel-blend is a blend of biodiesel fuel meeting ASTM D 6751 with petroleum-based diesel fuel, designated BXX, where XX represents the volume percentage of biodiesel fuel in the blend (Biodiesel, 2013). Studies using pure and blended biodiesels show that this biofuel can be used in diesel engine without any modification (Tazerout *et al*., 2009).

#### 1.2.1.1 Biodiesel and the environment

Biodiesel produced from vegetable oils is claimed to be carbon neutral. Plants absorb carbon dioxide as they grow, which could be ideally equated to carbon dioxide produced during combustion of biodiesel. This would hold if there are no energies involved in the production of biodiesel. In practice, oil seeds are more often cultivated in agricultural farms involving use of fertilizers and mechanical machines, where carbon dioxide is produced. Oil extraction and subsequent production of biodiesel also involves processes where carbon dioxide is generated. A study of life cycle analysis of biodiesel shows that the greenhouse gas emissions are between 22 and 59% of the emissions from petroleum diesel (Frondel and Peters, 2007). Studies show that biodiesel fuel reduces particulate matter exhaust by 75-83% as compared to petroleum diesel. However, the $NO_x$ emissions increase in case of biodiesel which is attributed to the unsaturation of fatty compounds. Emissions of carbon monoxide and hydrocarbons was also lower in case of biodiesel fuel (Knothe *et al*., 2006). A distinct feature of biodiesel is the reduced emission of sulphur compounds, which is lower by 20-50 times when compared to petroleum diesel (Dunn, 2001). The biodiesel has lower environmental impact compared to petroleum diesel as dramatic reductions are observed in the emissions of unburned hydrocarbons, carbon dioxide, carbon monoxide, sulphates, polycyclic aromatic hydrocarbons, nitrated polycyclic aromatic hydrocarbons, ozone-forming hydrocarbons, and particulate matter (Demirbas, 2009).

## 1.3 Objectives, Justification and Hypothesis

### 1.3.1 Objectives and Justification

Objectives of any research must be substantiated by due reasoning. By now it is established that biodiesel is best suited to replace petroleum diesel fuel. *Croton megalocarpus* is an indigenous tree, and the oil from its seed is a potential feedstock for biodiesel production. Hence there is a need to develop a process for transesterification of *Croton megalocarpus* oil to produce biodiesel fuel. Transesterification with homogeneous

catalysts needs elaborate downstream treatment and has environmental implications. Heterogeneous catalysts are more promising but only a very limited catalysts have been tested. Some catalysts that have shown good performance with other oil feedstock need to be tested for croton oil. Besides, microwave irradiation has been shown to be a better heat transfer mode, resulting into higher reaction rates. Kinetics data for transesterification are needed for any scale-up design; and continuous production is better than a batch process in terms of operations and economics. No such study using alkaline earth metal oxide catalysts, using conventional/microwave irradiation, of transesterification of *Croton megalocarpus* oil has been reported. Therefore the main and specific objectives can be given as:

**Main Objective**: To develop a process to transesterify Croton *megalocarpus* oil using alkaline earth catalysts and microwave irradiation.

**Specific objectives**

- To transesterify croton oil using alkaline earth catalysts using conventional and microwave irradiation
- To study the effect of reaction variables of the reaction
- To study reaction kinetics and obtain activation energies/ pre-exponential factors for the reactions
- To identify the conditions for optimal yield of fatty acid methyl esters
- To compare the yields for batch and flow reactors

### 1.3.2 Hypothesis

The outcome of the study should establish that *Croton megalocarpus* oil is a suitable feedstock for transesterification reaction. It should also show that the selected heterogeneous catalysts have a potential to replace conventional homogenous catalyst, and microwave irradiation is a superior heat transfer mode.

## 1.4 Organization of the thesis

Thesis is organized into eight chapters. The first, and the present, chapter introduces biofuels and gives its environmental advantages. This chapter also gives an idea about the scope of the present research and the rationale behind it. Chapter 2 is about literature review, and gives a comprehensive review of the publications related to the study.

Chapters 3 gives the characterization of *croton megalocarpus* oil and heterogeneous catalysts. Chapter 4 is about transesterification studies using homogenous NaOH catalyst. Chapters 5 deals with transesterification studies using BaO, SrO, CaO, MgO and BeO catalysts. Chapter 6 gives the results of transesterification using a plug flow reactor for NaOH and CaO catalysts. Chapter 7 gives the FAME properties as a biofuel. Chapter 8 is about conclusions made from the present study and recommendations for future work. A list of references, and appendices conclude the thesis.

# 2 LITERATURE REVIEW

## 2.1 Introduction

Historically the earliest biodiesel was vegetable oil, often called the *first generation* biodiesel. During the era of oil embargo, South Africa used a sunflower oil-petro diesel blend for vehicles. Percentage of sunflower oil ranged from 20-50% , and concentrations of oil above 50% was not suitable (Ma and Hanna, 1999). Blend of used cooking oil and petro diesel was successfully used for vehicles (Anon, 1982). Soybean oil, Rapeseed oil, Canola oil have also been used as diesel engine fuel, mostly in blended form (Adams *et al*., 1983; Peterson *et al*., 1983). The advantages of vegetable oil as diesel fuel are: liquid nature, good calorific value, ready availability and renewability. In spite of these good features, their use in diesel engines was restricted due to high viscosity which resulted in poor atomization, incomplete combustion, and carbon deposit on the injector and the valve seats, causing serious engine fouling. Viscosity of vegetable oil was reduced by blending it with solvents such as ethanol, methanol and 1-butanol and the resulting mixture performed quite close to petro diesel (Ma and Hanna, 1999; Demirbas, 2009). Vegetable oil or animal fat can be converted into biodiesel by application of heat (thermal decomposition), or through a chemical reaction (transesterification). Thermal decomposition known as Pyrolysis is the chemical decomposition of vegetable oils that occurs spontaneously at high enough temperatures. Pyrolysis produces gas and liquid products and leaves a solid residue richer in carbon. Thermal decomposition in presence of a catalyst is known as catalytic cracking. Catalytic cracking of palm oil in presence of Rare earth-Y catalyst yielded bio-gasoline and gas as fuel (Tamunaidu and Bhatia, 2007). Catalytic cracking of almost all common vegetable oils have been studied under a variety of catalysts employing different types of reactors. Reactor systems are complex, and the end products are a mixture of gasoline, petro-diesel and gaseous fuel (Hew *et al*., 2010; Taufiqurrahmi and Bhatia, 2011). Biodiesel produced by a chemical reaction, involves a reaction of oil/fat with an alcohol in presence of a catalyst, is known as transesterification.

## 2.2 Biodiesel by Transesterification: Reaction Chemistry

Transesterification, also called alcoholysis, is the displacement of alcohol from an ester by another alcohol in a process similar to hydrolysis, except that an alcohol is used instead of

water. This process has been widely used to reduce viscosity of triglycerides. The transesterification reaction is represented by the general equation:

$$\underset{\text{Ester}}{RCOOR'} + \underset{\text{Alcohol}}{R''OH} \leftrightarrow \underset{\text{Ester}}{RCOOR''} + \underset{\text{Alcohol}}{R'OH} \quad \ldots \quad (2.1)$$

If methanol is used in reaction 2.1, it is termed methanolysis. The reaction of triglyceride with an alcohol is represented by the general equation:

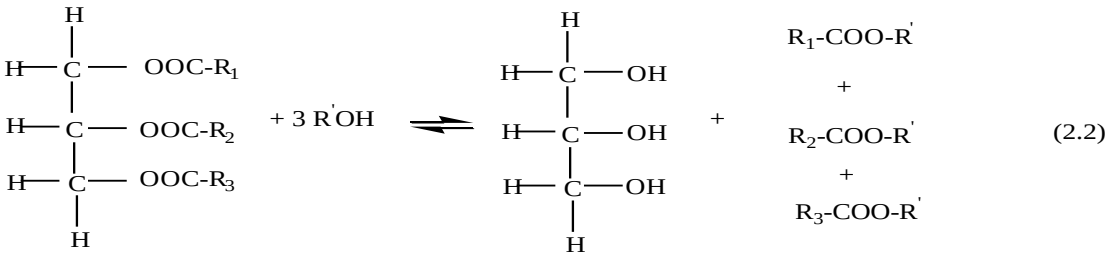


(2.2)

Triglyceride Alcohol Glycerol Fatty acid esters

Reaction 2.2 is carried out in presence of a catalyst. Fatty acid esters constitute the biodiesel. This reaction is reversible and is supposed to occur in three reversible steps. First is the conversion of triglycerides to diglycerides, second is the conversion of diglycerides to monoglycerides and the last is the monoglyceride to glycerol. Each step yields one molecule of methyl ester, as given in reactions 2.3, 2.4, and 2.5 (Adholeya and Dadhich, 2008):

$$\text{Triglyceride} + R'OH \overset{\text{catalyst}}{\rightleftharpoons} \text{diglyceride} + R'COOR_1 \quad (2.3)$$

$$\text{Diglyceride} + R'OH \overset{\text{catalyst}}{\rightleftharpoons} \text{monoglyceride} + R'COOR_2 \quad (2.4)$$

$$\text{Monoglyceride} + R'OH \overset{\text{catalyst}}{\rightleftharpoons} \text{glycerol} + R'COOR_3 \quad (2.5)$$

In reactions 2.2 to 2.5, R' is the alkyl group for the alcohol and $R_1$ , $R_2$ and $R_3$ are carbon chain of fatty acid. When methanol is used as the alcohol, the transesterification (or methanolysis) results in formation of fatty acid methyl esters (FAME). From stoichiometry, 3 mol of alcohol reacts with 1 mol of triglyceride to form 3 mol of fatty esters and 1 mol of glycerol. Reaction variables affecting the yield of FAME are: choice of

feedstock, choice of catalyst and its amount, reaction temperature and pressure, choice of alcohol, molar ratio of alcohol to oil, presence of co-solvents, mixing and heating modes. Choice of reaction system is also a variable since the transesterification can be carried out in a batch, continuous stirred tank, or a flow reactor.

## 2.3 Catalysts for Transesterification

Catalysts for transesterification can be categorized into homogeneous and heterogeneous. Homogeneous catalysts are further classified as: acidic, basic, and biocatalysts such as enzymes. Similarly heterogeneous catalysts are also classified into acidic and basic types.

### 2.3.1 Homogenous catalysts for transesterification

Homogeneous catalysts can be Brønsted acids and bases, biocatalysts and non-ionic organics.

#### 2.3.1.1 Homogeneous acid catalyzed transesterification

Brønsted acids like sulphuric, sulphonic and hydrochloric are the common acid catalysts for transesterification. These acids give very high yield of alkyl esters but the reactions require moderately high temperature, and are slow. Methanolysis of soybean oil, using 1mol% of sulphuric acid, gave a almost complete conversion (>99%) at 338K, at methanol to oil molar ratio of 30:1, in 50 hr. Similar reaction using ethanol required 18 hr at 351K, and that using butanol required 3 hr at 390K (Pryde, 1983). High alcohol:oil ratio makes the separation of glycerol difficult. Acid catalysts are suitable for high FFA oils and presence of moisture. Inexpensive feedstocks, such as waste cooking oil, containing high levels of FFAs cannot be directly used with the homogeneous base catalysts. Strong liquid acid catalysts are less sensitive to FFAs and can simultaneously conduct esterification and transesterification. Although they are slower and necessitate higher reaction temperatures, acid-catalyzed processes could produce biodiesel from low-cost feedstocks, lowering production costs. Figure 2.1 gives the reaction mechanism for a homogeneous acid catalyzed transesterification of triglycerides ( Lotero *et al*., 2005).

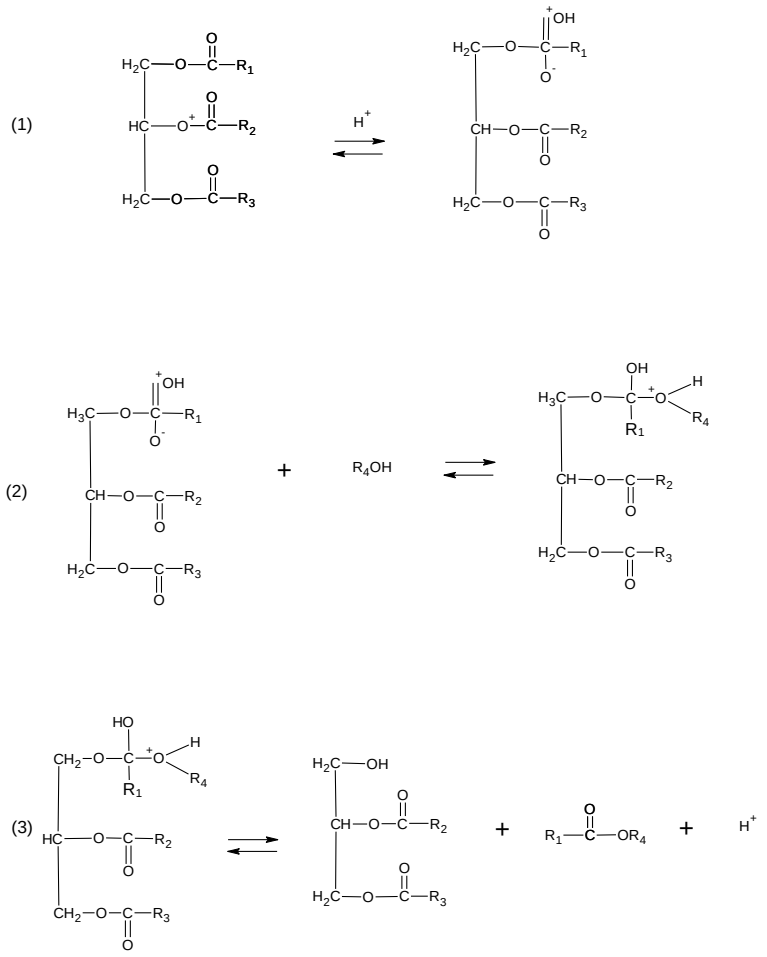


**Figure 2.1: Reaction mechanism for the homogeneous acid catalyzed transesterification of triglycerides ( Lotero et al., 2005)**

In Figure 2.1, reaction (1) is the protonation of the carbonyl group by the acid catalyst, reaction (2) is the nucleophilic attraction of the alcohol forming a tetrahedral intermediate, and reaction (3) gives the proton migration and breakdown of the intermediate. This sequence is repeated twice for $R_2$ and $R_3$. Reaction (1) is the key step in the catalyst-reactant interaction. However, this initial chemical pathway in turn increases the electrophilicity of the adjoining carbon atom, resulting in the intermediate molecules susceptible to nucleophilic attack. This is supposed to explain the slow reaction rates for such catalysts (Lam *et al*., 2010). Figure 2.2 gives a block diagram for acid catalyzed biodiesel production.

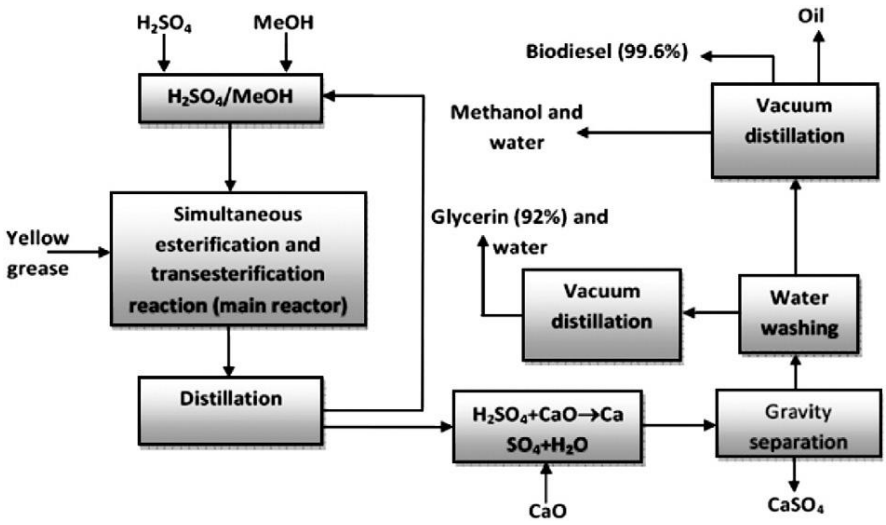


**Figure 2.2: Block diagram for an acid-catalyzed biodiesel production process (Helwani et al., 2009)**

### 2.3.1.2 Homogeneous base catalyzed transesterification

The conventional homogenous basic catalysts are alkali such as sodium hydroxide, alkali metal alkoxides (such as sodium or potassium methoxide and ethoxide) and potassium hydroxide. Base catalyzed transesterification is much faster than acid catalyzed and is most often used. Leung and Guo (2006) reported a yield of 88.8% for frying oil in 0.33 hr at 333K, using 1.1 wt% NaOH catalyst. Pinzi et al. (2011) optimized the transesterification of six different vegetable oils: maize oil, sunflower oil, orujo olive oil, coconut oil, linseed oil and palm oil, using methanol and catalyst KOH. The optimum reaction parameters for the six oils were found to be (in order of the oils listed), Yield (wt%): 98.67, 99.70, 98.02, 90.01, 97.71, 98.91; Reaction temperature (K): 320.5, 332.8, 318, 333, 326, 338; Catalyst concentration (wt%): 1.92, 1.81, 1.6, 1.7, 1.8, 1.8; Methanol to oil molar ratio: 5.4, 5.4, 6.03, 6.6, 6.02, 6.15. In a similar optimization study involving rapeseed oil, a very good conversion into FAME was obtained at 0.6 wt% KOH, 323K, in 90 min (Ferella et al., 2010). Noureddini and Zhu (1997) studied kinetics of transesterification of soybean oil using NaOH catalyst. Kinetics of palm oil transesterification using NaOH and KOH have been reported by Leevijit et al. (2004) and, Darnoko and Cheryan (2000). Kinetics of methanolysis of sunflower oil using KOH catalyst has been reported by Vicente (2005), and by use of NaOH catalyst by Marjanović *et al*. (2010). NaOH and KOH catalysts were use to study kinetics of transesterification of *Camelina Sativa* oil (Patil *et al*., 2010b).

Butyl ester yield of 71.88 wt% was reported for transesterification of *Jatropha Curcas* using NaOH, at 378K using 1:20 molar ratio of oil to butanol (Jha, 2007). Wagutu *et al*. (2009) studied the methanolysis of indigenous oil crops, *Jatropha curcas* L, *Croton megalocarpus*, *Calodendrum capense*, *Cocos nucifera* using NaOH catalyst, and also studied the properties of FAME. Study of biodiesel production from *Croton megalocarpus* using KOH catalyst gave a conversion of 88% at 1 wt% of catalyst, at 333K and in 60 min (Kafuku and Mbarawa, 2010). Sodium methoxide catalyzed transesterification is very rapid and vegetable oil can be completely transesterified in 2-5 min at room temperature. Potassium methoxide was found to be even more active at similar reaction conditions (Ramadhas, 2004). Transesterification of sunflower oil using sodium methoxide gave a 100% yield at 0.5 wt% catalyst, using alcohol to oil ratio 25% w/w, in 60 min (KoohiKamali, 2012). Figure 2.3 shows the mechanism for a base-catalyzed reaction. Reaction (1) is the production of active species, $RO^-$ ; reaction (2) depicts the nucleophilic attack of $RO^-$ to carbonyl group on triglycerides, forming a tetrahedral intermediate; reaction (3) is the intermediate breakdown; and reaction (4) is the regeneration of the $RO^-$ active species. The sequence is repeated for $R_2$ and $R_3$ (Lam *et al*., 2010).

Reaction (1) is crucial where an alkoxide ion is created, which acts as a strong nucleophile. This results in faster reaction rates as compared to acid catalysts. Figure 2.4 gives a bock diagram for a base catalyzed biodiesel production process.

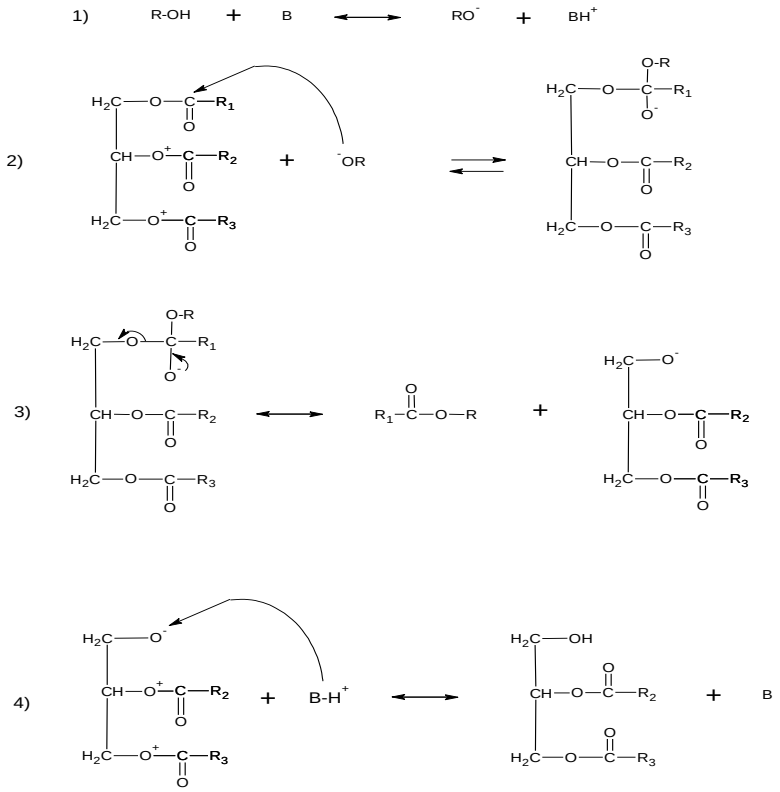


B: Base catalyst. $R_1$ , $R_2$ , $R_3$ : Carbon chain of fatty acid. $R_4$ : Alkyl group of alcohol

**Figure 2.3: Reaction mechanism for the homogeneous base catalyzed transesterification of triglycerides (Lam et al., 2010)**

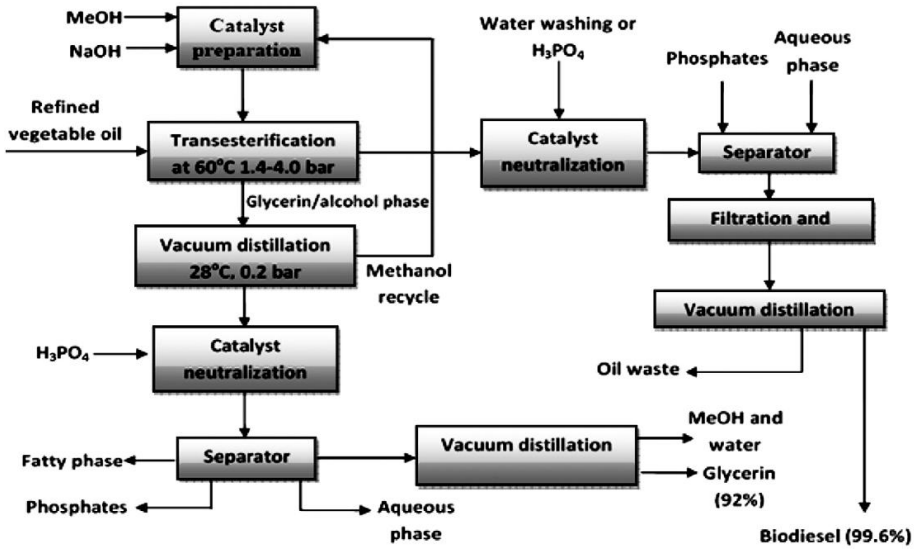


**Figure 2.4: Block diagram for a base-catalyzed biodiesel production process (Helwani et al., 2009)**

#### 2.3.1.3 Homogeneous acid and base catalyzed two-step transesterification

Characteristic features of a typical acid and base transesterification are summarized in Table 2.1.

**Table 2.1: Typical reaction conditions for a base-catalyzed transesterification and an acid-catalyzed transesterification for a triglyceride (Zhang et al., 2003)**

| | Acid catalyzed | Base catalyzed |
|---|---|---|
| **FFA** | > 4% | < 0.5% |
| **Methanol:oil (molar)** | 50:1 | 6:1 |
| **Temperature, K** | 353 | 333 - 338 |
| **Pressure, bar** | 4 | 1.4 – 4.1 |
| **Catalyst (wt%)** | $H_2SO_4$ (10) | NaOH (0.5 – 2) |
| **Conversion (%)** | > 95% in 4 hr | > 95% in 1 hr |

From Table 2.1, acid catalysts are suited for a high FFA feedstock, but have a slow reaction rate. Similarly base catalysts have a fast reaction rate, but require a low FFA. A two-step process combines both catalysts for feedstocks containing high FFA. Initially, acid catalyst is employed to convert FFAs to ester through esterification, and the FFA content drops to less than 0.5 wt%. In step 2, an alkali catalyst is used to transesterify the oil to take advantage of fast reaction rate, low catalyst requirement, and low methanol:oil requirement. *Jatropha curcas* oil (FFA 21.5%) was treated with 1wt% $H_2SO_4$ in step 1, and by 1 wt% NaOH in step 2, to give a yield of 21.2% of methyl ester during esterification and 90.1% from transesterification (Jain and Sharma, 2010). Waste cooking oil (FFA 21.84%) was similarly transesterified by treating with $H_2SO_4$ and NaOH, and a yield of 85-96% of biodiesel is reported (Jain *et al*., 2011; Kumar *et al*, 2011; Patil *et al*., 2009). A disadvantage of this two-stage process is that the catalyst need to be removed at the end of each stage, requiring two separation steps.

#### 2.3.1.4 Biocatalysis catalyzed transesterification

FAME from acid oil, residue oil from vegetable oil refining, was produced by submerged fermentation using genetically modified *Aspergillus oryzae/Aspergillus niger* microorganism as a catalyst giving a 88.7% yield (Chen *et al*., 2008). Methanolysis of

salad oil was carried out using Candida lipase catalyst giving a 90% FAME yield (Nie *et al*., 2006). Soybean oil was transesterified using fungus whole cell catalyst (Arai *et al*., 2010), and by using lipase ionic liquid catalyst (Ha *et al*., 2007). Immobilized lipase catalyst was employed for transesterification of Canola oil (Dizge and Keskinler, 2008). Other studies have been by using commercially produced enzymes catalysts (Hernández-Martin and Otero, 2008), various lipases as catalysts (Kaieda *et al*., 2001), enzymatic catalyst for sunflower oil (Ognjanovic *et al*., 2009). Immobilized *Candida antarctica* Lipase catalyzed transesterification of *Croton megalocarpus* oil gave a 98.71% yield at 30% enzyme (Mirie *et al*., 2012). One problem with enzymatic catalysis is its poor tolerance to methanol. Step wise addition of methanol was used to overcome this problem with encouraging results (Shimada *et al*., 1999). Biocatalysts are eco-friendly and have high potential but the present challenges are the high cost, poor stability and slow reaction rates (Bajaj *et al*, 2010).

#### 2.3.1.5 Non-ionic base catalyzed transesterification

In order to obtain milder reaction conditions and to simplify process, a number of organic bases have been developed and are used as a catalyst for organic synthesis including transesterification. Among these bases, amines such as triethylamine, piperidine, 1,2,2,6,6-pentamethylpiperidine, pentamethylpiperidine, pyridine, 2,6-di-tert-butylpyridine, and DMAP (4-dimethyl-aminopyridine); amidines such as DBU (1,8-diazabicycloundec-7-ene), DBN (1,5-diazobicyclonon-5-ene); guanidines such as TBD (1,5,7-triazobicyclo[4.4.0]dec-5-ene, TMG (1,1,3,3-tetramethylguanidine), PGB (1,1,2,3,3-pentabutylguanidine), 1,3-diphenylguanidine, 1,2,3-triphenylguanidine, aminoguanidines, and nitroguanidines; triamino(imino)phosphoranes such as BEMP (tert-butylimino-diethylamino-2-diethylamino-1,3-dimethyl-perhydro-1,3,2-diazophosphorane) are frequently used in organic synthesis and have been used for transesterification reactions. Yields comparable to alkaline catalysts have been obtained and the reaction is not affected by presence of FFA, and there is no soap formation (Adholeya and Dadhich, 2008; Schuchardt et al., 1998).

### 2.3.2 Heterogeneous catalysts for transesterification

Homogeneous catalysts require elaborate downstream treatment involving neutralization, washing and drying. They are not easy to separate as they dissolve fully in the glycerol layer and partially in the biodiesel (Ebiura *et al.* 2005). Separation process is expensive involving operations such as distillation which makes the separation process uneconomical and often not attempted. With increasing environmental regulations and emphasis on clean technology such catalysts have distinct disadvantage. Heterogeneous solid catalysts are noncorrosive with no adverse environmental effect. They can be easily separated and recycled and are suited for continuous production. Heterogeneous catalysts are highly selective and their activity depends upon their surface properties (Gera *et al.,* 2009). Solid catalysts are broadly classified into two types, acid and base.

#### 2.3.2.1 Heterogeneous acid catalysts

Solid acid catalysts are suited to oils with high free fatty acid contents (eg., waste cooking oils) since these catalyze both esterification and transesterification reactions (Leung *et al*., 2010; Suwannakarn *et al*., 2009). Acid ion exchange resins have been successfully used to produce ethyl oleate biodiesel from triolein. In a study, the anion-exchange resins exhibited much higher catalytic activity as compared to cation-exchange resins, and the resin could be recycled without loss of activity (Kitakawa *et al*., 2007). In another study, commercial Nafion® acid resin was used to transesterify triacetin with methanol (Lopez *et al*., 2007). Reaction rate with these resins is found to be slower compared to basic catalysts and require higher temperatures (Lotero *et al*., 2005). Sulphated and tungstated zirconia, and sulphated tin oxide are another type of acid catalysts. They have been tested for the transesterification of soybean oil giving yield close to 100% and a long activity period (Yadav and Nair, 1999; Furuta *et al*., 2004). Metal complexes containing tungsten, silica, caesium, zinc have been used as acid catalysts for rapeseed oil, yellow horn oil and oleic acid. Conversion is reported to be high, ranging from 88% to 100% (Narasimharao *et al*., 2007a; Xu *et al*., 2008; Zhang *et al*., 2010; Oliviera *et al*., 2010). Zeolites are another group of solids used as acid catalysts. Zeolites are microporous crystalline solids with well defined structures containing silicon, aluminium, and oxygen in their framework and cations (Sharma and Singh, 2011). The acid strength in zeolites can be adjusted such that it fits the reaction requirements (Jothiramalingam *et al*., 2011). Zeolite catalysts require

elaborate preparation procedure as reported for transesterification of methyl octanoate and soybean oil added with oleic acid. For methyl octanoate, a reaction temperature of 773K and a time of 20 min, gave a 100% conversion; whereas for soybean oil-oleic acid mixture, reaction temperature was 333K and time 1 min, to get a 80% conversion (Danuthai *et al*., 2009; Chung and Park, 2009). In general, acid catalysts require a long reaction time and a high temperature, and show weak catalytic activity (Patil and Deng, 2009). Another major drawback for acid catalysts, which arises from reaction mechanism, is its sensitivity to presence of water. Any presence of water slows down the main reaction giving rise to unwanted side reactions (Narasimharao *et al*., 2007b). Basic heterogeneous catalysts consist of single component metal oxides, zeolites, supported alkali metals, clays and non-oxides.

#### 2.3.2.2 Heterogeneous basic catalysts

Basic catalysts give a higher reaction rate as compared to acidic catalysts, whether they are homogeneous or heterogeneous (Freedman *et al*., 1984). The higher activity is explained by the generation of highly active alkoxide ion ($RO^-$) when the alcohol reacts with the base catalyst. Fig 2.5 gives the mechanism of alkali-catalyzed transesterification of triglycerides with alcohol. Reaction (1) is a 'pre-step' leading to the formation of alkoxide ion, where B is the base catalyst and R is the short alkyl group belonging to alcohol (Sridharan and Mathai, 1974). Reaction (2) gives the 'first step' of the reaction in which alkoxide ion reacts with the carbonyl carbon of triglyceride molecule forming a tetrahedral intermediate ion, where R', R" and R"' are the long chain alkyl groups. In the 'second step', the intermediate ion rearranges to give a diglyceride and alkyl ester molecule, given by reaction (3). Reaction (4), gives the 'third step' where the diglyceride ion reacts with the protonated base catalyst, generating a diglyceride molecule and the original base is recovered (Schuchardt *et al*., 1998).

Heterogeneous basic catalysts are sensitive to free fatty acids (FFA) in the feedstock. Soap formation decreases the biodiesel yield if the FFA content in oil exceeds 2% by mass (Lam *et al*., 2010). Water is another component which adversely affects the biodiesel yield. Water reacts with alkyl esters to produce carboxylic acids, which react with alkaline metals to form sodium or potassium salts similar to a soap, reducing alkyl ester yield and making glycerol recovery difficult (Freedman, *et al*., 1986). Zeolite and silica gel have been used in

the catalyst to absorb water to offset the adverse effect of water (Cao *et al*., 2008; Li *et al*., 2009).

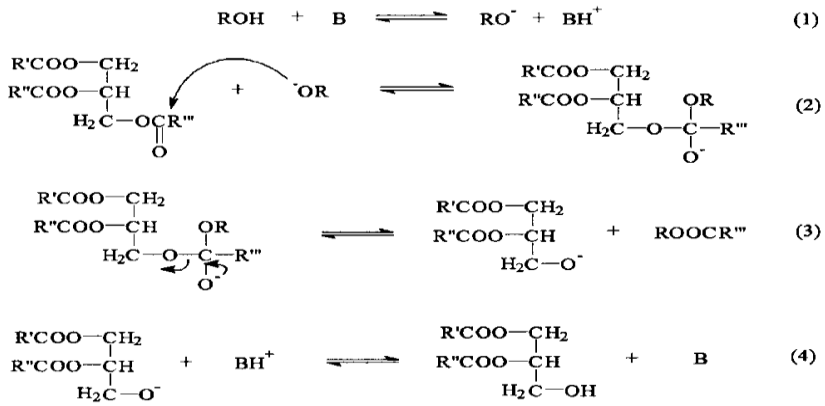

**Figure 2.5: Mechanism of alkali-catalyzed transesterification of triglycerides with alcohol (Schuchardt et al., 1998).**

#### 2.3.2.2.1 Classification of Heterogeneous Basic Catalysts

Hideshi Hattori (2004) studied a wide spectrum of solid basic catalysts. His work included pre-treatment methods, and their relative reactivity for ten typical organic reactions, including transesterification of ethyl acetate. Hattori classified heterogeneous basic catalysts into five types as given in Table 2.2.

Homogenous catalysts are of uniform structure and composition, and have the advantage of reproducibility. Heterogeneous catalysts, on the other hand, are solids of non-uniform structure. Structure and surface properties depend on the method of preparation and pre-treatment prior to use. Surface properties including surface defects are responsible for the active sites, where reaction takes place. Prolong use, poisoning, blocks the active sites making the catalyst inactive (Bond, 1993).

**Table 2.2: Types of heterogeneous basic catalysts (Hattori, 2004)**

| SN | Type | Material |
|---|---|---|
| **1** | Single component metal oxides | Alkali metal oxides<br>Alkaline earth oxides<br>Rare earth oxides<br>$ThO_2$, $ZrO_2$, ZnO, $TiO_2$ |
| **2** | Zeolites | Alkali ion-exchanged zeolite<br>Alkali ion-supported zeolite |

| | | |
|---|---|---|
| **3** | Supported alkali metal<br>(or alkaline earth metal) | Alkali metal ions on alumina<br>Alkali metal ions on silica<br>Alkali metal on alkaline earth oxides<br>Alkali metals and alkali metal hydroxides on alumina |
| **4** | Clay minerals | Hydrotalcites<br>Crysolite<br>Sepiolite |
| **5** | Non-oxides | Alkaline alkoxide<br>Alkaline carbonate<br>Guanidine-containing catalysts |

#### 2.3.2.2.2 Single Component Metal Oxide Catalysts and their Compounds

For most basic materials, the surfaces are covered with water and carbon dioxide in air, and do not exhibit their intrinsic catalytic activities. Removal of the adsorbed species from the surface is essential to reveal oxide surfaces. SrO and BaO easily form peroxides on contact with oxygen, so removal of oxygen is also required to reveal the surface basic sites (Hattori, 2004). A pre-treatment at high temperature is required to remove the adsorbed species, and to decompose hydroxides, carbonates and peroxides. The nature of surface basic sites varies with the severity of the of pre-treatment conditions (Hattori, 2001).

Calcium oxide is one of the most studied heterogeneous base catalyst for transesterification reaction. Producing biodiesel using CaO as a solid base catalyst has many advantages, such as higher activity, mild reaction conditions, reusability, easy availability and low cost. Pretreatment temperatures for removal of adsorbed water and carbon dioxide from CaO surface are 700K and 1000K respectively (Tanabe *et al*., 1971). Transesterification of soybean oil and methanol was carried out using CaO as a solid base catalyst. Figure 2.6 gives the reaction mechanism for CaO catalyzed transesterification. Reaction (1) is the abstraction of proton from methanol by the basic sites to form methoxide anion. This methoxide anion attacks carbonyl carbon in a molecule of the triglyceride leading to the formation of alkoxycarbonyl intermediate (Reaction 2). In reaction (3) the alkoxycarbonyl intermediate is transformed into a more stable form, FAME and anion of diglyceride; and in reaction (4) the methoxide cation attracts the anion of diglyceride leading to the formation of diglyceride. The sequence is repeated twice for $R_2$ and $R_3$.

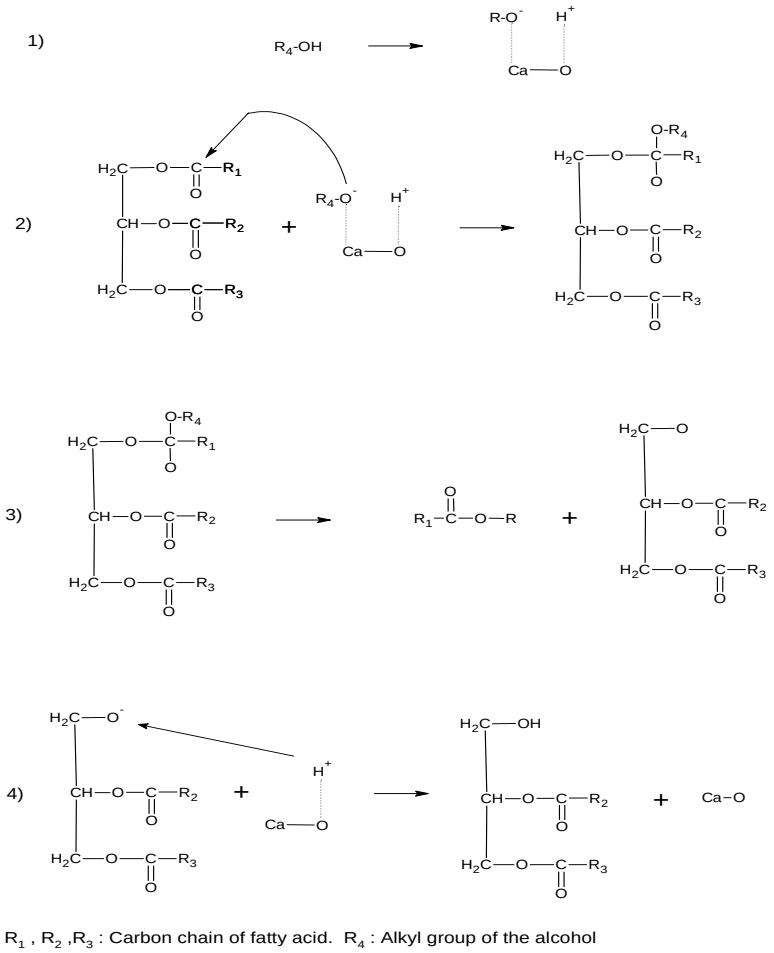


**Figure 2.6: Reaction mechanism for CaO as heterogeneous base catalyst (Lam et al., 2010)**

One interesting feature of CaO catalyst is the effect of water in the reaction system. While the presence of water has adverse affect on yield of FAME for most catalyst systems, CaO performs better in the presence of small amount of water. In the presence of a little water in methanol, CaO reacts to generate methoxide ion, which is highly active and is the real catalyst. A reaction mechanism for transesterification over CaO catalyst in presence of little water is given in Fig 2.7. At a basic site of CaO catalyst, surface $O^{2-}$ extracts $H^+$ from $H_2O$ from surface $OH^-$ (Reaction (1)), which is easily extracted by reactants in chemical reactions. Then, the $OH^-$ extracts $H^+$ from methanol to generate methoxide anion and $H_2O$ (Eq. 2). Also, $O^{2-}$ can also extract $H^+$ from hydroxyl group of methanol to form surface methoxide anions (Reaction (3)). However, if too much water (exceeding 2.8 wt% of

soybean oil) is added to methanol, the FAME is hydrolyzed to generate fatty acid and methanol.

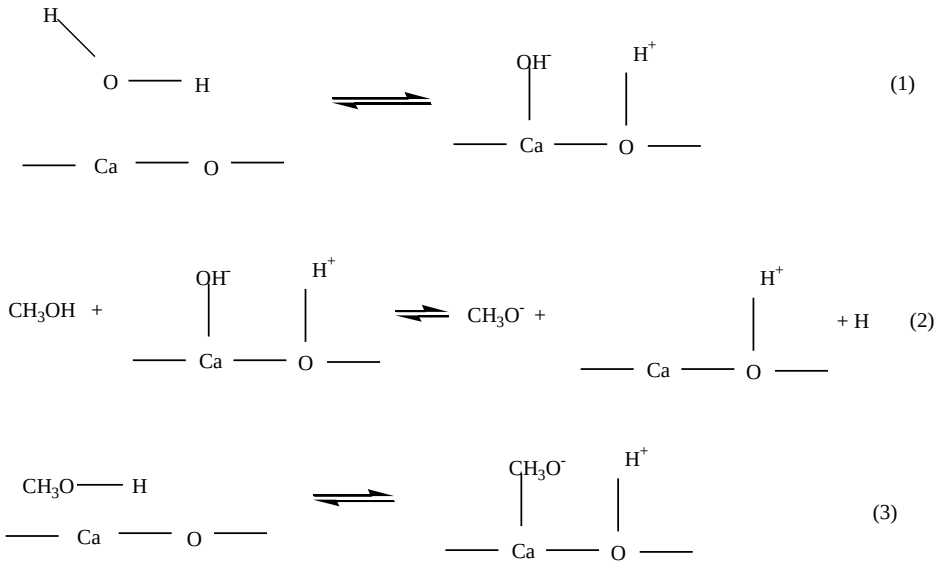


**Figure 2.7: Reaction mechanism for transesterification over CaO catalyst in presence of little water (Liu et al., 2008a)**

In the study a 12:1 molar ratio of methanol to oil, 8 wt% CaO catalyst, temperature of 338K, reaction time of 1.5 h, gave the maximum yield of 95% (Liu *et al*., 2008a). Transesterification of soybean oil using nanopowder CaO and microwave irradiation gave 96.6% conversion, at methanol to oil ratio 6:1, 338K temperature, reaction time 60 min, and 3 wt% catalyst (Hsiao *et al*., 2011). In a study involving transesterification of Jatropha oil, CaO was dipped in ammonium carbonate solution and calcined to get a super-base catalyst, of base strength of more than 26.5. For optimum conditions, calcinations temperature was 1173K, reaction temperature 343K, reaction time 2.5 h, catalyst concentration 1.5 wt%, methanol to oil ratio 9:1, and the conversion 93% (Zhu *et al*., 2006). Another study, using a similarly prepared super-base CaO catalyst, for transesterification of Jatropha oil gave a maximum yield of 95% for a 12:1 molar ratio of methanol to oil, 1.5 wt% of catalyst, temperature 343K, time 2 h, and water 2 wt%. Under supercritical conditions (473K and 24bar), the reaction time was reduced to 1 h, and yield increased to 96% in presence of super-base CaO catalyst (Hawash *et al*., 2011). This is in contrast to some other transesterification studies under supercritical conditions where the

catalyst was not employed and very high conversions obtained (Patil *et al*., 2010a; Demirbas, 2006; Yang, 2004; Kafuku *et al*., 2011).

Transesterification of *Camelina sativa* oil was studied using BaO, SrO, MgO, and CaO catalyst under conventional and microwave irradiation. The result of comparative experiments using conventional heating showed that the most effective catalyst was 1 wt% BaO which gave >80% yield of camelina to biodiesel conversion in 3 h at 373K. The FAME yields for BaO, SrO, CaO and MgO were 83%, 80%, 30% and 22%, respectively. The relative order of effectiveness of the catalysts was BaO > SrO > CaO > MgO (Patil and Deng, 2009; Patil *et al*., 2009). Under microwave irradiation, the FAME yields for BaO and SrO were 94% and 80% respectively. It was noted that microwave irradiation reduced the amount of methanol required, reduced the reaction time, but increased the catalyst amount (Patil *et al*., 2011), and SrO at 2 wt% gave a higher yield as compared to BaO at 1.5 wt%, although BaO has higher relative activity (Patil *et al*., 2010b). The relative activities of alkaline earth oxides compare well, with exception of CaO and MgO, as reported elsewhere, which gives the relative activities for transesterification of ethyl acetate with methanol as BaO > SrO > MgO > CaO (Hattori, 2004). Reaction mechanism for SrO catalyzed follows steps very similar to CaO catalyzed transesterification. The most crucial step is the formation of ionic complex when SrO comes in contact with methanol, similar to reaction (1) in Figure 2.6 for CaO, Sr replacing Ca in the reaction (Semwal *et al*., 2011). In a study on transesterification of ethyl acetate with methanol, magnesium oxide has been identified as a good alternative to homogeneous catalysts for biodiesel production (Dossin *et al*., 2006a). A simulation study indicated that a continuous production of 100,000 tonnes of biodiesel per year can be achieved at 323K in a continuous stirred reactor of 25 $m^3$ containing 5700 kg of MgO catalyst (Dossin *et al*., 2006b). Performances of MgO, CaO, BaO, PbO, and $MnO_2$ for transesterification of soybean oil at high pressure and temperature were studied. A maximum biodiesel yield of 85% was obtained by BaO in 14 min, whereas PbO, $MnO_2$, CaO, and MgO gave maximum yields of 84%, 80%, 78%, and 66%, respectively at 488K (Singh and Fernando, 2007). A similar high temperature, high pressure transesterification study of soybean oil involved seven metal oxide catalysts, PbO, ZnO, CaO, MgO, $PbO_2$, $Tl_2O_3$, and $Pb_3O_4$. Lead oxide catalysts were found to be most favourable towards the transesterification and gave yield

>89%. MgO and $Pb_3O_4$ showed an increasing FAME yield trend from 348 to 498K. MgO had the highest surface area, highest basicity, and relatively low leaching (Singh and Fernando, 2008). Transition metal oxides, zirconium oxide, titanium and zinc oxide have been tested as catalyst due to their strong acidic properties (Zabeti *et al*., 2009a). Transition metal solid base catalysts are moderately active and are of limited interest for transesterification reaction (Jitputti *et al*., 2006). However, metal oxides prepared with calcium show strong basic character, and have been tested for transesterification reaction. The calcium-containing catalysts, $CaTiO_3$, $CaMnO_3$, $Ca_2Fe_2O_5$, $CaZrO_3$, and $CaO–CeO_2$ , showed high activities and approximately 90% yields of FAME from rapeseed oil. In a catalytic durability test it was found that $CaZrO_3$ and $CaO–CeO_2$ show high durability and have the potential to be used in biodiesel production processes as heterogeneous base catalysts (Kawashima *et al*., 2008). Mesoporous $Li/ZrO_2$, $Na/ZrO_2$, $K/ZrO_2$, $Mg/ZrO_2$, and $Ca/ZrO_2$ were synthesized and tested for soybean oil transesterification. $Mg/ZrO_2$, and $Ca/ZrO_2$ showed no activity, $Na/ZrO_2$ showed little activity, and $Li/ZrO_2$, $K/ZrO_2$ gave FAME yield of 98% at temperature 923-1023K (Ding *et al*., 2011). A study of metals in homogeneous form showed the catalytic activity decrease in the order: $Sn^{+2} \gg Zn^{+2} > Pb^{+2} \cong Hg^{+2}$ (Abreu *et al*., 2004). Inspired by the high activity of $Sn^{+2}$, a solid SnO was used as a base catalyst for soybean oil. The yield of FAME was 56.5 to 94.7% for reaction time of 1 to 5 h. The catalyst was recycled up to four times without any loss of activity (Abreu *et al*., 2005). Magnesium methoxide was used as a solid base catalyst for transesterification of soybean oil. The reaction temperature varied from 323-338K, keeping methanol to oil ratio at 9:1, and catalyst concentration of 8 wt% (Huang *et al*., 2009). Transesterification of rapeseed oil was studied using alkaline earth metal compounds: calcium oxide, calcium methoxide and barium hydroxide. Tetrahydrofuran was used as a cosolvent to increase the solubility of methanol in oil. The results showed that barium hydroxide was most active, giving a conversion of 75% in 30 min, and >90% in 1.5 h; calcium methoxide was medially active, giving a conversion of 55% in 30 min, and 80% in 1 h, and 93% at equilibrium; solid CaO had the slowest rate, but the equilibrium conversion reached after 2.5 h had similar conversion. Magnesium oxide and calcium hydroxide showed no catalytic activity for rapeseed oil transesterification (Gryglewicz, 1999). Another study of transesterification of soybean oil and poultry fat using

nanocrystalline CaO catalyst gave a FAME yield of 2% for soybean oil, and *none* for poultry fat (Reddy *et al*., 2006). This review highlights the large variations in observed activities of alkaline earth oxide catalysts. Table 2.3 summarizes the FAME yield for alkaline earth oxide catalysts for a variety of feedstock at varying operating conditions.

**Table 2.3: Alkaline earth oxide catalysts in transesterification**

| Catalyst | Feedstock | Cat wt.% | MeOH:oil ratio | T(K) | Time (min) | FAME Yield, % | Reference |
|---|---|---|---|---|---|---|---|
| **MgO** | *J. curcas* | 3 | 25 | 393 | 180 | 64 | Taufiq-Yap *et al*.. 2011 |
| **MgO** | Sunflower | - | 12 | 323 | 1440 | 3.5a 2.5b | Arzamendi *et al*., 2008 |
| **MgO** | Soybean | 2.5 | 0.3(vol) | 488 | 120 | 66 | Singh & Fernando, 2007 |
| **MgO** | Soybean | 5 | 55 | 403 | 420 | 60 | Antunes *et al*., 2008 |
| **MgO** | Rapeseed | - | 4.5 | 340 | 150 | nil | Gryglewicz, 1999 |
| **MgO** | Soybean | 5 | 12 | 333 | 420 | 13.5 | Puna *et al*., 2010 |
| **MgO** | Camelina Sativa | 0.25-2 | 3-15 | 313-403 | 30-180 | 5-20 | Patil & Deng, 2009 |
| **MgO** | Palm | 5 | 9 | 333 | 90 | 3 | Babak *et al*., 2013 |
| **MgO** | Triacetin | 2 | 6 | 333 | 480 | 18 | Lopez *et al*., 2005 |
| **Nano MgO** | Soybean | 3 | 36 | 523 | 12 | 98 | Wang and Yang, 2007 |
| **CaO** | *J. curcas* | 3 | 25 | 393 | 180 | 96 | Taufiq-Yap *et al*., 2011 |
| **CaO** | Sunflower | - | 12<br>12 | 323<br>323 | 600<br>1440 | 90a<br>1.5b | Arzamendi *et al*., 2008 |
| **CaO** | Sunflower | 3 | 13 | 333 | 100 | 94 | Granados *et al*., 2007 |
| **CaO** | Sunflower | 1<br>5 | -<br>41 | 335<br>525 | 180<br>1200 | 5<br>99 | Demirbas, 2007 |
| **CaO** | Sunflower | 1 | 6 | 823 | 120 | 98 | Veljkovic *et al*., 2009 |
| **CaO** | Soybean | 8 | 12 | 338 | 180 | 80 | Liu *et al*., 2008 |
| **CaO** | Soybean | - | - | - | 120 | 99 (in $N_2$) | Kouzu *et al*., 2009 |
| **CaO** | Soybean | 1 | 12 | - | 120 | 99 (in $N_2$)<br><10 (in Air) | Kouzu *et al*., 2008a |
| **CaO** | Soybean | - | 12 | reflux | 120 | 93 | Kouzu *et al*., 2008b |
| **CaO** | Soybean | - | 27 | 298 | - | 2 | Reddy *et al*., 2006 |
| **CaO** | Soybean | 5 | 12 | 333 | 420 | 93.3 | Puna *et al*., 2010 |
| **CaO** | Soybean | 0.58 | 39 | 573 | - | 97 | Lee *et al*., 2009 |
| **CaO** | Soybean | 2.5 | 0.3(vol) | 488 | 30 | 75 | Singh & Fernando, 2007 |
| **CaO** | Rapeseed | - | 4.5 | 340 | 150 | 75 | Gryglewicz, 1999 |
| **CaO** | Rapeseed | 0.7 | 0.26 (wt) | 333 | 180 | 90 | Kawashima *et al*., 2009 |
| **CaO** | WCO | - | - | - | 120 | 99 (in $N_2$) | Kouzu *et al*., 2008a |
| **CaO** | Poultry fat | - | 27 | 298 | - | nil | Reddy *et al*., 2006 |
| **CaO** | Camelina Sativa | 0.25-2 | 3-15 | 313-403 | 30-180 | 10-20 | Patil & Deng, 2009 |
| **CaO** | Palm | 5 | 9 | 333 | 90 | 35 | Babak *et al*., 2013 |
| **CaO (oyster** | Soybean | 25 | 6 | 343 | 300 | 70 | Nakatani *et al*., 2009 |

| | | | | | | | |
|---|---|---|---|---|---|---|---|
| **shell)** | | | | | | | |
| **CaO (egg shell)** | Soybean | 3 | 9 | 338 | 180 | 95 | Wei *et al*., 2009 |
| **CaO (mud crab shell)** | Palm olein | 5 | 0.5 (wt) | 338 | 150 | 95 | Boey *et al*., 2009 |
| **CaO (mollusk shell)** | Palm olein | 10 | 18 | 233 | 120 | 90 | Viriya-empikul *et al*., 2010 |
| **CaO (crab & cockle shell)** | Chicken fat | 4.9 | 0.55(wt) | - | 180 | 98 | Boey *et al*., 2011 |
| **CaO (egg shell)** | Palm olein | 15 | 18 | 900W | 4 | 96.7 (microwave) | Khemthong *et al*., 2012 . |
| **CaO (egg and sea shells)** | Miscellaneous | 4 | 6 | - | 120 | 98 | Sarin *et al*., 2009 |
| **Nano-CaO** | Soybean | 3 | 7 | 338 | 60 | 96.9 | Hsiao *et al*., 2011 |
| **SrO** | Camelina Sativa | 0.25-2 | 3-15 | 313-403 | 30-180 | 25-80 | Patil & Deng, 2009 |
| **SrO** | Camelina Sativa | 2 | 9 | - | 4 | 95 (micro wave) | Patil *et al*., 2010b |
| **SrO** | Palm | 5 | 9 | 333 | 90 | 91 | Babak *et al*., 2013 |
| **SrO** | Soybean | 3 | 12 | 338 | 30 | 95 | Liu *et al*., 2007 |
| **BaO** | Camelina Sativa | 0.25-2 | 3-15 | 313-403 | 30-180 | 30-85 | Patil & Deng, 2009 |
| **BaO** | Camelina Sativa | 1.5 | 9 | - | 4 | 93 (micro wave) | Patil *et al*., 2010b |
| **BaO** | Palm | 5 | 9 | 333 | 90 | 95 | Babak *et al*., 2013 |
| **BaO** | Soybean | 2.5 | 0.3(vol) | 488 | 15 | 95 | Singh & Fernando, 2007 |

Note: a- Catalyst not calcined; b- Catalyst calcined at 773K for 12 h

#### 2.3.2.2.3 Zeolite Heterogeneous Catalysts

Zeolites are microporous, aluminosilicate minerals having a porous structure that can accommodate a wide variety of cations, such as $Na^{+}$, $K^{+}$, $Ca^{2+}$, $Mg^{2+}$ and others (Muerbach *et al*., 2003). They are available both in natural and synthetic form. The transesterification of soybean oil with methanol to methyl esters was carried out using NaX zeolites loaded with KOH as a solid base catalyst. The NaX zeolite did not present any particular catalytic activity, most likely due to the lack of strong basic sites on which the transesterification reaction could occur. However, loading of KOH onto the NaX zeolite produced a dramatic increment of basic strengths on the KOH/NaX catalyst. Best result was obtained with NaX zeolite loaded with 10% KOH, followed by heating at 393K for 3 h. When the

transesterification reaction was carried out at reflux of methanol (338K), with a 10:1 molar ratio of methanol to soybean oil, a reaction time of 8 h and a catalyst amount of 3 wt%, the conversion of soybean oil was 85.6% (Xie *et al*., 2007). Transesterification of soybean oil was studied using two types of zeolite, NaX faujasite zeolite and ETS-10 zeolite as catalyst at temperatures of 333, 393 and 423K. Stock zeolites were exchanged with K and Ce; NaX containing occluded sodium oxide ($NaO_x$/NaX) and occluded sodium azide ($NaO_x$/NaX). The catalysts were calcined at 773K prior to use in order to increase activity. The ETS-10 catalysts provided higher conversions than the Zeolite-X type catalysts. The increased conversions were attributed to the higher basicity of ETS-10 zeolites and larger pore structures that improved intra-particle diffusion. Methyl ester yield increased with an increase in temperature from 333 to 423K (Suppes *et al*., 2004). Soybean oil was transesterified with methanol using Mg MCM-41 zeolite, Mg-Al hydrocalcite, and K impregnated zirconia. Mg-Al hydrocalcite showed the highest activity, giving 97% conversion. For the K impregnated zirconia, the activity increased as K increased indicating the higher basicity increased activity (Georgogianni *et al*., 2009). In another study of soybean oil transesterification with methanol using modified zeolites such as Y, A, and clinoptilolite as natural zeolite catalyst; it was revealed that modified zeolite Y gave a higher conversion of 98.4% as compared to the natural zeolite clinoptilolite which gave 86.9% conversion (Farzaneh and Raashtizadeh, 2010). Transesterification of *Jatropha curcas* seed oil with methanol was studied using artificial zeolites loaded with potassium acetate as a catalyst. After calcinations for 5 h at 823K, the catalyst loaded with 47 wt% potassium acetate exhibited the highest efficiency. Optimum conditions were at oil to methanol ratio 1:10, catalyst 2 wt%, reaction time 4 h, at reflux temperature (Xue *et al*., 2009). Transesterification of sunflower oil was studied using NaX zeolite (Si/Al = 1.23) as a carrier for nano CaO particles. CaO mass percent ranged from 5-25%. Reactions were carried out at atmospheric conditions and at reflux temperature of methanol, at methanol to sunflower oil ratio of 6:1, for 6 hr. Highest yield for methyl ester was 93.5%, obtained at 16 wt% of CaO (Martinez *et al*., 2011). Zeolite Y with different $Al_2O_3$ content was tested as a catalyst to produce biodiesel from used vegetable oil and methanol. The methanol to oil ratio was 6:1 and the reactions were carried out at atmospheric pressure. The temperature varied from 473 – 749K. Product obtained had lower viscosity. Higher

temperature gave viscosity close to biodiesel (Brito *et al*., 2007). Activity of zeolite as a catalyst was tested as compared to alkali metal and alkaline earth catalysts, CaO, MgO, $Ba(OH)_2$, Li/CaO, for transesterification of vegetable oil. $Ba(OH)_2$ gave the highest activity among all the catalysts (Dalai *et al*., 2008).

#### 2.3.2.2.4 Supported Alkali/ Alkaline Earth Metals

Alkali and alkaline earth metal Na, K, Ba, Ca, Mg, and their carbonates, hydroxides, halides and nitrates can be supported on alumina and silica (Endalew *et al*., 2011). Potassium hydroxide supported on alumina was prepared by mixing alumina and the alkali, and separating and drying the solid. Some examples of supported alkali/alkaline earth metals are also given in previous section (Suppes *et al*., 2004; Martinez *et al*., 2011). Catalytic activities of alumina loaded potassium compounds, KI, KF, $K_2CO_3$ and $KNO_3$ with 35 wt% loading, were tested for the transesterification of canola oil with methanol and ethanol. Synthesized $KF/Al_2O_3$ catalyst showed the highest activity in the transesterification of canola oil with methanol and gave much stable methyl ester content during the reaction with the highest yield of 99.6% at the end of the 8 h reaction time at 333K, with a methanol to oil ratio of 15:1 and a catalyst amount of 3 wt% (Boz and Kara, 2009). Castor oil was transesterified with methanol using $Al_2O_3$/50% KOH catalyst. More than 90% conversion was obtained at 333K, in 1 h, using conventional heating, at methanol to oil ratio of 6:1, and catalyst 10 wt%. The same reaction carried out using microwave irradiation (40W) give a 95% conversion in 5 min at similar conditions (Perin *et al*., 2008). Transesterification of soybean oil with methanol was studied using alumina loaded with potassium iodide as a solid base catalyst. After loading KI of 35 wt% on alumina followed by calcination at 773 K for 3 h, the catalyst gave the highest basicity and the best catalytic activity with a conversion of 96% under the optimum reaction conditions (Xie and Li, 2006). Transesterification of soybean oil over KF loaded onto $\gamma$-$Al_2O_3$ heterogeneous basic catalyst was carried out. The best reaction conditions were at a load ratio of KF 72.68 wt%, methanol to oil ratio 12:1, temperature 338 K, mass of catalyst 2 wt%, reaction time 3 h, and the yield of biodiesel exceeded 99% (Teng *et al*., 2009). The transesterification of palm oil to FAME was studied using KOH loaded on $Al_2O_3$ and NaY zeolite supports as heterogeneous catalysts. The 25 wt% $KOH/Al_2O_3$ and 10 wt% KOH/NaY catalysts were suggested to be the best formula due to their biodiesel yield of

91.07% at temperatures below 343K within 2–3 h at a 1:15 molar ratio of palm oil to methanol and a catalyst amount of 3–6 wt%. The leaching of potassium species in both spent catalysts was observed (Noiroj *et al*., 2009). Mesoporous γ-alumina was used as a support for sodium azide, $NaN_3$, to yield a superbasic catalyst that showed high activity for soybean oil transesterification (Bota *et al*., 2010). Transesterification of palm kernel oil with methanol over mixed oxides of Ca and Zn, CaO·ZnO catalysts was studied. The mixed oxides had a relatively small particle sizes and high surface areas, compared to pure CaO and ZnO. At 60 °C (catalyst 10 wt%, methanol to oil molar ratio of 30, reaction time 1 h), the FAME content of >94% could be achieved over CaO·ZnO catalyst with the Ca/Zn ratio of 0.25 (Ngamcharussrivichai *et al*., 2009). Transesterification of palm oil was carried out using $CaO/Al_2O_3$ composite catalyst. It was shown that both the calcination temperature and the amount of calcium oxide loaded on the support had significant positive effects on the biodiesel yield. The maximum basicity and biodiesel yield obtained were about 194 mmol/g and 94% respectively, and the catalyst showed high performance at moderate operating conditions and its activity was maintained after two cycles (Zabeti *et al*., 2009b). Transesterification of palm kernel oil and coconut oil with methanol was investigated using various $Al_2O_3$-supported alkali and alkaline earth metal oxides, $LiNO_3/Al_2O_3$, $NaNO_3/Al_2O_3$ and $KNO_3/Al_2O_3$ . Effect of calcinations temperature on catalyst activity was studied. $Ca(NO_3)_2/Al_2O_3$ calcined at 723K yielded the FAME content as high as 94%, and calcined $Mg(NO_3)_2/Al_2O_3$ catalyst possessed an inactive magnesium-aluminate phase, resulting in very low FAME formation (Benjapornkulaphong *et al*., 2009). In another major study, novel mesoporous $Al_2O_3$-, $SiO_2$-supported solid base catalysts containing Ca, K as active elements were synthesized by a single-step sol-gel method. The synthesized catalysts possess a large BET surface area in the range of 180-400$m^2$/g and a mesoporous pore size in the range of 60-120Å. A 100% yield was obtained in 30min when 1wt% K/Al-0.6 or Ca/Al-4.0 catalyst was used. Ca-loaded catalysts exhibited a higher stability than K-loaded catalysts. The amount of Ca leaching was reduced significantly with the Ca/Al or Si molar ratio (Zhao, 2010).

#### 2.3.2.2.5 Clay Minerals

Classic clay mineral used as heterogeneous catalyst is hydrotalcite. Hydrotalcite is a layered double hydroxide of general formula $(Mg_6Al_2(CO_3)(OH)_{16}\cdot 4(H_2O)$. It is

dimorphous and has anion exchange capabilities (Bejoy, 2001). Hydrotalcites of Mg and Al (Mg/Al ratio 3) modified with Zn, Sn, Ba, Mn, Ce, and Ca with 5 wt% catalyst were used for transesterification of soy oil with methanol, at 343K, time 3 h, and methanol to oil ratio 9:1. Good results regarding biodiesel yield and product quality were obtained (Gomes *et al*., 2008). Transesterification of canola oil with methanol was studied using Mg-Al hydrotalcites as solid base catalysts. The highest triglyceride conversion rate of 71.9% was achieved after 9 h of reaction at 333K, with a 6:1 molar ratio of methanol to canola oil and a 3 wt% catalyst with 125-150 $\mu$m particles. Hydrotalcites were prepared by the co-precipitation method using ($Mg(NO_3)_2$), ($Al(NO_3)_3$), and $Na_2CO_3$ (Ilgen *et al*., 2007). Transesterification of palm oil was studied using KF/hydrotalcite solid base catalysts. At 338 K, with palm oil/methanol molar ratio of 12:1, reaction time of 3 h, and catalyst amount of 3 wt %, the yield of FAME reached 85%; and when the reaction time prolonged to 5 h, the yield became 92% (Gao *et al*., 2008). Transesterification of soybean oil to biodiesel was carried out using Mg-Al hydrotalcite as heterogeneous catalyst. The Mg-Al hydrotalcite with Mg/Al molar ratio of 3.0 was synthesized by co-precipitation method. The best conditions for hydrotalcite preparation and transesterification reactions were as follows: calcination temperature 823K, molar ratio of soybean oil to methanol of 6:1, reaction time 360 min, and catalyst dosage 5%, the yield of FAME 78% (Chang *et al*., 2008). In another study on transesterification of soybean oil, new solid base catalysts were prepared by substituting $Fe^{3+}$ ions substitute for a fraction of the $Al^{3+}$ ions in the Mg/Al layered double hydroxide lattices of hydrotalcites and calcining to give porous metal oxides. These iron-doped porous metal oxides are much stronger bases than those derived from undoped or $Ga^{3+}$ doped hydrotalcites and are effective catalysts for the methanol transesterification of triacetin (glycerol triacetate) and of soybean oil (Macala *et al*., 2008). Heterogeneous base catalyst derived from Mg–Al hydrotalcite was investigated for the conversion of poultry lipids to biodiesel. This solid base showed high activity for triglyceride transesterification with methanol without signs of catalyst leaching. Both temperature (333–393K) and methanol-to-lipid molar ratio (6:1–60:1) affected the reaction rate in a positive manner. The use of a co-solvent (hexane, toluene, tetrahydrofuran), however, gave rise to a change in triglyceride conversion profile which cannot be explained solely by a dilution effect. By re-calcination in air, complete catalyst

regeneration was achieved (Liu *et al*., 2007). In another study, vegetable and used frying oil were transesterified using pure hydrotalcite and hydrotalcite modified for increasing its alkali behavior and reactivity. Effect of temperature, mixing speed, reaction time, catalyst pretreatment, catalyst concentration, alcohol to feed-stock ratio, and percent hydrotalcite modification through introduction of sodium to structure, were investigated (Labarta *et al*., 2009). Production of biodiesel via transesterification of castor oil using metal oxides as solid catalysts was investigated using hydrotalcite derived Mg-Al mixed oxide as a heterogeneous catalyst and the effect of reaction parameters in transesterification reaction were observed (Yaacob and Farhah, 2010). Activities of hydrotalcite, Cs-sepiolite and Cs-MCM-41 have been compared as a heterogeneous catalyst for transesterification of triglycerides, at 513K for 5 h, and the activities were found to be in the order: hydrotalcite (92% conversion) > Cs-sepiolite (45% conversion) > Cs-MCM-41 (26% conversion) (Au and Dai, 2012).

#### 2.3.2.2.6 Non-Oxides

Some studies involving metal halides, hydroxides, carbonates and their combinations have already been given in previous sections. A major category of non-oxide catalysts are non-metallic organic compounds, mainly guanidine containing catalysts. Guanidines are a group of organic compounds sharing a common functional group with the general structure $(R^1R^2N)(R^3R^4N)C=N-R^5$. The central bond within this group is that of an imine, and the group is related structurally to amidines and ureas (Sherrington, 2001). A new catalyst based on amines (guanidine carbonate) for transesterification of vegetable oils was tested and it was found that conversions of >95% could be reached within one reaction step in less than one hour. Particularly in transesterification of oils containing free fatty acids, guanidine carbonate showed significant advantages as no soap formation was observed. The process is applied in an industrial pilot plant with a capacity of approx. 1t/h (Greve, n.d.). In another work to develop polymeric catalysts, three polycationic systems were studied, composed of poly(hexamethylene biguanide) (PHMBG, pKa in water ~11), branched polyethyleneimine (PEI, pKa, 9.7), and poly(N-vinylguanidine) (PVG, pKa ~13). Comparison of the methanolysis rates in anhydrous conditions revealed that uncross-linked PHMBG was a remarkably efficient catalyst, enabling 100% triglyceride conversion within 0.5 h at 343K. The PHMBG-based networks also demonstrated 100% conversion, but the

kinetics were 1.5- to 2.4-fold lower than those with uncross-linked PHMBG (which is soluble in methanol) due to the less efficient heterogeneous catalysis by the cross-linked networks (Bromberg *et al*., 2010). For transesterification of soybean oil, guanidines were successfully grafted on gel-type polystyrene matrix by covalent bonding and the catalyst gave high conversion, but the reaction time was prolonged. However, the heterogenized guanidines slowly leached out from polymer resulting in a continuous loss in catalytic activity (Schuchardt *et al*., 1996). To contain the loss of activity due to side reactions, the biguanides were confined to polystyrene, yielding a more reactive solid base than the polymer-supported guanidines, and with a reactivity which was stable for at least 10 cycles (Gelbard and Vielfaure-Joly, 2000; Gelbard and Vielfaure-Joly, 2001). In another work, guanidine functionalized polymers were also used for transesterification of methyl fatty ester with glycerol targeting the formation of monoglycerides (Jerome *et al*., 2004).

### 2.3.3 Non-catalytic transesterification

Non-catalytic transesterification for FAME is carried out by using methanol in supercritical state (T > 512.6K, P > 8.907 MPa). Supercritical methanol is believed to solve the problems associated with the two-phase nature of normal methanol/oil mixtures by forming a single phase as a result of lower dielectric constant of methanol in the supercritical state. Reactions in such a state are very fast and non-catalytic (Demirbas, 2009; Demirbas, 2003). Supercritical transesterification of *Camelina sativa* oil at 563K gave a yield of 90% biodiesel in the absence of any catalyst (Patil *et al*., 2010a). *Croton megalocarpus* oil transesterified non-catalytically at 603K yielded 74.91% FAME (Kafuku *et al*., 2011). Non-catalytic supercritical methanol method involves simpler purification, has a lower reaction time, is less energy intensive, and is environmentally superior (Saka and Kusdiana, 2001). However, requirement of high temperature and pressure has limited supercritical studies to laboratory scale so far.

## 2.4 Transesterification Process Variables

Fatty acid esters production depends upon the choice of feedstock, alcohol and catalyst as the reaction constituents. Operating variables include: oil-to-alcohol ratio, reaction temperature and pressure, catalyst concentration, reaction time, mixing intensity, co-solvents, and catalyst preparation conditions. The type of reactor system, heating methods

such as conventional or microwave, normal or ultrasound mixing etc., are part of reactor operation variables (Islam *et al*., 2013).

### 2.4.1 Feedstock

Biodiesel can be made from any plant oil or animal fat. However some oils are better that the others. Oils such as soybean, palm, palm kernel, ground nut, beef tallow etc have been successfully converted into biodiesel. However, there has been a debate in using edible oils to convert into fuel. Preference is given to the use of oil as food, especially in the third world. Therefore, one of the requirements for an acceptable feedstock is that it should not be edible. The non-edible feed stocks are oils from: *Jatropha curcus*, *Pongamia pinnata*, castor, cotton seed, linseed, *Croton megalocarpus*, algae etc. Waste cooking oils also fall in this category. Oils can be classified according to the number of carbon atoms and number of double bonds. Table 2.4 gives the percentage fatty acid compositions of some oils based on carbon atoms and double bonds (Demirbas, 2003).

**Table 2.4: Fatty Acid Composition (wt%) of Various Oils (no of C atoms: no of double bonds)**

| Fat or Oil | 12:0 | 14:0 | 16:0 | 18:0 | 18:1 | 18:2 | 18:3 | 20:0 | 20:1 | 22:1 |
|---|---|---|---|---|---|---|---|---|---|---|
| **Soybean** | . | . | 6-10 | 2-5 | 20-30 | 50-60 | 5-11 | . | . | . |
| **Corn** | . | 1-2 | 8-12 | 2-5 | 19-49 | 34-62 | . | . | . | . |
| **Peanut** | . | . | 8-9 | 2-3 | 50-65 | 20-30 | . | . | . | . |
| **Olive** | . | . | 9-10 | 2-3 | 73-84 | 10-12 | | . | . | . |
| **Cottonseed** | . | 0-2 | 20-25 | 1-2 | 23-35 | 40-50 | . | . | . | . |
| **Butter** | . | 7-10 | 24-26 | 10-13 | 28-31 | 1-2.5 | 2-5 | . | . | . |
| **Lard** | . | 1-2 | 28-30 | 12-18 | 40-50 | 7-13 | 0-1 | . | . | . |
| **Tallow** | . | 3-6 | 24-32 | 20-25 | 37-43 | 2-3 | . | . | . | . |
| **Linseed** | . | . | 4-7 | 2-4 | 25-40 | 35-40 | 25-60 | . | . | . |
| **Yellow grease** | . | 2 | 23 | 13 | 44 | 7 | 1 | . | . | . |
| **Coconut** | 45-53 | 17-21 | 7-10 | 2-4 | 5-10 | 1-3 | . | . | . | . |
| **Palm oil** | . | . | 44 | 5 | 39 | 10 | . | . | . | . |
| **Palm kernel** | 48 | 16 | 8 | . | 15 | 3 | . | . | . | . |
| **Pongamia P.** | . | . | 4-8 | 3-9 | 45-71 | 11-18 | . | 2-5 | 10-12 | 4-5 |

Fatty acids without double bonds are called saturated fats. A high saturation level is indicated from high fractions of saturated fatty acids (C14:0, C16:0, C18:0), raising the cloud point, cetane number, calorific value and stability of the biofuel; and lowering the

$NO_x$ emissions. Fatty acids containing double bonds are called unsaturated. The double bonding site is somewhat unstable and can break off or be chemically altered in the presence of heat and water. Unsaturated fats tend to spoil faster than saturated fats. High unsaturation level due to increased levels of unsaturated fatty acids (C18:2, C18:3) tends to reduce biofuel cloud point, cetane number, calorific value and increases $NO_x$ emissions (Tyson, 2006).

Three aspects are significant to decide whether a given feedstock is 'green' or environmentally benign: (i) what was the land use or cover prior to the planting of biodiesel feedstock, (ii) how much fossil fuel is used in growing the feedstock, and (iii) competition with food feedstock. Some common plant species (Jatropha, Castor, Palm, *Croton megalocarpus*) currently being promoted for biodiesel have been studied in view of the above three requirements (Milch, n.d.). Jatropha is endemic to India and the oil is inedible. There are always dangers in importing a foreign plant species in a country, and for that reasons Australia has banned it. Cultivation requires substantive inputs in fertilizer, irrigation, herbicides etc. Castor oil is inedible so do not compete with food. Oil yields are 200-2,750 kg/ha. Plant requires irrigation, or substantive water supply. Plant is subject to fungal and bugs attack. Plant depleted the soil quickly, and fertilizers are required to sustain yield. Seeds are toxic and dangerous if consumed by humans and animals. Also, the castor oil is too viscous to produce a good biofuel. Palm oil competes with food. *Croton megalocarpus* tree is indigenous to East Africa. Its large scale plantation would not have adverse ecological effect. Tree has a productive life of about 50 years, fruits drop by itself, and the oil is inedible. The roots are deep and fertilizers are not needed. In another study, vegetable oil production for five oil bearing plant species, *Aleurites moluccana, Croton megalocarpus, Jatropha carcas, Moringa oliphera and Pachira glabra,* were investigated. All five varieties were found to contain acceptable but different oil content ranging from 20 to 33 wt%, and seed/nut acreage yield of 3 t/ha/y to 12.5 t/ha/y. Upstream processing was needed for *A. moluccana* to break open nuts to release the kernel, and dehulling for both *C. megalocarpus* and *J. curcas* to release the seeds, before extracting the vegetable oil, while the seeds of both *M. oleifera* and *P. glabra* did not need upstream processing. The multi-criterion-decision-analysis ranked *C. megalocarpus* as the plant with the highest vegetable oil production potential of 1.8 t/ha/y, followed by *M. oliefera*, *J. curcas* (1

t/ha/y), *A. moluccana,* and *P. glabra*.( Kibazohi and Sangwan, 2011). Aliyu *et al*. (2010) also studied the potential of *croton megalocarpus* and concluded that the croton oil has a strong potential as a source for biodiesel.

### 2.4.2 Alcohol and Alcohol-to-Oil ratio

Alcohols are primary and secondary monohydric aliphatic alcohols having 1-8 carbon atoms. Among alcohols that can be used in the transesterification process are methanol, ethanol, propanol, butanol and amyl alcohol. Methanol and ethanol are used most frequently, especially methanol because of its low cost and its physical and chemical advantages (polar and shortest chain alcohol). It can quickly react with triglycerides and sodium hydroxide is quickly dissolved in it (Ma and Hanna, 1999). From Reaction 2.2, three moles of alcohol are needed to transesterify one mole of triglyceride, as per the stoichiometry. In practice, a higher molar ratio of alcohol-to-oil is needed to drive the reaction towards 'right' to get a higher yield. Section 2.3 gives numerous examples of alcohol:oil ratios used in transesterification studies. A methanol:oil molar ratio of 6:1 is found to be quite satisfactory for homogeneous alkaline catalysts (NaOH, KOH). Homogeneous acid catalysts and heterogeneous catalysts usually require a higher alcohol ratio for a good yield. For transesterification of soybean oil with methanol, a 42:1 methanol-to-oil molar ratio was used for 5wt% $Zn/I_2$ catalyst giving a 93% yield in 22h (Li and Xie, 2006), and a 36:1 ratio was used for Nano-MgO catalyst at 3% catalyst, 3 bar to give a yield of 98% in 0.2h (Wang and Yang, 2007). FAME from Triolein was obtained using Anion exchange resin catalyst using a 20:1 methanol:triolein ratio giving a 85% yield (Shibasaki-Kitakawa *et al*, 2007). On a more moderate side, methanol:oil ratios ranging from 16:1 to 6:1 have been used for: soybean oil - catalyst $KI/SiO_2$ (Samart *et al*., 2009), catalyst Mg-Al hydrotalcite ( Xie *et al*., 2006), catalyst Calcium methoxide (Liu *et al*., 2008b), catalyst $K_2CO_3/MgO$ (Liang et al., 2009), catalyst Na/NaOH/ $Al_2O_3$ (Kim *et al*., 2004); jatropha oil- catalyst $KNO_3/Al_2O_3$ (Vyas *et al*., 2009); rapeseed oil- catalyst $ZnL_2$/Cordierite (Kolaczkowski *et al*., 2009), catalyst $LiNO_3/CaO$ (MacLeod *et al*., 2008); palm oil- catalyst $KAl(SO_4)_2.12\ H_2O$ (Aderemi and Hameed, 2009), catalyst Montomorillonite KSF (Kansedo *et al*., 2009), catalyst $25\%KOH/Al_2O_3$ and 10%KOH/NaY (Noiroj *et al*., 2009), catalyst KF/ZnO (Hameed *et al*., 2009); sunflower oil- catalyst Calcium zincate (Rubio-Caballero *et al*., 2009), catalyst CaO (Granados *et al*.,

2007), catalyst $K_2CO_3$/ $Al_2O_3$-$SiO_2$ (Lukic *et al*., 2009), catalyst $CaO/SiO_2$ (Albuquerque *et al*., 2008); palm kernel oil- catalyst $SO_4/ZrO_2$ (Jitputti *et al*., 2006), catalyst CaO/Dolomite (Ngamcharussrivichai *et al*., 2007). As the molar ratio of methanol is increased, the reaction rate and the yield increases, but the excess methanol mixes with glycerol bringing about separation challenges.

### 2.4.3 Heating mode and reaction temperature

Simulation study of transesterification of triglyceride with methanol gives the enthalpy of reaction as 10.742 kJ $mol^{-1}$, which is slightly endothermic (Zhang *et al*., 2012). Hence a rise in temperature would favour the FAME formation. For catalytic reactions, a higher temperature reduces the viscosity and increases mass transfer rates, resulting into faster reaction rates. However, the highest operating temperature is somehow limited to the boiling temperature of methanol. If temperatures are raised substantially above the methanol boiling point, methanol goes into vapour phase, reducing the yield of FAME and leading to saponification of triglycerides (Eevera *et al*., 2009). Usual temperature range for transesterification for FAME is between 323 – 423K (Leung and Guo, 2006; Ma and Hanna, 1999). For the same reaction temperature, better results are observed when the heating mode is through microwave irradiation.

#### 2.4.3.1 Microwave irradiation

Mode of heat transfer is another process variable that has been under investigation in the recent times. Conventional heating is through conduction and convection using temperature controlled heating mantle, water bath or some other heat exchanger. Conventional heating methods are energy inefficient leading to high production costs. Microwave irradiation is an energy efficient, quick heating process for transesterification (Reefat *et al*., 2008). Microwave irradiation for biodiesel production is considered green chemistry due to savings in energy consumption, reaction time, solvent needs; coupled with higher conversion and better selectivity (Gude *et al*., 2014)

Microwave irradiation is the electromagnetic irradiation with frequency range of 0.3-300 GHz. They lie in the electromagnetic spectrum between infrared waves and radio waves between 0.01 and 1m. In general, in order to avoid interference, industrial and domestic microwave apparatus are regulated to 12.24 cm, corresponding to a frequency of 2.45 GHz, but other frequency allocations do exist. One reason for this is that near to this

frequency, the microwave energy absorption by liquid water is maximum. Energy associated with microwaves ($1.24x10^{-6}$ – $1.24x10^{-3}$ eV) is lower than the energy of Brownian motion ($2.7x10^{-3}$ eV at 310K) which is not strong enough to even break chemical bonds as such microwaves cannot induce chemical reactions. Microwaves as an energy source, produce heat by their interaction with the materials at molecular level without altering the molecular structure. In conventional heating, heat transferred to the sample volume is utilized to increase temperature of the surface of the vessel followed by the internal materials. Therefore, a large portion of the energy supplied through conventional energy source is lost to the environment through conduction of materials and convective currents. Heating effect in the conventional method is heterogeneous and depends on viscosity, conductive and convective heat transfer coefficients and density, resulting in higher surface temperatures (Reefat and El Sheltawy, 2008). Microwave heating offers several advantages over conventional heating such as non-contact heating (reduction of overheating of material surfaces), energy transfer instead of heat transfer (penetrative radiation), reduced thermal gradients, material selective and volumetric heating, fast start-up and stopping and reverse thermal effect, i.e. heat starts from the interior of material body. Microwaves transfer energy into materials by dipolar polarization, ionic conduction and interfacial polarization mechanisms to cause localized and rapid superheating of reaction materials. If a molecule possesses a dipole moment, when it is exposed to microwave irradiation the dipole tries to align with the applied electric field. Since the electric field is oscillating, the dipoles constantly try to realign to follow this movement. At 2.45 GHz, molecules have time to align with the electric field but not to follow the oscillating field exactly. If a molecule is charged, then the electric field component of the microwave irradiation moves the ions back and forth through the sample while also colliding them into each other. This movement again generates heat. In addition, because the energy is interacting with the molecules at a very fast rate, the molecules do not have time to relax and the heat generated can be, for short time, much greater than the overall recorded temperature of the bulk reaction mixture. In essence, there would be instantaneous localized superheating. In terms of biodiesel production, the resultant effect could include: more effective heating, fast heating of catalysts, reduced

equipment size, faster response to process heating control, faster start-up, increased production, and elimination of process steps (Gude *et al*., 2013).

Demirbas (2002), and Sinnwell & Ritter (2007) have reported 5 – 1000 times increase in reaction rates under microwave irradiation. Such increase can be justified through thermodynamics of reaction. Arrhenius equation for reaction rate constant, *k*:

$$k = A\, e^{-E/RT} \qquad \text{(Levenspiel, 1972)} \qquad ...2.6$$

In Equation 2.6, *E*, the activation energy, is the difference of Gibbs energy $\Delta G$. Hence,

$$k = A\, e^{-\Delta G/RT} \qquad \ldots 2.7$$

Reaction rate can be increased by increasing *frequency factor* A, which is the molecular mobility that depends on frequency of the vibrations of reacting molecules. This is directly related to microwave action.

Alternatively, reaction rate can also be increased by decreasing $\Delta G$ ( $= \Delta H - T\Delta S$ ). Since microwave irradiation effects are highly irreversibly, $\Delta S$ is large. Also temperature T is high (superheating). Combined effect leads to lowering of Gibbs energy of change (Perreux and Loupy, 2001).

Barnard et al. (2007) estimated the energy consumption in a continuous flow microwave irradiated biodiesel production in a scientific microwave oven, for 4 l reactor, 7.2 l/min flow rate and 6:1 methanol to oil ratio. It was found that microwave irradiated heating was more energy efficient than the conventional heated apparatus. Using the same microwave oven, batch and continuous-flow preparation of biodiesel derived from vegetable oil and 1-butanol was reported. Reaction was carried out at atmospheric pressure, in a continuous mode for flow rates up to 2.3 l/min using a 4 l reactor vessel. Both new and used vegetable oil was used at 6:1 1-butanol to oil ratio. Catalyst was sulphuric acid and potassium hydroxide (Leadbeater et al., 2008). Microwave activation has also been reported for enzymatic catalysts. The enzymatic microwave assisted biodiesel synthesis from macauba (*Acrocomia aculeate*) oil and ethanol using Novozyme 435 and Lipozyme IM was studied using statistical design of experiments. The investigation variables were reaction temperature, time and enzyme loading. A significant effect of the reaction time in reducing the catalytic activity was observed which interpreted in terms of enzyme deactivation due to microwave exposure. The enzyme loading also played an important role, however the effect of temperature was minor appearing only in the effect of variable interactions. The

resulting comparison between biocatalyst activity in absence and presence of microwave showed that the activity increased about one order of magnitude due to microwave (Nogueira *et al*., 2010). Sunflower oil and Waste vegetable oils (WWOs) were converted into biodiesel by microwave irradiation and a study was made about optimum reaction time and the performance of biodiesel produced. Oils were reacted with methanol in presence of potassium/ sodium methoxide catalyst. Catalyst loading was 0.5% and 1.0% w.w., reaction time was for 1-3 h under reflux at 333-343K. For conventional heating, reaction time was 60 min, separation time was 480 min and yield 96%; whereas for microwave irradiation the respective times were 2 min and 30 min, and yield of 100%. It was observed that for microwave irradiation, the yield was 100% at 2 min, and started to drop later. At a time of 4 min, the yield was about 60%. Exceeding of optimum reaction time reduced the yield and also the quality of biodiesel produced (Reefat *et al*., 2008). In a study of continuous transethylation of vegetable oils by microwave irradiation Lertsathapornsuk *et al*. (2005) prepared fatty acid ethyl esters (FAEE) from coconut, rice bran and used palm oils in a modified home-made microwave oven (800 W). Good yields of FAEEs were obtained with 1.0% sodium hydroxide (in excess) as a catalyst. With the alcohol to oil ratio of 9:1, 100% conversion is obtained within 30s for coconut oil, 94% conversion for rice bran and 83% conversion for used frying oil. Percent conversion is slightly increased for used frying oil but not for rice bran oil when the reaction time is increased to 60s. The temperatures of the reaction mixtures rapidly increased to the boiling point of alcohol within 30s and increased slightly above the boiling point of the alcohol, to 356.5K at 60s. When the used frying oil was thinned with kerosene (1:1 v/v), percent conversion was 92% in 30s, which was slightly higher than the un-thinned oil. Percent conversion remained constant at longer reaction times. Reaction temperature was lower than the un-thinned oil (344 K at 30s and 353.3 K at 60s). Transesterification of castor oil by microwave irradiation was studied by Perin *et al*. (2008). Reaction was carried out in presence of methanol or ethanol, using a molar ratio of alcohol/castor bean oil of 6:1, and 10wt.% of acidic silica gel or basic alumina (in relation to the oil mass) as catalyst. Under acid catalysis, the reaction occurred with satisfactory yields using sulphuric acid immobilized in silicon dioxide, methanol under conventional conditions (333 K for 3 h) as well as using microwave irradiation for 30 min. The best results were obtained under basic

conditions ($Al_2O_3$/50%KOH) using methanol and conventional (333 K, stirring, 1h) or microwave condition (5 min). In comparison with conventional heating, the catalyzed alcoholysis assisted by microwaves was much faster and led to higher yields of the desired fatty esters. In a study involving ultrasonic mixing and closed microwave irradiation to assist transesterification of soybean oil, it was observed that the optimal reaction conditions corresponded to 1 min ultrasonic mixing and 2 min closed microwave irradiation. The optimal reaction conditions that can reach 97.7% of conversion rate were- amount of catalyst used 1.0wt.%; reaction temperature 333K; and methanol to oil ratio 6:1 (Hsiao *et al*., 2010). Microwave assisted catalytic transesterification of *Camelina sativa* oil using both homogenous and heterogeneous catalysts has been reported. Three different types of catalysts: homogeneous catalysts (NaOH and KOH), heterogeneous metal oxide catalysts (BaO and SrO), and sol-gel derived catalyst ($BaCl_2$/AA and $SrCl_2$/AA) were evaluated for their efficiency in biodiesel production. For maximum biodiesel yield, the conditions were: for KOH - methanol to oil ratio 1:9, catalyst concentration 1 wt.%, reaction time 60s; for NaOH- methanol ratio of 1:9, catalyst concentration 0.5 wt.%, reaction time 60s; for BaO- methanol ratio to oil ratio of 1:9, catalyst concentration 1.5 wt.%, reaction time 4 min; for SrO- methanol to oil ratio of 1:9, catalyst concentration of 2 wt.%, reaction time 4 min. In case of sol-gel derived catalysts, different catalyst holding rates of 1-10 mmol/g were evaluated. Low biodiesel yields of 10-25% on the sol-gel derived catalysts were obtained. Satyanarayanareddy and Regupathi (2013) studied microwave assisted batch and continuous transesterification of karanja (*Pongamia pinnata*) oil using KOH homogeneous catalyst. RSM was applied for optimization of the variables.

Attempts have been made to compare the energy requirements for conventional and microwave irradiation. The estimations are based on various assumptions, and therefore should be used with caution. On the basis of energy consumptions in the transesterification processes with both conventional heating and microwave heating methods, evaluations showed that microwave heating consumes less than 10% of the energy to achieve the same yield as conventional heating (Patil *et al*., 2010b; Patil *et al*., 2011 ). A continuous transesterification process using conventional heating is estimated to consume 94.3 kJ/L of energy (Chand *et al*., 2010), where as a continuous microwave irradiated process consumes 26 kJ/L (Barnard *et al*., 2007). In a transesterification study using waste cooking oil and

employing microwave and ultrasound irradiation, energy consumption of 0.3- 1.3 kJ/g has been reported ( Martinez-Guerra and Gude, 2014). Power requirement depends upon the power output of the microwave reactor. Microwave irradiation studies so far have been on lab scale devices using very small reactor volumes, which limits the scaled up estimates.

### 2.4.4 Reaction Time

A study with groundnut oil, sunflower oil and soybean oil, with methanol to oil ratio of 6:1, sodium methoxide catalyst 0.5% (w/w) and at temperature of 333 K, gave a 60% yield within one minutes and about 98% yield after one hour showing that the conversion rate increased with time (Freedman, 1984). A similar study with beef tallow had a very slow reaction rate in the first five minutes, and a maximum value at 15 minutes. Slow mass transfer rate between methanol and tallow in the early period was suspected to be the cause (Ma and Hanna, 1999). For heterogeneous catalysts, in conventional heating, the reaction rate increases to about 180 min, and remains constant thereafter (Leung and Guo, 2006). For microwave irradiation, the time for highest reaction rate can be 3-5 min, as mentioned in Section 2.4.3.1 (Patil et al., 2011). If reaction time is exceeded beyond a certain optimum, the yield begins to drop due to increase in reverse reaction and formation of soap (Eevera *et al*., 2009; Maa *et al*., 1998).

### 2.4.5 Mixing

Mixing increases mass transfer rate. In a study on effect of mixing on beef tallow, because melted beef tallow and sodium hydroxide-methanol are immiscible there was no reaction without mixing. When reaction mixture was mixed at substantive speed, reaction time controlled the yield. This suggested that the mixing speed exceeded the threshold speed. At lower mixing speeds, reaction time was longer. It was observed that the smaller the droplet size, higher the reaction rate (Ma and Hanna, 1999; Stamenkovic´*et al*., 2007 ). In another study of the transesterification of Jatropha curcas oil in homogeneous catalyst, it was observed that the reaction is diffusion controlled. Without mixing, the reactants and catalysts form distinct layers and no reaction takes place. Rate of formation of butyl ester increases almost linearly with the revolution rate of mixer impeller in the early stages of reaction; whereas at later stages, the effect of mixing speed is not so predominant and very soon the conversion becomes independent of stirring speed (Kumar V and Kumar J, 2008). In a study of alkali catalyzed transesterification of *Pongamia pinnata* oil it was found that

the yield became independent of stirring speed after 360 rpm (Meher *et al*., 2006). A perfect mixing with no mass transfer resistance was observed at 600 rpm for NaOH catalyzed transesterification of sunflower oil (Marjanović *et al*., 2010; Vicente *et al*., 2005). Noureddini and Zhu (1997) also reported a negligible mass-transfer controlled region at a mixing speed of 600 rpm for soybean oil transesterification. Jain and Sharma (2010) obtained a complete mixing at 400 rpm for base catalyzed transesterification of *Jatropha curcas* oil. In another study for *Jatropha curcas* oil transesterification, beyond 150 rpm mixing rate had no effect on yield (Jha *et al*., 2007). For sunflower oil transesterification, mass transfer resistance was noticeable at 200 rpm, which became insignificant at mixing speed of 400 rpm and above (Bambase *et al*., 2007). The above studies show that complete mixing was observed for mixing speeds ranging from 150 to 600 rpm. A mixing speed of 600 rpm can be safely taken to be sufficient to eliminate mass transfer resistance for homogeneously catalyzed transesterification.

#### 2.4.5.1 Ultrasonic mixing

Hsiao *et al*. (2010) employed ultrasonic mixing equipment operating at 20 kHz and 600 W output. Ultrasonic field induced an effective emulsification and mass transfer so that the rate of ester formation under ultrasonic mixing was higher than that under normal stirring condition. An ultrasonic mixing of 10 min gave a 90.2% conversion of soybean into FAME under conventional heating. A combination of ultrasonic mixing of 1 min, and microwave irradiation of 2 min, gave a 97.7% FAME conversion. Notably, microwave irradiation alone with no mixing gave a maximum conversion of 21% in 10 min.

### 2.4.6 Co-solvents

Transesterification reactions involving homogeneous catalysts involve two immiscible phases, oil and catalyst-alcohol solution, whereas it becomes a three-phase system when an heterogeneous catalyst is used. In such cases, mass transfer resistances can become rate controlling unless very efficient mixing is employed. A co-solvent which is miscible to both alcohol and oil can reduce such resistance, and thereby increase reaction rate. Solvents such as hexane, ethers and tetrahydrofuran have been tested with encouraging results. Transesterification of camelina oil using supercritical methanol with hexane as a co-solvent was investigated to study the methyl ester conversion process. It was found that co-solvents play a vital role in reducing the severity of critical operational parameters and

maximize the biodiesel yield (Patil *et al*., 2010a). In another study, homogeneous transesterification of sunflower oil was studied in presence of KOH catalyst and tetrahydrofuran as a co-solvent; and heterogeneously base-catalyzed transesterification was investigated with CaO catalyst and co-solvents such as tetrahydrofuran, n-hexane, dioxane, diethyl ether, triethanolamine, ethyl acetate and methyl ethyl ketone. For homogenous catalysis, methanolysis increased with increasing the tetrahydrofuran concentration up to 50% of the oil mass, which was due to the self-enhancement of the interfacial area as the result of decreasing the mean drop size. No effect of tetrahydrofuran present at the concentration of 20% on the rate of CaO-catalyzed methanolysis was observed, but at higher tetrahydrofuran concentrations, the reaction was delayed and the final FAME yield was decreased. Of all tested co-solvents, only n-hexane and tetrahydrofuran slightly improved the methanolysis reaction in its initial period, triethanolamine and ethyl acetate had no effect, while diethyl ether, dioxane and methyl ethyl ketone negatively influenced the reaction rate and the FAME yield (Todorovic´ *et al*., 2012). A *BIOX* co-solvent process developed by Professor David Boocock of the University of Toronto uses tetrahydrofuran as the co-solvent. The patented process is a continuous process which is not feedstock specific, and gives up to 99% conversion in seconds at ambient temperature (Demirbas, 2009).

### 2.4.7 Reactor system

Batch reactors have advantage of easy control but are used for small and medium production rates. The CSTRs are used for large production rates, mostly in cascade of 2 or 3 (Bacovsky *et al*., 2007). The first reactor may be of larger volume so that the mixture spends more time in it, thus achieving a higher conversion. Biodiesel phase from produce is separated and sent to the second reactor to give a high yield of the order of 98% (Muniyappa *et al*., 1996). PFRs have been tested in laboratory studies but commercial installations are not existing. In a study, a PFR gave a biodiesel yield of 91.7% in 19 min of residence time, at 338K, using 1.2 wt% of KOH, and methanol to rapeseed oil ratio of 6:1 (Lu *et al*., 2010).

## 2.5 Raction Kinetics

### 2.5.1 Introduction

Chemical kinetics of a reaction is needed for chemical reactor design for an industrial process. A reactor design needs information about the reaction rate constants, reaction order and activation energies. Study of kinetics looks into the factors that influence the reaction rate and comes up with these information. Designs are simplified for reaction systems involving very fast or instantaneous reactions. In such systems an equilibrium state may be assumed whereby kinetics information is not needed, and thermodynamics of reaction is sufficient for reactor design (Levenspiel, 1972). However, transesterification reaction is known to be a slow reaction and obviously does not fall into this category.

Transesterification reactions can be written in the following stoichiometric form.

Overall reaction: $A + 3B \leftrightharpoons_{k_2}^{k_1} 3R + S$ …(2.8)

The reaction (5.1) occurs in three steps:

Step 1 $A + B \leftrightharpoons_{k_4}^{k_3} DG + R_1$ …(2.9)

Step 2 $DG + B \leftrightharpoons_{k_6}^{k_5} MG + R_2$ …(2.10)

Step 3 $MG + B \leftrightharpoons_{k_8}^{k_7} S + R_3$ …(2.11)

In the above, $A$ is a triglyceride (TG), $DG$ is diglyceride, $MG$ is monoglyceride. $R$, $R_1$, $R_2$, $R_3$ represent FAME, $B$ is methanol and $S$ is glycerol. $k_1$ , $k_3$, $k_5$ and $k_7$ are the forward reaction rate constants, and $k_2$ , $k_4$ , $k_6$ and $k_8$ are the reverse reaction rate constants.

Reactions are usually catalytic since reaction rates are slow. Exceptions are the reactions carried under supercritical conditions where a catalyst may not be needed, but such operating conditions are too expensive for large scale production. Reaction mechanisms for homogeneous and heterogeneous catalyst systems are different and hence treated separately.

### 2.5.2 Reaction Kinetics for Homogeneous Catalysts

In the published literature observed reaction rates show a lot of variance. Complications arise due to mass transfer limitations in the two phase reacting system. One of the earliest pioneering work on homogeneous reaction kinetics is of Noureddini and Zhu (1997) for transesterification of soybean oil using NaOH catalyst. Differential reaction rates for the three-step reactions were correlated with experimental data and reaction rate constants, and

activation energies, for forward and reverse reactions obtained. Initial reaction rates were slow and it was due to mass transfer limitations. Reaction rate increased with mixing intensity (Reynolds number) in this region of slow reaction. A second phase was when the reaction becomes fast, and was kinetics controlled. Kinetics was second order and mixing Reynolds number had little effect in this region. A third phase was when the reactions slow down once again which was attributed to equilibrium state where reverse reactions come into play. Darnoko and Cheryan (2000) observed a pseudo second order reaction in the first 30 minutes, and first or zero order in the later part for transesterification of palm oil using KOH catalyst. Integrated form of rate equations based on triglyceride, diglyceride and monoglyceride concentrations were used for data analysis and forward reaction rate constants and activation energies for the three-step reactions have been reported. In a similar study of palm oil transesterification (Leevijit *et al*., 2004), it was observed that reverse reactions were insignificant, and at high mixing intensity (Re = 2000) the mass transfer controlled region was negligible. A second order reaction was observed, and forward and reverse reaction rate constants for the three-step reaction were obtained. Transesterification kinetics of sunflower with methanol was studied by Vicente *et al*. (2005), Bambase *et al*. (2007), and with ethanol by Marjanović *et al*.(2010). Vicente *et al*. (2005) included the catalyst (KOH) concentration in the reaction rate by defining an effective rate constant which was a multiple of catalyst concentration and the rate constant. This unconventional approach to kinetics resulted in a second order reaction kinetics. Reaction rate constants and energies of activation were reported. Bambase *et al*. (2007) used NaOH catalyst and observed a second order rate. Mass transfer limitations were minimal for stirring speeds of 400-600 rpm. Reaction rate constants for forward and reverse three-step reactions were reported. Marjanović *et al*.(2010) used NaOH catalyst and reported reaction kinetics for the overall reaction (Equation 2.1). Mass transfers limitations were neglected. Initial reaction phase was modelled as irreversible second order, and the later phase as a reversible second order. Reaction rate constants and activation energies were reported. Similar results are reported for methanolysis of sunflower oil using KOH catalyst by Stamenkovic´ *et al*. (2008) at low temperatures of 283- 303K, using the overall reaction. Jain and Sharma (2010) studied the two-stage esterification/ transesterification of *Jatropha curcas* oil with methanol using $H_2SO_4$/ NaOH

catalysts. They used the overall reaction and obtained a first order reaction rate for both stages. Reaction rate constants for both the stages are reported. Jain *et al*. (2011) studied the two stage esterification/ transesterification of waste cooking oil with methanol using $H_2SO_4$/ NaOH catalysts. They used the overall reaction and observed a first order reaction rate for both stages. Reaction rate constants for both the stages were reported. A supercritical non-catalytic, and homogenous catalytic using KOH, transesterification of *Croton megalocarpus* oil with methanol gave a first order reaction for the overall reaction (Kafuku *et al*., 2011).

The above mentioned kinetic studies on soybean oil, sunflower oil, palm oil, *Jatropha curcas* oil, waste cooking oil and *Croton megalocarpus* oil show that the observed reaction order varied from zero to two. Initially the reaction system consists of two phases and mass transfer controls, but very soon the reaction system becomes pseudo homogeneous and chemical reaction becomes rate controlling. Initial studies focussed on detailed reaction kinetics for the three reaction steps which yields reaction rate constants for forward and reaction rates and activation energies for the three reactions. However, most of the recent studies ignore the reaction steps and work on the overall transesterification reaction. The justification, besides the obvious simplified mathematical modelling, is that the design of a reaction system to produce FAME would need rate data for the overall reaction rate rather than the reaction constants for intermediate steps. This is the approach adapted in the present study.

### 2.5.3 Reaction Kinetics for Heterogeneous Catalysts

#### 2.5.3.1 Literature summary

Literature has already been briefly reviewed above in this chapter. Intention here is to summarize the mechanism details. There have been fewer studies involving heterogeneous catalysts as compared to homogeneous catalytic systems. One reason is that application of solid catalysts for transesterification is relatively recent, another is the complex three-phase reaction system that further complicates reaction mechanism. Dossin *et al*. (2006a, 2006b) studied kinetics of transesterification of ethyl acetate with methanol over MgO catalyst. A perfect mixing was assumed with methanol adsorption as rate determining. Eley-Rideal mechanism, where methanol was adsorbed on metal surface and ethyl acetate was in liquid phase, fitted to the experimental data. Activation energy was obtained which indicated that

the MgO catalyzed reaction was faster than homogeneous base catalyzed reaction. Transesterification of soybean oil over MgO, CaO, BaO, PbO, and $MnO_2$ catalysts was studied by Singh and Fernando (2007). A general rate equation based on overall reaction (Equation 2.1) was used, and integrated form fitted to experimental data. Reaction was of first-order with respect to methanol and zero-order with respect to triglyceride for PbO, MgO, $MnO_2$, CaO; and of first-order with respect to methanol and second-order with respect to triglyceride for BaO. Reaction rate constants were obtained assuming reaction to be irreversible. A similar approach to reaction modelling was used by Patil *et al*. (2011) for transesterification kinetics of *Camelina sativa* oil over BaO, CaO, MgO, SrO catalysts, using conventional and microwave heating. For conventional heating the observed reaction rate orders were: second-order with respect to triglyceride and first-order with respect to methanol for BaO and SrO; zero-order with respect to triglyceride and first-order with respect to methanol for CaO; second-order with respect to triglyceride and zero-order with respect to methanol for MgO. For microwave heating the observed reaction rate orders were: second-order with respect to triglyceride and first-order with respect to methanol for BaO, and second-order with respect to triglyceride and zero-order with respect to methanol for SrO. Veljkovic´*et al*. (2009) studied the methanolysis of sunflower oil catalyzed by CaO. A simplified model was used assuming pseudo-first order rates for methanol adsorption and triglyceride surface reaction. Resulting integrated form of first order rate equation satisfied the experimental data. Mass transfer resistance was eliminated by intensive mixing. Kafuku *et al*. (2011) assumed a first order reaction rate for transesterification of *Croton megalocarpus* oil over sulphated $SnO_2$ catalyst and reported activation energy and reaction rate constant. Wang and Yang (2007) studied the transesterification of soybean oil in supercritical and subcritical methanol using constant molar methanol ratio. The overall stoichiometric equation was used for kinetics modelling, and since methanol concentration was assumed to be constant, a first-order rate equation in terms of triglyceride concentration was written. Kouzu *et al*. (2008) studied transesterification of soybean oil over CaO catalyst and noted that the reaction rate was a function of soybean oil concentration. Reaction rate constant was obtained based on this observation of first-order reaction with respect to oil, using the overall stoichiometry. Because of the complex reaction system, most of the studies have been on the overall

reaction kinetics, and there are a lot of variations in reported kinetic models and observed reaction orders.

### 2.5.3.2 Reaction Mechanism

Reaction system for transesterification for FAME consists of three immiscible phases in feedstock: triglyceride, methanol, and a solid catalyst. After completion of reaction, FAME and glycerol are also immiscible. In a solid-liquid-liquid system, the resistance to reaction could be due to the following seven steps ( Boudart, 1984):

(i) Diffusion of reactant molecules through bulk liquid phase to catalyst surface
(ii) Diffusion of reactant molecules through liquid-solid surface or catalyst pore
(iii) Adsorption of reactant molecules on catalyst active sites
(iv) Chemical reaction at catalyst surface
(v) Desorption of product molecules from catalyst active sites
(vi) Diffusion of product molecules through liquid-solid surface or catalyst pore
(vii) Diffusion of reactant molecules through catalyst surface to bulk liquid phase

The slowest of the above steps determine the reaction rate, called rate controlling. Other steps are assumed fast, and always in equilibrium.

In transesterification kinetics studies, resistances in steps (i), (ii), (vi) and (vii) are eliminated by the use of efficient mixing. A criterion for perfect mixing in a batch slurry reactor is (Thoenes, 1994) :

$$N_I > \left(12\frac{g}{d_I}\right)^{0.5} \left(\frac{\rho_{p,wet} - \rho_L}{\rho_L}\right)^{0.5} \left(\frac{d_p}{d_I}\right)^{0.165} \epsilon_s^{0.25} \qquad ...(2.12)$$

In equation 2.12, $N_I$ = impeller speed ($s^{-1}$), $d_I$ = impeller diameter (m), g = acceleration of gravity ($m^2s^{-1}$) , $\rho_{p,wet}$ = density of catalyst filled with liquid (kg $m^{-3}$), $\rho_L$ = density of liquid (kg $m^{-3}$), $d_p$ = particle diameter (m), and $\varepsilon_s$ = catalyst fraction in slurry.

Once mass transfer resistance is eliminated by intensive mixing conforming to above criterion, the parameters affecting the reaction rate are adsorption of reactants, surface reaction and product desorption. Several theories are proposed but the two main theories are Langmuir- Hinshelwood and Eley-Rideal. Langmuir- Hinshelwood mechanism for catalytic processes postulated that the rate of heterogeneous reaction is controlled by the reaction of the adsorbed molecules, and that all the adsorption and desorption processes are in equilibrium. The Eley-Rideal mechanism, on the other hand, envisaged that a

heterogeneous reaction could take place between strongly adsorbed atoms (chemisorbed), and molecules held to the surface by weak, van der Waals forces (physical adsorption) (Thomas and Thomas, 1967). Both mechanisms have been used to explain heterogeneous reaction mechanism but for the vast majority of surface catalytic reactions, including transesterification, it has been accepted that the Langmuir–Hinshelwood mechanism is preferred (Baxter and Hu, 2002).

#### 2.5.3.2.1 Langmuir–Hinshelwood mechanism

Based on the reaction mechanism for catalyst CaO as given in Figure 2.5, both triglyceride molecule and methanol molecule can be chemisorbed on the basic catalyst surface before the surface reaction takes place. Based on a chemisorption model proposed for ethyl acetate (Hattori *et al*., 2000) it can be presumed that triglyceride molecule will also be chemisorbed on a basic catalyst since it also has –C=O group, similar to ethyl acetate. Secondly, a chemisorbed methanol molecule may not be able to react to a free large triglyceride molecule, in which a long alkyl group is attached to the carbon atom in the –C=O group, in bulk phase. This suggests that reaction with chemisorbed methanol is more likely when the triglyceride is immobilized on the catalyst surface through chemisorption. This scenario leads to Langmuir–Hinshelwood mechanism where transesterification takes place between chemisorbed triglyceride and methanol molecules. Overall reaction given by equation 2.1 can be assumed to take place in five-steps:

Chemisorption $B + * \underset{k_{desB}}{\overset{k_{adsB}}{\rightleftharpoons}} B*$ 2.13

$A + * \underset{k_{desA}}{\overset{k_{adsA}}{\rightleftharpoons}} A*$ 2.14

Surface reaction $A* + 3B* \xrightarrow{k_{SR}} 3R* + S*$ 2.15

Desorption $R* \underset{k_{adsR}}{\overset{k_{desR}}{\rightleftharpoons}} R + *$ 2.16

$S* \underset{k_{adsS}}{\overset{k_{desS}}{\rightleftharpoons}} S + *$ 2.17

In the above scheme asterisk (*) represents an active-site on catalyst surface; $k_{ads}$ and $k_{des}$ are adsorption and desorption rate constants for species A, B, R and S; and $k_{SR}$ is the surface reaction rate constant. B*, A*, R* and S* represent adsorbed species. A reaction kinetic model based on equations 2.13 -2.17 is obtained based on the following assumptions:

(i) Reaction system is completely mixed such that mass transfer resistance for reactants and products in bulk is negligible.

(ii) Alkaline earth metal oxides are microporous solids with relatively small external surfaces as given in Table 3.13. Hence the adsorption may be assumed to be of first order Langmuir type (Section 3.2.2.2).

(iii) For such reactions methanol is always in surplus which leads to an assumption that fraction of catalyst surface occupied by chemisorbed methanol is constant.

(iv) Reverse surface reaction is negligible since reactant methanol is in excess. This is justified by published reaction rate constants for reverse reactions (Noureddini and Zhu, 1997; Darnoko and Cheryan, 2000; Leevijit *et al*., 2004).

(v) Adsorption and desorption steps are in equilibrium. Also, since fraction of adsorbed methanol on catalyst surface has been assumed constant, surface reaction follows a pseudo-first order with respect to triglyceride, and is rate controlling.

(vi) Concentrations of intermediate monoglyceride and diglyceride are negligible, and do not affect overall kinetics.

Rate of disappearance of triglyceride (A), $-r_A = -\frac{d[A]}{dt} = k_{SR}\, f_B\, [A*]$ ...(2.18)

where $f_B$ is the fraction of solid surface occupied by methanol (B).

Rate of adsorption of triglyceride on solid surface = $k_{adsA}$ [A]( $1 - f$ ) ...(2.19)

where $f$ total fraction of solid surface occupied.

Adsorbed triglyceride is used up in surface reaction and also possibly desorbed, which is given by: $k_{SR}\, f_B\, [A*] + k_{desA}[A*]$ ...(2.20)

Equating equations (2.19) and (2.20),

$$k_{adsA}\,[\mathrm{A}](1 - f) = k_{SR}\, f_B\, [A*] + k_{desA}[A*] \quad \ldots(2.21)$$

we get, $[A*] = \frac{k_{adsA}\,[\mathrm{A}](1 - f)}{k_{SR}\, f_B + k_{desA}}$ …(2.22)

Substitute for [A*] in equation (2.18), we get

$$-r_A = -\frac{d[A]}{dt} = k_{SR}\, f_B\, \frac{k_{adsA}\,[\mathrm{A}](1 - f)}{k_{desA} + k_{SR}\, f_B} = \left[\frac{k_{SR}\, k_{adsA}\, f_B\,(1-f)}{k_{desA} + k_{SR}\, f_B}\right][A] \quad \ldots(2.23)$$

We define, $k_{obs} = \left[\frac{k_{SR}\, k_{adsA}\, f_B\,(1-f)}{k_{desA} + k_{SR}\, f_B}\right]$ , where $k_{obs}$ is the observed reaction rate constant.

Equation (2.23) now becomes,

$$-r_A = -\frac{d[A]}{dt} = k_{obs}\,[A] \quad \ldots(2.24)$$

It shows that the observed rate is a first order with respect to triglyceride.

If the initial concentration of triglyceride is $[A]_o$ , and $x_A$ is the conversion of triglyceride into FAME, then $[A] = [A]_o\,(1 - x_A)$ ...(2.25)

And equation (2.24) is integrated to give

$$-\ln(1 - x_A) = k_{obs}\, t + C_1 \quad \ldots(2.26)$$

$C_1$ is the integration constant. If the feed does not contain any FAME in the beginning, $C_1 = 0$. And, $-\ln(1 - x_A) = k_{obs}\, t$ ...(2.27)

Equation (2.27) is the integrated form of the rate equation for Langmuir–Hinshelwood mechanism.

### 2.5.4 General Rate Equation

Langmuir–Hinshelwood mechanism predicts a first order rate with respect to triglyceride concentration. However, as seen in Section 2.5.3.1, the observed rate varies from zero to second order with respect to methanol and triglyceride. Also, the observed rates are different for conventional heating and microwave irradiation. A general rate equation has been developed (Singh and Fernando, 2007; Patil *et al*., 2011) which can take care of varying reaction orders with respect to methanol and triglyceride. This rate equation is applicable to both homogeneous and heterogeneous catalyst systems since it is based on the overall reaction. Overall stoichiometry (Equation 2.1) is written for a forward reaction, assuming negligible reverse reaction.

Overall reaction: $\mathrm{A} + 3\mathrm{B} \xrightarrow{\mathrm{k}} 3\mathrm{R} + \mathrm{S}$ …(2.28)

Rate of reaction, written as rate of disappearance of triglyceride, *A* is:

$$-r_A = -\frac{d[A]}{dt} = k\,[A]^m\,[B]^n \qquad ...(2.29)$$

In equation (2.29), *m* and *n* are the reaction orders with respect to triglyceride and methanol respectively, *k* is the reaction rate constant, and *t* is the time. By taking mass balance on triglyceride,

$$[A] = [A]_o\,(1 - x_A) \qquad ...(2.30)$$

In equation (2.30), $[A]_o$ is the initial triglyceride concentration, and $x_A$ is the conversion.

Similar mass balance on methanol gives,

$$[B] = [B]_o - 3\,x_A\,[A]_o = [A]_o\,(\alpha_B - 3\,x_A) \qquad …(2.31)$$

Here, $\alpha_B = [B]_o / [A]_o$

Equations 2.30 and 2.31, when substituted in 2.29, give:

$$\frac{dx_A}{dt} = k\,[A]_o^{(m+n-1)}\,(1 - x_A)^m\,(\alpha_B - 3x_A)^n \qquad …(2.32)$$

Or, $$\int \frac{dx_A}{(1-x_A)^m\,(\alpha_B - 3x_A)^n} = k\,[A]_o^{(m+n-1)} \int dt \qquad …(2.33)$$

Limits for the integral are: $x_A = 0$ at $t = 0$; and $x_A = x_A$ at $t$.

Integral has been evaluated for overall order varying from 0 to 3, for different combinations of *m* and *n*, and the integrated form of rate equation is given in Table 2.1. Appendix B gives the detailed algebra.

**Table 2.1 : Integrated form of rate equation (Eqn 2.33)**

| Case | Overall order | *m* | *n* | Rate equation | Equation number |
|---|---|---|---|---|---|
| 1 | 0 | 0 | 0 | $[A]_o\, x_A = k\, t$ | 2.34 |
| 2 | 1 | 1 | 0 | $\ln\left(\frac{1}{1-x_A}\right) = k\, t$ | 2.35 |
| 3 | 1 | 0 | 1 | $-\frac{1}{3} ln\left(\frac{\alpha_B - 3x_A}{\alpha_B}\right) = k\, t$ | 2.36 |
| 4 | 2 | 1 | 1 | $\frac{1}{(\alpha_B - 3)} ln\left(\frac{\alpha_B - 3x_A}{(1-x_A)\alpha_B}\right) = k\, [A]_o\, t$ | 2.37 |
| 5 | 2 | 2 | 0 | $\left(\frac{x_A}{1-x_A}\right) = k\, [A]_o\, t$ | 2.38 |
| 6 | 2 | 0 | 2 | $\frac{x_A}{(\alpha_B - 3x_A)\alpha_B} = k\, [A]_o\, t$ | 2.39 |
| 7 | 3 | 2 | 1 | $\frac{1}{(\alpha_B - 3)}\left(\frac{x_A}{1-x_A} - \frac{3}{\alpha_B - 3} ln\frac{(\alpha_B - 3x_A)}{(1-x_A)\alpha_B}\right) = k\, [A]_o^2\, t$ | 2.40 |
| 8 | 3 | 1 | 2 | $\frac{1}{(3-\alpha_B)}\left(\frac{3x_A}{(\alpha_B - 3x_A)\alpha_B} - \frac{1}{3-\alpha_B} ln\frac{(1-x_A)\alpha_B}{(\alpha_B - 3x_A)}\right) = k\, [A]_o^2\, t$ | 2.41 |
| 9 | 3 | 3 | 0 | $\frac{(2-x_A)x_A}{(1-x_A)^2} = 2\, k\, [A]_o^2\, t$ | 2.42 |
| 10 | 3 | 0 | 3 | $\frac{1}{(\alpha_B - 3x_A)^2} - \frac{1}{{\alpha_B}^2} = 6\, k\, [A]_o^2\, t$ | 2.43 |

Equations 2.34 to 2.43 in Table 2.1 are equations of straight line. A plot of left-hand-side, a function of conversion $x_A$, versus time *t* would be a straight line for the appropriate *m* and *n*. Reaction rate constant, *k* , can be obtained by the slope.

### 2.5.4.1 Activation energy for the reaction

Chemical reaction rate constant, *k* , is a temperature dependent term. The temperature dependency is well represented by Arrhenius' law (Levenspiel, 1972):

$$k = k_o\, e^{-E/RT} \qquad \ldots 2.6$$

An alternate expression of Arrhenius' law is:

$$k = k_o'\, T^m\, e^{-E/RT} \qquad 0 \le m \le 1 \qquad 2.44$$

The exponential term in the above equation (2.44) is so much more temperature-sensitive than the $T^m$ term, the variation of k caused by the later is effectively masked, and the expression reduces to equation 2.6. Equation 2.6, in logarithmic form is:

$$\ln k = \ln k_o - E/\mathrm{RT} \quad \ldots \quad 2.45$$

Hence a plot of ln *k* versus 1/T is a straight line with a slope of (–*E*/R).

### 2.5.4.2 Enthalpy and Gibbs Energy

Standard Enthalpy of Formation and Standard Gibbs Energy of Formation (at 298.15K) for Croton megalocarpus oil triglyceride were estimated for fatty acid mass composition given in Table 3.11 (Chapter 3), and using published fatty acid ester thermodynamic data (Yancy-Caballero and Guirardello, 2013). The estimated values were: $\Delta H^o_{f\,298}$ = –1576.11 kJ/mol and $\Delta G^o_{f\,298}$ = –125.76 kJ/mol. Similar calculations for Croton megalocarpus oil Fatty Acid Methyl Esters gave molar average values as: $\Delta H^o_{f\,298}$ = –541.31 kJ/mol and $\Delta G^o_{f\,298}$ = –69.97 kJ/mol. Standard Enthalpy and Gibbs energy changes (at 298.15K) for the transesterification reaction (Eqn 2.2) were estimated as: $\Delta H^o_{298}$ = –22.95 kJ/mol and $\Delta G^o_{298}$ = –44.29 kJ/mol. The entropy change at 298.15K was, $\Delta S_{298}$ = 0.0716 kJ/mol K.

Enthalpy change for the reaction shows that the reaction is slightly exothermic. Gibbs energy change is negative indicating that the reaction is spontaneous. However, considering absolute value of Gibbs energy change, the reaction rate would be extremely low.

# 3 CHARACTERIZATION OF *CROTON MEGALOCARPUS* OIL AND ALKALINE EARTH CATALYSTS

## 3.1 Characterization of *Croton megalocarpus* oil

Characteristic physical properties of *Croton megalocarpus* oil are required to appropriately design the transesterification reaction. Such properties are also need to scale-up the process from lab to pilot and to industrial scale. Characterization of croton *megalocarpus* oil was carried out by using standard analytical techniques.

### 3.1.1 Materials

The fruits harvested from Croton trees from Kesses region (Uasin Gishu) were sun dried and outer shell removed to obtain the seeds. These seeds were used to study the oil content. Croton oil was also obtained from Help-Self-Help Group, Nairobi.

General laboratory reagents were of analytical grade. Equipment employed are mentioned under the specific tests.

### 3.1.2 Characterization methods and Results

Experimental methods to determine various characteristic physical properties, and subsequent results are given below (Kumar *et al*., 2013). Results from similar studies from other counties are also provided for comparison purposes. Properties are likely to vary since the oil is a natural product.

#### 3.1.2.1 Oil content of Croton seeds

Mechanical extraction and Solvent extraction were employed to estimate the yield of oil.

##### 3.1.2.1.1 Mechanical extraction

The seeds were heated for about 20 minutes in an oven (WTC binder) at a 373-378K. A locally fabricated Ram press was used to manually extract the oil. Extraction yielded a 15.5 wt% oil (on seed basis). The yield was low due to poor efficiency of press.

##### 3.1.2.1.2 Solvent extraction

Soxhlet apparatus was used for solvent extraction. Hexane and Diethyl ether were used as solvent. Hexane gave a yield of 49.2 wt%, and diethyl ether gave a yield of 49.8 wt% of oil (seed basis). Table 3.1 gives the results and also cites published data.

**Table 3.1: Oil content of Croton seeds**

| | Present work | Literature |
|---|---|---|
| **Oil, wt%** | 49.8 | Wagutu *et al*., 2009); 32.6 (Kibazohi and Sangwan, 2011) |

### 3.1.2.2 Density

Oil density was measured as per ASTM D4052 by DMA 4500M Density meter. Results are given in Table 3.2, which also cites published data.

**Table 3.2: Density of Croton oil**

| | Present work | Literature |
|---|---|---|
| **Density ($kg\ m^{-3}$)** | **929.2 (293K)** | 871.8(353K), 864.9(363K), 858.0(373K) (Wu *et al*., 2012); 918 (298K) (Kafuku and Mbarawa, 2010), (Wagutu *et al*., 2009); 924 (mechanical extraction), 904 (chem. extraction) 288K (Aliyu *et al*., 2010); 916.8 (Kafuku *et al*., 2011) |

### 3.1.2.3 Viscosity

Kinematic viscosity of oil was measured as per ASTM D445, by Automatic viscometer CAV2200. Table 3.3 gives the measured viscosity, and also gives published data.

**Table 3.3: Viscosity of Croton oil**

| | Present work | Literature |
|---|---|---|
| **Viscosity** | **Kinematic: 28.52 cST (313K), 7.12 cST (373K)**<br>**Dynamic: 0.0265 Pa.s (313K), 0.0066 Pa.s (373K)** | 27.7 cST (313K) (Wagutu *et al*., 2009); 49.4 cST (313K) (Kafuku *et al*., 2011); 30.37 cST (313K) (mechanical extraction), 23.48 cST (313K) (chem. extraction) (Aliyu *et al*., 2010) |

### 3.1.2.4 Refractive Index

Refractive index of Croton oil was obtained by Abbe refractometer. Table 3.4 gives the refractive index, and also cites value from literature.

**Table 3.4: Refractive Index**

| | Present study | Literature |
|---|---|---|
| **Refractive index** | **1.4737 (293K)** | 1.4728 (Wagutu *et al*., 2009) |

### 3.1.2.5 Sulphur Content

Sulphur content of Croton oil was estimated by use of Sulfur-in-Oil Analyzer SLFA-2100/2800, HORIBA. Table 3.5 gives the measured Sulphur content, and also cites values from literature.

**Table 3.5: Sulphur content**

| | Present study | Literature |
|---|---|---|
| **S** | **0.001205 wt%** | 0.001 vol % (mechanical ex--traction), 0.0017 (chem. extraction) (Aliyu *et al*., 2010) |

### 3.1.2.6 Water Content

*Water content* or *moisture content* is the quantity of water contained in a material. Water content was measured by standard methods, and was found to be 0.007wt%.

### 3.1.2.7 Ash content

Ash content is the non-volatile inorganic matter of a compound which remains after subjecting it to a high decomposition temperature. Alumina, iron, silica, and other noncombustible impurities contained in oil and left after its burning. Ash content is measured as a percent by weight of oil. Table 3.6 gives the ash content of the Croton oil found by standard method, and also cites data from literature.

**Table 3.6: Ash Content**

| | Present study | Literature |
|---|---|---|
| **Ash** | **0.087 wt%** | <0.01 vol % (mechanical extraction and chem. extraction) (Aliyu *et al*., 2010) |

### 3.1.2.8 Acid value

Acid value (or "neutralization number" or "acid number" or "acidity") is the mass of potassium hydroxide (KOH) in milligrams that is required to neutralize one gram of chemical substance. The acid value is a measure of the amount of carboxylic acid groups in a chemical compound, such as a fatty acid, or in a mixture of compounds. It is the quantity of base, expressed in milligrams of potassium hydroxide, that is required to neutralize the acidic constituents in 1 g of sample. Acid value was obtained by standard titration method. Table 3.7 gives the Acid value (mg KOH/g) of Croton oil, and also cites data from literature.

**Table 3.7: Acid value**

| | Present study | Literature |
|---|---|---|
| **Acid value** | **2.00** | 4.8 (Kafuku *et al*,. 2011); 3.334 (Kafuku and Mbarawa, 2010); 1.7 (Wagutu *et al*., 2009); 1.4 (mechanical extraction), 5.1 (chem. extraction) (Aliyu *et al*., 2010) |

### 3.1.2.9 Free Fatty Acid (FFA)

The free fatty acid is determined from the acid value obtained. FFA is taken to be one-half of the acid value. FFA of croton oil is therefore 1.00

### 3.1.2.10 Saponification value

Saponification value represents the number of milligrams of potassium hydroxide required to saponify 1g of fat under the specified conditions. It is a measure of the average molecular weight (or chain length) of all the fatty acids present. Saponification value was obtained by standard titration method. Table 3.8 gives the Saponification value of Croton oil, and also cites data from literature.

**Table 3.8: Saponification value**

| | Present study | Literature |
|---|---|---|
| **Saponification value** | **192.1** | Wagutu *et al*., 2009); 194.9 (Kafuku *et al*,. 2011) |

### 3.1.2.11 Iodine value

Iodine value, also called Iodine Number, is a measure of the degree of unsaturation of an oil, fat, or wax. It is the amount of iodine, in grams, that is taken up by 100 grams of the oil, fat, or wax This unsaturation is in the form of double bonds, which react with iodine compounds. The higher the iodine number, the more C=C bonds are present in the fat.

Iodine value was obtained by Wijs' method. Table 3.9 gives the Iodine value and a value from literature.

**Table 3.9: Iodine Value**

| | Present study | Literature |
|---|---|---|
| **Iodine value, mg/g** | 139.2 | 137.5 (Wagutu *et al*., 2009) |

### 3.1.2.12 Calorific value

The calorific *value* (or energy *value* or *heating value*) of a substance is the amount of heat released during the combustion of a specified amount of it. Calorific value obtained by standard method is given in Table 3.10, which also gives values from literature.

**Table 3.10: Calorific value**

| | Present study | Literature |
|---|---|---|
| **Calorific value (Gross)** | **41.0 MJ/kg** | 43.06 MJ/kg (mechanical extraction), 40.28 (chem. extraction) (Aliyu *et al*., 2010), 39.65 MJ/kg (Lujaji *et al*, 2010) |

#### 3.1.2.13 Peroxide Value

Peroxide value is an indication of deterioration of oils. Oils with higher peroxide values are more unsaturated than those with lower peroxide values. Peroxide value obtained by standard methods was found to be 8.66.

#### 3.1.2.14 Fatty acid composition and Molar mass

Fatty acid composition of croton oil was analyzed by gas chromatography (Shimadzu 9A, 10m glass packed column with DEGS, column temp. 443 K, Det/Inj temp. 493 K, run time 50 min, carrier gas Nitrogen flow rate 50ml/min). Table 3.11 gives the fatty acid composition.

**Table 3.11: Fatty acid composition of Croton megalocarpus oil**

| | Common name(Fatty acid) | Mass % |
|---|---|---|
| **C8:0** | Caprylic acid | **0.09** |
| **C10:0** | Caproic acid (Decanoic acid) | **0.08** |
| **C12:0** | Lauric acid (Dodecanoic acid) | **0.09** |
| **C14:0** | Myristic acid (Tetradecanoic) | **0.26** |
| **C16:0** | Palmitic acid (Hexadecanoic) | **8.39** |
| **C18:0** | Stearic acid (Octadecanoic) | **3.15** |
| **C18:1 cis** | Oleic acid (cis-9-Octadecenoic) | **12.16** |
| **C18:2 cis** | Linoleic acid (all cis-9,12 Octadecadienoic) | **70.97** |
| **C18:3 n3** | α- linolenic acid (all cis-9,12,15-Octadecatrienoic) | **3.89** |
| | **Total** | **99.08** |

Molar mass of the oil based on the above composition was estimated to be 870.86 kg/mol.

## 3.2 Characterization of Heterogeneous Catalysts

### 3.2.1 Introduction

The characterization of heterogeneous catalysts involves study of morphology, physical properties, surface properties, bulk properties, particle size distribution and mechanical properties. The variety of techniques available for these studies are tremendous and a detailed description is not appropriate here. A brief account of the techniques relevant to

the present study would be given in the following. Theoretical details would be kept to a minimum and the emphasis would on the applications (Leofanti *et al*., 1997; Haber, 1991).

### 3.2.2 Morphology and Physical Properties

#### 3.2.2.1 Pore Structure and Surface Area

Surface area measurement is an important expedient in predicting catalyst performance even though only a small fraction of the surface area determined by physical techniques is chemically active. Besides surface area, equally important, especially for nonmetallic catalysts, is the pore structure, which, although contributing to the total surface area, must be regarded as a separate factor. This is because, in a given catalyst, the distribution of pore sizes may be such that some of the catalyst is completely inaccessible to large reactant molecules and, furthermore, may restrict the rate of conversion to products by impeding the diffusion of reactant in the internal pore structure (Thomas and Thomas, 1967). IUPAC classified pores according to their pore-width as given in Table 3.12 (Sing, 1985):

**Table 3.12: Pore size classification**

| Pores | Pore width, w |
|---|---|
| **Ultra-micropore** | $w \leq 0.7$ nm (7 Å) |
| **Micropore** | 0.7 nm (7 Å) < w < 2 nm (20 Å) |
| **Mesopore** | 2 nm (20 Å) < w < 50 nm (500 Å) |
| **Macropore** | $w \geq 50$ nm (500 Å) |

#### 3.2.2.2 Adsorption, Adsorption Isotherms and Hysteresis

All adsorptions can be divided into two main types, physical adsorption (or, physisorption) and chemical adsorption (or, chemisorption). Adsorption isotherms relate quantity of fluid adsorbed as a function of pressure (or, concentration) at equilibrium conditions. IUPAC has recommended six types of adsorption as shown in Figure 3.1 (Kaneko, 1994; Sing, 1982).

The type I isotherm corresponds to the so called Langmuir isotherm. Such isotherms are given by microporous solids having relatively small external surfaces. The type II isotherm is the most familiar, the multilayer adsorption which assumes that the first monolayer

adsorption serves as a site for second, third, and multilayer adsorption. The adsorption in the second, and subsequent layers is similar to condensation. Point B, the beginning of the almost linear middle section of the isotherm, is often taken to indicate the stage at which monolayer coverage is complete and multilayer adsorption about to begin. The type III isotherm arises from nonporous or macroporous surfaces. The type IV isotherm gives useful information on the mesopore structure through its hysteresis loop, that is, non-overlapping adsorption and desorption branches. Type V isotherm is close to type IV but for a very weak adsorbent-adsorbate interaction. The type VI isotherm is the stepped adsorption isotherm which comes from adsorption on different faces of a crystalline solid having non-porous uniform surface.

Above a relative pressure of about 0.2, porous adsorbents desorb a larger quantity of vapour at a given relative pressure than that corresponding to adsorption. A plot of adsorbed/desorbed vapour volume against relative pressure shows a hysteresis loop. Hysteresis appearing in the multilayer range of physisorption isotherm is usually associated with capillary condensation. Such hysteresis loops may exhibit a wide variety of shapes as shown in Fig 3.2 (Sing, 1982).

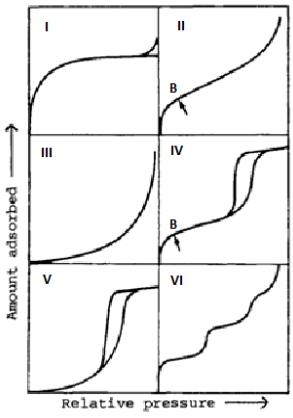


**Figure 3.1: IUPAC Classification of Adsorption Isotherms**

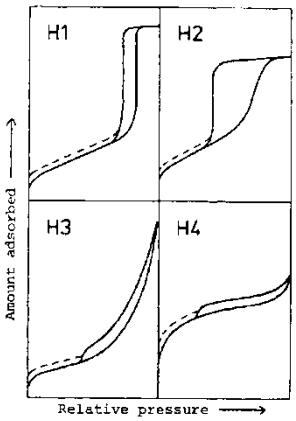


**Figure 3.2: Types of Hysterisis Loops**

### 3.2.2.3 Vapour adsorption at low temperature

Method commonly uses adsorption of nitrogen at 77 K (saturation temperature). Three main methods are: Langmuir and BET isotherms, t-plot, and BJH plots.

#### 3.2.2.3.1 Langmuir and BET isotherms

Microporous material exhibit Type I isotherm which assumes monolayer adsorption, given by Langmuir adsorption equation. For multilayer adsorption, a more common occurrence, Type II (S shaped) isotherm is given by Brunauer, Emmett and Teller (BET) adsorption equation.

The BET equation is given as (Thomas and Thomas, 1967):

$$\frac{1}{v(1-x)} = \frac{1}{v_m} + \frac{1}{v_m\, c}\,\frac{(1-x)}{x} \qquad \text{where} \quad x = \frac{p}{p_{sat}}$$

or, $$\frac{1}{v\left(\frac{P_{sat}}{P}-1\right)} = \frac{1}{v_m\, c} + \frac{c-1}{v_m\, c}\,\frac{P}{P_{sat}} \qquad \text{...3.1}$$

The intercept of a plot of the left-hand side of Equation 3.1 against relative pressure ($P/P_{sat}$) is the reciprocal of ($v_m\, c$), thereby giving the monolayer volume, and hence the surface area of the adsorbate. BET equation is best suited for type II adsorption. For most systems the BET equation is applicable in the $p/p_{sat}$ range of 0.05 – 0.3. BET equation is the most commonly used equation for surface area estimation and is applied to all types of isotherms.

Under exceptional circumstances involving monolayer physical and chemical adsorption, Langmuir model of adsorption enables estimate of $v_m$, the volume of adsorbate occupying one monolayer. The Langmuir equation (Thomas and Thomas, 1967) is given as:

$$\frac{p}{v} = \frac{1}{b\, v_m} + \frac{p}{v_m} \qquad \text{...3.2}$$

A plot of $p/v$ versus $p$ is a straight line, and $v_m$ is obtained from the slope.

The BET method although strictly derived for micropores, is applied to mesopores and macropores as well.

#### 3.2.2.3.2 t-Plot method

An adsorbent is never covered with an adsorbed film of uniform thickness. However, it is often assumed that the film thickness on pore walls is uniform, which enables one to obtain 'statistical thickness' $t$ from adsorption isotherms. t-plot is a comparison plot comparing an isotherm to standard Type II isotherm (given by BET equation). In the t-plot analysis, the

adsorbed amount, $W_a$, of the standard isotherm is converted to the average thickness, *t*, of adsorbed film with the equation

$$t = (W_a / W_m)\ \sigma_t \qquad ...3.3$$

where subscript *m* refers to a monolayer. Here $\sigma_t$ is the thickness of a single adsorbed layer ($\sigma_t$ = 0.354 nm for $N_2$). Then, $p/p_o$ is transformed into *t*, so that the abscissa of the *t* plot is expressed by *t* instead of $p/p_o$. If the isotherm under test is also described by multilayer adsorption, the *t* plot is a straight line passing through the origin, whose slope is proportionate to the surface area. The deviation from the linearity of the *t* plot gives information on the sort of pores, the average pore size, the surface area, and the pore volume. However, the *t* plot analysis has a limited applicability to the microporous system due to the absence of explicit monolayer adsorption (Kaneko, 1994). In practice, thickness *t* values are obtained by thickness equations obtained for a given adsorbent. Thickness equation for nitrogen adsorption at 77K for a non-porous surface given by de Boer is:

$$t = \left[\frac{13.99}{\log\left(\frac{p}{p_o}\right) + 0.034}\right]^{1/2} \qquad ...3.4$$

Another equation is the Halsey equation for nitrogen adsorption at 77 K

$$t = 3.54\left[\frac{5}{\ln\left(\frac{p}{p_o}\right)}\right]^{1/3} \qquad ...3.5$$

t-plot method is applicable to mesopores and macropores for surface area, and to micropores for pore volume (Mircopore Analysis, n.d.).

#### 3.2.2.3.3 Barret-Joyner-Halenda (BJH) Method

This method usually applies to mesopores. The classic Kelvin equation gives a relationship between the relative pressure and capillary radius for capillary condensation:

$$ln\frac{p}{p_o} = \frac{2\gamma\,\bar{V}}{r\,RT} \qquad ...3.6$$

Since multilayer adsorption usually accompanies capillary condensation in solid pores, the Kelvin equation does not give the correct radius, since the pore radius is effectively reduced by the thickness of the adsorbed multilayer. Many researchers developed a method for the calculation of the pore size distribution on the basis of Kelvin equation with a correction term for the thickness of the multilayer adsorbed film. Barret-Joyner-Halenda

(BJH) is one such method which gives plots of cumulative pore area, cumulative pore volume, differential plot of derivative of pore area, differential plot of derivative of pore volume; versus pore size (or, log of pore size) (Thomas and Thomas, 1967).

### 3.2.3 Materials and Methods

Alkaline earth catalysts, Beryllium oxide (BeO, 99.98%), Magnesium oxide (MgO, 99%), Nano Magnesium oxide (Nano MgO, 99.8%), Calcium oxide (CaO, 96%), Nano Calcium oxide (Nano CaO, 98%), Strontium oxide (SrO, 99.9%), Barium oxide (BaO, 97%) of analytical grade were from Sigma Aldrich.

Because of more emphasis given to Calcium oxide, one new sample of CaO was prepared by mixing about 100gm of analytical grade CaO with 250 ml of deionized water and heating under reflux at 70$^{o}$C (343 K) for three hours. Resulting Calcium hydroxide ( $CaO + H_2O \rightarrow Ca(OH)_2$ ) was filtered and dried in an oven (WTB Binder) overnight at 100$^{o}$C (373 K). This dried hydroxide was then calcined in a furnace (ELSKLO- LNT 20) at 700$^{o}$C (973 K) for three hours under atmospheric conditions, to convert calcium hydroxide into oxide once again. The calcium oxide thus obtained is named Re-Oxidized Calcium oxide and abbreviated as CaO-RO. This would be referred to as CaO-RO hereafter.

BET (Brunauer, Emmett, and Teller) surface area and total pore volume of the catalyst samples were achieved in a Micromeritics TriStar 3000 Surface Area and Porosity System analyzer by the low-temperature $N_2$ adsorption method. Prior to analysis, the samples were degassed at 120°C (393 K) overnight (12 h) under a continuous flow of $N_2$ gas to remove the adsorbed contaminants and moisture from the surface and pores of the material.

### 3.2.4 Results and Discussion

#### 3.2.4.1 Surface Area of Catalysts

**Single point BET:**

This involves determining specific surface area using a single point on the isotherm. A single point value for adsorbed volume at relative pressure of 0.3 is used to estimate the surface area according to the following expression (Particle Analytical, 2013):

$$S_{1\,Pt} = \frac{V_m\, N\, a}{m\,(22400)} \qquad \ldots 3.7$$

where $S_{1\ Pt}$ is the single-point surface area ($m^2/g$).

Figure 3.3 is a plot of BET equation as per Equation 3.1. Catalyst samples included BeO, MgO, nano-MgO, CaO, nano-CaO, CaO-RO, SrO and BaO. The slope and intercept from the plot is used to estimate the BET Surface area as per Section 3.2.2.3.1.

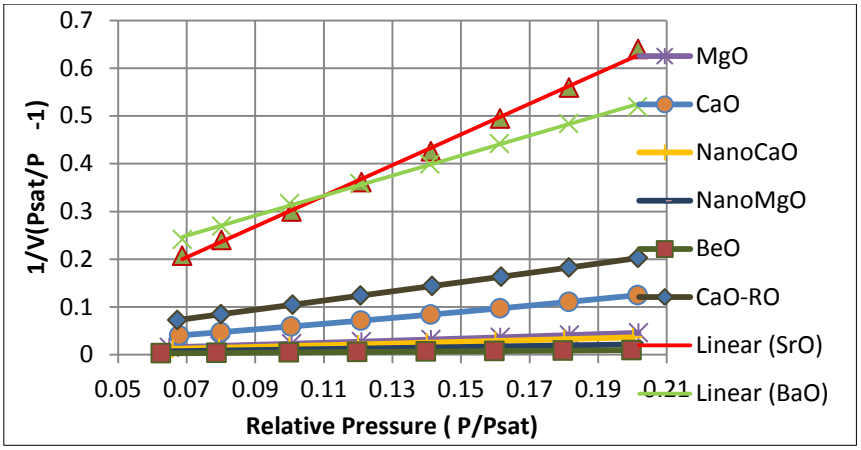


**Figure 3.3: BET plot for catalysts**

Table 3.13 gives the Surface area estimated from Equation 3.7, and the BET equation for the eight catalyst samples.

**Table 3.12: Single-point and BET Surface Area**

| Catalyst | Surface Area | |
|---|---|---|
| | Single Point Surface Area, $m^2/g$ | BET Surface Area, $m^2/g$ |
| **BaO** | 1.69 | 1.98 |
| **SrO** | 1.37 | 1.36 |
| **Nano CaO** | 23.90 | 24.15 |
| **CaO-RO** | 4.33 | 4.47 |
| **CaO** | 7.02 | 6.96 |
| **Nano MgO** | 39.89 | 40.83 |
| **MgO** | 19.13 | 19.54 |
| **BeO** | 90.07 | 92.33 |

From Figure 3.3 it is clear that BET equation satisfies the experimental adsorption data. Areas obtained from Single-point method and BET equation are very close. Table 4.2 shows that BeO has the highest specific surface area, followed by Nono MgO, Nano CaO, MgO, CaO, CaO-RO, BaO and SrO respectively.

### 3.2.4.2 Porosity of Catalysts

Porosity is another characteristic property of heterogeneous catalysts. A catalyst with large surface area should have a high porosity although there is no direct correlation between the two. Equation 3.8 is a correlation that gives porosity as function of pore radius, surface area and density (Froment and Bischoff , 1990).

$$\varepsilon_p = \frac{r_p S_{BET} \rho_p}{4 + r_p S_{BET} \rho_p} \qquad ...3.8$$

In that above, $\varepsilon_p$ is the particle porosity; $r_p$ = average catalyst pore radius, m; $S_{BET}$ = BET Surface area, $m^2/g$; and $\rho_p$ = catalyst density, $kg/m^3$. Table 3.14 gives the estimated porosity by the use of Eqn 4.8. BET surface area are from Table 4.2, and pore sizes are from BJH Desorption data.

**Table 3.13: Porosity of Catalysts**

| Catalyst | Pore radius, $r_p$ (BJH Desorp) | | $S_{BET}$ | | Solid density | | Porosity $\varepsilon_p$ |
|---|---|---|---|---|---|---|---|
| | nm | m | $m^2\ g^{-1}$ | $m^2\ kg^{-1}$ | $g\ ml^{-1}$ | $kg\ m^{-3}$ | |
| **BaO** | 9.88 | 9.88E-09 | 1.981 | 1981.6 | 5.72 | 5720 | 0.03 |
| **SrO** | 24.95 | 2.50E-08 | 1.361 | 1361.1 | 4.70 | 4700 | 0.04 |
| **Nano CaO** | 11.25 | 1.13E-08 | 24.149 | 24149 | 3.3 | 3300 | 0.18 |
| **CaO-RO** | 16.28 | 1.63E-08 | 4.47 | 4470 | 3.1 | 3100 | 0.05 |
| **CaO** | 17.125 | 1.71E-08 | 6.96 | 6960 | 3.3 | 3300 | 0.09 |
| **Nano MgO** | 11.6 | 1.16E-08 | 40.83 | 40830 | 3.6 | 3600 | 0.30 |
| **MgO** | 10.65 | 1.07E-08 | 19.545 | 19545.5 | 3.6 | 3600 | 0.16 |
| **BeO** | 11.305 | 1.13E-08 | 92.33 | 92330 | 3.01 | 3010 | 0.44 |

Alkaline earth oxides have low porosity with exceptions of Nano MgO and BeO. Beryllium oxide has the highest porosity, and Barium oxide the least. The porosity vary as: BeO > Nano MgO > Nano CaO > MgO > CaO > CaO-RO > SrO > BaO.

### 3.2.4.3 Particle Size Distribution and Pore Size Distribution

#### 3.2.4.3.1 t-plot and Adsorption/Desorption Plots

Figure 3.4 gives the t-plot for the heterogeneous catalysts. Quantity adsorbed is highest for BeO, followed by MgO, Nano CaO, Nano MgO, CaO, CaO-RO, BaO and SrO. Adsorption for BaO and SrO is very small. With exception of BeO, plots are very close to linear, with tangents passing through the origin. However, the plots show distinct curvature at early stages of adsorption, indicating monolayer adsorption in the beginning, followed by multilayer adsorption. The tangents pass through the origin indicating a multilayer homogenous adsorption. For the case of BeO, the tangent does not pass through the origin indication a multilayer non-homogeneous adsorption.

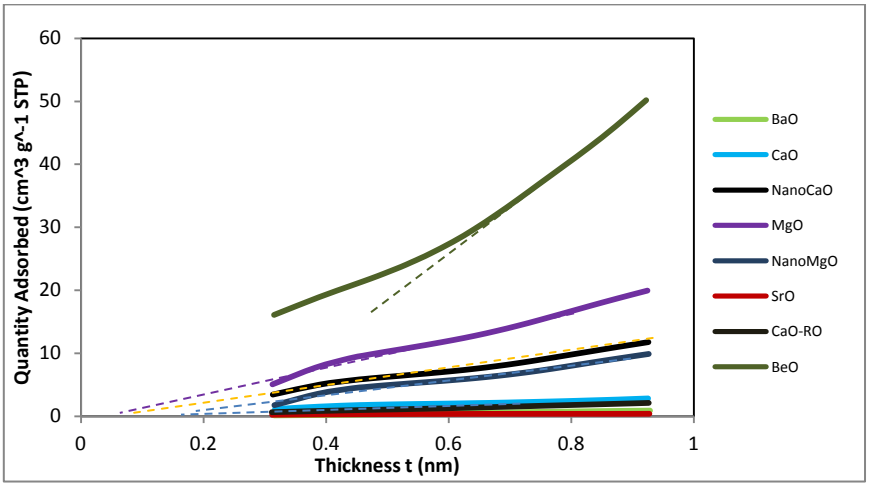


**Figure 3.4: t- plot**

Figure 3.5 is the **Isotherm Plot** which shows the adsorbed quantity (of $N_2$) as a function of pressure for the catalysts. BeO has the highest adsorption, followed by Nano MgO, Nano CaO, MgO, CaO, CaO-RO, BaO and SrO respectively. The curves resemble Type II Isotherm in Fig 3.1, which is a case for multilayer adsorption. With reference to the Nano MgO curve, adsorption begins from '*D*' as pressure is increased. At '*C*', the monolayer coverage is complete and multilayer begins. Between *B –A*, complete rapid multilayer

condensation takes place. At '*A*', all capillaries are completely filled with condensed adsorbate in liquid phase.

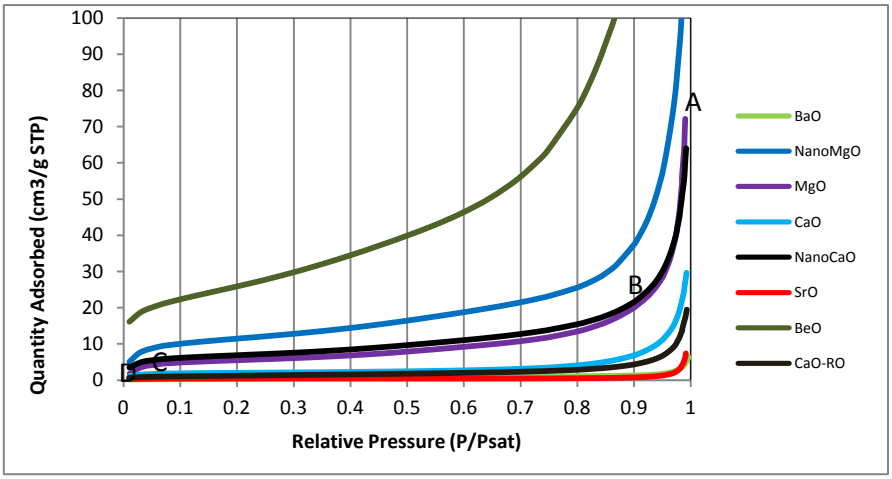


**Figure 3.5: Isotherm Plot**

When the pressure is reduced from saturation pressure, the liquefied adsorbate begins to evaporate known as *desorption*. For a given system, desorption curve lies above the adsorption curve. A combined plot of adsorption/desorption is known as hysteresis loop as shown in Fig 3.2.

Figure 3.6 shows the Hysteresis loop for the catalysts. Comparing to Fig 3.2, the hysteresis loop resembles the Type H3 loop. This does not exhibit any limiting adsorption at high relative pressure, and is observed with aggregates of plate-like particles giving rise to slit-shaped pores.

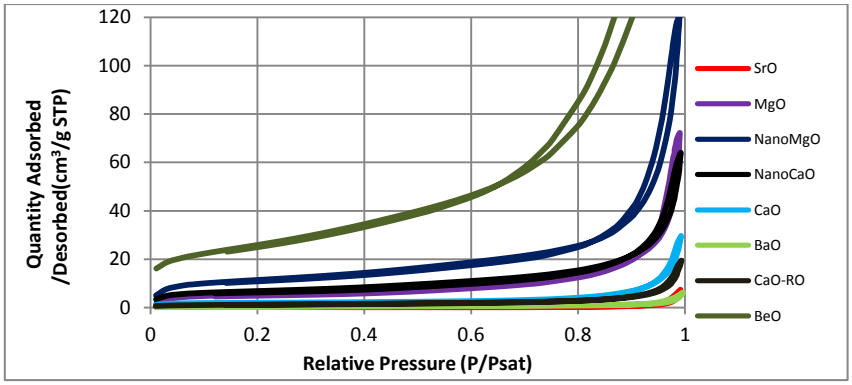


**Figure 3.6: Isotherm Plot- Adsorption/ Desorption Hysteresis Barret-Joyner-Halenda (BJH) Plots**

Figures 3.7 to 3.14 are the BJH plots for Cumulative pore area, Differential pore area, Cumulative pore volume and Differential pore volume, for adsorption and desorption respectively.

Figure 3.7 is the BJH plot for **adsorption cumulative pore area**. From the plot the BJH adsorption surface area for various catalysts are:

- BeO pores between 3 – 110 nm width = 102 $m^2/g$
- Nano-MgO pores between 3 – 200 nm width = 33 $m^2/g$
- Nano-CaO pores between 3 – 200 nm width = 18.5 $m^2/g$
- MgO pores between 3 – 200 nm width = 17 $m^2/g$
- CaO pores between 4 – 200 nm width = 5 $m^2/g$
- CaO-RO pores between 3-200 nm width = 4 $m^2/g$
- BaO pores between 0 – 200 nm width = 2 $m^2/g$
- SrO pores between 8 – 200 nm width = <1 $m^2/g$

Above values compare well with specific surface area in Table3.13.

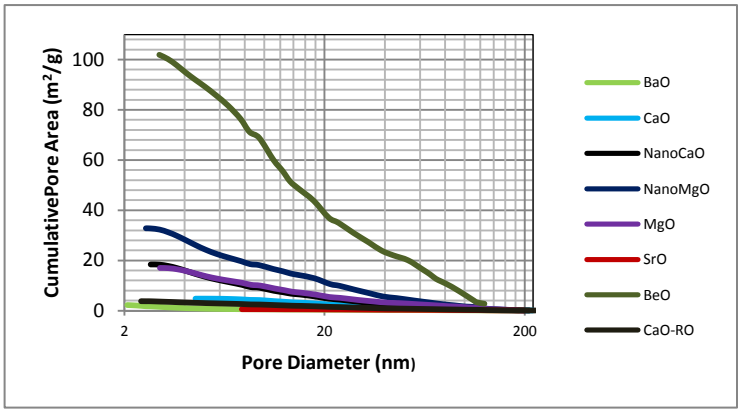


**Figure 3.7: BJH Adsorption Cumulative Pore Area**

Figure 3.8 is the BJH **adsorption plot for differential pore area** for catalysts. It is a plot of dA/d(logD) versus log of Pore diameter (D), where A is the area. From the plot, BeO has the highest pore area which corresponds to pore size of 8-16 nm; for nano MgO, nano CaO and MgO, highest pore area are for the pores of 4- 6 nm size. No such observation can be made for CaO, CaO-RO, SrO and BaO as there are no distinct peaks. Pore area for SrO is negligible.

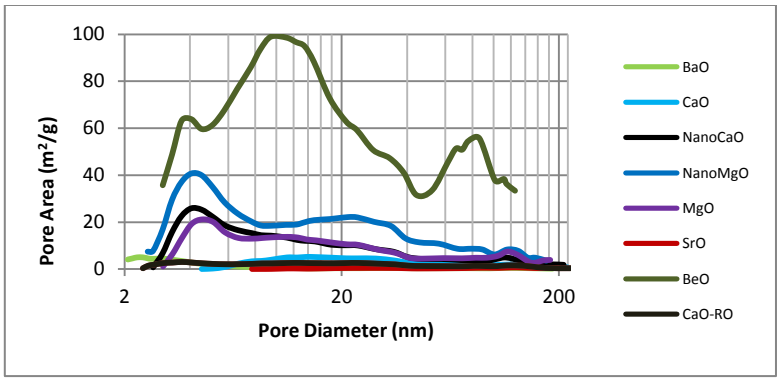


**Figure 3.8: BJH Adsorption dA/d(logD) Pore Area**

BJH **Cumulative pore volume for adsorption** is given in Figure 3.9. From the plot, one observes that the BJH cumulative volume of pores for the various catalysts are:

- BeO pores between 2 – 116 nm width = 0.69 $cm^3/g$
- Nano MgO pores between 2.5 – 200 nm width = 0.19 $cm^3/g$
- MgO pores between 3 – 200 nm width = 0.11 $cm^3/g$
- Nano CaO pores between 3 – 200 nm width = 0.1 $cm^3/g$
- CaO pores between 4.5 – 200 nm width = 0.045 $cm^3/g$
- CaO-RO pores between 2.5- 200 nm width = 0.03 $cm^3/g$
- BaO pores between 2 – 200 nm width = 0.01 $cm^3/g$
- SrO pores between 8 – 200 nm width = 0.01 $cm^3/g$

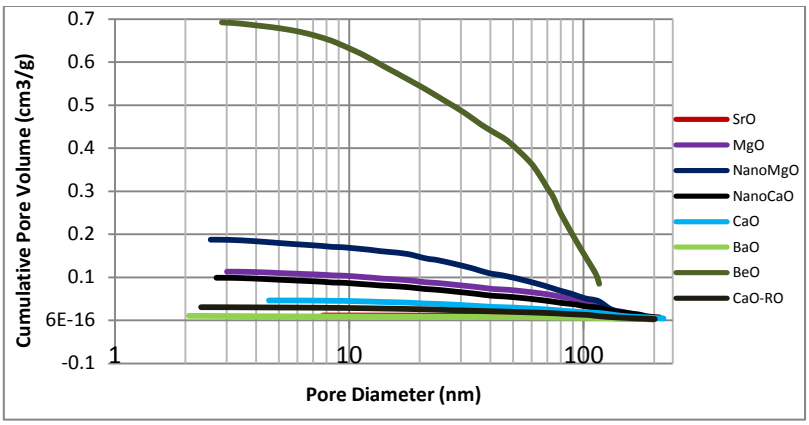


**Figure 3.9: BJH Adsorption Cumulative Pore Volume**

Figure 3.10 gives the BJH **adsorption plot for differential pore volume**. From the plot, the highest BJH pore volume is for BeO, which corresponds to pore size of about 80 nm.

For most of the other catalysts maximum pore volumes correspond to pore sizes of 100 – 200 nm.

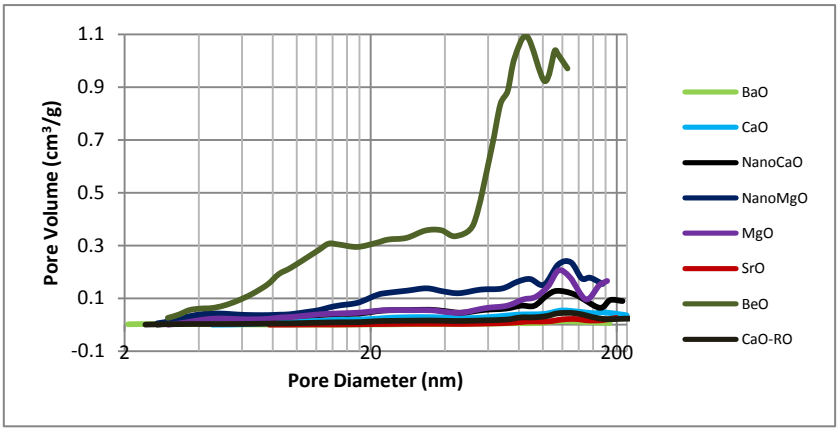


**Figure 3.10: BJH Adsorption dV/d(logD) Pore Volume**

Next four plots are for desorption. Figure 3.11 is the BJH plot for **desorption cumulative pore area**. From the plot the BJH desorption surface area for various catalysts are:

- BeO pores between 4-120 nm width = 128 $m^2/g$
- Nano-MgO pores between 3 – 200 nm width = 32.5 $m^2/g$
- Nano-CaO pores between 3 – 200 nm width = 17.5 $m^2/g$
- MgO pores between 3 – 200 nm width = 17 $m^2/g$
- CaO pores between 4 – 200 nm width = 5.5 $m^2/g$
- CaO-RO pores between 3-170 nm width = 3.8 $m^2/g$
- BaO pores between 0 – 200 nm width = 1.5 $m^2/g$
- SrO pores between 8 – 200 nm width = 1 $m^2/g$

The above values are in agreement with the similar area obtained from BJH Adsorption cumulative pore area, Fig 3.7, with an exception for BeO which depicts a higher area in case of BJH Desorption.

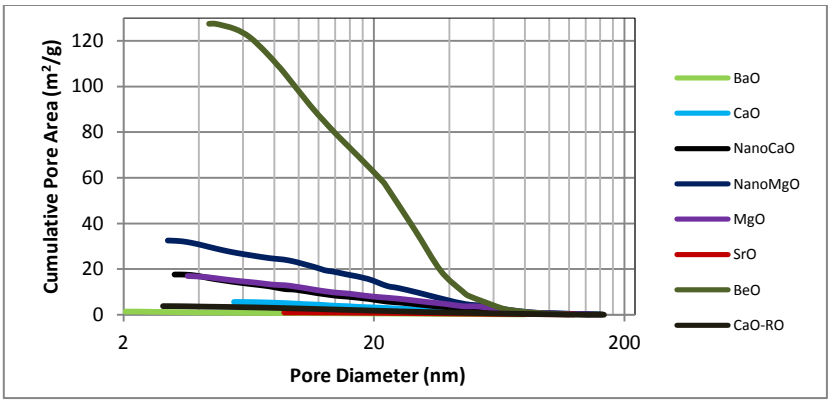


**Figure 3.11: BJH Desorption Cumulative Pore Area**

Figure 3.12 gives the BJH **desorption plot for differential pore area** for catalysts. It is a plot of dA/d(logD) versus log of Pore diameter (D). BeO has the highest pore area of 170 $m^2/g$ and most of the pores are between 8-50 nm size. For nano MgO most of the pores lie between 20 - 40 nm size. Most of the pores of Nano CaO are of 4 nm size. It is difficult to draw such conclusions for other catalysts as their plots lack distinct peaks. Results for adsorption and desorption cumulative pore area plots in this case are in disagreement, most notable is the high pore area for the case of BeO.

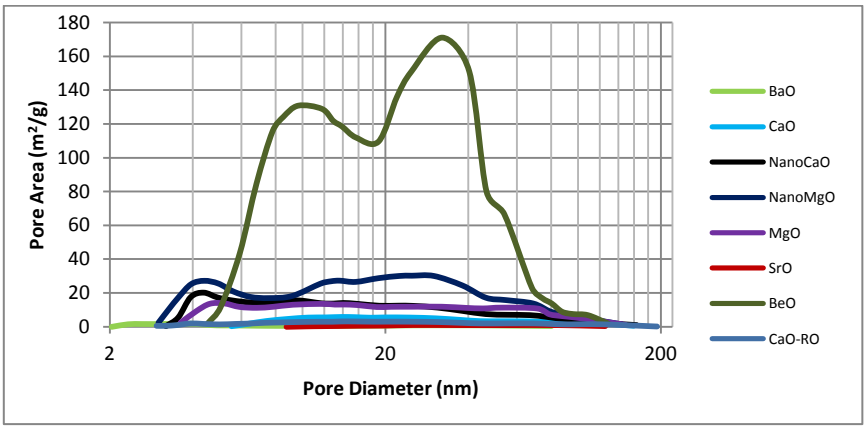


**Figure 3.12: BJH Desorption dA/d(logD) Pore Area**

BJH **Cumulative pore volume for desorption** is given in Figure 3.13. From the plot, one observes that the BJH total volume of pores for the various catalysts are:

- BeO pores between 4 -120 nm width = 0.72 $cm^3/g$
- Nano MgO pores between 3 – 160 nm width = 0.19 $cm^3/g$
- MgO pores between 4 – 160 nm width = 0.118 $cm^3/g$

- Nano CaO pores between 6 – 160 nm width = 0.1 $cm^3/g$
- CaO pores between 4.5 – 150 nm width = 0.05 $cm^3/g$
- CaO-RO pores between 3 – 165 nm width = 0.03 $cm^3/g$
- BaO pores between 2 – 160 nm width = 0.008 $cm^3/g$
- SrO pores between 9 – 160 nm width = 0.012 $cm^3/g$

The observed values are in close agreement with a similar data obtained for adsorption case (Fig 3.9).

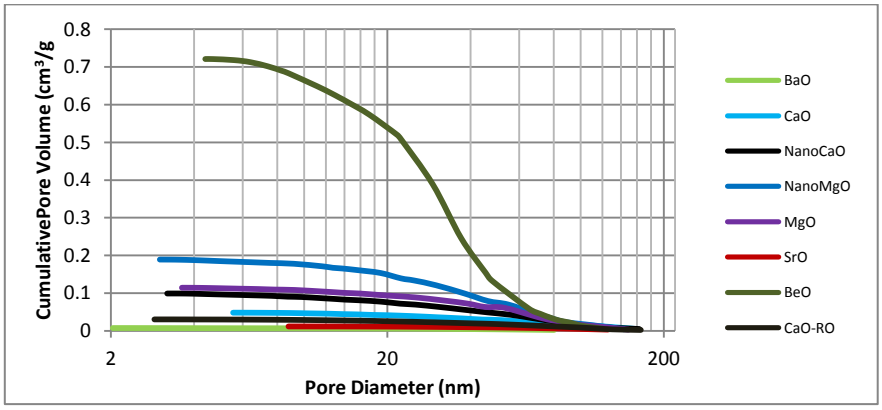


**Figure 3.13: BJH Desorption Cumulative Pore Volume**

Figure 3.14 gives the BJH **adsorption plot for differential pore volume**. From the plot, the highest BJH pore volume for: BeO lie between 20—80 nm, nano MgO lie between 30 – 80 nm, MgO and CaO lie at about 70 nm, CaO lie at 100 nm, CaO-RO lie at 120 nm. No such observation can be made for BaO and SrO. Observations are in slight disagreement with a similar plot for adsorption case (Fig 3.10).

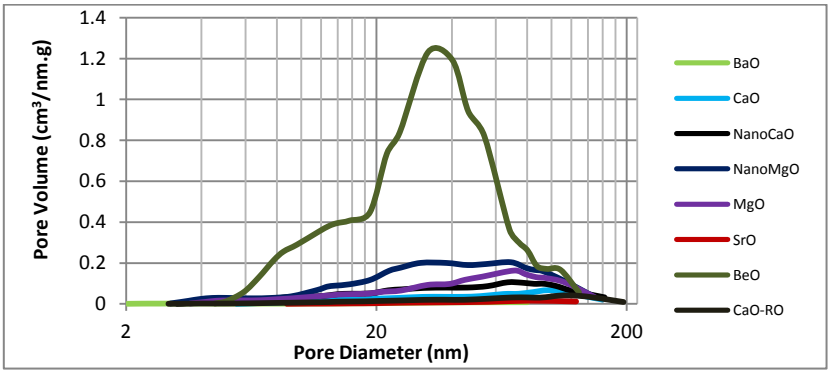


**Figure 3.14: BJH Desorption dV/d(logD) Pore Volume**

### 3.2.5 Microscopy

Scanning Electron Microscopy (SEM) and Transmission Electron Microscopy (TEM) are qualitative techniques which give a direct view of the solid catalyst. The images give an idea about the shape, size, crystalline habit, homogeneity, and composition. The images produced in both SEM and TEM are highly magnified and offer high resolution. SEM scans the surface of the sample by releasing electrons and making the electrons bounce or scatter upon impact. The machine collects the scattered electrons and produces an image. TEM processes the sample by directing an electron beam through the sample. The result is seen using a fluorescent screen. SEM images are three-dimensional and are accurate representations while TEM pictures are two-dimensional but of a higher resolution.

#### 3.2.5.1 Materials and Methods

TEM analysis was conducted on a JEOL 2100 F TEM instrument, operated at 200 kV. For TEM, the powder sample was sonicated in ethanol for 5 min, followed by depositing the solution on a Cu-grid with holey carbon film. The material is dispersed in ethanol using a bath sonicator to form a suspension. One or two droplets were dropped onto a holey carbon supported copper grid and allowed to dry. TEM imaging was performed on a dry sample.

#### 3.2.5.2 Results and Discussion

##### 3.2.5.2.1 Beryllium oxide

Figure 3.15 gives two images of BeO at different resolutions. Highly porous nature of the catalyst is clearly visible in the pictures.

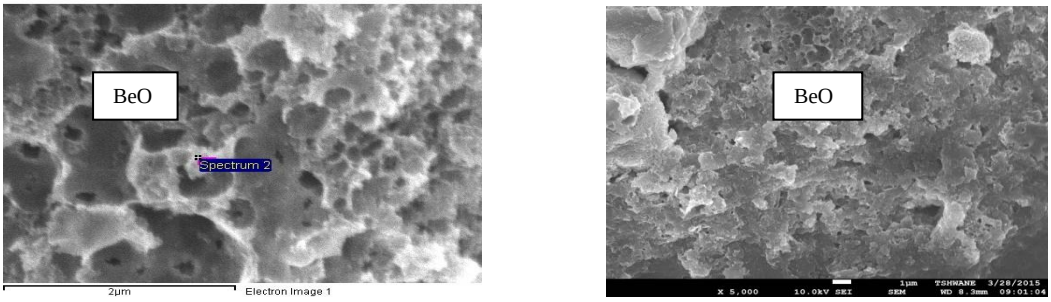


**Figure 3.15: TEM images of BeO**

### 3.2.5.2.2 Magnesium oxide

Figure 3.16 gives two TEM images of MgO at varying resolution. No clear indication in noted of crystal size or structure, instead an amorphous nature is observed.

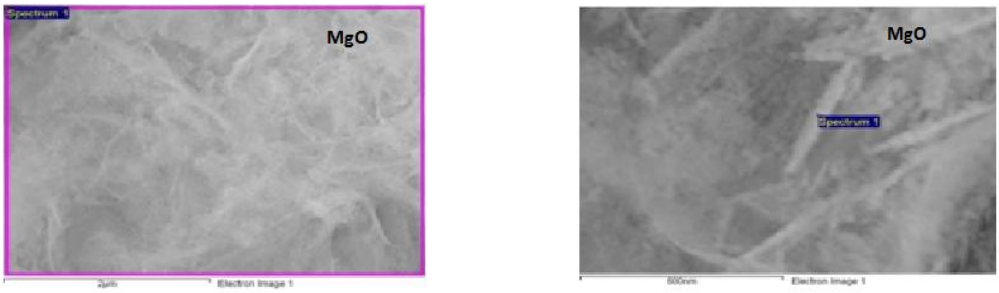


**Figure 3.16: TEM images of MgO**

### 3.2.5.2.3 Nano Magnesium oxide

Figure 3.17 gives two TEM images of Nano MgO particles. Particles are distinct, uniform and cylindrical in shape.

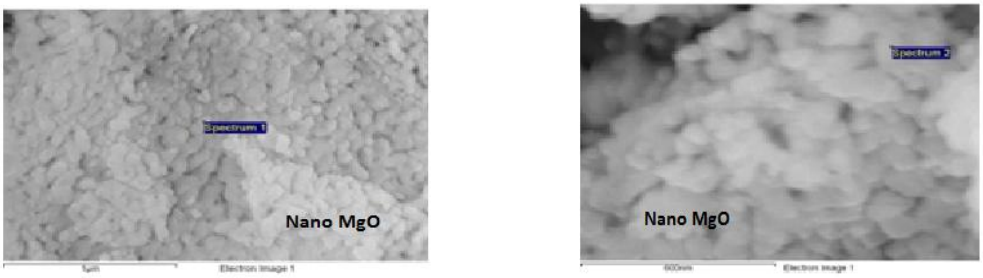


**Figure 3.17: TEM images of Nano MgO**

### 3.2.5.2.4 Calcium oxide

Figure 3.18 are two TEM image of CaO crystals. Crystals are round cylindrical, of size 1 – 2 μm.

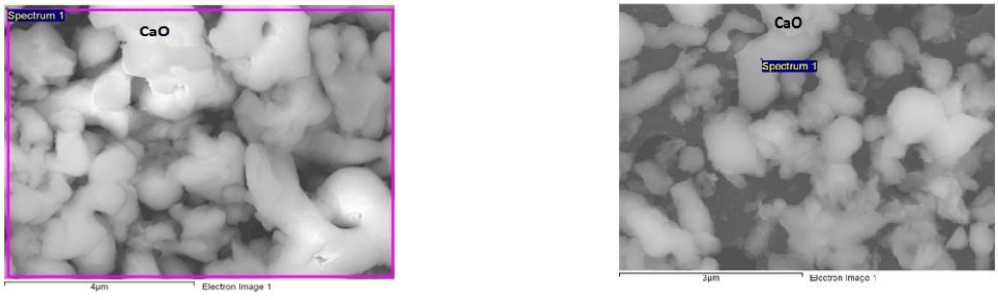


**Figure 3.18: TEM images of CaO**

### 3.2.5.2.5 Re-oxidized Calcium oxide

Figure 3.19 is a TEM image of Re-oxidized CaO (CaO-RO). Particle shapes are similar to that of CaO as in Fig 3.18 but seem to be conglomerated.

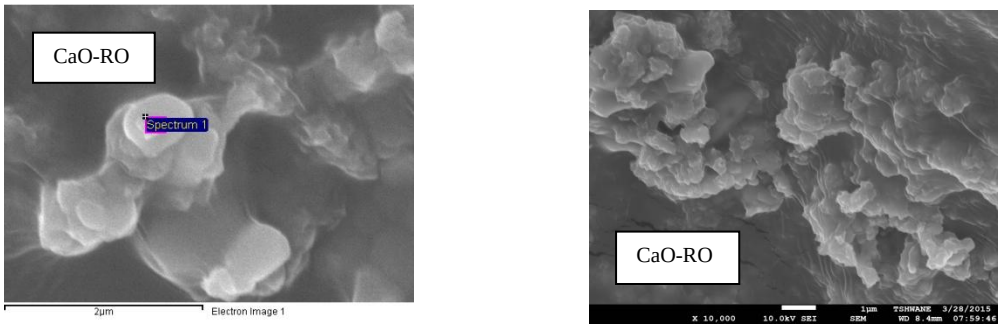


**Figure 3.19: TEM image of CaO RO**

### 3.2.5.2.6 Nano Calcium oxide

Figure 3.20 are two TEM images of Nano CaO. Particle shapes are similar to that of CaO as in Fig 3.18.

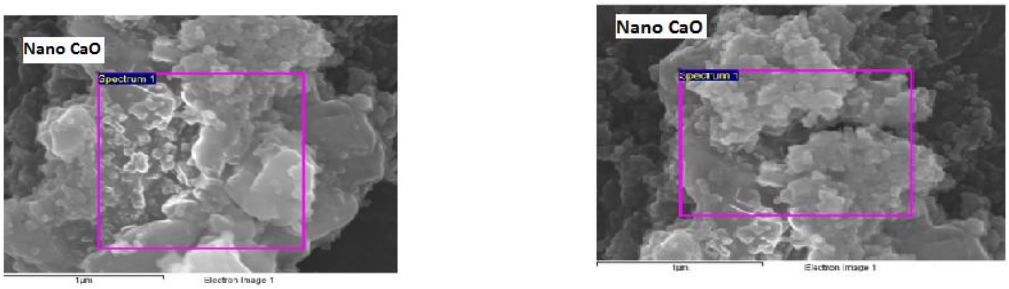


**Figure 3.20: TEM images of Nano CaO**

### 3.2.5.2.7 Strontium oxide

Figure 3.21 gives two TEM images for SrO. No distinct particle shape is visible. Particles form an agglomerate.

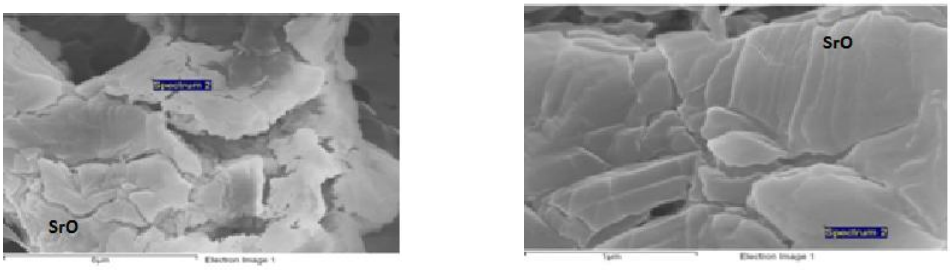


**Figure 3.21: TEM images of SrO**

#### 3.2.5.2.8 Barium oxide

Figure 3.22 gives two TEM images for BaO. Particles form agglomerate and no distinct shape is identifiable.

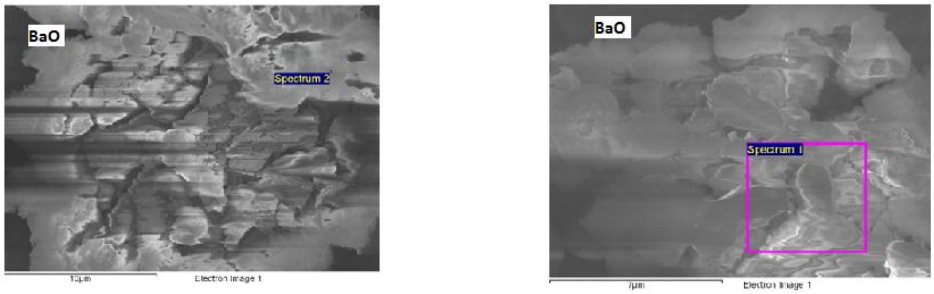


**Figure 3.22: TEM images of BaO**

### 3.2.6 Bulk Properties

Bulk properties provide insight on the nature of surface sites. Analysis include elemental analysis techniques, spectroscopic and diffraction techniques and thermal analysis (Leofanti *et al*., 1997). Bulk properties to be considered here are the chemical composition and crystal structure.

#### 3.2.6.1 Elemental Analysis

There are several methods for such an analysis. Elemental analysis was not relevant in the present study since catalyst samples were of analytical grade of high purity. The purity of catalysts supplied by Sigma Aldrich was as follows: BeO (99.98%), MgO (99%), Nano MgO (99%), CaO (extra pure), Nano CaO (98%), SrO (99.9%) and BaO (97%).

#### 3.2.6.2 X-ray Diffraction

Most catalysts are crystalline solids, metal oxides, supported metals, salts and so on. X-ray powder diffraction allows us to evaluate the nature of crystalline phases, their concentration, and the crystallite size.

##### 3.2.6.2.1 Materials and Methods

The crystalline phases of the samples were determined by X-ray diffraction (PAnalytical XPERT-PRO diffractometer) measurement, using Ni filtered CuKa radiation (k = 1.5406 Å), with a variable slit at 35 kV, 50 mA. Spectra were analyzed with the help of published literature (NBS Monograph 25, 1981; Xu *et al*., 2001; Wan Isahak *et al*., 2010; Kouzu *et al*., 2010; Kawashima *et al*., 2009; Taufiq-Yap *et al*., 2011).

For calcination studies, about 10g of CaO catalyst was calcined in a muffle furnace under atmospheric conditions, for three hours. The optimum calcination time has been reported to be 2-4 h. Longer time results in sintering of catalyst leading to lowering of surface area (Viriya-empikul *et al*., 2010). Calcination was carried out at varying temperatures of 500 (773 K), 700 (973 K), 800 (1073 K) and 900$^{o}$ C (1173. K). The sample was removed from the furnace after three hours and allowed to cool in a desiccator. Once cooled, the sample was removed from desiccator and stored in an air tight container. The calcined calcium oxide was analyzed for composition by X-ray diffraction.

#### 3.2.6.2.2 Results and Discussion

##### 3.2.6.2.2.1 Beryllium oxide

Figure 3.23 gives the XRD spectra of Beryllium oxide catalyst. It shows a pure specimen.

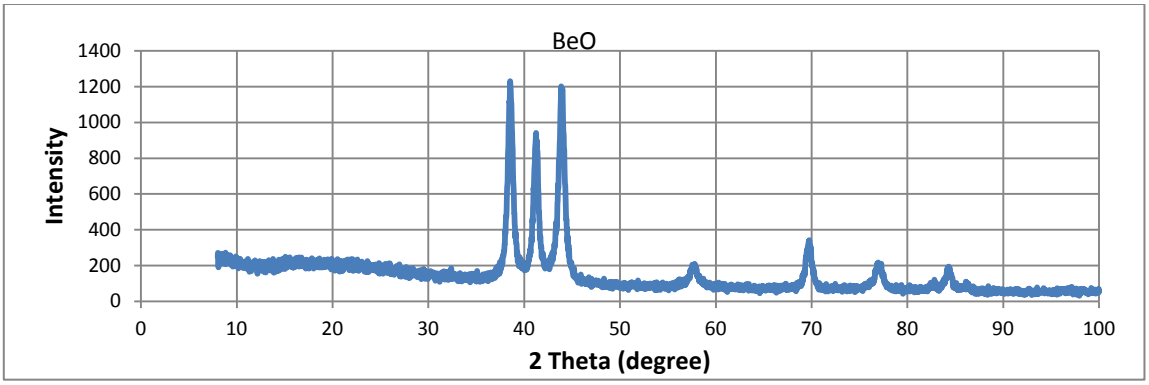


**Figure 3.23: XRD Spectra for BeO**

##### 3.2.6.2.2.2 Magnesium oxide

Figure 3.24 gives the XRD spectra of Magnesium oxide catalyst. Magnesium is present in oxide form and there are no indications of any other species.

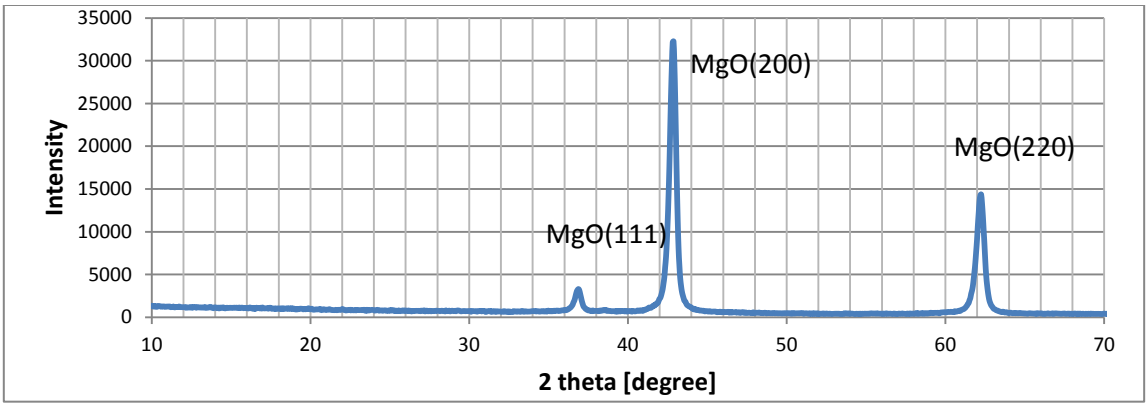


**Figure 3.24: XRD Spectra for MgO**

### 3.2.6.2.2.3 Nano Magnesium oxide

Figure 3.25 is a XRD spectra for Nano Magnesium oxide catalyst. When compared to the spectra for MgO (Fig 3.24), this contains several additional peaks. Nano MgO being more reactive, reacts readily with atmospheric moisture, carbon dioxide and oxygen to form hydroxide, carbonate etc., giving rise to other peaks.

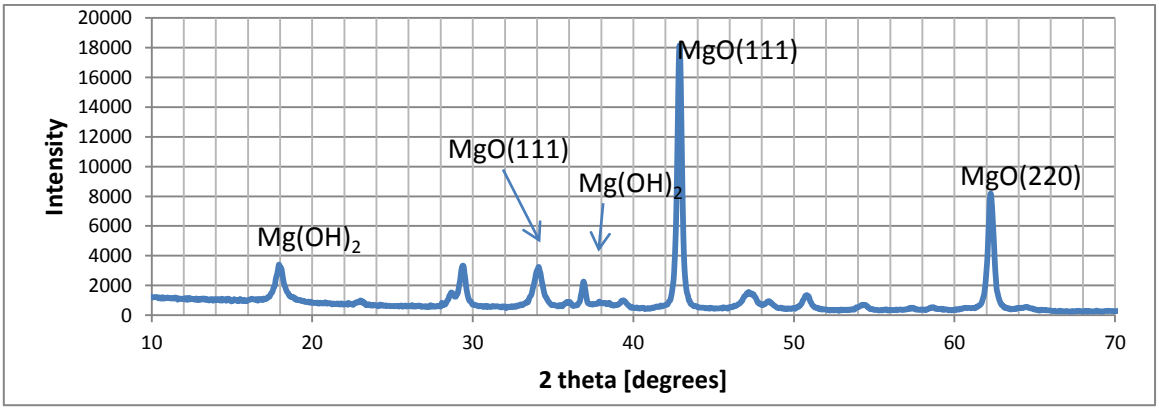


**Figure 3.25: XRD Spectra for Nano MgO**

### 3.2.6.2.2.4 Calcium oxide

Figure 3.26 gives the XRD spectra for Calcium oxide catalyst. Calcium oxide is known to contain carbonate and hydroxide as impurity when exposed to atmospheric moisture, oxygen and carbon dioxide. The other peaks in the spectra are due to the presence of such compounds.

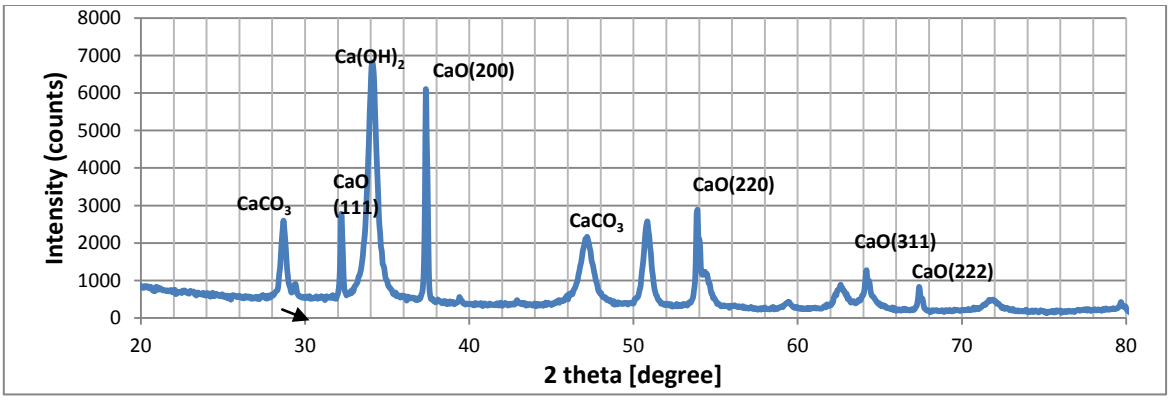


**Figure 3.26: XRD Spectra for CaO**

### 3.2.6.2.2.5 Calcination of Calcium oxide

XRD spectra of CaO (Fig 3.26) shows presence of carbonate ($CaCO_3$) and hydroxide ($Ca(OH)_2$) as impurities. This observation is also made from XRD spectra of Nano CaO as presented in the following section, and given in Fig 3.28. When such samples of CaO ( or Nano CaO) are subjected to high temperatures (calcined), carbonate and hydroxide forms are converted to oxides [$CaCO_3 \rightarrow CaO + CO_2$ ; $Ca(OH)_2 \rightarrow CaO + H_2O$]. In the present study, calcination was carried out at temperatures of 500 (773 K), 700 (973 K), 800 1073 K), and 900$^oC$ (1173 K), for a constant period of three hours. Fig 4.27 gives the XRD plots for *uncalcined* CaO, and for CaO calcined at these temperatures.. It gives the effect of temperature on CaO composition. The bottom most XRD plot in Fig 3.27 corresponds to uncalcined CaO, which is characterized by substantive presence of calcium carbonate and calcium hydroxide. Plot above to this is the sample calcined at 500$^o$ C (773 K). It depicts small presence of carbonate and hydroxide. Calcination plot for 700$^o$ C (973 K) still have peaks for carbonate and hydroxide, although they are very small. XRD plots for temperatures of 800 (1073 K) and 900$^o$ C (1173 K) are almost identical, showing a pure sample of CaO. Carbonate and hydroxide have been totally converted into oxide. The study shows that calcination of calcium oxide, containing carbonate and hydroxide as impurity, at 800 - 900 $^o$C (1073 – 1173 K), converts calcium carbonate and calcium hydroxide into calcium oxide, resulting in pure CaO catalyst. A sample of uncalcined Nano CaO similarly contains unwanted carbonate and hydroxide impurities ( Fig 3.28), and the findings of calcination temperature also hold for it (Kumar *et al*., 2014).

### 3.2.6.2.2.6 Nano Calcium oxide

Nano Calcium oxide is more reactive as compared to Calcium oxide because of larger specific surface area. It readily reacts with atmospheric moisture, carbon dioxide and oxygen. A sample of Nano CaO is most likely to contain hydroxide and carbonate of calcium as impurity. Peaks corresponding to $Ca(OH)_2$ ($2\theta = 34.1^o$), $CaCO_3$ ($2\theta = 29.4^o$, $47.5^o$, $48.5^o$) predominate, whereas peaks for CaO ( $2\theta = 32.2^o$, $37.3^o$, $53.8^o$) are small. This shows that carbonate and hydroxide predominate in the sample (Figure 3.28).

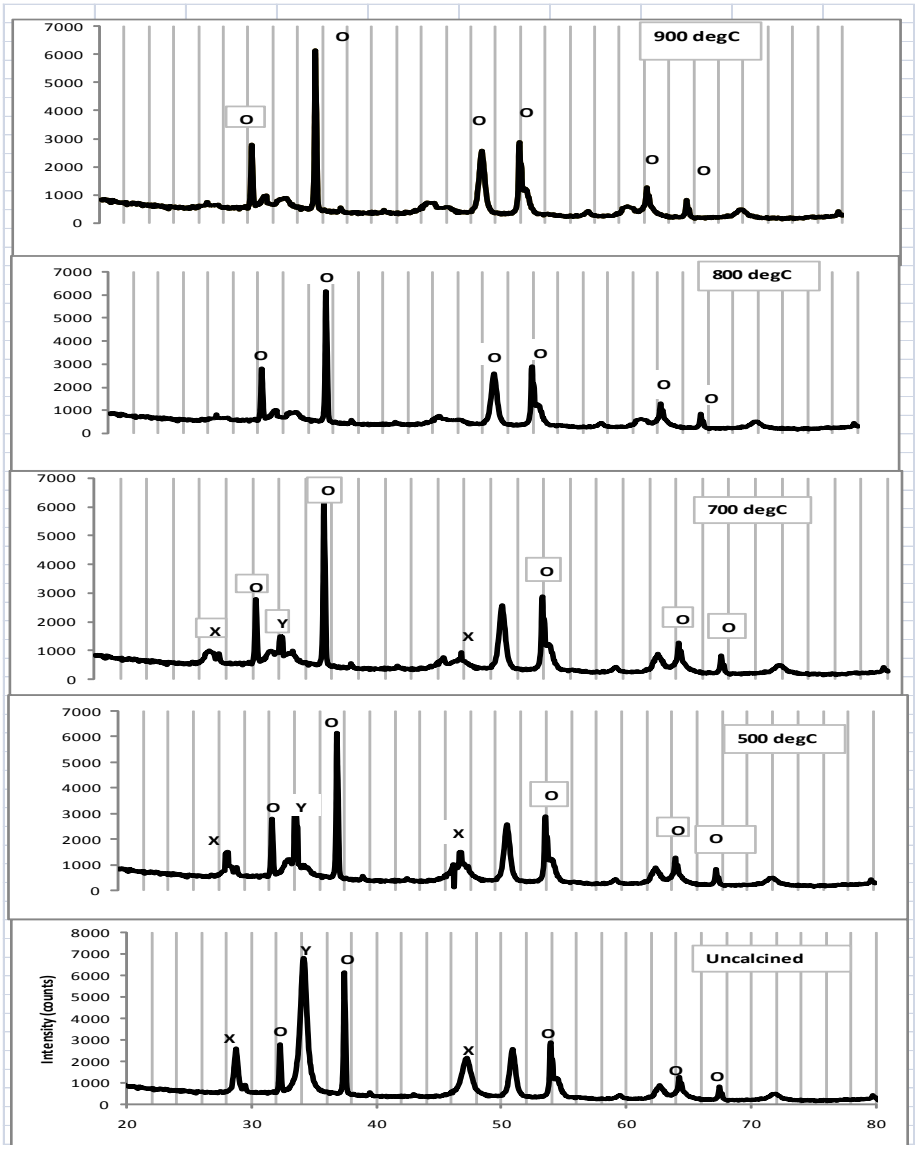


**Figure 3.27: Effect of calcination temperature on CaO composition**

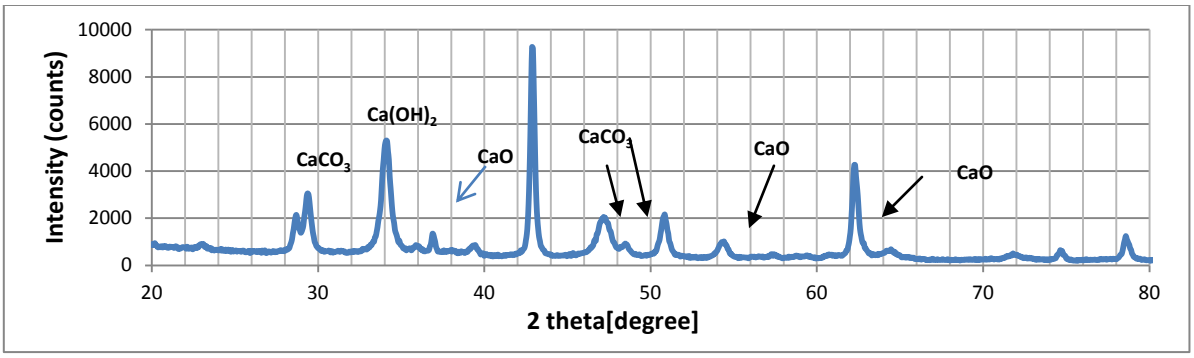


**Figure 3.28; XRD Spectra for Nano CaO**

### 3.2.6.2.2.7 Reoxidized Calcium oxide

Figure 3.29 is the spectra for calcined (at 700$^{o}$ C for 3 hours) Re-oxidized Calcium oxide (CaO-RO). Comparing to Figures 3.26 and 3.27, the sample mostly consists of oxide of calcium. Peaks corresponding to $Ca(OH)_2$ ($2\theta = 34.1^{o}$), and $CaCO_3$ ($2\theta = 29.4^{o}, 47.5^{o}$) are small when compared to peaks for CaO. Because of high reactivity of CaO, carbonate and hydroxide are formed whenever the sample is exposed to atmosphere.

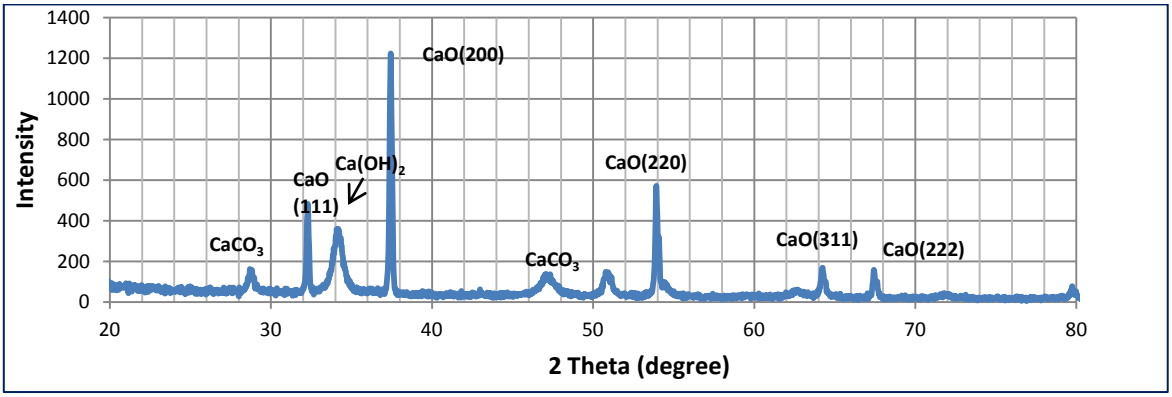


**Figure 3.29: XRD Spectra for CaO-RO**

### 3.2.6.2.2.8 Strontium oxide

Figure 3.30 gives the XRD spectra for Strontium oxide catalyst. The specimen seems to contain some amount of Strontium sulphate as impurity.

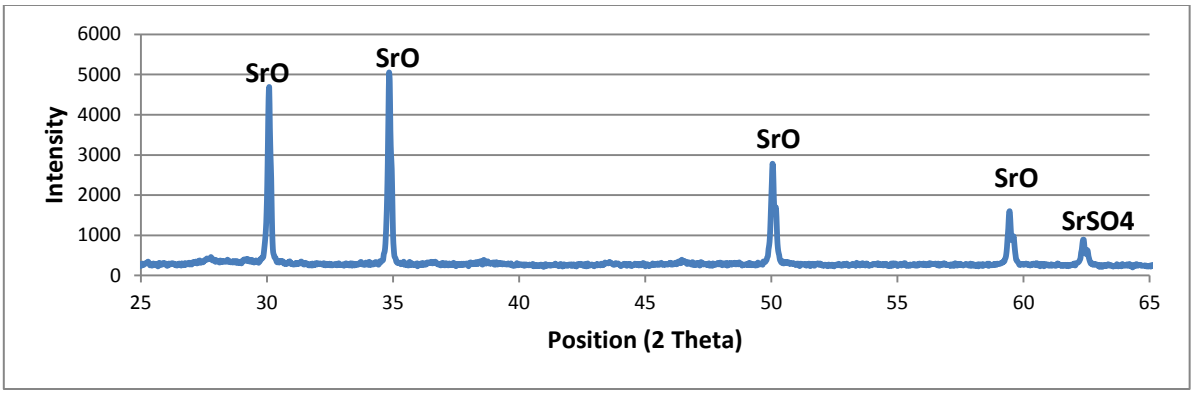


**Figure 3.30: XRD Specra for SrO**

### 3.2.6.2.2.9 Barium oxide

XRD spectra for BaO given in Figure 3.31 is very noisy and very few peaks could be identified. BaO is known to be very reactive and readily reacts with atmospheric moisture, carbon dioxide, oxygen to form $BaO_2$, $Ba(OH)_2$, $BaCO_3$. Such reactions can take place during sample preparation. These unwanted components in the sample may be responsible for unexpected peaks in the spectra.

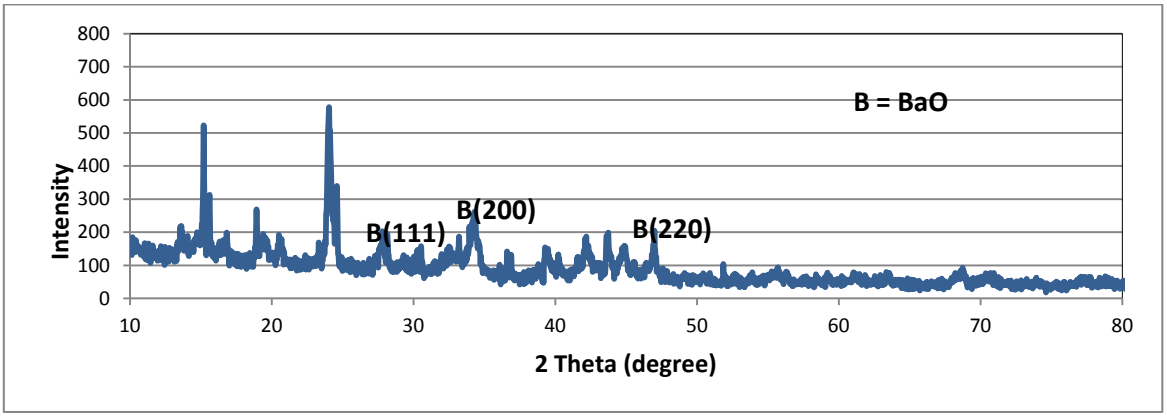


**Figure 3.31: XRD Spectra for BaO**

## 3.2.7 Surface Chemical Characterization: Basicity and Acidity of solid surface

### 3.2.7.1 Introduction

Acid and basic properties of solid catalysts affect their activity for a particular reaction. On a given surface, one type (acidic or basic) may prevail but both are always present (conjugate acidic and basic pairs). For transesterification reaction both acidic and basic catalysts have been tried with varying success. A catalyst is said to be acidic or basic based depending on its pH value. For an acidic catalyst, strength of an acid is defined as the

ability of a solid surface to convert an adsorbed neutral base to its conjugate acid. Similarly for a basic catalyst, basic strength of a solid surface is defined as its ability to convert an adsorbed electrically neutral acid to its conjugate base. The acid or base strength may be estimated following the colour changes of the indicators, or by such techniques as IR or NMR spectroscopies (Haber, 1991). Indicator method gives a semi-quantitative estimate of acidity or basicity.

An 'indicator' method to determine the acidity/basicity of a solid catalyst was originally proposed by Hammett (Matsuzaki and Masahiro, 1969; Kijeński and Zadrożny, 1979; Tanabe and Yamaguchi, 1963). When a neutral base (B) is brought in contact with an acid catalyst ($H^+$), the equilibrium reaction is: $B + H^+ \leftrightarrow BH^+$, and the Hammett acidity function ($H_o$) is given by:

$$H_o = pK_{BH^+} + log\frac{[B]}{[BH^+]} \quad ...3.9$$

$pK_{BH^+}$ is the logarithm of dissociation constant $K_{BH^+}$.

For a basic catalyst ($\bar{B}$), the equilibrium reaction with an acid indicator (BH) is:

$BH + \bar{B} \leftrightarrow B^- + \bar{B}H^+$ , and the Hammett basic strength is given by:

$$H_- = pK_{BH} + log\frac{[B^-]}{[BH]} \quad ...3.10$$

Here $pK_{BH}$ is the logarithm of the dissociation constant of the indicator.

For base catalysts, the catalytic activity is a strong function of its basicity. The solid catalyst is brought into contact with an indicator and the colour change indicates the basicity. The amount of basicity is measured by titration with 0.1 N benzoic acid in benzene/ iso-octane using Bromothymol Blue (BTB) or Phenolphthalein as an indicator. Basicity is expressed in terms of mmol (of benzoic acid) per gram (of catalyst). Table 3.15 gives some Hammett indicators for basicity measurement.

**Table 3.14: Hammett Indicators for Basicity Measurement**

| **Indicators** | **Colour** | | **pK** |
|---|---|---|---|
| | Acid form | Basic form | |
| **Bromothymol Blue** | Yellow | Green | 7.2 |
| **Phenolphthalein** | Colourless | Red | 8.2 |
| **2,4,6,Trinitroaniline** | Yellow | Reddish Orange | 12.1 |

| | | | |
|---|---|---|---|
| **2,4,Dinitroaniline** | Yellow | Violet | 15 |
| **4Chloro-2-nitroaniline** | Yellow | Orange | 17.2 |
| **4-Nitroaniline** | Yellow | Orange | 18.4 |
| **4-Chloroaniline** | Colourless | Pink | 26.5 |

### 3.2.7.2 Materials and Method

Hammett indicators 4-Chloroaniline, 4-Nitroaniline, 2,4-Dinitroaniline, Bromothymol Blue (BTB), and solvent Methanol (analytical grade) were from Sigma Aldrich. Hammett indicator Phenolphthalein, Universal indicator (maximum pK = 11), Benzoic acid, Benzene were of laboratory grade, obtained from Gelsup Nairobi. Calcination was done under atmospheric conditions in a muffle furnace (ELSKLO- LNT 20).

Hammett indicator solutions were prepared by dissolving approximately 5mg of each indicator in 50 ml of methanol. Methanol was chosen as the solvent as it is representative of reaction conditions. Bromothymol blue (BTB) indictor solution used in titration was obtained by dissolving 128mg of BTB in 100 ml of benzene. 0.1 N solution of benzoic acid (pK = + 4.17) in benzene was used as titrating acid.

To measure the base strength, about 25 mg of catalyst sample were shaken with 1 ml of Hammett indicator, and left to equilibrate for 2 hours. The colour on the catalyst was then noted. The base strength of the catalyst will be higher than that of the indicator with the highest pK that changes colour on contact with the catalyst, but lower than the indicator with the lowest pK that does not change colour on contact with the catalyst.

The basicity of catalysts were determined by Hammett indicator titration method. A weighed amount (about 500 mg) of catalyst was mixed with 20ml of benzene in a 250 ml conical flask and shaken. This was titrated against 0.01 N benzoic acid, using BTB or phenolphthalein as indicator. For BTB indicator the end point is when the green colour on catalyst particle disappears, and for phenolphthalein indicator the end point is when the pink colour on catalyst particle disappears. The titration needed to be performed very slowly as the colour change on catalyst particle was not instant but gradual. The moles of benzoic acid needed to neutralize the alkaline catalyst particles are equivalent to the basicity of the catalyst, expressed in mmol $g^{-1}$ (Zhao, 2010).

Catalyst samples of MgO, Nano MgO, CaO, Nano CaO and CaO-RO were calcined at 700$^{o}$C (973.15K) for 3 hours to convert carbonate and hydroxides into oxide form. BeO, SrO and BaO were used as obtained.

### 3.2.7.3 Results and Discussion

#### 3.2.7.3.1 Basic Strength ($H_-$) and Basicity

Basic strengths were observed as per Hammett indictor method and Basicity was obtained by titration against benzoic acid. Table 3.16 gives the results.

**Table 3.15: Basic Strength and Basicity of Catalysts**

| Catalyst | Basic Strength, $H_-$ | Basicity, mmol/g |
|---|---|---|
| **BaO** | $15 < H_- < 18.4$ | 0.0961 |
| **SrO** | $15 < H_- < 18.4$. | 0.0841 |
| **Nano CaO** | $11 < H_- < 15$ | 0.0625 |
| **CaO-RO** | $11 < H_- < 15$ | 0.0535 |
| **CaO** | $11 < H_- < 15$ | 0.0441 |
| **Nano MgO** | $11 < H_- < 15$ | 0.0361 |
| **MgO** | $11 < H_- < 15$ | 0.0289 |
| **BeO** | $8 < H_- < 8.2$ | 0 |

### 3.2.8 Summary

Characteristic physical and chemical properties of croton oil and heterogeneous catalysts were determined through studies of surface properties, microscopy, X- ray diffraction and chemical analysis.

# 4 HOMOGENEOUS SODIUM HYDROXIDE CATALYSIS IN THE TRANSESTERIFICATION OF CROTON *MEGALOCARPUS* OIL

## 4.1 Introduction

Transesterification reactions of croton *megalocarpus* oil and methanol were carried out in a batch reactor using sodium hydroxide as a catalyst, employing conventional heating and microwave irradiation. Reactions were performed to study the effect of operating variables on FAME yield, to study the reaction kinetics, and to identify the conditions for optimal yield.

## 4.2 Materials and Methods

### 4.2.1 Materials

Croton *megalocarpus* oil was solvent-extracted from croton nuts in department lab, and also obtained from Help Self-Help Centre Nairobi. Analytical grade sodium hydroxide was obtained from Gelsup, Nairobi. Analytical grade methanol was from Sigma Aldrich. GC grade solvents n-heptane, hexane; GC standards methyl heptadecanoate, triolein, methyl myristate, methyl palmitate, methyl stearate, methyl oleate, methyl linoleate were from Sigma Aldrich. Equipment included analytical balance, water bath (Stuart RE 300B, accuracy ± 1$^{o}$C), mechanical stirrer (Stuart SS10, 0-2000 rpm), domestic microwave oven (Shivaki, SMW-103, 1300W), voltage regulator, microwave leak detector, magnetic stirrer (Hanna), thermocouple thermometer (Hanna HI9055), centrifuge (Hettich D-7200), Teflon® tubing, standard laboratory glassware.

FAME was analyzed using a Gas chromatograph (MRC GC3420A) with flame ionization detector, capillary column Agilent CP-Sil 88 (60m x 0.25mm x 0.36mm, coating 0.2μm); carrier gas was nitrogen and other gases were hydrogen and air. Gases were of analytical grade. Data analysis was done using Peak-ABC chromatography data handling system. Polymath 6.10, Matlab R2006b, DesignExpert9 were used for experiment design and data analysis.

### 4.2.2 Experimental setup

#### 4.2.2.1 Conventional heating

For Transesterification with conventional heating (WB), a 3-neck round bottom flask (250 ml) was used as the batch reactor which was kept in a constant temperature water bath. A water-cooled reflux condenser was used to condense methanol vapours. Reactants were mixed by mechanical stirrer fitted with a stainless steel impeller of diameter 0.03m, operating at 750 rpm. The mixing speed was sufficient to eliminate mass transfer resistance and ensure complete mixing (see Section 2.4.5). Fig 4.1a, 4.1b give the experimental setup.

**Figure 4.1: a- Experimental Setup (WB)**

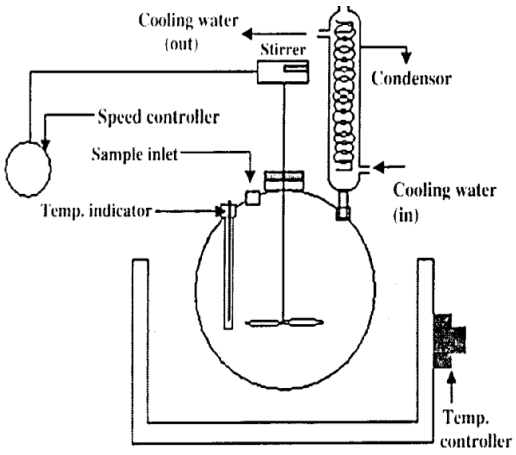


**Fig 4.1b: Experimental setup schematic diagram (WB)**

#### 4.2.2.2 Microwave Irradiation

For studies with microwave irradiation (MW), a domestic microwave oven was modified as shown in Fig 4.2a and 4.2b. A voltage regulator (Variac) was used to control the input power, an electromagnetic stirrer with Teflon® coated stirring magnet was used to provide the stirring, temperature sensor was a Teflon® covered thermocouple. Water cooled condenser was used to condense methanol. Modified oven was tested for microwave leakage using a microwave leak-detector and the irradiation level was found to be within the safely limit ( < 5 $mW/cm^2$). Three-neck round bottom flask (250 ml) was used as a reactor. Oven also contained a water reservoir ( 500 ml beaker/ conical flask) to act as a

sink to absorb excess microwave irradiation. Samples were drawn using a hypodermic syringe.

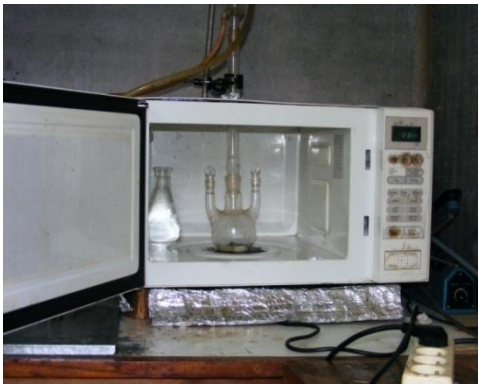

**Figure 4.2:a Experimental setup (MW)**

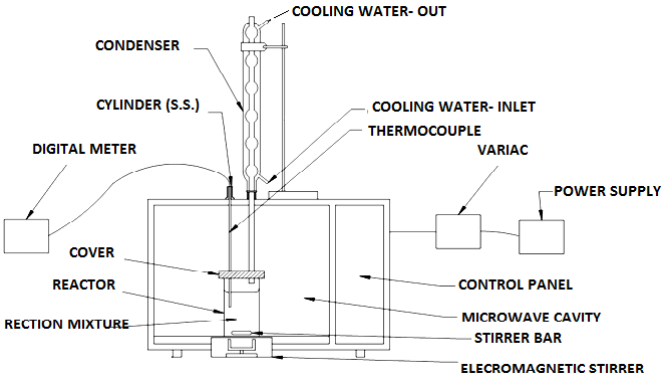


**Fig 4.2b: Experimental setup- schematic diagram (MW)**

### 4.2.3 Experimental Procedure

#### 4.2.3.1 Conventional Heating

Weighed amount of croton *megalocarpus* oil was added to the reactor and heated in the water bath to the reaction temperature. Weighed amount of sodium hydroxide catalyst and measured volume of methanol were heated separately to the desired temperature allowing the solid catalyst to dissolve completely. The sodium hydroxide-methanol solution was then added to the oil. The mechanical stirrer was immediately started, and the reaction timed at this point. At the end of the desired reaction time, the round bottom flask was immersed in ice bath to quench the reaction. The contents were then transferred to a separating funnel and some warm distilled water was added and contents shaken. The separating funnel was kept in a stand allowing the two phases to separate. Oily phase containing FAME was the top phase. Glycerol, unreacted methanol and the added water formed the bottom aqueous phase. Aqueous phase was removed and discarded. The oily phase was similarly washed two, or more, times with warm water till the aqueous phase was free from any alkalinity, as tested by adding phenolphthalein indicator to a small portion of aqueous phase. Presence of alkali changed the solution colour to ink. The oily phase containing FAME was dried in an oven at 90$^{o}$C (363K) for 1 hour to remove any dissolved methanol. The dried FAME sample was kept in a deep freezer pending analysis by GC. For kinetic studies, samples were periodically removed using a hypodermic syringe and treated as above.

#### 4.2.3.2 Microwave irradiation

Procedure was almost similar to the case of conventional heating. Methanol and NaOH were mixed prior to being added to croton oil kept in the reactor in microwave. Stirring was vigorous to eliminate mass transfer resistances and to prevent hot-spots within the reacting media. For studies involving effect of power, power setting of 20, 40, 60, 80, 100% were used. For kinetic studies, constant temperatures were maintained by controlling input voltage through a voltage regulator. This temperature control through manual input voltage control was satisfactory only for a short reaction time. Attempts to maintain a lower temperature by reducing the in-built microwave power setting were not successful as the microwave kept on switching off-and-on at lower power settings -resulting in temperature fluctuations. Secondly, the microwave had to be switched off every time a sample was withdrawn. After an experimental run, the oven was allowed to cool to ambient temperature before reuse.

### 4.2.4 FAME Analysis

Product FAME sample was analyzed by gas chromatography for total FAME according to EN-14103 (BRUKER Chemical Analysis Application Note # CA-270358). Approximately 250mg of sample was accurately weighed in a 10ml vial, and 5 ml of methyl heptadecanoate solution (10 mg/ml- as internal standard) was added using a pipette. 1 μL of this was injected in a split ratio 1:100. Nitrogen carrier gas flow rate was 45 ml/min, hydrogen 30 ml/min, and air 300 ml/min. Initial column temperature was 120$^{o}$C (393K) for 2 min, and the ramped at the rate of 10K/min to 220$^{o}$C (493K ) and kept there. Injector temperature was 250$^{o}$C (523K) and Detector temperature was 300$^{o}$C (573K). Run time was 30 min. FAME content was calculated using the following formula (BRUKER Chemical Analysis Application Note # CA-270358):

$$\text{FAME} = \left(\frac{(\sum A)-AEI}{AEI}\right)\left(\frac{CEI \times VEI}{m}\right) \times 100\ \% \qquad \text{...4.1}$$

where, $\sum A$ = total peak area for methyl esters

$AEI$ = peak area of methyl heptadecanoate (internal standard)

$CEI$ = concentration of methyl heptadecanoate solution (mg/ml)

$VEI$ = volume of methyl heptadecanoate solution (ml)

$m$ = mass of the sample (mg)

Fig 4.3 gives an illustrative chromatogram for Croton *megalocarpus* FAME.

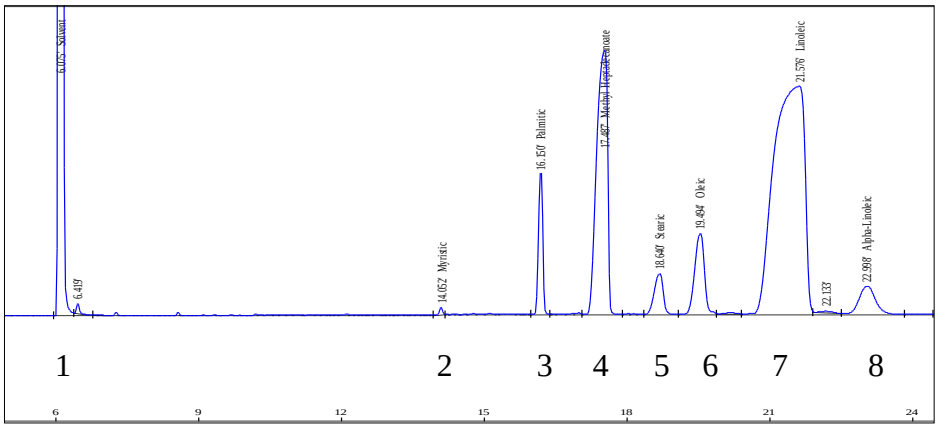


**Figure 4.3: FAME Chromatogram** ( Peaks: 1- Solvent Hexane, 2- Myristic acid, 3- Palmitic acid, 4- Methyl heptadecanoate (IS), 5- Stearic acid, 6- Oleic acid, 7- Linoleic acid, 8- Linolenic acid)

## 4.3 Results and Discussions

### 4.3.1 Studies with conventional heating

This section deals with transesterification reactions carried out with conventional heating employing a water bath as heat source.

#### 4.3.1.1 Effect of operation variables on FAME yield

Operating variables studied were (i) Methanol to triglyceride molar ratio, (ii) Catalyst concentration, and (iii) Reaction temperature. Effect of reaction time on FAME yield was studied under reaction kinetics. Stirring speed was kept constant at 750 rpm, which was large enough to rule out mass transfer resistances.

##### 4.3.1.1.1 Effect of methanol to triglyceride molar ratio on FAME yield

Methanol to oil molar ratio was varied as 3:1, 6:1, 9:1, 12:1, 15:1. Batch consisted of 30 ml of Croton *megalocarpus* oil (FFA = 1.7), NaOH catalyst 1% by mass of oil. Reaction temperature was 70$^{o}$C (343K), and reaction time 2 h. Fig 4.4 gives the FAME yield as a function of methanol: oil ratio.

The reaction stoichiometry requires three moles of methanol to one mole of triglyceride. However, due to reversible nature of the reaction (Eqn 2.2, Chapter 2), an excess amount of methanol is employed to promote the forward reaction. Fame yield was 48.1% for a 3:1 methanol:oil ratio. Yield increased to 96% when the ratio was increased to 6:1. At higher ratios the yield began to decline, and the highest ratio of 15:1 corresponded to a 66.8% yield. When methanol is in large excess, the unreacted fraction mixes with product

glycerol, hindering the separation. The glycerol in the solution drives the equilibrium back to the left-side resulting in lower yields. It is also reported that in large excess of methanol, glycerol forms an emulsion with FAME, leading to glycerol-FAME separation problems and lowering the yield (Jain *et al*., 2011). Lastly, large surplus of methanol reduces the effective percentage of catalyst in the reaction mixture, thereby lowering the yield (Bambase *et al*., 2007).

#### 4.3.1.1.2 Effect of Catalyst concentration on FAME yield

Transesterification of Croton *megalocarpus* oil was carried out with varying catalyst concentrations. Batch consisted of 30 ml of Croton *megalocarpus* oil (FFA = 1.7), methanol to oil ratio of 6:1, reaction temperature 70$^{o}$C (343K), reaction time 2 h, and NaOH concentrations of 0.5, 1, 1.5, 2 mass% respectively. A FAME yield of 58.6% was obtained for NaOH concentration of 0.5 mass%. The yield increased to 96.0% when NaOH concentration was raised to 1 mass%. Further increase in NaOH concentration resulted in a drop in yield. Yields for 1.5 and 2 mass% were 89 and 79.6% respectively. The highest FAME yield corresponded to 1 mass% of catalyst. At higher ( > 1mass%) catalyst concentrations, soap formation was observed bringing about problems in phase separation. Recovery of FAME therefore dropped as catalyst concentration was increased beyond 1 mass%, resulting in lower yields. Fig 4.5 gives the FAME yield as a function of NaOH concentration.

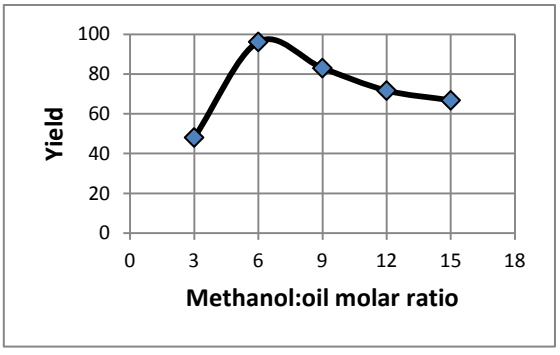


**Figure 4.4: FAME yield as a function of Methanol: oil ratio**

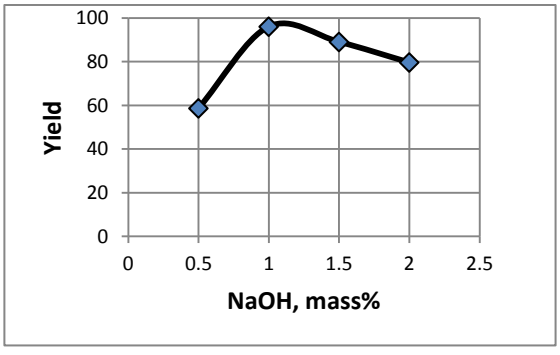


**Figure 4.5: FAME yield as a function of NaOH concentration (WB)**

#### 4.3.1.1.3 Effect of temperature on FAME yield

In the absence of mass transfer limitations, reaction temperature is a major factor dominating reaction kinetics. Reaction temperature was increased in the range of 40 – 70$^{o}$C (313 – 343 K). Reactions at temperatures higher than 70$^{o}$C (313K) brings about problems of phase contact as the temperature exceeds the normal boiling point of methanol. A reaction carried out at 80$^{o}$C resulted in a coagulated mass of oil since the methanol was in vapour phase. Reactions were carried out at constant catalyst concentration of 1 mass%, methanol to oil molar ratio 6:1, and reaction time 1 h. Reaction temperatures were 40, 50, 60 and 70$^{o}$C (313, 323, 333, 343 K) respectively. Yield increased with the increase in reaction temperature. Yield at 40$^{o}$C (313K) was 78.1%, which rose to 85% at 50$^{o}$C (323K). Yields at 60 and 70$^{o}$C (333 and 343K) were fairly close, 96 and 97.1%. It shows that at temperatures above 60$^{o}$C (333K), the yield almost stabilized and became constant. The results are given in Fig 4.6.

### 4.3.1.2 Reaction Kinetics

Transesterification reaction was carried out at temperatures of 40, 50, 60, 70$^{o}$C (313, 323, 333, 343 K) keeping other variables constant at: methanol to oil ratio 6:1, NaOH 1 mass%, reaction time 3 h. Amount of oil used in each run was 100 ml, and samples (of 1 ml) were drawn at time intervals of 15, 30, 45, 60, 90, 120, 150, 180 min. Regression analysis was used to identify the most probable reaction order, and the regression coefficients were used to obtain reaction rate constant. Arrhenius equation was used to estimate the activation energy for the reaction.

#### 4.3.1.2.1 Effect of Time on FAME yield

Fig 4.7 gives the FAME yield as a function of time at different reaction temperatures, for the reaction period of 3 h. Yield vs. time plot for temperatures of 60 and 70$^{o}$C (333 and 343K) ran very close to each other, and final yields were 97 and 98%. For 50$^{o}$C (323K) the yields were initially lower, but increased to reach almost same level (91%) at the end of reaction period. Yields at various temperatures became almost constant after 1 hr of reaction time.

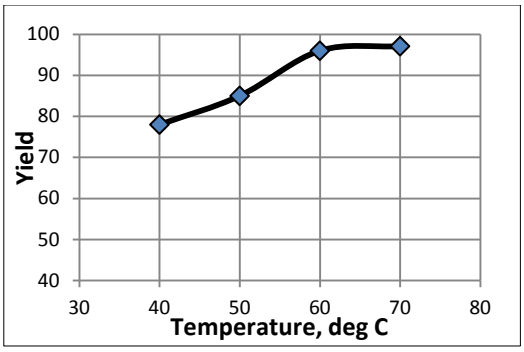


**Figure 4.6: FAME yield as a function of temperatures (WB)**

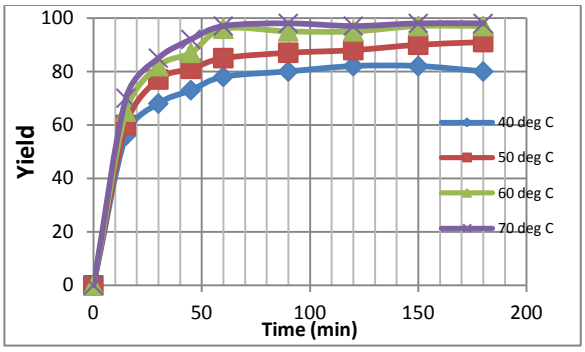


**Figure 4.7: Variation of Yield with time at various reaction temperature (WB)**

#### 4.3.1.2.2 Order of reaction

Equations 2.34 to 2.43 (Chapter 2) are integrated forms of reaction orders from 'zero' to 'three'. L.H.S. of these equations is a function of conversion, or Yield ($F(x_A)$); and the R.H.S. is a function of reaction time, *t*. These equations are in the form of y = mx (passing through origin). For all the ten cases, y (or $F(x_A)$) was plotted against x ( or *t*) and the coefficient of determination obtained. Highest correlation coefficient, $R^2$, was noted to determine the order of reaction. Table 4.1 gives the coefficients of correlation ,$R^2$, for all the ten cases, at each temperature. General rate equation is (Eqn 2.29): $-r_A = -\frac{d[A]}{dt} = k\,[A]^m\,[B]^n$ .

**Table 4.1: Coefficients of correlation, R2, for various reaction orders (WB)**

| | 0th Order | 1st Order | | 2nd Order | | | 3rd Order | | | |
|---|---|---|---|---|---|---|---|---|---|---|
| **Temp °C** | Case 1 | Case 2 (m=1, n=0) | Case 3 (m=0, n=1) | Case 4 (m=1, n=1) | Case 5 (m=2, n=0) | Case 6 (m=0, n=2) | Case 7 (m=2, n=1) | Case 8 (m=1, n=2) | Case 9 (m=3, n=0) | Case 10 (m=0, n=3) |
| **40** | 0.4063 | 0.5539 | 0.4469 | 0.5986 | 0.6987 | 0.4898 | 0.7878 | 0.6299 | **0.7777** | 0.5336 |
| **50** | 0.4171 | 0.6605 | 0.4677 | 0.7240 | **0.9155** | 0.5226 | 0.9066 | 0.7619 | 0.9870 | 0.5797 |
| **60** | 0.4098 | 0.7479 | 0.4620 | 0.7968 | **0.8522** | 0.5175 | 0.7094 | 0.8148 | 0.4538 | 0.5730 |
| **70** | 0.3728 | 0.6763 | 0.4175 | 0.7175 | **0.7946** | 0.4650 | 0.7555 | 0.7286 | 0.6925 | 0.5129 |

In the above Table, largest correlation coefficients for the four temperatures are in **bold**. At 40°C (313K), largest value corresponded to Case 9, whereas for the remaining three temperatures it was for Case 5. Hence the overall order of reaction (rate of disappearance

of triglyceride) was most likely to be ‘second’; order with respect to triglyceride was ‘two’, and order with respect to methanol was ‘zero’.

A second order kinetics has been reported for homogenous NaOH/ KOH catalysts for transesterification of palm oil and methanol (Leevijit *et al*., 2004), sunflower oil with methanol (Vicente *et al*., 2005; Stamenkovic´ *et al*., 2008; Bambase *et al*., 2007), sunflower oil with ethanol (Marjanović *et al*., 2010), soybean oil with methanol (Noureddini and Zhu, 1997). A first order kinetics for transesterification is reported for $H_2SO_4$/ NaOH catalysts and methanol for *Jatropha curcas* oil (Jain and Sharma, 2010), waste cooking oil (Jain *et al*., 2011). Some studies report kinetic order varying with reaction progress. For transesterification of palm oil using KOH catalyst, Darnoko and Cheryan (2000) observed a pseudo second order reaction in initial part, and first or zero order in the later part. Freedman *et al*. (1986) reported a fourth order and second order kinetics for transesterification of soybean oil with methanol using sodium methoxide catalyst. Fourth order kinetics was explained through a shunt-reaction in which 3 moles of methanol directly attacks one mole of triglyceride and FAME is formed in a single step, bypassing formation of di- and mono-glyceride intermediates.

#### 4.3.1.2.3 Rate constant and Activation energy

Case 5 in Table 4.1 refers to Eqn 2.38 (Chapter 2): $\left(\frac{x_A}{1-x_A}\right) = k\,[A]_o\,t$. A plot of F($x_A$) vs. *t* for 70$^o$C (343K) is given in Fig 4.8.

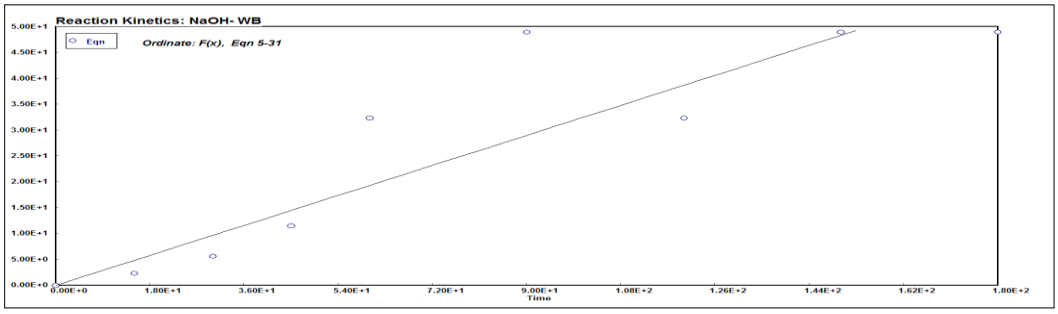


**Figure 4.8: Plot of kinetic equation 5.31 (WB)** (Ordinate: $\left(\frac{x_A}{1-x_A}\right)$, Abscissa: *t*. )

Correlation constants ($= k\,[A]_o$) for Eqn 2.38 for the four temperatures were used to estimate reaction constant *k* as given in Table 4.2.

**Table 4.2: Reaction constant k (WB)**

| temp C | temp K | [Ao]k | [Ao] | k (in min) | k (in s) |
|---|---|---|---|---|---|
| | | | | | |
| **40** | 313.15 | 0.036496 | 0.734034 | 0.0497 | 0.000829 |
| **50** | 323.15 | 0.065104 | 0.734034 | 0.0887 | 0.001478 |
| **60** | 333.15 | 0.246002 | 0.734034 | 0.3351 | 0.005586 |
| **70** | 343.15 | 0.348918 | 0.734034 | 0.4753 | 0.007922 |

Activation energy was obtained from the slope of the plot of ln*k* vs. 1/T (Arrhenius plot, Section 2.5.4.1). Fig 4.9 gives the plot.

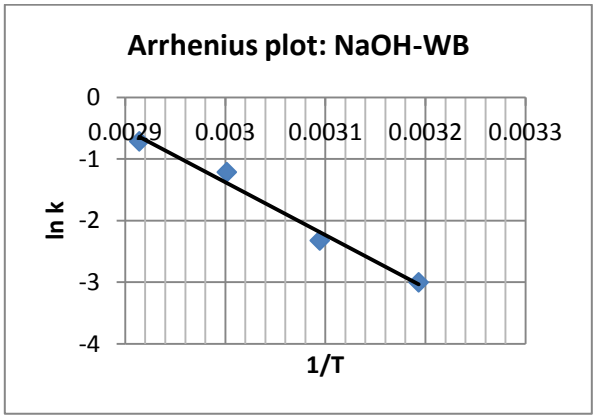


**Figure 4.9: Arrhenius plot for NaOH catalyst (WB)**

The slope is 8573.08 ( $R^2$ = 0.9826), which gave the Activation energy, $E$ = 71.27 kJ/mol; and intercept gave pre-exponential factor, $A = 3.72 \times 10^{10}$.

#### 4.3.1.3 Optimization studies

Optimization studies involve exploring the process variables for maximum yield. Experimental data are fitted into an appropriate correlation, which is then plotted in surface and contour plots that depict optimal conditions.

##### 4.3.1.3.1 Experimental Design

Reaction temperature, methanol to oil ratio, and catalyst concentration were chosen to be the key process variables for FAME yield. RSM (Appendix A) was used to investigate the influence of these three independent variables on FAME yield. A five-level, three-factor Central Composite Design (CCD) was used to optimize these 3 independent variables to achieve maximum FAME yield. Table 4.3 gives the independent variables and levels used for experimental design.

**Table 4.3: Independent variables and their levels in CCD (WB)**

| Independent variables | Codes | Variable levels | | | | |
|---|---|---|---|---|---|---|
| | | -α= -1.682 | -1 | 0 | 1 | +α= 1.682 |
| Catalyst amount (wt%) | X1 | 0.16 | 0.5 | 1 | 1.5 | 1.84 |
| Temperature (°C) | X2 | 43 | 50 | 60 | 70 | 77 |
| Methanol:oil molar ratio | X3 | 1 | 3 | 6 | 9 | 11 |

A total of 20 experiments, including 6 replications at the centre point, were conducted. Replicates at the centre point give pure error. Reaction time was kept constant at 2 h.

#### 4.3.1.3.2 Experimental results and data analysis

Table 4.4 gives the details of a set of 20 experiments in terms of actual and coded levels as per CCD, and experimental and predicted FAME yields.

**Table 4.4: CCD matrix with experimental FAME yield (WB)**

| Run | Level of variables [actual(coded)] | | | Expt. Yield | Quadratic Model (Eqn 6.3) |
|---|---|---|---|---|---|
| | Catalyst,% X1 | Temp, (°C) X2 | Methanol :oil X3 | | Y |
| **1** | 1(0) | 60(0) | 6(0) | 96 | 95.6 |
| **2** | 1(0) | 43(-1.68) | 6(0) | 83.5 | 83.7 |
| **3** | 0.5(-1) | 70(1) | 9(1) | 85.1 | 85.8 |
| **4** | 1(0) | 60(0) | 11(1.68) | 78.9 | 78.4 |
| **5** | 1.84(1.68) | 60(0) | 6(0) | 82.9 | 82.2 |
| **6** | 1(0) | 60(0) | 1(-1.68) | 86.8 | 87.2 |
| **7** | 0.5(-1) | 50(-1) | 3(-1) | 90.6 | 90.7 |
| **8** | 1(0) | 60(0) | 6(0) | 95.5 | 95.6 |
| **9** | 1.5(1) | 70(1) | 9(1) | 91.1 | 91.1 |
| **10** | 1.5(1) | 70(1) | 3(-1) | 84.01 | 84.8 |
| **11** | 1(0) | 60(0) | 6(0) | 96 | 95.6 |
| **12** | 1.5(1) | 50(-1) | 3(-1) | 85 | 84.4 |
| **13** | 0.16(-1.68) | 60(0) | 6(0) | 82.6 | 83.1 |
| **14** | 1(0) | 60(0) | 6(0) | 95.2 | 95.6 |
| **15** | 1.5(1) | 50(-1) | 9(1) | 74.3 | 75.2 |
| **16** | 1(0) | 60(0) | 6(0) | 96.2 | 95.6 |
| **17** | 0.5(-1) | 50(-1) | 9(1) | 74.6 | 73.9 |
| **18** | 1(0) | 77(1.68) | 6(0) | 94.6 | 94.2 |
| **19** | 1(0) | 60(0) | 6(0) | 95.2 | 95.6 |
| **20** | 0.5(-1) | 70(1) | 3(-1) | 88.1 | 87.2 |

Data in Table 4.4 were tested for fit for a linear, two-factor interaction (2FI), quadratic and cubic polynomials. Table 4.5 gives the result.

**Table 4.5: Summary for model fit- Sequential model sum of squares (WB)**

| Source | Sum of Squares | df | Mean Square | F Value | p-value Prob > F | |
|---|---|---|---|---|---|---|
| **Mean vs Total** | 1.541E+005 | 1 | 1.541E+005 | | | |
| **Linear vs Mean** | 227.36 | 3 | 75.79 | 1.64 | 0.2195 | |
| **2FI vs Linear** | 155.73 | 3 | 51.91 | 1.16 | 0.3632 | |
| **Quadratic vs 2FI** | 576.00 | 3 | 192.00 | 273.44 | < 0.0 | Suggested |
| **Cubic vs Quadratic** | 5.12 | 4 | 1.28 | 4.03 | 0.0636 | Aliased |
| **Residual** | 1.90 | 6 | 0.32 | | | |
| **Total** | 1.551E+005 | 20 | 7753.72 | | | |

Based on the F value and p-value, Quadratic model was suggested. Cubic was aliased.

A full quadratic model for yield (Eqn 4.2) was tested.

$$Y = b_0 + \sum_{i=1}^{n} b_i X_i + \sum_{i=1}^{n} b_{ii} X_i^2 + \sum_{1=1}^{n-1} \sum_{j=i+1}^{n} b_{ij} X_i X_j \quad \ldots 4.2$$

Table 4.6 gives Analysis of Variance (ANOVA)

**Table 4.6: ANOVA for Response Surface Quadratic model (WB)**

| **Analysis of variance table [Partial sum of squares - Type III]** | | | | | | |
|---|---|---|---|---|---|---|
| **Source** | **Sum of Squares** | **df** | **Mean Square** | **F Value** | **p-value Prob > F** | |
| **Model** | 959.09 | 9 | 106.57 | 151.77 | < 0.0001 | significant |
| ***X1-NaOH*** | *0.89* | *1* | *0.89* | *1.27* | *0.2866* | |
| ***X2-Temp*** | *132.12* | *1* | *132.12* | *188.17* | *< 0.0001* | |
| ***X3-Meth: oil*** | *94.35* | *1* | *94.35* | *134.37* | *< 0.0001* | |
| ***X1 X2*** | *7.62* | *1* | *7.62* | *10.86* | *0.0081* | |
| ***X1 X3*** | *29.61* | *1* | *29.61* | *42.17* | *< 0.0001* | |
| ***X2 X3*** | *118.50* | *1* | *118.50* | *168.77* | *< 0.0001* | |
| ***X1^2*** | *300.36* | *1* | *300.36* | *427.78* | *< 0.0001* | |
| ***X2^2*** | *78.77* | *1* | *78.77* | *112.19* | *< 0.0001* | |
| ***X3^2*** | *295.73* | *1* | *295.73* | *421.18* | *< 0.0001* | |
| **Residual** | 7.02 | 10 | 0.70 | | | |
| ***Lack of Fit*** | *5.17* | *5* | *1.03* | *2.80* | *0.1416* | *not significant* |
| ***Pure Error*** | *1.85* | *5* | *0.37* | | | |
| **Cor Total** | 966.12 | 19 | | | | |

| | | | |
|---|---|---|---|
| **Std. Dev.** | **0.84** | **R-Squared** | **0.9927** |
| **Mean** | 87.78 | Adj R-Squared | 0.9862 |
| **C.V. %** | 0.95 | Pred R-Squared | 0.9519 |
| **PRESS** | 46.47 | Adeq Precision | 36.646 |

The Model F-value of 151.77 implied the model was significant. There was only a 0.01% chance that an F-value this large could occur due to noise. Values of "Prob > F" less than 0.0500 indicate model terms are significant. In this case X2, X3, X1.X2, X1.X3, X2.X3, X1^2, X2^2, X3^2 were significant model terms. Values greater than 0.1000 indicate the model terms are not significant. Although X1 was not significant, it cannot be dropped because it was part of model hierarchy.

The "Lack of Fit F-value" of 2.80 implies there was a 14.16% chance that a "Lack of Fit F-value" this large could occur due to noise. P-value for lack-of-fit was > 0.05, hence it was insignificant which implies that there was no evidence that the model did not fit.

The "Pred R-Squared" of 0.9519 was in reasonable agreement with the "Adj R-Squared" of 0.9962; i.e. the difference was less than 0.2. "Adeq Precision" measures the signal to noise ratio. A ratio greater than 4 is desirable. The ratio of 36.646 indicated an adequate signal. This model can be used to predict Yield as a function of variables X1, X2, and X3.

Table 4.7 gives the values of coefficients for the model.

**Table 4.7: Coefficients for the full quadratic model (WB)**

| | **Coefficient** | | **Standard** | **95% CI** | **95% CI** |
|---|---|---|---|---|---|
| **Factor** | **Estimate** | **df** | **Error** | **Low** | **High** |
| **Intercept** | 95.59 | 1 | 0.34 | 94.83 | 96.35 |
| **X1- NaOH** | -0.26 | 1 | 0.23 | -0.76 | 0.25 |
| **X2- Temp** | 3.11 | 1 | 0.23 | 2.61 | 3.62 |
| **X3- Meth:oil** | -2.63 | 1 | 0.23 | -3.13 | -2.12 |
| **X1.X2** | 0.98 | 1 | 0.30 | 0.32 | 1.64 |
| **X1.X3** | 1.92 | 1 | 0.30 | 1.26 | 2.58 |
| **X2.X3** | 3.85 | 1 | 0.30 | 3.19 | 4.51 |
| **X1^2** | -4.57 | 1 | 0.22 | -5.06 | -4.07 |
| **X2^2** | -2.34 | 1 | 0.22 | -2.83 | -1.85 |
| **X3^2** | -4.53 | 1 | 0.22 | -5.02 | -4.04 |

Since all the terms were significant, no further reductions were needed. Hence the model was: Yield, $Y = 95.59 - 0.26\ X1 + 3.11\ X2 - 2.63\ X3 + 0.98\ X1.X2 + 1.92\ X1.X3 + 3.85\ X2.X3 - 4.57\ X1^2 - 2.34\ X2^2 - 4.53\ X3^2$ …4.3

Predicted FAME yields obtained from Eqn 4.3 is given in Table 4.4. Eqn 4.3 can be used for response surface plots.

#### 4.3.1.3.3 Response Surface and Contour Plots

Fig 4.10 gives a plot for Yield as a function of Temperature and Catalyst composition. The optima lies close to a temperature of 70$^{o}$C (343K) and a catalyst concentration of 1.5 mass%. Fig 4.11 gives a plot for Yield as a function of Methanol to oil mole ratio and Catalyst composition. The optima lies close to a mole ratio of 7 and a catalyst concentration of 1.5 mass%. Fig 4.12 is a plot for Yield as a function of temperature and mole ratio. It indicates that a maxima corresponds to a temperature of 70$^{o}$C (343K), and a mole ratio of 7. The observations made in the RSM plots therefore confirm that the experimental values were in good agreement with the predicted values.

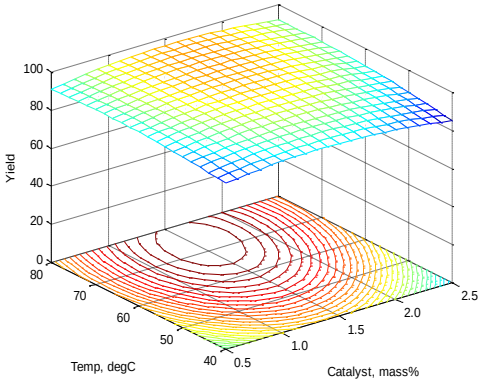


**Figure 4.10: RSM plot: Effect of Catalyst conc. and Temperature on Yield (WB)**

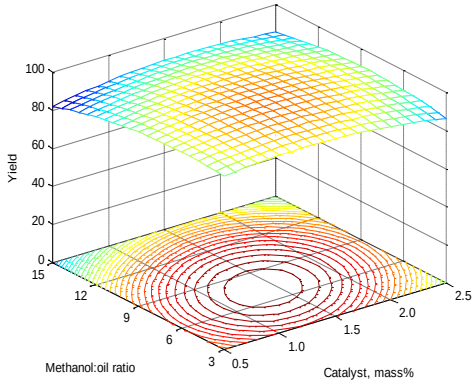


**Figure 4.11: RSM plot: Effect of Catalyst conc. and Methanol:oil ratio on Yield (WB)**

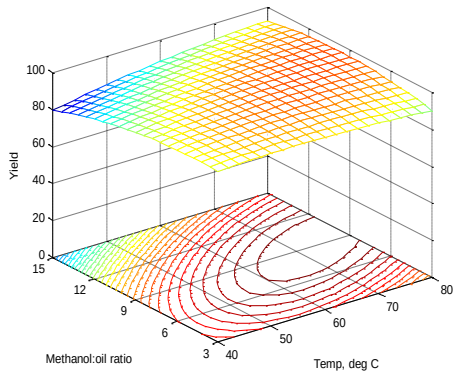


**Figure 4.12: RSM plot: Effect of Methanol:oil ratio and Temp on Yield (WB)**

### 4.3.2 Studies with Microwave Irradiation

This section deals with transesterification of Croton *megalocarpus* oil using homogeneous NaOH catalyst with microwave irradiation.

#### 4.3.2.1 Effect of operation variables on FAME yield

Operating variables studied were (i) Methanol to triglyceride molar ratio, (ii) Catalyst concentration, (iii) Reaction time, (iv) Reaction temperature, and (v) Microwave Power. Stirring was through an electromagnetic stirrer operating at full speed. Mixing was very vigorous and mass transfer resistance was ruled out. Twenty five ml of oil was used in each run with exception of kinetic studies where 50 ml of oil was used. Effect of reaction temperature is reported under Section 4.3.2.2 (Reaction Kinetics).

##### 4.3.2.1.1 Effect of methanol: triglyceride molar ratio on FAME yield

Methanol to oil molar ratio was varied as 6:1, 9:1, 12:1, 15:1. Batch consisted of 25 ml of Croton *megalocarpus* oil (FFA = 1.7), NaOH catalyst 1% by mass of oil. Microwave power was at full, and reaction time was 1 min. Fig 4.13 gives the FAME yield as a function of Methanol: oil ratio.

As mentioned in Sec 4.3.1.1.1, an excess of methanol is used in transesterification to drive the reaction in forward direction. Yield was 90.5% at the ratio of 6:1. Yield increased to 96.5% when the methanol was increased to 9:1 molar ratio. At higher methanol to oil ratios of 12:1 and 15:1, yield did not increase any further, instead a slight drop was observed. Yield for 15:1 ratio was found to be 91.1%. Reasons for a decrease in yield at higher methanol concentration are: excess methanol mixing with glycerol leading to poor

separation, glycerol forming an emulsion with FAME in presence of excess methanol leading to poor separation, and finally large methanol reducing the effective concentration of the catalyst in the reaction mixture. Literature references are given in Section 4.3.1.1.1.

#### 4.3.2.1.2 Effect of catalyst concentration on FAME yield

Transesterification of Croton *megalocarpus* oil was carried out with varying NaOH concentrations. Batch consisted of 25 ml of Croton *megalocarpus* oil (FFA = 1.7), methanol to oil ratio of 6:1, microwave power- full, reaction time- 1 min. NaOH concentrations were 0.5, 1.0, 1.5, 2.0 mass% of oil. NaOH was mixed with methanol before being added to the oil. Fig 4.14 gives the FAME yield as a function of NaOH concentration.

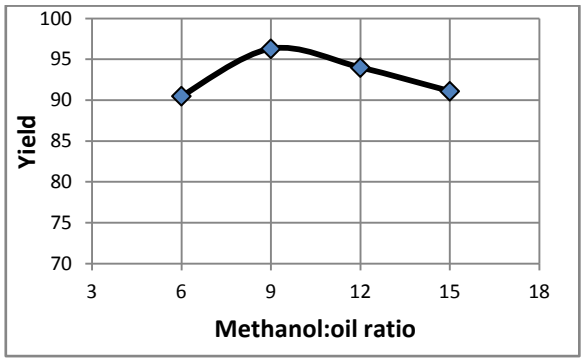


**Figure 4.13: FAME yield as a function of Methanol: oil ratio (MW)**

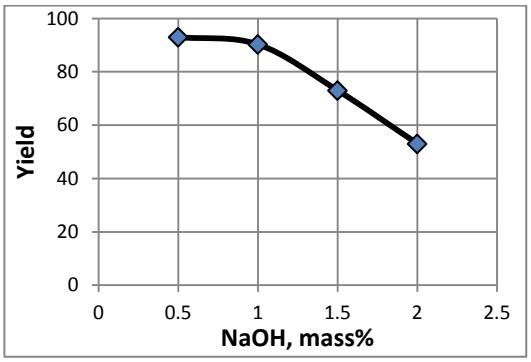


**Figure 4.14: FAME yield as a function of NaOH concentration (MW)**

Highest yield of 93% was obtained when catalyst concentration was 0.5 mass%. As the catalyst concentration was increased to 1.0, 1.5, 2.0% the yield dropped to 90.3, 73, 53% respectively. At catalyst concentrations of 1.5 and 2%, the product FAME consisted of soap which needed several washings. Excess sodium hydroxide reacts with oil to form soap, which lowers the yield of FAME. No significant soap was noticed at 1 mass% NaOH concentration.

#### 4.3.2.1.3 Effect of reaction time on FAME yield

Batch consisted of 25 ml of Croton *megalocarpus* oil (FFA = 1.7), methanol to oil ratio of 6:1, 1 mass% NaOH and full microwave power. Reaction times were 30, 45, 60, 90, 120, 180s. The Variation of FAME yield with reaction time is given in Fig 4.15.

FAME yield increased as the reaction time was increased from 30s to 45s. However, the yield soon stabilized and attained a constant value ranging from 90 – 92%. Between reaction times of 45s and 60s, the increase in yield was only 2%, from 90% to 92% of FAME; which dropped to 91% at a time of 120s, and to 90.5% at a time of 180s. This goes to show that the reaction attained a steady state at times above 45s, and the yield became constant.

#### 4.3.2.1.4 Effect of microwave power

Microwave reactor had built in power settings of 20, 40, 60, 80, 100%. Reactions were carried out at these power settings at methanol to oil ratio of 6:1, 1 mass% of NaOH, and a time of 60s. Fig 4.16 gives the effect of microwave power on FAME yield. As anticipated, yield increased with the rise of power since microwave power is directly related to microwave irradiation. The increase was steep when power was increased from 20% to 40%, and to 60%. After a power level of 60% the rise in yield was gradual. The increase in FAME yield from 60 to 100% of power was only 5%, from 85 to 93% of FAME.

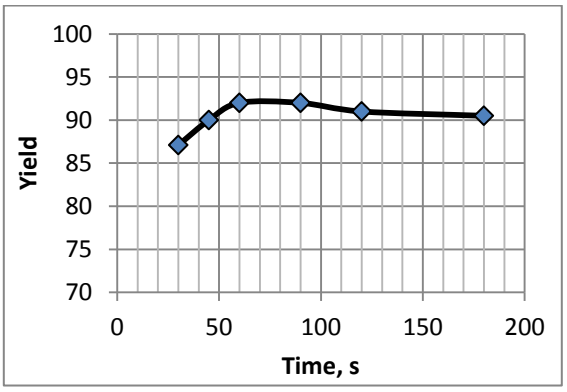


**Figure 4.15: Effect of reaction time on Yield (MW)**

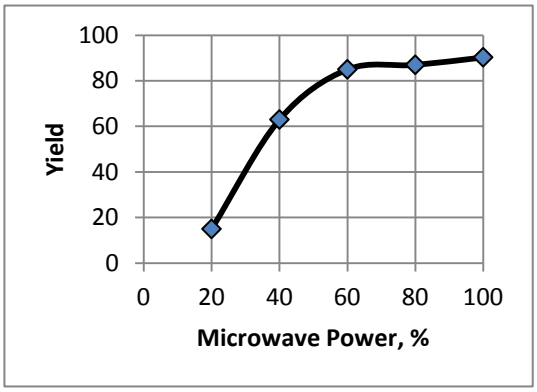


**Figure 4.16: Effect of microwave power on yield**

#### 4.3.2.2 Reaction Kinetics

In the study of reaction kinetics the parameters were, methanol to oil ratio - 6:1, NaOH concentration -1 mass%. Reactions were carried out at temperatures of 50, 60 and 70$^{o}$C (323, 333, 343K). Samples were drawn at 30, 45, 60 and 90s.

#### 4.3.2.2.1 Effect of Time on FAME yield

Fig 4.17 is a plot of FAME yield vs. reaction time at varying reaction temperatures. For reaction temperature of 50°C (323K), reaction rate was considerably slow in the early period of 60s; thereafter it rose steeply between 60 to 90s to give a yield of 75% at the end. Yield vs. time curves for 60 and 70°C (333 and 343K) were fairly close, and followed the same pattern. Final yield at 60 and 70°C (333 and 343K) were 90 and 94.5% respectively.

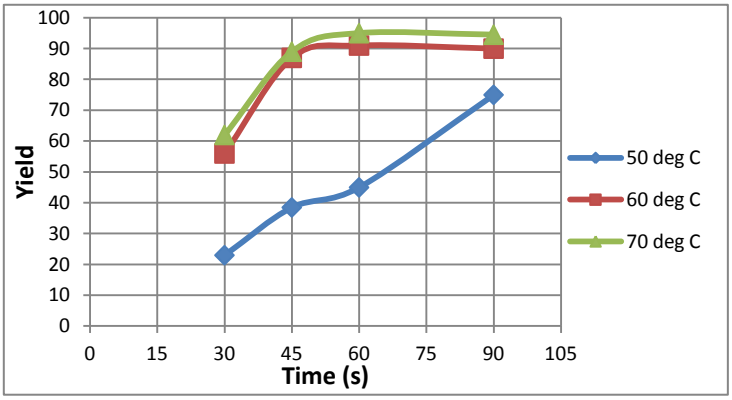


**Figure 4.17: Variation of Yield with time at various temperatures (MW)**

#### 4.3.2.2.2 Order of reaction

Eqn 2.29 (Chapter 2) gives the overall reaction rate in terms of rate of disappearance of triglyceride as: $-r_A = -\frac{d[A]}{dt} = k\,[A]^m\,[B]^n$. Kinetic data for Fig 4.17 were used to find the best fit into integrated form of Eqn 2.29. Integrated form of rate equation for reaction order varying from 'zero' to 'three' are given in Eqns. 2.34- 2.43. Highest correlation coefficient ($R^2$) was identified as outlined in Section 4.3.1.2.2, which corresponded to the most likely rate equation. Table 4.8 gives the coefficients of correlation for all reaction orders, Cases 1 to 10, at the three temperatures.

**Table 4.8: Coefficients of correlation, $R^2$, for various reaction orders (MW)**

| | **0th Order** | **1st Order** | | **2nd Order** | | | **3rd Order** | | | |
|---|---|---|---|---|---|---|---|---|---|---|
| **Temp °C** | Case 1 | Case 2 (m=1, n=0) | Case 3 (m=0, n=1) | Case 4 (m=1, n=1) | Case 5 (m=2, n=0) | Case 6 (m=0, n=2) | Case 7 (m=2, n=1) | Case 8 (m=1, n=2) | Case 9 (m=3, n=0) | Case 10 (m=0, n=3) |
| **50** | **.9922** | .8663 | .9826 | .9097 | .5281 | .9639 | .4439 | .7425 | .1347 | .9354 |
| **60** | .7603 | **.8060** | .7733 | .8012 | .7739 | .7840 | .7184 | .7943 | .5950 | .7920 |
| **70** | .7618 | **.8533** | .7803 | .8483 | .6973 | .7969 | .6736 | .8412 | .4220 | .8109 |

Highest correlation coefficients have been bolded in Table 4.8. Kinetic data at 50$^{o}$C (323K) suggested a zero order reaction, and kinetic data at 60 and 70$^{o}$C (333 and 343K) suggested a first order reaction. Zero order option has been ruled out as it neither has any theoretical justification, nor any literature support ( Section 2.5.2). Overall reaction order, defined as rate of disappearance of triglyceride, was therefore a first order. It was first order with respect to triglyceride and zero order with respect to methanol (m = 1, n = 0). Some of the published literature supporting a first order reaction for NaOH catalyst are from Jain and Sharma (2010) for *Jatropha curcas* oil, and Jain *et al*. (2011) for waste cooking oil.

#### 4.3.2.2.3 Rate constant and Activation energy

Integrated form of the first order rate equation identified in previous section is given by Eqn 2.35:$\ln\left(\frac{1}{1-x_A}\right) = k\,t$ . Hence a plot of $\ln\left(\frac{1}{1-x_A}\right)$ vs. time *t* should be a straight line, and reaction rate constant *k* given by the slope. Fig 4.18 gives such a plot for temperature of 70$^{o}$C (343K) ($R^2$ = 0.8533).

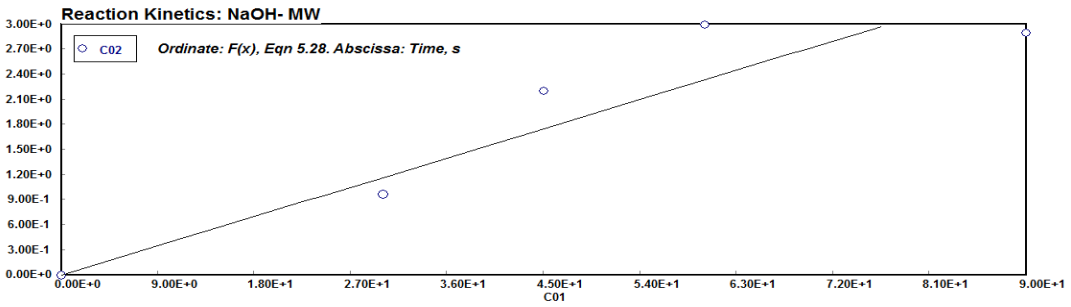


**Figure 4.18: : Plot of kinetic equation 5.28 (MW)** (Ordinate: $\mathbf{ln\left(\frac{1}{1-x_A}\right)}$ , abscissa: *t* )

Correlation constants for Eqn 2.35 for temperatures 40, 50 and 60$^{o}$C (313, 323, 333K). were used to estimate reaction constant *k* as given in Table 4.9.

**Table 4.9: Reaction constant k (MW)**

| Temp $^{o}$C | T (K) | Const =1/ k | k (per s) | k (per min) |
|---|---|---|---|---|
| **50** | 323.15 | 73.67 | 0.013574 | 8.14E-01 |
| **60** | 333.15 | 29.376 | 0.034041 | 2.04E+00 |
| **70** | 343.15 | 24.537 | 0.040755 | 2.45E+00 |

Activation energy (*E*) was obtained from the slope of the plot of ln*k* vs. 1/T (Arrhenius plot, Section 2.5.4.1). Fig 4.19 gives the plot.

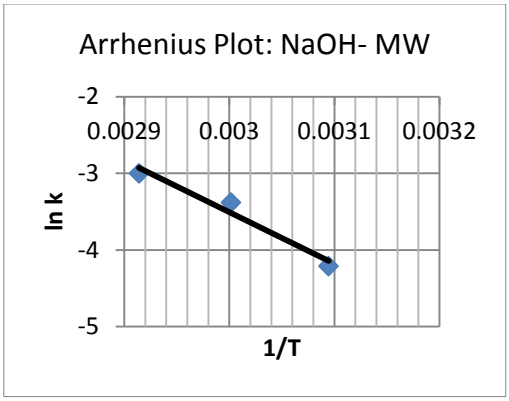


**Figure 4.19: Arrhenius plot for NaOH catalyst (MW)**

The plot has a slope of 6134.8 ($R^2$ = 0.8804) which gave the activation energy, $E$ as 51.0 kJ/mole, and the intercept gave pre-exponential factor, $A$ = 2.68x$10^6$.

#### 4.3.2.3 Optimization studies

As mentioned in Section 4.3.1.3, optimization involves identifying the experimental parameters for maximum yield. A statistical experimental design was used to fit experimental data into a correlation. The correlation can be used to predict the yield for a given set of experimental variables, and to plot response surface and contour plots.

##### 4.3.2.3.1 Experimental Design

Transesterification was carried out at full microwave power, and the reaction variables were: catalyst concentration (mass%), reaction time (s), and methanol to oil molar ratio. A five-level, three-factor Central Composite Design (CCD) was used to optimize these 3 independent variables to achieve maximum FAME yield. Table 4.10 gives the independent variables and levels used for experimental design. RSM was used to further investigate the influence of these 3 independent variables on FAME yield.

**Table 4.10: Independent variables and levels for CCD (MW)**

| Independent variables | Codes | Variable levels | | | | |
|---|---|---|---|---|---|---|
| | | -α= -1.682 | -1 | 0 | 1 | +α= 1.682 |
| **Catalyst amount (%)** | X1 | 0.16 | 0.5 | 1 | 1.5 | 1.84 |
| **Time (s)** | X2 | 10 | 30 | 60 | 90 | 110 |
| **Methanol:oil ratio** | X3 | 4 | 6 | 9 | 12 | 14 |

A total of 20 experiments, including 6 replications at the centre point, were conducted. Replicates at the centre point give pure error.

#### 4.3.2.3.2 Experimental results and data analysis

Table 4.11 gives the details of a set of 20 experiments in terms of actual and coded levels as per CCD, and experimental and predicted FAME yields.

**Table 4.11: CCD matrix with experimental FAME yield (MW)**

| Run | Level of variables [actual(coded)] | | | Experimental Yield | Quadratic Model (Eqn 6.4) |
|---|---|---|---|---|---|
| | Catalyst,% | Time (s) | Methanol :oil | | **Y** |
| | X1 | X2 | X3 | | |
| **1** | 1(0) | 60(0) | 9(0) | 96.3 | 96.1 |
| **2** | 1(0) | 10(-1.68) | 9(0) | 74.9 | 75.4 |
| **3** | 0.5(-1) | 90(1) | 12(1) | 73.5 | 72.7 |
| **4** | 1(0) | 60(0) | 14(1.68) | 75.1 | 75.3 |
| **5** | 1.84(1.68) | 60(0) | 9(0) | 67.1 | 67.2 |
| **6** | 1(0) | 60(0) | 4(-1.68) | 69.8 | 69.7 |
| **7** | 0.5(-1) | 30(-1) | 6(-1) | 63.5 | 62.5 |
| **8** | 1(0) | 60(0) | 9(0) | 95.5 | 96.1 |
| **9** | 1.5(1) | 90(1) | 12(1) | 83.7 | 84.6 |
| **10** | 1.5(1) | 90(1) | 6(-1) | 65.0 | 64.3 |
| **11** | 1(0) | 60(0) | 9(0) | 95.8 | 96.1 |
| **12** | 1.5(1) | 30(-1) | 6(-1) | 68.0 | 68.7 |
| **13** | 0.16(-1.68) | 60(0) | 9(0) | 51.9 | 51.9 |
| **14** | 1(0) | 60(0) | 9(0) | 95.9 | 96.1 |
| **15** | 1.5(1) | 30(-1) | 12(1) | 83.1 | 82.0 |
| **16** | 1(0) | 60(0) | 9(0) | 97.0 | 96.1 |
| **17** | 0.5(-1) | 30(-1) | 12(1) | 48.3 | 48.9 |
| **18** | 1(0) | 110(1.68) | 9(0) | 92.0 | 91.7 |
| **19** | 1(0) | 60(0) | 9(0) | 96.3 | 96.1 |
| **20** | 0.5(-1) | 90(1) | 6(-1) | 78.3 | 79.3 |

Data in Table 4.11 were tested for fit for a linear, two-factor interaction (2FI), quadratic and cubic polynomials. Table 4.12 gives the result.

**Table 4.12: Summary for model fit- Sequential model sum of squares (MW)**

| Source | Sequential p-value | Lack of Fit p-value | Adjusted R-Squared | Predicted R-Squared | |
|---|---|---|---|---|---|
| **Linear** | 0.4706 | < 0.0001 | -0.0188 | -0.2796 | |
| **2FI** | 0.5071 | < 0.0001 | -0.0549 | -0.7445 | |
| **Quadratic** | < 0.0001 | 0.0602 | 0.9968 | 0.9869 | Suggested |
| **Cubic** | 0.0208 | 0.7875 | 0.9990 | 0.9985 | Aliased |

**Sequential Model Sum of Squares [Type I]**

| Source | Sum of Squares | df | Mean Square | F Value | p-value Prob > F | |
|---|---|---|---|---|---|---|
| **Mean vs Total** | 1.234E+005 | 1 | 1.234E+005 | | | |
| **Linear vs Mean** | 637.91 | 3 | 212.64 | 0.88 | 0.4706 | |
| **2FI vs Linear** | 611.03 | 3 | 203.68 | 0.82 | 0.5071 | |
| **Quadratic vs 2FI** | 3232.37 | 3 | 1077.46 | 1405.67 | < 0.0001 | Suggested |
| **Cubic vs Quadratic** | 6.27 | 4 | 1.57 | 6.74 | 0.0208 | Aliased |
| **Residual** | 1.40 | 6 | 0.23 | | | |
| **Total** | 1.279E+005 | 20 | 6395.34 | | | . |

Looking at $R^2$ values, Cubic model has the highest value but it is aliased, so should not be selected. Next highest $R^2$ was for a Quadratic model ( $R^2$ = 0.9985), which was the suggested model. Criterion of p-value, Prob > F was less than 0.0500, indicating that the Quadratic model terms were significant. Quadratic was the highest order polynomial where the model terms were significant and the model was not aliased. Table 4.13 is the ANOVA for a Response Surface Quadratic Model.

**Table 4.13: ANOVA for Response Surface Quadratic model (MW)**

**Analysis of variance table [Partial sum of squares - Type III]**

| Source | Sum of Squares | df | Mean Square | F Value | p-value Prob > F | |
|---|---|---|---|---|---|---|
| **Model** | 4481.30 | 9 | 497.92 | 649.60 | < 0.0001 | significant |
| ***X1-NaOH*** | *279.32* | *1* | *279.32* | *364.41* | *< 0.0001* | |
| ***X2-Time*** | *320.80* | *1* | *320.80* | *418.53* | *< 0.0001* | |
| ***X3-Meth:oil*** | *37.78* | *1* | *37.78* | *49.28* | *< 0.0001* | |
| ***X1.X2*** | *224.72* | *1* | *224.72* | *293.17* | *< 0.0001* | |
| ***X1.X3*** | *361.81* | *1* | *361.81* | *472.02* | *< 0.0001* | |
| ***X2.X3*** | *24.50* | *1* | *24.50* | *31.96* | *0.0002* | |
| ***X1^2*** | *2410.93* | *1* | *2410.93* | *3145.34* | *< 0.0001* | |
| ***X2^2*** | *285.25* | *1* | *285.25* | *372.14* | *< 0.0001* | |
| ***X3^2*** | *1006.17* | *1* | *1006.17* | *1312.67* | *< 0.0001* | |
| **Residual** | 7.67 | 10 | 0.77 | | | |
| ***Lack of Fit*** | *6.29* | *5* | *1.26* | *4.58* | *0.0602* | *not significant* |
| ***Pure Error*** | *1.37* | *5* | *0.27* | | | |
| **Cor Total** | 4488.97 | 19 | | | | |

The Model F-value of 649.60 implied the model was significant. There was only a 0.01% chance that an F-value this large could occur due to noise. Values of "Prob > F" less than 0.0500 indicated model terms were significant. In this case X1, X2, X3, X1.X2, X1.X3, X2.X3, X1^2, X2^2, X3^2 were significant model terms. The "Lack of Fit F-value" of 4.58 implied there was a 6.02% chance that a "Lack of Fit F- value" this large could occur due to noise. The p-value for lack-of-fit was greater than 0.05, hence it was not significant. Table 4.14 gives the $R^2$ values for the Quadratic model.

**Table 4.14: $R^2$ Values (MW)**

| | | | |
|---|---|---|---|
| Std. Dev. | 0.88 | R-Squared | 0.9983 |
| Mean | 78.55 | Adj R-Squared | 0.9968 |
| C.V. % | 1.11 | Pred R-Squared | 0.9869 |
| PRESS | 58.86 | Adeq Precision | 76.275 |

The "Pred R-Squared" of 0.9869 was in reasonable agreement with the "Adj R-Squared" of 0.9968; i.e. the difference was less than 0.2. "Adeq Precision" measures the signal to noise ratio. A ratio greater than 4 is desirable. In this case, the ratio of 76.275 indicated an adequate signal. The full Quadratic model (Eqn 4.2) can therefore be used for design purposes, to predict the yield as a function of selected operation variables. Table 4.15 gives the terms for the quadratic model.

**Table 4.15: Coefficients for the Quadratic Model (MW)**

| | Coefficient | | Standard | 95% CI | 95% CI | |
|---|---|---|---|---|---|---|
| **Factor** | **Estimate** | **df** | **Error** | **Low** | **High** | **VIF** |
| **Intercept** | 96.13 | 1 | 0.36 | 95.34 | 96.93 | |
| **X1-NaOH** | 4.52 | 1 | 0.24 | 3.99 | 5.05 | 1.0 |
| **X2-Time** | 4.85 | 1 | 0.24 | 4.32 | 5.37 | 1.0 |
| **X3-Meth:oil** | 1.66 | 1 | 0.24 | 1.14 | 2.19 | 1.0 |
| **X1.X2** | -5.30 | 1 | 0.31 | -5.99 | -4.61 | 1.0 |
| **X1.X3** | 6.73 | 1 | 0.31 | 6.04 | 7.41 | 1.0 |
| **X2.X3** | 1.75 | 1 | 0.31 | 1.06 | 2.44 | 1.0 |
| **X1^2** | -12.93 | 1 | 0.23 | -13.45 | -12.42 | 1.0 |
| **X2^2** | -4.45 | 1 | 0.23 | -4.96 | -3.94 | 1.0 |
| **X3^2** | -8.36 | 1 | 0.23 | -8.87 | -7.84 | 1.0 |

Since all the terms were significant, no reductions were needed. The model was:

$$\text{Yield, } Y = 96.13 + 4.52\,X1 + 4.85\,X2 + 1.66\,X3 - 5.30\,X1.X2 + 6.73\,X1.X3 + 1.75\,X2.X3 - 12.92\,X1^2 - 4.45\,X2^2 - 8.36\,X3^2 \quad \ldots 4.4$$

Table 4.11 gives the predicted FAME yields based on Eqn 4.4. Eqn 4.4 can be used for response surface plots.

#### 4.3.2.3.3 Response Surface and Contour Plots

Fig 4.20, 4.21, 4.22 give the RSM Surface and contour plots. Fig 4.20 gives response surface and contour plot for FAME yield (Y) as a function of Catalyst concentration (X1) and Reaction time (X2). It shows that the maximum yield corresponded to a catalyst concentration of about 1%, and a time of about 50s. These values were close to experimentally observed values. Fig 4.21 gives a response surface and contour plot for FAME yield (Y) as a function of Catalyst concentration (X1) and Methanol to oil ratio (X3). Optima was at a catalyst concentration of 1-1.25%, and a methanol: oil ratio slightly above 9:1. This was in agreement with experimental observations.

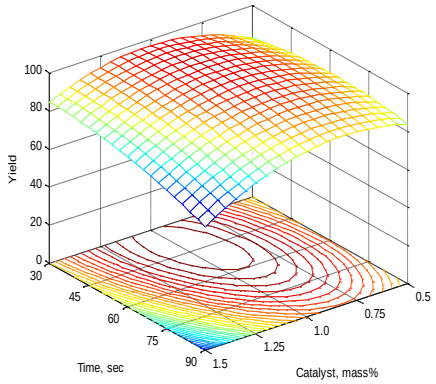


**Figure 4.20: RSM plot- Effect of Catalyst conc. and Time on Yield (MW)**

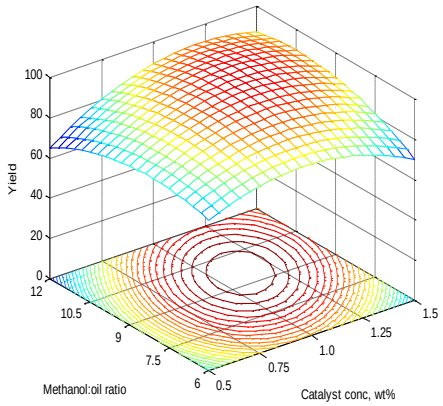


**Figure 4.21: RSM plot- Effect of Catalyst conc. and Methanol:oil ratio on Yield (MW)**

Fig 4.22 is a response surface and contour plot for FAME yield (Y) as a function of Reaction time (X2) and Methanol to oil ratio (X3). A methanol:oil ratio of 9:1, and a time of 45s corresponded to the maximum yield. These values were in agreement with the experimental observations.

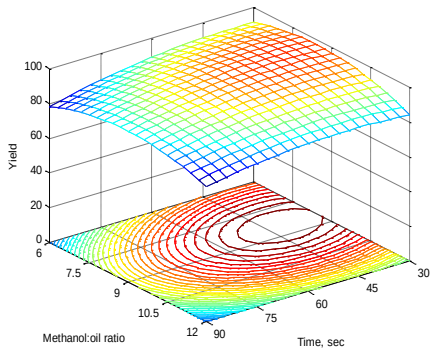


**Figure 4.22: RSM plot- Effect of Time and Methanol:oil ratio on Yield (MW)**

## 4.4 Summary

Transesterification of Croton *megalocarpus* was studied using homogenous NaOH catalyst under conventional water bath and microwave irradiation. When water bath was used, best results corresponded to a methanol to oil ratio of 6:1, catalyst concentration of 1mass%, a reaction temperature of 60-70$^{o}$C (333- 343K), and a reaction time of 1 h. Reaction was found to be of 2nd order with respect to triglyceride and zero order with respect to methanol. Reaction rate constant and activation energy were obtained. CCD was used to correlate FAME yield as function of reaction variables in a second order quadratic equation. RSM plots identified reaction variables for optimal yield.

When microwave irradiation was used, highest yield was obtained at 9:1 methanol to oil ratio, 0.5% NaOH catalyst, and reaction time of 1 min. Microwave power below 60% was inefficient in providing the necessary heating. Reaction order for the case of microwave irradiation was 1$^{st}$ order with respect to triglyceride and zero order with respect to methanol. Reaction rate constant and activation energy were obtained. CCD was used to correlate FAME yield as a function of reaction variables in a second order quadratic equation. RSM plots gave regions of highest yield for microwave irradiation.

# 5 HETEROGENEOUS ALKALINE EARTH OXIDE CATALYSIS IN THE TRANSESTERIFICATION OF *CROTON MEGALOCARPUS* OIL

## 5.1 Introduction

Elements Barium, Strontium, Calcium, Magnesium and Berillium are in Group 2A (alkaline earth metals) of the Periodic table. All members of this group are very reactive and are thus never found in the free state in nature. Transesterification of croton *megalocarpus* was carried out using heterogeneous oxides as a catalyst using both conventional heating and microwave irradiation. Effect of operating variables on the FAME yield, conditions for maximum yield and reaction kinetics were studied.

## 5.2 Materials and Methods

### 5.2.1 Materials

Analytical grade BaO (97%), SrO (99.9%), Nano CaO (98%), CaO (96%), Nano MgO (99.8%), MgO (99%), and BeO (99.98%) were obtained from Sigma Aldrich. CaO RO was synthesized in the lab. BaO and SrO were used as such while other samples were calcined at 700$^{o}$C (973K) for 3h before use. Other materials were as mentioned in Section 4.2.1.(Chapter 4).

### 5.2.2 Experimental setup

Experimental setup for conventional and microwave irradiation has already been described under Section 4.2.2.1 and 4.2.2.2 of Chapter 4. Criterion for a perfect mixing in a batch slurry reactor, in terms of minimum mixing speed, is given by Eqn 2.12 (Dossin *et al*., 2006a):

$$N_I > \left(12\frac{g}{d_I}\right)^{0.5} \left(\frac{\rho_{p,wet}-\rho_L}{\rho_L}\right)^{0.5} \left(\frac{d_p}{d_I}\right)^{0.165} \epsilon_s^{0.25} \qquad ...2.12$$

Where, $N_I$ = impeller speed ($s^{-1}$), $d_I$ = impeller diameter (m), g = acceleration of gravity ($m^2s^{-1}$) = 9.81, $\rho_{p,wet}$ = density of catalyst filled with liquid (kg $m^{-3}$), $\rho_L$ = density of liquid (kg $m^{-3}$), $d_p$ = particle diameter (m), $\varepsilon_s$ = catalyst fraction in slurry.

For BaO, $d_p \approx 3$ μm (Fig 3.21, Chapter 3), $\rho_{p,wet}$ = 5720 kg $m^{-3}$ ( taken as solid density since porosity is very small). For stirrer impeller, $d_I$ = 0.03m. For oil, $\rho_L$ = 930 kg $m^{-3}$. Assuming a 1% catalyst and 9:1 methanol:oil ratio, $\varepsilon_s$ = 0.0077. Substituting the data in

Eqn 2.12, minimum speed for perfect mixing was 9.22 $s^{-1}$, or 553 rpm. For SrO, particle size was estimated from BET surface area data assuming the particle to be non-porous and spherical. The assumption of non porous particle was justified due to its very low porosity ( $\varepsilon = 0.04$). BET surface area is related to particle diameter, D by Eqn 5.1 (Rouquerol *et al*., 1999):

$$SSA\ (BET) = \frac{6}{\rho_p\, d_p} \qquad ...5.1$$

Where SSA(BET) is BET specific surface area ($m^2\ kg^{-1}$), $\rho_p$ is particle density ($kg\ m^{-3}$), and $d_p$ = particle diameter (m). For SrO, SSA(BET) = 1361 $m^2\ kg^{-1}$ (Table 3.13, Chapter 3), $\rho_p$ = 4700 kg $m^{-3}$ (Sigma Aldrich property data), giving particle diameter $d_p$ = 0.94 μm. For Eqn 2.12, $\rho_{p,wet}$ = 4700 kg $m^{-3}$ ( taken as solid density since porosity was very small). Assuming a 1% catalyst and 9:1 methanol:oil ratio, $\varepsilon_s$ = 0.0077, substituting the data in equation 2.12, minimum speed for perfect mixing was 6.75 $s^{-1}$, or 405 rpm. Calculations for a 1% CaO and 9:1 methanol to oil feed, $d_p$ = 1μm = $1x10^{-6}$ m, $\rho_{p,wet}$ = 3400 kg $m^{-3}$, $\varepsilon_s$ = 0.0077, gave minimum speed as $N_I$ > 331 rpm. Similar calculation at 2% CaO gave, $N_I$ > 394 rpm. Minimum speed requirement of Nano CaO would be even lower due to smaller particle size. Calculations for a 1% MgO and 9:1 methanol to oil feed, $\rho_L$ = 930 kg $m^{-3}$, $d_p$ = 1.1 μm = $1.1x10^{-6}$ m, $\rho_{p,wet}$ = 3750 kg $m^{-3}$, $\varepsilon_s$ = 0.0077 ; gave minimum speed as $N_I$ > 358 rpm. Similar calculation at 2% MgO gave, $N_I$ > 426 rpm. Minimum stirring speed would be even lower for Nano MgO. For BeO particle size was estimated from BET surface area data, assuming the particle to be non-porous and spherical. For BeO, SSA(BET) = 92,330 $m^2\ kg^{-1}$ (Table 3.13, Chapter 3), $\rho_p$ = 3010 kg $m^{-3}$ (Sigma Aldrich data), giving particle diameter $d_p$ = 0.21 μm, $\rho_{p,wet}$ = 3010 kg $m^{-3}$. Assuming a 1% catalyst and 9:1 methanol:oil ratio, $\varepsilon_s$ = 0.0077, minimum speed for perfect mixing was 5.25 $s^{-1}$, or 315 rpm. The stirrer was operated at 800 rpm which ensured perfect mixing and ruled out mass transfer resistances for all catalyst samples.

### 5.2.3 Experimental Procedure

#### 5.2.3.1 Conventional Heating

Figure 4.1a and 4.1b (Chapter 4) show the experimental setup. Weighed amount of *croton megalocarpus* oil was added to the reactor and heated in the water bath to the reaction

temperature. Weighed amount of oxide catalyst and measured volume of methanol were heated separately in a round bottom flask in a water bath at desired temperature, under reflux and mechanical stirring, for 1 hour. This was to activate the catalyst through complete mixing with methanol. Oxide reacts with methanol to form methoxide, which catalyzes the reaction. The catalyst and methanol mixture was then added to the oil. The mechanical stirrer was immediately started, and the reaction timed at this point. At the end of the desired reaction time, the round bottom flask was immersed in ice bath to quench the reaction. The contents were then centrifuged for thirty minutes to separate the FAME, methanol and solid catalyst fraction. Clear FAME collected at the top over glycerol and unreacted methanol which formed the bottom aqueous fraction. Spent catalyst settled at the bottom of centrifuge tube. FAME was decanted from the centrifuge tube and heated at $90^{o}$C (363K) in an oven, for 1 h, to drive off dissolved methanol. The dried FAME sample was kept in a deep freezer pending analysis by GC. For kinetic studies, samples were removed using a hypodermic syringe periodically and treated as above.

In the study of **effect of operating variables**, variables studied were (i) Methanol to triglyceride molar ratio, (ii) Catalyst concentration, and (iii) Reaction temperature. **Effect of reaction time** on FAME yield was studied under reaction kinetics. Stirring speed was kept constant at 800 rpm.

**Effect of catalyst concentration** on FAME yield was studied using catalyst concentrations of 0.5, 1, 1.5, 2, 3 mass% based on oil mass. Batch consisted of 30 ml of Croton *megalocarpus* oil (FFA = 1.7), methanol to oil ratio of 9:1, reaction temperature $70^{o}$C (343K), reaction time 2 h.

In the study of **effect of methanol to oil molar ratio**, the ratio was varied as 6:1, 9:1, 12:1, 15:1. Batch consisted of 30 ml of Croton *megalocarpus* oil (FFA = 1.7), catalyst 1% by mass of oil. Reaction temperature was $70^{o}$C (343K), and reaction time 2 h.

In the study of **effect of reaction temperature**, mass transfer resistances were eliminated by using high stirring speed, leaving surface reaction as being a rate controlling step. Reaction temperature was increased in the range of 40 – $70^{o}$C (313 – 343 K). Reaction at a higher temperature of $80^{o}$C (353K) resulted in a coagulated mass of oil since the reaction temperature was higher than the normal boiling point of methanol, resulting in methanol being in vapour phase and poor contact with triglyceride. Reactions were carried out at

constant catalyst concentration of 1 mass%, methanol to oil molar ratio of 9:1, and reaction time of 2 h.

In order to **study the reaction kinetics**, transesterification was carried out at constant temperatures of 40, 50, 60, 70$^{o}$C (313, 323, 333, 343 K). Other variables were kept constant at: methanol to oil ratio 9:1, catalyst at 1 mass%, reaction time of 3 h. Each run consisted of 100 ml of oil, and product samples (of 1 ml) were drawn at time intervals of 15, 30, 45, 60, 90, 120, 150, 180 min. Regression analysis was used to identify the reaction order, and the regression coefficients were used to obtain reaction rate constant. Activation energy was estimated by use of Arrhenius equation.

**Reaction order, Activation Energy and Pre-exponentail factor**: Reaction order was obtained by fitting the kinetic data into integrated reaction rate equations. Equations 2.34 – 2.43 (Chapter 2) are the integrated form of rate equations covering overall reaction orders from 'zero' to 'three'. L.H.S. of these equations are functions of conversion or Yield, F($x_A$); and the R.H.S. is a function of reaction time, *t*. These equations are in the form of y = mx (passing through origin). For all the ten cases, y (or F($x_A$)) is correlated with *x* (or time *t*) and the coefficient-of-determination obtained for a linear regression passing through origin. This was done for all the four temperatures. Highest correlation coefficient, $R^2$, at a given temperature indicated the reaction order. Activation energy *E* was obtained from the slope of the plot of ln*k* vs. 1/T (Arrhenius plot, Section 2.5.4.1), and intercept gave Pre-exponentail factor, *A*.

**Optimization studies:** Experiments were designed to study the effect of reaction variables on the yield and thereafter graphically present conditions for a maximum yield through RSM. Experimental data were fitted into an appropriate correlation, which was then plotted in surface and contour plots depicting optimal conditions. A five-level, three-factor Central Composite Design (CCD) (Appendix A) was used to optimize the process variables of reaction temperature, methanol to oil ratio, and catalyst concentration. Reaction time was kept constant at 2h. Table 5.1 gives the independent variables and levels used for experimental design.

**Table 5.1: : Independent variables and their levels in CCD (WB)**

| Independent variables | Codes | Variable levels | | | | |
|---|---|---|---|---|---|---|
| | | -α= -1.682 | -1 | 0 | 1 | +α= 1.682 |
| **CATALYST CONC, %** | X1 | 0.16 | 0.5 | 1 | 1.5 | 1.84 |
| **TEMPERATURE, $^{o}$C** | X2 | 43 | 50 | 60 | 70 | 77 |
| **METH:OIL MOL RATIO** | X3 | 4 | 6 | 9 | 12 | 14 |

A total of 20 experiments, including 6 replications at the centre point, were performed in randomized order. Replicates at the centre point give pure error.

### 5.2.3.2 Microwave Irradiation

Figure 4.2a and 4.2b (Chapter 4) show the experimental setup Procedure was almost similar to the case of conventional heating. Methanol and oxide catalysts were activated through heating in a round bottom flask in a water bath for 1 hour at desired temperature, under reflux and mechanical stirring, prior to being added to the reactor in microwave. Stirring in microwave was vigorous to prevent hot-spots within the reacting media. For studies involving effect of power, power setting of 40, 60, 80, 100% were used. For kinetic studies, constant temperatures were maintained by controlling input voltage through a voltage regulator. This temperature control through manual input voltage control was satisfactory only for a short reaction time. Attempts to maintain a lower temperature by reducing the in-built microwave power setting were not successful as the microwave kept on switching off-and-on at lower power settings, resulting in temperature fluctuations. The microwave was switched off whenever a sample was withdrawn. After an experimental run the oven was allowed to cool to ambient temperature before reuse. The reaction mixture was centrifuged for 30 minutes and clear FAME decanted from top. Bottom layer of centrifuge tube contained the glycerol, methanol with solid catalyst settled at the bottom. FAME was dried for 1 h at 90$^{o}$C (363K) in an oven to remove dissolved methanol. For kinetic studies, samples were periodically removed using a hypodermic syringe and treated as above.

In the study of **effect of operation vatiobles**, variables identified for the study were (i) Methanol to triglyceride molar ratio, (ii) Catalyst concentration, (iii) Reaction time, (iv) Reaction temperature, and (v) Microwave Power. Stirring was through an electromagnetic

stirrer operating at full speed. Mixing was very vigorous and mass transfer resistances were ruled out. Twenty five ml of oil was used in each run with exception of kinetic studies where 50 ml of oil was used.

In the study of **effect of methanol to oil molar ratio** reactions were carried out with 1 mass% of catalyst for 5 min at full microwave power. Methanol to oil ratios were 6:1, 9:1, 12:1, and 15:1. Batch consisted of 25 ml of Croton *megalocarpus* oil (FFA = 1.7).

Effect of **catalyst concentration** was studied by varying catalyst concentration from 0.5 to 3.0 mass% of oil. Methanol to oil molar ratio was 9:1, and reaction time was 5 min at full microwave power.

**Optimization Studies**: As in the case of conventional heating, a five-level, three-factor Central Composite Design (CCD) was used to optimize the process variables of catalyst concentration (Coded X1), reaction time (Coded X2), and methanol to oil ratio (Coded X3). Reactions were conducted at full microwave power. Table 5.2 gives the independent variables and levels used for experimental design.

**Table 5.2: Independent variables and their levels in CCD (MW)**

| Independent variables | Codes | Variable levels | | | | |
|---|---|---|---|---|---|---|
| | | $-\alpha = -1.682$ | -1 | 0 | 1 | $+\alpha = 1.682$ |
| **CATALYST, %** | X1 | 0.16 | 0.5 | 1 | 1.5 | 1.84 |
| **TIME, MIN** | X2 | 0.5 | 1.5 | 3 | 4.5 | 5.5 |
| **METH:OIL MOL RATIO** | X3 | 4 | 6 | 9 | 12 | 14 |

A total of 20 experiments, including 6 replications at the centre point, were performed in randomized order. Replicates at the centre point give pure error.

### 5.2.4 FAME Analysis

FAME was analyzed as per the procedure described in Section 4.2.4 (Chapter 4).

## 5.3 Results and Discussions

This section gives results and discussions for the studies with BaO, SrO, Nano CaO, CaO RO, CaO, Nano MgO, MgO and BeO catalysts, for conventional heating and microwave irradiation.

### 5.3.1 Studies with Conventional Heating- Barium oxide catalyst

This section deals with transesterification reactions carried out with conventional heating employing a water bath as a heat source.

#### 5.3.1.1 Effect of operation variables on FAME yield

##### 5.3.1.1.1 Effect of methanol to triglyceride molar ratio on FAME yield

A FAME yield of 69.2% corresponded to a 6:1 molar ratio. It increased to 82.1% when the ratio was increased to 9:1. The highest yield of 83.0% was obtained for a ratio of 12:1. As the methanol: oil ratio was increased further to 15:1, the yield dropped slightly to 81.5%. Fig 5.1 gives the FAME yield as a function of methanol to oil ratio.

Initially excess of methanol drives the transesterification reaction (Eqn 2.2, Chapter 2) towards left, increasing the yield. But an excess of methanol dilutes the catalyst percentage in the reaction system and unreacted methanol mixes with glycerol bringing about separation problems. Also, in presence of surplus methanol, glycerol forms emulsion with FAME, lowering the yield. Literature for these observations has been sighted in Section 5.3.1.1.1, Chapter 5. Patil *et al*. (2009) have reported a maximum FAME yield of 83% at 9:1 methanol:oil ratio for BaO catalyst for *Camelina sativa* oil, and the yield dropped slightly as the ratio was increased.

##### 5.3.1.1.2 Effect of catalyst concentration on FAME yield

A BaO concentration of 0.5 mass% gave an yield of 72%. Yield increased when concentration was raised to 1 mass%, to 81% of FAME. Further increase in catalyst concentration did not result into any substantive increase in yield. Observed increase in FAME yield was only 1% when catalyst concentration was increased from 1mass% to 2 mass%, and it remained unchanged when the concentration was increased to 3 mass%. Fig 5.2 gives the effect of catalyst concentration on FAME yield. Patil *et al*. (2009) have reported a 83% FAME yield for *Camelina sativa* oil at 3h, $100^{o}$C (373K), 1 mass% BaO catalyst, and 9:1 methanol to oil ratio.

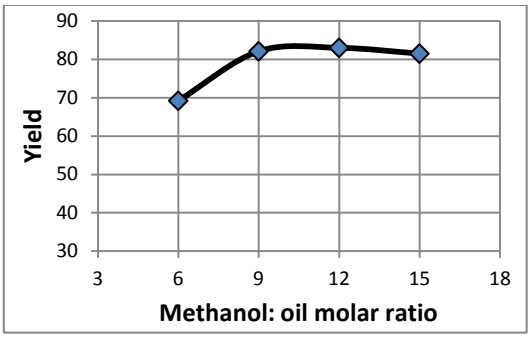


**Figure 5.1: Effect of Methanol: oil ratio on Yield (WB)**

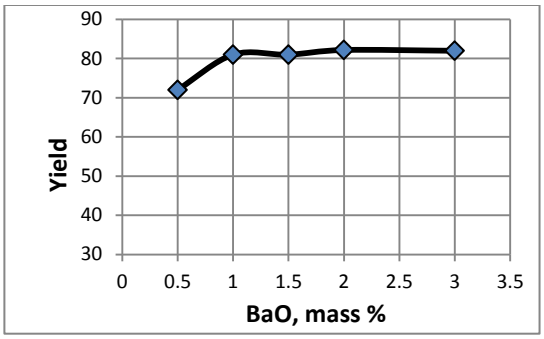


**Figure 5.2: Effect of BaO concentration on FAME yield (WB)**

#### 5.3.1.1.3 Effect of temperature on FAME yield

An yield of 53% was obtained at 40$^{o}$C (313K), and it increased as the temperature was increased. The increase in yield was substantive from 40 – 60$^{o}$C (313 – 333 K), and increase was little when temperature was increased to 70$^{o}$C. A state of equilibrium was reached at 60$^{o}$C (333 K) and no further increase in yield was noted. Fig 5.3 gives the effect of reaction temperature on FAME yield.

### 5.3.1.2 Reaction Kinetics

#### 5.3.1.2.1 Effect of Time on FAME yield

FAME yield for temperatures of 40, 50, 60, 70$^{o}$C (313, 323, 333, 343 K) is plotted as a function of time as given in Fig 5.4.

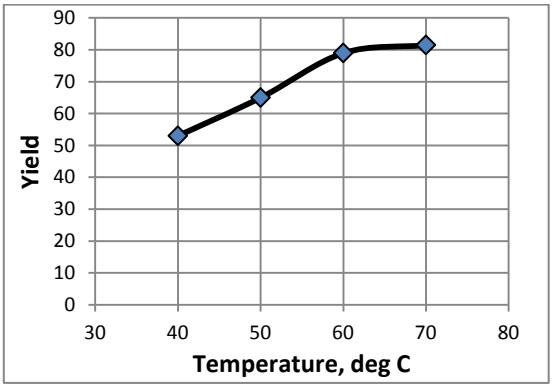


**Figure 5.3: Effect of reaction temp. on yield (WB)**

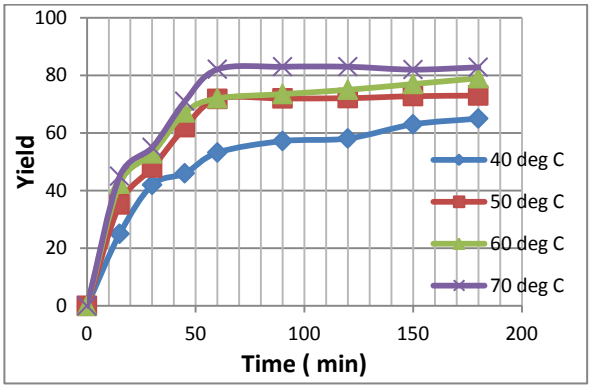


**Figure 5.4: Variation of Yield with time at various temperatures (WB)**

Yields increased with increase in temperature. Yield at 40°C (313K) was much lower compared to yields at 50, 60 and 70°C (323, 333 and 334K). For 50, 60 and 70°C (323, 333 and 334K), the yield curves became almost horizontal after a time period of 1 h, and there were not much increase in yield. Final yields for temperatures of 40, 50, 60 and 70°C (313, 323, 333 and 334K) were 65, 73, 79 and 82.8% respectively.

#### 5.3.1.2.2 Order of reaction

Table 5.3 gives the coefficients of correlation, $R^2$, for all the ten cases of reaction orders, for all temperatures. Indices *m* and *n* refer to the general rate equation: $-r_A = -\frac{d[A]}{dt} = k\,[A]^m\,[B]^n$ (Eqn 2.29).

**Table 5.3: Coefficients of correlation, R2, for various reaction orders (WB)**

| | **0th Order** | **1st Order** | | **2nd Order** | | | **3rd Order** | | | |
|---|---|---|---|---|---|---|---|---|---|---|
| **Temp °C** | Case 1 | Case 2 (m=1, n=0) | Case 3 (m=0, n=1) | Case 4 (m=1, n=1) | Case 5 (m=2, n=0) | Case 6 (m=0, n=2) | Case 7 (m=2, n=1) | Case 8 (m=1, n=2) | Case 9 (m=3, n=0) | Case 10 (m=0, n=3) |
| **40** | 0.6352 | 0.7581 | 0.6632 | 0.7858 | 0.8735 | 0.6914 | 0.8952 | 0.8140 | **0.9550** | 0.7195 |
| **50** | 0.5282 | 0.6318 | 0.5507 | 0.6508 | 0.7136 | 0.5728 | **0.7650** | 0.6680 | 0.7604 | 0.5941 |
| **60** | 0.5233 | 0.6844 | 0.5529 | 0.7150 | 0.8409 | 0.5831 | **0.9629** | 0.7421 | 0.9438 | 0.6134 |
| **70** | 0.5041 | 0.6346 | 0.5299 | 0.6528 | 0.7062 | 0.5550 | **0.7099** | 0.6668 | 0.7067 | 0.5790 |

Highest coefficient-of-correlation at each temperature is given in **bold**. Regression analysis for the reaction at 40°C (313K) suggested a third order reaction with m = 3; whereas reactions at 50, 60 and 70°C (323, 333 and 343K) indicated a third order reaction with m = 2, n = 1. From this analysis, the most likely overall reaction order was 'three', second order with respect to triglyceride and first order with respect to methanol (Case 7 in Table 5.3). The 'slope' in this case is = k $[A_o]^2$ The rate equation, in terms of rate of disappearance of triglyceride, is: $-r_A = -\frac{d[A]}{dt} = k\,[A]^2\,[B]$, where *A* is triglyceride.

#### 5.3.1.2.3 Rate constant and Activation energy

Integrated form of rate reaction in Case 7 (Table 5.3) is Eqn 2.40:

$$\frac{1}{(\alpha_B - 3)}\left(\frac{x_A}{1 - x_A} - \frac{3}{\alpha_B - 3}\right) ln\frac{(\alpha_B - 3x_A)}{(1 - x_A)\alpha_B} = k\,[A]_o^2\,t$$

L.H.S is F($x_A$) and RHS is a function of time *t*. Regression linear plot for F($x_A$) vs. *t* for 70$^o$C (343K) is given in Fig 5.5.The ordinate is L.H.S expression of Eqn 2.40, and abscissa is *t*. Reaction constant *k* is given by the slope of the plot ($R^2$ = 0.7099).

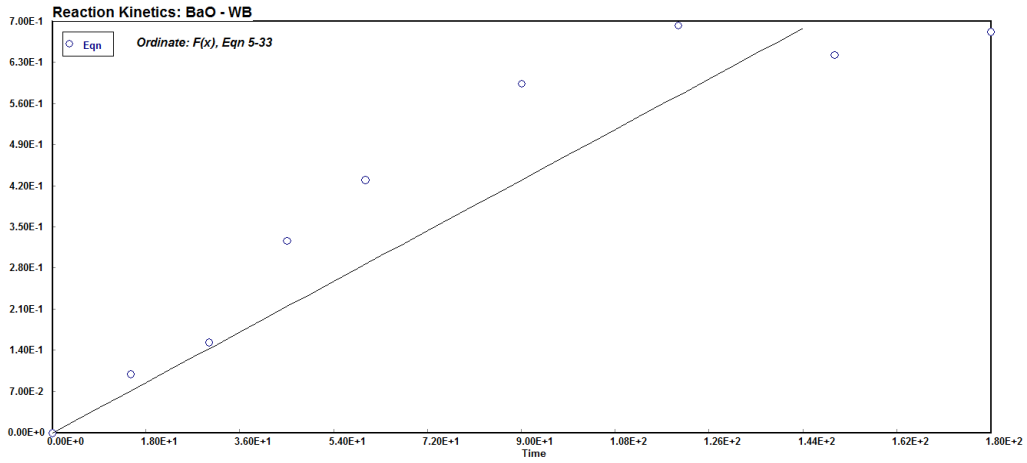


**Figure 5.5: Plot of kinetic equation 5.33 (WB)**

Correlation constants (k $[A_o]^2$ ) for Eqn 2.40 for the four temperatures were used to estimate reaction constant *k* as given in Table 5.4.

**Table 5.4: Reaction constant k (WB)**

| Temp $^o$C | Temp K | $[Ao]^2$ .k | [Ao] | k |
|---|---|---|---|---|
| | | | g/cm3 | (in min) |
| **40** | 313.15 | 0.001603 | 0.6663 | 3.61E-03 |
| **50** | 323.15 | 0.003003 | 0.6663 | 6.76E-03 |
| **60** | 333.15 | 0.003558 | 0.6663 | 8.02E-03 |
| **70** | 343.15 | 0.005655 | 0.6663 | 1.27E-02 |

. Fig 5.6 gives the plot.

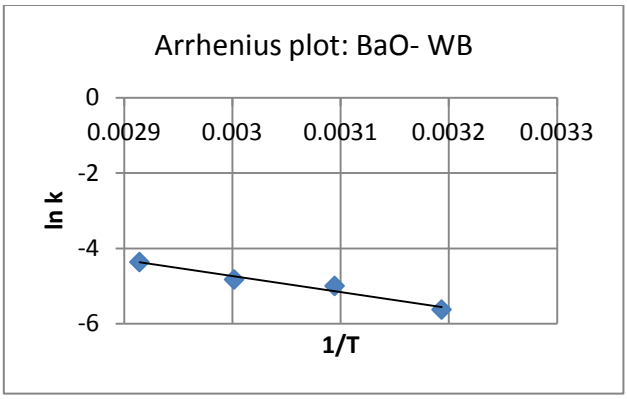


**Figure 5.6: Arrhenius plot for BaO catalyst (WB)**

The slope was 4255.47 ( $R^2$ = 0.9615), which gave the Activation energy, *E* = 35.38 kJ/mol; and the intercept gave pre-exponential factor $A = 3.07 \times 10^3$.

There is not much published literature on use of BaO as a transesterification catalyst. Singh and Fernando (2007) used BaO for soybean oil transesterification in a high pressure reactor and have reported an overall third order kinetics, second order with respect to triglyceride and first order with respect to methanol. Reaction constant *k* (at 215$^o$C) was found to be 0.0085 $g^2$ $mol^{-2}$ $min^{-1}$. In a transesterification study of *Camelina sativa* oil on BaO catalyst, the reaction was of a similar order, and reaction constant was 0.0526 $g^2$ $mol^{-2}$ $min^{-1}$ (reaction temperature not given) (Patil *et al*., 2011). The present work is in agreement with the published literature on BaO kinetics.

### 5.3.1.3 Optimization studies

#### 5.3.1.3.1 Experimental results and data analysis

Table 5.5 gives the details of a set of 20 experiments in terms of actual and coded levels, as per CCD, and the FAME yields obtained in experimental studies. Last column of the Table also gives the predicted yield based on the quadratic correlation (Eqn 4.2).

**Table 5.5: CCD matrix with experimental FAME yield (WB)**

| Run | Level of variables [actual(coded)] | | | Expt. Yield | Quadratic Model (Eqn 5.2) |
|---|---|---|---|---|---|
| | Catalyst,% X1 | Temp, ($^o$C) X2 | Methanol :oil X3 | | Y |
| **1** | 1(0) | 60(0) | 9(0) | 81.3 | 81.7 |
| **2** | 1(0) | 43(-1.68) | 9(0) | 60.9 | 60.8 |
| **3** | 0.5(-1) | 70(1) | 12(1) | 76.1 | 77.0 |
| **4** | 1(0) | 60(0) | 14(1.68) | 74.2 | 74.1 |

| | | | | | |
|---|---|---|---|---|---|
| **5** | 1.84(1.68) | 60(0) | 9(0) | 74.01 | 73.9 |
| **6** | 1(0) | 60(0) | 4(-1.68) | 58.6 | 59.0 |
| **7** | 0.5(-1) | 50(-1) | 6(-1) | 52.9 | 53.8 |
| **8** | 1(0) | 60(0) | 9(0) | 83.1 | 81.7 |
| **9** | 1.5(1) | 70(1) | 12(1) | 78.9 | 77.8 |
| **10** | 1.5(1) | 70(1) | 6(-1) | 61.1 | 62.0 |
| **11** | 1(0) | 60(0) | 9(0) | 81.9 | 81.7 |
| **12** | 1.5(1) | 50(-1) | 6(-1) | 72.5 | 71.4 |
| **13** | 0.16(-1.68) | 60(0) | 9(0) | 57.9 | 58.3 |
| **14** | 1(0) | 60(0) | 9(0) | 81.5 | 81.7 |
| **15** | 1.5(1) | 50(-1) | 12(1) | 66.5 | 67.9 |
| **16** | 1(0) | 60(0) | 9(0) | 81.7 | 81.7 |
| **17** | 0.5(-1) | 50(-1) | 12(1) | 57 | 55.9 |
| **18** | 1(0) | 77(1.68) | 9(0) | 70.1 | 70.5 |
| **19** | 1(0) | 60(0) | 9(0) | 81 | 81.7 |
| **20** | 0.5(-1) | 70(1) | 6(-1) | 57 | 55.5 |

Data in Table 7.4 were tested for fit for a linear, two-factor interaction (2FI), quadratic and cubic polynomials. Table 7.5 gives the result.

**Table 5.6: Summary for model fit- Sequential model sum of squares (WB)**

| **Sequential Model Sum of Squares [Type I]** | | | | | | |
|---|---|---|---|---|---|---|
| **Source** | **Sum of Squares** | **df** | **Mean Square** | **F Value** | **p-value Prob > F** | |
| **Mean vs Total** | 99152.77 | 1 | 99152.77 | | | |
| **Linear vs Mean** | 681.31 | 3 | 227.10 | 2.63 | 0.0860 | |
| **2FI vs Linear** | 266.03 | 3 | 88.68 | 1.03 | 0.4110 | |
| **Quadratic vs 2FI** | 1104.45 | 3 | 368.15 | 275.92 | < 0.0001 | Suggested |
| **Cubic vs Quadratic** | 10.46 | 4 | 2.62 | 5.45 | 0.0337 | Aliased |
| **Residual** | 2.88 | 6 | 0.48 | | | |
| **Total** | 1.012E+005 | 20 | 5060.90 | | | |

For linear and 2FI, p value > 0.05, hence they did not qualify for regression. For Quadratic and Cubic, the F and p values satisfy the conditions, but cubic was aliased hence should not be chosen. The appropriate model for the given set of data was full Quadratic model (Eqn 4.2, Chapter 4) : $Y = b_0 + \sum_{i=1}^{n} b_i X_i + \sum_{i=1}^{n} b_{ii} X_i^2 + \sum_{1=1}^{n-1} \sum_{j=i+1}^{n} b_{ij} X_i X_j$

Y is the Yield, $X_i$ are coded variables as given in Table 5.1.

Table 5.7 gives Analysis of Variance (ANOVA) for a full quadratic model.

**Table 5.7: ANOVA for Response Surface Quadratic model (WB)**

| **ANOVA for Response Surface Quadratic model** | | | | | |
|---|---|---|---|---|---|
| **Analysis of variance table [Partial sum of squares - Type III]** | | | | | |
| **Source** | **Sum of Squares** | **df** | **Mean Square** | **F Value** | **p-value Prob > F** |

| | | | | | | |
|---|---|---|---|---|---|---|
| **Model** | 2051.79 | 9 | 227.98 | 170.86 | < 0.0001 | significant |
| ***X1-BaO*** | *291.49* | *1* | *291.49* | *218.47* | *< 0.0001* | |
| ***X2-Temp*** | *115.25* | *1* | *115.25* | *86.37* | *< 0.0001* | |
| ***X3-Meth:oil*** | *274.58* | *1* | *274.58* | *205.79* | *< 0.0001* | |
| ***X1.X2*** | *61.61* | *1* | *61.61* | *46.17* | *< 0.0001* | |
| ***X1.X3*** | *16.24* | *1* | *16.24* | *12.18* | *0.0058* | |
| ***X2.X3*** | *188.18* | *1* | *188.18* | *141.04* | *< 0.0001* | |
| ***X1^2*** | *440.83* | *1* | *440.83* | *330.39* | *< 0.0001* | |
| ***X2^2*** | *466.84* | *1* | *466.84* | *349.89* | *< 0.0001* | |
| ***X3^2*** | *416.11* | *1* | *416.11* | *311.87* | *< 0.0001* | |
| **Residual** | 13.34 | 10 | 1.33 | | | |
| ***Lack of Fit*** | *10.67* | *5* | *2.13* | *3.99* | *0.0776* | *not significant* |
| ***Pure Error*** | *2.67* | *5* | *0.53* | | | |
| **Cor Total** | 2065.13 | 19 | | | | |

The Model F-value of 170.86 implied the model was significant. There was only a 0.01% chance that an F-value this large could occur due to noise. Values of "Prob > F" less than 0.0500 indicated model terms were significant. In this case X1, X2, X3, X1.X2, X1.X3, X2.X3, X1^2, X2^2, X3^2 were significant model terms. The "Lack of Fit F-value" of 3.99 implied there was a 7.76% chance that a "Lack of Fit F-value" this large could occur due to noise. Lack of fit was not very good, but p = 0.0776 (> 0.05) indicated that it was acceptable. Hence lack-of-fit was insignificant. Table 5.8 gives the R-square values for the model.

**Table 5.8: R-Square values (WB)**

| **Std. Dev.** | **1.16** | **R-Squared** | **0.9935** |
|---|---|---|---|
| **Mean** | 70.41 | Adj R-Squared | 0.9877 |
| **C.V. %** | 1.64 | Pred R-Squared | 0.9515 |
| **PRESS** | 100.08 | Adeq Precision | 34.221 |

The "Predicted R-Squared" of 0.9515 was in reasonable agreement with the "Adjusted R-Squared" of 0.9877; i.e. the difference was less than 0.2."Adeq Precision" measures the signal to noise ratio. A ratio greater than 4 is desirable. For this model a ratio of 34.221 indicated an adequate signal. This model can be used for design purposes as it adequately represented the experimental data. Table 5.9 gives the coefficients for the model.

**Table 5.9: Coefficients for the full quadratic model (WB)**

| | **Coefficient** | | **Standard** | **95% CI** | **95% CI** |
|---|---|---|---|---|---|
| **Factor** | **Estimate** | **df** | **Error** | **Low** | **High** |
| **Intercept** | 81.74 | 1 | 0.47 | 80.69 | 82.79 |
| **X1-BaO** | 4.62 | 1 | 0.31 | 3.92 | 5.32 |
| **X2-Temp** | 2.90 | 1 | 0.31 | 2.21 | 3.60 |

| | | | | | |
|---|---|---|---|---|---|
| **X3-Meth:oil** | 4.48 | 1 | 0.31 | 3.79 | 5.18 |
| **X1.X2** | -2.78 | 1 | 0.41 | -3.68 | -1.87 |
| **X1.X3** | -1.42 | 1 | 0.41 | -2.33 | -0.52 |
| **X2.X3** | 4.85 | 1 | 0.41 | 3.94 | 5.76 |
| **X1^2** | -5.53 | 1 | 0.30 | -6.21 | -4.85 |
| **X2^2** | -5.69 | 1 | 0.30 | -6.37 | -5.01 |
| **X3^2** | -5.37 | 1 | 0.30 | -6.05 | -4.69 |

Since all the terms were significant, no further reductions were needed. Hence the model was: Yield, $Y = 81.74 + 4.62\ X1 + 2.90\ X2 + 4.48\ X3 - 2.78\ X1.X2 - 1.42\ X1.X3 + 4.85\ X2.X3 - 5.53\ X1^2 - 5.69\ X2^2 - 5.37\ X3^2$ …5.2

Predicted yields based on this model are given in Table 5.5. Eqn 5.2 can be used for response surface plots.

#### 5.3.1.3.2 Response Surface and Contour Plots

Fig 5.7 is a RSM plot giving response surface and contours for FAME yield as a function of BaO catalyst concentration and reaction temperature. The optima was close to catalyst concentration of 1 mass% and a temperature of 60$^{o}$C (333K). These fairly agreed with the experimental observations.

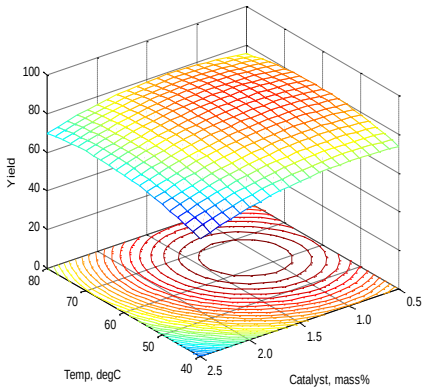


**Figure 5.7: RSM plot- Effect of BaO conc. and Temp. on Yield (WB)**

Fig 5.8 is a RSM plot giving response surface and contours for FAME yield as a function of BaO catalyst concentration and methanol to oil ratio. The optima was close to catalyst concentration of 1 mass% and a methanol to oil ratio of 9:1. These agreed well with the experimental observations.

Fig 5.9 is a RSM plot giving response surface and contours for FAME yield as a function of reaction temperature and methanol to oil ratio. The optima was close to a temperature of 70$^{o}$C (343K) and a methanol to oil ratio of 9:1. This is in an agreement with the experimental observations.

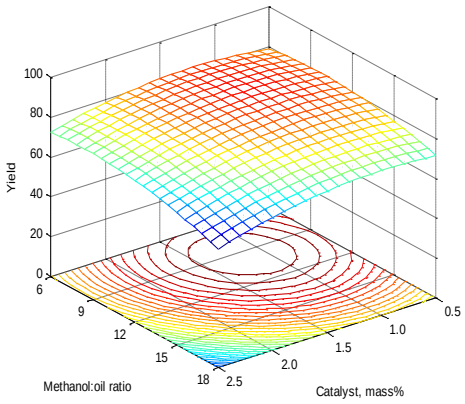


**Figure 5.8: RSM plot- Effect of BaO conc. and Methanol:oil ratio on on Yield (WB)**

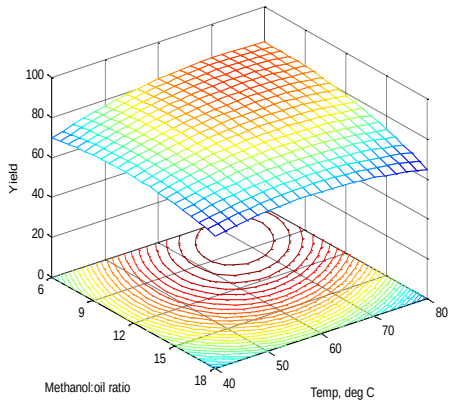


**Figure 5.9: RSM plot- Effect of Methanol:oil Yield (WB) ratio and Temp.**

### 5.3.2 Studies with Microwave Irradiation- Barium oxide catalyst

This section deals with transesterification of Croton *megalocarpus* oil using heterogeneous BaO catalyst with microwave irradiation.

#### 5.3.2.1 Effect of operation variables on FAME yield

##### 5.3.2.1.1 Effect of methanol to triglyceride molar ratio on FAME yield

FAME yield increased with the increase of methanol to oil ratio from 6 to 9, and from 9 to 12. Maximum FAME yield of 77.2% corresponded to the ratio of 12:1. Yield dropped to 73.0% as the methanol ratio was increased to 15:1. This drop of yield beyond a certain methanol to oil ratio has been observed in earlier such studies. Reasons given were: dilution of catalyst at excess methanol, glycerol forming an emulsion with FAME in presence of excess methanol reducing FAME separation, and methanol dissolving in glycerol bringing about separation problems (Section 4.3.2.1.1). A maximum FAME yield of 94% has been reported for microwave irradiated transesterification of *Camelina sativa* oil at 9:1 methanol:oil ratio, 1.5 mass% BaO catalyst; and the yield dropped as the methanol to oil ratio was further increased (Patil *et al*., 2010). Under combined effect of

microwave and ultrasound irradiation highest FAME yield was obtained at 4.5:1 methanol to oil ratio, at 1 mass% BaO catalyst, for used vegetable oil transesterification. Yield began to drop as the methanol:oil ratio was increased beyond 4.5 due to dilution of BaO at higher methanol ratio (Martinez-Guerra and Gude, 2014). Fig 5.10 gives the fame yield as a function of methanol to oil ratio.

#### 5.3.2.1.2 Effect of catalyst concentration on FAME yield

Fig 5.11 gives FAME yield as a function of BaO concentration. FAME yield initially increased with the increase in BaO concentration and highest yield of 78.5% was at 2 mass% BaO. Yield slightly dropped to 76% when the BaO concentration was increased to 3 mass%. Figure shows that the yield became almost constant at BaO concentration above 1 mass%. As already mentioned in previous section, Patil *et al*.(2010) have reported an optimum concentration of 1.5 mass% BaO and 4 min reaction time, for 94% yield of FAME from *Camelina Sativa* oil using microwave irradiation.

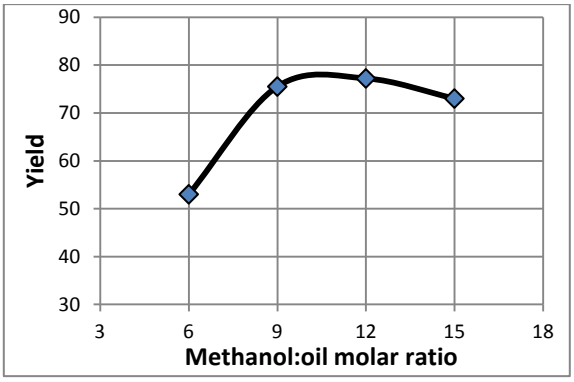


**Figure 5.10: FAME yield as a function of Methanol:oil ratio (MW)**

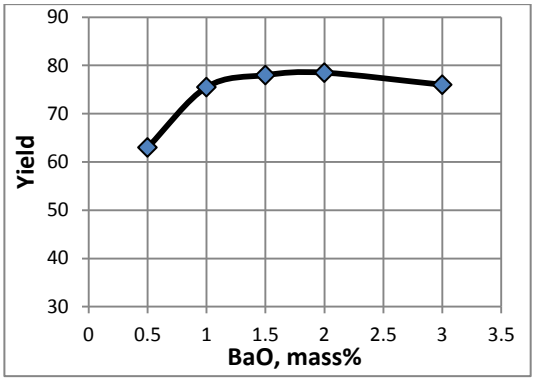


**Figure 5.11: FAME yield as a function of BaO concentration (MW)**

#### 5.3.2.1.3 Effect of reaction time on FAME yield

Transesterification was carried out with 1 mass% BaO, 9:1 methanol to oil molar ratio at full microwave power. An yield of 62.7% was obtained after 30s of reaction time. Maximum yield of 76.9% corresponded to 3 min of time. After 3 min, a slight drop in yield was noted. Such slight drop in yield after a certain reaction time have also been reported by other studies with microwave irradiation (Patil *et al*., 2010; Martinez-Guerra and Gude, 2014 ). Although no specific reasons have been given to such a decrease, it

could be due to the reversible nature of the reaction. Fig 5.12 gives the effect of reaction time on FAME yield at full microwave power.

#### 5.3.2.1.4 Effect of microwave power

Microwave reactor had built in power settings of 20, 40, 60, 80, 100%. Reactions were carried out at microwave power of 40, 60, 80 and 100%, at methanol to oil ratio of 9:1, 1 mass% of BaO, and a reaction time of 5 min. Fig 5.13 gives the effect of microwave power on FAME yield. As expected, yield increased with the rise of power since microwave power is directly related to microwave irradiation. The increase was more steep when power was increased from 40- 80%. After a power level of 80% the rise in yield was gradual. The increase in FAME yield from 80 to 100% of power was from 68.2 to 75.5% .

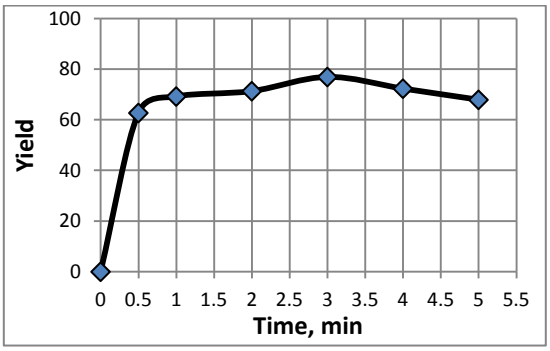


**Figure 5.12: Effect of reaction time on Yield (MW)**

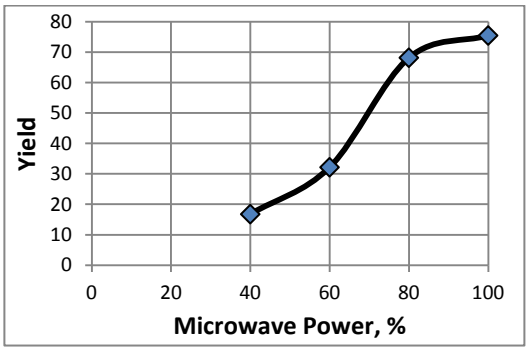


**Figure 5.13: Effect of microwave power on FAME yield**

### 5.3.2.2 Reaction Kinetics

Transesterification reactions were carried out at constant temperatures of 50, 60 and 70$^{o}$C (323, 333, 343K). Constant reaction parameters were methanol to oil ratio - 9:1, BaO concentration -1 mass%. Samples were drawn at 30, 45, 60 and 90s.

#### 5.3.2.2.1 Effect of Time on FAME yield

Fig 5.14 is a plot of FAME yield vs. reaction time at varying reaction temperatures. Nature of yield vs time curves were similar at all the three temperatures. Yields at 60 and 70$^{o}$C (333 and 343K) were close to each other. After an initial period of accelerated increase, yield became almost constant with time after 60s. Yields at the end of 60 s for the temperatures of 50, 60 and 70$^{o}$C (323, 333, 343K) were, 51.3, 63.0, 68.5%; while yields at the end of 90 s for these temperatures were, 55.2, 67.3, 71.7% respectively.

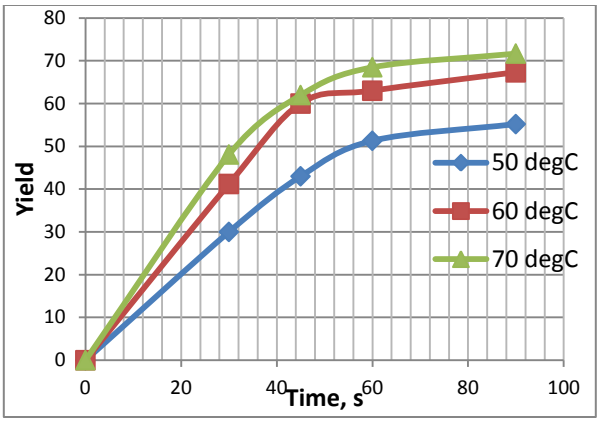


**Figure 5.14: Variation of Yield with time at various temperatures (MW)**

#### 5.3.2.2.2 Order of reaction

Table 5.10 gives the coefficients of correlation, $R^2$, for all the ten cases of reaction orders, for all temperatures. Indices *m* and *n* refer to the general rate equation: $-r_A = -\frac{d[A]}{dt} = k\,[A]^m\,[B]^n$ (Eqn 2.29).

**Table 5.10: Coefficients of correlation, $R^2$, for various reaction orders (MW)**

| | 0th Order | 1st Order | | 2nd Order | | | 3rd Order | | | |
|---|---|---|---|---|---|---|---|---|---|---|
| **Temp °C** | Case 1 | Case 2 (m=1, n=0) | Case 3 (m=0, n=1) | Case 4 (m=1, n=1) | Case 5 (m=2, n=0) | Case 6 (m=0, n=2) | Case 7 (m=2, n=1) | Case 8 (m=1, n=2) | Case 9 (m=3, n=0) | Case 10 (m=0, n=3) |
| **50** | .8719 | .9238 | .8858 | .9341 | .9577 | .8991 | **.9617** | .9436 | .9603 | .9114 |
| **60** | .8056 | .8768 | .8219 | .8899 | .9297 | .8376 | **.9360** | .9016 | .9293 | .8527 |
| **70** | .7923 | ..8851 | .8120 | .9017 | .9517 | .8315 | **.9580** | .9161 | .9514 | .9505 |

Highest correlation coefficients are in bold in Table 5.10. The most likely order of reaction was 'three'; second order with respect to triglyceride, and first order with respect to methanol (Case 7). The integrated form of rate equation is Eqn 2.40 (Chapter 2) given as: $\frac{1}{(\alpha_B-3)}\left(\frac{x_A}{1-x_A}-\frac{3}{\alpha_B-3}\right) ln\frac{(\alpha_B-3x_A)}{(1-x_A)\alpha_B} = k\,[A]_o^2\,t$. The slope in this case is = k $[A_o]^2$.

#### 5.3.2.2.3 Rate constant and Activation energy

L.H.S. of Eqn 2.40,( $\frac{1}{(\alpha_B-3)}\left(\frac{x_A}{1-x_A}-\frac{3}{\alpha_B-3}\right) ln\frac{(\alpha_B-3x_A)}{(1-x_A)\alpha_B}$ ) is a function of conversion $x_A$, $F(x_A)$, or the yield. A plot of $F(x_A)$ vs time *t* is a straight line passing through the origin. Regression linear plot for $F(x_A)$ vs. *t* for 70°C (343K) is given in Fig 5.15. The ordinate is,

$\frac{1}{(\alpha_B-3)}\left(\frac{x_A}{1-x_A}-\frac{3}{\alpha_B-3}\right)ln\frac{(\alpha_B-3x_A)}{(1-x_A)\alpha_B}$ ) and abscissa is *t*. Reaction constant *k* is given by the slope of the plot ($R^2$ = 0.9580).

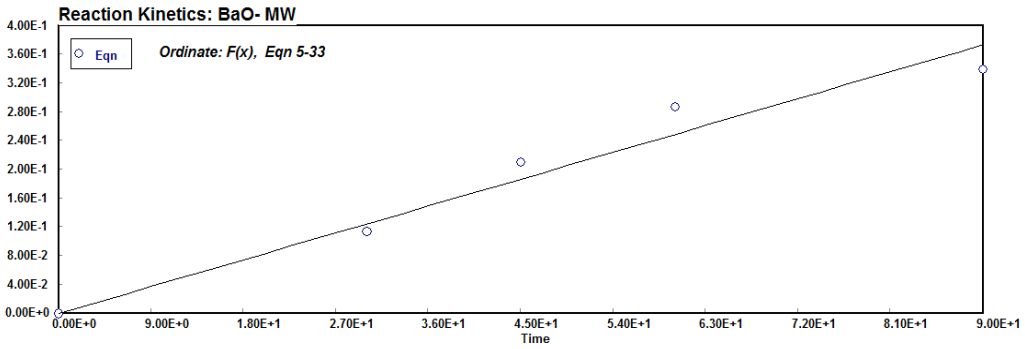


**Figure 5.15: Plot of kinetic equation 5.33 (MW)**

Correlation constants (k $[A_o]^2$ ) for Eqn 2.40 for the three temperatures were used to estimate reaction constant *k* as given in Table 5.11.

**Table 5.11: Reaction constant k (MW)**

| Temp, °C | Temp K | $[Ao]^2$ .k | [Ao] | k |
|---|---|---|---|---|
| | | | g/cm3 | in min |
| **50** | 323.15 | 0.001902 | 0.6663 | 2.57E-01 |
| **60** | 333.15 | 0.003405 | 0.6663 | 4.60E-01 |
| **70** | 343.15 | 0.004209 | 0.6663 | 5.69E-01 |

Activation energy was obtained from the slope of the plot of ln*k* vs. 1/T (Arrhenius plot, Section 2.5.4.1). Fig 5.16 gives the plot ($R^2$ = 0.9408).

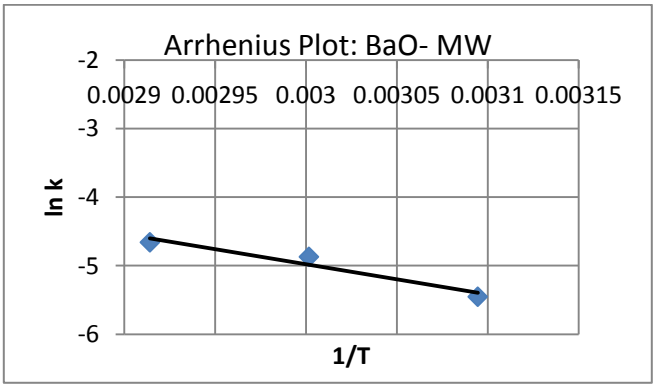


**Figure 5.16: Arrhenius plot for BaO (MW)**

Slope of the plot was 4422.3, giving Activation energy, $E$ = 36.77 kJ/mol; and the intercept gave the pre-exponential factor, $A = 2.38 \times 10^5$.

#### 5.3.2.3 Optimization studies

##### 5.3.2.3.1 Experimental Design

##### 5.3.2.3.2 Experimental results and data analysis

Table 5.12 gives the details of a set of 20 experiments in terms of actual and coded levels, as per CCD, and the FAME yields obtained in transesterification studies. Last column in the Table also gives the Predicted yield calculated from Reduced Quadratic Model (Eqn 5.3).

**Table 5.12: CCD matrix with experimental FAME yield (MW)**

| Run | Level of variables [actual(coded)] | | | Experimental Yield | Reduced Model (Eqn 5.3) |
|---|---|---|---|---|---|
| | Catalyst,% | Time (min) | Methanol :oil | | Y |
| | X1 | X2 | X3 | | |
| **1** | 1(0) | 3(0) | 9(0) | 75.1 | 75.3 |
| **2** | 1(0) | 0.5(-1.68) | 9(0) | 62.7 | 63.4 |
| **3** | 0.5(-1) | 4.5(1) | 12(1) | 62.1 | 63.4 |
| **4** | 1(0) | 3(0) | 14(1.68) | 68.1 | 67.1 |
| **5** | 1.84(1.68) | 3(0) | 9(0) | 74.1 | 72.8 |
| **6** | 1(0) | 3(0) | 4(-1.68) | 56.7 | 57.6 |
| **7** | 0.5(-1) | 1.5(-1) | 6(-1) | 61.9 | 61.8 |
| **8** | 1(0) | 3(0) | 9(0) | 76.9 | 75.3 |
| **9** | 1.5(1) | 4.5(1) | 12(1) | 77.5 | 78.1 |
| **10** | 1.5(1) | 4.5(1) | 6(-1) | 56.1 | 58.1 |
| **11** | 1(0) | 3(0) | 9(0) | 74.1 | 75.3 |
| **12** | 1.5(1) | 1.5(-1) | 6(-1) | 69.1 | 67.5 |
| **13** | 0.16(-1.68) | 3(0) | 9(0) | 54.5 | 55.7 |
| **14** | 1(0) | 3(0) | 9(0) | 75.0 | 75.3 |
| **15** | 1.5(1) | 1.5(-1) | 12(1) | 66.5 | 67.8 |
| **16** | 1(0) | 3(0) | 9(0) | 74.8 | 75.3 |
| **17** | 0.5(-1) | 1.5(-1) | 12(1) | 54.5 | 53.1 |
| **18** | 1(0) | 5.5(1.68) | 9(0) | 64.9 | 64.1 |
| **19** | 1(0) | 3(0) | 9(0) | 75.6 | 75.3 |

| | | | | | |
|---|---|---|---|---|---|
| **20** | 0.5(-1) | 4.5(1) | 6(-1) | 54.1 | 52.4 |

Data in Table 5.12 were tested for fit for a linear, two-factor interaction (2FI), quadratic and cubic polynomials. Table 5.13 gives the result.

**Table 5.13: Summary for model fit- Sequential model sum of squares (MW)**

| **Summary for model fit** | | | | | | |
|---|---|---|---|---|---|---|
| **Source** | **Sequential p-value** | **Lack of Fit p-value** | **Adjusted R-Squared** | **Predicted R-Squared** | | |
| **Linear** | 0.0752 | < 0.0001 | 0.2188 | 0.0200 | | |
| **2FI** | 0.2465 | < 0.0001 | 0.2930 | -0.2837 | | |
| **Quadratic** | < 0.0001 | 0.0603 | 0.9652 | 0.8702 | | Suggested |
| **Cubic** | 0.0201 | 0.9064 | 0.9896 | 0.9930 | | Aliased |
| **Sequential Model Sum of Squares [Type I]** | | | | | | |
| **Source** | **Sum of Squares** | **df** | **Mean Square** | **F Value** | **p-value Prob > F** | |
| **Mean vs Total** | 89017.82 | 1 | 89017.82 | | | |
| **Linear vs Mean** | 463.45 | 3 | 154.48 | 2.77 | 0.0752 | |
| **2FI vs Linear** | 235.85 | 3 | 78.62 | 1.56 | 0.2465 | |
| **Quadratic vs 2FI** | 630.32 | 3 | 210.11 | 84.58 | < 0.0001 | Suggested |
| **Cubic vs Quadratic** | 20.37 | 4 | 5.09 | 6.84 | 0.0201 | Aliased |
| **Residual** | 4.47 | 6 | 0.74 | | | |
| **Total** | 90372.29 | 20 | 4518.61 | | | " |

Cubic has the highest $R^2$, followed by $R^2$ for Quadratic model. However, cubic was not suitable being aliased. For linear and 2FI, p value > 0.05, hence they did not qualify for regression. For Quadratic and Cubic, the F and p values satisfied the conditions, but cubic was once again aliased and hence should not be chosen. The appropriate model for the given set of data was full Quadratic model (Eqn 4.2, Chapter 4) :

$$Y = b_0 + \sum_{i=1}^{n} b_i X_i + \sum_{i=1}^{n} b_{ii} X_i^2 + \sum_{1=1}^{n-1} \sum_{j=i+1}^{n} b_{ij} X_i X_j$$

Y is the Yield, $X_i$ are coded variables as given in Table 5.2.

Table 5.14 gives Analysis of Variance (ANOVA) for a full quadratic model.

**Table 5.14: ANOVA for Response Surface Quadratic model (MW)**

| **ANOVA for Response Surface Quadratic model** | | | | | | |
|---|---|---|---|---|---|---|
| **Analysis of variance table [Partial sum of squares - Type III]** | | | | | | |
| **Source** | **Sum of Squares** | **df** | **Mean Square** | **F Value** | **p-value Prob > F** | |
| **Model** | 1329.62 | 9 | 147.74 | 59.47 | < 0.0001 | significant |

| | | | | | | |
|---|---|---|---|---|---|---|
| ***X1-Catalyst*** | *354.34* | *1* | *354.34* | *142.63* | *< 0.0001* | |
| ***X2-Time*** | *0.16* | *1* | *0.16* | *0.066* | *0.8020* | |
| ***X3-Meth.:oil*** | *108.95* | *1* | *108.95* | *43.85* | *< 0.0001* | |
| ***X1.X2*** | *0.41* | *1* | *0.41* | *0.16* | *0.6949* | |
| ***X1.X3*** | *41.40* | *1* | *41.40* | *16.67* | *0.0022* | |
| ***X2.X3*** | *194.04* | *1* | *194.04* | *78.11* | *< 0.0001* | |
| ***X1^2*** | *217.51* | *1* | *217.51* | *87.55* | *< 0.0001* | |
| ***X2^2*** | *237.75* | *1* | *237.75* | *95.70* | *< 0.0001* | |
| ***X3^2*** | *299.22* | *1* | *299.22* | *120.45* | *< 0.0001* | |
| **Residual** | 24.84 | 10 | 2.48 | | | |
| ***Lack of Fit*** | *20.39* | *5* | *4.08* | *4.58* | *0.0603* | *not significant* |
| ***Pure Error*** | *4.46* | *5* | *0.89* | | | |
| **Cor Total** | 1354.47 | 19 | | | | |

The Model F-value of 59.47 implies the model was significant. There was only a 0.01% chance that an F-value this large could occur due to noise. Values of "Prob > F" less than 0.0500 indicate model terms are significant. In this case X1, X3, X1.X3, X2.X3, X1^2, X2^2, X3^2 were significant model terms. The model could therefore be reduced by dropping insignificant terms, X2 and X1.X2. However, X2 (Time) could not be dropped since it was part of model hierarchy. Hence X1.X2 was dropped and tested the reduced model for ANOVA.

**Reduced model:** X1.X2 term was dropped from the full quadratic model. Table 5.15 gives the ANOVA for the reduced model.

**Table 5.15: ANOVA for Response Surface Quadratic (Reduced) model (MW)**

| **ANOVA for Response Surface Reduced Quadratic model** | | | | | | |
|---|---|---|---|---|---|---|
| **Analysis of variance table [Partial sum of squares - Type III]** | | | | | | |
| | **Sum of** | | **Mean** | **F** | **p-value** | |
| **Source** | **Squares** | **df** | **Square** | **Value** | **Prob > F** | |
| **Model** | 1329.22 | 8 | 166.15 | 72.39 | < 0.0001 | significant |
| ***X1-Catalyst*** | *354.34* | *1* | *354.34* | *154.38* | *< 0.0001* | |
| ***X2-Time*** | *0.16* | *1* | *0.16* | *0.072* | *0.7937* | |
| ***X3-Meth.:oil*** | *108.95* | *1* | *108.95* | *47.47* | *< 0.0001* | |
| ***X1.X3*** | *41.40* | *1* | *41.40* | *18.04* | *0.0014* | |
| ***X2.X3*** | *194.04* | *1* | *194.04* | *84.54* | *< 0.0001* | |
| ***X1^2*** | *217.51* | *1* | *217.51* | *94.76* | *< 0.0001* | |
| ***X2^2*** | *237.75* | *1* | *237.75* | *103.58* | *< 0.0001* | |
| ***X3^2*** | *299.22* | *1* | *299.22* | *130.37* | *< 0.0001* | |
| **Residual** | 25.25 | 11 | 2.30 | | | |
| ***Lack of Fit*** | *20.79* | *6* | *3.47* | *3.89* | *0.0788* | *not significant* |
| ***Pure Error*** | *4.46* | *5* | *0.89* | | | |
| **Cor Total** | 1354.47 | 19 | | | | |

The Model F-value of 72.39 implied the model was significant. There was only a 0.01% chance that an F-value this large could occur due to noise. Values of "Prob > F" less than 0.0500 indicate model terms are significant. In this case X1, X3, X1.X3, X2.X3, X1^2, X2^2, X3^2 were significant model terms. The "Lack of Fit F-value" of 3.89 implied there was a 7.88% chance that a "Lack of Fit F- value" this large could occur due to noise. Lack of fit was not very good but it was not significant, and acceptable ($p > 0.05$). Table 5.16 gives the $R^2$ values for the reduced model.

**Table 5.16: R-Square values (MW)**

| **Std. Dev.** | **1.52** | **R-Squared** | **0.9814** |
|---|---|---|---|
| **Mean** | 66.72 | Adj R-Squared | 0.9678 |
| **C.V. %** | 2.27 | Pred R-Squared | 0.9132 |
| **PRESS** | 117.57 | Adeq Precision | 25.274 |

The "Pred R-Squared" of 0.9132 was in reasonable agreement with the "Adj R-Squared" of 0.9678; i.e. the difference was less than 0.2. "Adeq Precision" measures the signal to noise ratio. A ratio greater than 4 is desirable. Reduced quadratic model had a ratio of 25.274 which indicated an adequate signal. This model can be used for design purposes. Table 5.17 gives the coefficients for the reduced quadratic model.

**Table 5.17: Coefficients for the Reduced Quadratic model (MW)**

| | **Coefficient** | | **Standard** | **95% CI** | **95% CI** | |
|---|---|---|---|---|---|---|
| **Factor** | **Estimate** | **df** | **Error** | **Low** | **High** | **VIF** |
| **Intercept** | 75.25 | 1 | 0.62 | 73.89 | 76.61 | |
| **X1-BaO** | 5.09 | 1 | 0.41 | 4.19 | 6.00 | 1.00 |
| **X2-Time** | 0.11 | 1 | 0.41 | -0.79 | 1.01 | 1.00 |
| **X3-Meth.:oil** | 2.82 | 1 | 0.41 | 1.92 | 3.73 | 1.00 |
| **X1.X3** | 2.27 | 1 | 0.54 | 1.10 | 3.45 | 1.00 |
| **X2.X3** | 4.92 | 1 | 0.54 | 3.75 | 6.10 | 1.00 |
| **X1^2** | -3.88 | 1 | 0.40 | -4.76 | -3.01 | 1.02 |
| **X2^2** | -4.06 | 1 | 0.40 | -4.94 | -3.18 | 1.02 |
| **X3^2** | -4.56 | 1 | 0.40 | -5.43 | -3.68 | 1.02 |

Since all the terms in the reduced model were significant, no further reductions were needed. Hence the model was:

Yield, $Y = 75.25 + 5.09\ X1 + 0.11\ X2 + 2.82\ X3 + 2.27\ X1.X3 + 4.92$

$X2.X3 - 3.88\ X1^2 - 4.06\ X2^2 - 4.56\ X3^2$ …5.3

Reduced model was used to calculate predicted yields given in Table 5.12. Eqn 5.3 can be used for response surface plots.

#### 5.3.2.3.3 Response Surface and Contour Plots

Fig 5.17, 5.18 and 5.19 give the RSM surface and contour plots based on Eqn 5.3. In Fig 5.17, optimal FAME yield corresponded to a catalyst concentration of 1 mass% and a reaction time of 3 min. These agreed well with experimental observations.

Fig 5.18 indicated catalyst concentration of 0.5-1% and methanol to oil ratio of 9:1 for maximum FAME yield. This agreed with experimental observations.

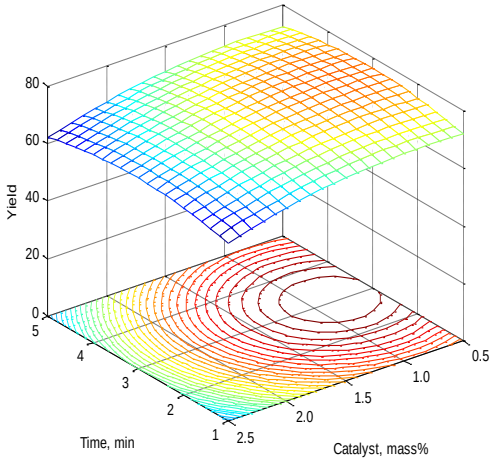


**Figure 5.17: RSM plot- Effect of BaO conc. and Time on Yield (MW)**

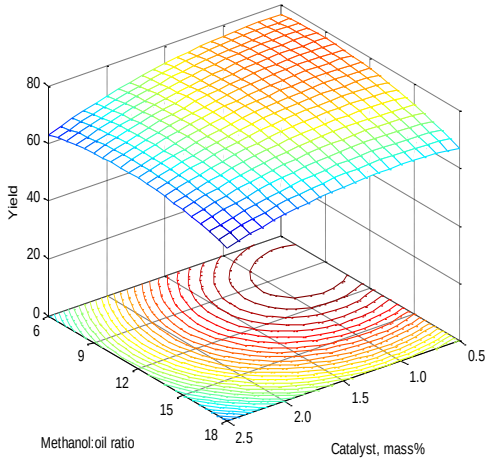


**Figure 5.18: RSM plot- Effect of BaO conc. and methanol:oil ratio on Yield (MW)**

Fig 5.19 identified region of maximum yield corresponding to methanol to oil ratio of 9:1, and reaction time > 3 min. These were in agreement with experimental findings.

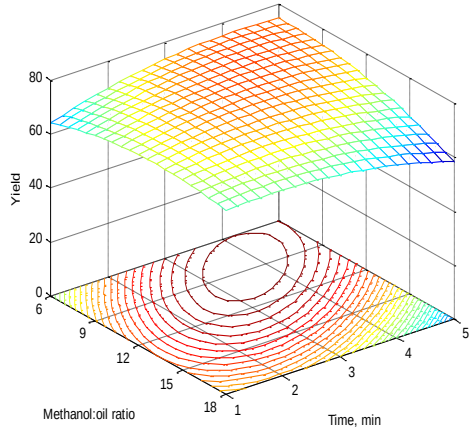


**Figure 5.19: RSM plot- Effect of Time and methanol:oil ratio on Yield (MW)**

### 5.3.3 Studies with Conventional Heating- Strontium oxide catalyst

This section deals with transesterification reactions carried out with conventional heating employing a water bath as heat source.

#### 5.3.3.1 Effect of operation variables on FAME yield

Operating variables studied were (i) Methanol to triglyceride molar ratio, (ii) Catalyst concentration, and (iii) Reaction temperature. Effect of reaction time on FAME yield was studied under reaction kinetics. Stirring speed was kept constant at 800 rpm.

##### 5.3.3.1.1 Effect of methanol to triglyceride molar ratio on FAME yield

Methanol to oil molar ratio was varied as 6:1, 9:1, 12:1, 15:1. Batch consisted of 30 ml of Croton *megalocarpus* oil (FFA = 1.7), SrO catalyst 1% by mass of oil. Reaction temperature was 70$^{o}$C (343K), and reaction time 2 h. A FAME yield of 58.4% corresponded to a 6:1 molar ratio. It increased to 75.2% when the ratio was increased to 9:1. The highest yield of 77.2% was obtained for a ratio of 12:1. As the methanol:oil ratio was increased further to 15:1, no increase in yield was noted. Instead the yield dropped slightly to 75.6%. Fig 5.20 gives the FAME yield as a function of methanol:oil ratio.

Initially excess of methanol drives the transesterification reaction (Eqn 2.2, Chapter 2) towards left, increasing the yield. But an excess of methanol dilutes the catalyst percentage in the reaction system and unreacted methanol mixes with glycerol bringing about separation problems. Also, in presence of surplus methanol glycerol forms emulsion with FAME lowering the yield. Literatures for these observations have been sighted in Section 4.3.1.1.1, Chapter 4.

##### 5.3.3.1.2 Effect of catalyst concentration on FAME yield

Effect of catalyst concentration on FAME yield was studied using SrO concentrations of 0.5 – 3 mass% based on oil mass. Batch consisted of 30 ml of Croton *megalocarpus* oil (FFA = 1.7), methanol to oil ratio of 9:1, reaction temperature 70$^{o}$C (343K), reaction time 2 h, and SrO concentrations of 0.5, 1, 1.5, 2 mass% . A SrO concentration of 0.5 mass% gave an yield of 63%. Yield increased when concentration was raised to 1 mass%, to 75.1% of FAME. Increase in FAME yield was only 1% when catalyst concentration was increased from 1mass% to 1.5 mass%. Further increase in catalyst concentration did not result into any increase in yield and it remained in the range of 75-76%. Fig 5.21 gives the

effect of catalyst concentration on FAME yield. Patil *et al*. (2009) have reported about 80% yield of *Camelina sativa* oil to FAME in 3h at 100$^{o}$C (373K), at 0.5 mass% SrO catalyst, and 9:1 methanol to oil ratio.

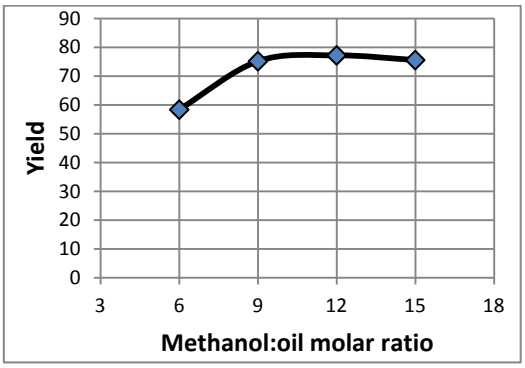


**Figure 5.20: Effect of Methanol:oil ratio on Yield (WB)**

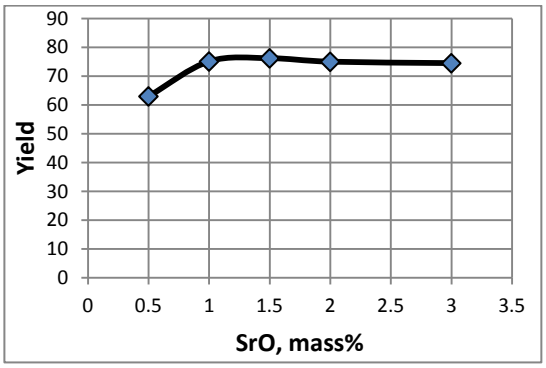


**Figure 5.21: Effect of SrO concentration on FAME yield (WB)**

#### 5.3.3.1.3 Effect of temperature on FAME yield

Reaction temperature is one of the most important parameters in transesterification studies. In this study, mass transfer resistances have been eliminated by using high stirring speed, leaving surface reaction as being a rate controlling step. Reaction temperatures were increased in the range of 40 – 70$^{o}$C (313 – 343 K). Reactions were carried out at constant catalyst concentration of 1 mass%, methanol to oil molar ratio of 9:1, and reaction time of 2 h. Reaction temperatures were 40, 50, 60 and 70$^{o}$C (313, 323, 333, 343 K) respectively. An yield of 52.0% was obtained at 40$^{o}$C (313K), and it increased steadily as the temperature was increased. Yields at 50, 60 and 70$^{o}$C (323, 333, 343K) were 66.8, 71.1 and 75.1% of FAME respectively. Patil *et al*. (2009) have reported a maximum yield at 60$^{o}$C (323K) for *Camelina sativa* oil transesterification for SrO catalyst. Fig 5.22 gives the effect of reaction temperature on FAME yield.

### 5.3.3.2 Reaction Kinetics

#### 5.3.3.2.1 Effect of Time on FAME yield

FAME yield for temperatures of 40, 50, 60, 70$^{o}$C (313, 323, 333, 343 K) was plotted as a function of time as given in Fig 5.23. Yields increased with increase in temperature. Conversions curve at 40$^{o}$C (313K) show a slow start but the rates increased later to catch up with higher temperature curves. Yields became almost constant after a time period of 2

h for reactions at 50, 60 and 70°C (323, 333 and 334K). Final yields for temperatures of 40, 50, 60 and 70°C (313, 323, 333 and 334K) after 3 h were 58.4, 64.3, 69.3 and 73.8% respectively.

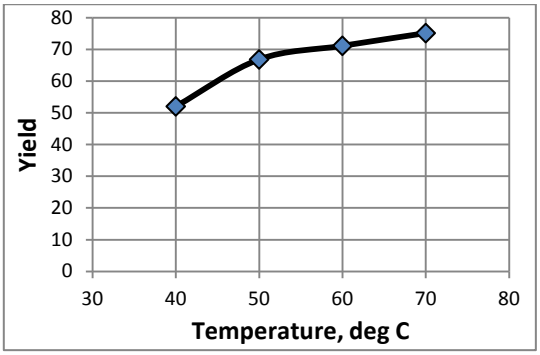


**Figure 5.22: Effect of reaction temperature on temperatures (WB)**

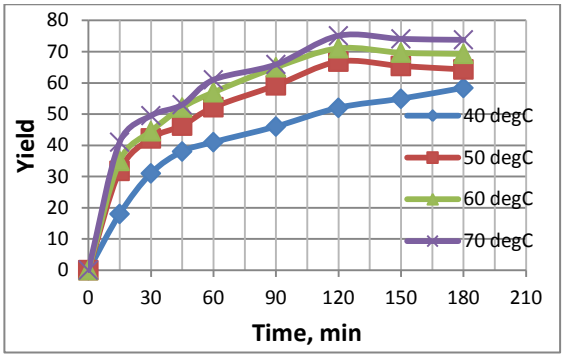


**Figure 5.23: Variation of Yield with Time at various FAME yield (WB)**

#### 5.3.3.2.2 Order of reaction

Table 5.18 gives the coefficients of correlation, $R^2$, for all the ten cases of reaction orders, and for all temperatures. Indices *m* and *n* refer to the general rate equation: $-r_A = -\frac{d[A]}{dt} = k\,[A]^m\,[B]^n$ (Eqn 2.29, Chapter 2).

**Table 5.18: Coefficients of correlation, R2, for various reaction orders (WB)**

| | 0th Order | 1st Order | | 2nd Order | | | 3rd Order | | | |
|---|---|---|---|---|---|---|---|---|---|---|
| **Temp °C** | Case 1 | Case 2 (m=1, n=0) | Case 3 (m=0, n=1) | Case 4 (m=1, n=1) | Case 5 (m=2, n=0) | Case 6 (m=0, n=2) | Case 7 (m=2, n=1) | Case 8 (m=1, n=2) | Case 9 (m=3, n=0) | Case 10 (m=0, n=3) |
| **40** | 0.7396 | 0.8436 | 0.766 | 0.8676 | 0.9321 | 0.7921 | **0.9489** | 0.8924 | 0.9355 | 0.8177 |
| **50** | 0.6204 | 0.7432 | 0.6494 | 0.7687 | 0.8389 | 0.6781 | **0.8533** | 0.7934 | 0.8472 | 0.7061 |
| **60** | 0.6059 | 0.7439 | 0.6366 | 0.7711 | 0.8509 | 0.6672 | **0.8654** | 0.7966 | 0.8598 | 0.6972 |
| **70** | 0.5921 | 0.7589 | 0.627 | 0.79 | 0.8811 | 0.662 | **0.894** | 0.8179 | 0.8502 | 0.6966 |

Highest coefficient-of-correlation at each temperature is given in **bold**. Regression analysis for the reactions at all the four temperatures suggested a third order reaction with m = 2, n = 1. Hence the overall reaction order was 'three', second order with respect to triglyceride and first order with respect to methanol (Case 7 in Table 5.18). The 'slope' in this case is k

$[A_o]^2$ The rate equation, in terms of rate of disappearance of triglyceride, is: $-r_A = -\frac{d[A]}{dt} = k\,[A]^2\,[B]$, where *A* is triglyceride and *B* is methanol.

#### 5.3.3.2.3 Rate constant and Activation energy

Integrated form of rate equation in Case 7 (Table 5.18) is Eqn 2.40 (Chapter 2):

$$\frac{1}{(\alpha_B - 3)}\left(\frac{x_A}{1 - x_A} - \frac{3}{\alpha_B - 3}\right) ln\frac{(\alpha_B - 3x_A)}{(1 - x_A)\alpha_B} = k\,[A]_o^2\,t$$

L.H.S is F($x_A$) and RHS is a function of time *t*. Regression linear plot for F($x_A$) vs. *t* for 70°C (343K) is given in Fig 5.24. The ordinate is $\frac{1}{(\alpha_B-3)}\left(\frac{x_A}{1-x_A} - \frac{3}{\alpha_B-3}\right) ln\frac{(\alpha_B-3x_A)}{(1-x_A)\alpha_B}$, and abscissa is *t*. Reaction constant *k* is given by the slope of the plot ($R^2$ = 0.8940).

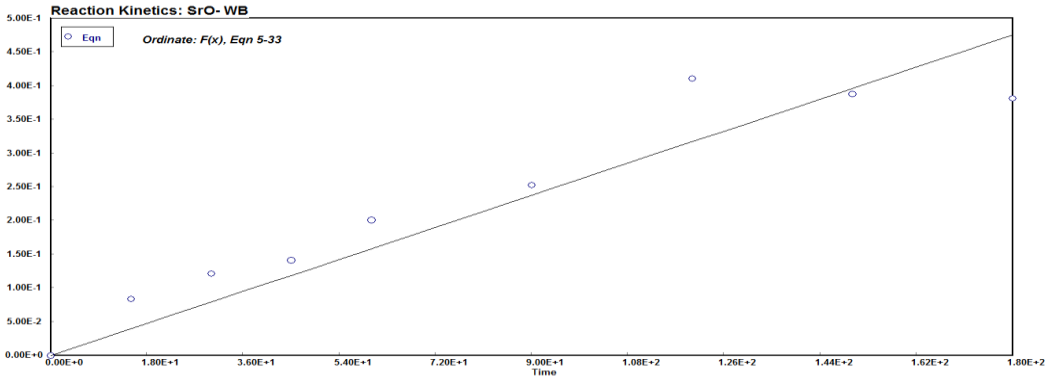


**Figure 5.24: Plot of kinetic equation 2.40 (WB)**

Correlation constants (k $[A_o]^2$ ) for Eqn 5.33 for the four temperatures were used to estimate reaction constant *k* as given in Table 5.19.

**Table 5.19: Reaction constant k (WB)**

| Temp °C | Temp K | $[Ao]^2$ .k | [Ao] | k |
|---|---|---|---|---|
| | | | g/cm3 | (in min) |
| **40** | 313.15 | 0.001104 | 0.6663 | 2.49E-03 |
| **50** | 323.15 | 0.001811 | 0.6663 | 4.08E-03 |
| **60** | 333.15 | 0.002267 | 0.6663 | 5.11E-03 |
| **70** | 343.15 | 0.002749 | 0.6663 | 6.19E-03 |

Activation energy was obtained from the slope of the plot of ln*k* vs. 1/T (Arrhenius plot, Section 2.5.4.1, Chapter 2). Fig 5.25 gives the plot.

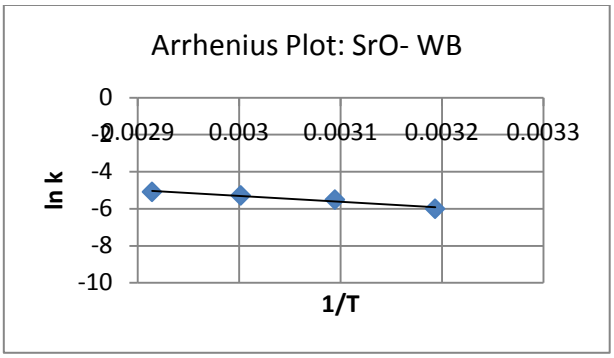


**Figure 5.25: Arrhenius plot for SrO catalyst (WB)**

The slope was 3200.7 ( $R^2$ = 0.9558), which gave the Activation energy, *E* = 26.61 kJ/mol; and intercept gave pre-exponential factor *A* = 73.7.

There is not much published literature on use of SrO as a transesterification catalyst. In a transesterification study of *Camelina sativa* oil using SrO catalyst and conventional heating, the reaction was of a similar order, and reaction constant was 0.0493 $g^2$ $mol^{-2}$ $min^{-1}$ (reaction temperature not mentioned) (Patil *et al*., 2011).

### 5.3.3.2.4 Optimization studies- experimental results and data analysis

Table 5.20 gives the details of a set of 20 experiments in terms of actual and coded levels, as per CCD, and the FAME yields obtained in transesterification studies. Table also gives predicted yield calculated from Reduced Model given by Eqn 5.4.

**Table 5.20: CCD matrix with experimental FAME yield (WB)**

| Run | Level of variables [actual(coded)] | | | Expt. Yield Y | Reduced Model (Eqn 5.4) |
|---|---|---|---|---|---|
| | Catalyst,% X1 | Temp, ($^o$C) X2 | Methanol :oil X3 | | Y |
| **1** | 1(0) | 60(0) | 9(0) | 71.5 | 72.3 |
| **2** | 1(0) | 43(-1.68) | 9(0) | 59.5 | 59.5 |
| **3** | 0.5(-1) | 70(1) | 12(1) | 69.3 | 68.7 |
| **4** | 1(0) | 60(0) | 14(1.68) | 74.3 | 73.5 |
| **5** | 1.84(1.68) | 60(0) | 9(0) | 72.0 | 71.1 |
| **6** | 1(0) | 60(0) | 4(-1.68) | 49.6 | 51.2 |
| **7** | 0.5(-1) | 50(-1) | 6(-1) | 47.0 | 45.8 |
| **8** | 1(0) | 60(0) | 9(0) | 72.9 | 72.3 |
| **9** | 1.5(1) | 70(1) | 12(1) | 73.9 | 74.6 |
| **10** | 1.5(1) | 70(1) | 6(-1) | 64.9 | 64.4 |
| **11** | 1(0) | 60(0) | 9(0) | 71.3 | 72.3 |
| **12** | 1.5(1) | 50(-1) | 6(-1) | 62.5 | 62.5 |
| **13** | 0.16(-1.68) | 60(0) | 9(0) | 50.3 | 52.0 |
| **14** | 1(0) | 60(0) | 9(0) | 72.1 | 72.3 |

| | | | | | |
|---|---|---|---|---|---|
| **15** | 1.5(1) | 50(-1) | 12(1) | 67.3 | 68.1 |
| **16** | 1(0) | 60(0) | 9(0) | 73.8 | 72.3 |
| **17** | 0.5(-1) | 50(-1) | 12(1) | 62.1 | 62.1 |
| **18** | 1(0) | 77(1.68) | 9(0) | 65.8 | 66.6 |
| **19** | 1(0) | 60(0) | 9(0) | 72.5 | 72.3 |
| **20** | 0.5(-1) | 70(1) | 6(-1) | 49.0 | 47.6 |

Data in Table 5.20 were tested for fit for a linear, two-factor interaction (2FI), quadratic and cubic polynomials. Table 5.21 gives the result.

**Table 5.21: Summary for model fit- Sequential model sum of squares (WB)**

| **Summary (detailed tables shown below)** | | | | | | |
|---|---|---|---|---|---|---|
| | **Sequential** | **Lack of Fit** | | **Adjusted** | **Predicted** | |
| **Source** | **p-value** | **p-value** | | **R-Squared** | **R-Squared** | |
| **Linear** | 0.0004 | 0.0002 | | 0.6104 | 0.5372 | |
| **2FI** | 0.6034 | 0.0001 | | 0.5820 | 0.3205 | |
| **Quadratic** | < 0.0001 | 0.1322 | | 0.9805 | 0.9380 | Suggested |
| **Cubic** | 0.1275 | 0.2282 | | 0.9886 | 0.7784 | Aliased |
| **Sequential Model Sum of Squares [Type I]** | | | | | | |
| | **Sum of** | | **Mean** | **F** | **p-value** | |
| **Source** | **Squares** | **df** | **Square** | **Value** | **Prob > F** | |
| **Mean vs Total** | 84708.13 | 1 | 84708.13 | | | |
| **Linear vs Mean** | 1105.64 | 3 | 368.55 | 10.92 | 0.0004 | |
| **2FI vs Linear** | 69.37 | 3 | 23.12 | 0.64 | 0.6034 | |
| **Quadratic vs 2FI** | 453.68 | 3 | 151.23 | 89.37 | < 0.0001 | Suggested |
| **Cubic vs Quadratic** | 10.98 | 4 | 2.75 | 2.77 | 0.1275 | Aliased |
| **Residual** | 5.94 | 6 | 0.99 | | | |
| **Total** | 86353.74 | 20 | 4317.69 | | | |

Highest $R^2$ was for a Cubic model but it was aliased. Next highest $R^2$ was for a Quadratic model. Considering the F value and p-value, Quadratic model was suggested. Cubic was not considered being aliased. The appropriate model for the given set of data was full Quadratic model (Eqn 4.2, Chapter 4) : $Y = b_0 + \sum_{i=1}^{n} b_i X_i + \sum_{i=1}^{n} b_{ii} X_i^2 + \sum_{1=1}^{n-1} \sum_{j=i+1}^{n} b_{ij} X_i X_j$ . Y is the Yield, $X_i$ are coded variables as given in Table 5.1. Table 5.22 gives Analysis of Variance (ANOVA) for a full quadratic model.

**Table 5.22: ANOVA for Response Surface Quadratic model (WB)**

| **ANOVA for Response Surface Quadratic model** |
|---|

| Analysis of variance table [Partial sum of squares - Type III] | | | | | |
|---|---|---|---|---|---|
| | Sum of | | Mean | F | p-value |
| Source | Squares | df | Square | Value | Prob > F |
| **Model** | 1628.69 | 9 | 180.97 | 106.94 | < 0.0001 |
| ***X1-SrO*** | *442.02* | *1* | *442.02* | *261.21* | *< 0.0001* |
| ***X2-Temp*** | *60.71* | *1* | *60.71* | *35.88* | *0.0001* |
| ***X3-Meth:oil*** | *602.91* | *1* | *602.91* | *356.29* | *< 0.0001* |
| ***X1.X2*** | *5.000E-003* | *1* | *5.000E-003* | *2.955E-003* | *0.9577* |
| ***X1.X3*** | *58.32* | *1* | *58.32* | *34.46* | *0.0002* |
| ***X2.X3*** | *11.05* | *1* | *11.05* | *6.53* | *0.0286* |
| ***X1^2*** | *209.09* | *1* | *209.09* | *123.56* | *< 0.0001* |
| ***X2^2*** | *154.92* | *1* | *154.92* | *91.55* | *< 0.0001* |
| ***X3^2*** | *179.19* | *1* | *179.19* | *105.89* | *< 0.0001* |
| **Residual** | 16.92 | 10 | 1.69 | | |
| ***Lack of Fit*** | *12.61* | *5* | *2.52* | *2.92* | *0.1322* |
| ***Pure Error*** | *4.32* | *5* | *0.86* | | |
| **Cor Total** | 1645.61 | 19 | | | |

The Model F-value of 106.94 implied the model was significant. There was only a 0.01% chance that an F-value this large could occur due to noise. Values of "Prob > F" less than 0.0500 indicate model terms are significant. In this case X1, X2, X3, X1.X3, X2.X3, X1^2, X2^2, X3^2 were significant model terms. The "Lack of Fit F-value" of 2.92 implied the Lack of Fit was not significant relative to the pure error. There was a 13.22% chance that a "Lack of Fit F-value" this large could occur due to noise. Non-significant lack of fit was good.

**Reduced Model:** In the full quadratic model, the term X1.X2 was not significant and model was simplified by dropping this interacting effect of X1 and X2. The model was analyzed for ANOVA after dropping X1.X2 from the full quadratic expression. Table 5.23 gives the results.

**Table 5.23: ANOVA for Response Surface for Reduced Quadratic model (WB)**

| ANOVA for Response Surface Reduced Quadratic model | | | | | | |
|---|---|---|---|---|---|---|
| Analysis of variance table [Partial sum of squares - Type III] | | | | | | |
| | Sum of | | Mean | F | p-value | |
| Source | Squares | df | Square | Value | Prob > F | |
| **Model** | 1628.69 | 8 | 203.59 | 132.30 | < 0.0001 | significant |
| ***X1-SrO*** | *442.02* | *1* | *442.02* | *287.25* | *< 0.0001* | |
| ***X2-Temp*** | *60.71* | *1* | *60.71* | *39.46* | *< 0.0001* | |
| ***X3-Meth:oil*** | *602.91* | *1* | *602.91* | *391.81* | *< 0.0001* | |
| ***X1.X3*** | *58.32* | *1* | *58.32* | *37.90* | *< 0.0001* | |
| ***X2.X3*** | *11.04* | *1* | *11.04* | *7.18* | *0.0214* | |
| ***X1^2*** | *209.09* | *1* | *209.09* | *135.88* | *< 0.0001* | |
| ***X2^2*** | *154.92* | *1* | *154.92* | *100.68* | *< 0.0001* | |
| ***X3^2*** | *179.19* | *1* | *179.19* | *116.45* | *< 0.0001* | |

| | | | | | | |
|---|---|---|---|---|---|---|
| **Residual** | 16.93 | 11 | 1.54 | | | |
| ***Lack of Fit*** | *12.61* | *6* | *2.10* | *2.44* | *0.1736* | *not significant* |
| ***Pure Error*** | *4.32* | *5* | *0.86* | | | |
| **Cor Total** | 1645.61 | 19 | | | | |

The Model F-value of 132.30 implies the model was significant. There is only a 0.01% chance that an F-value this large could occur due to noise. Values of "Prob > F" less than 0.0500 indicate model terms are significant. In this case X1, X2, X3, X1.X3, X2.X3, X1^2, X2^2, X3^2 were significant model terms. The "Lack of Fit F-value" of 2.44 implied the Lack of Fit was not significant relative to the pure error. There was a 17.36% chance that a "Lack of Fit F-value" this large could occur due to noise. Table 5.24 gives R-Square values.

**Table 5.24: R-Square values (WB)**

| | | | |
|---|---|---|---|
| **Std. Dev.** | **1.24** | **R-Squared** | **0.9897** |
| **Mean** | 65.08 | **Adj R-Squared** | 0.9822 |
| **C.V. %** | 1.91 | **Pred R-Squared** | 0.9519 |
| **PRESS** | 79.23 | **Adeq Precision** | 34.709 |

In Table 5.24, the "Pred R-Squared" of 0.9519 was in reasonable agreement with the "Adj R-Squared" of 0.9822; i.e. the difference was less than 0.2. "Adeq Precision" measures the signal to noise ratio. A ratio greater than 4 is desirable. Present model had a ratio of 34.709 which indicated an adequate signal. This model can be used for design purposes. Table 5.25 gives the coefficients for the reduced model.

**Table 5.25: Coefficients for the Reduced Quadratic Model (WB)**

| | Coefficient | | Standard | 95% CI | 95% CI |
|---|---|---|---|---|---|
| **Factor** | **Estimate** | **df** | **Error** | **Low** | **High** |
| **Intercept** | 72.33 | 1 | 0.51 | 71.21 | 73.44 |
| **X1-SrO** | 5.69 | 1 | 0.34 | 4.95 | 6.43 |
| **X2-Temp** | 2.11 | 1 | 0.34 | 1.37 | 2.85 |
| **X3-Meth:oil** | 6.64 | 1 | 0.34 | 5.91 | 7.38 |
| **X1.X3** | -2.70 | 1 | 0.44 | -3.67 | -1.73 |
| **X2.X3** | 1.18 | 1 | 0.44 | 0.21 | 2.14 |
| **X1^2** | -3.81 | 1 | 0.33 | -4.53 | -3.09 |
| **X2^2** | -3.28 | 1 | 0.33 | -4.00 | -2.56 |
| **X3^2** | -3.53 | 1 | 0.33 | -4.24 | -2.81 |

Since all the terms in the reduced model are significant, no further reductions were needed. Hence the model was:

$$\text{Yield, } Y = 72.33 + 5.69\,X1 + 2.11\,X2 + 6.64\,X3 - 2.70\,X1.X3 + 1.18\,X2.X3 - 3.81\,X1^2 - 3.28\,X2^2 - 3.53\,X3^2 \quad \ldots 5.4$$

Reduced model was used to estimate Predicted yield given in Table 5.20. Eqn 5.4 was used for response surface plots.

#### 5.3.3.2.5 Response Surface and Contour Plots

Fig 5.26 is a RSM plot giving response surface and contours for FAME yield as a function of SrO catalyst concentration and reaction temperature. The optima was close to catalyst concentration of 1.25 -1.5 mass% and a temperature of 60 -70$^{o}$C (333 -343K). These agreed with the experimental observations.

Fig 5.27 is a RSM plot giving response surface and contours for FAME yield as a function of SrO catalyst concentration and methanol to oil ratio. The optima was close to catalyst concentration of 1.25 mass% and a methanol to oil ratio of 10.5:1. These agreed well with the experimental observations.

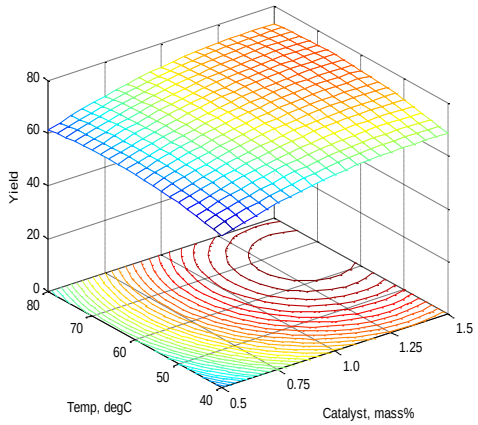


**Figure 5.26: RSM plot- Effect of SrO conc. and Temperature on Yield (WB)**

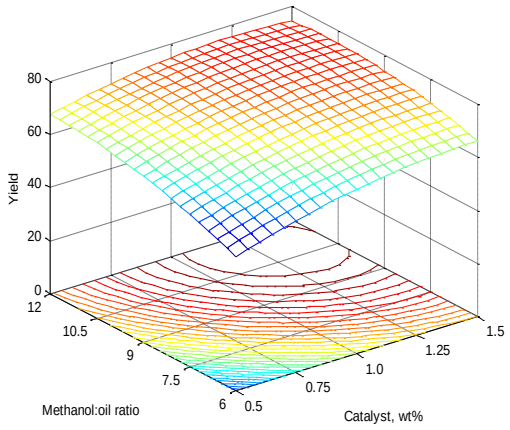


**Figure 5.27: RSM plot- Effect of Catalyst conc. and Methanol:oil ratio on Yield (WB)**

Fig 5.28 is a RSM plot giving response surface and contours for FAME yield as a function of reaction temperature and methanol to oil ratio. The optima was close to a temperature of

70$^{o}$C (343K) and a methanol to oil ratio of 11:1. These agreed well with the experimental findings.

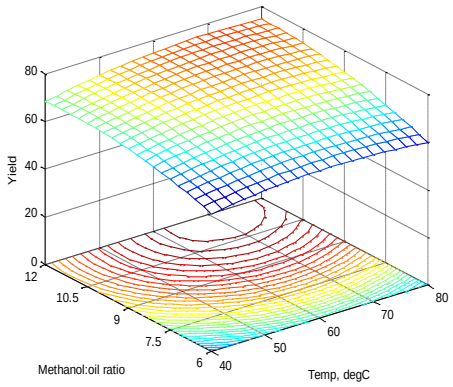


**Figure 5.28: RSM plot- Effect of Methanol:oil ratio and Temperature on Yield (WB)**

### 5.3.4 Studies with Microwave Irradiation- Strontium oxide catalyst

This section deals with transesterification of Croton *megalocarpus* oil using heterogeneous SrO catalyst with microwave irradiation. Studies include effect of operation variables on FAME yield, transesterification reaction kinetics and optimization.

#### 5.3.4.1 Effect of operation variables on FAME yield

##### 5.3.4.1.1 Effect of methanol to triglyceride molar ratio on FAME yield

Transesterification reaction (Eqn 2.2, Chapter 2) is a reversible reaction requiring 3 moles methanol to each mole of triglyceride. In practice an excess of methanol is always employed to drive the reaction in the forward direction to favour FAME formation. Reactions were carried out with 1mass% of SrO catalyst for 5 min at full microwave power. Methanol to oil ratios were 6:1, 9:1, 12:1, 15:1. Batch consisted of 25 ml of Croton *megalocarpus* oil (FFA = 1.7). Fig 5.29 gives the fame yield as a function of methanol to oil ratio.

FAME yield increased with the increase of methanol to oil ratio from 6 to 9, and from 9 to 12. Maximum FAME yield of 72.9% corresponded to the ratio of 12:1. Yield dropped slightly as the methanol ratio was increased to 15:1, to 71.2%. This drop in yield beyond a certain methanol to oil ratio has been observed in earlier such studies. Reasons given were: dilution of catalyst at excess methanol, glycerol forming an emulsion with FAME in presence of excess methanol reducing FAME separation, and methanol dissolving in

glycerol bringing about separation problems (Kim *et al*., 2004). There is very limited published work on use of SrO catalyst for transesterification under microwave. A maximum FAME yield of 98% is reported for microwave irradiated transesterification of *Camelina sativa* oil at 9:1 methanol to oil ratio, 1.5 mass% SrO catalyst; and the yield dropped as the methanol to oil ratio was increased further (Patil *et al*., 2010).

#### 5.3.4.1.2 Effect of catalyst concentration on FAME yield

Fig 5.30 gives FAME yield as a function of SrO concentration. FAME yield increased with the increase in SrO concentration. The increase was more prominent from 0.5 – 1.0 mass% SrO, after which there was no substantive change. A maximum yield of 68.7% corresponding to 2 mass% SrO. Patil *et al*.(2010) have reported an optimum concentration of 1.5 mass% SrO and 4 min reaction time for 98% yield of FAME from *Camelina Sativa* oil using microwave irradiation.

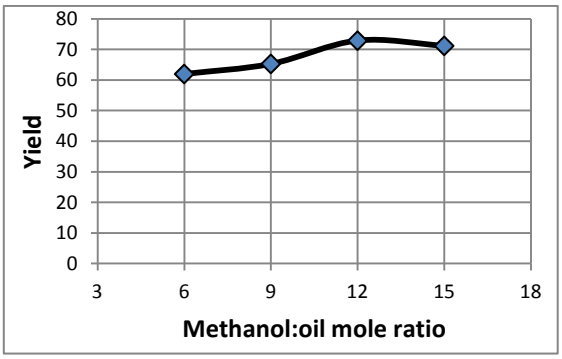


**Figure 5.29: FAME yield as a function of Methanol: oil ratio (MW)**

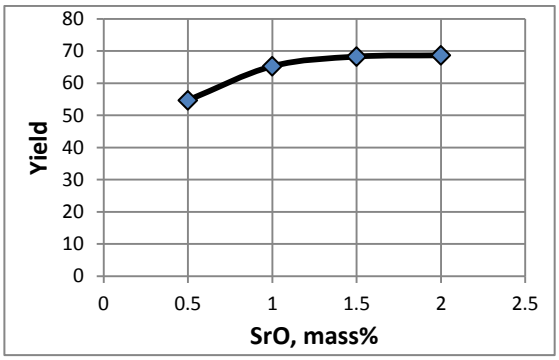


**Figure 5.30: FAME yield as a function of SrO concentration (MW)**

#### 5.3.4.1.3 Effect of reaction time on FAME yield

An yield of 45.1% was obtained after 30s of reaction time. Yield increased with time although the increase was very little after 2 min of reaction time. FAME yields at 2, 3, 4 and 5 min were 66.0, 68.1, 67.9 and 68.7% respectively. Fig 5.31 gives the effect of reaction time on FAME yield at full microwave power and it shows that the reaction time had little effect on yield after 2 min of reaction time.

#### 5.3.4.1.4 Effect of microwave power

Fig 5.32 gives the effect of microwave power on FAME yield. Yield increased with the rise in power since microwave power is directly related to microwave irradiation. The increase was more steep when power was increased from 40 to 80%. After a power level of

80%, the rise in yield was small. The increase in FAME yield from 80 to 100% of power was from 66.3 to 68.7% .

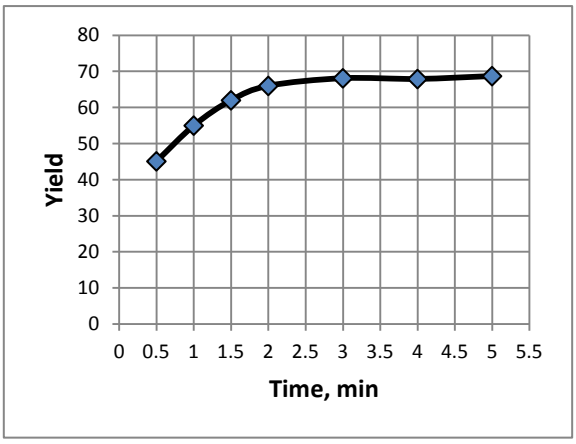


**Figure 5.31: Effect of reaction time on Yield**

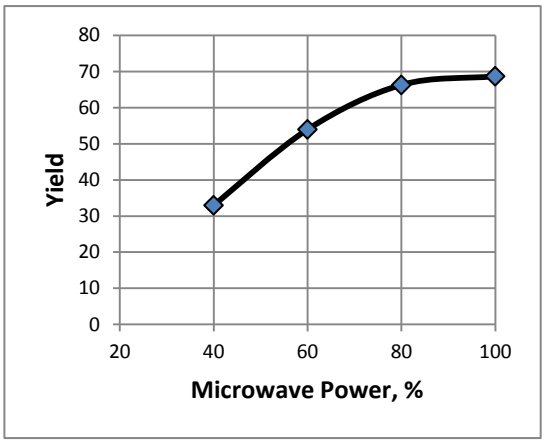


**Figure 5.32: The effect of microwave power on Yield**

#### 5.3.4.1.5 Effect of Time on FAME yield

Fig 5.33 is a plot of FAME yield vs. reaction time at varying reaction temperatures. Conversions at 50$^{o}$C (323K) were much lower and the FAME yield at the end of 90s was 48%. Reactions at 60$^{o}$C (333K) were also slow in the beginning but increased later to give almost the same yield as that at 70$^{o}$C (343K). The final yields at the end of 90s, at 60$^{o}$C (333K) and 70$^{o}$C (343K) were 65.0 and 68.3% respectively.

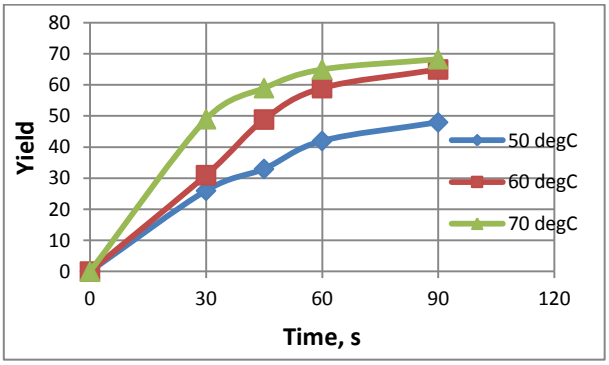


**Figure 5.33: Variation of Yield with time at various temperatures (MW)**

#### 5.3.4.1.6 Order of reaction

Table 5.26 gives the coefficients of correlation for all reaction orders, Cases 1 to 10, at the three temperatures.

**Table 5.26: Coefficients of correlation, R2, for various reaction orders (MW)**

| | 0th Order | 1st Order | | 2nd Order | | | 3rd Order | | | |
|---|---|---|---|---|---|---|---|---|---|---|
| **Temp °C** | Case 1 | Case 2 (m=1, n=0) | Case 3 (m=0, n=1) | Case 4 (m=1, n=1) | Case 5 (m=2, n=0) | Case 6 (m=0, n=2) | Case 7 (m=2, n=1) | Case 8 (m=1, n=2) | Case 9 (m=3, n=0) | Case 10 (m=0, n=3) |
| **50** | .9083 | .9542 | .9215 | .9638 | .9835 | .9340 | **.9872** | .9731 | .9870 | .9455 |
| **60** | .9003 | .9547 | .9149 | .9615 | .9620 | .9281 | **.9625** | .9613 | .9240 | .9395 |
| **70** | .7714 | .8618 | .7905 | .8803 | .9402 | .8098 | **.9517** | .8977 | .8775 | .8291 |

Highest correlation coefficients are in bold numbers in Table 5.26. The most likely order of reaction was 'three'; second order with respect to triglyceride, and first order with respect to methanol (Case 7). The integrated form of rate equation is Eqn 2.40 (Chapter 2) given as: $\frac{1}{(\alpha_B-3)}\left(\frac{x_A}{1-x_A}-\frac{3}{\alpha_B-3}\right) ln\frac{(\alpha_B-3x_A)}{(1-x_A)\alpha_B} = k\,[A]_o^2\,t$ . The slope in this case is = k $[A_o]^2$.

### 5.3.4.1.7 Rate constant and Activation energy

L.H.S. of Eqn 2.40,( $\frac{1}{(\alpha_B-3)}\left(\frac{x_A}{1-x_A}-\frac{3}{\alpha_B-3}\right) ln\frac{(\alpha_B-3x_A)}{(1-x_A)\alpha_B}$ ) is a function of conversion $x_A$ , F($x_A$), or the yield. A plot of F($x_A$) vs time *t* is a straight line passing through the origin. Regression linear plot for F($x_A$) vs. *t* for 70°C (343K) is given in Fig 5.34. The ordinate is, $\frac{1}{(\alpha_B-3)}\left(\frac{x_A}{1-x_A}-\frac{3}{\alpha_B-3}\right) ln\frac{(\alpha_B-3x_A)}{(1-x_A)\alpha_B}$ ) and abscissa is *t*. Reaction constant *k* is given by the slope of the plot ($R^2$ = 0.9517).

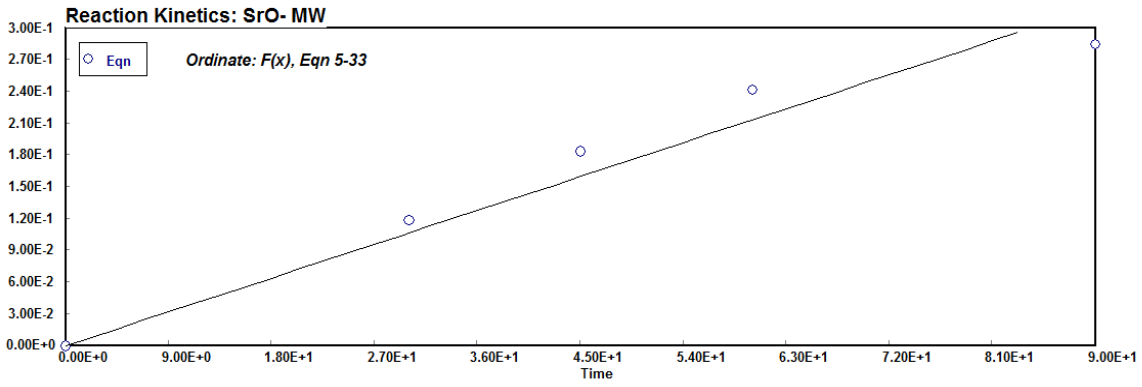


**Figure 5.34: Plot of kinetic equation 2.40 (MW)**

Correlation constants (k $[A_o]^2$ ) for Eqn 2.40 for the three temperatures were used to estimate reaction constant *k* as given in Table 5.27.

**Table 5.27: Reaction constant k (MW)**

| Temp, °C | Temp K | $[Ao]^2$ .k | [Ao] | k |
|---|---|---|---|---|
| | | | g/cm3 | in min |
| **50** | 323.15 | 0.00133 | 0.6663 | 1.80E-01 |
| **60** | 333.15 | 0.00275 | 0.6663 | 3.72E-01 |
| **70** | 343.15 | 0.003611 | 0.6663 | 4.88E-01 |

Activation energy is obtained from the slope of the plot of ln*k* vs. 1/T (Arrhenius plot, Section 2.5.4.1). Fig 5.35 gives the plot ($R^2$ = 0.9437).

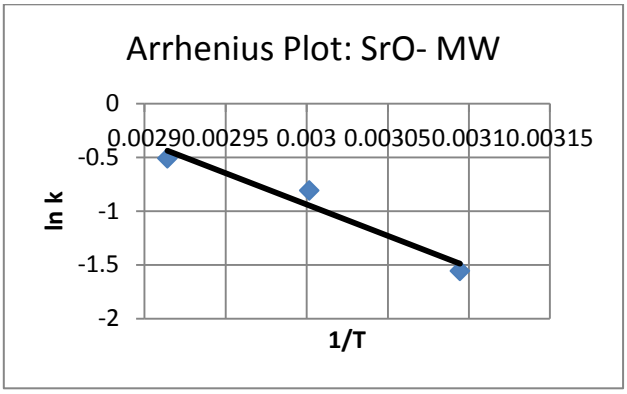


**Figure 5.35: Arrhenius plot for SrO (MW)**

Slope of the plot was 5558.85, giving Activation energy, *E* = 46.22 kJ/mol; and intercept gave pre-exponential factor $A = 5.67 \times 10^6$.

### 5.3.4.1.8 Optimization studies- experimental results and data analysis

Table 5.28 gives the details of a set of 20 experiments in terms of actual and coded levels, as per CCD, and the FAME yields obtained in transesterification studies. Table also gives the Predicted yield obtained from Reduced model given by Eqn 5.5.

**Table 5.28: CCD matrix with experimental FAME yield (MW)**

| Run | Level of variables [actual(coded)] | | | Experimental Yield | Reduced Model (Eqn 5.5) |
|---|---|---|---|---|---|
| | Catalyst,% | Time (min) | Methanol :oil | | Y |
| | X1 | X2 | X3 | | |
| **1** | 1(0) | 3(0) | 9(0) | 68.5 | 68.4 |
| **2** | 1(0) | 0.5(-1.68) | 9(0) | 56.6 | 56.6 |

| | | | | | |
|---|---|---|---|---|---|
| **3** | 0.5(-1) | 4.5(1) | 12(1) | 56.5 | 56.9 |
| **4** | 1(0) | 3(0) | 14(1.68) | 61.3 | 61.0 |
| **5** | 1.84(1.68) | 3(0) | 9(0) | 66.7 | 66.7 |
| **6** | 1(0) | 3(0) | 4(-1.68) | 51.1 | 51.5 |
| **7** | 0.5(-1) | 1.5(-1) | 6(-1) | 54.3 | 54.7 |
| **8** | 1(0) | 3(0) | 9(0) | 68.3 | 68.4 |
| **9** | 1.5(1) | 4.5(1) | 12(1) | 71.4 | 71.3 |
| **10** | 1.5(1) | 4.5(1) | 6(-1) | 51.8 | 52.2 |
| **11** | 1(0) | 3(0) | 9(0) | 68.1 | 68.4 |
| **12** | 1.5(1) | 1.5(-1) | 6(-1) | 62.2 | 61.5 |
| **13** | 0.16(-1.68) | 3(0) | 9(0) | 49.0 | 49.5 |
| **14** | 1(0) | 3(0) | 9(0) | 68.0 | 68.4 |
| **15** | 1.5(1) | 1.5(-1) | 12(1) | 60.9 | 61.3 |
| **16** | 1(0) | 3(0) | 9(0) | 68.9 | 68.4 |
| **17** | 0.5(-1) | 1.5(-1) | 12(1) | 47.1 | 47.0 |
| **18** | 1(0) | 5.5(1.68) | 9(0) | 57.1 | 57.9 |
| **19** | 1(0) | 3(0) | 9(0) | 68.3 | 68.4 |
| **20** | 0.5(-1) | 4.5(1) | 6(-1) | 46.1 | 45.4 |

Data in Table 5.28 were tested for fit for a linear, two-factor interaction (2FI), quadratic and cubic polynomials. Table 5.29 gives the result.

**Table 5.29: Summary for model fit- Sequential model sum of squares (MW)**

| **Summary for model fit** | | | | | |
|---|---|---|---|---|---|
| | **Sequential** | **Lack of Fit** | **Adjusted** | **Predicted** | |
| **Source** | **p-value** | **p-value** | **R-Squared** | **R-Squared** | |
| **Linear** | 0.0492 | < 0.0001 | 0.2627 | 0.0810 | |
| **2FI** | 0.2430 | < 0.0001 | 0.3345 | -0.1625 | |
| **Quadratic** | < 0.0001 | 0.1020 | 0.9967 | 0.9874 | Suggested |
| **Cubic** | 0.0387 | 0.9646 | 0.9987 | 0.9994 | Aliased |
| **Sequential Model Sum of Squares [Type I]** | | | | | |
| | **Sum of** | | **Mean** | **F** | **p-value** |
| **Source** | **Squares** | **df** | **Square** | **Value** | **Prob > F** | |
| **Mean vs Total** | 72264.24 | 1 | 72264.24 | | | |
| **Linear vs Mean** | 490.05 | 3 | 163.35 | 3.26 | 0.0492 | |
| **2FI vs Linear** | 213.93 | 3 | 71.31 | 1.58 | 0.2430 | |
| **Quadratic vs 2FI** | 586.32 | 3 | 195.44 | 859.88 | < 0.0001 | Suggested |

| | | | | | | |
|---|---|---|---|---|---|---|
| **Cubic vs Quadratic** | 1.76 | 4 | 0.44 | 5.12 | 0.0387 | Aliased |
| **Residual** | 0.52 | 6 | 0.086 | | | |
| **Total** | 73556.82 | 20 | 3677.84 | | " | |

Cubic had the highest $R^2$ (0.9994), followed by $R^2$ for Quadratic model (0.9874). However, cubic was not suitable because of being aliased. Considering the F and p-values, a Quadratic model was suggested. The appropriate model for the given set of data was full Quadratic model (Eqn 4.2, Chapter 4) :

$$Y = b_0 + \sum_{i=1}^{n} b_i X_i + \sum_{i=1}^{n} b_{ii} X_i^2 + \sum_{1=1}^{n-1} \sum_{j=i+1}^{n} b_{ij} X_i X_j$$

Y is the FAME yield, $X_i$ are coded variables as given in Table 5.2.

Table 5.30 gives Analysis of Variance (ANOVA) for a full quadratic model.

**Table 5.30: ANOVA for Response Surface Quadratic model (MW)**

| **ANOVA for Response Surface Quadratic model** | | | | | | |
|---|---|---|---|---|---|---|
| **Analysis of variance table [Partial sum of squares - Type III]** | | | | | | |
| **Source** | **Sum of Squares** | **df** | **Mean Square** | **F Value** | **p-value Prob > F** | |
| **Model** | 1290.31 | 9 | 143.37 | 630.77 | < 0.0001 | significant |
| ***X1-SrO*** | *380.30* | *1* | *380.30* | *1673.21* | *< 0.0001* | |
| ***X2-Time*** | *0.34* | *1* | *0.34* | *1.48* | *0.2522* | |
| ***X3-Methanol:oil*** | *109.41* | *1* | *109.41* | *481.36* | *< 0.0001* | |
| ***X1.X2*** | *0.15* | *1* | *0.15* | *0.67* | *0.4336* | |
| ***X1.X3*** | *28.50* | *1* | *28.50* | *125.40* | *< 0.0001* | |
| ***X2.X3*** | *185.28* | *1* | *185.28* | *815.17* | *< 0.0001* | |
| ***X1^2*** | *198.39* | *1* | *198.39* | *872.86* | *< 0.0001* | |
| ***X2^2*** | *238.00* | *1* | *238.00* | *1047.12* | *< 0.0001* | |
| ***X3^2*** | *265.68* | *1* | *265.68* | *1168.89* | *< 0.0001* | |
| **Residual** | 2.27 | 10 | 0.23 | | | |
| ***Lack of Fit*** | *1.76* | *5* | *0.35* | *3.41* | *0.1020* | *not significant* |
| ***Pure Error*** | *0.52* | *5* | *0.10* | | | |
| **Cor Total** | 1292.58 | 19 | | | | |

The Model F-value of 630.77 implied the model was significant. There was only a 0.01% chance that an F-value this large could occur due to noise. Values of "Prob > F" less than 0.0500 indicate model terms are significant. In this case X1, X3, X1.X3, X2.X3, X1^2, X2^2, X3^2 were significant model terms. X3 and X1.X2 were not significant because p-values were > 0.1000.

**Reduced model:** Model was simplified by dropping non-significant terms which were X1 and X1.X2. However X1 could not be dropped since it was part of model hierarchy. Hence X1.X2 being the cross coefficient of SrO concentration and Time was dropped from the full quadratic model. Table 5.31 gives the ANOVA for the reduced model.

**Table 5.31: ANOVA for Response Surface Quadratic (Reduced) model (MW)**

| **ANOVA for Response Surface Reduced Quadratic model** | | | | | | |
|---|---|---|---|---|---|---|
| **Analysis of variance table [Partial sum of squares - Type III]** | | | | | | |
| | **Sum of** | | **Mean** | **F** | **p-value** | |
| **Source** | **Squares** | **df** | **Square** | **Value** | **Prob > F** | |
| **Model** | 1290.15 | 8 | 161.27 | 731.79 | < 0.0001 | significant |
| ***X1-SrO*** | *380.30* | *1* | *380.30* | *1725.69* | *< 0.0001* | |
| ***X2-Time*** | *0.34* | *1* | *0.34* | *1.52* | *0.2429* | |
| ***X3-Methanol:oil*** | *109.41* | *1* | *109.41* | *496.46* | *< 0.0001* | |
| ***X1.X3*** | *28.50* | *1* | *28.50* | *129.33* | *< 0.0001* | |
| ***X2.X3*** | *185.28* | *1* | *185.28* | *840.74* | *< 0.0001* | |
| ***X1^2*** | *198.39* | *1* | *198.39* | *900.24* | *< 0.0001* | |
| ***X2^2*** | *238.00* | *1* | *238.00* | *1079.96* | *< 0.0001* | |
| ***X3^2*** | *265.68* | *1* | *265.68* | *1205.55* | *< 0.0001* | |
| **Residual** | 2.42 | 11 | 0.22 | | | |
| ***Lack of Fit*** | *1.91* | *6* | *0.32* | *3.09* | *0.1182* | *not significant* |
| ***Pure Error*** | *0.52* | *5* | *0.10* | | | |
| **Cor Total** | 1292.58 | 19 | | | | |

The Model F-value of 731.79 implied the model was significant. There was only a 0.01% chance that an F-value this large could occur due to noise. Values of "Prob > F" less than 0.0500 indicate model terms are significant. In this case X1, X3, X1.X3, X2.X3, X1^2, X2^2, X3^2 were significant model terms. The "Lack of Fit F-value" of 3.09 implied the Lack of Fit was not significant. There was a 11.82% chance that a "Lack of Fit F- value" this large could occur due to noise. Table 5.32 gives the $R^2$ values for the reduced model.

**Table 5.32: R-Square values**

| | | | |
|---|---|---|---|
| **Std. Dev.** | **0.47** | **R-Squared** | **0.9981** |
| **Mean** | 60.11 | **Adj R-Squared** | 0.9968 |
| **C.V. %** | 0.78 | **Pred R-Squared** | 0.9920 |
| **PRESS** | 10.34 | **Adeq Precision** | 82.052 |

The "Pred R-Squared" of 0.9920 was in reasonable agreement with the "Adj R-Squared" of 0.9968; i.e. the difference was less than 0.2. "Adeq Precision" measures the signal to noise ratio. A ratio greater than 4 is desirable. This model's ratio of 82.052 indicated an adequate

signal. This model can be used for design purposes. Table 5.33 gives the coefficients for the reduced quadratic model.

**Table 5.33: Coefficients for the Reduced Quadratic model**

| Factor | Coefficient Estimate | df | Standard Error | 95% CI Low | 95% CI High |
|---|---|---|---|---|---|
| **Intercept** | 68.35 | 1 | 0.19 | 67.93 | 68.77 |
| **X1-SrO** | 5.28 | 1 | 0.13 | 5.00 | 5.56 |
| **X2-Time** | 0.16 | 1 | 0.13 | -0.12 | 0.44 |
| **X3-Methanol:oil** | 2.83 | 1 | 0.13 | 2.55 | 3.11 |
| **X1.X3** | 1.89 | 1 | 0.17 | 1.52 | 2.25 |
| **X2.X3** | 4.81 | 1 | 0.17 | 4.45 | 5.18 |
| **X1^2** | -3.71 | 1 | 0.12 | -3.98 | -3.44 |
| **X2^2** | -4.06 | 1 | 0.12 | -4.34 | -3.79 |
| **X3^2** | -4.29 | 1 | 0.12 | -4.56 | -4.02 |

Since all the terms in the reduced model were significant, no further reductions were needed. Hence the model was:

$$\text{Yield, } Y = 68.35 + 5.28\,X1 + 0.16\,X2 + 2.83\,X3 + 1.89\,X1.X3 + 4.81\,X2.X3 - 3.71\,X1^2 - 4.06\,X2^2 - 4.29\,X3^2 \quad \ldots 5.5$$

Reduced model was used to compute Predicted yield as given in Table 5.28. In the following section, Eqn 5.5 was used for response surface plots.

#### 5.3.4.1.9 Response Surface and Contour Plots

Fig 5.36, 5.37 and 5.38 give the RSM surface and contour plots based on Eqn 5.5.

In Fig 5.36, FAME yield increased with increasing SrO concentration and did not change much with time after an initial period of 1.5 min. Contour plot suggested optimal FAME yield corresponding to a catalyst concentration of >1.25 mass% and a reaction time of 3 min. In Eqn 5.5, coefficient for time (X2) is 0.16 (insignificant) which accounts for weak affect of 'time' variable. These agreed well with experimental observations.

Fig 5.37 is a RSM plot for effect of SrO concentration and methanol to oil ratio on FAME yield. Contour plot indicated catalyst concentration of >1.25% and methanol to oil ratio of 10.5:1 for the maximum FAME yield. This agreed with experimental observations.

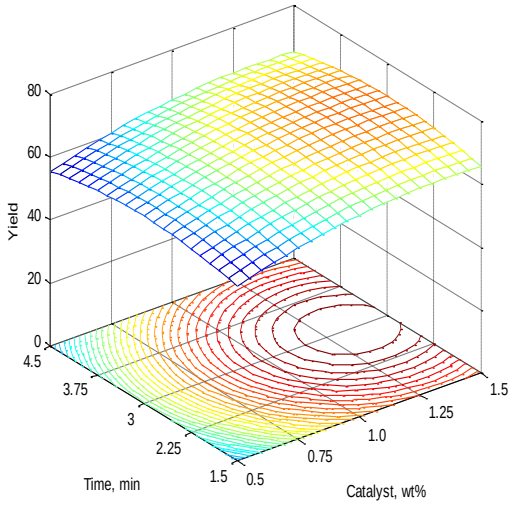


**Figure 5.36: RSM plot- Effect of SrO conc. and Time on Yield (MW)**

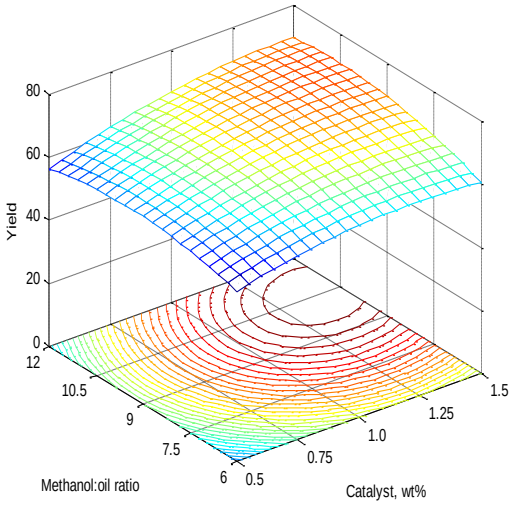


**Figure 5.37: RSM plot- Effect of SrO conc and Methanol:oil ratio on Yield (MW)**

Contour plot in Fig 5.38 identified region of maximum yield corresponding to methanol to oil ratio of 10.5:1, and reaction time > 3 min. These were in agreement with experimental findings.

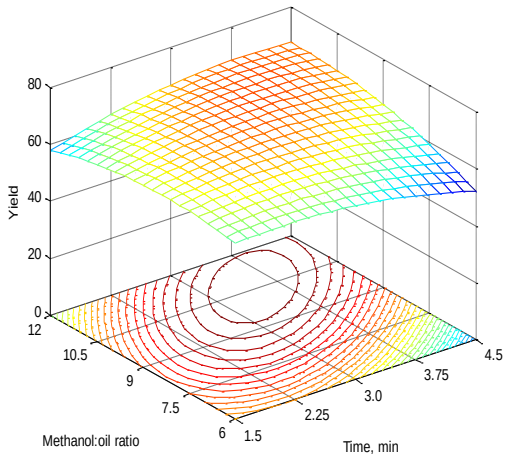


**Figure 5.38: RSM plot- Effect of Time and Methanol:oil ratio on Yield (MW)**

### 5.3.5 Studies with conventional heating- Nano calcium oxide, Re-oxidized calcium oxide and Calcium oxide catalysts

This section deals with transesterification studies carried out with conventional heating employing a water bath as a heat source.

#### 5.3.5.1 Effect of operation variables on FAME yield

Effect of reaction operating variables on FAME yield are presented in this section. Results are presented in form of figures containing yield data for all the three catalysts. This would help in getting a feel of relative activities of the three catalysts. Operating variables studied were (i) Methanol to triglyceride molar ratio, (ii) Catalyst concentration, and (iii) Reaction temperature. Effect of reaction time on FAME yield was studied under reaction kinetics.

##### 5.3.5.1.1 Effect of Methanol to triglyceride mole ratio on FAME yield

Methanol to oil molar ratio was varied as 6:1, 9:1, 12:1, 15:1. Batch consisted of 30 ml of Croton *megalocarpus* oil (FFA = 1.7), catalyst 1% by mass of oil. Reaction temperature was 70$^{o}$C (343K), and reaction time 2 h. Fig 5.39 gives the FAME yield for Nano CaO, CaO RO and CaO as a function methanol to oil molar ratio.

Nano CaO showed the highest activity followed by CaO RO and CaO. Highest yield corresponded to a methanol to oil ratio of 9:1 for all the three catalysts. The highest yields obtained for Nano CaO, CaO RO and CaO were 73.2, 41.5 and 31.5% respectively. The yield decreased at methanol ratios higher than 9:1. At very high methanol ratios, glycerol dissolves in excessive methanol and subsequently inhibits the forward reaction (Viriya-empikul *et al*., 2010). Other explanation for reducing yield is that catalyst concentration decreases with excess methanol (Liu *et al*., 2008; Bambase *et al*., 2007). Excess methanol affects the interphase area between alcohol and oil due to their immiscibility leading to a drop in yield (Babak *et al*., 2013). There is no reported study for the use of these catalysts for Croton *megalocarpus* oil. Hsiao *et al*. (2011) obtained a 96.9% FAME yield with Nano CaO on soybean oil at 7:1 methanol to oil ratio, at 65$^{o}$C (338K). Extreme variations in yield have been reported for CaO catalyst transesterification. It ranges from ‘no conversion’ (Reddy *et al*., 2006) to 99% conversion (Kouze *et al*., 2008). Table 2.3 (Chapter 2) gives an extensive account of various reported studies. Variations in

pretreatment of CaO is one major reason for yield inconsistencies. Calcination under inert atmosphere gives a far higher activity compared to incineration under atmospheric conditions. CaO RO was a new catalyst tested and it gave a better performance as compared to CaO.

#### 5.3.5.1.2 Effect of catalyst concentration on FAME yield

Effect of catalyst concentration on FAME yield was studied using catalyst concentrations of 0.5 – 3 mass% based on oil mass. Batch consisted of 30 ml of Croton *megalocarpus* oil (FFA = 1.7), methanol to oil ratio of 9:1, reaction temperature 70$^{o}$C (343K), reaction time 2 h, and catalyst concentrations varied as 0.5, 1, 1.5, 2, 3 mass%. Fig 5.40 gives the effect of Nano CaO, CaO RO and CaO concentrations on FAME yield. For Nano CaO and CaO, maximum yields of 74.9 and 32.6% respectively were obtained at 1.5 mass%. For CaO RO the maximum yield of 43% was at 2 mass% catalyst, which was slightly above the yield of 42.8% obtained at 1.5 mass%. For all the three catalyst samples, yield declined at higher catalyst ratios of 2.5 and 3 mass%. This decline in yield was more noticeable for Nano CaO and CaO (about 5%), but was negligible for CaO-RO (1.5%). Higher concentrations of calcium catalysts lead to calcium soap formation resulting into lowering of yield (Hsiao *et al.*, 2011).

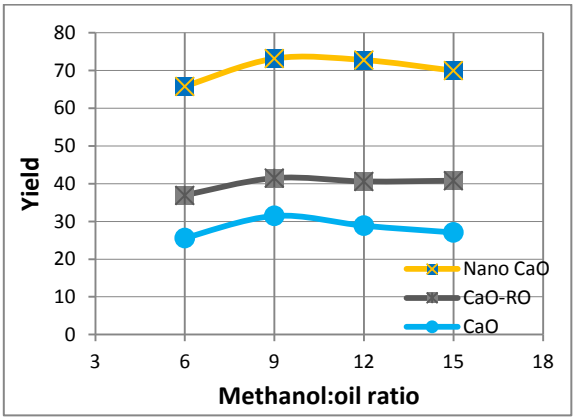


**Figure 5.39: Effect of Meth. :oil ratio on Yield(WB)**

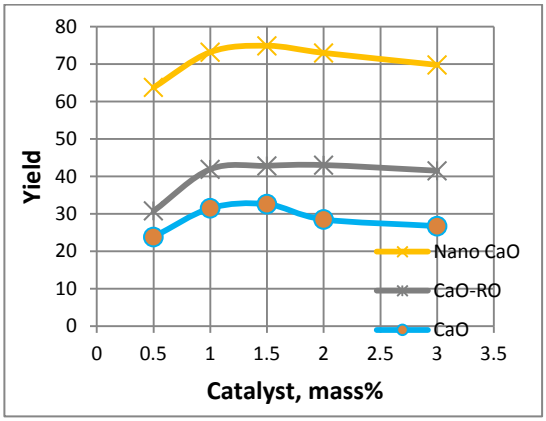


**Figure 5.40: Effect of Catalyst conc. on Yield**

#### 5.3.5.1.3 Effect of Temperature on FAME yield

Fig 5.41 gives the effect of reaction temperature on FAME yield. Mass transfer resistances have been eliminated by using high stirring speed, leaving surface reaction as being a rate

controlling step. Reactions were carried out at constant catalyst concentration of 1 mass%, methanol to oil molar ratio of 9:1, and reaction time of 2 h. Reaction temperatures were 40, 50, 60 and 70$^{o}$C (313, 323, 333, 343 K) respectively.

FAME yield increased with temperature for Nano CaO, CaO-RO and CaO catalysts. Increase in rate was more noticeable when temperatures were increased from 40 to 50, and from 50 to 60$^{o}$C (313 to 323, and 323 to 333K). After 60$^{o}$C (333K) the yield increased marginally. For Nano CaO, CaO RO and CaO, the yields at 60$^{o}$C (333K) were 69.8, 39.0 and 30.8%; and at 70$^{o}$C (343K) were 73.2; 41.5; and 31.5% respectively. Nano CaO was found to be the most effective catalyst followed by CaO RO and CaO.

#### 5.3.5.2 Reaction Kinetics

Results for Nano CaO, CaO RO and CaO are presented separately in the following sections.

##### 5.3.5.2.1 Nano Calcium oxide

###### 5.3.5.2.1.1 Effect of Time on FAME yield

Fig 5.42 is a plot of FAME yields for Nano CaO catalyst at temperatures of 40, 50, 60, 70$^{o}$C (313, 323, 333, 343 K) for a time period of 3h. Yields increased with reaction temperature and with time. At 40$^{o}$C (313K) the initial reaction rates were far lower when compared to 50, 60 and 70$^{o}$C (323, 333 and 343 K) as shown by the slopes at the origin for the conversion curves. The final yields at the end of 3h for the temperatures of 40, 50, 60, 70$^{o}$C (313, 323, 333, 343 K) were 52.4, 68.0, 71.8 and 74.5% respectively. At 70$^{o}$C (343K) the yield became almost constant after 2h, increasing only by 1%, from 73.2 to 74.5%. Similar trend was noted at 60$^{o}$C (333K) as well. At lower temperatures of 40 and 50$^{o}$C (313 and 323K) corresponding increase in yield was 4 – 7%.

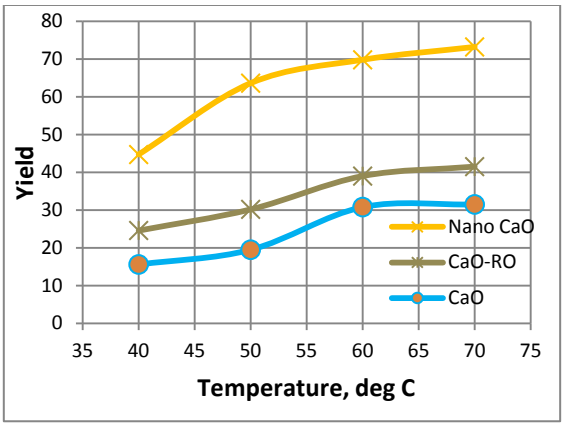


**Figure 5.41: Effect of Reaction temp. on Yield (WB)**

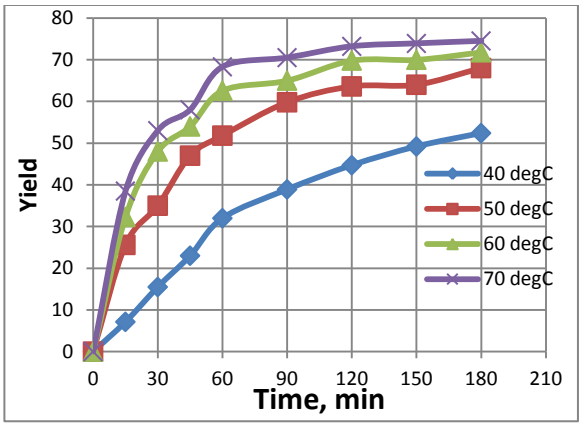


**Figure 5.42: Variation of Yield with time at various temperatures for Nano CaO (WB)**

#### 5.3.5.2.1.2 Order of reaction

Kinetic data (Fig 5.42) were fitted into integrated forms of reaction rate equations to get the reaction order. Equations 2.34 – 2.43 (Chapter 2) are the integrated form of rate equations covering overall reaction orders from 'zero' to 'three'. L.H.S. of these equations are functions of conversion or Yield, F($x_A$); and the R.H.S. is function of reaction time, *t*. These equations are in the form of y = mx (passing through origin). For all the ten cases, F($x_A$) is correlated with time *t*, and the coefficient-of-determination obtained for a linear regression passing through the origin. This was done for temperatures of 40, 50, 60 and 70$^o$C (313, 323, 333 and 334K). Equation with the highest correlation coefficient ($R^2$), at a given temperature was taken to be representing the most likely reaction order. Table 5.34 gives the coefficients of correlation, $R^2$, for all the ten cases of reaction orders, and for all temperatures. Indices *m* and *n* refer to the general rate equation: $-r_A = -\frac{d[A]}{dt} = k\,[A]^m\,[B]^n$ (Eqn 2.29, Chapter 2), where *A* is triglyceride and *B* is methanol.

**Table 5.34: Coefficients of correlation, R2, for various reaction orders for Nano CaO (WB)**

| | 0th Order | 1st Order | | 2nd Order | | | 3rd Order | | | |
|---|---|---|---|---|---|---|---|---|---|---|
| **Temp $^o$C** | Case 1 | Case 2 (m=1, n=0) | Case 3 (m=0, n=1) | Case 4 (m=1, n=1) | Case 5 (m=2, n=0) | Case 6 (m=0, n=2) | Case 7 (m=2, n=1) | Case 8 (m=1, n=2) | Case 9 (m=3, n=0) | Case 10 (m=0, n=3) |

| | | | | | | | | | | |
|---|---|---|---|---|---|---|---|---|---|---|
| **40** | 0.901 | 0.955 | 0.9166 | 0.9658 | 0.9884 | 0.931 | **0.9924** | 0.9762 | 0.9915 | 0.9444 |
| **50** | 0.6929 | 0.8201 | 0.7225 | 0.8464 | 0.9248 | 0.7517 | **0.9413** | 0.8718 | 0.919 | 0.7801 |
| **60** | 0.5915 | 0.734 | 0.6214 | 0.7633 | 0.8647 | 0.6515 | **0.8857** | 0.7911 | 0.8489 | 0.6814 |
| **70** | 0.5434 | 0.6906 | 0.5727 | 0.7196 | 0.8261 | 0.6024 | **0.8465** | 0.7463 | 0.8144 | 0.632 |

In Table 5.34, Case 7 had the highest $R^2$ values for all the four temperatures (in bold). This corresponded to an overall third order reaction, second order with respect to triglyceride and first order with respect to methanol. The 'slope' in this case is = k $[A_o]^2$ The rate equation, in terms of rate of disappearance of triglyceride, was: $-r_A = -\frac{d[A]}{dt} = k\,[A]^2\,[B]$.

#### 5.3.5.2.1.3 Rate constant and Activation energy

Integrated form of rate of reaction in Case 7 (Table 5.34) is Eqn 2.40 (Chapter 2):

$$\frac{1}{(\alpha_B - 3)}\left(\frac{x_A}{1 - x_A} - \frac{3}{\alpha_B - 3}\right) ln\frac{(\alpha_B - 3x_A)}{(1 - x_A)\alpha_B} = k\,[A]_o^2\,t$$

L.H.S is F($x_A$) or F(yield) and RHS is a function of time *t*. Regression linear plot for F($x_A$) vs. *t* for 70°C (343K) for Nano CaO is given in Fig 5.43. The ordinate is $\frac{1}{(\alpha_B-3)}\left(\frac{x_A}{1-x_A} - \frac{3}{\alpha_B-3}\right) ln\frac{(\alpha_B-3x_A)}{(1-x_A)\alpha_B}$, and abscissa is *t*. Reaction constant *k* is given by the slope of the plot ($R^2$ = 0.8465).

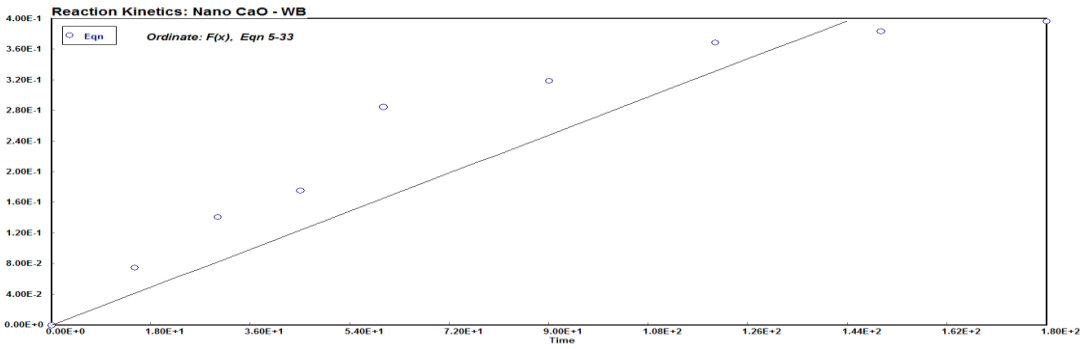


**Figure 5.43: Plot of kinetic equation 2.40 for Nano CaO (WB)**

Correlation constants (k $[A_o]^2$ ) for Eqn 2.40 for the four temperatures were used to estimate reaction constant *k* ( $cm^6\ mol^{-2}\ min^{-1}$) as given in Table 5.35.

**Table 5.35: Reaction rate constant k for Nano CaO (WB)**

| Temp °C | Temp K | $[Ao]^2$ .k | [Ao] | k |
|---|---|---|---|---|

| | | | g/cm3 | (in min) |
|---|---|---|---|---|
| **40** | 313.15 | 0.0008 | 0.6663 | 1.80E-03 |
| **50** | 323.15 | 0.001762 | 0.6663 | 3.97E-03 |
| **60** | 333.15 | 0.002367 | 0.6663 | 5.33E-03 |
| **70** | 343.15 | 0.002511 | 0.6663 | 5.65E-03 |

Activation energy was obtained from the slope of the plot of ln*k* vs. 1/T (Arrhenius plot, Section 2.5.4.1, Chapter 2). Fig 5.44 gives the plot.

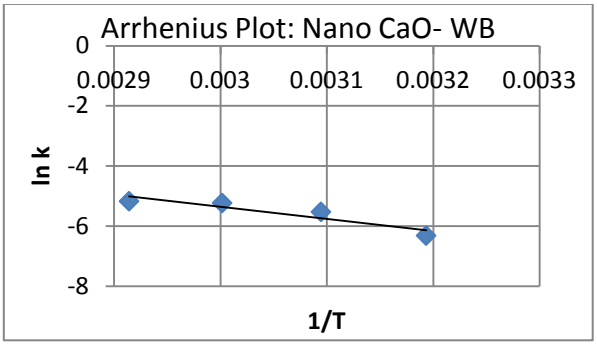


**Figure 5.44: Arrhenius plot for Nano CaO catalyst (WB)**

The slope was 4047.84 ( $R^2$ = 0.8550), which gave the Activation energy, *E* = 33.65 kJ/mol, and intercept gave pre-exponential factor, *A* = 880.

### 5.3.5.2.2 Re-oxidized Calcium oxide

#### 5.3.5.2.2.1 Effect of Time on FAME yield

Fig 5.45 gives FAME yield for CaO RO catalyst at temperatures of 40, 50, 60, 70$^o$C (313, 323, 333, 343 K) for a time period of 3h. Yields increased with reaction temperature and with time. Yields became almost constant after 2h for temperatures of 40, 60 and 70$^o$C (313, 333, 343 K). Final yields after 3h at 40, 50, 60, 70$^o$C (313, 323, 333, 343 K) were 25.5, 34.6, 40.8 and 41.8% of FAME. The yields at 60, 70$^o$C (333, 343 K) were very close.

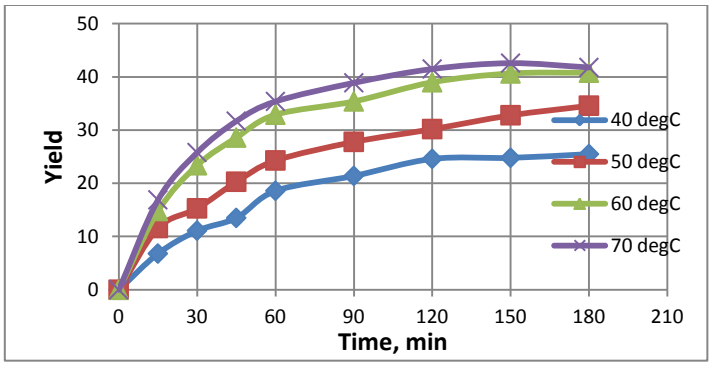


**Figure 5.45: Variation of Yield with time at various temperatures for CaO-RO (WB)**

#### 5.3.5.2.2.2 Order of reaction

Kinetics data in Fig 5.45 were fitted into integrated forms of reaction rate equations to get the reaction order as given earlier in Section 5.3.5.2.1.2. Table 5.36 gives the coefficients of correlation, $R^2$, for all the ten cases of reaction orders.

**Table 5.36: Coefficients of correlation, $R^2$, for various reaction orders for CaO-RO**

| | 0th Order | 1st Order | | 2nd Order | | | 3rd Order | | | |
|---|---|---|---|---|---|---|---|---|---|---|
| **Temp °C** | Case 1 | Case 2 (m=1, n=0) | Case 3 (m=0, n=1) | Case 4 (m=1, n=1) | Case 5 (m=2, n=0) | Case 6 (m=0, n=2) | Case 7 (m=2, n=1) | Case 8 (m=1, n=2) | Case 9 (m=3, n=0) | Case 10 (m=0, n=3) |
| **40** | 0.7977 | 0.8273 | 0.8068 | 0.8358 | 0.8548 | 0.8157 | **0.8626** | 0.8461 | 0.8799 | 0.8245 |
| **50** | 0.7765 | 0.8267 | 0.7912 | 0.8406 | 0.8736 | 0.8058 | **0.8862** | 0.8571 | 0.9152 | 0.8201 |
| **60** | 0.6816 | 0.743 | 0.6987 | 0.7597 | 0.8023 | 0.7156 | **0.8177** | 0.7789 | 0.8562 | 0.7325 |
| **70** | 0.6338 | 0.6941 | 0.6503 | 0.7103 | 0.7526 | 0.6667 | **0.7676** | 0.7289 | 0.806 | 0.6831 |

In Table 5.36, Case 7 has the highest $R^2$ values for all the four temperatures (in bold). This corresponds to an overall third order reaction, second order with respect to triglyceride and first order with respect to methanol. The 'slope' in this case is = k $[A_o]^2$

#### 5.3.5.2.2.3 Rate constant and Activation energy

Integrated form of rate reaction in Case 7 (Table 5.36) is Eqn 2.40 (Chapter 2):

$$\frac{1}{(\alpha_B - 3)}\left(\frac{x_A}{1 - x_A} - \frac{3}{\alpha_B - 3}\right) ln\frac{(\alpha_B - 3x_A)}{(1 - x_A)\alpha_B} = k\,[A]_o^2\,t$$

L.H.S is F($x_A$) or F(yield) and RHS is a function of time *t*. Regression linear plot for F($x_A$) vs. *t* for 70°C (343K) for CaO RO is given in Fig 5.46. The ordinate is $\frac{1}{(\alpha_B-3)}\left(\frac{x_A}{1-x_A}\right.$ –

$\frac{3}{\alpha_B - 3}\Big) ln \frac{(\alpha_B - 3x_A)}{(1-x_A)\alpha_B}$, and abscissa is *t*. Reaction constant *k* is given by the slope of the plot ($R^2$ = 0.7676).

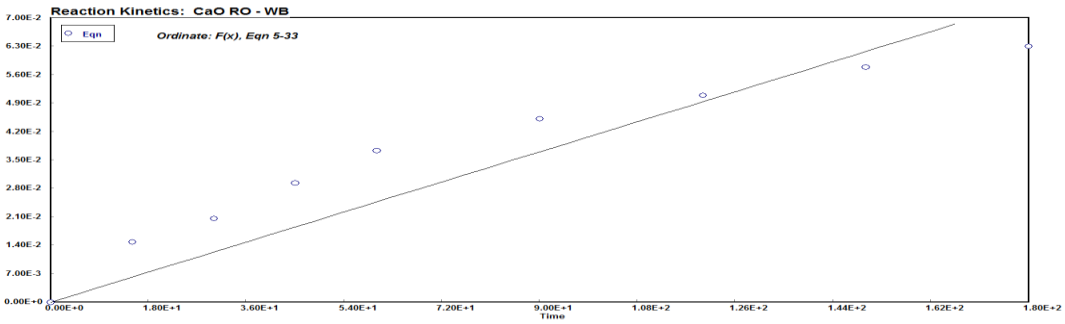


**Figure 5.46: Plot of kinetic equation 2.40 for CaO RO (WB)**

Correlation constants (k $[A_o]^2$ ) for Eqn 2.40 for the four temperatures were used to estimate reaction rate constant *k* ($cm^6\ mol^{-2}\ min^{-1}$) as given in Table 5.37.

**Table 5.37: Reaction rate constant for CaO RO (WB)**

| Temp °C | Temp K | $[Ao]^2$ .k | [Ao] | k |
|---|---|---|---|---|
| | | | g/cm3 | (in min) |
| **40** | 313.15 | 0.000291 | 0.6663 | 6.56E-04 |
| **50** | 323.15 | 0.000429 | 0.6663 | 9.67E-04 |
| **60** | 333.15 | 0.000631 | 0.6663 | 1.42E-03 |
| **70** | 343.15 | 0.000707 | 0.6663 | 1.59E-03 |

Activation energy was obtained from the slope of the plot of ln*k* vs. 1/T (Arrhenius plot, Section 2.5.4.1, Chapter 2). Fig 5.47 gives the plot.

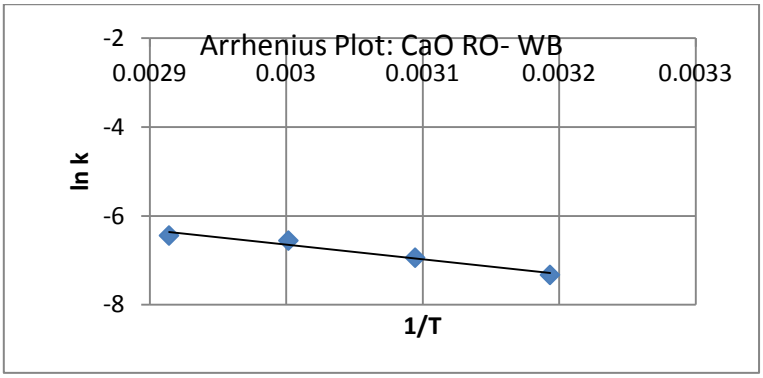


**Figure 5.47: Arrhenius plot for CaO-RO catalyst (WB)**

The slope was 3289.87 ( $R^2$ = 0.9636), which gave the Activation energy, *E* = 27.35 kJ/mol, and intercept gave pre-exponential factor, *A* = 25.

#### 5.3.5.2.3 Calcium oxide

##### 5.3.5.2.3.1 Effect of Time on FAME yield

Fig 5.48 gives FAME yield for CaO catalyst at temperatures of 40, 50, 60, 70°C (313, 323, 333, 343 K) for a time period of 3h. Yields increased with reaction temperature and with time. Yields were poor at temperature of 40°C (313K). There were little variations in yield after 2h for temperatures of 40, 60 and 70°C (313, 333, 343 K). Final yields after 3h at 40, 50, 60, 70°C (313, 323, 333, 343 K) were 17.3, 24.6, 29.2 and 31.8% of FAME. Figure shows that the yields at 60, 70°C (333, 343 K) were close.

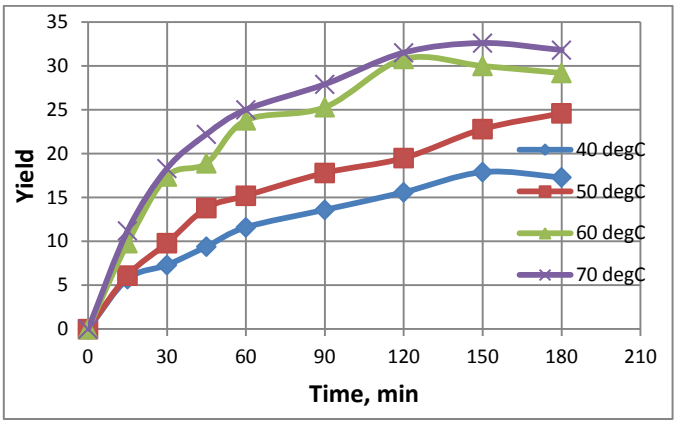


**Figure 5.48: Variation of Yield with time at various temperatures for CaO (WB)**

##### 5.3.5.2.3.2 Order of reaction

Kinetics data for Fig 5.48 were fitted into integrated forms of reaction rate equations to get the reaction order as given earlier in Section 9.3.1.2.1.2. Table 5.38 gives the coefficients of correlation, $R^2$, for all the ten cases of reaction orders.

**Table 5.38: Coefficients of correlation, $R^2$, for various reaction orders for CaO (WB)**

| | 0th Order | 1st Order | | 2nd Order | | | 3rd Order | | | |
|---|---|---|---|---|---|---|---|---|---|---|
| **Temp °C** | Case 1 | Case 2 (m=1, n=0) | Case 3 (m=0, n=1) | Case 4 (m=1, n=1) | Case 5 (m=2, n=0) | Case 6 (m=0, n=2) | Case 7 (m=2, n=1) | Case 8 (m=1, n=2) | Case 9 (m=3, n=0) | Case 10 (m=0, n=3) |
| **40** | 0.8185 | 0.8403 | 0.8254 | 0.8569 | 0.8611 | 0.8322 | **0.8673** | 0.8552 | 0.8605 | 0.839 |
| **50** | 0.8375 | 0.8686 | 0.847 | 0.8777 | 0.8978 | 0.8565 | **0.9061** | 0.8888 | 0.9041 | 0.8659 |

| | | | | | | | | | | |
|---|---|---|---|---|---|---|---|---|---|---|
| **60** | 0.7005 | 0.7378 | 0.7117 | 0.7478 | 0.7727 | 0.7227 | **0.7823** | 0.761 | 0.7739 | 0.7336 |
| **70** | 0.6962 | 0.741 | 0.7093 | 0.7537 | 0.7841 | 0.7223 | **0.796** | 0.7689 | 0.724 | 0.7352 |

In Table 5.38, Case 7 had the highest $R^2$ values at all the four temperatures (in bold). This corresponded to an overall third order reaction, second order with respect to triglyceride and first order with respect to methanol. The 'slope' in this case is = k $[A_o]^2$.

#### 5.3.5.2.3.3 Rate constant and Activation energy

Integrated form of reaction rate in Case 7 (Table 5.38) is Eqn 2.40 (Chapter 2):

$$\frac{1}{(\alpha_B - 3)}\left(\frac{x_A}{1 - x_A} - \frac{3}{\alpha_B - 3}\right) ln\frac{(\alpha_B - 3x_A)}{(1 - x_A)\alpha_B} = k\,[A]_o^2\,t$$

L.H.S is F($x_A$) or F(yield) and RHS is a function of time *t*. Regression linear plot for F($x_A$) vs. *t* for 70°C (343K) for CaO is given in Fig 5.49. The ordinate is $\frac{1}{(\alpha_B-3)}\left(\frac{x_A}{1-x_A} - \frac{3}{\alpha_B-3}\right) ln\frac{(\alpha_B-3x_A)}{(1-x_A)\alpha_B}$, and abscissa is *t*. Reaction constant *k* is given by the slope of the plot ($R^2$ = 0.7960).

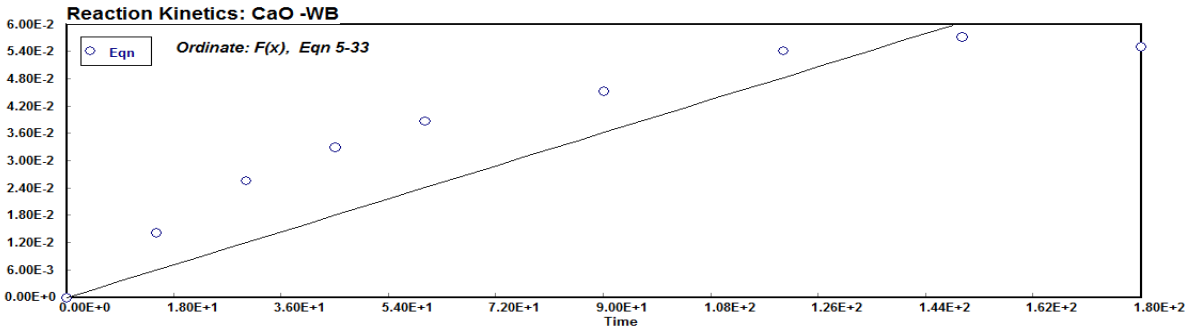


**Figure 5.49: Plot of kinetic equation 2.40 for CaO (WB)**

Correlation constants (k $[A_o]^2$ ) for Eqn 2.40 for the four temperatures were used to estimate reaction rate constant *k* ($cm^6\ mol^{-2}\ min^{-1}$) as given in Table 5.39.

**Table 5.39: Reaction rate constant for CaO (WB)**

| Temp °C | Temp K | $[Ao]^2$ .k | [Ao] | k |
|---|---|---|---|---|
| | | | g/cm3 | (in min) |
| **40** | 313.15 | 0.000175 | 0.6663 | 3.94E-04 |
| **50** | 323.15 | 0.000247 | 0.6663 | 5.57E-04 |
| **60** | 333.15 | 0.000394 | 0.6663 | 8.87E-04 |
| **70** | 343.15 | 0.000436 | 0.6663 | 9.83E-04 |

Activation energy was obtained from the slope of the plot of ln*k* vs. 1/T (Arrhenius plot, Section 2.5.4.1, Chapter 2). Fig 5.50 gives the plot.

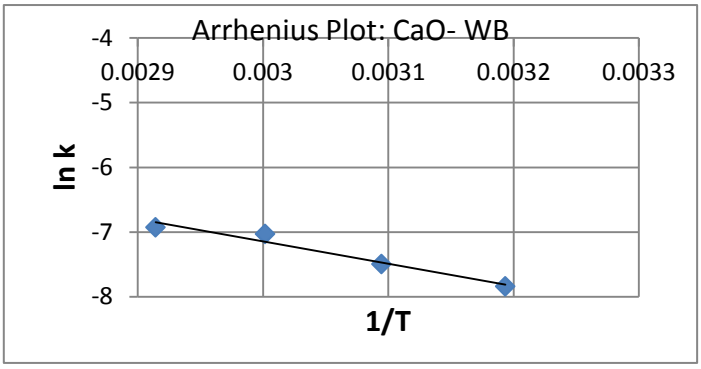


**Figure 5.50: Arrhenius plot for CaO catalyst (WB)**

The slope was 3457.33 ( $R^2$ = 0.9592), which gave the Activation energy, *E* = 28.74 kJ/mol, intercept gave pre-exponential factor, *A* = 25.3.

Literature on transesterification kinetics of CaO catalysts is limited. Singh and Fernando (2007) reported a first order reaction with respect to methanol with *k* = 0.0046 $min^{-1}$ at high pressure and high temperature (215$^oC$, 488K) for soybean oil. Patil *et al*. (2011) also report a first order reaction with respect to methanol and *k* = 0.0006 $min^{-1}$ for *Camelina sativa* oil at 100$^oC$ (373K).

#### 5.3.5.2.3.4 Optimization studies- Experimental results and data analysis

Table 5.40 gives the details of a set of 20 experiments in terms of actual and coded levels, as per CCD, and the FAME yields obtained in transesterification studies. Table also gives Predicted yield as per Quadratic model given by Eqn 5.6.

**Table 5.40: CCD matrix with experimental FAME yield for Nano CaO (WB)**

| Run | Level of variables [actual(coded)] | | | Expt. Yield Y | Quadratic Model (Eqn 5.6) |
|---|---|---|---|---|---|
| | Catalyst,% X1 | Temp, ($^oC$) X2 | Methanol :oil X3 | | Y |
| **1** | 1(0) | 60(0) | 9(0) | 69.3 | 69.8 |
| **2** | 1(0) | 43(-1.68) | 9(0) | 54.1 | 53.8 |
| **3** | 0.5(-1) | 70(1) | 12(1) | 65.3 | 66.3 |
| **4** | 1(0) | 60(0) | 14(1.68) | 66.2 | 65.4 |
| **5** | 1.84(1.68) | 60(0) | 9(0) | 70.1 | 70.0 |
| **6** | 1(0) | 60(0) | 4(-1.68) | 58.9 | 59.6 |
| **7** | 0.5(-1) | 50(-1) | 6(-1) | 52.5 | 53.1 |

| | | | | | |
|---|---|---|---|---|---|
| **8** | 1(0) | 60(0) | 9(0) | 70.0 | 69.8 |
| **9** | 1.5(1) | 70(1) | 12(1) | 73.5 | 73.0 |
| **10** | 1.5(1) | 70(1) | 6(-1) | 70.5 | 70.9 |
| **11** | 1(0) | 60(0) | 9(0) | 69.7 | 69.8 |
| **12** | 1.5(1) | 50(-1) | 6(-1) | 61.5 | 60.6 |
| **13** | 0.16(-1.68) | 60(0) | 9(0) | 58.1 | 58.1 |
| **14** | 1(0) | 60(0) | 9(0) | 69.1 | 69.8 |
| **15** | 1.5(1) | 50(-1) | 12(1) | 57.9 | 59.1 |
| **16** | 1(0) | 60(0) | 9(0) | 70.2 | 69.8 |
| **17** | 0.5(-1) | 50(-1) | 12(1) | 58.1 | 57.8 |
| **18** | 1(0) | 77(1.68) | 9(0) | 69.5 | 69.7 |
| **19** | 1(0) | 60(0) | 9(0) | 70.5 | 69.8 |
| **20** | 0.5(-1) | 70(1) | 6(-1) | 59.2 | 58.0 |

Data in Table 5.40 were tested for fit for a linear, two-factor interaction (2FI), quadratic and cubic polynomials. Table 5.41 gives the result.

**Table 5.41: Summary for model fit- Sequential model sum of squares for Nano CaO (WB)**

| **Summary (detailed tables shown below)** | | | | | | |
|---|---|---|---|---|---|---|
| | **Sequential** | **Lack of Fit** | | **Adjusted** | **Predicted** | |
| **Source** | **p-value** | **p-value** | | **R-Squared** | **R-Squared** | |
| **Linear** | 0.0006 | < 0.0001 | | 0.5858 | 0.5002 | |
| **2FI** | 0.5558 | < 0.0001 | | 0.5631 | 0.2003 | |
| **Quadratic** | < 0.0001 | 0.0555 | | 0.9800 | 0.9221 | Suggested |
| **Cubic** | 0.0188 | 0.7948 | | 0.9942 | 0.9914 | Aliased |
| **Sequential Model Sum of Squares [Type I]** | | | | | | |
| | **Sum of** | | **Mean** | **F** | **p-value** | |
| **Source** | **Squares** | **df** | **Square** | **Value** | **Prob > F** | |
| **Mean vs Total** | 83747.68 | 1 | 83747.68 | | | |
| **Linear vs Mean** | 515.80 | 3 | 171.93 | 9.96 | 0.0006 | |
| **2FI vs Linear** | 39.52 | 3 | 13.17 | 0.72 | 0.5558 | |
| **Quadratic vs 2FI** | 228.42 | 3 | 76.14 | 91.43 | < 0.0001 | Suggested |
| **Cubic vs Quadratic** | 6.87 | 4 | 1.72 | 7.05 | 0.0188 | Aliased |
| **Residual** | 1.46 | 6 | 0.24 | | | |
| **Total** | 84539.76 | 20 | 4226.99 | | | |

Highest $R^2$ is for a Cubic model but it was aliased. Next highest $R^2$ was for a Quadratic model. Considering the F value and p-value, Quadratic model was suggested. Cubic was not considered being aliased. The appropriate model for the given set of data was full Quadratic model (Eqn 4.2, Chapter 4) :

$$Y = b_0 + \sum_{i=1}^{n} b_i X_i + \sum_{i=1}^{n} b_{ii} X_i^2 + \sum_{1=1}^{n-1} \sum_{j=i+1}^{n} b_{ij} X_i X_j \qquad ..4.2$$

Y is the Yield, $X_i$ are coded variables as given in Table 5.1. Table 5.42 gives Analysis of Variance (ANOVA) for a full quadratic model.

**Table 5.42: ANOVA for Response Surface Quadratic model for Nano CaO (WB)**

| **ANOVA for Response Surface Quadratic model** | | | | | | |
|---|---|---|---|---|---|---|
| **Analysis of variance table [Partial sum of squares - Type III]** | | | | | | |
| | **Sum of** | | **Mean** | **F** | **p-value** | |
| **Source** | **Squares** | **df** | **Square** | **Value** | **Prob > F** | |
| **Model** | 783.75 | 9 | 87.08 | 104.57 | < 0.0001 | significant |
| ***X1-Nano CaO*** | *172.11* | *1* | *172.11* | *206.67* | *< 0.0001* | |
| ***X2-Temp*** | *303.68* | *1* | *303.68* | *364.66* | *< 0.0001* | |
| ***X3-Meth:oil*** | *40.02* | *1* | *40.02* | *48.05* | *< 0.0001* | |
| ***X1.X2*** | *14.31* | *1* | *14.31* | *17.18* | *0.0020* | |
| ***X1.X3*** | *18.91* | *1* | *18.91* | *22.71* | *0.0008* | |
| ***X2.X3*** | *6.30* | *1* | *6.30* | *7.57* | *0.0205* | |
| ***X1^2*** | *59.53* | *1* | *59.53* | *71.49* | *< 0.0001* | |
| ***X2^2*** | *116.70* | *1* | *116.70* | *140.13* | *< 0.0001* | |
| ***X3^2*** | *95.96* | *1* | *95.96* | *115.23* | *< 0.0001* | |
| **Residual** | 8.33 | 10 | 0.83 | | | |
| ***Lack of Fit*** | *6.89* | *5* | *1.38* | *4.78* | *0.0555* | *not significant* |
| ***Pure Error*** | *1.44* | *5* | *0.29* | | | |
| **Cor Total** | 792.08 | 19 | | | | |

The Model F-value of 104.57 implied the model was significant. There was only a 0.01% chance that an F-value this large could occur due to noise. Values of "Prob > F" less than 0.0500 indicate model terms are significant. In this case X1, X2, X3, X1.X2, X1.X3, X2.X3, X1^2, X2^2, X3^2 were significant model terms. The "Lack of Fit F-value" of 4.78 implied there was a 5.55% chance that a "Lack of Fit F-. value" this large could occur due to noise. Lack of fit was not very good but since p-value > 0.05, it was insignificant and acceptable. Table 5.43 gives R-Square values.

**Table 5.43: R-Square values for Nano CaO (WB)**

| **Std. Dev.** | **0.91** | **R-Squared** | **0.9895** |
|---|---|---|---|
| **Mean** | 64.71 | **Adj R-Squared** | 0.9800 |
| **C.V. %** | 1.41 | **Pred R-Squared** | 0.9221 |
| **PRESS** | 61.70 | **Adeq Precision** | 30.922 |

The "Pred R-Squared" of 0.9221 was in reasonable agreement with the "Adj R-Squared" of 0.9800; i.e. the difference was less than 0.2. "Adeq Precision" measures the signal to noise ratio. A ratio greater than 4 is desirable. Ratio of 30.922 in the present model indicated an

adequate signal. This model can be used for design purposes. Table 5.44 gives the coefficients for the reduced model.

**Table 5.44: Coefficients for the Quadratic Model for Nano CaO (WB)**

| | Coefficient | | Standard | 95% CI | 95% CI |
|---|---|---|---|---|---|
| **Factor** | **Estimate** | **df** | **Error** | **Low** | **High** |
| **Intercept** | 69.80 | 1 | 0.37 | 68.97 | 70.63 |
| **X1-Nano CaO** | 3.55 | 1 | 0.25 | 3.00 | 4.10 |
| **X2-Temp** | 4.72 | 1 | 0.25 | 4.17 | 5.27 |
| **X3-Meth:oil** | 1.71 | 1 | 0.25 | 1.16 | 2.26 |
| **X1.X2** | 1.34 | 1 | 0.32 | 0.62 | 2.06 |
| **X1.X3** | -1.54 | 1 | 0.32 | -2.26 | -0.82 |
| **X2.X3** | 0.89 | 1 | 0.32 | 0.17 | 1.61 |
| **X1^2** | -2.03 | 1 | 0.24 | -2.57 | -1.50 |
| **X2^2** | -2.85 | 1 | 0.24 | -3.38 | -2.31 |
| **X3^2** | -2.58 | 1 | 0.24 | -3.12 | -2.04 |

Since all the terms in the model were significant, no reductions were needed. Hence the model was: Yield, $Y = 69.80 + 3.55\ X1 + 4.72\ X2 + 1.71\ X3 + 1.34\ X1.X2 - 1.54\ X1.X3 + 0.89\ X2.X3 - 2.03\ X1^2 - 2.85\ X2^2 - 2.58\ X3^2$ …5.6

Quadratic model was used to calculate Predicted yield given in Table 5.40. Eqn 5.6 can be used for response surface plots.

#### 5.3.5.2.3.5 Response Surface and Contour Plots

Equation 5.6 adequately represented the FAME yield for transesterification of Croton *megalocarpus* oil using Nano CaO catalyst, as a function of the three process variables. This full quadratic model has been used for RSM surface and contour plots to identify areas for optimal yield. Fig 5.51 is plot for FAME yield as functions of Nano CaO concentration (X1) and Temperature (X2). The plot goes to show that for optimum yield, Nano CaO ≈ 1.5% and Temperature > $80^oC$ (353K).

Fig 5.52 identified the area for optimal FAME yield as the one where Nano CaO was 1.25 – 1.5%, and methanol to oil molar ratio was 9:1.

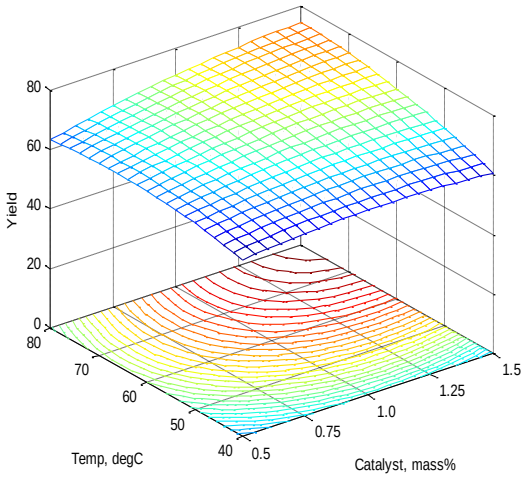


**Figure 5.51: RSM plot- Effect of Nano CaO conc. and Temp on Yield (WB)**

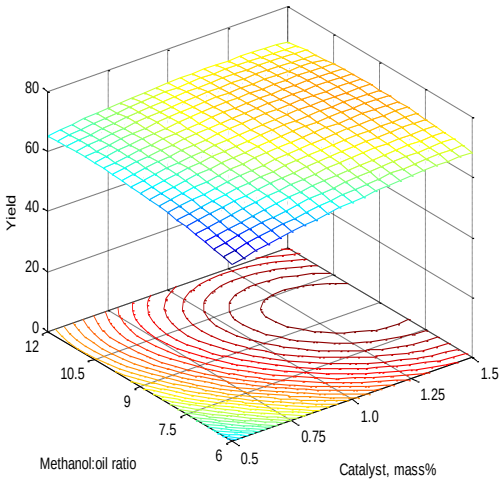


**Figure 5.52: RSM plot- Effect of Nano CaO conc. and Meth:oil ratio on Yield (WB)**

Fig 5.53 identified the area of optimal FAME yield where temperature was 70 – 80$^{o}$C (343 -353K) and methanol to oil ratio was between 9:1 and 10.5:1.

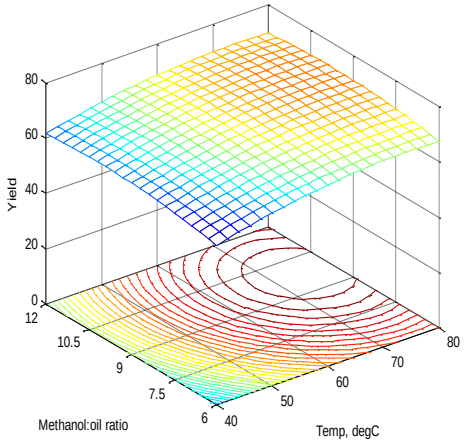


**Figure 5.53: RSM plot- Effect of Temp and Meth:oil ratio on Yield for Nano CaO (WB)**

The plots were in quantitative agreement with experimental observations. Experiments showed that a high temperature, high catalyst concentration and methanol:oil ratio of about 9:1 led to optimum yield.

#### 5.3.5.2.3.6 Optimization studies- experimental results and data analysis- CaO RO

Table 5.45 gives the details of a set of 20 experiments in terms of actual and coded levels, as per CCD, and the FAME yields obtained in transesterification studies. Table also gives Predicted yield as per Reduced quadratic model (Eqn 5.7).

**Table 5.45: CCD matrix with experimental FAME yield for CaO RO (WB)**

| Run | Level of variables [actual(coded)] | | | Expt. Yield Y | Reduced Model (Eqn 5.7) |
|---|---|---|---|---|---|
| | Catalyst,% X1 | Temp, ($^oC$) X2 | Methanol :oil X3 | | Y |
| **1** | 1(0) | 60(0) | 9(0) | 40.5 | 40.6 |
| **2** | 1(0) | 43(-1.68) | 9(0) | 29.1 | 29.1 |
| **3** | 0.5(-1) | 70(1) | 12(1) | 36.5 | 36.7 |
| **4** | 1(0) | 60(0) | 14(1.68) | 38.9 | 39.0 |
| **5** | 1.84(1.68) | 60(0) | 9(0) | 41.0 | 40.8 |
| **6** | 1(0) | 60(0) | 4(-1.68) | 32.0 | 32.0 |
| **7** | 0.5(-1) | 50(-1) | 6(-1) | 24.2 | 24.6 |
| **8** | 1(0) | 60(0) | 9(0) | 40.8 | 40.6 |
| **9** | 1.5(1) | 70(1) | 12(1) | 41.9 | 41.6 |
| **10** | 1.5(1) | 70(1) | 6(-1) | 38.9 | 39.4 |
| **11** | 1(0) | 60(0) | 9(0) | 40.8 | 40.6 |
| **12** | 1.5(1) | 50(-1) | 6(-1) | 32.9 | 32.5 |
| **13** | 0.16(-1.68) | 60(0) | 9(0) | 29.9 | 30.1 |
| **14** | 1(0) | 60(0) | 9(0) | 40.4 | 40.6 |
| **15** | 1.5(1) | 50(-1) | 12(1) | 38.1 | 38.7 |
| **16** | 1(0) | 60(0) | 9(0) | 39.9 | 40.6 |
| **17** | 0.5(-1) | 50(-1) | 12(1) | 31.5 | 30.8 |
| **18** | 1(0) | 77(1.68) | 9(0) | 39.9 | 39.9 |
| **19** | 1(0) | 60(0) | 9(0) | 40.9 | 40.6 |
| **20** | 0.5(-1) | 70(1) | 6(-1) | 34.9 | 34.5 |

Data in Table 5.45 were tested for fit for a linear, two-factor interaction (2FI), quadratic and cubic polynomials. Table 5.46 gives the result.

**Table 5.46: Summary for model fit- Sequential model sum of squares for CaO RO (WB)**

| Summary (detailed tables shown below) | | | | | |
|---|---|---|---|---|---|
| | **Sequential** | **Lack of Fit** | **Adjusted** | **Predicted** | |
| **Source** | **p-value** | **p-value** | **R-Squared** | **R-Squared** | |
| **Linear** | 0.0002 | < 0.0001 | 0.6408 | 0.5805 | |
| **2FI** | 0.7592 | < 0.0001 | 0.5947 | 0.2886 | |
| **Quadratic** | < 0.0001 | 0.1717 | 0.9905 | 0.9660 | Suggested |
| **Cubic** | 0.0780 | 0.7979 | 0.9954 | 0.9933 | Aliased |

| Sequential Model Sum of Squares [Type I] | | | | | | |
|---|---|---|---|---|---|---|
| Source | Sum of Squares | df | Mean Square | F Value | p-value Prob > F | |
| Mean vs Total | 26864.45 | 1 | 26864.45 | | | |
| Linear vs Mean | 337.65 | 3 | 112.55 | 12.30 | 0.0002 | |
| 2FI vs Linear | 12.21 | 3 | 4.07 | 0.39 | 0.7592 | |
| Quadratic vs 2FI | 131.82 | 3 | 43.94 | 182.17 | < 0.0001 | Suggested |
| Cubic vs Quadratic | 1.71 | 4 | 0.43 | 3.63 | 0.0780 | Aliased |
| Residual | 0.71 | 6 | 0.12 | | | |
| Total | 27348.54 | 20 | 1367.43 | | | |

Highest $R^2$ was for a Cubic model but it was aliased. Next highest $R^2$ was for a Quadratic model. Considering the F value and p-value, Quadratic model was suggested. Cubic was not considered being aliased. The appropriate model for the given set of data was full Quadratic model (Eqn 4.2, Chapter 4) :

$$Y = b_0 + \sum_{i=1}^{n} b_i X_i + \sum_{i=1}^{n} b_{ii} X_i^2 + \sum_{1=1}^{n-1} \sum_{j=i+1}^{n} b_{ij} X_i X_j$$

Y is the Yield, $X_i$ are coded variables as given in Table 5.1. Table 5.47 gives Analysis of Variance (ANOVA) for a full quadratic model.

**Table 5.47: ANOVA for Response Surface Quadratic model for CaO-RO (WB)**

| ANOVA for Response Surface Quadratic model | | | | | | |
|---|---|---|---|---|---|---|
| Analysis of variance table [Partial sum of squares - Type III] | | | | | | |
| Source | Sum of Squares | df | Mean Square | F Value | p-value Prob > F | |
| Model | 481.68 | 9 | 53.52 | 221.89 | < 0.0001 | significant |
| *X1-CaO-RO* | *137.72* | *1* | *137.72* | *570.96* | *< 0.0001* | |
| *X2-Temp* | *139.60* | *1* | *139.60* | *578.77* | *< 0.0001* | |
| *X3-Meth:oil* | *60.33* | *1* | *60.33* | *250.13* | *< 0.0001* | |
| *X1.X2* | *4.35* | *1* | *4.35* | *18.04* | *0.0017* | |
| *X1.X3* | *0.061* | *1* | *0.061* | *0.25* | *0.6252* | |
| *X2.X3* | *7.80* | *1* | *7.80* | *32.34* | *0.0002* | |
| *X1^2* | *46.23* | *1* | *46.23* | *191.68* | *< 0.0001* | |
| *X2^2* | *65.20* | *1* | *65.20* | *270.30* | *< 0.0001* | |
| *X3^2* | *46.23* | *1* | *46.23* | *191.68* | *< 0.0001* | |
| Residual | 2.41 | 10 | 0.24 | | | |
| *Lack of Fit* | *1.72* | *5* | *0.34* | *2.47* | *0.1717* | *not significant* |
| *Pure Error* | *0.69* | *5* | *0.14* | | | |
| Cor Total | 484.09 | 19 | | | | |

The Model F-value of 221.89 implied the model was significant. There was only a 0.01% chance that an F-value this large could occur due to noise. Values of "Prob > F" less than 0.0500 indicate model terms are significant. In this case X1, X2, X3, X1.X2, X2.X3, X1^2, X2^2, X3^2 were significant model terms. The "Lack of Fit F-value" of 2.47 implied the Lack of Fit was not significant relative to the pure error. There was a 17.17% chance that a "Lack of Fit F-value" this large could occur due to noise. Non-significant lack of fit was good. Since X1.X3 was not significant, it was dropped from the full quadratic model to simplify the model.

**Reduced Model:** X1.X3 was dropped from the model and ANOVA performed to test the reduced model. Table 5.48 gives ANOVA for the reduced model.

**Table 5.48: ANOVA for Response Surface Reduced Quadratic model for CaO-RO (WB)**

| **ANOVA for Response Surface Quadratic model** | | | | | | |
|---|---|---|---|---|---|---|
| **Analysis of variance table [Partial sum of squares - Type III]** | | | | | | |
| | **Sum of** | | **Mean** | **F** | **p-value** | |
| **Source** | **Squares** | **df** | **Square** | **Value** | **Prob > F** | |
| **Model** | 481.62 | 8 | 60.20 | 267.75 | < 0.0001 | significant |
| ***X1-CaO-RO*** | *137.72* | *1* | *137.72* | *612.51* | *< 0.0001* | |
| ***X2-Temp*** | *139.60* | *1* | *139.60* | *620.88* | *< 0.0001* | |
| ***X3-Meth:oil*** | *60.33* | *1* | *60.33* | *268.33* | *< 0.0001* | |
| ***X1.X2*** | *4.35* | *1* | *4.35* | *19.35* | *0.0011* | |
| ***X2.X3*** | *7.80* | *1* | *7.80* | *34.70* | *0.0001* | |
| ***X1^2*** | *46.23* | *1* | *46.23* | *205.63* | *< 0.0001* | |
| ***X2^2*** | *65.20* | *1* | *65.20* | *289.97* | *< 0.0001* | |
| ***X3^2*** | *46.23* | *1* | *46.23* | *205.63* | *< 0.0001* | |
| **Residual** | 2.47 | 11 | 0.22 | | | |
| ***Lack of Fit*** | *1.78* | *6* | *0.30* | *2.13* | *0.2118* | *not significant* |
| ***Pure Error*** | *0.69* | *5* | *0.14* | | | |
| **Cor Total** | 484.09 | 19 | | | | |

The Model F-value of 267.75 implied the model was significant. There was only a 0.01% chance that an F-value this large could occur due to noise. Values of "Prob > F" less than 0.0500 indicated model terms were significant. In this case X1, X2, X3, X1.X2, X2.X3, X1^2, X2^2, X3^2 were significant model terms. The "Lack of Fit F-value" of 2.13 implied the Lack of Fit was not significant relative to the pure error. There was a 21.18% chance that a "Lack of Fit F-value" this large could occur due to noise. Non-significant lack of fit was good. Table 5.49 gives the R-square terms for the reduced model.

**Table 5.49: R-square for Reduced Quadratic Model for CaO RO (WB)**

| | | | |
|---|---|---|---|
| **Std. Dev.** | **0.47** | **R-Squared** | **0.9949** |
| **Mean** | 36.65 | **Adj R-Squared** | 0.9912 |
| **C.V. %** | 1.29 | **Pred R-Squared** | 0.9798 |
| **PRESS** | 9.76 | **Adeq Precision** | 53.282 |

The "Pred R-Squared" of 0.9798 was in reasonable agreement with the "Adj R-Squared" of 0.9912; i.e. the difference was less than 0.2. "Adeq Precision" measures the signal to noise ratio. A ratio greater than 4 is desirable. This model's ratio of 53.282 indicated an adequate signal. This model can be used for design purposes. Table 5.50 gives the coefficients for the reduced model.

**Table 5.50: Coefficients for the Reduced Quadratic Model for CaO RO (WB)**

| | Coefficient | | Standard | 95% CI | 95% CI | |
|---|---|---|---|---|---|---|
| **Factor** | **Estimate** | **df** | **Error** | **Low** | **High** | **VIF** |
| **Intercept** | 40.55 | 1 | 0.19 | 40.12 | 40.97 | |
| **X1-CaO-RO** | 3.18 | 1 | 0.13 | 2.89 | 3.46 | 1.00 |
| **X2-Temp** | 3.20 | 1 | 0.13 | 2.91 | 3.48 | 1.00 |
| **X3-Meth:oil** | 2.10 | 1 | 0.13 | 1.82 | 2.38 | 1.00 |
| **X1.X2** | -0.74 | 1 | 0.17 | -1.11 | -0.37 | 1.00 |
| **X2.X3** | -0.99 | 1 | 0.17 | -1.36 | -0.62 | 1.00 |
| **X1^2** | -1.79 | 1 | 0.12 | -2.07 | -1.52 | 1.02 |
| **X2^2** | -2.13 | 1 | 0.12 | -2.40 | -1.85 | 1.02 |
| **X3^2** | -1.79 | 1 | 0.12 | -2.07 | -1.52 | 1.02 |

Since all the terms in the reduced model were significant, no further reductions were needed. Hence the model was:

$$\text{Yield, } Y = 40.55 + 3.18\,X1 + 3.20\,X2 + 2.10\,X3 - 0.74\,X1.X2 - 0.99\,X2.X3 - 1.79\,X1^2 - 2.13\,X2^2 - 1.79\,X3^2 \quad \ldots 5.7$$

Reduced quadratic model was used to compute Predicted yield given in Table 5.45. In the following section Eqn 5.7 was used for response surface plots.

### 5.3.5.2.3.7 Response Surface and Contour Plots for CaO RO

Eqn 5.7 was used for RSM surface and contour plots. Fig 5.54 is a RSM surface and contour plot for FAME yield as function of CaO-RO concentration and Temperature. Optima was at CaO-RO > 1.5% and Temperature 70- 80$^{o}$C (343 – 353K). Yield increased with increasing CaO-RO concentration and reaction temperature. This general trend was noted in experimental results.

Fig 5.55 is a RSM surface and contour plot for FAME yield as function of CaO-RO concentration and methanol to oil ratio. Optima was at CaO-RO ≈ 1.5% and methanol to oil ratio 10.5 – 12. This agreed with experimental observations.

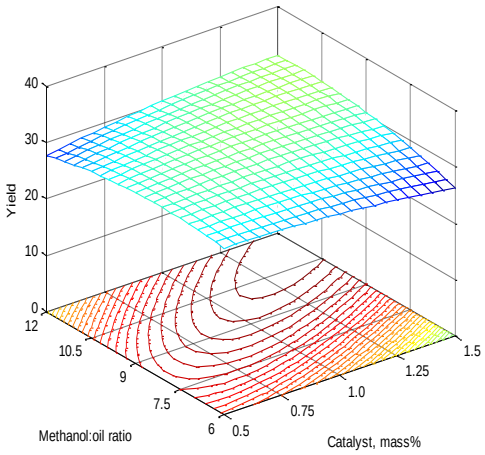


**Figure 5.54: RSM plot- Effect of CaO RO conc. and Temperature on Yield (WB)**

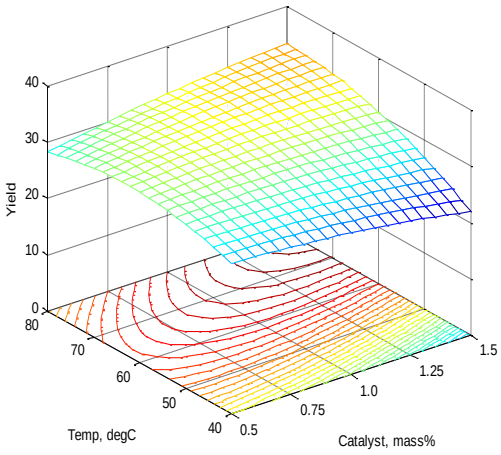


**Figure 5.55: RSM plot- Effect of CaO RO and Methanol:oil ratio on Yield (WB)**

Fig 5.56 is a RSM surface and contour plot for FAME yield as function of Temperature and methanol to oil ratio. Optima was at a temperature > 70$^{o}$C (343K) and methanol to oil ratio 10.5. Yield increased as temperature was increased from 40 to 70$^{o}$C (313 to 343K), and when methanol to oil ratio was increased from 6:1 to 11:1 during experimental studies. Hence the RSM plot concurred with the experimental findings.

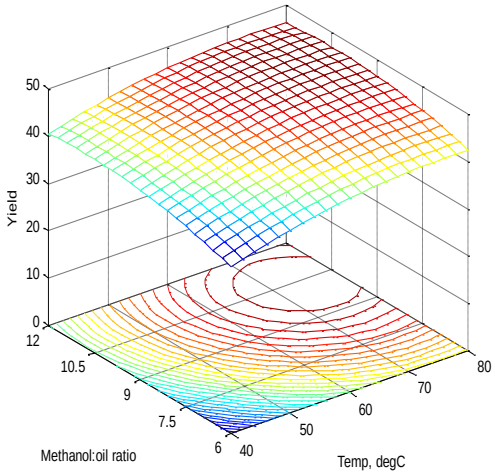


**Figure 5.56: RSM plot- Effect of Temp. and Methanol:oil ratio on Yield for CaO-RO (WB)**

#### 5.3.5.2.3.8 Optimization studies- experimental results and data analysis for CaO

Table 5.51 gives the details of a set of 20 experiments in terms of actual and coded levels, as per CCD, and the FAME yields obtained in transesterification studies. Table also gives Predicted yields as per the Quadratic model (Eqn 5.8).

**Table 5.51: CCD matrix with experimental FAME yield for CaO (WB)**

| Run | Level of variables [actual(coded)] | | | Expt. Yield | Quadratic Model (Eqn 5.8) |
|---|---|---|---|---|---|
| | Catalyst,% X1 | Temp, ($^oC$) X2 | Methanol :oil X3 | | Y |
| **1** | 1(0) | 60(0) | 9(0) | 31.8 | 31.3 |
| **2** | 1(0) | 43(-1.68) | 9(0) | 18.5 | 18.6 |
| **3** | 0.5(-1) | 70(1) | 12(1) | 22.9 | 22.7 |
| **4** | 1(0) | 60(0) | 14(1.68) | 27.0 | 27.2 |
| **5** | 1.84(1.68) | 60(0) | 9(0) | 30.5 | 29.3 |
| **6** | 1(0) | 60(0) | 4(-1.68) | 25.2 | 24.2 |
| **7** | 0.5(-1) | 50(-1) | 6(-1) | 24.2 | 24.3 |
| **8** | 1(0) | 60(0) | 9(0) | 31.9 | 31.3 |
| **9** | 1.5(1) | 70(1) | 12(1) | 32.4 | 32.7 |
| **10** | 1.5(1) | 70(1) | 6(-1) | 29.6 | 30.8 |
| **11** | 1(0) | 60(0) | 9(0) | 31.3 | 31.3 |
| **12** | 1.5(1) | 50(-1) | 6(-1) | 15.2 | 15.6 |
| **13** | 0.16(-1.68) | 60(0) | 9(0) | 27.8 | 28.3 |
| **14** | 1(0) | 60(0) | 9(0) | 31.0 | 31.3 |
| **15** | 1.5(1) | 50(-1) | 12(1) | 24.8 | 25.1 |
| **16** | 1(0) | 60(0) | 9(0) | 31.2 | 31.3 |
| **17** | 0.5(-1) | 50(-1) | 12(1) | 26.8 | 26.0 |
| **18** | 1(0) | 77(1.68) | 9(0) | 29.5 | 28.7 |
| **19** | 1(0) | 60(0) | 9(0) | 30.6 | 31.3 |
| **20** | 0.5(-1) | 70(1) | 6(-1) | 28.7 | 28.8 |

Data in Table 5.51 were tested for fit for a linear, two-factor interaction (2FI), quadratic and cubic polynomials. Table 5.52 gives the result.

**Table 5.52: Summary for model fit- Sequential model sum of squares for CaO (WB)**

| Summary (detailed tables shown below) | | | | | |
|---|---|---|---|---|---|
| | **Sequential** | **Lack of Fit** | **Adjusted** | **Predicted** | |
| **Source** | **p-value** | **p-value** | **R-Squared** | **R-Squared** | |
| **Linear** | 0.0837 | < 0.0001 | 0.2073 | -0.0847 | |
| **2FI** | 0.0574 | < 0.0001 | 0.4414 | -0.0413 | |
| **Quadratic** | < 0.0001 | 0.0555 | 0.9677 | 0.8879 | Suggested |
| **Cubic** | 0.0920 | 0.1026 | 0.9833 | 0.4805 | Aliased |

| Sequential Model Sum of Squares [Type I] | | | | | | |
|---|---|---|---|---|---|---|
| Source | Sum of Squares | df | Mean Square | F Value | p-value Prob > F | |
| Mean vs Total | 15174.54 | 1 | 15174.54 | | | |
| Linear vs Mean | 135.77 | 3 | 45.26 | 2.66 | 0.0837 | |
| 2FI vs Linear | 116.55 | 3 | 38.85 | 3.24 | 0.0574 | |
| Quadratic vs 2FI | 149.15 | 3 | 49.72 | 71.67 | < 0.0001 | Suggested |
| Cubic vs Quadratic | 4.78 | 4 | 1.20 | 3.33 | 0.0920 | Aliased |
| Residual | 2.15 | 6 | 0.36 | | | |
| Total | 15582.95 | 20 | 779.15 | | | |

Highest $R^2$ Adjusted was for a Cubic model but it was aliased. However its Predicted R-Square was low. Highest acceptable R-Square was for a Quadratic model. Considering the F value and p-value, Quadratic model was suggested. Cubic was not considered being aliased. The appropriate model for the given set of data was full Quadratic model (Eqn 4.2, Chapter 4) : $Y = b_0 + \sum_{i=1}^{n} b_i X_i + \sum_{i=1}^{n} b_{ii} X_i^2 + \sum_{1=1}^{n-1} \sum_{j=i+1}^{n} b_{ij} X_i X_j$ , Y is the Yield, $X_i$ are coded variables as given in Table 5.1. Table 5.53 gives Analysis of Variance (ANOVA) for a full quadratic model.

**Table 5.53: ANOVA for Response Surface Quadratic model for CaO (WB)**

| ANOVA for Response Surface Quadratic model | | | | | | |
|---|---|---|---|---|---|---|
| Analysis of variance table [Partial sum of squares - Type III] | | | | | | |
| Source | Sum of Squares | df | Mean Square | F Value | p-value Prob > F | |
| Model | 401.47 | 9 | 44.61 | 64.31 | < 0.0001 | significant |
| *X1-CaO* | *1.14* | *1* | *1.14* | *1.64* | *0.2293* | |
| *X2-Temp* | *123.69* | *1* | *123.69* | *178.31* | *< 0.0001* | |
| *X3-Meth:oil* | *10.95* | *1* | *10.95* | *15.78* | *0.0026* | |
| *X1.X2* | *57.25* | *1* | *57.25* | *82.52* | *< 0.0001* | |
| *X1.X3* | *30.42* | *1* | *30.42* | *43.85* | *< 0.0001* | |
| *X2.X3* | *28.88* | *1* | *28.88* | *41.63* | *< 0.0001* | |
| *X1^2* | *11.04* | *1* | *11.04* | *15.92* | *0.0026* | |
| *X2^2* | *104.76* | *1* | *104.76* | *151.02* | *< 0.0001* | |
| *X3^2* | *55.01* | *1* | *55.01* | *79.30* | *< 0.0001* | |
| Residual | 6.94 | 10 | 0.69 | | | |
| *Lack of Fit* | *5.74* | *5* | *1.15* | *4.78* | *0.0555* | *not significant* |
| *Pure Error* | *1.20* | *5* | *0.24* | | | |
| Cor Total | 408.41 | 19 | | | | |

The Model F-value of 64.31 implied the model was significant. There was only a 0.01% chance that an F-value this large could occur due to noise. Values of "Prob > F" less than 0.0500 indicate model terms are significant. In this case X2, X3, X1.X2, X1.X3, X2.X3,

X1^2, X2^2, X3^2 were significant model terms. The "Lack of Fit F-value" of 4.78 implied there was a 5.55% chance that a "Lack of Fit F- value" this large could occur due to noise. Lack of fit was not very good but it was not significant, and hence acceptable. Term X1 (CaO concentration) was not significant but it could not be dropped since it was part of model hierarchy. Also it was noted that the cross coefficients of X1, i.e., X1.X1 and X1.X3 were significant. Hence X1 was retained and full quadratic model used. Table 5.54 gives the R-Square terms for the model.

**Table 5.54: R-Square values for CaO (WB)**

| | | | |
|---|---|---|---|
| **Std. Dev.** | **0.83** | **R-Squared** | **0.9830** |
| **Mean** | 27.55 | **Adj R-Squared** | 0.9677 |
| **C.V. %** | 3.02 | **Pred R-Squared** | 0.8879 |
| **PRESS** | 45.76 | **Adeq Precision** | 28.966 |

The "Pred R-Squared" of 0.8879 was in reasonable agreement with the "Adj R-Squared" of 0.9677; i.e. the difference was less than 0.2. "Adeq Precision" measures the signal to noise ratio. A ratio greater than 4 is desirable. Present ratio of 28.966 indicated an adequate signal. This model can be used for design purposes. Table 5.55 gives the coefficients for the reduced model.

**Table 5.55: Coefficients for the Full Quadratic Model- CaO (WB)**

| | Coefficient | | Standard | 95% CI | 95% CI |
|---|---|---|---|---|---|
| **Factor** | **Estimate** | **df** | **Error** | **Low** | **High** |
| **Intercept** | 31.32 | 1 | 0.34 | 30.56 | 32.07 |
| **X1-CaO** | 0.29 | 1 | 0.23 | -0.21 | 0.79 |
| **X2-Temp** | 3.01 | 1 | 0.23 | 2.51 | 3.51 |
| **X3-Meth:oil** | 0.90 | 1 | 0.23 | 0.39 | 1.40 |
| **X1.X2** | 2.68 | 1 | 0.29 | 2.02 | 3.33 |
| **X1.X3** | 1.95 | 1 | 0.29 | 1.29 | 2.61 |
| **X2.X3** | -1.90 | 1 | 0.29 | -2.56 | -1.24 |
| **X1^2** | -0.88 | 1 | 0.22 | -1.36 | -0.39 |
| **X2^2** | -2.70 | 1 | 0.22 | -3.18 | -2.21 |
| **X3^2** | -1.95 | 1 | 0.22 | -2.44 | -1.46 |

Since all the terms in the model were significant, no reductions were needed. Hence the model was:

Yield, $Y = 31.32 + 0.29\ X1 + 3.01\ X2 + 0.90\ X3 + 2.68\ X1.X2 + 1.95\ X1.X3 - 1.90\ X2.X3 - 0.88\ X1^2 - 2.70\ X2^2 - 1.95\ X3^2$ …5.8

Full quadratic model was used to compute Predicted yields given in Table 5.51. Eqn 5.8 was used for response surface plots.

#### 5.3.5.2.3.9 Response Surface and Contour Plots

Quadratic model Eqn 5.8 was used to plot RSM surface and contour plots. Fig 5.57 is a RSM surface and contour plot for Yield as a function of CaO catalyst and Temperature. Optima for FAME yield was at CaO > 1.5% and Temperature 70 – 80$^{o}$C (343 -353K). This was the general trend observed in lab studies.

Fig 5.58 is a RSM surface and contour plot showing effect of Methanol to oil ratio and CaO concentration on FAME Yield. Maxima was at CaO ≈ 1.5% and Methanol to oil > 10.5. These observations agreed with experimental results.

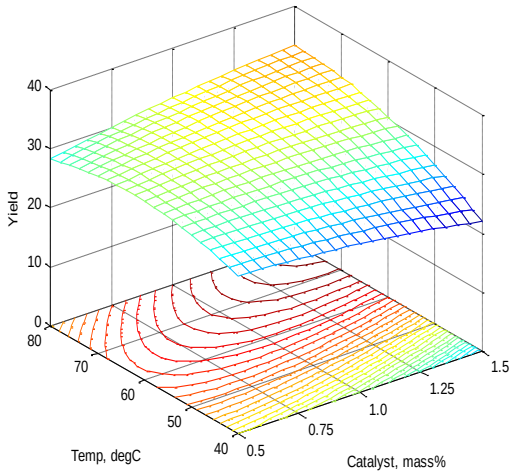


**Figure 5.57: RSM plot- Effect of Temperature and CaO concentration on Yield (WB)**

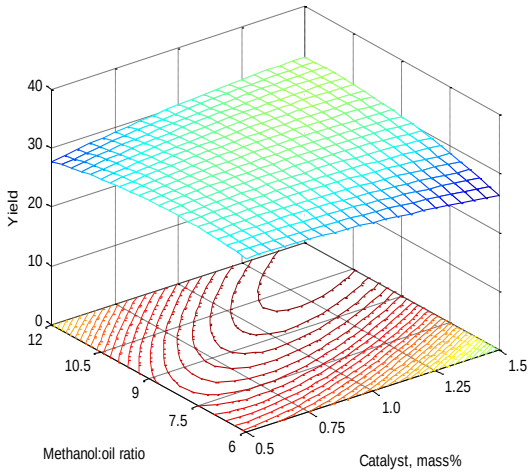


**Figure 5.58: RSM plot- Effect of Methanol:oil ratio and CaO conc. on Yield (WB)**

Fig 5.59 is a RSM surface and contour plot showing effect of Temperature and Methanol to oil ratio on FAME yield. For maximum yield, temperature and methanol to oil ratio were suggested to be at 70$^{o}$C (343K) and 9:1 respectively. These agreed with experimental results.

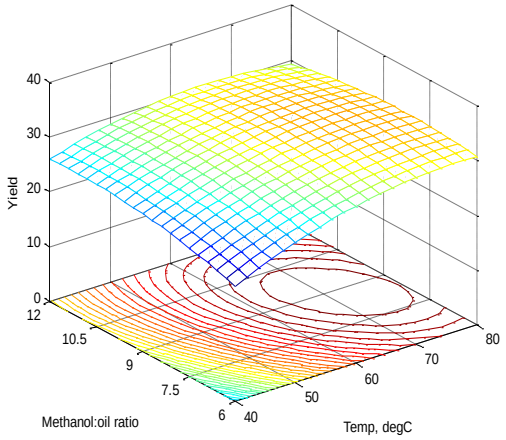


**Figure 5.59: RSM plot- Effect of Temperature and Meth:oil ratio on Yield for CaO (WB)**

### 5.3.6 Studies with Microwave Irradiation- Nano calcium oxide, Roxidized calcium oxide and Calcium oxide catalysts

This section deals with transesterification studies carried out with microwave irradiation.

#### 5.3.6.1 Effect of operation variables on FAME yield

This section presents effects of operation variables of (i) Methanol to triglyceride molar ratio, (ii) Catalyst concentration, (iii) Reaction time, and (iv) Microwave power. Effect of reaction temperature on FAME yield is presented under Reaction kinetics. Results are presented in form of figures containing yield data for all the three catalysts, Nano CaO, CaO-RO and CaO.

##### 5.3.6.1.1 Effect of methanol to triglyceride molar ratio

Methanol to oil molar ratio was varied as 6:1, 9:1, 12:1, 15:1. Batch consisted of 30 ml of Croton *megalocarpus* oil (FFA = 1.7), catalyst 1% by mass of oil. Reaction time was 5 min at full microwave power. Fig 5.60 gives the FAME yield for Nano CaO, CaO-RO and CaO as a function methanol to oil molar ratio. Stoichiometric requirement of methanol for transesterification is 3 mole to one mole of triglyceride, but methanol is used in excess to drive the reaction in forward direction. Yields for all the three catalysts increased when methanol ratio was increased from 6:1 to 9:1, and it remained more or less constant when the ratio was further increased to 12:1 and 15:1, with a slight decline at 15:1 ratio. Yields for Nano CaO, CaO-RO and CaO at 12:1 ratio were 58.3, 24.3 and 19.5%; whereas the

yields at 15:1 ratio were 57.3, 23.1 and 18.6%. The explanations for this decline in yield at large excess of methanol have already been given in earlier sections.

#### 5.3.6.1.2 Effect of catalyst concentration on FAME yield

Fig 5.61 gives the effect of catalyst concentrations on FAME yield. Concentration of Nano CaO was varied from 0.5 – 3 mass% whereas concentrations of CaO-RO and CaO changed from 0.5 – 2 mass%. Batch consisted of 30 ml of Croton *megalocarpus* oil (FFA = 1.7), 9:1 methanol to oil ratio, reaction time of 5 min at full microwave power. Yields increased with increase in catalyst concentration from 0.5 to 1 mass%. When catalyst concentration was increased further from 1 to 1.5%: the yield for Nano CaO increased from 61.5 to 62.1%, the yield for CaO-RO increased from 23.6 to 24.5%, and yield for CaO increased from 18.6 to 19.8%. This showed that there was little effect of increased catalyst concentration on yield for concentrations above 1 mass%. Highest yield for Nano CaO was 62.7% at 3 mass% , for CaO-RO 24.6% at 1.5 mass%, and for CaO 19.8% at 1.5 mass%.

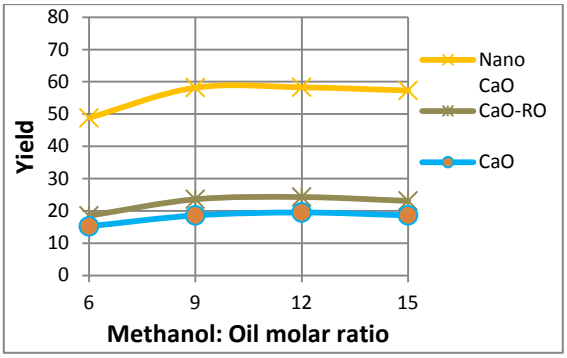


**Figure 5.60: Effect of Meth. :oil ratio on Yield (MW)**

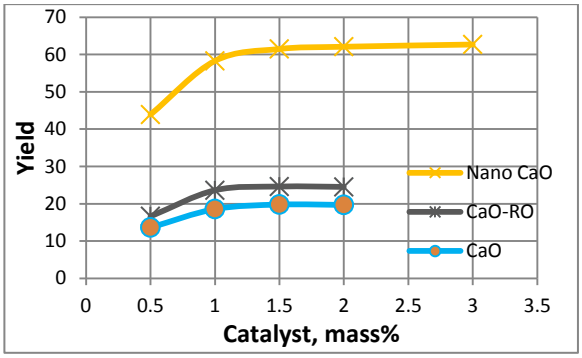


**Figure 5.61: Effect of Catalyst concentration on FAME yield (MW)**

#### 5.3.6.1.3 Effect of reaction time on FAME yield

Fig 5.62 gives the effect of reaction time on FAME yield. Transesterification was carried out with 1 mass% catalyst, 9:1 methanol to oil molar ratio at full microwave power. For Nano CaO yield steadily increased with time and the final yield at the end of 5 min was 58.3%. For CaO-RO and CaO, yields stabilized, with little increase, after 2 min of reaction time. The increase in yields for CaO-RO and CaO from a time of 2 min to 5 min were: 19.5 to 23.6; and 15.2 to 18.6%. Reaction rates were very high in the beginning and they stabilized as the time proceeded. Literature on microwave irradiated transesterification

using calcium oxide catalysts is very limited. Hsiao *et al*. (2011) used nanopowder CaO for soybean microwave transesterification and obtained a 96.6% yield at 7:1 methanol to oil ratio, 3 mass% catalyst at 65$^{o}$C (338K) in 1 h. Khemthong *et al*. (2012) used industrial eggshell waste (99.2 wt% CaO) as a catalyst for palm oil transesterification and 96.7% yield of FAME was obtained in 4 min, 15% catalyst, 18:1 methanol:oil ratio under microwave. Patil *et al.* (2011) found activity of CaO very poor under microwave irradiation for transesterification of *Camelina sativa* oil.

#### 5.3.6.1.4 Effect of microwave power

Fig 5.63 gives the effect of microwave power on yield. Microwave reactor had built in power settings of 20, 40, 60, 80, 100%. Reactions were carried out at microwave power of 40, 60, 80 and 100%, at methanol to oil ratio of 9:1, 1 mass% of catalyst, and a reaction time of 5 min. Yields for Nano CaO, CaO RO and CaO catalysts increased with power. The increase in yield was more pronounced when power increased from 40 to 80%. Between 80 - 100% power, yields were almost constant. Yields for Nano CaO, CaO RO and CaO at 80% power were 56.8, 22.8, 17.88%; and at 100% power were 58.3, 23.6 and 18.6% respectively.

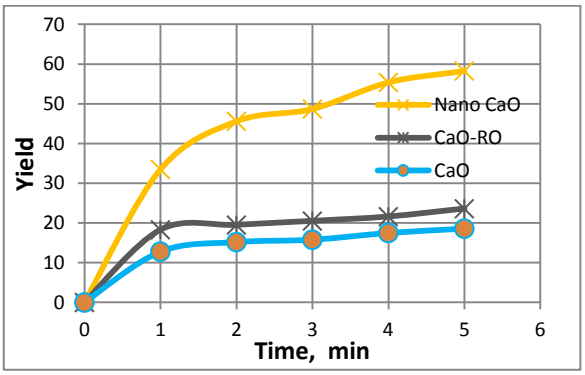


**Figure 5.62: Effect of Reaction Time on Yield (MW)**

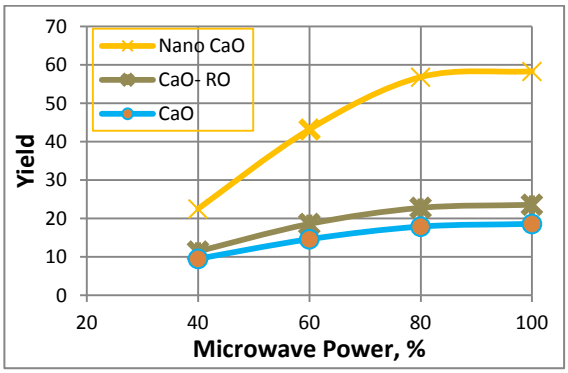


**Figure 5.63: Effect of Microwave power on Yield**

### 5.3.6.2 Reaction Kinetics

Transesterification reactions were carried out at constant temperatures of 50, 60 and 70$^{o}$C (323, 333, 343K). Other variables were kept constant at methanol to oil ratio 9:1, catalyst concentration 1 mass%, and full power. Samples were drawn at 30, 45, 60 and 90s. Studies with Nano CaO, CaO RO and CaO are presently in the following sections.

#### 5.3.6.2.1 Nano Calcium oxide

#### 5.3.6.2.1.1 Effect of Time on FAME yield

Fig 5.64 gives the FAME yield for Nano CaO catalyst at 50, 60 and 70$^{o}$C (323, 333, 343K). Yield increased with the rise in reaction temperature. The reaction rate was higher in early stages of reaction as shown by the steeper slopes of the curves at the origin. The final yields for at 50, 60 and 70$^{o}$C (323, 333, 343K) were 39.7, 52.9 and 55.0% of FAME respectively.

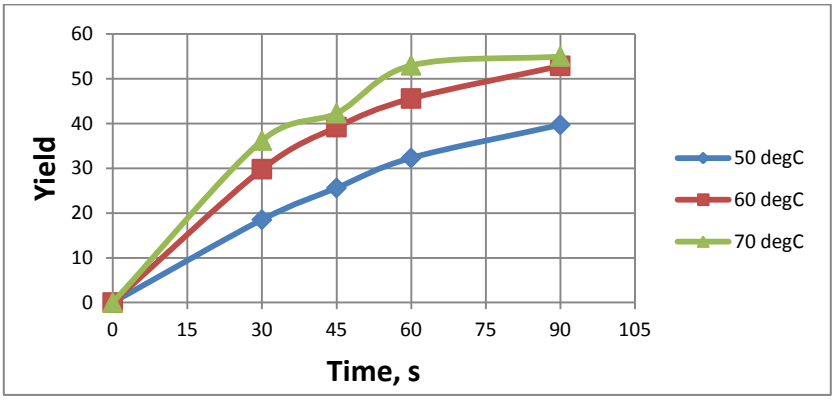


**Figure 5.64: Variation of Yield with time for Nano CaO (MW)**

#### 5.3.6.2.1.2 Order of reaction

Kinetic data for Fig 5.64 were used to find the best fit into integrated form of Eqn 2.29 (Chapter 2) which is given as $-r_A = -\frac{d[A]}{dt} = k\,[A]^m\,[B]^n$, where $A$ is triglyceride and $B$ is methanol. These equations (Eqns 2.34- 2.43, Chapter 2) cover reaction orders ranging from 'zero' to 'three'. Highest correlation coefficient ($R^2$) at each temperature was identified as outlined in Section 5.3.5.2.1.2, which corresponded to the most likely rate equation. Table 5.56 gives the coefficients of correlation for all reaction orders, Cases 1 to 10, at the three temperatures.

**Table 5.56: Coefficients of correlation, $R^2$, for various reaction orders for Nano CaO (MW)**

| | 0th Order | 1st Order | | 2nd Order | | | 3rd Order | | | |
|---|---|---|---|---|---|---|---|---|---|---|
| **Temp °C** | Case 1 | Case 2 (m=1, n=0) | Case 3 (m=0, n=1) | Case 4 (m=1, n=1) | Case 5 (m=2, n=0) | Case 6 (m=0, n=2) | Case 7 (m=2, n=1) | Case 8 (m=1, n=2) | Case 9 (m=3, n=0) | Case 10 (m=0, n=3) |
| **50** | 0.9509 | 0.98 | 0.9601 | 0.9859 | 0.9959 | 0.9684 | **0.9973** | 0.9914 | 0.9942 | 0.98 |
| **60** | 0.8882 | 0.9469 | 0.9041 | 0.9594 | 0.9876 | 0.9194 | **0.9932** | 0.9716 | 0.9927 | 0.9434 |
| **70** | 0.8256 | 0.8843 | 0.849 | 0.8969 | 0.9277 | 0.8557 | **0.9444** | 0.9093 | 0.9439 | 0.870 |

Highest correlation coefficients are in bold numbers in Table 5.56. The most likely order of reaction was 'three' . Second order with respect to triglyceride, and first order with respect to methanol (Case 7). The integrated form of rate equation is Eqn 2.40 (Chapter 2) given as: $\frac{1}{(\alpha_B-3)}\left(\frac{x_A}{1-x_A}-\frac{3}{\alpha_B-3}\right) ln\frac{(\alpha_B-3x_A)}{(1-x_A)\alpha_B} = k\,[A]_o^2\,t$ . The slope in this case is = k $[A_o]^2$.

#### 5.3.6.2.1.3 Rate constant and Activation energy

L.H.S. of Eqn 2.40, ( $\frac{1}{(\alpha_B-3)}\left(\frac{x_A}{1-x_A}-\frac{3}{\alpha_B-3}\right) ln\frac{(\alpha_B-3x_A)}{(1-x_A)\alpha_B}$ ) is a function of conversion $x_A$ , F($x_A$), or the yield. A plot of F($x_A$) vs time *t* is a straight line passing through the origin. Regression linear plot for F($x_A$) vs. *t* for 70°C (343K) is given in Fig 5.65.The ordinate is, $\frac{1}{(\alpha_B-3)}\left(\frac{x_A}{1-x_A}-\frac{3}{\alpha_B-3}\right) ln\frac{(\alpha_B-3x_A)}{(1-x_A)\alpha_B}$ ) and abscissa is *t*. Reaction constant *k* is given by the slope of the plot ($R^2$ = 0.9444).

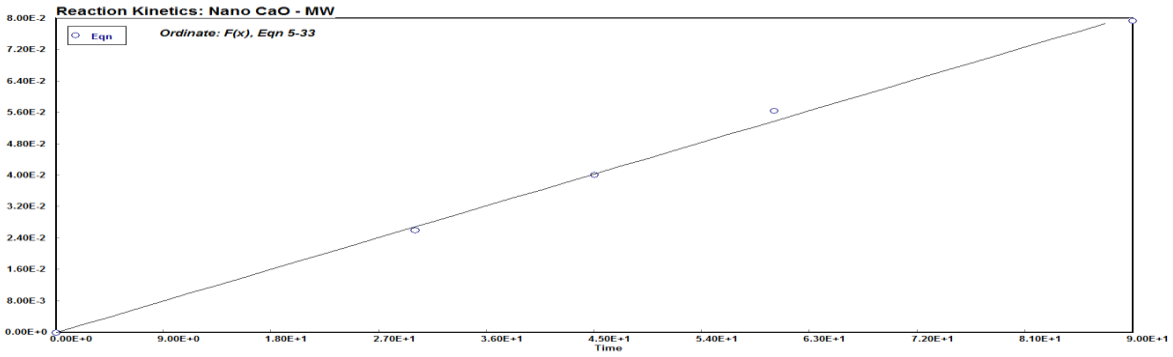


**Figure 5.65: Plot of kinetic equation 2.40 for Nano CaO (MW)**

Correlation constants (k $[A_o]^2$ ) for Eqn 2.40 for the three temperatures were used to estimate reaction constant *k* as given in Table 5.57.

**Table 5.57: Reaction constant k for Nano CaO (MW)**

| Temp, °C | Temp K | $[Ao]^2$ .k | [Ao] | k |
|---|---|---|---|---|
| | | | g/cm3 | in min |
| **50** | 323.15 | 0.000898 | 0.6663 | 1.21E-01 |
| **60** | 333.15 | 0.001632 | 0.6663 | 2.21E-01 |
| **70** | 343.15 | 0.00198 | 0.6663 | 2.68E-01 |

Activation energy was obtained from the slope of the plot of ln*k* vs. 1/T (Arrhenius plot, Section 2.5.4.1). Fig 5.66 gives the plot ($R^2$ = 0.9294).

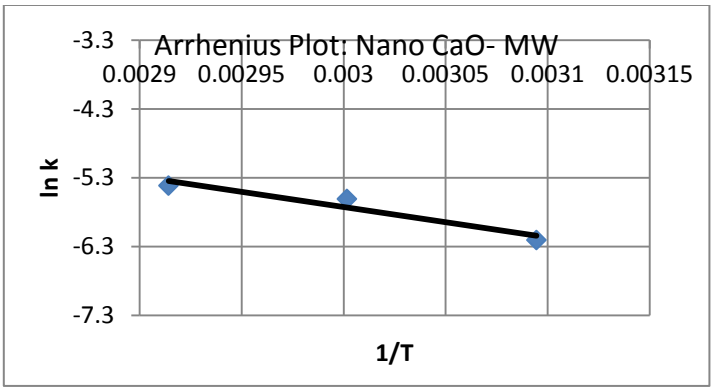


**Figure 5.66: Arrhenius plot for Nano CaO (MW)**

Slope of the plot was 4404.5, giving Activation energy, $E$ = 36.62 kJ/mol, and intercept gave the pre-exponential factor, $A$ = 1790.

#### 5.3.6.2.2 Re-oxidized Calcium oxide

##### 5.3.6.2.2.1 Effect of Time on FAME yield

Fig 5.67 is a plot of FAME yield with time at temperatures of 50, 60 and 70$^{o}$C (323, 333, 343 K) for CaO RO catalyst. Yield increased with increasing temperature and time. Highest yields at the end of 90s for temperatures of 50, 60 and 70$^{o}$C (323, 333, 343 K) were 11.5, 17.3 and 19.3% respectively.

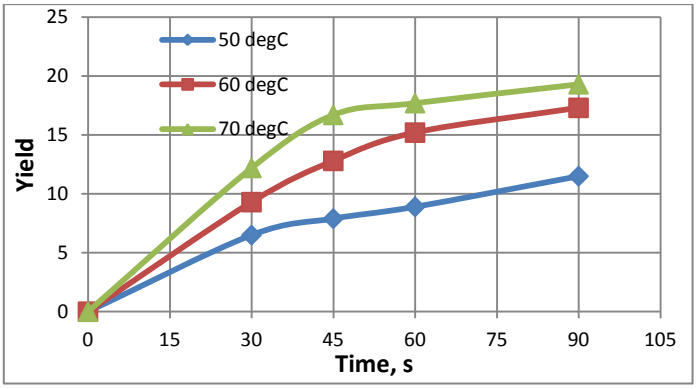


**Figure 5.67: Variation of yield with time for CaO-RO (MW)**

##### 5.3.6.2.2.2 Order of reaction

Table 5.58 gives the coefficients of correlation for all reaction orders, Cases 1 to 10, at the three temperatures.

**Table 5.58: Coefficients of correlation, R2, for various reaction orders for CaO RO (MW)**

| | 0th Order | 1st Order | | 2nd Order | | | 3rd Order | | | |
|---|---|---|---|---|---|---|---|---|---|---|
| **Temp °C** | Case 1 | Case 2 (m=1, n=0) | Case 3 (m=0, n=1) | Case 4 (m=1, n=1) | Case 5 (m=2, n=0) | Case 6 (m=0, n=2) | Case 7 (m=2, n=1) | Case 8 (m=1, n=2) | Case 9 (m=3, n=0) | Case 10 (m=0, n=3) |
| **50** | 9079 | 0.9183 | 0.9113 | 0.9215 | 0.92825 | 0.9146 | **0.9314** | 0.9256 | 0.9278 | 0.9178 |
| **60** | 0.9713 | 0.9729 | 0.9719 | 0.9732 | 0.9734 | 0.9724 | **0.9735** | 0.9734 | 0.9731 | 0.9728 |
| **70** | 0.9089 | 0.9196 | 0.9124 | 0.9228 | 0.9297 | 0.9157 | **0.9327** | 0.9269 | 0.9315 | 0.919 |

Highest correlation coefficients are in bold numbers in Table 5.58. The most likely order of reaction was 'three'; second order with respect to triglyceride, and first order with respect to methanol (Case 7). The integrated form of rate equation is Eqn 2.40 (Chapter 2) given as: $\frac{1}{(\alpha_B-3)}\left(\frac{x_A}{1-x_A}-\frac{3}{\alpha_B-3}\right) ln\frac{(\alpha_B-3x_A)}{(1-x_A)\alpha_B} = k\,[A]_o^2\,t$ . The slope in this case is = k $[A_o]^2$.

#### 5.3.6.2.2.3 Rate constant and Activation energy

L.H.S. of Eqn 2.40, ( $\frac{1}{(\alpha_B-3)}\left(\frac{x_A}{1-x_A}-\frac{3}{\alpha_B-3}\right) ln\frac{(\alpha_B-3x_A)}{(1-x_A)\alpha_B}$ ) is a function of conversion $x_A$ , F($x_A$), or the yield. A plot of F($x_A$) vs time t is a straight line passing through the origin. Regression linear plot for F($x_A$) vs. *t* for 70°C (343K) is given in Fig 5.68. The ordinate is, $\frac{1}{(\alpha_B-3)}\left(\frac{x_A}{1-x_A}-\frac{3}{\alpha_B-3}\right) ln\frac{(\alpha_B-3x_A)}{(1-x_A)\alpha_B}$ ) and abscissa is *t*. Reaction constant *k* is given by the slope of the plot ($R^2$ = 0.9327).

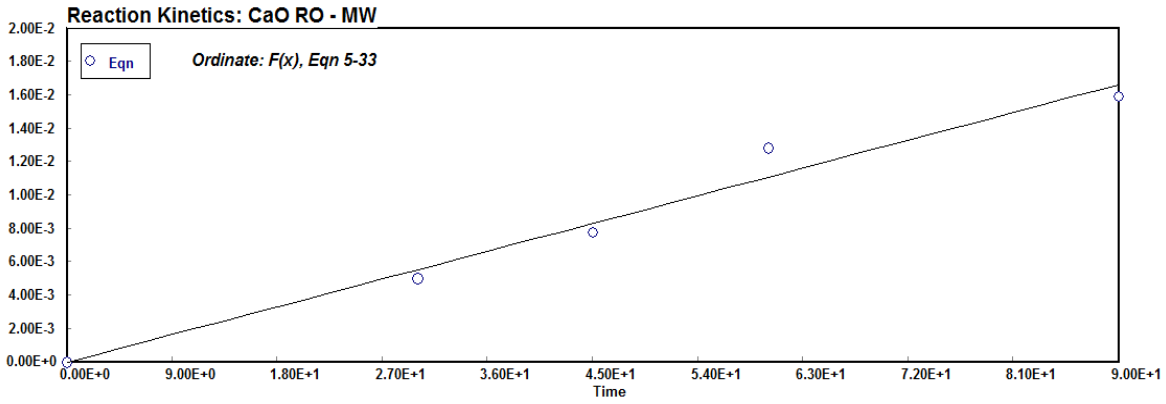


**Figure 5.68: Plot of kinetic equation 2.40 for CaO RO (MW)**

Correlation constants (k $[A_o]^2$ ) for Eqn 2.40 for the three temperatures were used to estimate reaction constant *k* as given in Table 5.59.

**Table 5.59: Reaction constant k for CaO RO (MW)**

| Temp, °C | Temp K | $[Ao]^2$ .k | [Ao] | k |
|---|---|---|---|---|

| | | | g/cm3 | in min |
|---|---|---|---|---|
| **50** | 323.15 | 0.000186 | 0.6663 | 2.51E-02 |
| **60** | 333.15 | 0.000187 | 0.6663 | 2.52E-02 |
| **70** | 343.15 | 0.000291 | 0.6663 | 3.93E-02 |

Activation energy was obtained from the slope of the plot of ln*k* vs. 1/T (Arrhenius plot, Section 2.5.4.1). Fig 5.69 gives the plot ($R^2$ = 0.7442).

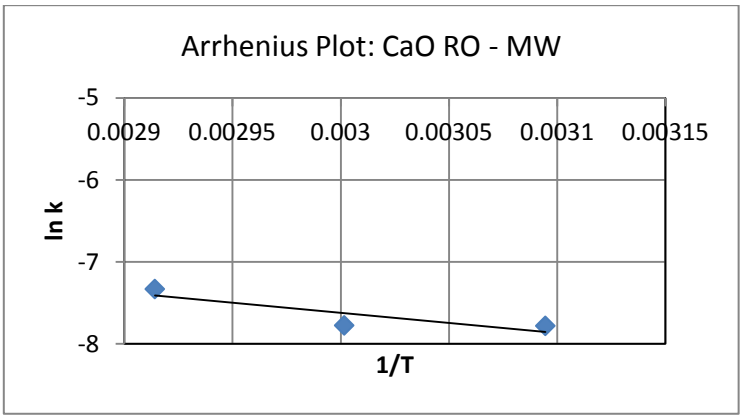


**Figure 5.69; Arrhenius plot for CaO-RO (MW)**

Slope of the plot was 1589.41, giving Activation energy, *E* = 20.49 kJ/mol; and intercept gave pre-exponential factor *A* = 47.8.

### 5.3.6.2.3 Calcium oxide

#### 5.3.6.2.3.1 Effect of Time on FAME yield

Transesterification reactions were carried out at constant temperatures of 50, 60 and 70$^{o}$C (323, 333, 343K) using CaO catalyst. Other variables were kept constant at methanol to oil ratio 9:1, CaO concentration 1 mass%, and full power. Samples were drawn at 30, 45, 60 and 90s. Fig 5.70 is a plot of FAME yield vs. reaction time at varying reaction temperatures. Yields in general were low. At 50$^{o}$C (323K), the yield at the end of 90s was 4.5%, which rose to 12.3% and 14.3% for 60 and 70$^{o}$C (333 and 343K) respectively.

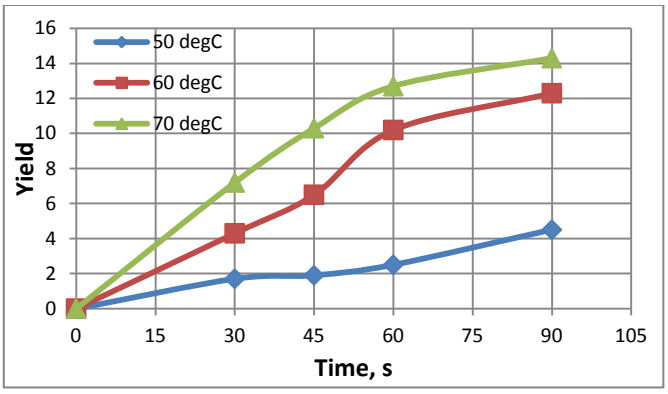


**Figure 5.70: Variation of Yield with Time for CaO (MW)**

#### 5.3.6.2.3.2 Order of reaction

Table 5.60 gives the coefficients of correlation for all reaction orders, Cases 1 to 10, at the three temperatures.

**Table 5.60: Coefficients of correlation, R2, for various reaction orders for CaO (MW)**

| | 0th Order | 1st Order | | 2nd Order | | | 3rd Order | | | |
|---|---|---|---|---|---|---|---|---|---|---|
| **Temp °C** | Case 1 | Case 2 (m=1, n=0) | Case 3 (m=0, n=1) | Case 4 (m=1, n=1) | Case 5 (m=2, n=0) | Case 6 (m=0, n=2) | Case 7 (m=2, n=1) | Case 8 (m=1, n=2) | Case 9 (m=3, n=0) | Case 10 (m=0, n=3) |
| **50** | **0.97** | 0.9681 | 0.9694 | 0.9674 | 0.966 | 0.9688 | 0.9652 | 0.9665 | 0.9636 | 0.9682 |
| **60** | 0.9713 | 0.9729 | 0.9719 | 0.9732 | 0.9734 | 0.9724 | **0.9735** | 0.9734 | 0.9731 | 0.9728 |
| **70** | 0.909 | 0.9196 | 0.9124 | 0.9228 | 0.9297 | 0.9157 | **0.9327** | 0.9269 | 0.932 | 0.919 |

Highest correlation coefficients are in bold numbers in Table 5.60. The suggested order at 50°C (323K) was a 'zero order', whereas it was a 'third' order at 60 and 70°C (333 and 343K). A zero order transesterification was not supported by other studies in this work, and by published literature. The most likely order of reaction is 'three'; second order with respect to triglyceride, and first order with respect to methanol (Case 7). The integrated form of rate equation is Eqn 2.40 (Chapter 2) given as:

$\frac{1}{(\alpha_B-3)}\left(\frac{x_A}{1-x_A}-\frac{3}{\alpha_B-3}\right) ln\frac{(\alpha_B-3x_A)}{(1-x_A)\alpha_B} = k\,[A]_o^2\,t$ . The slope in this case is = k $[A_o]^2$.

#### 5.3.6.2.3.3 Rate constant and Activation energy

L.H.S. of Eqn 2.40,( $\frac{1}{(\alpha_B-3)}\left(\frac{x_A}{1-x_A}-\frac{3}{\alpha_B-3}\right) ln\frac{(\alpha_B-3x_A)}{(1-x_A)\alpha_B}$ ) is a function of conversion $x_A$ , F($x_A$), or the yield. A plot of F($x_A$) vs time t is a straight line passing through the origin. Regression

linear plot for F($x_A$) vs. $t$ for 70°C (343K) is given in Fig 5.71.The ordinate is, $\frac{1}{(\alpha_B-3)}\left(\frac{x_A}{1-x_A}-\frac{3}{\alpha_B-3}\right)ln\frac{(\alpha_B-3x_A)}{(1-x_A)\alpha_B}$ ) and abscissa is $t$. Reaction constant $k$ is given by the slope of the plot ($R^2$ = 0.9327).

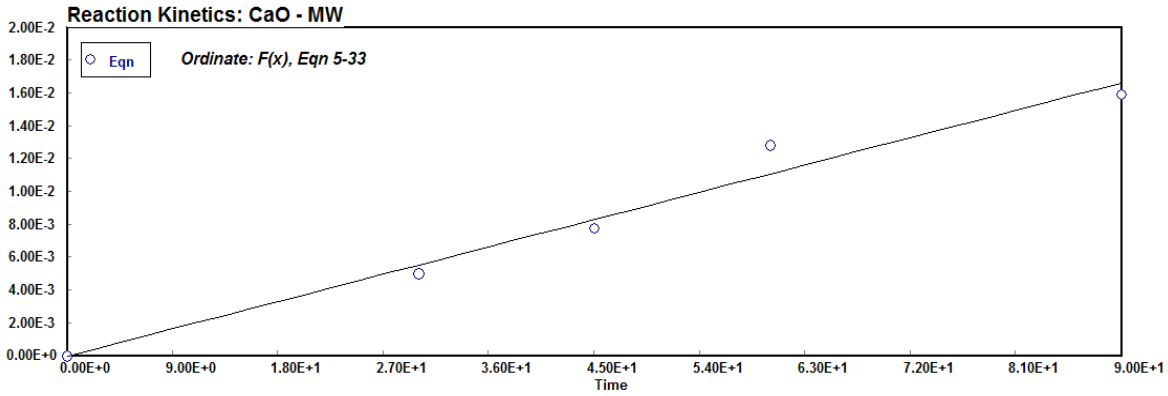


**Figure 5.71: Plot of kinetic equation 2.40 for CaO (MW)**

Correlation constants (k $[A_o]^2$ ) for Eqn 2.40 for the three temperatures were used to estimate reaction constant $k$ as given in Table 5.61.

**Table 5.61: Reaction constant k for CaO (MW)**

| Temp, °C | Temp K | $[Ao]^2$ .k | [Ao] | k |
|---|---|---|---|---|
| | | | g/cm3 | in min |
| **50** | 323.15 | 5.54E-05 | 0.6663 | 7.49E-03 |
| **60** | 333.15 | 0.000187 | 0.6663 | 2.52E-02 |
| **70** | 343.15 | 0.000248 | 0.6663 | 3.35E-02 |

Activation energy was obtained from the slope of the plot of ln$k$ vs. 1/T (Arrhenius plot, Section 2.5.4.1). Fig 5.72 gives the plot ($R^2$ = 0.8969).

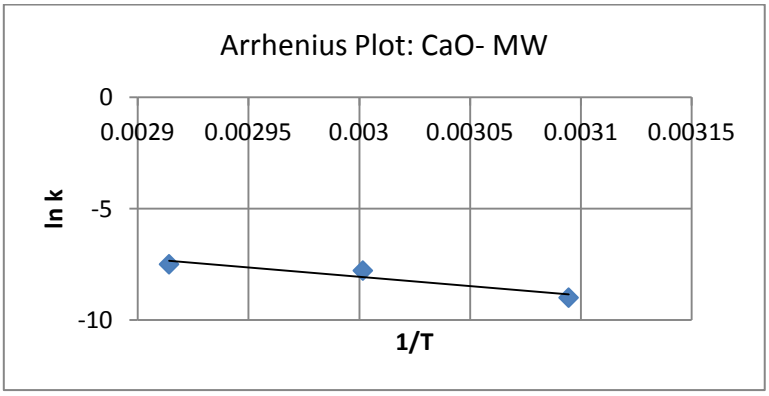


**Figure 5.72: Arrhenius plot for CaO (MW)**

Slope of the plot was 8456.66, giving Activation energy, $E$ = 70.3 kJ/mol; and intercept gave pre-exponential factor $A = 2.44 \times 10^7$.

### 5.3.6.3 Optimization studies

#### 5.3.6.3.1 Nano CaO- experimental results and data analysis

Table 5.62 gives the details of a set of 20 experiments in terms of actual and coded levels, as per CCD, and the FAME yields obtained in transesterification studies. Last column of the Table gives Predicted yield obtained from the Reduced quadratic model (Eqn 5.9).

**Table 5.62: CCD matrix with experimental FAME yield for Nano CaO (MW)**

| Run | Level of variables [actual(coded)] | | | Experimental Yield | Reduced Model (Eqn 5.9) |
|---|---|---|---|---|---|
| | Catalyst,% | Time (min) | Methanol :oil | | Y |
| | X1 | X2 | X3 | | |
| **1** | 1(0) | 3(0) | 9(0) | 52.1 | 52.0 |
| **2** | 1(0) | 0.5(-1.68) | 9(0) | 43.8 | 44.0 |
| **3** | 0.5(-1) | 4.5(1) | 12(1) | 52.7 | 53.2 |
| **4** | 1(0) | 3(0) | 14(1.68) | 54.7 | 54.7 |
| **5** | 1.84(1.68) | 3(0) | 9(0) | 56.3 | 57.1 |
| **6** | 1(0) | 3(0) | 4(-1.68) | 48.9 | 49.3 |
| **7** | 0.5(-1) | 1.5(-1) | 6(-1) | 43.0 | 43.1 |
| **8** | 1(0) | 3(0) | 9(0) | 52.9 | 52.0 |
| **9** | 1.5(1) | 4.5(1) | 12(1) | 59.7 | 59.3 |
| **10** | 1.5(1) | 4.5(1) | 6(-1) | 55.4 | 56.1 |
| **11** | 1(0) | 3(0) | 9(0) | 52.5 | 52.0 |
| **12** | 1.5(1) | 1.5(-1) | 6(-1) | 49.4 | 49.2 |
| **13** | 0.16(-1.68) | 3(0) | 9(0) | 45.3 | 46.9 |
| **14** | 1(0) | 3(0) | 9(0) | 52.0 | 52.0 |
| **15** | 1.5(1) | 1.5(-1) | 12(1) | 52.6 | 52.4 |
| **16** | 1(0) | 3(0) | 9(0) | 52.4 | 52.0 |
| **17** | 0.5(-1) | 1.5(-1) | 12(1) | 46.7 | 46.3 |
| **18** | 1(0) | 5.5(1.68) | 9(0) | 55.1 | 55.5 |
| **19** | 1(0) | 3(0) | 9(0) | 51.5 | 52.0 |
| **20** | 0.5(-1) | 4.5(1) | 6(-1) | 51.8 | 50.0 |

Data in Table 5.62 were tested for fit for a linear, two-factor interaction (2FI), quadratic and cubic polynomials. Table 5.63 gives the result.

**Table 5.63: Summary for model fit- Sequential model sum of squares for Nano CaO (MW)**

| **Summary (detailed tables shown below)** | | | | | | |
|---|---|---|---|---|---|---|
| | **Sequential** | **Lack of Fit** | **Adjusted** | | **Predicted** | |
| **Source** | **p-value** | **p-value** | **R-Squared** | | **R-Squared** | |
| **Linear** | < 0.0001 | 0.0247 | 0.9360 | | 0.9118 | |
| **2FI** | 0.7117 | 0.0168 | 0.9289 | | 0.8821 | |
| **Quadratic** | 0.0141 | 0.0743 | 0.9665 | | 0.8789 | Suggested |
| **Cubic** | 0.4026 | 0.0292 | 0.9689 | | -0.4057 | Aliased |
| **Sequential Model Sum of Squares [Type I]** | | | | | | |
| | **Sum of** | | **Mean** | **F** | **p-value** | |
| **Source** | **Squares** | **df** | **Square** | **Value** | **Prob > F** | |
| **Mean vs Total** | 52916.33 | 1 | 52916.33 | | | |
| **Linear vs Mean** | 321.57 | 3 | 107.19 | 93.67 | < 0.0001 | |
| **2FI vs Linear** | 1.77 | 3 | 0.59 | 0.46 | 0.7117 | |
| **Quadratic vs 2FI** | 10.54 | 3 | 3.51 | 5.86 | 0.0141 | Suggested |
| **Cubic vs Quadratic** | 2.65 | 4 | 0.66 | 1.19 | 0.4026 | Aliased |
| **Residual** | 3.34 | 6 | 0.56 | | | |
| **Total** | 53256.20 | 20 | 2662.81 | | | |

Cubic model was out of consideration, being aliased. Quadratic model had highest Adjusted $R^2$ and hence was suggested. Table 5.64 gives the analysis of variance (ANOVA) for a full quadratic model.

**Table 5.64: ANOVA for Full Quadratic Model for Nano CaO (MW)**

| **ANOVA for Response Surface Quadratic model** | | | | | | |
|---|---|---|---|---|---|---|
| **Analysis of variance table [Partial sum of squares - Type III]** | | | | | | |
| | **Sum of** | | **Mean** | **F** | **p-value** | |
| **Source** | **Squares** | **df** | **Square** | **Value** | **Prob > F** | |
| **Model** | 333.88 | 9 | 37.10 | 61.90 | < 0.0001 | significant |
| ***X1-Nano CaO*** | *125.50* | *1* | *125.50* | *209.40* | *< 0.0001* | |
| ***X2-Time*** | *161.09* | *1* | *161.09* | *268.79* | *< 0.0001* | |
| ***X3-Methanol:oil*** | *34.97* | *1* | *34.97* | *58.35* | *< 0.0001* | |
| ***X1.X2*** | *0.36* | *1* | *0.36* | *0.60* | *0.4555* | |
| ***X1.X3*** | *1.05* | *1* | *1.05* | *1.75* | *0.2148* | |
| ***X2.X3*** | *0.36* | *1* | *0.36* | *0.60* | *0.4555* | |
| ***X1^2*** | *1.57* | *1* | *1.57* | *2.62* | *0.1364* | |
| ***X2^2*** | *9.40* | *1* | *9.40* | *15.68* | *0.0027* | |
| ***X3^2*** | *7.779E-003* | *1* | *7.779E-003* | *0.013* | *0.9116* | |
| **Residual** | 5.99 | 10 | 0.60 | | | |
| ***Lack of Fit*** | *4.81* | *5* | *0.96* | *4.08* | *0.0743* | *not significant* |
| ***Pure Error*** | *1.18* | *5* | *0.24* | | | |

| | | |
|---|---|---|
| **Cor Total** | 339.87 | 19 |

The Model F-value of 61.90 implies the model was significant. There was only a 0.01% chance that an F-value this large could occur due to noise. Values of "Prob > F" less than 0.0500 indicated model terms were significant. In this case X1, X2, X3, X2^2 were significant model terms. The insignificant terms X1.X2, X1.X3, X2.X3, X1^2 and X3^2 were dropped to simplify the model. The reduced model was tested for ANOVA once again.

**ANOVA for Reduced Model**

Table 5.65 gives ANOVA for the reduced model.

**Table 5.65: ANOVA for Reduced Quadratic Model for Nano CaO (MW)**

| **ANOVA for Response Surface Reduced Quadratic model** | | | | | | |
|---|---|---|---|---|---|---|
| **Analysis of variance table [Partial sum of squares - Type III]** | | | | | | |
| **Source** | **Sum of Squares** | **df** | **Mean Square** | **F Value** | **p-value Prob > F** | |
| **Model** | 330.49 | 4 | 82.62 | 132.05 | < 0.0001 | significant |
| ***X1-Nano CaO*** | *125.50* | *1* | *125.50* | *200.59* | *< 0.0001* | |
| ***X2-Time*** | *161.09* | *1* | *161.09* | *257.47* | *< 0.0001* | |
| ***X3-Methanol:oil*** | *34.97* | *1* | *34.97* | *55.90* | *< 0.0001* | |
| ***X2^2*** | *8.92* | *1* | *8.92* | *14.26* | *0.0018* | |
| **Residual** | 9.39 | 15 | 0.63 | | | |
| ***Lack of Fit*** | *8.21* | *10* | *0.82* | *3.48* | *0.0905* | *not significant* |
| ***Pure Error*** | *1.18* | *5* | *0.24* | | | |
| **Cor Total** | 339.87 | 19 | | | | |

The Model F-value of 132.05 implies the model was significant. There was only a 0.01% chance that an F-value this large could occur due to noise. Values of "Prob > F" less than 0.0500 indicate model terms are significant. In this case A, B, C, B^2 were significant model terms. The "Lack of Fit F-value" of 3.48 implied there was a 9.05% chance that a "Lack of Fit F-value" this large could occur due to noise. Lack of fit was not very good but it was insignificant and acceptable since p-value > 0.05. Table 5.66 gives the R-Square for the reduced model.

**Table 5.66: R-Square for reduced model for Nano CaO (MW)**

| | | | |
|---|---|---|---|
| **Std. Dev.** | **0.79** | **R-Squared** | **0.9724** |
| **Mean** | 51.44 | **Adj R-Squared** | 0.9650 |
| **C.V. %** | 1.54 | **Pred R-Squared** | 0.9476 |
| **PRESS** | 17.82 | **Adeq Precision** | 40.788 |

The "Pred R-Squared" of 0.9476 was in reasonable agreement with the "Adj R-Squared" of 0.9650; i.e. the difference was less than 0.2. "Adeq Precision" measures the signal to noise ratio. A ratio greater than 4 is desirable. For this model the ratio of 40.788 indicated an adequate signal. This model can be used for design purposes. Table 5.67 gives the coefficients for the reduced model.

**Table 5.67: Coefficients for the reduced model for Nano CaO (MW)**

| | Coefficient | | Standard | 95% CI | 95% CI | |
|---|---|---|---|---|---|---|
| **Factor** | **Estimate** | **df** | **Error** | **Low** | **High** | **VIF** |
| **Intercept** | 51.97 | 1 | 0.23 | 51.49 | 52.45 | |
| **X1-Nano CaO** | 3.03 | 1 | 0.21 | 2.58 | 3.49 | 1.00 |
| **X2-Time** | 3.43 | 1 | 0.21 | 2.98 | 3.89 | 1.00 |
| **X3-Methanol:oil** | 1.60 | 1 | 0.21 | 1.14 | 2.06 | 1.00 |
| **X2^2** | -0.78 | 1 | 0.21 | -1.22 | -0.34 | 1.00 |

The reduced model was: Yield, $Y = 51.97 + 3.03\ X1 + 3.43\ X2 + 1.60\ X3 – 0.78\ X2^2$

…5.9

The reduced model showed no interaction between the reaction variables and also lacked most of the curvature terms. It was very close to a linear relationship. Reduced model was used to compute Predicted yield given in Table 5.62.

#### 5.3.6.3.1.1 Respond Surface and Contour Plots

Equation 5.9 was used for RSM surface and contour plots. Figs 5.73, 5.74 and 5.75 give the plots. These plots fail to identify the region for optima. The functional relationship for Yield (Eqn 5.9) is almost a linear relationship with only one curvature term. The reason could be that the range of operation variables (Nano CaO concentration, Reaction time and Methanol to oil ratio in Table 5.2) chosen for optimization study were limited and optima possibly lies beyond it. Fig 5.73 is a RSM plot for FAME yield as a function of Nano CaO concentration and reaction time. It shows that the yield increases with increasing catalyst concentration and reaction time- almost linearly.

Fig 5.74 is a RSM surface and contour plot showing FAME yield as functions of Nano CaO concentration and methanol to oil ratio. Yield increased with the increase in these variables. From the plot, catalyst concentration has a larger contribution towards an increase in yield as compared to methanol ratio.

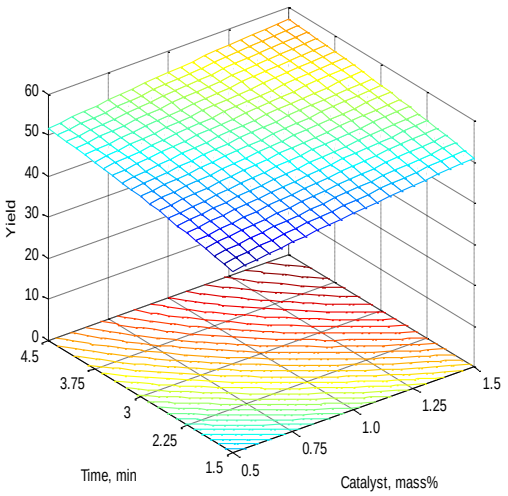


**Figure 5.73: RSM plot- Effect of Time and and Nano CaO conc. on Yield (MW)**

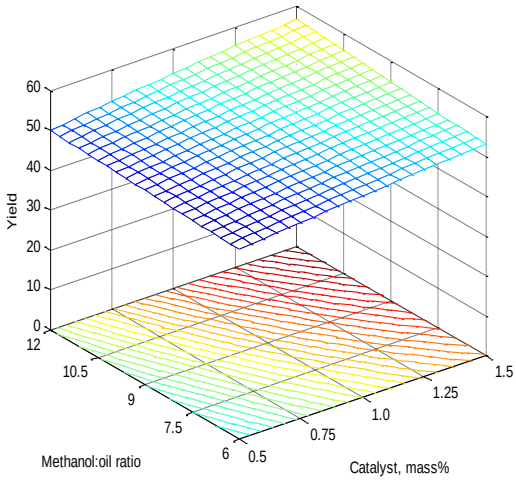


**Figure 5.74: RSM plot- Effect of Meth:oil ratio Nano CaO conc. on Yield (MW)**

Fig 5.75 is a RSM surface and contour plot with variables as methanol to oil ratio and reaction time. Yield increased with increasing time and methanol ratio. Reaction time was a more significant variable as compared to methanol ratio.

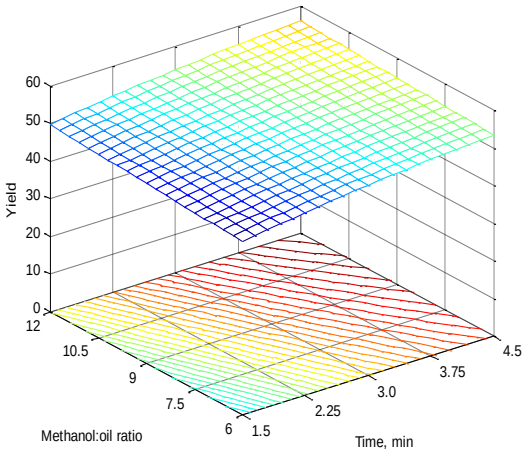


**Figure 5.75: RSM plot- Effect of Meth:oil ratio and Time on Yield for Nano CaO (MW)**

#### 5.3.6.3.1.1 Re-oxidized CaO- experimental results and data analysis

Table 5.68 gives the details of a set of 20 experiments in terms of actual and coded levels as per CCD, and the FAME yields obtained in transesterification studies. Table also gives Predicted yield obtained from the Reduced quadratic model (Eqn 5.10).

**Table 5.68: CCD matrix with experimental FAME yield for CaO-RO (MW)**

| Run | Level of variables [actual(coded)] | | | Experimental Yield | Reduced Model (Eqn 5.10) |
|---|---|---|---|---|---|
| | Catalyst,% | Time (min) | Methanol :oil | | **Y** |
| | X1 | X2 | X3 | | |
| **1** | 1(0) | 3(0) | 9(0) | 23.6 | 23.7 |
| **2** | 1(0) | 0.5(-1.68) | 9(0) | 22.5 | 20.9 |
| **3** | 0.5(-1) | 4.5(1) | 12(1) | 19.3 | 20.1 |
| **4** | 1(0) | 3(0) | 14(1.68) | 18.5 | 19.1 |
| **5** | 1.84(1.68) | 3(0) | 9(0) | 22.1 | 21.6 |
| **6** | 1(0) | 3(0) | 4(-1.68) | 18.6 | 17.8 |
| **7** | 0.5(-1) | 1.5(-1) | 6(-1) | 18.2 | 19.2 |
| **8** | 1(0) | 3(0) | 9(0) | 23.9 | 23.7 |
| **9** | 1.5(1) | 4.5(1) | 12(1) | 24.9 | 25.1 |
| **10** | 1.5(1) | 4.5(1) | 6(-1) | 21.9 | 22.5 |
| **11** | 1(0) | 3(0) | 9(0) | 22.9 | 23.7 |
| **12** | 1.5(1) | 1.5(-1) | 6(-1) | 17.3 | 17.8 |
| **13** | 0.16(-1.68) | 3(0) | 9(0) | 18.3 | 18.6 |
| **14** | 1(0) | 3(0) | 9(0) | 22.8 | 23.7 |
| **15** | 1.5(1) | 1.5(-1) | 12(1) | 20.8 | 20.4 |
| **16** | 1(0) | 3(0) | 9(0) | 23.9 | 23.7 |
| **17** | 0.5(-1) | 1.5(-1) | 12(1) | 19.8 | 18.3 |
| **18** | 1(0) | 5.5(1.68) | 9(0) | 25.8 | 26.4 |
| **19** | 1(0) | 3(0) | 9(0) | 24.0 | 23.7 |
| **20** | 0.5(-1) | 4.5(1) | 6(-1) | 21.6 | 21.0 |

Data in Table 5.68 were tested for fit for a linear, two-factor interaction (2FI), quadratic and cubic polynomials. Table 5.69 gives the result.

**Table 5.69: Summary for model fit- Sequential model sum of squares for CaO-RO (MW)**

| Summary for model fit | | | | | |
|---|---|---|---|---|---|
| | Sequential | Lack of Fit | Adjusted | Predicted | |
| Source | p-value | p-value | R-Squared | R-Squared | |
| Linear | 0.1327 | 0.0010 | 0.1548 | -0.1581 | |
| 2FI | 0.5302 | 0.0007 | 0.1170 | -0.5379 | |
| Quadratic | < 0.0001 | 0.1010 | 0.9012 | 0.6587 | Suggested |
| Cubic | 0.0715 | 0.3101 | 0.9534 | 0.3240 | Aliased |
| **Sequential Model Sum of Squares [Type I]** | | | | | |
| | Sum of | | Mean | F | p-value |
| Source | Squares | df | Square | Value | Prob > F |
| Mean vs Total | 9275.12 | 1 | 9275.12 | | |
| Linear vs Mean | 35.10 | 3 | 11.70 | 2.16 | 0.1327 |
| 2FI vs Linear | 13.10 | 3 | 4.37 | 0.77 | 0.5302 |
| Quadratic vs 2FI | 67.25 | 3 | 22.42 | 35.40 | < 0.0001 |
| Cubic vs Quadratic | 4.54 | 4 | 1.13 | 3.80 | 0.0715 |
| Residual | 1.79 | 6 | 0.30 | | |
| Total | 9396.91 | 20 | 469.85 | | " |

Cubic had the highest $R^2$ (0.9534), followed by $R^2$ for Quadratic model (0.9012). However, cubic was not suitable because of being aliased. Considering the F and p-values, a Quadratic model was suggested. Cubic was aliased. The appropriate model for the given set of data was full Quadratic model (Eqn 4.2, Chapter 4) :

$$Y = b_0 + \sum_{i=1}^{n} b_i X_i + \sum_{i=1}^{n} b_{ii} X_i^2 + \sum_{1=1}^{n-1} \sum_{j=i+1}^{n} b_{ij} X_i X_j \quad \ldots 4.2$$

Y is the FAME Yield, $X_i$ are coded variables as given in Table 5.2.

Table 5.70 gives Analysis of Variance (ANOVA) for a full quadratic model.

**Table 5.70: ANOVA for Response Surface Quadratic model for CaO RO (MW)**

| ANOVA for Response Surface Quadratic model | | | | | | |
|---|---|---|---|---|---|---|
| **Analysis of variance table [Partial sum of squares - Type III]** | | | | | | |
| | Sum of | | Mean | F | p-value | |
| Source | Squares | df | Square | Value | Prob > F | |
| **Model** | 115.45 | 9 | 12.83 | 20.26 | < 0.0001 | significant |
| ***X1-Catalyst*** | *11.24* | *1* | *11.24* | *17.75* | *0.0018* | |
| ***X2-Time*** | *21.54* | *1* | *21.54* | *34.01* | *0.0002* | |
| ***X3-Methanol:oil*** | *2.32* | *1* | *2.32* | *3.67* | *0.0845* | |
| ***X1.X2*** | *4.20* | *1* | *4.20* | *6.64* | *0.0276* | |
| ***X1.X3*** | *6.48* | *1* | *6.48* | *10.23* | *0.0095* | |
| ***X2.X3*** | *2.42* | *1* | *2.42* | *3.82* | *0.0791* | |
| ***X1^2*** | *22.29* | *1* | *22.29* | *35.21* | *0.0001* | |

| | | | | | | |
|---|---|---|---|---|---|---|
| ***X2^2*** | *0.34* | *1* | *0.34* | *0.53* | *0.4831* | |
| ***X3^2*** | *48.11* | *1* | *48.11* | *75.98* | *< 0.0001* | |
| **Residual** | 6.33 | 10 | 0.63 | | | |
| ***Lack of Fit*** | *4.90* | *5* | *0.98* | *3.43* | *0.1010* | *not significant* |
| ***Pure Error*** | *1.43* | *5* | *0.29* | | | |
| **Cor Total** | 121.79 | 19 | | | | |

The Model F-value of 20.26 implied the model was significant. There was only a 0.01% chance that an F-value this large could occur due to noise. Values of "Prob > F" less than 0.0500 indicated model terms were significant. In this case X1, X2, X1.X2, X1.X3, X1^2, X3^2 were significant model terms. Insignificant terms were X3, X2.X3, X2^2. The model could possibly be reduced by dropping these terms. It was not advisable to drop X3 since it was part of model hierarchy. Hence X2.X3, X2^2 were dropped and the reduced model tested for ANOVA.

**Reduced model:**. Table 5.71 gives the ANOVA for the reduced model where X2.X3, X2^2 had been dropped.

**Table 5.71: ANOVA for Response Surface Reduced Quadratic model for CaO RO (MW)**

| **ANOVA for Response Surface Reduced Quadratic model** | | | | | | |
|---|---|---|---|---|---|---|
| **Analysis of variance table [Partial sum of squares - Type III]** | | | | | | |
| | **Sum of** | | **Mean** | **F** | **p-value** | |
| **Source** | **Squares** | **df** | **Square** | **Value** | **Prob > F** | |
| **Model** | 112.70 | 7 | 16.10 | 21.26 | < 0.0001 | significant |
| ***X1-Catalyst*** | *11.24* | *1* | *11.24* | *14.84* | *0.0023* | |
| ***X2-Time*** | *21.54* | *1* | *21.54* | *28.44* | *0.0002* | |
| ***X3-Methanol:oil*** | *2.32* | *1* | *2.32* | *3.07* | *0.1054* | |
| ***X1.X2*** | *4.20* | *1* | *4.20* | *5.55* | *0.0363* | |
| ***X1.X3*** | *6.48* | *1* | *6.48* | *8.56* | *0.0127* | |
| ***X1^2*** | *23.07* | *1* | *23.07* | *30.46* | *0.0001* | |
| ***X3^2*** | *49.40* | *1* | *49.40* | *65.23* | *< 0.0001* | |
| **Residual** | 9.09 | 12 | 0.76 | | | |
| ***Lack of Fit*** | *7.66* | *7* | *1.09* | *3.83* | *0.0792* | *not significant* |
| ***Pure Error*** | *1.43* | *5* | *0.29* | | | |
| **Cor Total** | 121.79 | 19 | | | | |

The Model F-value of 21.26 implied the model was significant. There was only a 0.01% chance that an F-value this large could occur due to noise. Values of "Prob > F" less than 0.0500 indicate model terms are significant. In this case X1, X2, X1.X2, X1.X3, X1^2, X3^2 were significant model terms. The "Lack of Fit F-value" of 3.83 implied there was a 7.92% chance that a "Lack of Fit F- value" this large could occur due to noise. Lack of fit

was not very good but it was not significant and acceptable since p-value > 0.05. Table 5.72 gives the $R^2$ values for the reduced model.

**Table 5.72: R-Square values for CaO RO (MW)**

| | | | |
|---|---|---|---|
| **Std. Dev.** | **0.87** | **R-Squared** | **0.9254** |
| **Mean** | 21.54 | **Adj R-Squared** | 0.8818 |
| **C.V. %** | 4.04 | **Pred R-Squared** | 0.7009 |
| **PRESS** | 36.43 | **Adeq Precision** | 14.566 |

The "Pred R-Squared" of 0.7009 was in reasonable agreement with the "Adj R-Squared" of 0.8818; i.e. the difference was less than 0.2. "Adeq Precision" measures the signal to noise ratio. A ratio greater than 4 is desirable. This model had a ratio of 14.566 which indicated an adequate signal. This model can be used for design purposes. Table 5.73 gives the coefficients for the reduced quadratic model.

**Table 5.73: Coefficients for the Reduced Quadratic model for CaO-RO (MW)**

| | Coefficient | | Standard | 95% CI | 95% CI |
|---|---|---|---|---|---|
| **Factor** | **Estimate** | **df** | **Error** | **Low** | **High** |
| **Intercept** | 23.65 | 1 | 0.30 | 23.00 | 24.31 |
| **X1-Catalyst** | 0.91 | 1 | 0.24 | 0.39 | 1.42 |
| **X2-Time** | 1.26 | 1 | 0.24 | 0.74 | 1.77 |
| **X3-Meth:oil** | 0.41 | 1 | 0.24 | -0.10 | 0.93 |
| **X1.X2** | 0.72 | 1 | 0.31 | 0.055 | 1.40 |
| **X1.X3** | 0.90 | 1 | 0.31 | 0.23 | 1.57 |
| **X1^2** | -1.26 | 1 | 0.23 | -1.76 | -0.76 |
| **X3^2** | -1.84 | 1 | 0.23 | -2.34 | -1.35 |

Since all the terms in the reduced model were significant, no further reductions were needed. Hence the model was:

$$\text{Yield, } Y = 23.65 + 0.91\,X1 + 1.26\,X2 + 0.41\,X3 + 0.72\,X1.X2 + 0.90\,X1.X3 - 1.26\,X1^2 - 1.84\,X3^2 \quad \ldots 5.10$$

Reduced model was used to obtain Predicted yield given in Table 5.68. In the following section, Eqn 5.10 was used for response surface plots.

#### 5.3.6.3.1.2 Response Surface and Contour Plots

Fig 5.76 is a RSM surface and contour plot for FAME yield as a function of CaO RO catalyst mass% and Time. Yield increased with time and with increasing catalyst

concentration. No optima was found within the range of independent variables in this case. This general observation agreed with experimental findings.

Fig 5.77 is RSM surface and contour plot for FAME yield as function of CaO-RO concentration and Methanol to oil ratio. Maxima was at methanol:oil ratio of > 9:1 and CaO RO of 1.25%. Experimental data were in agreement with this observation.

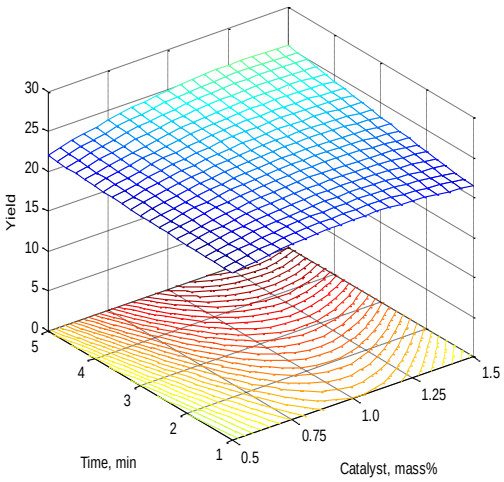


**Figure 5.76: RSM plot- Effect of CaO-RO and Time on Yield (MW)**

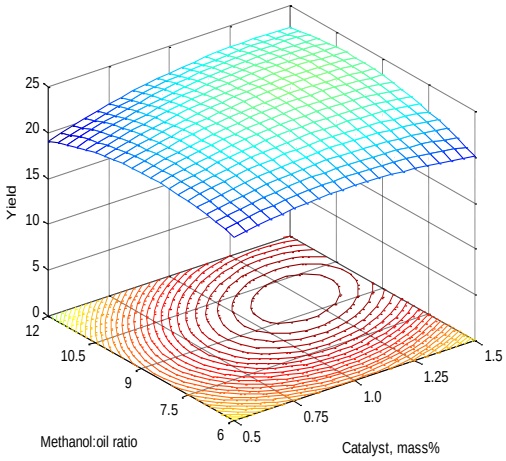


**Figure 5.77: RSM plot- Effect of Meth:oil ratio and CaO RO conc. on Yield (MW)**

Fig 5.78 is a RSM surface and contour plot for Yield as function of methanol to oil ratio and time. Optima was at time > 5 min, and at methanol ratio of 9:1. This fully agreed with experimental data.

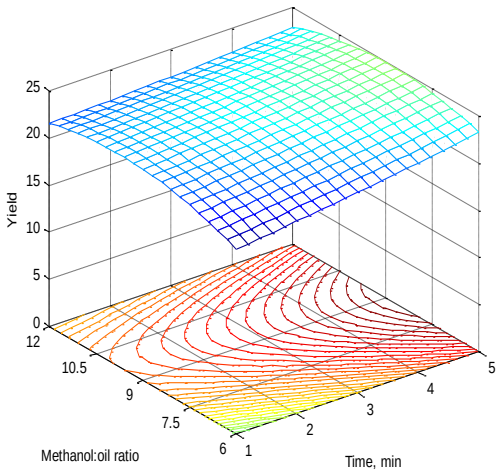


**Figure 5.78: RSM plot- Effect of Meth:oil ratio and Time on Yield for CaO RO (MW)**

#### 5.3.6.3.1.1 CaO- Experimental results and data analysis

Table 5.74 gives the details of a set of 20 experiments in terms of actual and coded levels as per CCD, and the FAME yields obtained in transesterification studies. Last column of the Table gives Predicted yield computed using the Reduced quadratic model (Eqn 5.11).

**Table 5.74: CCD matrix with experimental FAME yield for CaO (MW)**

| Run | Level of variables [actual(coded)] | | | Experimental Yield | Reduced Model (Eqn 5.11) |
|---|---|---|---|---|---|
| | Catalyst,% | Time (min) | Methanol :oil | | Y |
| | X1 | X2 | X3 | | |
| **1** | 1(0) | 3(0) | 9(0) | 18.6 | 18.9 |
| **2** | 1(0) | 0.5(-1.68) | 9(0) | 16.0 | 16.1 |
| **3** | 0.5(-1) | 4.5(1) | 12(1) | 16.8 | 16.8 |
| **4** | 1(0) | 3(0) | 14(1.68) | 18.2 | 18.1 |
| **5** | 1.84(1.68) | 3(0) | 9(0) | 18.2 | 18.4 |
| **6** | 1(0) | 3(0) | 4(-1.68) | 12.9 | 13.5 |
| **7** | 0.5(-1) | 1.5(-1) | 6(-1) | 10.8 | 11.5 |
| **8** | 1(0) | 3(0) | 9(0) | 18.9 | 18.9 |
| **9** | 1.5(1) | 4.5(1) | 12(1) | 20.5 | 20.1 |
| **10** | 1.5(1) | 4.5(1) | 6(-1) | 18.6 | 18.4 |
| **11** | 1(0) | 3(0) | 9(0) | 19.1 | 18.9 |
| **12** | 1.5(1) | 1.5(-1) | 6(-1) | 16.1 | 15.0 |
| **13** | 0.16(-1.68) | 3(0) | 9(0) | 12.3 | 12.7 |
| **14** | 1(0) | 3(0) | 9(0) | 19.2 | 18.9 |
| **15** | 1.5(1) | 1.5(-1) | 12(1) | 17.6 | 18.5 |
| **16** | 1(0) | 3(0) | 9(0) | 18.4 | 18.9 |
| **17** | 0.5(-1) | 1.5(-1) | 12(1) | 15.8 | 15.1 |
| **18** | 1(0) | 5.5(1.68) | 9(0) | 19.8 | 20.3 |
| **19** | 1(0) | 3(0) | 9(0) | 19.3 | 18.9 |
| **20** | 0.5(-1) | 4.5(1) | 6(-1) | 15.5 | 14.9 |

Data in Table 5.74 were tested for fit for a linear, two-factor interaction (2FI), quadratic and cubic polynomials. Table 5.75 gives the result.

**Table 5.75: Summary for model fit- Sequential model sum of squares for CaO (MW)**

| Summary for model fit | | | | |
|---|---|---|---|---|
| | **Sequential** | **Lack** | **Adjusted** | **Predicted** |

| | | of Fit | | | |
|---|---|---|---|---|---|
| **Source** | **p-value** | **p-value** | **R-Squared** | **R-Squared** | |
| **Linear** | 0.0003 | 0.0009 | 0.6229 | 0.5266 | |
| **2FI** | 0.8473 | 0.0005 | 0.5629 | 0.2892 | |
| **Quadratic** | < 0.0001 | 0.0553 | 0.9431 | 0.7794 | Suggested |
| **Cubic** | 0.0831 | 0.1137 | 0.9716 | 0.1572 | Aliased |

**Sequential Model Sum of Squares [Type I]**

| **Source** | **Sum of Squares** | **df** | **Mean Square** | **F Value** | **p-value Prob > F** | |
|---|---|---|---|---|---|---|
| **Mean vs Total** | 5866.34 | 1 | 5866.34 | | | |
| **Linear vs Mean** | 89.41 | 3 | 29.80 | 11.46 | 0.0003 | |
| **2FI vs Linear** | 2.42 | 3 | 0.81 | 0.27 | 0.8473 | |
| **Quadratic vs 2FI** | 35.26 | 3 | 11.75 | 29.96 | < 0.0001 | Suggested |
| **Cubic vs Quadratic** | 2.75 | 4 | 0.69 | 3.51 | 0.0831 | Aliased |
| **Residual** | 1.17 | 6 | 0.20 | | | |
| **Total** | 5997.36 | 20 | 299.87 | | | |

Cubic had the highest Adjusted $R^2$ (0.9716), followed by Adjusted $R^2$ for Quadratic model (0.9431). However, cubic was not suitable because of being aliased. Considering the F and p-values, a Quadratic model was suggested. Cubic was aliased. The appropriate model for the given set of data was full Quadratic model (Eqn 4.2, Chapter 4) :

$$Y = b_0 + \sum_{i=1}^{n} b_i X_i + \sum_{i=1}^{n} b_{ii} X_i^2 + \sum_{1=1}^{n-1} \sum_{j=i+1}^{n} b_{ij} X_i X_j \quad \ldots 4.2$$

Y is the FAME Yield, $X_i$ are coded variables as given in Table 5.2.

Table 5.76 gives Analysis of Variance (ANOVA) for a full quadratic model.

**Table 5.76: ANOVA for Response Surface Quadratic model for CaO (MW)**

**ANOVA for Response Surface Quadratic model**

**Analysis of variance table [Partial sum of squares - Type III]**

| **Source** | **Sum of Squares** | **df** | **Mean Square** | **F Value** | **p-value Prob > F** | |
|---|---|---|---|---|---|---|
| **Model** | 127.09 | 9 | 14.12 | 36.00 | < 0.0001 | significant |
| ***X1-CaO*** | *41.56* | *1* | *41.56* | *105.92* | *< 0.0001* | |
| ***X2-Time*** | *22.49* | *1* | *22.49* | *57.32* | *< 0.0001* | |
| ***X3-Methanol:oil*** | *25.37* | *1* | *25.37* | *64.67* | *< 0.0001* | |
| ***X1.X2*** | *0.011* | *1* | *0.011* | *0.029* | *0.8689* | |
| ***X1.X3*** | *1.05* | *1* | *1.05* | *2.68* | *0.1327* | |
| ***X2.X3*** | *1.36* | *1* | *1.36* | *3.47* | *0.0921* | |
| ***X1^2*** | *21.10* | *1* | *21.10* | *53.80* | *< 0.0001* | |
| ***X2^2*** | *1.10* | *1* | *1.10* | *2.82* | *0.1243* | |
| ***X3^2*** | *17.57* | *1* | *17.57* | *44.78* | *< 0.0001* | |
| **Residual** | 3.92 | 10 | 0.39 | | | |

| | | | | | | |
|---|---|---|---|---|---|---|
| ***Lack of Fit*** | *3.25* | *5* | *0.65* | *4.79* | *0.0553* | *not significant* |
| ***Pure Error*** | *0.68* | *5* | *0.14* | | | |
| **Cor Total** | 131.02 | 19 | | | | |

The Model F-value of 36.00 implied the model was significant. There was only a 0.01% chance that an F-value this large could occur due to noise. Values of "Prob > F" less than 0.0500 indicate model terms are significant. In this case X1, X2, X3, X1^2, X3^2 were significant model terms. Terms X1.X2, X1.X3, X2.X3, X2^2 were not significant. These terms could be dropped to simplify the model. Terms X1.X2, X1.X3, X2^2 were dropped first, while retaining X2.X3 since Prob > F was 0.0921( < 0.1000). This was named Reduced Model-1.

**Reduced model-1:**. Dropped X1.X2, X1.X3 and X2^2 . Table 5.77 gives the ANOVA for the reduced model.

**Table 5.77: ANOVA for Response Surface Reduced Quadratic model-1 for CaO (MW)**

| **ANOVA for Response Surface Reduced Quadratic model 1** | | | | | | |
|---|---|---|---|---|---|---|
| **Analysis of variance table [Partial sum of squares - Type III]** | | | | | | |
| | **Sum of** | | **Mean** | **F** | **p-value** | |
| **Source** | **Squares** | **df** | **Square** | **Value** | **Prob > F** | |
| **Model** | 124.93 | 6 | 20.82 | 44.45 | < 0.0001 | significant |
| ***X1-CaO*** | *41.56* | *1* | *41.56* | *88.71* | *< 0.0001* | |
| ***X2-Time*** | *22.49* | *1* | *22.49* | *48.00* | *< 0.0001* | |
| ***X3-Methanol:oil*** | *25.37* | *1* | *25.37* | *54.15* | *< 0.0001* | |
| ***X2X3*** | *1.36* | *1* | *1.36* | *2.91* | *0.1120* | |
| ***X1^2*** | *20.36* | *1* | *20.36* | *43.46* | *< 0.0001* | |
| ***X3^2*** | *16.87* | *1* | *16.87* | *36.01* | *< 0.0001* | |
| **Residual** | 6.09 | 13 | 0.47 | | | |
| ***Lack of Fit*** | *5.41* | *8* | *0.68* | *4.99* | *0.0465* | *significant* |
| ***Pure Error*** | *0.68* | *5* | *0.14* | | | |
| **Cor Total** | 131.02 | 19 | | | | |

The Model F-value of 44.45 implied the model was significant. There was only a 0.01% chance that an F-value this large could occur due to noise. Values of "Prob > F" less than 0.0500 indicate model terms are significant. In this case X1, X2, X3, X1^2, X3^2 were significant model terms. The "Lack of Fit F-value" of 4.99 implied the Lack of Fit was significant. There was only a 4.65% chance that a "Lack of Fit F-value" this large could occur due to noise. This showed that the present reduced model failed lack-of-fit test. Also

p-value for X2.X3 had gone worse. In another attempt to simplify the model, X2.X3 was dropped as well. This was called as Reduced Model-2, and tested for ANOVA.

**Reduced Model-2:** Dropped X1.X2, X2.X3, X1.X3 and X2^2. Table 5.78 gives ANOVA.

**Table 5.78: ANOVA for Response Surface Reduced Quadratic model2 for CaO (MW)**

| ANOVA for Response Surface Reduced Quadratic model2 | | | | | | |
|---|---|---|---|---|---|---|
| **Analysis of variance table [Partial sum of squares - Type III]** | | | | | | |
| | **Sum of** | | **Mean** | **F** | **p-value** | |
| **Source** | **Squares** | **df** | **Square** | **Value** | **Prob > F** | |
| **Model** | 123.57 | 5 | 24.71 | 46.43 | < 0.0001 | significant |
| ***X1-CaO*** | *41.56* | *1* | *41.56* | *78.08* | *< 0.0001* | |
| ***X2-Time*** | *22.49* | *1* | *22.49* | *42.25* | *< 0.0001* | |
| ***X3-Methanol:oil*** | *25.37* | *1* | *25.37* | *47.67* | *< 0.0001* | |
| ***X1^2*** | *20.36* | *1* | *20.36* | *38.25* | *< 0.0001* | |
| ***X3^2*** | *16.87* | *1* | *16.87* | *31.70* | *< 0.0001* | |
| **Residual** | 7.45 | 14 | 0.53 | | | |
| ***Lack of Fit*** | *6.77* | *9* | *0.75* | *5.56* | *0.0367* | *significant* |
| ***Pure Error*** | *0.68* | *5* | *0.14* | | | |
| **Cor Total** | 131.02 | 19 | | | | |

The Model F-value of 46.43 implied the model was significant. There was only a 0.01% chance that an F-value this large could occur due to noise. Values of "Prob > F" less than 0.0500 indicate model terms are significant. In this case X1, X2, X3, X1^2, X3^2 were significant model terms. The "Lack of Fit F-value" of 5.56 implied the Lack of Fit was significant. There was only a 3.67% chance that a "Lack of Fit F-value" this large could occur due to noise. In this Reduced Model-2 lack-of-fit had became worse when compared to Reduced model-1. In another attempt to simplify, only X1.X2 was dropped (largest p-value in full model) while retaining all other terms. This was named as Reduced Model-3.

**Reduced Model-3**: Dropped X1.X2. ANOVA is given in Table 5.79.

**Table 5.79: ANOVA for Response Surface Reduced Quadratic model3 for CaO (MW)**

| ANOVA for Response Surface Reduced Quadratic model-3 | | | | | | |
|---|---|---|---|---|---|---|
| **Analysis of variance table [Partial sum of squares - Type III]** | | | | | | |
| | **Sum of** | | **Mean** | **F** | **p-value** | |
| **Source** | **Squares** | **df** | **Square** | **Value** | **Prob > F** | |
| **Model** | 127.08 | 8 | 15.89 | 44.41 | < 0.0001 | significant |
| ***X1-CaO*** | *41.56* | *1* | *41.56* | *116.18* | *< 0.0001* | |
| ***X1-Time*** | *22.49* | *1* | *22.49* | *62.87* | *< 0.0001* | |

| | | | | | | |
|---|---|---|---|---|---|---|
| ***X3-Methanol:oil*** | *25.37* | *1* | *25.37* | *70.93* | *< 0.0001* | |
| ***X1.X3*** | *1.05* | *1* | *1.05* | *2.94* | *0.1145* | |
| ***X2.X3*** | *1.36* | *1* | *1.36* | *3.81* | *0.0770* | |
| ***X1^2*** | *21.10* | *1* | *21.10* | *59.01* | *< 0.0001* | |
| ***X2^2*** | *1.10* | *1* | *1.10* | *3.09* | *0.1066* | |
| ***X3^2*** | *17.57* | *1* | *17.57* | *49.12* | *< 0.0001* | |
| **Residual** | 3.93 | 11 | 0.36 | | | |
| ***Lack of Fit*** | *3.26* | *6* | *0.54* | *4.01* | *0.0746* | *not significant* |
| ***Pure Error*** | *0.68* | *5* | *0.14* | | | |
| **Cor Total** | 131.02 | 19 | | | | |

The Model F-value of 44.41 implies the model was significant. There was only a 0.01% chance that an F-value this large could occur due to noise. Values of "Prob > F" less than 0.0500 indicate model terms are significant. In this case X1, X2, X3, X1^2, X3^2 were significant model terms. The "Lack of Fit F-value" of 4.01 implied there is a 7.46% chance that a "Lack of Fit F- value" this large could occur due to noise. Lack-of-fit was not significant. Another reduction was attempted by dropping X1.X2 and X1.X3, named Reduced Model-4.

**Reduced Model-4**: Dropped X1.X2 and X1.X3 but retained X2^2. Table 5.80 gives the ANOVA.

**Table 5.80: ANOVA for Response Surface Reduced Quadratic model-4 for CaO (MW)**

| **ANOVA for Response Surface Reduced Quadratic model-4** | | | | | | |
|---|---|---|---|---|---|---|
| **Analysis of variance table [Partial sum of squares - Type III]** | | | | | | |
| | **Sum of** | | **Mean** | **F** | **p-value** | |
| **Source** | **Squares** | **df** | **Square** | **Value** | **Prob > F** | |
| **Model** | 126.03 | 7 | 18.00 | 43.34 | < 0.0001 | Significant |
| ***X1-CaO*** | *41.56* | *1* | *41.56* | *100.02* | *< 0.0001* | |
| ***X2-Time*** | *22.49* | *1* | *22.49* | *54.12* | *< 0.0001* | |
| ***X3-Methanol:oil*** | *25.37* | *1* | *25.37* | *61.06* | *< 0.0001* | |
| ***X2.X3*** | *1.36* | *1* | *1.36* | *3.28* | *0.0954* | |
| ***X1^2*** | *21.10* | *1* | *21.10* | *50.80* | *< 0.0001* | |
| ***X2^2*** | *1.10* | *1* | *1.10* | *2.66* | *0.1290* | |
| ***X3^2*** | *17.57* | *1* | *17.57* | *42.28* | *< 0.0001* | |
| **Residual** | 4.99 | 12 | 0.42 | | | |
| ***Lack of Fit*** | *4.31* | *7* | *0.62* | *4.54* | *0.0574* | *not significant* |
| ***Pure Error*** | *0.68* | *5* | *0.14* | | | |
| **Cor Total** | 131.02 | 19 | | | | |

The Model F-value of 43.34 implied the model was significant. There was only a 0.01% chance that an F-value this large could occur due to noise. Values of "Prob > F" less than

0.0500 indicate model terms are significant. In this case X1, X2, X3, X1^2, X3^2 were significant model terms. The "Lack of Fit F-value" of 4.54 implied there is a 5.74% chance that a "Lack of Fit F- value" this large could occur due to noise. Lack-of-fit was not good but it was insignificant and acceptable. This was taken to be the final model since it met the lack-of-fit requirements. Table 5.81 gives the R-Square values for this reduced model.

**Table 5.81: R-Square values for Reduced Model-4 for CaO (MW)**

| **Std. Dev.** | **0.64** | **R-Squared** | **0.9619** |
|---|---|---|---|
| **Mean** | 17.13 | **Adj R-Squared** | 0.9397 |
| **C.V. %** | 3.76 | **Pred R-Squared** | 0.8767 |
| **PRESS** | 16.15 | **Adeq Precision** | 21.539 |

The "Pred R-Squared" of 0.8767 was in reasonable agreement with the "Adj R-Squared" of 0.9397; i.e. the difference was less than 0.2. "Adeq Precision" measures the signal to noise ratio. A ratio greater than 4 is desirable. Model ratio of 21.539 indicated an adequate signal. This model can be used for design purposes. Table 5.82 gives the coefficients for this model

**Table 5.82: Coefficients for Reduced Model-4- for CaO (MW)**

| | **Coefficient** | | **Standard** | **95% CI** | **95% CI** |
|---|---|---|---|---|---|
| **Factor** | **Estimate** | **df** | **Error** | **Low** | **High** |
| **Intercept** | 18.90 | 1 | 0.26 | 18.32 | 19.47 |
| **X1-CaO** | 1.74 | 1 | 0.17 | 1.36 | 2.12 |
| **X2-Time** | 1.28 | 1 | 0.17 | 0.90 | 1.66 |
| **X3-Methanol:oil** | 1.36 | 1 | 0.17 | 0.98 | 1.74 |
| **X2X3** | -0.41 | 1 | 0.23 | -0.91 | 0.084 |
| **X1^2** | -1.21 | 1 | 0.17 | -1.58 | -0.84 |
| **X2^2** | -0.28 | 1 | 0.17 | -0.65 | 0.093 |
| **X3^2** | -1.10 | 1 | 0.17 | -1.47 | -0.73 |

Reduced Model-4 was the final model since any further reduction made lack-of-fit significant. Hence the Reduced Quadratic model was:

Yield, $Y = 18.90 + 1.74\ X1 + 1.28\ X2 + 1.36\ X3 - 0.41 X2.X3 - 1.21\ X1^2 - 0.28\ X2^2$

$- 1.10\ X3\text{^}2$ …5.11

Reduced Model-4 was used to estimate Predicted yield given in Table 5.74. In the following section, Eqn 5.11 was used for response surface plots.

#### 5.3.6.3.1.2 Response Surface and Contour Plots

Fig 5.79 is a RSM surface and contour plot for FAME yield as function of CaO concentration and reaction time. Optima was at time > 5 min and CaO > 1.25%. This was in agreement with experimental observations. Fig 5.80 is a RSM plot for FAME yield as function of CaO concentration and methanol to oil ratio. It depicted the area for maximum yield corresponding to CaO > 1.25% and methanol:oil ratio of 10.5. This was in agreement with experimental data.

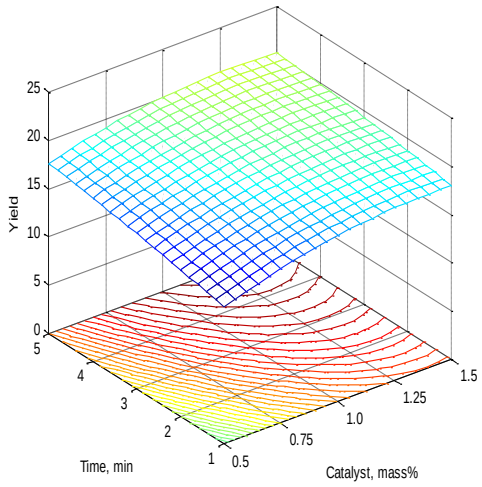


**Figure 5.79: RSM plot- Effect of CaO conc. and Time on Yield (MW)**

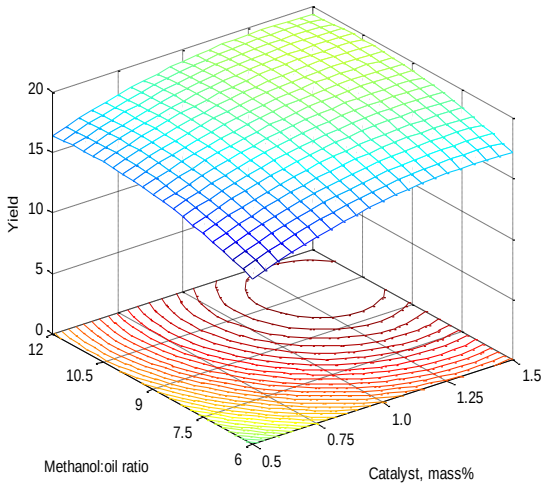


**Figure 5.80: RSM plot- Effect of. CaO conc. and Methanol:oil ratio on Yield (MW)**

Fig 5.81 is a RSM surface and contour plot for FAME yield as function of methanol:oil ratio and reaction time. Maxima corresponded to time > 5 min, and methanol:oil ratio 9 – 10.5. This was in agreement with experimental studies.

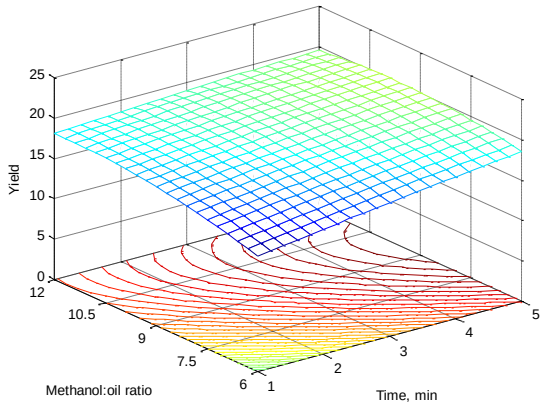


**Figure 5.81: RSM plot- Effect of Time and Methanol:oil ratio on Yield for CaO (MW)**

### 5.3.7 Studies with conventional heating- Nano magnesium oxide and Magnesium oxide catalysts

This section deals with transesterification studies carried out with conventional heating employing a water bath as heat source.

#### 5.3.7.1 Effect of operation variables on FAME yield

##### 5.3.7.1.1 Effect of Methanol to triglyceride mole ratio

Fig 5.82 gives the FAME yield for Nano MgO, and MgO as a function methanol to oil molar ratio.

Nano MgO gave a higher yield as compared to MgO. The highest yield was at 9:1 methanol to oil ratio, 24.5% for Nano MgO and 19.4% for MgO. The yield decreased at higher methanol ratio but the decrease was slight, of about 1%. At very high methanol ratios, glycerol dissolves in excessive methanol and subsequently inhibits the forward reaction (Viriya-empikul *et al*., 2010). Other explanation for reduced yield is that catalyst concentration decreases with excess methanol (Liu *et al*., 2008; Bambase *et al*., 2007). Excess methanol affects the interphase area between alcohol and oil due to their immiscibility leading to a drop in yield (Babak *et al*., 2013). There is no published study for the use of MgO catalyst for Croton *megalocarpus* oil. Yields for transesterification of other oils have been low at atmospheric conditions.

##### 5.3.7.1.2 Effect of catalyst concentration

Fig 5.83 gives the effect of Nano MgO and MgO concentrations on FAME yield. For both Nano MgO and MgO yield rose with increasing catalyst concentration from 0.5 mass% to

1.5 mass%. After that the yield remained almost constant. The highest yield obtained for Nano MgO and MgO catalysts was 25.6 and 20.6% respectively, which was at 1.5 mass% catalyst. A slight decrease in yield at higher catalyst concentration was observed for Nano MgO, from 25.6% to 24% at 3 mass% catalyst, a drop of just 1.6%.

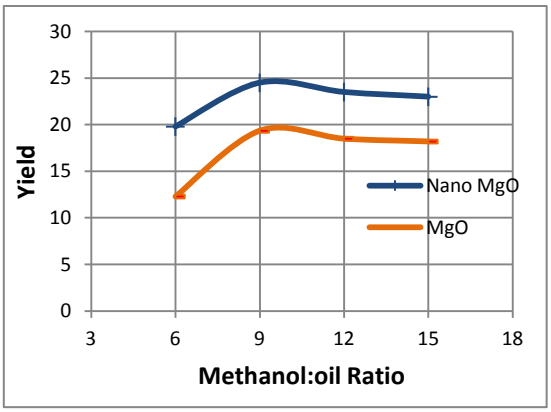


**Figure 5.82: Effect of Methanol.:oil ratio on Yield (WB)**

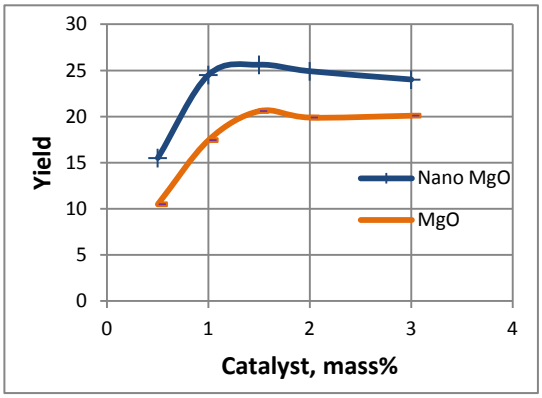


**Figure 5.83: Effect of Catalyst concentration on Yield (WB)**

#### 5.3.7.1.3 Effect of Temperature

Fig 5.84 gives the effect of reaction temperature on FAME yield. Yield increased with increasing temperature. Highest yield for Nano MgO was 24.5% and for MgO was 20% at 70$^{o}$C (343 K). The FAME yield increased rapidly as temperature was raised from 40$^{o}$C (313K) to 60$^{o}$C (333 K) and became constant between 60 and 70$^{o}$C (333 and 343 K).

Literature on use of MgO catalysts for transesterification is limited. High yields have been reported for reactions carried out at high temperature and pressure. Reaction temperatures of 120$^{o}$C (393K) – 215$^{o}$C (488K) have reported FAME yields of 60 – 64% for MgO catalyst (Taufiq-Yap *et al*.. 2011, Singh & Fernando, 2007; Antunes *et al*., 2008). For Nano MgO, yield at 250$^{o}$C (523 K) was 98% (Wang and Yang, 2007). For reactions at normal pressure, reported FAME yield for MgO catalyst range from 0 – 20% (Arzamendi *et al*., 2008; Gryglewicz, 1999; Puna *et al*., 2010; Patil & Deng, 2009; Lopez *et al*., 2005; Babak *et al*., 2013). In these studies, methanol to oil ratio ranged from 3 to 55, and catalyst 0.25 to 5 mass%. Table 2.3 (Chapter 2) lists some studies on MgO and Nano MgO catalysts.

### 5.3.7.2 Reaction Kinetics

Results for Nano MgO and MgO are presented separately in the following sections.

#### 5.3.7.2.1 Nano Magnesium oxide

##### 5.3.7.2.1.1 Effect of Time on FAME yield

Fig 5.85 is a plot of FAME yields at temperatures of 40, 50, 60, 70$^{o}$C (313, 323, 333, 343 K) for a time period of 3h. Yield increased with reaction temperature and with time.

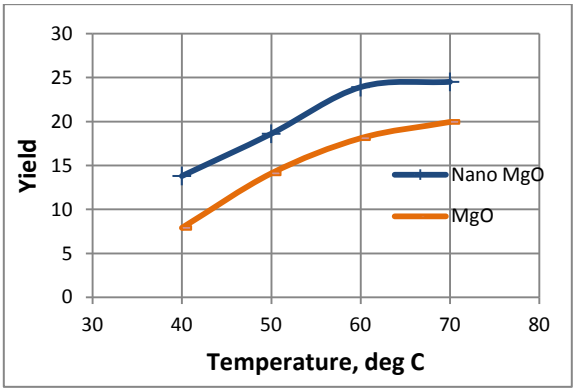


**Figure 5.84: Effect of Reaction temperature on Yield (WB)**

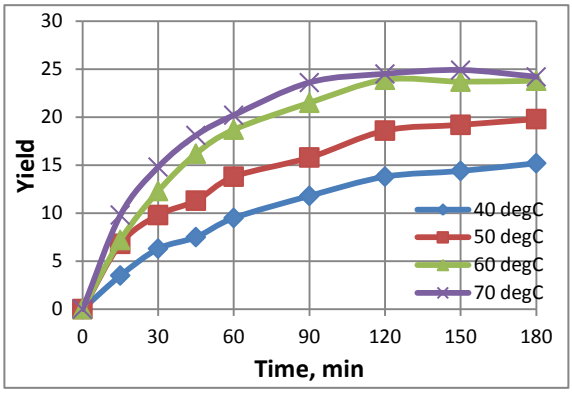


**Figure 5.85: Variation of Yield with time at various temperatures for Nano MgO (WB)**

FAME yields increased with reaction temperature and with time. After an early increase in reaction rates, yields became almost constant after 2h of reaction time. The final yields at the end of 3h for the temperatures of 40, 50, 60, 70$^{o}$C (313, 323, 333, 343 K) were 15.2, 19.8, 23.8 and 24.2% respectively.

##### 5.3.7.2.1.2 Order of reaction

Table 5.83 gives the coefficients of correlation, $R^2$, for all the ten cases of reaction orders, and for all temperatures.

**Table 5.83: Coefficients of correlation, R2, for various reaction orders for Nano MgO (WB)**

| | 0$^{th}$ Order | 1$^{st}$ Order | | | 2$^{nd}$ Order | | | 3$^{rd}$ Order | | |
|---|---|---|---|---|---|---|---|---|---|---|
| **Temp $^{o}$C** | Case 1 | Case 2 (m=1, | Case 3 (m=0, | Case 4 (m=1, | Case 5 (m=2, n=0) | Case 6 (m=0, | Case 7 (m=2, | Case 8 (m=1, n=2) | Case 9 (m=3, n=0) | Case 10 (m=0, |

| | | n=0) | n=1) | n=1) | | n=2) | n=1) | | | n=3) |
|---|---|---|---|---|---|---|---|---|---|---|
| **40** | 0.8496 | 0.8666 | 0.855 | 0.8718 | 0.8828 | 0.8604 | **0.8878** | 0.8784 | 0.8782 | 0.8657 |
| **50** | 0.7725 | 0.7993 | 0.7809 | 0.8074 | 0.8252 | 0.7892 | **0.833** | 0.8176 | 0.8299 | 0.7974 |
| **60** | 0.7162 | 0.7447 | 0.7249 | 0.7532 | 0.7723 | 0.7335 | **0.7803** | 0.7636 | 0.7784 | 0.7421 |
| **70** | 0.6393 | 0.669 | 0.6483 | 0.6779 | 0.6982 | 0.6572 | **0.7068** | 0.6888 | 0.7063 | 0.6662 |

In Table 5.83, Case 7 had the highest $R^2$ values for all the four temperatures (in bold numbers). This corresponded to an overall third order reaction, second order with respect to triglyceride and first order with respect to methanol. The 'slope' in this case is = k $[A_o]^2$ The rate equation, in terms of rate of disappearance of triglyceride, is: $-r_A = -\frac{d[A]}{dt} = k\,[A]^2\,[B]$. Singh and Fernando (2007) found the reaction order to be first order with methanol for high pressure (215$^o$C) transesterification of soybean oil with MgO catalyst. Patil *et al*. (2011) observed a second order reaction with respect to methanol for *Camelina sativa* transesterification with MgO catalyst.

#### 5.3.7.2.1.3 Rate constant and Activation energy

Integrated form of rate reaction in Case 7 (Table 5.83) is Eqn 2.40 (Chapter 2):

$$\frac{1}{(\alpha_B - 3)}\left(\frac{x_A}{1 - x_A} - \frac{3}{\alpha_B - 3}\right) ln\frac{(\alpha_B - 3x_A)}{(1 - x_A)\alpha_B} = k\,[A]_o^2\,t$$

L.H.S is F($x_A$) or F(yield) and RHS is a function of time *t*. Regression linear plot for F($x_A$) vs. *t* for 70$^o$C (343K) for Nano MgO is given in Fig 5.86.The ordinate is $\frac{1}{(\alpha_B-3)}\left(\frac{x_A}{1-x_A} - \frac{3}{\alpha_B-3}\right) ln\frac{(\alpha_B-3x_A)}{(1-x_A)\alpha_B}$, and abscissa is *t*. Reaction constant *k* was given by the slope of the plot ($R^2$ = 0.7068).

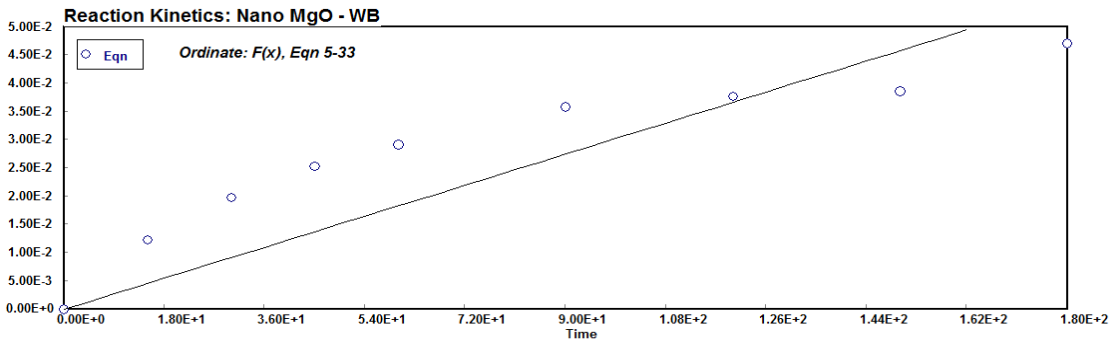


**Figure 5.86: Plot of kinetic equation 2.40 for Nano MgO (WB)**

Correlation constants (k $[A_o]^2$ ) for Eqn 2.40 for the four temperatures were used to estimate reaction constant *k* ($g^2$ $mol^{-2}$ $min^{-1}$) as given in Table 5.84.

**Table 5.84: Reaction rate constant k for Nano MgO (WB)**

| Temp °C | Temp K | $[Ao]^2$ .k | [Ao] | k |
|---|---|---|---|---|
| | | | g/cm3 | (in min) |
| **40** | 313.15 | 0.000143 | 0.6663 | 3.22E-04 |
| **50** | 323.15 | 0.00021 | 0.6663 | 4.72E-04 |
| **60** | 333.15 | 0.000289 | 0.6663 | 6.52E-04 |
| **70** | 343.15 | 0.000319 | 0.6663 | 7.18E-04 |

Activation energy was obtained from the slope of the plot of ln*k* vs. 1/T (Arrhenius plot, Section 2.5.4.1, Chapter 2). Fig 5.87 gives the plot.

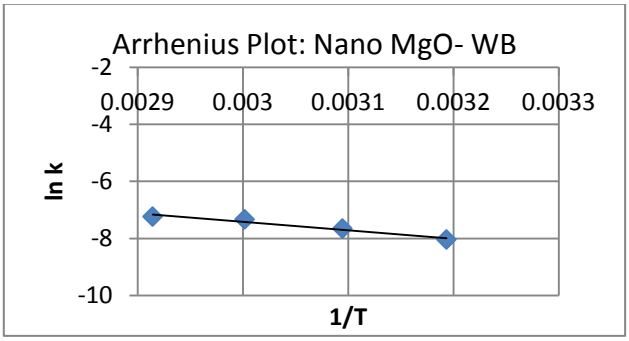


**Figure 5.87: Arrhenius plot for Nano MgO catalyst (WB)**

The slope was 2950.96 ( $R^2$ = 0.9560), which gave the Activation energy, *E* = 24.53 kJ/mol; and intercept gave pre-exponential factor, *A* = 4.18.

### 5.3.7.2.2 Magnesium oxide

#### 5.3.7.2.2.1 Effect of Time on FAME yield

Fig 5.88 gives FAME yield for MgO catalyst at temperatures of 40, 50, 60, 70°C (313, 323, 333, 343 K) for a time period of 3h. Yield increased with reaction temperature and with time. Reactions at 40°C (313K) proceeded slower when compared to those at 50, 60, 70°C (323, 333, 343 K). Final yields after 3h at 40, 50, 60, 70°C (313, 323, 333, 343 K) were 8.3, 14.8, 18.5 and 19.5% of FAME. The yields at 60, 70°C (333, 343 K) were very close.

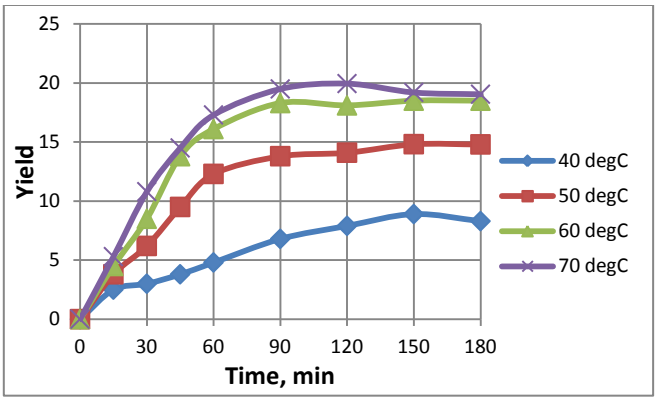


**Figure 5.88: Variation of Yield with time at various temperatures for MgO (WB)**

#### 5.3.7.2.2.2 Order of reaction

Table 5.85 gives the coefficients of correlation, $R^2$, for all the ten cases of reaction orders

**Table 5.85: Coefficients of correlation, R2, for various reaction orders for MgO (WB)**

| | **0th Order** | **1st Order** | | **2nd Order** | | | **3rd Order** | | | |
|---|---|---|---|---|---|---|---|---|---|---|
| **Temp °C** | Case 1 | Case 2 (m=1, n=0) | Case 3 (m=0, n=1) | Case 4 (m=1, n=1) | Case 5 (m=2, n=0) | Case 6 (m=0, n=2) | Case 7 (m=2, n=1) | Case 8 (m=1, n=2) | Case 9 (m=3, n=0) | Case 10 (m=0, n=3) |
| **40** | 0.8669 | 0.8747 | 0.8695 | 0.8771 | 0.8821 | 0.872 | **0.8844** | 0.8802 | 0.8831 | 0.8744 |
| **50** | 0.7359 | 0.7502 | 0.7404 | 0.7546 | 0.7641 | 0.7449 | **0.76835** | 0.7602 | 0.7676 | 0.7494 |
| **60** | 0.6792 | 0.6949 | 0.6841 | 0.6996 | 0.7101 | 0.6889 | **0.7148** | 0.7056 | 0.7049 | 0.6938 |
| **70** | 0.6369 | 0.6529 | 0.6419 | 0.6578 | 0.6683 | 0.6469 | **0.6729** | 0.6638 | 0.6729 | 0.6518 |

In Table 5.85, Case 7 had the highest $R^2$ values at all the four temperatures ( in bold numbers). This corresponded to an overall third order reaction, second order with respect to triglyceride and first order with respect to methanol. The 'slope' in this case is = k $[A_o]^2$.

#### 5.3.7.2.2.3 Rate constant and Activation energy

Integrated form of rate reaction in Case 7 (Table 5.85) is Eqn 2.40 (Chapter 2):

$$\frac{1}{(\alpha_B - 3)}\left(\frac{x_A}{1 - x_A} - \frac{3}{\alpha_B - 3}\right) ln\frac{(\alpha_B - 3x_A)}{(1 - x_A)\alpha_B} = k\,[A]_o^2\,t$$

L.H.S is F($x_A$) and RHS is a function of time *t*. Regression linear plot for F($x_A$) vs. *t* for 70°C (343K) for MgO is given in Fig 5.89. The ordinate is $\frac{1}{(\alpha_B-3)}\left(\frac{x_A}{1-x_A} - \frac{3}{\alpha_B-3}\right) ln\frac{(\alpha_B-3x_A)}{(1-x_A)\alpha_B}$, and abscissa is *t*. Reaction constant *k* is given by the slope of the plot ($R^2$ = 0.6729).

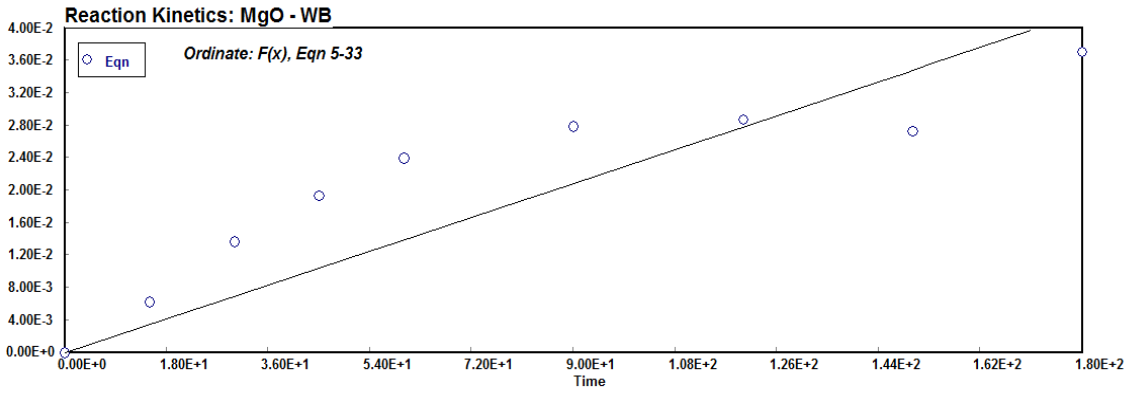


**Figure 5.89: Plot of kinetic equation 2.40 for MgO (WB)**

Correlation constants (k $[A_o]^2$ ) for Eqn 2.40 for the four temperatures were used to estimate reaction rate constant *k* ($cm^6$ $mol^{-2}$ $min^{-1}$) as given in Table 5.86.

**Table 5.86: Reaction rate constant for MgO (WB)**

| Temp $^oC$ | Temp K | $[Ao]^2$ .k | [Ao] | k |
|---|---|---|---|---|
| | | | g/cm3 | (in min) |
| **40** | 313.15 | 7.54E-05 | 0.6663 | 1.70E-04 |
| **50** | 323.15 | 0.000159 | 0.6663 | 3.58E-04 |
| **60** | 333.15 | 0.000219 | 0.6663 | 4.94E-04 |
| **70** | 343.15 | 0.00024 | 0.6663 | 5.41E-04 |

Activation energy was obtained from the slope of the plot of ln*k* vs. 1/T (Arrhenius plot, Section 2.5.4.1, Chapter 2). Fig 5.90 gives the plot.

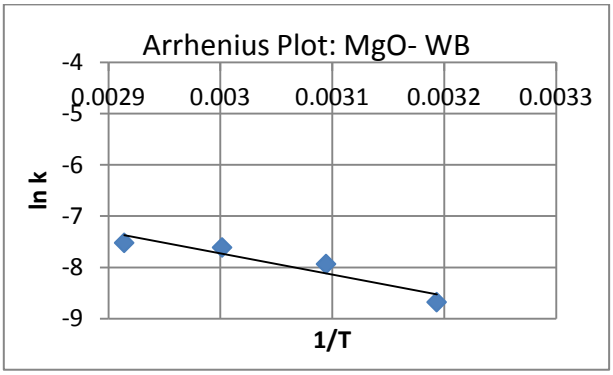


**Figure 5.90: Arrhenius plot for MgO (WB)**

The slope was 4121.16 ( $R^2$ = 0.88677), which gave the Activation energy, *E* = 34.3 kJ/mol, and intercept gave pre-exponential factor, *A* = 103.

### 5.3.7.3 Optimization studies

Following sections give optimization studies for Nano MgO and MgO separately.

#### 5.3.7.3.1 Nano Magnesium oxide- experimental results and data analysis

Table 5.87 gives the details of a set of 20 experiments in terms of actual and coded levels, as per CCD, and the FAME yields obtained in transesterification studies. Last column in the Table gives Predicted yield obtained from Reduced quadratic model (Eqn 5.12).

**Table 5.87: CCD matrix with experimental FAME yield for Nano MgO (WB)**

| Run | Level of variables [actual(coded)] | | | Expt. Yield Y | Reduced Model (Eqn 5.12) |
|---|---|---|---|---|---|
| | Catalyst,% X1 | Temp, ($^{o}$C) X2 | Methanol :oil X3 | | Y |
| **1** | 1(0) | 60(0) | 9(0) | 23.8 | 23.6 |
| **2** | 1(0) | 43(-1.68) | 9(0) | 15.9 | 16.3 |
| **3** | 0.5(-1) | 70(1) | 12(1) | 16.8 | 16.7 |
| **4** | 1(0) | 60(0) | 14(1.68) | 21.2 | 21.7 |
| **5** | 1.84(1.68) | 60(0) | 9(0) | 24.8 | 24.2 |
| **6** | 1(0) | 60(0) | 4(-1.68) | 16.2 | 16.2 |
| **7** | 0.5(-1) | 50(-1) | 6(-1) | 11.3 | 10.5 |
| **8** | 1(0) | 60(0) | 9(0) | 23.1 | 23.6 |
| **9** | 1.5(1) | 70(1) | 12(1) | 23.5 | 23.2 |
| **10** | 1.5(1) | 70(1) | 6(-1) | 23.9 | 23.3 |
| **11** | 1(0) | 60(0) | 9(0) | 23.7 | 23.6 |
| **12** | 1.5(1) | 50(-1) | 6(-1) | 16.5 | 17.0 |
| **13** | 0.16(-1.68) | 60(0) | 9(0) | 12.2 | 13.3 |
| **14** | 1(0) | 60(0) | 9(0) | 24.1 | 23.6 |
| **15** | 1.5(1) | 50(-1) | 12(1) | 23.2 | 23.6 |
| **16** | 1(0) | 60(0) | 9(0) | 22.2 | 23.6 |
| **17** | 0.5(-1) | 50(-1) | 12(1) | 18.3 | 17.2 |
| **18** | 1(0) | 77(1.68) | 9(0) | 21.2 | 21.3 |
| **19** | 1(0) | 60(0) | 9(0) | 24.2 | 23.6 |
| **20** | 0.5(-1) | 70(1) | 6(-1) | 16.9 | 16.8 |

Data in Table 5.87 were tested for fit for a linear, two-factor interaction (2FI), quadratic and cubic polynomials. Table 5.88 gives the result.

**Table 5.88: Summary for model fit- Sequential model sum of squares for Nano CaO (WB)**

| Summary (detailed tables shown below) | | | | |
|---|---|---|---|---|
| | Sequential | Lack of Fit | Adjusted | Predicted |
| Source | p-value | p-value | R-Squared | R-Squared |
| **Linear** | 0.0015 | 0.0016 | 0.5354 | 0.4399 |

| | | | | | | |
|---|---|---|---|---|---|---|
| **2FI** | 0.4599 | 0.0013 | | 0.5281 | 0.2492 | |
| **Quadratic** | < 0.0001 | 0.3876 | | 0.9655 | 0.9103 | Suggested |
| **Cubic** | 0.3508 | 0.3506 | | 0.9698 | 0.6219 | Aliased |
| **Sequential Model Sum of Squares [Type I]** | | | | | | |
| **Source** | **Sum of Squares** | **df** | **Mean Square** | **F Value** | **p-value Prob > F** | |
| **Mean vs Total** | 8120.45 | 1 | 8120.45 | | | |
| **Linear vs Mean** | 208.80 | 3 | 69.60 | 8.30 | 0.0015 | |
| **2FI vs Linear** | 23.43 | 3 | 7.81 | 0.92 | 0.4599 | |
| **Quadratic vs 2FI** | 104.52 | 3 | 34.84 | 56.00 | < 0.0001 | Suggested |
| **Cubic vs Quadratic** | 2.96 | 4 | 0.74 | 1.36 | 0.3508 | Aliased |
| **Residual** | 3.27 | 6 | 0.54 | | | |
| **Total** | 8463.42 | 20 | 423.17 | | | |

Highest Adjusted $R^2$ was for a Cubic model but it was aliased. Next highest Adjusted $R^2$ was for a Quadratic model. Considering the F value and p-value, Quadratic model was suggested. Cubic was not considered being aliased. The appropriate model for the given set of data was full Quadratic model (Eqn 4.2, Chapter 4) : $Y = b_0 + \sum_{i=1}^{n} b_i X_i + \sum_{i=1}^{n} b_{ii} X_i^2 + \sum_{1=1}^{n-1} \sum_{j=i+1}^{n} b_{ij} X_i X_j$ , Y is the Yield, $X_i$ are coded variables as given in Table 5.1. Table 5.89 gives Analysis of Variance (ANOVA) for a full quadratic model.

**Table 5.89: ANOVA for Response Surface Quadratic model for Nano MgO (WB)**

| **ANOVA for Response Surface Quadratic model** | | | | | | |
|---|---|---|---|---|---|---|
| **Analysis of variance table [Partial sum of squares - Type III]** | | | | | | |
| **Source** | **Sum of Squares** | **df** | **Mean Square** | **F Value** | **p-value Prob > F** | |
| **Model** | 336.75 | 9 | 37.42 | 60.14 | < 0.0001 | significant |
| ***X1-Nano MgO*** | *142.99* | *1* | *142.99* | *229.85* | *< 0.0001* | |
| ***X2-Temp*** | *29.04* | *1* | *29.04* | *46.67* | *< 0.0001* | |
| ***X3-Meth:oil*** | *36.77* | *1* | *36.77* | *59.10* | *< 0.0001* | |
| ***X1.X2*** | *0.98* | *1* | *0.98* | *1.58* | *0.2380* | |
| ***X1.X3*** | *5.000E-003* | *1* | *5.000E-003* | *8.037E-003* | *0.9303* | |
| ***X2.X3*** | *22.45* | *1* | *22.45* | *36.08* | *0.0001* | |
| ***X1^2*** | *43.21* | *1* | *43.21* | *69.45* | *< 0.0001* | |
| ***X2^2*** | *42.33* | *1* | *42.33* | *68.04* | *< 0.0001* | |
| ***X3^2*** | *39.75* | *1* | *39.75* | *63.90* | *< 0.0001* | |
| **Residual** | 6.22 | 10 | 0.62 | | | |
| ***Lack of Fit*** | *3.53* | *5* | *0.71* | *1.31* | *0.3876* | *not significant* |
| ***Pure Error*** | *2.70* | *5* | *0.54* | | | |
| **Cor Total** | 342.97 | 19 | | | | |

The Model F-value of 60.14 implied the model was significant. There was only a 0.01% chance that an F-value this large could occur due to noise. Values of "Prob > F" less than

0.0500 indicate model terms are significant. In this case X1, X2, X3, X2.X3, X1^2, X2^2, X3^2 were significant model terms. The terms X1.X2 and X1.X3 were not significant and the model was simplified by dropping them from the full quadratic model. These two terms were dropped and the resulting reduced model tested for ANOVA.

**Reduced Model:** X1.X2 and X1.X3 were dropped. ANOVA for reduced model is given in Table 5.90.

**Table 5.90: ANOVA for Response Surface Reduced Quadratic Model for Nano MgO (WB)**

| **ANOVA for Response Surface Reduced Quadratic model** | | | | | | |
|---|---|---|---|---|---|---|
| **Analysis of variance table [Partial sum of squares - Type III]** | | | | | | |
| | **Sum of** | | **Mean** | **F** | **p-value** | |
| **Source** | **Squares** | **df** | **Square** | **Value** | **Prob > F** | |
| **Model** | 335.76 | 7 | 47.97 | 79.88 | < 0.0001 | significant |
| ***X1-Nano MgO*** | *142.99* | *1* | *142.99* | *238.12* | *< 0.0001* | |
| ***X2-Temp*** | *29.04* | *1* | *29.04* | *48.35* | *< 0.0001* | |
| ***X3-Methanol:oil*** | *36.77* | *1* | *36.77* | *61.23* | *< 0.0001* | |
| ***X2X3*** | *22.45* | *1* | *22.45* | *37.38* | *< 0.0001* | |
| ***X1^2*** | *43.21* | *1* | *43.21* | *71.95* | *< 0.0001* | |
| ***X2^2*** | *42.33* | *1* | *42.33* | *70.49* | *< 0.0001* | |
| ***X3^2*** | *39.75* | *1* | *39.75* | *66.19* | *< 0.0001* | |
| **Residual** | 7.21 | 12 | 0.60 | | | |
| ***Lack of Fit*** | *4.51* | *7* | *0.64* | *1.20* | *0.4369* | *not significant* |
| ***Pure Error*** | *2.70* | *5* | *0.54* | | | |
| **Cor Total** | 342.97 | 19 | | | | |

The Model F-value of 79.88 implied the model was significant. There was only a 0.01% chance that an F-value this large could occur due to noise. Values of "Prob > F" less than 0.0500 indicate model terms are significant. In this case X1, X2, X3, X2X3, X1^2, X2^2, X3^2 were significant model terms. The "Lack of Fit F-value" of 1.20 implied the Lack of Fit was not significant relative to the pure error. There was a 43.69% chance that a "Lack of Fit F-value" this large could occur due to noise. Non-significant lack of fit was good. Table 5.91 gives the R-Square for the reduced model.

**Table 5.91: R-Square values for Nano MgO (WB)**

| | | | |
|---|---|---|---|
| **Std. Dev.** | **0.77** | **R-Squared** | **0.9790** |
| **Mean** | 20.15 | **Adj R-Squared** | 0.9667 |
| **C.V. %** | 3.85 | **Pred R-Squared** | 0.9289 |
| **PRESS** | 24.40 | **Adeq Precision** | 27.870 |

The "Pred R-Squared" of 0.9289 was in reasonable agreement with the "Adj R-Squared" of 0.9667; i.e. the difference was less than 0.2. "Adeq Precision" measures the signal to noise ratio. A ratio greater than 4 is desirable. This model's ratio of 27.870 indicated an adequate signal. This model can be used for design purposes. Table 5.92 gives the coefficients for the reduced model.

**Table 5.92: Coefficients for the Quadratic Model for Nano MgO (WB)**

| | Coefficient | | Standard | 95% CI | 95% CI |
|---|---|---|---|---|---|
| **Factor** | **Estimate** | **df** | **Error** | **Low** | **High** |
| **Intercept** | 23.64 | 1 | 0.32 | 22.95 | 24.33 |
| **X1-Nano MgO** | 3.24 | 1 | 0.21 | 2.78 | 3.69 |
| **X2-Temp** | 1.46 | 1 | 0.21 | 1.00 | 1.91 |
| **X3-Meth:oil** | 1.64 | 1 | 0.21 | 1.18 | 2.10 |
| **X2.X3** | -1.68 | 1 | 0.27 | -2.27 | -1.08 |
| **X1^2** | -1.73 | 1 | 0.20 | -2.18 | -1.29 |
| **X2^2** | -1.71 | 1 | 0.20 | -2.16 | -1.27 |
| **X3^2** | -1.66 | 1 | 0.20 | -2.11 | -1.22 |

Since all the terms in the model were significant, no further reductions were needed. Hence the model was:

$$\text{Yield, } Y = 23.64 + 3.24\,X1 + 1.46\,X2 + 1.64\,X3 - 1.68\,X2.X3 - 1.73\,X1^2 - 1.71\,X2^2 - 1.66\,X3^2 \quad \ldots 5.12$$

Reduced model was used to compute Predicted yield given in Table 5.87. In the following section, Eqn 5.12 was used for response surface plots.

#### 5.3.7.3.1.1 Response Surface and Contour Plots

Equation 5.12 adequately represents the FAME yield for transesterification of Croton *megalocarpus* oil, as a function of the three process variables. This reduced quadratic model has been used for RSM surface and contour plots to identify areas for optimal yield. Fig 5.91 is plot for FAME yield as functions of Nano MgO concentration (X1) and Temperature (X2). The plot indicated that for optimum yield, Nano MgO ≈ 1.5% and Temperature of 70$^{o}$C (343K). These findings agreed with experimental observations.

Fig 5.92 is a plot of Yield as functions of catalyst concentration and methanol ratio. It identified the area for optimal FAME yield as the one where Nano CaO ≈ 1.5 % and methanol to oil molar ratio was 10.5:1. This was in agreement with experimental data.

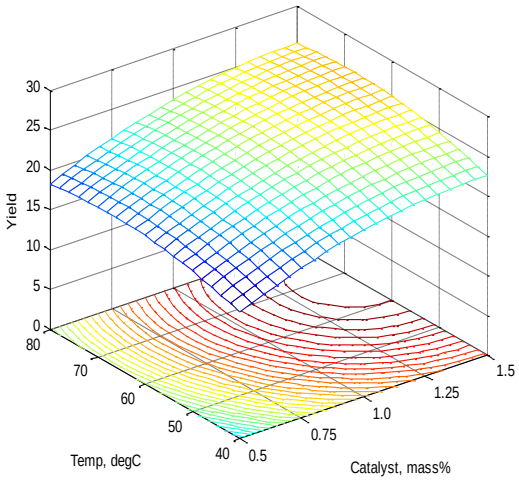


**Figure 5.91: RSM plot- Effect of Nano MgO conc. and Temperature on Yield (WB)**

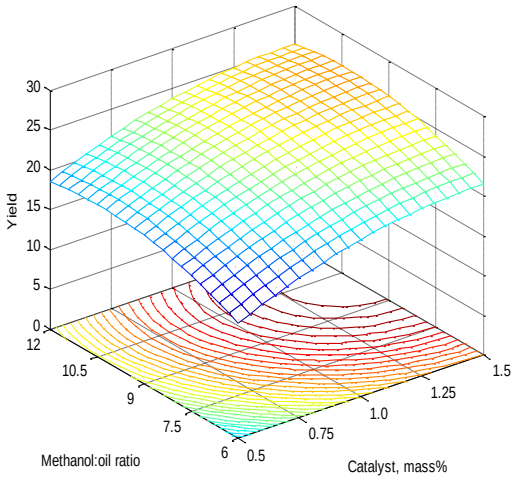


**Figure 5.92: RSM plot- Effect of Nano MgO conc. and Meth:oil ratio on Yield (WB)**

Fig 5.93 is a plot of Yield vs. methanol ratio and temperature. It identified the area of optimal FAME yield where temperature was 60 – 70$^{o}$C (343 -353K) and methanol to oil ratio was about 10:1, which was in agreement with experimental findings.

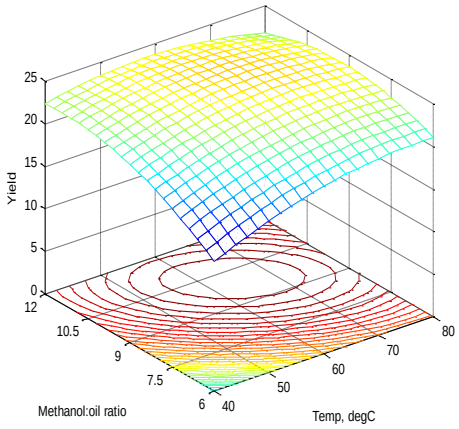


**Figure 5.93: RSM plot- Effect of Temp. and Meth:oil ratio on Yield for Nano MgO (WB)**

### 5.3.7.3.2 Magnesium oxide

#### 5.3.7.3.2.1 Experimental results and data analysis

Table 5.93 gives the details of a set of 20 experiments in terms of actual and coded levels, as per CCD, and the FAME yields obtained in transesterification studies. Last column gives the Predicted yield computed by Reduced quadratic model (Eqn 5.13).

**Table 5.93: CCD matrix with experimental FAME yield for MgO (WB)**

| Run | Level of variables [actual(coded)] | | | Expt. Yield Y | Reduced Model (Eqn 5.13) |
|---|---|---|---|---|---|
| | Catalyst,% X1 | Temp, ($^oC$) X2 | Methanol :oil X3 | | Y |
| **1** | 1(0) | 60(0) | 9(0) | 18.1 | 18.2 |
| **2** | 1(0) | 43(-1.68) | 9(0) | 9.0 | 9.5 |
| **3** | 0.5(-1) | 70(1) | 12(1) | 12.3 | 12.0 |
| **4** | 1(0) | 60(0) | 14(1.68) | 14.2 | 14.1 |
| **5** | 1.84(1.68) | 60(0) | 9(0) | 20.1 | 19.7 |
| **6** | 1(0) | 60(0) | 4(-1.68) | 11.2 | 11.5 |
| **7** | 0.5(-1) | 50(-1) | 6(-1) | 6.9 | 6.4 |
| **8** | 1(0) | 60(0) | 9(0) | 18.5 | 18.2 |
| **9** | 1.5(1) | 70(1) | 12(1) | 20.1 | 20.2 |
| **10** | 1.5(1) | 70(1) | 6(-1) | 17.5 | 17.2 |
| **11** | 1(0) | 60(0) | 9(0) | 18.5 | 18.2 |
| **12** | 1.5(1) | 50(-1) | 6(-1) | 14.2 | 14.4 |
| **13** | 0.16(-1.68) | 60(0) | 9(0) | 5.8 | 6.3 |
| **14** | 1(0) | 60(0) | 9(0) | 18.0 | 18.2 |
| **15** | 1.5(1) | 50(-1) | 12(1) | 13.9 | 14.4 |
| **16** | 1(0) | 60(0) | 9(0) | 18.3 | 18.2 |
| **17** | 0.5(-1) | 50(-1) | 12(1) | 6.9 | 6.4 |
| **18** | 1(0) | 77(1.68) | 9(0) | 16.5 | 16.5 |
| **19** | 1(0) | 60(0) | 9(0) | 18.0 | 18.2 |
| **20** | 0.5(-1) | 70(1) | 6(-1) | 9.2 | 9.2 |

Data in Table 5.93 were tested for fit for a linear, two-factor interaction (2FI), quadratic and cubic polynomials. Table 5.94 gives the result.

**Table 5.94: Summary for model fit- Sequential model sum of squares for MgO (WB)**

| **Summary (detailed tables shown below)** | | | | | |
|---|---|---|---|---|---|
| | **Sequential** | **Lack of Fit** | **Adjusted** | **Predicted** | |
| **Source** | **p-value** | **p-value** | **R-Squared** | **R-Squared** | |
| **Linear** | 0.0003 | < 0.0001 | 0.6232 | 0.5702 | |
| **2FI** | 0.9172 | < 0.0001 | 0.5533 | 0.2446 | |
| **Quadratic** | < 0.0001 | 0.1025 | 0.9946 | 0.9824 | Suggested |
| **Cubic** | 0.0759 | 0.2944 | 0.9974 | 0.9602 | Aliased |
| **Sequential Model Sum of Squares [Type I]** | | | | | |
| | **Sum of** | | **Mean** | **F** | **p-value** |
| **Source** | **Squares** | **df** | **Square** | **Value** | **Prob > F** |

| | | | | | | |
|---|---|---|---|---|---|---|
| **Mean vs Total** | 4124.19 | 1 | 4124.19 | | | |
| **Linear vs Mean** | 290.16 | 3 | 96.72 | 11.47 | 0.0003 | |
| **2FI vs Linear** | 4.99 | 3 | 1.66 | 0.17 | 0.9172 | |
| **Quadratic vs 2FI** | 128.69 | 3 | 42.90 | 356.36 | < 0.0001 | Suggested |
| **Cubic vs Quadratic** | 0.86 | 4 | 0.21 | 3.68 | 0.0759 | Aliased |
| **Residual** | 0.35 | 6 | 0.058 | | | |
| **Total** | 4549.24 | 20 | 227.46 | | | |

Highest Adjusted $R^2$ was for a Cubic model but it was aliased. Next highest Adjusted $R^2$ was for a Quadratic model. Considering the F value and p-value, Quadratic model was suggested. Cubic was not considered being aliased. The appropriate model for the given set of data was full Quadratic model (Eqn 4.2, Chapter 4) : $Y = b_0 + \sum_{i=1}^{n} b_i X_i + \sum_{i=1}^{n} b_{ii} X_i^2 + \sum_{1=1}^{n-1} \sum_{j=i+1}^{n} b_{ij} X_i X_j$ , Y is the Yield, $X_i$ are coded variables as given in Table 5.1. Table 5.95 gives Analysis of Variance (ANOVA) for a full quadratic model.

**Table 5.95: ANOVA for Response Surface Quadratic model for MgO (WB)**

| **ANOVA for Response Surface Quadratic model** | | | | | | |
|---|---|---|---|---|---|---|
| **Analysis of variance table [Partial sum of squares - Type III]** | | | | | | |
| | **Sum of** | | **Mean** | **F** | **p-value** | |
| **Source** | **Squares** | **df** | **Square** | **Value** | **Prob > F** | |
| **Model** | 423.84 | 9 | 47.09 | 391.22 | < 0.0001 | significant |
| ***X1-MgO*** | *217.09* | *1* | *217.09* | *1803.42* | *< 0.0001* | |
| ***X2-Temp*** | *65.08* | *1* | *65.08* | *540.67* | *< 0.0001* | |
| ***X3-Meth:oil*** | *7.99* | *1* | *7.99* | *66.37* | *< 0.0001* | |
| ***X1.X2*** | *0.41* | *1* | *0.41* | *3.36* | *0.0965* | |
| ***X1.X3*** | *0.080* | *1* | *0.080* | *0.66* | *0.4339* | |
| ***X2.X3*** | *4.50* | *1* | *4.50* | *37.38* | *0.0001* | |
| ***X1^2*** | *48.55* | *1* | *48.55* | *403.34* | *< 0.0001* | |
| ***X2^2*** | *52.37* | *1* | *52.37* | *435.01* | *< 0.0001* | |
| ***X3^2*** | *53.34* | *1* | *53.34* | *443.12* | *< 0.0001* | |
| **Residual** | 1.20 | 10 | 0.12 | | | |
| ***Lack of Fit*** | *0.93* | *5* | *0.19* | *3.40* | *0.1025* | *Not significant* |
| ***Pure Error*** | *0.27* | *5* | *0.055* | | | |
| **Cor Total** | 425.05 | 19 | | | | |

The Model F-value of 391.22 implied the model was significant. There was only a 0.01% chance that an F-value this large could occur due to noise. Values of "Prob > F" less than 0.0500 indicate model terms are significant. In this case X1, X2, X3, X2.X3, X1^2, X2^2, X3^2 were significant model terms. Insignificant terms were X1.X2 and X1.X3, which were dropped to simplify the model.

**Reduced Model:** Terms X1.X2 and X1.X3 were dropped from the full quadratic model and ANOVA performed to test the reduced model. Table 5.96 gives ANOVA for the reduced model.

**Table 5.96: ANOVA for Response Surface Reduced Quadratic model for MgO (WB)**

| ANOVA for Response Surface Quadratic model | | | | | | |
|---|---|---|---|---|---|---|
| **Analysis of variance table [Partial sum of squares - Type III]** | | | | | | |
| **Source** | **Sum of Squares** | **df** | **Mean Square** | **F Value** | **p-value Prob > F** | |
| **Model** | 423.36 | 7 | 60.48 | 429.75 | < 0.0001 | significant |
| ***X1-MgO*** | *217.09* | *1* | *217.09* | *1542.59* | *< 0.0001* | |
| ***X2-Temp*** | *65.08* | *1* | *65.08* | *462.47* | *< 0.0001* | |
| ***X3-Meth:oil*** | *7.99* | *1* | *7.99* | *56.77* | *< 0.0001* | |
| ***X2.X3*** | *4.50* | *1* | *4.50* | *31.98* | *0.0001* | |
| ***X1^2*** | *48.55* | *1* | *48.55* | *345.00* | *< 0.0001* | |
| ***X2^2*** | *52.37* | *1* | *52.37* | *372.10* | *< 0.0001* | |
| ***X3^2*** | *53.34* | *1* | *53.34* | *379.03* | *< 0.0001* | |
| **Residual** | 1.69 | 12 | 0.14 | | | |
| ***Lack of Fit*** | *1.42* | *7* | *0.20* | *3.70* | *0.0845* | *Not significant* |
| ***Pure Error*** | 0.27 | 5 | 0.055 | | | |
| **Cor Total** | *425.05* | *19* | | | | |

The Model F-value of 429.75 implied the model was significant. There was only a 0.01% chance that an F-value this large could occur due to noise. Values of "Prob > F" less than 0.0500 indicate model terms are significant. In this case X1, X2, X3, X2.X3, X1^2, X2^2, X3^2 were significant model terms. The "Lack of Fit F-value" of 3.70 implied there was a 8.45% chance that a "Lack of Fit F- value" this large could occur due to noise. Lack-of-fit was not significant, and was acceptable. Table 5.97 gives the R-square terms for the reduced model.

**Table 5.97: R-square for Reduced Quadratic Model for MgO (WB)**

| | | | |
|---|---|---|---|
| **Std. Dev.** | **0.38** | **R-Squared** | **0.9960** |
| **Mean** | 14.36 | **Adj R-Squared** | 0.9937 |
| **C.V. %** | 2.61 | **Pred R-Squared** | 0.9847 |
| **PRESS** | 6.51 | **Adeq Precision** | 58.660 |

The "Pred R-Squared" of 0.9847 was in reasonable agreement with the "Adj R-Squared" of 0.9937; i.e. the difference was less than 0.2. "Adeq Precision" measured the signal to noise ratio. A ratio greater than 4 is desirable. In this case the ratio of 58.660 indicated an

adequate signal. This model can be used for design purposes. Table 5.98 gives the coefficients for the reduced model.

**Table 5.98: Coefficients for the Reduced Quadratic Model for MgO (WB)**

| | Coefficient | | Standard | 95% CI | 95% CI |
|---|---|---|---|---|---|
| **Factor** | **Estimate** | **df** | **Error** | **Low** | **High** |
| **Intercept** | 18.23 | 1 | 0.15 | 17.90 | 18.56 |
| **X1-MgO** | 3.99 | 1 | 0.10 | 3.77 | 4.21 |
| **X2-Temp** | 2.18 | 1 | 0.10 | 1.96 | 2.40 |
| **X3-Meth:oil** | 0.76 | 1 | 0.10 | 0.54 | 0.99 |
| **X2.X3** | 0.75 | 1 | 0.13 | 0.46 | 1.04 |
| **X1^2** | -1.84 | 1 | 0.099 | -2.05 | -1.62 |
| **X2^2** | -1.91 | 1 | 0.099 | -2.12 | -1.69 |
| **X3^2** | -1.92 | 1 | 0.099 | -2.14 | -1.71 |

Since all the terms in the reduced model were significant, no further reductions were needed. Hence the model was:

$$\text{Yield, } Y = 18.23 + 3.99\,X1 + 2.18\,X2 + 0.76\,X3 + 0.75\,X2.X3 - 1.84\,X1^2 - 1.91\,X2^2 - 1.92\,X3^2 \quad \ldots 5.13$$

Reduced quadratic model was used to compute Predicted yield given in Table 5.93. In the following section Eqn 5.13 has been used for response surface plots.

#### 5.3.7.3.2.2 Response Surface and Contour Plots for MgO

Eqn 5.13 was used for RSM surface and contour plots. Fig 5.94 is a RSM surface and contour plot for FAME yield as function of MgO concentration and Temperature. Optima was at MgO > 1.5% and Temperature 70- 80$^{o}$C (343 – 353K). Yield increased with increasing CaO-RO concentration and reaction temperature. This agreed with experimental results.

Fig 5.95 is a RSM surface and contour plot for FAME yield as function of MgO concentration and methanol to oil ratio. Optima was at MgO ≈ 1.5% and methanol to oil ratio 9 – 10.5. This general trend was noted in experimental results.

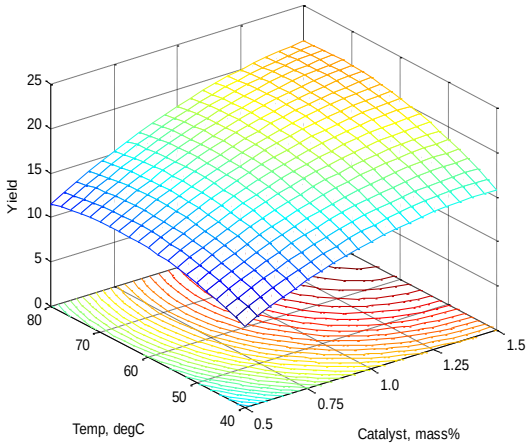


**Figure 5.94: RSM plot- Effect of MgO conc. and Temp. on Yield (WB)**

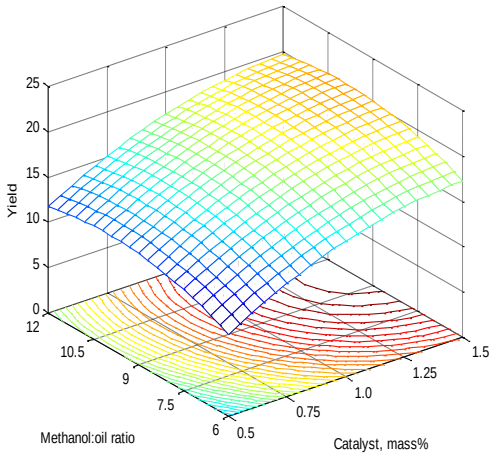


**Figure 5.95: RSM plot- Effect of MgO conc. and Meth:oil ratio on Yield (WB)**

Fig 5.96 is a RSM surface and contour plot for FAME yield as function of Temperature and methanol to oil ratio. Optima was at a temperature of 70$^{o}$C (343K) and methanol to oil ratio 9 - 10.5. The RSM plot concurred with the experimental findings.

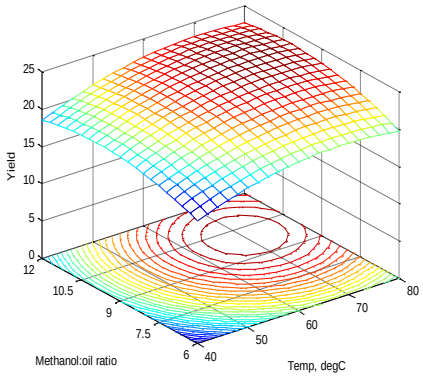


**Figure 5.96: RSM plot- Effect of Temp. and Meth:oil ratio on Yield for MgO (WB)**

### 5.3.8 Studies with Microwave Irradiation- Nano magnesium oxide and Magnesium oxide catalysts

This section deals with transesterification studies carried out with microwave irradiation.

#### 5.3.8.1 Effect of operation variables on FAME yield

##### 5.3.8.1.1 Effect of methanol to triglyceride molar ratio

Fig 5.97 gives the FAME yield for Nano MgO and MgO as a function methanol to oil molar ratio. Stoichiometric requirement of methanol for transesterification is 3 mole to one mole of triglyceride, but excess is used to drive the reaction in forward direction. Yields for Nano MgO were 5.8, 6.5, 6.3 and 5.0 % FAME at methanol ratios of 6, 9, 12 and 15. Similarly yields for MgO were 4.2, 5.3, 5.5 and 5.0% FAME at methanol ratios of 6, 9, 12, 15 respectively. It showed that yields for Nano MgO were just slightly higher than that for MgO, and the highest yield were for methanol to oil ratio of 9:1 – 12:1. Yields slightly declined when methanol to oil ratio was increased to 15:1. The explanations for decline in yield at large excess of methanol have already been given in earlier sections. The yield obtained were in general low.

#### 5.3.8.1.2 Effect of catalyst concentration on FAME yield

Fig 5.98 gives the effect of catalyst concentrations on FAME yield. Yield increased with increasing catalyst concentration for both Nano MgO and MgO. However the yields in general were low. Highest yield for Nano MgO and MgO at 2 mass% was 7.5 and 6.5% respectively.

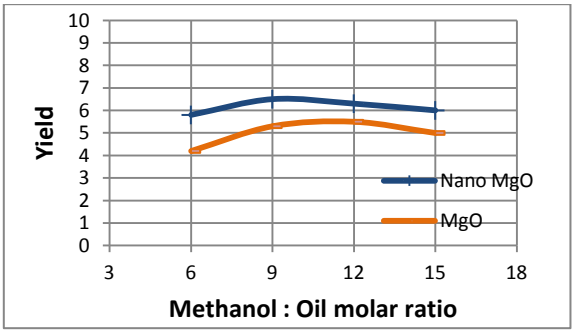


**Figure 5.97: Effect of Methanol:oil ratio on Yield (MW)**

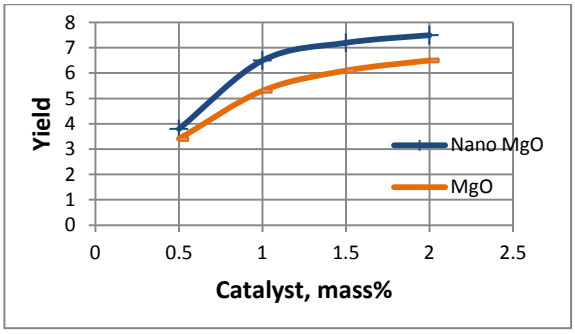


**Figure 5.98: Effect of Catalyst concentration on FAME yield (MW)**

#### 5.3.8.1.3 Effect of reaction time on FAME yield

Fig 5.99 gives the effect of reaction time on FAME yield. For Nano MgO and MgO, yield steadily increased with time and the final yield at the end of 5 min was 6.5 and 5.3 respectively.

#### 5.3.8.1.4 Effect of microwave power

Fig 5.100 gives the effect of microwave power on yield. As anticipated, yields for Nano MgO and MgO catalysts increased with power. The yield was more pronounced in power

increase from 40 to 80%. After 80% power, yields became almost constant. Yields for Nano MgO and MgO at 100% power were 6.5 and 5.3% respectively.

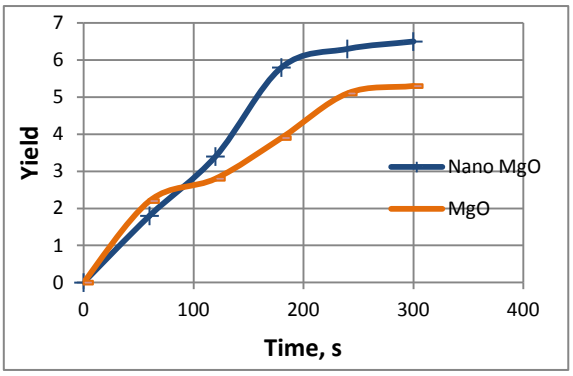


**Figure 5.99: Effect of Reaction Time on Yield (MW)**

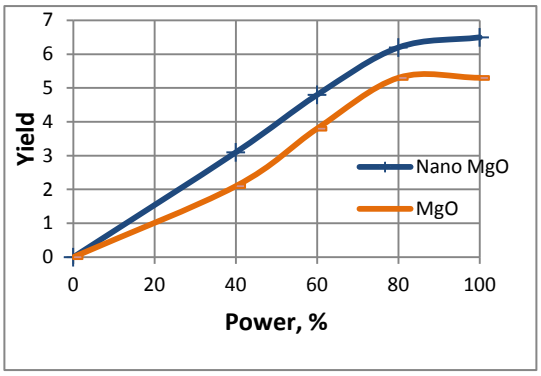


**Figure 5.100: Effect of Microwave power on Yield**

### 5.3.8.2 Reaction Kinetics

Kinetics studies for Nano MgO and MgO are presented separately in the following sections.

#### 5.3.8.2.1 Nano Magnesium oxide

##### 5.3.8.2.1.1 Effect of Time on FAME yield

Fig 5.101 gives the FAME yield for Nano MgO catalyst at 50, 60 and 70$^{o}$C (323, 333, 343K). Yield increased with the rise in reaction temperature. As the figure shows, yields were very low.

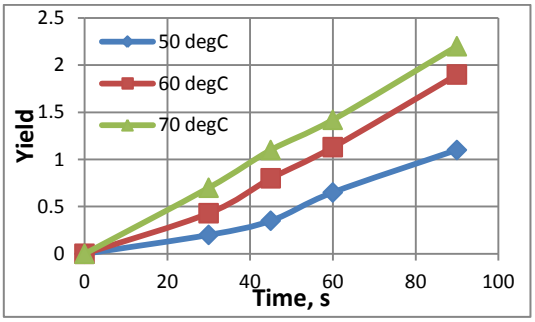


**Figure 5.101: Variation of Yield with time for Nano MgO (MW)**

##### 5.3.8.2.1.2 Order of reaction

Table 5.99 gives the coefficients of correlation for all reaction orders, Cases 1 to 10, at the three temperatures.

**Table 5.99: Coefficients of correlation, R2, for various reaction orders for Nano MgO (MW)**

| | 0th Order | 1st Order | | 2nd Order | | | 3rd Order | | | |
|---|---|---|---|---|---|---|---|---|---|---|
| **Temp °C** | Case 1 | Case 2 (m=1, n=0) | Case 3 (m=0, n=1) | Case 4 (m=1, n=1) | Case 5 (m=2, n=0) | Case 6 (m=0, n=2) | Case 7 (m=2, n=1) | Case 8 (m=1, n=2) | Case 9 (m=3, n=0) | Case 10 (m=0, n=3) |
| **50** | 0.9094 | 0.9081 | **0.9098** | 0.9077 | 0.9068 | 0.9085 | 0.9064 | 0.9071 | 0.9055 | 0.9081 |
| **60** | 0.9094 | 0.9081 | **0.9098** | 0.9077 | 0.9068 | 0.9085 | 0.9064 | 0.9071 | 0.9055 | 0.9081 |
| **70** | 0.9693 | 0.9689 | **0.9698** | 0.9684 | 0.9675 | 0.9694 | 0.967 | 0.9678 | 0.966 | 0.9689 |

Highest correlation coefficients are in bold numbers in Table 5.99. The most likely order of reaction was 'first' . Zero order with respect to triglyceride, and first order with respect to methanol (Case 3). The integrated form of rate equation is Eqn 2.36 (Chapter 2) given as: $-\frac{1}{3} ln\left(\frac{\alpha_B - 3x_A}{\alpha_B}\right) = k\, t$. The slope in this case is k.

### 5.3.8.2.1.3 Rate constant and Activation energy

L.H.S. of Eqn 2.36,$\left(-\frac{1}{3} ln\left(\frac{\alpha_B - 3x_A}{\alpha_B}\right)\right)$ is a function of conversion $x_A$ , F($x_A$), or the yield. A plot of F($x_A$) vs time $t$ is a straight line passing through the origin. Regression linear plot for F($x_A$) vs. $t$ for 70°C (343K) is given in Fig 5.102.The ordinate is, $-\frac{1}{3} ln\left(\frac{\alpha_B - 3x_A}{\alpha_B}\right)$ and abscissa is $t$. Reaction constant $k$ is given by the slope of the plot ($R^2$ = 0.9698).

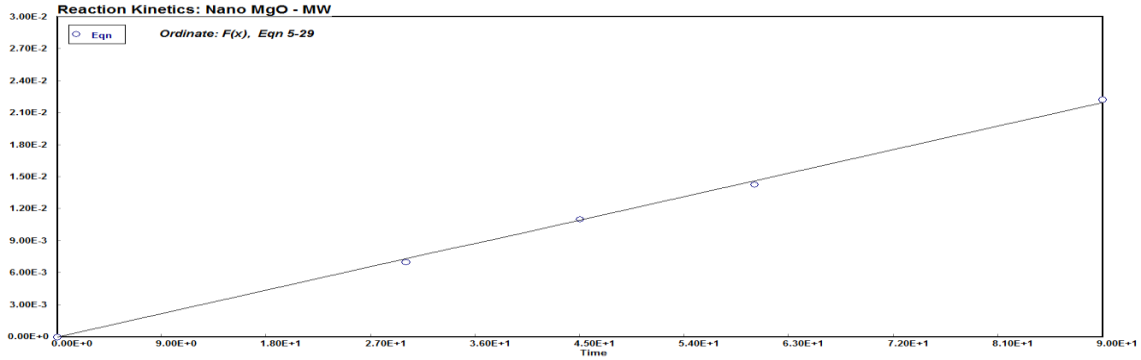


**Figure 5.102: Plot of kinetic equation 2.36 for Nano MgO (MW)**

Correlation constants (k) for Eqn 2.36 for the three temperatures were used to estimate reaction constant $k$ as given in Table 5.100.

**Table 5.100: Reaction constant k for Nano MgO (MW)**

| Temp, °C | Temp K | k |
|---|---|---|

| | | in min |
|---|---|---|
| **50** | 323.15 | 7.50E-04 |
| **60** | 333.15 | 1.33E-03 |
| **70** | 343.15 | 1.62E-03 |

Activation energy was obtained from the slope of the plot of ln*k* vs. 1/T (Arrhenius plot, Section 5.4.1). Fig 5.103 gives the plot ($R^2$ = 0.9358).

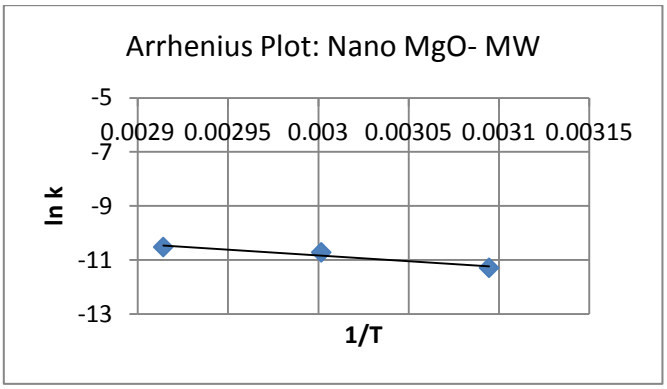


**Figure 5.103: Arrhenius plot for Nano MgO (MW)**

Slope of the plot was 4279.83, giving Activation energy, *E* = 35.6 kJ/mol. Intercept of the plot gave pre-exponential factor, *A* = 7.5.

#### 5.3.8.2.2 Magnesium oxide

##### 5.3.8.2.2.1 Effect of Time on FAME yield

Fig 5.104 is a plot of FAME yield with time at temperatures of 50, 60 and 70$^{o}$C (323, 333, 343 K). Yield increased with increasing temperature and time. Highest yield at the end of 90s for temperatures of 50, 60 and 70$^{o}$C (323, 333, 343 K) was 1.05, 1.5 and 2% respectively. The yields were very low.

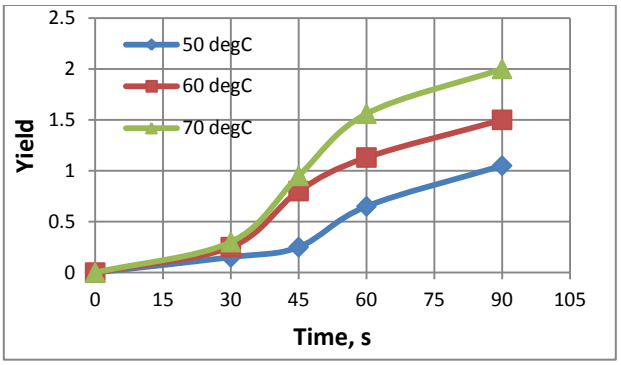


**Figure 5.104: Variation of yield with time for MgO (MW)**

#### 5.3.8.2.2.2 Order of reaction

Table 5.101 gives the coefficients of correlation for all reaction orders, Cases 1 to 10, at the three temperatures.

**Table 5.101: Coefficients of correlation, $R^2$, for various reaction orders for MgO (MW)**

| | $0^{th}$ Order | $1^{st}$ Order | | $2^{nd}$ Order | | | $3^{rd}$ Order | | | |
|---|---|---|---|---|---|---|---|---|---|---|
| **Temp °C** | Case 1 | Case 2 (m=1, n=0) | Case 3 (m=0, n=1) | Case 4 (m=1, n=1) | Case 5 (m=2, n=0) | Case 6 (m=0, n=2) | Case 7 (m=2, n=1) | Case 8 (m=1, n=2) | Case 9 (m=3, n=0) | Case 10 (m=0, n=3) |
| **50** | 0.8241 | 0.8233 | **0.8242** | 0.8228 | 0.8219 | 0.8237 | 0.8215 | 0.8222 | 0.8206 | 0.8233 |
| **60** | 0.9371 | 0.9372 | **0.9373** | 0.9371 | 0.937 | 0.9373 | 0.9369 | 0.937 | 0.9368 | 0.9372 |
| **70** | 0.9173 | 0.917 | **0.9174** | 0.9167 | 0.9163 | 0.9172 | 0.9161 | 0.9165 | 0.9157 | 0.917 |

Highest correlation coefficients are in bold numbers in Table 5.101. The most likely order of reaction was 'first', zero order with respect to triglyceride and first order with respect to methanol (Case 3). The integrated form of rate equation is Eqn 2.36 (Chapter 2) given as: $-\frac{1}{3} ln\left(\frac{\alpha_B - 3x_A}{\alpha_B}\right) = k\,t$. The slope in this case is k. There is no published literature on transesterification kinetics of MgO under microwave irradiation. Low yield was a reason for lack of interest in such a study (Patil *et al*., 2011).

#### 5.3.8.2.2.3 Rate constant and Activation energy

L.H.S. of Eqn 2.36,( $-\frac{1}{3} ln\left(\frac{\alpha_B - 3x_A}{\alpha_B}\right)$) is a function of conversion $x_A$ , F($x_A$), or the yield. A plot of F($x_A$) vs time t is a straight line passing through the origin. Regression linear plot

for F($x_A$) vs. *t* for 70°C (343K) is given in Fig 5.105.The ordinate is $-\frac{1}{3}ln\left(\frac{\alpha_B - 3x_A}{\alpha_B}\right)$ and abscissa is *t*. Reaction constant *k* is given by the slope of the plot ($R^2$ = 0.9174).

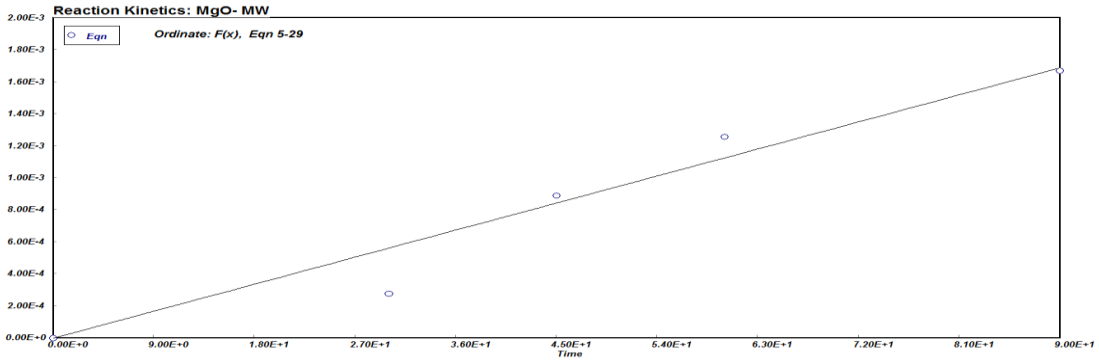


**Figure 5.105: Plot of kinetic equation 2.36 for MgO (MW)**

Correlation constants (k) for Eqn 2.36 for the three temperatures were used to estimate reaction constant *k* as given in Table 5.102.

**Table 5.102: Reaction constant k for MgO**

| Temp, °C | Temp K | k |
|---|---|---|
| | | in min |
| **50** | 323.15 | 7.20E-04 |
| **60** | 333.15 | 1.15E-03 |
| **70** | 343.15 | 1.53E-03 |

Activation energy is obtained from the slope of the plot of ln*k* vs. 1/T (Arrhenius plot, Section 5.4.1). Fig 5.106 gives the plot ($R^2$ = 0.9857).

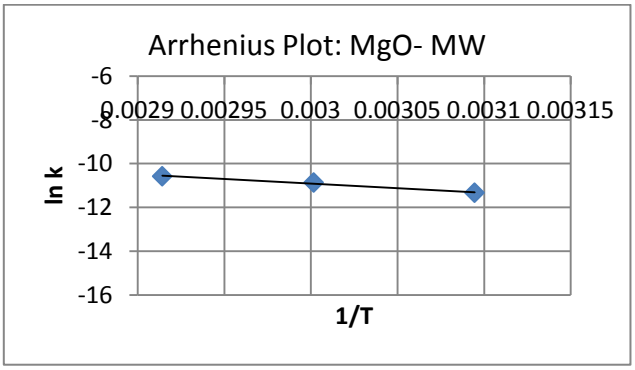


**Figure 5.106: Arrhenius plot for MgO (MW)**

Slope of the plot was 4173.83, giving Activation energy, *E* = 34.7 kJ/mol; and intercept gave pre-exponential factor, *A* = 299.

### 5.3.8.3 Optimization studies- experimental results and data analysis Nano MgO

Table 5.103 gives the details of a set of 20 experiments in terms of actual and coded levels, as per CCD, and the FAME yields obtained in transesterification studies. Last column of the Table gives Predicted yield obtained from the Reduced quadratic model (Eqn 5.14).

**Table 5.103: CCD matrix with experimental FAME yield for Nano MgO (MW)**

| Run | Level of variables [actual(coded)] | | | Experimental Yield | Reduced Model (Eqn 10.3) |
|---|---|---|---|---|---|
| | Catalyst,% | Time (min) | Methanol :oil | | **Y** |
| | X1 | X2 | X3 | | |
| **1** | 1(0) | 3(0) | 9(0) | 5.3 | 5.3 |
| **2** | 1(0) | 0.5(-1.68) | 9(0) | 3.1 | 3.4 |
| **3** | 0.5(-1) | 4.5(1) | 12(1) | 3.1 | 3.2 |
| **4** | 1(0) | 3(0) | 14(1.68) | 4.1 | 4.1 |
| **5** | 1.84(1.68) | 3(0) | 9(0) | 5.9 | 5.8 |
| **6** | 1(0) | 3(0) | 4(-1.68) | 2.5 | 2.6 |
| **7** | 0.5(-1) | 1.5(-1) | 6(-1) | 1.7 | 1.8 |
| **8** | 1(0) | 3(0) | 9(0) | 5.1 | 5.3 |
| **9** | 1.5(1) | 4.5(1) | 12(1) | 6.3 | 6.5 |
| **10** | 1.5(1) | 4.5(1) | 6(-1) | 6.3 | 6.4 |
| **11** | 1(0) | 3(0) | 9(0) | 5.4 | 5.3 |
| **12** | 1.5(1) | 1.5(-1) | 6(-1) | 3.0 | 2.7 |
| **13** | 0.16(-1.68) | 3(0) | 9(0) | 2.0 | 2.1 |
| **14** | 1(0) | 3(0) | 9(0) | 5.5 | 5.3 |
| **15** | 1.5(1) | 1.5(-1) | 12(1) | 4.3 | 4.5 |
| **16** | 1(0) | 3(0) | 9(0) | 5.0 | 5.3 |
| **17** | 0.5(-1) | 1.5(-1) | 12(1) | 3.8 | 3.5 |
| **18** | 1(0) | 5.5(1.68) | 9(0) | 6.5 | 6.3 |
| **19** | 1(0) | 3(0) | 9(0) | 5.8 | 5.3 |
| **20** | 0.5(-1) | 4.5(1) | 6(-1) | 3.1 | 3.1 |

Data in Table 5.103 were tested for fit for a linear, two-factor interaction (2FI), quadratic and cubic polynomials. Table 5.104 gives the result.

**Table 5.104: Summary for model fit- Sequential model sum of squares for Nano MgO (MW)**

| **Summary (detailed tables shown below)** |
|---|

| Source | Sequential p-value | Lack of Fit p-value | Adjusted R-Squared | Predicted R-Squared | |
|---|---|---|---|---|---|
| **Linear** | 0.0004 | < 0.0001 | 0.6019 | 0.4718 | |
| **2FI** | 0.2059 | < 0.0001 | 0.6510 | 0.4162 | |
| **Quadratic** | < 0.0001 | 0.0692 | 0.9797 | 0.9284 | Suggested |
| **Cubic** | 0.0241 | 0.8764 | 0.9935 | 0.9947 | Aliased |

**Sequential Model Sum of Squares [Type I]**

| Source | Sum of Squares | df | Mean Square | F Value | p-value Prob > F | |
|---|---|---|---|---|---|---|
| **Mean vs Total** | 383.95 | 1 | 383.95 | | | |
| **Linear vs Mean** | 28.72 | 3 | 9.57 | 10.57 | 0.0004 | |
| **2FI vs Linear** | 4.17 | 3 | 1.39 | 1.75 | 0.2059 | |
| **Quadratic vs 2FI** | 9.85 | 3 | 3.28 | 71.08 | < 0.0001 | Suggested |
| **Cubic vs Quadratic** | 0.37 | 4 | 0.093 | 6.33 | 0.0241 | Aliased |
| **Residual** | 0.089 | 6 | 0.015 | | | |
| **Total** | 427.16 | 20 | 21.36 | | | |

Cubic model was out of consideration, being aliased. Quadratic model had highest Adjusted $R^2$ and hence suggested. Table 5.105 gives the analysis of variance (ANOVA) for a full quadratic model.

**Table 5.105: ANOVA for Full Quadratic Model for Nano MgO (MW)**

**ANOVA for Response Surface Quadratic model**

**Analysis of variance table [Partial sum of squares - Type III]**

| Source | Sum of Squares | df | Mean Square | F Value | p-value Prob > F | |
|---|---|---|---|---|---|---|
| **Model** | 42.75 | 9 | 4.75 | 102.78 | < 0.0001 | significant |
| ***X1-Nano MgO*** | *15.95* | *1* | *15.95* | *345.16* | *< 0.0001* | |
| ***X2-Time*** | *10.05* | *1* | *10.05* | *217.59* | *< 0.0001* | |
| ***X3-Methanol:oil*** | *2.72* | *1* | *2.72* | *58.79* | *< 0.0001* | |
| ***X1.X2*** | *2.65* | *1* | *2.65* | *57.24* | *< 0.0001* | |
| ***X1.X3*** | *0.080* | *1* | *0.080* | *1.73* | *0.2176* | |
| ***X2.X3*** | *1.45* | *1* | *1.45* | *31.27* | *0.0002* | |
| ***X1^2*** | *3.35* | *1* | *3.35* | *72.56* | *< 0.0001* | |
| ***X2^2*** | *0.48* | *1* | *0.48* | *10.31* | *0.0093* | |
| ***X3^2*** | *7.31* | *1* | *7.31* | *158.17* | *< 0.0001* | |
| **Residual** | 0.46 | 10 | 0.046 | | | |
| ***Lack of Fit*** | *0.37* | *5* | *0.075* | *4.25* | *0.0692* | *not significant* |
| ***Pure Error*** | *0.088* | *5* | *0.018* | | | |
| **Cor Total** | 43.21 | 19 | | | | |

The Model F-value of 102.78 implies the model was significant. There was only a 0.01% chance that an F-value this large could occur due to noise. Values of "Prob > F" less than 0.0500 indicate model terms are significant. In this case X1, X2, X3, X1.X2, X2.X3, X1^2,

X2^2, X3^2 were significant model terms. The term X1.X3 was not significant. It was dropped to simplify the model and the reduced model tested for ANOVA.

**Reduced Model:** Term X1.X3 was dropped from full quadratic model. Table 5.106 gives ANOVA for the reduced model.

**Table 5.106: ANOVA for Reduced Quadratic Model for Nano MgO (MW)**

| **ANOVA for Response Surface Reduced Quadratic model** | | | | | | |
|---|---|---|---|---|---|---|
| **Analysis of variance table [Partial sum of squares - Type III]** | | | | | | |
| | **Sum of** | | **Mean** | **F** | **p-value** | |
| **Source** | **Squares** | **df** | **Square** | **Value** | **Prob > F** | |
| **Model** | 42.67 | 8 | 5.33 | 108.22 | < 0.0001 | significant |
| ***X1-Nano MgO*** | *15.95* | *1* | *15.95* | *323.65* | *< 0.0001* | |
| ***X2-Time*** | *10.05* | *1* | *10.05* | *204.02* | *< 0.0001* | |
| ***X3-Methanol:oil*** | *2.72* | *1* | *2.72* | *55.12* | *< 0.0001* | |
| ***X1X2*** | *2.64* | *1* | *2.64* | *53.67* | *< 0.0001* | |
| ***X2X3*** | *1.44* | *1* | *1.44* | *29.32* | *0.0002* | |
| ***X1^2*** | *3.35* | *1* | *3.35* | *68.04* | *< 0.0001* | |
| ***X2^2*** | *0.48* | *1* | *0.48* | *9.67* | *0.0099* | |
| ***X3^2*** | *7.31* | *1* | *7.31* | *148.31* | *< 0.0001* | |
| **Residual** | 0.54 | 11 | 0.049 | | | |
| ***Lack of Fit*** | *0.45* | *6* | *0.076* | *4.30* | *0.0656* | *not significant* |
| ***Pure Error*** | *0.088* | *5* | *0.018* | | | |
| **Cor Total** | 43.21 | 19 | | | | |

The Model F-value of 108.22 implied the model was significant. There was only a 0.01% chance that an F-value this large could occur due to noise. Values of "Prob > F" less than 0.0500 indicate model terms are significant. In this case X1, X2, X3, X1.X2, X2.X3, X1^2, X2^2, X3^2 were significant model terms. The "Lack of Fit F-value" of 4.30 implied there was a 6.56% chance that a "Lack of Fit F- value" this large could occur due to noise. Lack of fit was not very good but it was insignificant and acceptable. Table 5.107 gives the R-Square for the reduced model.

**Table 5.107: R-Square for reduced model for Nano MgO (MW)**

| | | | |
|---|---|---|---|
| **Std. Dev.** | **0.22** | **R-Squared** | **0.9875** |
| **Mean** | 4.38 | **Adj R-Squared** | 0.9783 |
| **C.V. %** | 5.07 | **Pred R-Squared** | 0.9397 |
| **PRESS** | 2.60 | **Adeq Precision** | 32.026 |

The "Pred R-Squared" of 0.9397 was in reasonable agreement with the "Adj R-Squared" of 0.9783; i.e. the difference was less than 0.2. "Adeq Precision" measures the signal to noise ratio. A ratio greater than 4 is desirable. This model's ratio of 32.026 indicated an adequate

signal. This model can be used for design purposes. Table 5.108 gives the coefficients for the reduced model.

**Table 5.108: Coefficients for the reduced model for Nano MgO (MW)**

| | Coefficient | | Standard | 95% CI | 95% CI | |
|---|---|---|---|---|---|---|
| **Factor** | **Estimate** | **df** | **Error** | **Low** | **High** | **VIF** |
| **Intercept** | 5.32 | 1 | 0.091 | 5.12 | 5.52 | |
| **X1-Nano CaO** | 1.08 | 1 | 0.060 | 0.95 | 1.21 | |
| **X2-Time** | 0.86 | 1 | 0.060 | 0.73 | 0.99 | |
| **X3-Methanol:oil** | 0.45 | 1 | 0.060 | 0.31 | 0.58 | |
| **X1X2** | 0.58 | 1 | 0.078 | 0.40 | 0.75 | |
| **X2X3** | -0.42 | 1 | 0.078 | -0.60 | -0.25 | |
| **X1^2** | -0.48 | 1 | 0.058 | -0.61 | -0.35 | |
| **X2^2** | -0.18 | 1 | 0.058 | -0.31 | -0.053 | |
| **X3^2** | -0.71 | 1 | 0.058 | -0.84 | -0.58 | |

The full Quadratic model was given by (Eqn 4.2, Chapter 4) :

$$Y = b_0 + \sum_{i=1}^{n} b_i X_i + \sum_{i=1}^{n} b_{ii} X_i^2 + \sum_{1=1}^{n-1} \sum_{j=i+1}^{n} b_{ij} X_i X_j$$

And the reduced model, after dropping insignificant term X1.X3 was:

Yield, Y = 5.32 + 1.08 X1 + 0.86 X2 + 0.45 X3+ 0.58 X1X2 – 0.42X2X3

– 0.48 X1^2– 0.18 $X2^2$ – 0.71X3^2 …5.14

Reduced model was used to compute Predicted yield given in Table 5.103. Eqn 5.14 would be used to plot RSM surface and contour plots.

#### 5.3.8.3.1.1 Response Surface and Contour Plots

Equation 5.14 was used for RSM surface and contour plots. Figs 5.107, 5.108 and 5.109 give the plots. Fig 5.107 is a RSM plot for FAME yield as a function of Nano MgO concentration and reaction time. It shows that the yield increased with increasing catalyst concentration and reaction time, and optima was at Nano MgO> 1.5% and Time > 5 min. This agreed with experimental data.

Fig 5.108 is a RSM surface and contour plot showing FAME yield as functions of Nano MgO concentration and methanol to oil ratio. Maximum yield corresponded to Nano MgO > 1.5 % and methanol to oil ratio 9 – 10.5. These agreed with experimental findings.

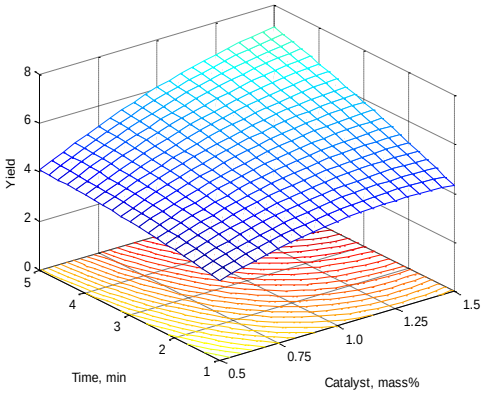


**Figure 5.107: RSM plot- Effect of Time and Nano MgO conc. on Yield (MW)**

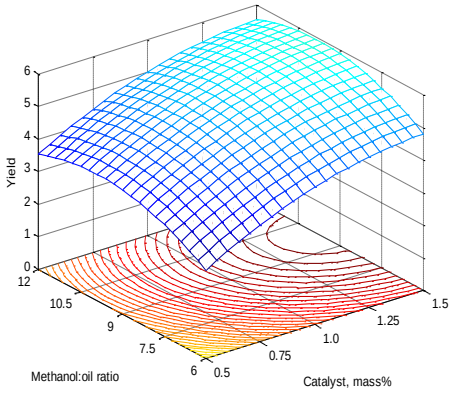


**Figure 5.108: RSM plot- Effect of Meth:oil ratio and Nano MgO conc. on Yield (MW)**

Fig 5.109 is a RSM surface and contour plot with variables as methanol to oil ratio and reaction time. Yield increased with increasing time and for maximum yield, Time > 5 min and methanol to oil ratio was about 9:1. These observations agreed with experimental results.

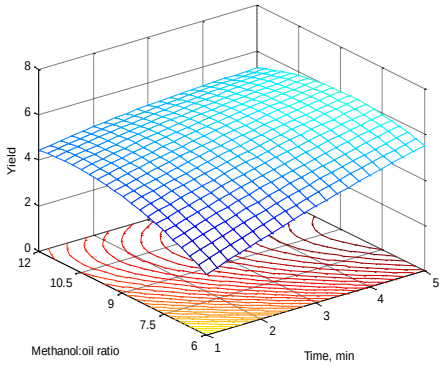


**Figure 5.109: RSM plot- Effect of Meth:oil ratio and Time on Yield for Nano MgO (MW)**

### 5.3.8.3.2 Optimization studies- experimental results and data analysis MgO

Table 5.109 gives the details of a set of 20 experiments in terms of actual and coded levels, as per CCD, and the FAME yields obtained in transesterification studies. Last column gives Predicted yield as per the Reduced quadratic model (Eqn 5.15).

**Table 5.109: CCD matrix with experimental FAME yield for MgO (MW)**

| Run | Level of variables [actual(coded)] | | | Experimental Yield | Reduced Model (Eqn 5.15) |
|---|---|---|---|---|---|
| | Catalyst,% | Time (min) | Methanol :oil | | Y |
| | X1 | X2 | X3 | | |
| **1** | 1(0) | 3(0) | 9(0) | 4.3 | 4.1 |
| **2** | 1(0) | 0.5(-1.68) | 9(0) | 2.9 | 2.8 |
| **3** | 0.5(-1) | 4.5(1) | 12(1) | 2.8 | 3.0 |
| **4** | 1(0) | 3(0) | 14(1.68) | 3.2 | 3.2 |
| **5** | 1.84(1.68) | 3(0) | 9(0) | 3.9 | 4.3 |
| **6** | 1(0) | 3(0) | 4(-1.68) | 2.2 | 2.4 |
| **7** | 0.5(-1) | 1.5(-1) | 6(-1) | 2.1 | 1.7 |
| **8** | 1(0) | 3(0) | 9(0) | 3.9 | 4.1 |
| **9** | 1.5(1) | 4.5(1) | 12(1) | 5.3 | 5.1 |
| **10** | 1.5(1) | 4.5(1) | 6(-1) | 5.4 | 5.2 |
| **11** | 1(0) | 3(0) | 9(0) | 4.2 | 4.1 |
| **12** | 1.5(1) | 1.5(-1) | 6(-1) | 2.2 | 2.4 |
| **13** | 0.16(-1.68) | 3(0) | 9(0) | 2.1 | 1.9 |
| **14** | 1(0) | 3(0) | 9(0) | 4.3 | 4.1 |
| **15** | 1.5(1) | 1.5(-1) | 12(1) | 3.8 | 3.3 |
| **16** | 1(0) | 3(0) | 9(0) | 3.9 | 4.1 |
| **17** | 0.5(-1) | 1.5(-1) | 12(1) | 2.2 | 2.7 |
| **18** | 1(0) | 5.5(1.68) | 9(0) | 5.5 | 5.4 |
| **19** | 1(0) | 3(0) | 9(0) | 3.87 | 4.1 |
| **20** | 0.5(-1) | 4.5(1) | 6(-1) | 3.1 | 3.0 |

Data in Table 5.109 were tested for fit for a linear, two-factor interaction (2FI), quadratic and cubic polynomials. Table 5.110 gives the result.

**Table 5.110: Summary for model fit- Sequential model sum of squares for MgO (MW)**

**Summary for model fit**

| Source | Sequential p-value | Lack of Fit p-value | Adjusted R-Squared | Predicted R-Squared | |
|---|---|---|---|---|---|
| **Linear** | 0.0004 | 0.0036 | 0.6078 | 0.4497 | |
| **2FI** | 0.2293 | 0.0041 | 0.6497 | 0.4513 | |
| **Quadratic** | 0.0001 | 0.1618 | 0.9361 | 0.7883 | Suggested |

| | | | | | | |
|---|---|---|---|---|---|---|
| **Cubic** | 0.1072 | 0.3937 | 0.9650 | | 0.6248 | Aliased |
| **Source** | | | | | | |
| **Mean vs Total** | 253.26 | 1 | 253.26 | | | |
| **Linear vs Mean** | 15.64 | 3 | 5.21 | 10.82 | 0.0004 | |
| **2FI vs Linear** | 2.11 | 3 | 0.70 | 1.64 | 0.2293 | |
| **Quadratic vs 2FI** | 4.81 | 3 | 1.60 | 20.41 | 0.0001 | Suggested |
| **Cubic vs Quadratic** | 0.53 | 4 | 0.13 | 3.06 | 0.1072 | Aliased |
| **Residual** | 0.26 | 6 | 0.043 | | | |
| **Total** | 276.61 | 20 | 13.83 | | | |

Cubic had the highest Adj $R^2$ (0.9650), followed by Adj $R^2$ for Quadratic model (0.9361). However, cubic was not suitable because of being aliased. Considering the F and p-values, a Quadratic model was suggested. Cubic was aliased. The appropriate model for the given set of data was full Quadratic model (Eqn 4.2, Chapter 4) :

$$Y = b_0 + \sum_{i=1}^{n} b_i X_i + \sum_{i=1}^{n} b_{ii} X_i^2 + \sum_{1=1}^{n-1} \sum_{j=i+1}^{n} b_{ij} X_i X_j$$

Y is the FAME Yield, $X_i$ are coded variables as given in Table 5.2.

Table 5.111 gives Analysis of Variance (ANOVA) for a full quadratic model.

**Table 5.111: ANOVA for Response Surface Quadratic model for MgO (MW)**

| **ANOVA for Response Surface Quadratic model** | | | | | | |
|---|---|---|---|---|---|---|
| **Analysis of variance table [Partial sum of squares - Type III]** | | | | | | |
| | **Sum of** | | **Mean** | **F** | **p-value** | |
| **Source** | **Squares** | **df** | **Square** | **Value** | **Prob > F** | |
| **Model** | 22.56 | 9 | 2.51 | 31.91 | < 0.0001 | significant |
| ***X1-MgO*** | *6.65* | *1* | *6.65* | *84.60* | *< 0.0001* | |
| ***X2-Time*** | *8.34* | *1* | *8.34* | *106.17* | *< 0.0001* | |
| ***X3-Methanol:oil*** | *0.65* | *1* | *0.65* | *8.29* | *0.0164* | |
| ***X1.X2*** | *1.20* | *1* | *1.20* | *15.29* | *0.0029* | |
| ***X1.X3*** | *0.36* | *1* | *0.36* | *4.60* | *0.0576* | |
| ***X2.X3*** | *0.55* | *1* | *0.55* | *7.02* | *0.0244* | |
| ***X1^2*** | *1.85* | *1* | *1.85* | *23.53* | *0.0007* | |
| ***X2^2*** | *0.063* | *1* | *0.063* | *0.80* | *0.3916* | |
| ***X3^2*** | *3.11* | *1* | *3.11* | *39.52* | *< 0.0001* | |
| **Residual** | 0.79 | 10 | 0.079 | | | |
| ***Lack of Fit*** | *0.57* | *5* | *0.11* | *2.57* | *0.1618* | *Not significant* |
| ***Pure Error*** | *0.22* | *5* | *0.044* | | | |
| **Cor Total** | 23.35 | 19 | | | | |

The Model F-value of 31.91 implies the model was significant. There was only a 0.01% chance that an F-value this large could occur due to noise. Values of "Prob > F" less than 0.0500 indicated model terms were significant. In this case X1, X2, X3, X1X2, X2X3, X1^2, X3^2 were significant model terms. Insignificant terms were, X1X3 and X2^2. Model was simplified by dropping these terms.

**Reduced model:** .Terms X1X3 and X2^2 were dropped from the full Quadratic model. Table 5.112 gives the ANOVA for the reduced model.

**Table 5.112: ANOVA for Response Surface Reduced Quadratic model for MgO (MW)**

| **ANOVA for Response Surface Reduced Quadratic model** | | | | | | |
|---|---|---|---|---|---|---|
| **Analysis of variance table [Partial sum of squares - Type III]** | | | | | | |
| **Source** | **Sum of Squares** | **df** | **Mean Square** | **F Value** | **p-value Prob > F** | |
| **Model** | 22.14 | 7 | 3.16 | 31.37 | < 0.0001 | significant |
| ***X1-MgO*** | *6.65* | *1* | *6.65* | *65.92* | *< 0.0001* | |
| ***X2-Time*** | *8.34* | *1* | *8.34* | *82.73* | *< 0.0001* | |
| ***X3-Methanol:oil*** | *0.65* | *1* | *0.65* | *6.46* | *0.0259* | |
| ***X1X2*** | *1.20* | *1* | *1.20* | *11.91* | *0.0048* | |
| ***X2X3*** | *0.55* | *1* | *0.55* | *5.47* | *0.0375* | |
| ***X1^2*** | *1.94* | *1* | *1.94* | *19.20* | *0.0009* | |
| ***X3^2*** | *3.23* | *1* | *3.23* | *31.99* | *0.0001* | |
| **Residual** | 1.21 | 12 | 0.10 | | | |
| ***Lack of Fit*** | *0.99* | *7* | *0.14* | *3.21* | *0.1087* | *Not significant* |
| ***Pure Error*** | *0.22* | *5* | *0.044* | | | |
| **Cor Total** | 23.35 | 19 | | | | |

The Model F-value of 31.37 implied the model was significant. There was only a 0.01% chance that an F-value this large could occur due to noise. Values of "Prob > F" less than 0.0500 indicate model terms are significant. In this case X1, X2, X3, X1X2, X2X3, X1^2, X3^2 were significant model terms. The "Lack of Fit F-value" of 3.21 implied the Lack of Fit was not significant relative to the pure error. There was a 10.87% chance that a "Lack of Fit F-value" this large could occur due to noise. Non-significant lack of fit is good. Table 5.113 gives the $R^2$ values for the reduced model.

**Table 5.113: R-Square values (MW)**

| | | | |
|---|---|---|---|
| **Std. Dev.** | **0.32** | **R-Squared** | **0.9482** |
| **Mean** | 3.56 | **Adj R-Squared** | 0.9180 |
| **C.V. %** | 8.92 | **Pred R-Squared** | 0.7834 |

| | | | |
|---|---|---|---|
| **PRESS** | 5.06 | **Adeq Precision** | 18.534 |

The "Pred R-Squared" of 0.7834 was in reasonable agreement with the "Adj R-Squared" of 0.9180; i.e. the difference was less than 0.2. "Adeq Precision" measures the signal to noise ratio. A ratio greater than 4 is desirable. This model's ratio of 18.534 indicated an adequate signal. This model can be used for design purposes. Table 5.114 gives the coefficients for the reduced quadratic model.

**Table 5.114: Coefficients for the Reduced Quadratic model for MgO (MW)**

| Factor | Coefficient Estimate | df | Standard Error | 95% CI Low | 95% CI High |
|---|---|---|---|---|---|
| **Intercept** | 4.13 | 1 | 0.11 | 3.89 | 4.37 |
| **X1-MgO** | 0.70 | 1 | 0.086 | 0.51 | 0.88 |
| **X2-Time** | 0.78 | 1 | 0.086 | 0.59 | 0.97 |
| **X3-Meth:oil** | 0.22 | 1 | 0.086 | 0.031 | 0.41 |
| **X1X2** | 0.39 | 1 | 0.11 | 0.14 | 0.63 |
| **X2X3** | -0.26 | 1 | 0.11 | -0.51 | -0.018 |
| **X1^2** | -0.36 | 1 | 0.083 | -0.55 | -0.18 |
| **X3^2** | -0.47 | 1 | 0.083 | -0.65 | -0.29 |

Since all the terms in the reduced model were significant, no further reductions were needed. Hence the model for yield (Y) was:

$$Y = 4.13 + 0.70\ X1 + 0.78\ X2 + 0.22\ X3 + 0.39\ X1.X2 - 0.26\ X2.X3 - 0.36\ X1^2 - 0.47\ X3^2 \quad \ldots 5.15$$

Reduced model was used to compute Predicted yields given in Table 5.109. In the following section, Eqn 5.15 was used for response surface plots.

#### 5.3.8.3.2.1 Response Surface and Contour Plots

Fig 5.110 is a RSM surface and contour plot for FAME yield as a function of MgO catalyst mass% and Time. Yield increased with time and with increasing catalyst concentration. No optima was found within the range of independent variables in this case, hence for optimum yield MgO > 1.5% and Time > 5 min. The general observation agreed with experimental results.

Fig 5.111 is RSM surface and contour plot for FAME yield as function of MgO concentration and Methanol to oil ratio. Maxima was at methanol:oil ratio of 9:1- 10.5:1

and MgO concentration > 1.5%. Experimental data were in agreement with this observation.

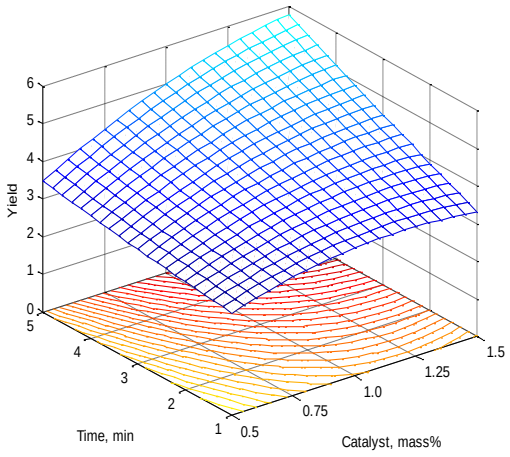


**Figure 5.110: RSM plot- Effect of MgO conc. and Time on Yield (MW)**

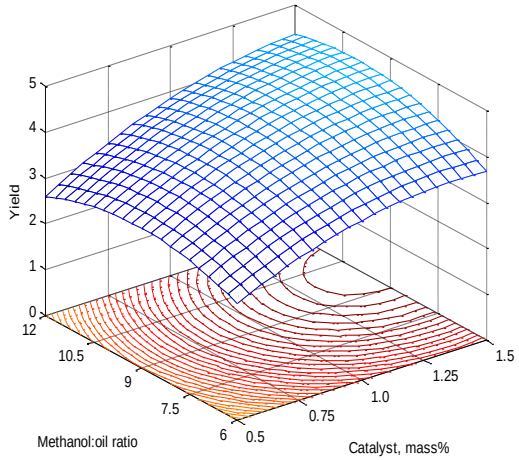


**Figure 5.111: RSM plot- Effect of Meth:oil ratio and MgO conc. on Yield (MW)**

Fig 5.112 is RSM surface and contour plot for Yield as function of methanol to oil ratio and time. Optima was at time > 5 min, and at methanol ratio of 9:1. This fully agreed with experimental data.

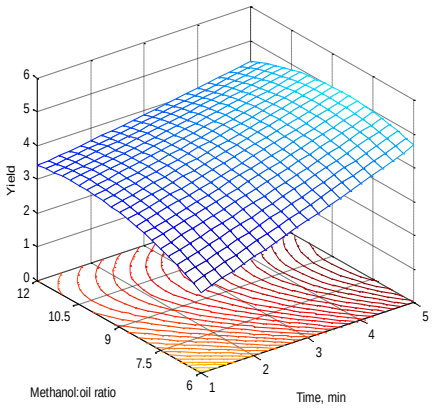


**Figure 5.112: RSM plot- Effect of Meth:oil ratio and Time on Yield for MgO (MW)**

### 5.3.9 Studies with Conventional Heating- Beryllium oxide catalyst

This section deals with transesterification reactions carried out with conventional heating employing a water bath as heat source.

### 5.3.9.1 Effect of operation variables on FAME yield

#### 5.3.9.1.1 Effect of methanol to triglyceride molar ratio on FAME yield

Fig 5.113 gives the FAME yield (%) as a function of methanol: oil ratio. Yields were low, and the highest yield of 4.5% FAME was at 12:1 methanol to oil ratio. A slight decline in yield was noted at 15:1 ratio. Initially excess of methanol drives the transesterification reaction (Eqn 2.2) towards left, increasing yield. But an excess of methanol dilutes the catalyst percentage in the reaction system and unreacted methanol mixes with glycerol bringing about separation problems. Also, in presence of surplus methanol, glycerol forms emulsion with FAME, lowering the yield. Literatures for these observations have been sighted in earlier sections.

#### 5.3.9.1.2 Effect of catalyst concentration on FAME yield

Highest yield of 4.8% was obtained at 2 mass% catalyst. However, there was not much variation in yield in the catalyst concentration ranging 1 – 3% (Fig 5.114).

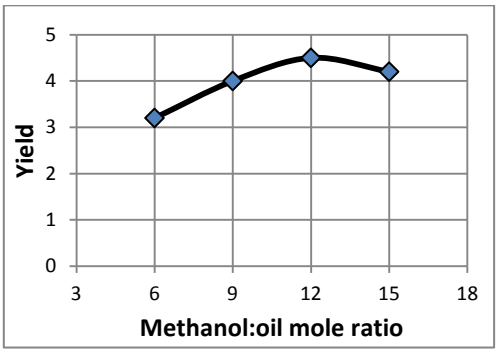


**Figure 5.113: Effect of Methanol to oil ratio on FAME yield (WB)**

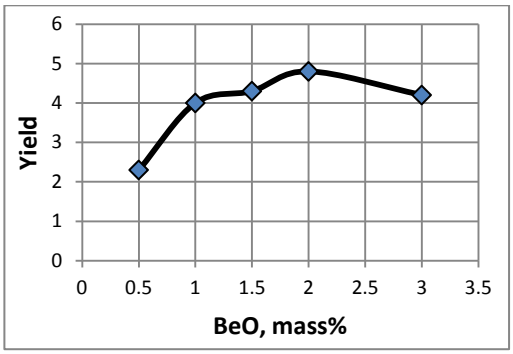


**Figure 5.114: : Effect of BeO concentration on FAME yield (WB)**

#### 5.3.9.1.3 Effect of temperature on FAME yield

Yield became almost constant after 60$^{o}$C (333K). Highest yield was at 70$^{o}$C (343K) to be 4% of FAME. Fig 5.115 gives the effect of reaction temperature on FAME yield (%).

### 5.3.9.2 Reaction Kinetics

#### 5.3.9.2.1 Effect of Time on FAME yield

FAME yields (%) for temperatures of 40, 50, 60, 70$^{o}$C (313, 323, 333, 343 K) were plotted as a function of time as given in Fig 5.116. Yields increased with increase in temperature, and with time. At 70$^{o}$C (343K) yield became almost constant after 1h. At other lower

temperatures, yields did not change much after 2h of reaction time. Yield curves for 60 and 70°C (333 and 343K) follow closely to each other.

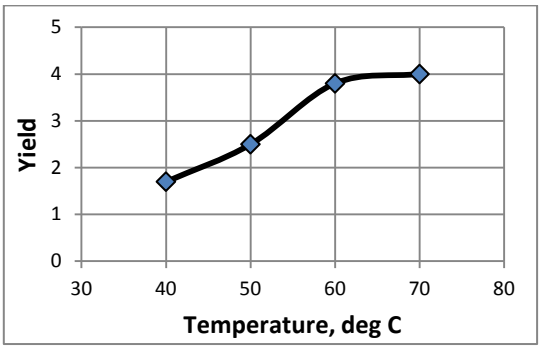


**Figure 5.115: Effect of reaction temperature on FAME yield (WB)**

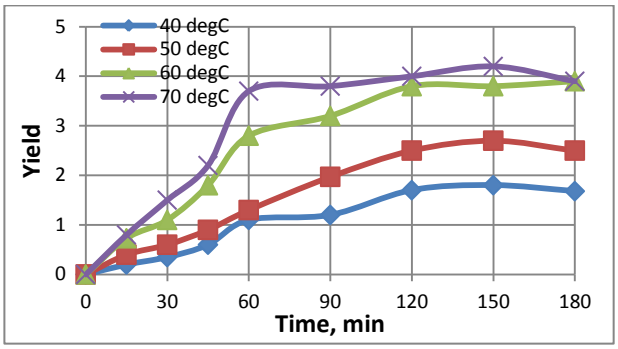


**Figure 5.116: Variation of Yield with time at various temperatures (WB)**

#### 5.3.9.2.2 Order of reaction

Table 5.115 gives the coefficients of correlation, $R^2$, for all the ten cases of reaction orders, and for all temperatures. Indices *m* and *n* refer to the general rate equation: $-r_A = -\frac{d[A]}{dt} = k\,[A]^m\,[B]^n$ (Eqn 2.29, Chapter 2).

**Table 5.115: Coefficients of correlation, $R^2$, for various reaction orders (WB)**

| | 0th Order | 1st Order | | 2nd Order | | | 3rd Order | | | |
|---|---|---|---|---|---|---|---|---|---|---|
| **Temp °C** | Case 1 | Case 2 (m=1, n=0) | Case 3 (m=0, n=1) | Case 4 (m=1, n=1) | Case 5 (m=2, n=0) | Case 6 (m=0, n=2) | Case 7 (m=2, n=1) | Case 8 (m=1, n=2) | Case 9 (m=3, n=0) | Case 10 (m=0, n=3) |
| **40** | 0.8986 | 0.8993 | 0.8988 | 0.8995 | 0.8999 | 0.899 | **0.9001** | 0.8998 | 0.9006 | 0.8993 |
| **50** | 0.9149 | 0.9158 | 0.9152 | 0.9161 | 0.9168 | 0.9155 | **0.9171** | 0.9166 | 0.917 | 0.9158 |
| **60** | 0.8477 | 0.8506 | 0.8486 | 0.8516 | 0.8535 | 0.8496 | **0.8565** | 0.8528 | 0.8564 | 0.8506 |
| **70** | 0.729 | 0.7313 | 0.7298 | 0.732 | 0.7335 | 0.7305 | **0.7342** | 0.7329 | 0.7336 | 0.7312 |

Highest coefficient-of-correlation at each temperature is given in bold. Regression analysis for the reactions at all the four temperatures suggested a third order reaction with *m* = 2, *n* = 1. Hence the overall reaction order was 'three', second order with respect to triglyceride and first order with respect to methanol (Case 7 in Table 5.115). The 'slope' in this case is = k $[A_o]^2$ The rate equation, in terms of rate of disappearance of triglyceride, is: $-r_A = -\frac{d[A]}{dt} = k\,[A]^2\,[B]$, where *A* is triglyceride and *B* is methanol.

#### 5.3.9.2.3 Rate constant and Activation energy

Integrated form of rate reaction in Case 7 (Table 5.115) is Eqn 2.40 (Chapter 2):

$$\frac{1}{(\alpha_B - 3)}\left(\frac{x_A}{1 - x_A} - \frac{3}{\alpha_B - 3}\right) ln\frac{(\alpha_B - 3x_A)}{(1 - x_A)\alpha_B} = k\,[A]_o^2\,t$$

L.H.S is F($x_A$) and RHS is a function of time *t*. Regression linear plot for F($x_A$) vs. *t* for 70$^o$C (343K) is given in Fig 11.5.The ordinate is $\frac{1}{(\alpha_B-3)}\left(\frac{x_A}{1-x_A} - \frac{3}{\alpha_B-3}\right) ln\frac{(\alpha_B-3x_A)}{(1-x_A)\alpha_B}$, and abscissa is *t*. Reaction constant *k* is given by the slope of the plot ($R^2$ = 0.7342).

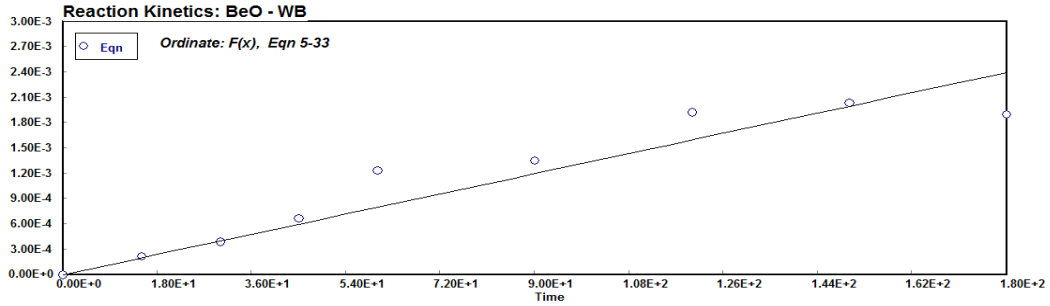


**Figure 5.117: Plot of kinetic equation 2.40 (WB)**

Correlation constants (k $[A_o]^2$ ) for Eqn 2.40 for the four temperatures were used to estimate reaction constant *k* as given in Table 5.116.

**Table 5.116: Reaction constant k (WB)**

| Temp $^o$C | Temp K | $[Ao]^2$ .k | [Ao] | k |
|---|---|---|---|---|
| | | | g/cm3 | (in min) |
| **40** | 313.15 | 1.39E-05 | 0.6663 | 3.12E-05 |
| **50** | 323.15 | 2.07E-05 | 0.6663 | 4.65E-05 |
| **60** | 333.15 | 3.37E-05 | 0.6663 | 7.58E-05 |
| **70** | 343.15 | 3.88E-05 | 0.6663 | 8.73E-05 |

Activation energy was obtained from the slope of the plot of ln*k* vs. 1/T (Arrhenius plot, Section 2.5.4.1, Chapter 2). Fig 5.118 gives the plot.

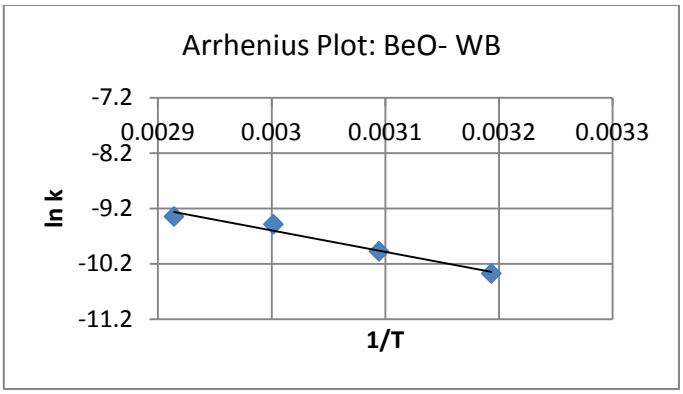


**Figure 5.118: Arrhenius plot for BeO catalyst (WB)**

The slope was 3856.75 ( $R^2$ = 0.9681), which gave the Activation energy, *E* = 32.1 kJ/mol; and intercept gave pre-exponential factor, *A* = 7.2.

### 5.3.9.3 Optimization studies- experimental results and data analysis for BeO

Table 5.117 gives the details of a set of 20 experiments in terms of actual and coded levels, as per CCD, and the FAME yields obtained in transesterification studies. Last column gives the Predicted yield computed from Reduced quadratic model (Eqn 5.16).

**Table 5.117: CCD matrix with experimental FAME yield for BeO (WB)**

| Run | Level of variables [actual(coded)] | | | Expt. Yield | Reduced Model (Eqn 5.16) |
|---|---|---|---|---|---|
| | Catalyst,% X1 | Temp, (°C) X2 | Methanol :oil X3 | | Y |
| **1** | 1(0) | 60(0) | 9(0) | 4.4 | 4.6 |
| **2** | 1(0) | 43(-1.68) | 9(0) | 3.2 | 3.1 |
| **3** | 0.5(-1) | 70(1) | 12(1) | 3.3 | 3.5 |
| **4** | 1(0) | 60(0) | 14(1.68) | 4.6 | 4.5 |
| **5** | 1.84(1.68) | 60(0) | 9(0) | 4.8 | 4.4 |
| **6** | 1(0) | 60(0) | 4(-1.68) | 3.8 | 3.7 |
| **7** | 0.5(-1) | 50(-1) | 6(-1) | 3.0 | 3.1 |
| **8** | 1(0) | 60(0) | 9(0) | 4.6 | 4.6 |
| **9** | 1.5(1) | 70(1) | 12(1) | 5.2 | 5.2 |
| **10** | 1.5(1) | 70(1) | 6(-1) | 3.8 | 3.9 |
| **11** | 1(0) | 60(0) | 9(0) | 4.5 | 4.6 |
| **12** | 1.5(1) | 50(-1) | 6(-1) | 3.2 | 3.2 |
| **13** | 0.16(-1.68) | 60(0) | 9(0) | 3.0 | 2.9 |
| **14** | 1(0) | 60(0) | 9(0) | 4.7 | 4.6 |
| **15** | 1.5(1) | 50(-1) | 12(1) | 4.5 | 4.6 |
| **16** | 1(0) | 60(0) | 9(0) | 4.9 | 4.6 |
| **17** | 0.5(-1) | 50(-1) | 12(1) | 2.9 | 2.8 |
| **18** | 1(0) | 77(1.68) | 9(0) | 4.0 | 4.2 |
| **19** | 1(0) | 60(0) | 9(0) | 4.5 | 4.6 |

| | | | | | |
|---|---|---|---|---|---|
| **20** | 0.5(-1) | 70(1) | 6(-1) | 3.8 | 3.8 |

Data in Table 5.117 were tested for fit for a linear, two-factor interaction (2FI), quadratic and cubic polynomials. Table 5.118 gives the result.

**Table 5.118: Summary for model fit- Sequential model sum of squares (WB)**

| **Summary (detailed tables shown below)** | | | | | | |
|---|---|---|---|---|---|---|
| | **Sequential** | **Lack of Fit** | | **Adjusted** | **Predicted** | |
| **Source** | **p-value** | **p-value** | | **R-Squared** | **R-Squared** | |
| **Linear** | 0.0051 | < 0.0001 | | 0.4542 | 0.2902 | |
| **2FI** | 0.1668 | < 0.0001 | | 0.5389 | 0.0837 | |
| **Quadratic** | < 0.0001 | 0.0519 | | 0.9842 | 0.9404 | Suggested |
| **Cubic** | 0.4673 | 0.0161 | | 0.9843 | 0.2133 | Aliased |
| **Sequential Model Sum of Squares [Type I]** | | | | | | |
| | **Sum of** | | **Mean** | **F** | **p-value** | |
| **Source** | **Squares** | **df** | **Square** | **Value** | **Prob > F** | |
| **Mean vs Total** | 322.00 | 1 | 322.00 | | | |
| **Linear vs Mean** | 5.15 | 3 | 1.72 | 6.27 | 0.0051 | |
| **2FI vs Linear** | 1.37 | 3 | 0.46 | 1.98 | 0.1668 | |
| **Quadratic vs 2FI** | 2.93 | 3 | 0.98 | 122.93 | < 0.0001 | Suggested |
| **Cubic vs Quadratic** | 0.032 | 4 | 8.028E-003 | 1.02 | 0.4673 | Aliased |
| **Residual** | 0.047 | 6 | 7.877E-003 | | | |
| **Total** | 331.53 | 20 | 16.58 | | | |

Highest Adjusted $R^2$ was for a Cubic model but it was aliased. Next highest Adj $R^2$ was for a Quadratic model. Considering the F value and p-value, Quadratic model was suggested. Cubic was not considered being aliased. The appropriate model for the given set of data was full Quadratic model (Eqn 4.2, Chapter 4) : $Y = b_0 + \sum_{i=1}^{n} b_i X_i + \sum_{i=1}^{n} b_{ii} X_i^2 + \sum_{1=1}^{n-1} \sum_{j=i+1}^{n} b_{ij} X_i X_j$ , Y is the Yield, $X_i$ are coded variables as given in Table 5.1. Table 5.119 gives Analysis of Variance (ANOVA) for a full quadratic model.

**Table 5.119: ANOVA for Response Surface Quadratic model (WB)**

| **ANOVA for Response Surface Quadratic model** | | | | | | |
|---|---|---|---|---|---|---|
| **Analysis of variance table [Partial sum of squares - Type III]** | | | | | | |
| | **Sum of** | | **Mean** | **F** | **p-value** | |
| **Source** | **Squares** | **df** | **Square** | **Value** | **Prob > F** | |
| **Model** | 9.45 | 9 | 1.05 | 132.29 | < 0.0001 | significant |
| ***X1-BeO*** | *2.91* | *1* | *2.91* | *366.94* | *< 0.0001* | |

| | | | | | | |
|---|---|---|---|---|---|---|
| ***X2-Temp*** | *1.28* | *1* | *1.28* | *161.32* | *< 0.0001* | |
| ***X3-Meth:oil*** | *0.96* | *1* | *0.96* | *120.46* | *< 0.0001* | |
| ***X1.X2*** | *1.250E-003* | *1* | *1.250E-003* | *0.16* | *0.6998* | |
| ***X1.X3*** | *1.36* | *1* | *1.36* | *171.50* | *< 0.0001* | |
| ***X2.X3*** | *0.011* | *1* | *0.011* | *1.42* | *0.2613* | |
| ***X1^2*** | *1.47* | *1* | *1.47* | *185.11* | *< 0.0001* | |
| ***X2^2*** | *1.55* | *1* | *1.55* | *195.50* | *< 0.0001* | |
| ***X3^2*** | *0.41* | *1* | *0.41* | *51.88* | *< 0.0001* | |
| **Residual** | 0.079 | 10 | 7.937E-003 | | | |
| ***Lack of Fit*** | *0.066* | *5* | *0.013* | *4.95* | *0.0519* | *not significant* |
| ***Pure Error*** | *0.013* | *5* | *2.667E-003* | | | |
| **Cor Total** | 9.53 | 19 | | | | |

The Model F-value of 132.29 implied the model was significant. There was only a 0.01% chance that an F-value this large could occur due to noise. Values of "Prob > F" less than 0.0500 indicate model terms are significant. In this case X1, X2, X3, X1.X3, X1^2, X2^2, X3^2 were significant model terms. Insignificant term X1.X2 and X2.X3 were dropped to simplify the model

**Reduced Model:** Insignificant terms X1.X2 and X2.X3 were dropped from the full Quadratic model. Table 5.120 gives ANOVA for the reduced model.

**Table 5.120: ANOVA for Response Surface for Reduced Quadratic model (WB)**

| **ANOVA for Response Surface Reduced Quadratic model** | | | | | | |
|---|---|---|---|---|---|---|
| **Analysis of variance table [Partial sum of squares - Type III]** | | | | | | |
| | **Sum of** | | **Mean** | **F** | **p-value** | |
| **Source** | **Squares** | **df** | **Square** | **Value** | **Prob > F** | |
| **Model** | 9.44 | 7 | 1.35 | 176.10 | < 0.0001 | significant |
| ***X1-BeO*** | *2.91* | *1* | *2.91* | *380.42* | *< 0.0001* | |
| ***X2-Temp*** | *1.28* | *1* | *1.28* | *167.25* | *< 0.0001* | |
| ***X3-Meth:oil*** | *0.96* | *1* | *0.96* | *124.89* | *< 0.0001* | |
| ***X1.X3*** | *1.36* | *1* | *1.36* | *177.80* | *< 0.0001* | |
| ***X1^2*** | *1.47* | *1* | *1.47* | *191.90* | *< 0.0001* | |
| ***X2^2*** | *1.55* | *1* | *1.55* | *202.68* | *< 0.0001* | |
| ***X3^2*** | *0.41* | *1* | *0.41* | *53.79* | *< 0.0001* | |
| **Residual** | 0.092 | 12 | 7.656E-003 | | | |
| ***Lack of Fit*** | *0.079* | *7* | *0.011* | *4.21* | *0.0665* | *not significant* |
| ***Pure Error*** | *0.013* | *5* | *2.667E-003* | | | |
| **Cor Total** | 9.53 | 19 | | | | |

The Model F-value of 176.10 implied the model was significant. There was only a 0.01% chance that an F-value this large could occur due to noise. Values of "Prob > F" less than 0.0500 indicated model terms were significant. In this case X1, X2, X3, X1.X3, X1^2,

X2^2, X3^2 were significant model terms. The "Lack of Fit F-value" of 4.21 implied there was a 6.65% chance that a "Lack of Fit F- value" this large could occur due to noise. Lack-of-fit was not very good but it was insignificant and acceptable. Table 5.121 gives R-Square values.

**Table 5.121: R-Square values (WB)**

| | | | |
|---|---|---|---|
| **Std. Dev.** | **0.087** | **R-Squared** | **0.9904** |
| **Mean** | 4.01 | **Adj R-Squared** | 0.9847 |
| **C.V. %** | 2.18 | **Pred R-Squared** | 0.9658 |
| **PRESS** | 0.33 | **Adeq Precision** | 42.663 |

In Table 5.121, the "Pred R-Squared" of 0.9658 was in reasonable agreement with the "Adj R-Squared" of 0.9847; i.e. the difference was less than 0.2. "Adeq Precision" measures the signal to noise ratio. A ratio greater than 4 is desirable. Present model's ratio of 42.663 indicated an adequate signal. This model can be used for design purposes. Table 5.122 gives the coefficients for the reduced model.

**Table 5.122: Coefficients for the Reduced Quadratic Model (WB)**

| | **Coefficient** | **Standard** | **95% CI** | **95% CI** |
|---|---|---|---|---|
| **Factor** | **Estimate** | **Error** | **Low** | **High** |
| **Intercept** | 4.57 | 0.036 | 4.49 | 4.65 |
| **X1-BeO** | 0.46 | 0.024 | 0.41 | 0.51 |
| **X2-Temp** | 0.31 | 0.024 | 0.25 | 0.36 |
| **X3-Meth:oil** | 0.26 | 0.024 | 0.21 | 0.32 |
| **X1.X3** | 0.41 | 0.031 | 0.35 | 0.48 |
| **X1^2** | -0.32 | 0.023 | -0.37 | -0.27 |
| **X2^2** | -0.33 | 0.023 | -0.38 | -0.28 |
| **X3^2** | -0.17 | 0.023 | -0.22 | -0.12 |

Since all the terms in the reduced model were significant, no further reductions were needed. Hence the model was:

$$\text{Yield, } Y = 4.57 + 0.46\,X1 + 0.31\,X2 + 0.26\,X3 + 0.41\,X1.X3 - 0.32\,X1^2 - 0.33\,X2^2 - 0.17\,X3^2 \quad \ldots 5.16$$

Reduced quadratic model was used to compute Predicted yields given in Table 5.117. Eqn 5.16 can be used for response surface plots.

#### 5.3.9.3.1 Response Surface and Contour Plots

Fig 5.119 is a RSM plot giving response surface and contours for FAME yield as a function of BeO Catalyst concentration and reaction temperature. The optima was in the catalyst concentration of 2 – 2.5 mass% and a temperature of 70$^{o}$C (343K). These agreed with the experimental observations.

Fig 5.120 is a RSM plot giving response surface and contours for FAME yield as a function of BeO catalyst concentration and methanol to oil ratio. Optima was beyond the range of experimental variables, yield increased with increasing BeO and increasing methanol. These agreed with the trends observed during experiments.

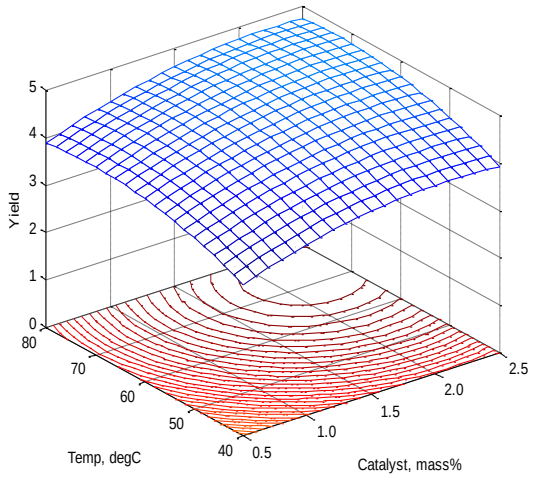


**Figure 5.119: RSM plot- Effect of BeO conc. and Temperature on Yield (WB)**

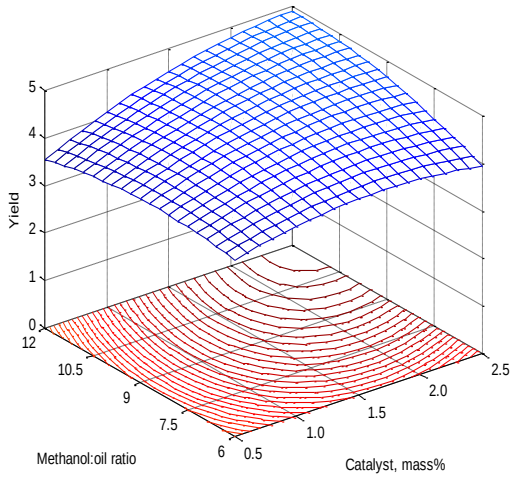


**Figure 5.120: : RSM plot- Effect of BeO conc. and Methanol:oil ratio on Yield (WB)**

Fig 5.121 is a RSM plot giving response surface and contours for FAME yield as a function of reaction temperature and methanol to oil ratio. The optima was close to a temperature of 70$^{o}$C (343K) and a methanol to oil ratio of 10.5:1. These agreed well with the experimental observations.

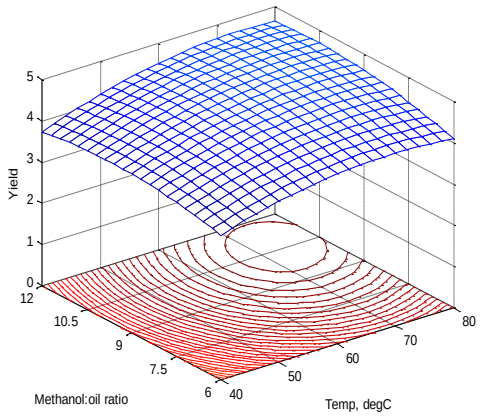


**Figure 5.121: RSM plot- Effect of Methanol:oil ratio and Temp. on Yield for BeO (WB)**

### 5.3.10 Studies with Microwave Irradiation- Beryllium oxide catalyst

This section deals with transesterification of Croton *megalocarpus* oil using heterogeneous BeO catalyst with microwave irradiation. Studies include effect of operation variables on FAME yield, transesterification reaction kinetics and optimization.

#### 5.3.10.1 Effect of operation variables on FAME yield

##### 5.3.10.1.1 Effect of methanol to triglyceride molar ratio on FAME yield

Fig 5.122 gives the FAME yield (%) as a function of methanol to oil ratio. FAME yield increased with the increase of methanol to oil ratio from 6 to 9, and from 9 to 12. Maximum FAME yield of 3.9% corresponded to the ratio of 12:1. Yield dropped slightly as the methanol ratio was increased to 15:1. The yields were low, and the drop was about 1%.

##### 5.3.10.1.2 Effect of catalyst concentration on FAME yield

Fig 5.123 gives FAME yield (%) as a function of BeO concentration. FAME yield increased with the increase in BeO concentration, maximum yield of 3.7% was at 2 mass% BeO.

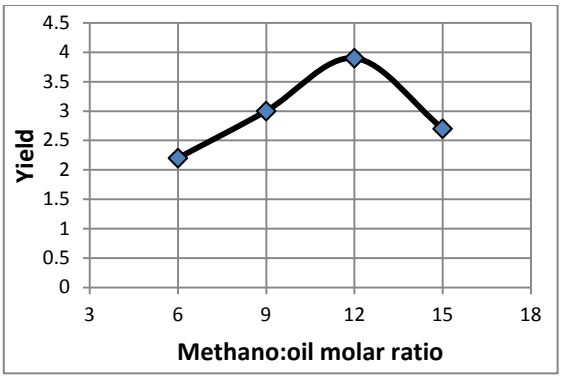


**Figure 5.122: FAME yield as a function of Methanol: oil ratio (MW)**

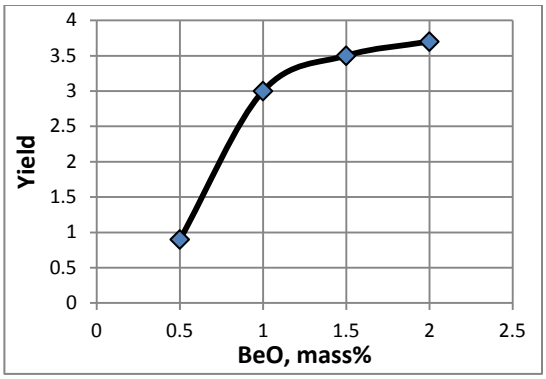


**Figure 5.123: FAME yield as a function of BeO concentration (MW)**

#### 5.3.10.1.3 Effect of reaction time on FAME yield

Yield increased with time and the yield at the end of 5 min was 3.2% of FAME. Fig 5.124 gives the effect of reaction time on FAME yield (%) at full microwave power.

#### 5.3.10.1.4 Effect of microwave power

Fig 5.125 gives the effect of microwave power on FAME yield. Yield increased with the rise of power since microwave power is directly related to microwave irradiation. The highest yield at 100% power was 3.2% of FAME.

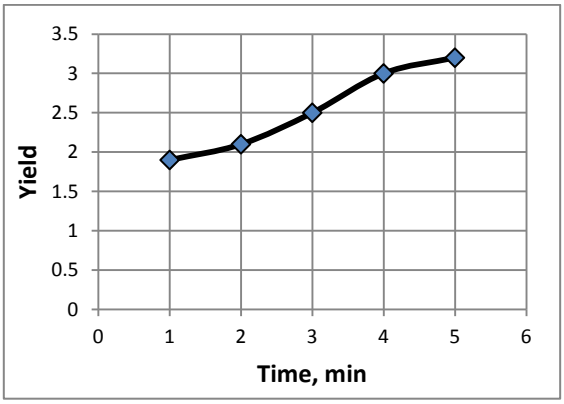


**Figure 5.124: Effect of reaction time on Yield (MW)**

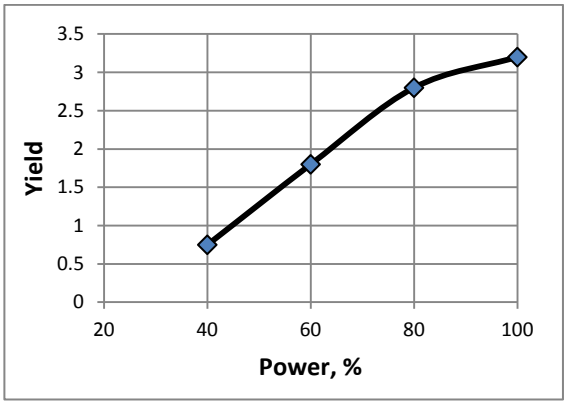


**Figure 5.125: The effect of microwave power on FAME yield**

### 5.3.10.2 Reaction Kinetics

#### 5.3.10.2.1 Effect of Time on FAME yield

Fig 5.126 is a plot of FAME yield (%) vs. reaction time at varying reaction temperatures. Conversions at 50$^{o}$C (323K) were much lower in the initial time of 45s, but accelerated

later. Reactions at 60°C (333K) were also slower in the beginning but increased later to give almost same yield as that at 70°C (343K).

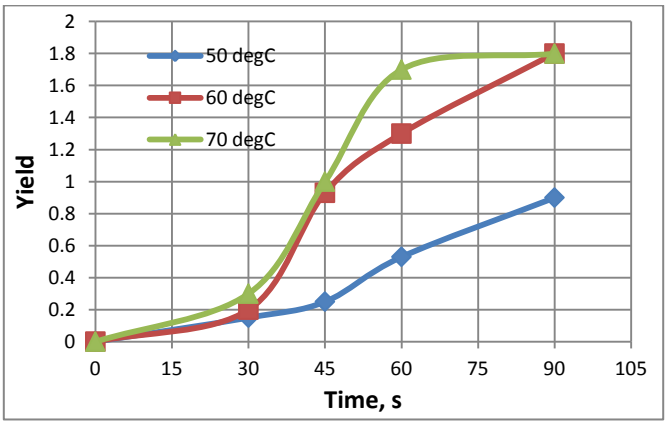


**Figure 5.126: Variation of Yield with time at various temperatures (MW)**

### 5.3.10.2.2 Order of reaction

Table 5.123 gives the coefficients of correlation for all reaction orders, Cases 1 to 10, at the three temperatures.

**Table 5.123: Coefficients of correlation, $R^2$, for various reaction orders**

| | 0th Order | 1st Order | | 2nd Order | | | 3rd Order | | | |
|---|---|---|---|---|---|---|---|---|---|---|
| **Temp °C** | Case 1 | Case 2 (m=1, n=0) | Case 3 (m=0, n=1) | Case 4 (m=1, n=1) | Case 5 (m=2, n=0) | Case 6 (m=0, n=2) | Case 7 (m=2, n=1) | Case 8 (m=1, n=2) | Case 9 (m=3, n=0) | Case 10 (m=0, n=3) |
| **50** | 0.8724 | 0.8717 | **0.8725** | 0.8713 | 0.8706 | 0.8721 | 0.8702 | 0.8708 | 0.8694 | 0.8717 |
| **60** | 0.9053 | 0.9053 | **0.9055** | 0.9052 | 0.9049 | 0.9054 | 0.9048 | 0.905 | 0.9046 | 0.9053 |
| **70** | 0.8625 | 0.8619 | **0.8623** | 0.8617 | 0.8613 | 0.8621 | 0.8611 | 0.8614 | 0.8607 | 0.8619 |

Highest correlation coefficients are in bold numbers in Table 5.123. The most likely order of reaction was 'first' . Zero order with respect to triglyceride, and first order with respect to methanol (Case 3). The integrated form of rate equation is Eqn 2.36 (Chapter 2) given as: $-\frac{1}{3} ln\left(\frac{\alpha_B - 3x_A}{\alpha_B}\right) = k\,t$. The slope in this case is = k.

### 5.3.10.2.3 Rate constant and Activation energy

L.H.S. of Eqn 2.36, $\left(-\frac{1}{3} ln\left(\frac{\alpha_B - 3x_A}{\alpha_B}\right)\right)$ is a function of conversion $x_A$ , $F(x_A)$, or the yield. A plot of $F(x_A)$ vs time t is a straight line passing through the origin. Regression linear plot

for F($x_A$) vs. $t$ for 70°C (343K) is given in Fig 5.127.The ordinate is, $-\frac{1}{3}ln\left(\frac{\alpha_B - 3x_A}{\alpha_B}\right)$ and abscissa is $t$. Reaction constant $k$ is given by the slope of the plot ($R^2$ = 0.8623).

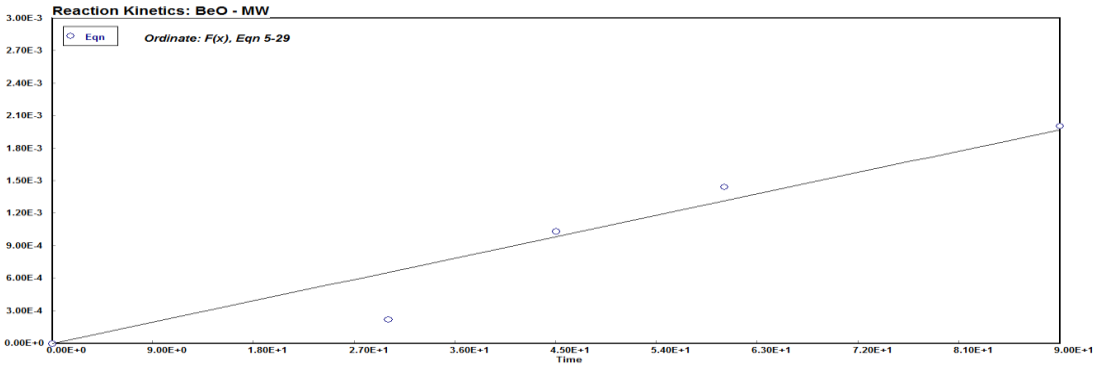


**Figure 5.127: Plot of kinetic equation 2.36 (MW)**

Correlation constants (k) for Eqn 2.36 for the three temperatures were used to estimate reaction constant $k$ as given in Table 5.124.

**Table 5.124: Reaction constant k (MW)**

| Temp, °C | Temp K | k |
|---|---|---|
| | | ( min) |
| **50** | 323.15 | 6.10E-04 |
| **60** | 333.15 | 1.35E-03 |
| **70** | 343.15 | 1.52E-03 |

Activation energy was obtained from the slope of the plot of ln$k$ vs. 1/T (Arrhenius plot, Section 5.4.1). Fig 5.128 gives the plot ($R^2$ = 0.8551).

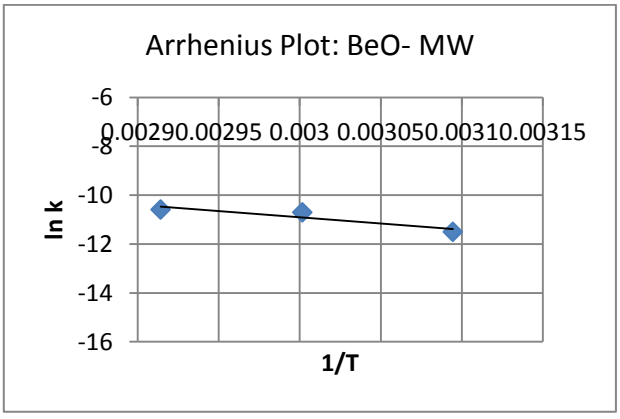


**Figure 5.128: Arrhenius plot for BeO (MW)**

Slope of the plot was 5091.31, giving Activation energy, $E$ = 42.3 kJ/mol, and intercept gave pre-exponential factor, $A$ = 78.6.

### 5.3.10.3 Optimization studies- experimenatal results and data analysis- BeO

Table 5.125 gives the details of a set of 20 experiments in terms of actual and coded levels, as per CCD, and the FAME yields obtained in transesterification studies. Last column gives the Predicted yield using Quadratic model given by Eqn 5.17.

**Table 5.125: CCD matrix with experimental FAME yield (MW)**

| Run | Level of variables [actual(coded)] | | | Experimental Yield | Quadratic model (Eqn 5.17) |
|---|---|---|---|---|---|
| | Catalyst,% | Time (min) | Meth :oil | | Y |
| | X1 | X2 | X3 | | |
| **1** | 1(0) | 3(0) | 9(0) | 2.5 | 2.4 |
| **2** | 1(0) | 0.5(-1.68) | 9(0) | 1.7 | 1.3 |
| **3** | 0.5(-1) | 4.5(1) | 12(1) | 1.7 | 1.5 |
| **4** | 1(0) | 3(0) | 14(1.68) | 1.8 | 1.8 |
| **5** | 1.84(1.68) | 3(0) | 9(0) | 2.7 | 2.7 |
| **6** | 1(0) | 3(0) | 4(-1.68) | 1.4 | 1.4 |
| **7** | 0.5(-1) | 1.5(-1) | 6(-1) | 1.2 | 1.1 |
| **8** | 1(0) | 3(0) | 9(0) | 2.3 | 2.4 |
| **9** | 1.5(1) | 4.5(1) | 12(1) | 3.5 | 3.4 |
| **10** | 1.5(1) | 4.5(1) | 6(-1) | 3.4 | 3.2 |
| **11** | 1(0) | 3(0) | 9(0) | 2.4 | 2.4 |
| **12** | 1.5(1) | 1.5(-1) | 6(-1) | 1.0 | 1.1 |
| **13** | 0.16(-1.68) | 3(0) | 9(0) | 1.1 | 1.1 |
| **14** | 1(0) | 3(0) | 9(0) | 2.3 | 2.4 |
| **15** | 1.5(1) | 1.5(-1) | 12(1) | 1.9 | 1.8 |
| **16** | 1(0) | 3(0) | 9(0) | 2.4 | 2.4 |
| **17** | 0.5(-1) | 1.5(-1) | 12(1) | 1.3 | 1.3 |
| **18** | 1(0) | 5.5(1.68) | 9(0) | 3.3 | 3.2 |
| **19** | 1(0) | 3(0) | 9(0) | 2.3 | 2.4 |
| **20** | 0.5(-1) | 4.5(1) | 6(-1) | 1.8 | 1.7 |

Data in Table 5.125 were tested for fit for a linear, two-factor interaction (2FI), quadratic and cubic polynomials. Table 5.126 gives the result.

**Table 5.126: Summary for model fit- Sequential model sum of squares (MW)**

| **Summary for model fit** | | | | | |
|---|---|---|---|---|---|
| | **Sequential** | **Lack of Fit** | **Adjusted** | **Predicted** | |
| **Source** | **p-value** | **p-value** | **R-Squared** | **R-Squared** | |
| **Linear** | 0.0001 | 0.0002 | 0.6708 | 0.5208 | |
| **2FI** | 0.0474 | 0.0003 | 0.7753 | 0.6371 | |
| **Quadratic** | < 0.0001 | 0.0524 | 0.9757 | 0.9094 | Suggested |
| **Cubic** | 0.0169 | 0.9200 | 0.9932 | 0.9958 | Aliased |
| **Sequential Model Sum of Squares [Type I]** | | | | | |
| | **Sum of** | | **Mean** | **F** | **p-value** |
| **Source** | **Squares** | **df** | **Square** | **Value** | **Prob > F** |
| **Mean vs Total** | 7.62 | 3 | 2.54 | 13.91 | 0.0001 |
| **Linear vs Mean** | 1.30 | 3 | 0.43 | 3.48 | 0.0474 |
| **2FI vs Linear** | 1.49 | 3 | 0.50 | 36.73 | < 0.0001 |
| **Quadratic vs 2FI** | 0.11 | 4 | 0.028 | 7.37 | 0.0169 |
| **Cubic vs Quadratic** | 0.023 | 6 | 3.800E-003 | | |
| **Residual** | 99.50 | 20 | 4.97 | | |
| **Total** | 88.96 | 1 | 88.96 | | |

Cubic had the highest Adj $R^2$ (0.9932), followed by Adj $R^2$ for Quadratic model (0.9757). However, cubic was not suitable because of being aliased. Considering the F and p-values, a Quadratic model was suggested. The appropriate model for the given set of data was full Quadratic model (Eqn 4.2, Chapter 4) :

$$Y = b_0 + \sum_{i=1}^{n} b_i X_i + \sum_{i=1}^{n} b_{ii} X_i^2 + \sum_{1=1}^{n-1} \sum_{j=i+1}^{n} b_{ij} X_i X_j$$

Y is the FAME Yield, $X_i$ are coded variables as given in Table 5.2.

Table 5.127 gives Analysis of Variance (ANOVA) for a full quadratic model.

**Table 5.127: ANOVA for Response Surface Quadratic model (MW)**

| **ANOVA for Response Surface Quadratic model** | | | | | | |
|---|---|---|---|---|---|---|
| **Analysis of variance table [Partial sum of squares - Type III]** | | | | | | |
| | **Sum of** | | **Mean** | **F** | **p-value** | |
| **Source** | **Squares** | **df** | **Square** | **Value** | **Prob > F** | |
| **Model** | 10.41 | 9 | 1.16 | 85.74 | < 0.0001 | significant |
| ***X1-BeO*** | *3.16* | *1* | *3.16* | *234.42* | *< 0.0001* | |
| ***X2-Time*** | *4.26* | *1* | *4.26* | *316.15* | *< 0.0001* | |
| ***X3-Methanol:oil*** | *0.19* | *1* | *0.19* | *14.42* | *0.0035* | |
| ***X1.X2*** | *1.07* | *1* | *1.07* | *79.03* | *< 0.0001* | |

| | | | | | | |
|---|---|---|---|---|---|---|
| ***X1.X3*** | *0.13* | *1* | *0.13* | *9.27* | *0.0124* | |
| ***X2.X3*** | *0.11* | *1* | *0.11* | *8.19* | *0.0169* | |
| ***X1^2*** | *0.42* | *1* | *0.42* | *31.11* | *0.0002* | |
| ***X2^2*** | *0.025* | *1* | *0.025* | *1.84* | *0.2048* | |
| ***X3^2*** | *1.09* | *1* | *1.09* | *80.76* | *< 0.0001* | |
| **Residual** | 0.13 | 10 | 0.013 | | | |
| ***Lack of Fit*** | *0.11* | *5* | *0.022* | *4.93* | *0.0524* | *not significant* |
| ***Pure Error*** | *0.023* | *5* | *4.550E-003* | | | |
| **Cor Total** | 10.54 | 19 | | | | |

The Model F-value of 85.74 implied the model was significant. There was only a 0.01% chance that an F-value this large could occur due to noise. Values of "Prob > F" less than 0.0500 indicate model terms are significant. In this case X1, X2, X3, X1X2, X1X3, X2X3, X1^2, X3^2 were significant model terms. X2^2 was not significant and it was dropped to simplify the model.

**Reduced Model:** X2^2 was dropped from full Quadratic model. Table 5.128 gives the ANOVA for the reduced model.

**Table 5.128: ANOVA for Response Surface Quadratic (Reduced) model (MW)**

| **ANOVA for Response Surface Reduced Quadratic model** | | | | | | |
|---|---|---|---|---|---|---|
| **Analysis of variance table [Partial sum of squares - Type III]** | | | | | | |
| | **Sum of** | | **Mean** | **F** | **p-value** | |
| **Source** | **Squares** | **df** | **Square** | **Value** | **Prob > F** | |
| **Model** | 10.38 | 8 | 1.30 | 89.40 | < 0.0001 | significant |
| ***X1-BeO*** | *3.16* | *1* | *3.16* | *217.79* | *< 0.0001* | |
| ***X2-Time*** | *4.26* | *1* | *4.26* | *293.72* | *< 0.0001* | |
| ***X3-Methanol:oil*** | *0.19* | *1* | *0.19* | *13.39* | *0.0038* | |
| ***X1.X2*** | *1.07* | *1* | *1.07* | *73.42* | *< 0.0001* | |
| ***X1.X3*** | *0.13* | *1* | *0.13* | *8.61* | *0.0136* | |
| ***X2X3*** | *0.11* | *1* | *0.11* | *7.61* | *0.0186* | |
| ***X1^2*** | *0.44* | *1* | *0.44* | *30.62* | *0.0002* | |
| ***X3^2*** | *1.13* | *1* | *1.13* | *78.07* | *< 0.0001* | |
| **Residual** | 0.16 | 11 | 0.015 | | | |
| ***Lack of Fit*** | *0.14* | *6* | *0.023* | *5.02* | *0.0487* | *significant* |
| ***Pure Error*** | *0.023* | *5* | *4.550E-003* | | | |
| **Cor Total** | 10.54 | 19 | | | | |

The Model F-value of 89.40 implied the model was significant. There was only a 0.01% chance that an F-value this large could occur due to noise. Values of "Prob > F" less than 0.0500 indicate model terms are significant. In this case X1, X2, X3, X1.X2, X1.X3, X2.X3, X1^2, X3^2 were significant model terms. The "Lack of Fit F-value" of 5.02 implied the Lack of Fit was significant. In this case the reduced model did not meet the

required statistical criterion and therefore was not recommended. The full Quadratic model was hence retained. Table 5.129 gives the R-Square values for the full quadratic model.

**Table 5.129: R-Square values**

| | | | |
|---|---|---|---|
| **Std. Dev.** | **0.12** | **R-Squared** | **0.9872** |
| **Mean** | 2.11 | **Adj R-Squared** | 0.9757 |
| **C.V. %** | 5.51 | **Pred R-Squared** | 0.9094 |
| **PRESS** | 0.96 | **Adeq Precision** | 29.464 |

The "Pred R-Squared" of 0.9094 was in reasonable agreement with the "Adj R-Squared" of 0.9757; i.e. the difference was less than 0.2. "Adeq Precision" measures the signal to noise ratio. A ratio greater than 4 is desirable. Present model's ratio of 29.464 indicated an adequate signal. This model can be used for design purposes. Table 5.130 gives the coefficients for full Quadratic model.

**Table 5.130: Coefficients for the Full Quadratic model (MW)**

| | Coefficient | | Standard | 95% CI | 95% CI |
|---|---|---|---|---|---|
| **Factor** | **Estimate** | **df** | **Error** | **Low** | **High** |
| **Intercept** | 2.38 | 1 | 0.047 | 2.28 | 2.49 |
| **X1-BeO** | 0.48 | 1 | 0.031 | 0.41 | 0.55 |
| **X2-Time** | 0.56 | 1 | 0.031 | 0.49 | 0.63 |
| **X3-Meth:oil** | 0.12 | 1 | 0.031 | 0.049 | 0.19 |
| **X1.X2** | 0.37 | 1 | 0.041 | 0.27 | 0.46 |
| **X1.X3** | 0.13 | 1 | 0.041 | 0.034 | 0.22 |
| **X2X3** | -0.12 | 1 | 0.041 | -0.21 | -0.026 |
| **X1^2** | -0.17 | 1 | 0.031 | -0.24 | -0.10 |
| **X2^2** | 0.041 | 1 | 0.031 | -0.027 | 0.11 |
| **X3^2** | -0.27 | 1 | 0.031 | -0.34 | -0.21 |

Since all the terms in the full quadratic model were significant, the model was:

$$\text{Yield, } Y = 2.38 + 0.48\ X1 + 0.56\ X2 + 0.12\ X3 + 0.37\ X1.X2 + 0.13 X1.X3 - 0.12\ X2.X3 - 0.17\ X1^2 + 0.041\ X2^2 - 0.27\ X3^2 \quad \ldots 5.17$$

Predicted yield values in Table 5.125 were obtained by use of Quadratic model. In the following section, Eqn 5.17 was used for response surface plots.

### 5.3.10.3.1 Response Surface and Contour Plots

Fig 5.129, 5.130 and 5.131 give the RSM surface and contour plots based on Eqn 5.17. In Fig 5.129, FAME yield increased with increasing BeO concentration and with reaction time. Region of maximum yield in this case was beyond the range of reaction variables. Hence for maximum FAME yield, BeO > 2.5%, and reaction time > 5 min.

Fig 5.130 is a RSM plot for effect of BeO concentration and methanol to oil ratio on FAME yield. Contour plot indicated catalyst concentration of >2.5% and methanol to oil ratio of 10.5:1 for the maximum FAME yield. This agreed with experimental observations.

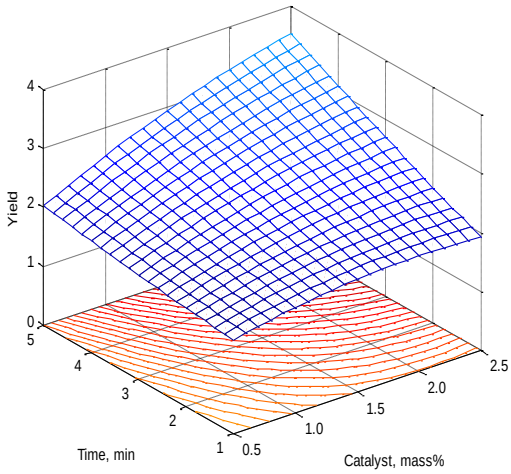


**Figure 5.129: RSM plot- Variation of Yield with BeO conc. and Time (MW)**

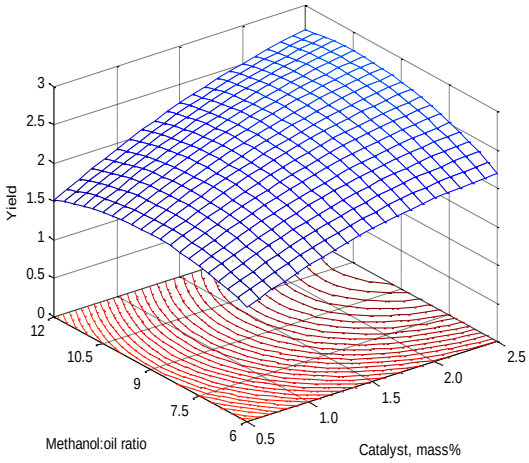


**Figure 5.130: RSM plot- Variation of Yield with BeO conc and methanol: oil ratio (MW)**

Contour plot in Fig 5.131 identified region of maximum yield corresponding to methanol to oil ratio of 9:1, and reaction time > 5 min. These were in qualitative agreement with experimental findings.

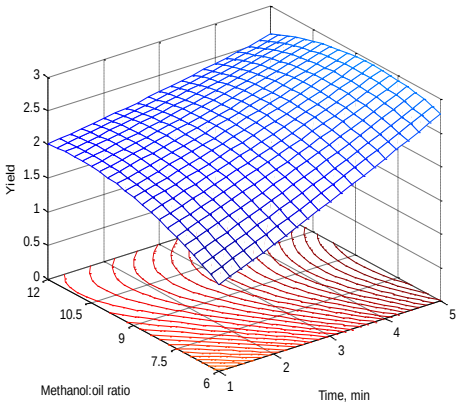


**Figure 5.131: RSM plot- Variation of Yield with Time and methanol:oil ratio for BeO (MW)**

# 6 CONTINUOUS TRANSESTERIFICATION OF *CROTON MEGALOCARPUS* OIL USING HOMOGENEOUS SODIUM HYDROXIDE AND HETEROGENEOUS CALCIUM OXIDE CATALYSTS

## 6.1 Introduction

Transesterification of Croton *megalocarpus* oil was carried out in a plug flow reactor using conventional heating and microwave irradiation. Studies were made for both homogeneous NaOH and heterogeneous CaO catalysts. Among the alkaline earth oxides, calcium oxide was selected because of its special status, being the most abundant, easily available, low cost and easy to handle compound.

## 6.2 Materials and Methods

### 6.2.1 Materials

Calcium oxide (96%) was obtained from Sigma Aldrich. Prior to use, CaO was calcined at 700$^{o}$C (973K) in a muffle furnace under atmospheric conditions for 3 h. Copper tubing ( ID 0.005m) and polytetrafluoroethylene ( Teflon®) tubing ( ID 0.005m) were used for tubular reactor. Peristaltic pump (Cole Palmer Model 77202-50) was employed to control reactor feed rate. Other materials have already been mentioned in Section 4.2.1 of Chapter 4.

### 6.2.2 Experimental Setup

#### 6.2.2.1 Conventional Heating

For transesterification with conventional heating a tubular reactor was fabricated using a 1.7m length of copper tube ( ID 0.005m ) coiled in spiral shape. This tubular flow reactor was kept in a constant temperature water bath. NaOH was mixed with methanol in a round bottom flask. Methanol, NaOH and croton *megalocarpus* oil were sent to a cylindrical container and mixed by a mechanical stirrer, to form reactor feed. Peristaltic pump was used to transfer the feed mixture to the tubular rector at desired rate. Tubular reactor was placed in a constant temperature water bath. Product samples were collected from the exit end of the reactor. Fig 6.1a and 6.1b give the experimental setup.

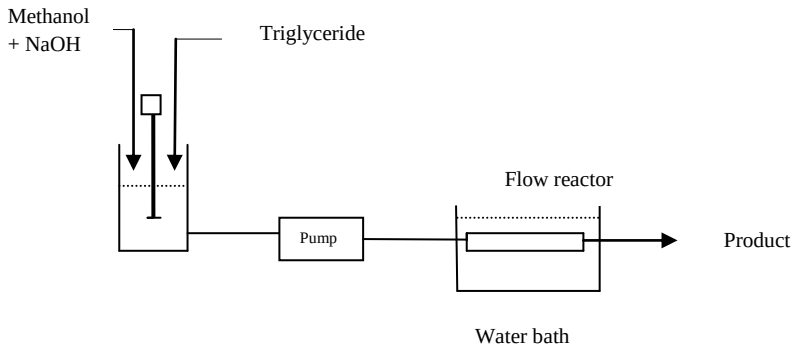


**Figure 6.1:a Schematic diagram of experimental setup (conventional heating)**

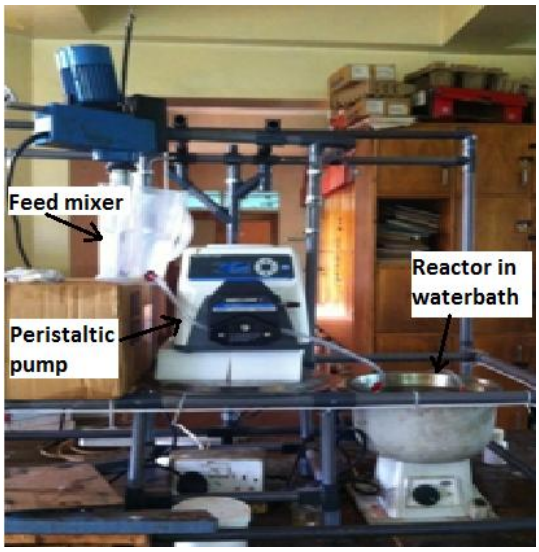


**Fig 6.1b: Experimental setup (conventional heating)**

### 6.2.2.2 Microwave Irradiation

For studies under microwave irradiation, a 1.7m long, 0.005m ID, polytetrafluoroethylene (Teflon®) tubing was used for the reactor. Tube was coiled in a spiral shape and held at the bottom of microwave oven by fixing it to a plywood board by use of copper wire. Spiral shape ensured a plug flow in the laminar region. Feed entrance and exit was though holes at the top and bottom of the oven. A polyethylene tubing of 0.012 m diameter and 0.65m length was coiled and installed inside the oven chamber to act as radiation sink. Water was circulated through it to absorb surplus radiation. Oven would switch-off sensing excess radiation if water was not circulated continuously. Methanol and catalyst were premixed, and later mixed with oil and sent to the reactor through a peristaltic pump in the manner

already described above in Section 6.2.2.1. Fig 6.2a and 6.2b show the experimental setup for microwave irradiation.

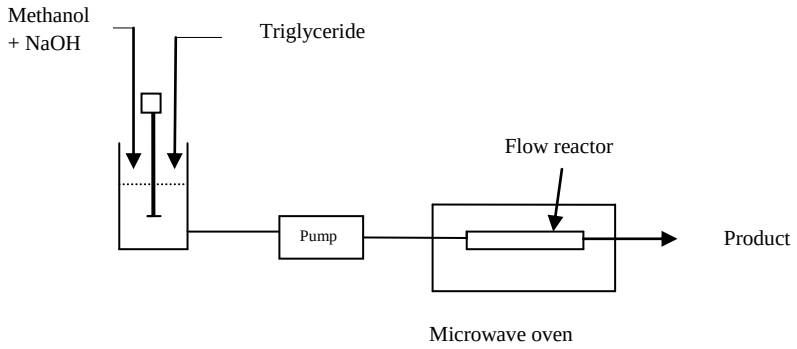


**Figure 6.2a: Schematic diagram of experimental setup (microwave irradiation)**

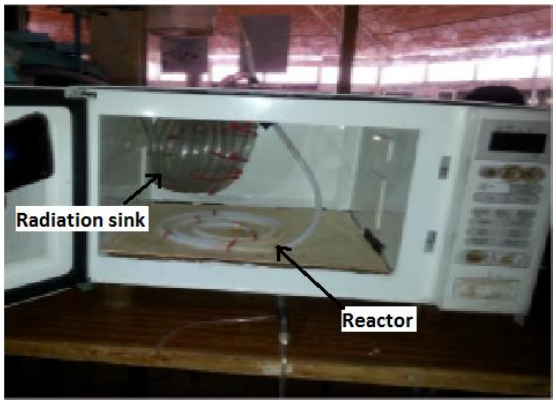


**Fig 6.2b: Tubular reactor and radiation sink in the microwave oven**

### 6.2.3 Experimental Procedure

#### 6.2.3.1 Conventional Heating

Weighed amount of catalyst was added to measured amount of methanol and the mixture stirred using mechanical stirrer for one hour at room temperature. In case of homogeneous catalyst, NaOH goes into solution; and for the case of CaO, a slurry was formed. This mixture was added to croton *megalocarpus* oil in a cylindrical container and stirred vigorously by a mechanical stirrer. In 15 min of stirring, oil and methanol blend into a single phase. Once it was observed that the two phases have coalesced, it was sent to the reactor in water bath at 60$^{o}$C (333K) through a peristaltic pump. Reaction variables chosen were: residence time, catalyst concentration, and methanol to triglyceride ratio. Residence time was varied as 3min ( equivalent to volumetric flow rate of 11.1 cm$^{3}$ min$^{-1}$), 6 min

(equivalent to volumetric flow rate of 5.6 $cm^3$ $min^{-1}$), and 9 min (equivalent to volumetric flow rate of 3.7 $cm^3$ $min^{-1}$); catalyst concentration was varied as 0.5, 1.0 and 1.5 mass% of triglyceride; and methanol to oil molar ratio was varied as 6:1, 9:1, 12:1. Effect of one variable was studied at a time, keeping other variables at centre point. Collected samples for homogeneous catalyst were treated as mentioned in Section 4.2.3.1 (Chapter 4), and samples for heterogeneous catalyst were treated as mentioned in Section 5.2.3.1 (Chapter 5).

Reynolds number was estimated to ascertain that the flow under the chosen residence times was laminar. Calculations for diameter d = 0. 005 m, length l = 1.7m, and lowest residence time = 3 min gave volumetric flow rate = 11.1 $cm^3$ $min^{-1}$, and velocity v = 0.0094 m $s^{-1}$. Using data for methanol, density $\rho$ = 792 kg $m^{-3}$, and viscosity at 60$^o$C (333K) = 0.0004 kg $m^{-1}$ $s^{-1}$ (Appendix 10, McCabe, Smith and Harriott, 1985), gave Reynolds number Re = 93. Similar calculation based on oil properties gave Re = 2.2. At higher residence times, velocities would be lower resulting into lower values of Re. Taking Re = 2100 as a threshold value for laminar flow in a pipe, we conclude that the flows under experimental conditions were fully laminar and plug flow.

#### 6.2.3.2 Microwave Irradiation

Method for microwave irradiation was similar to that of conventional heating except that there was no attempt to maintain a constant temperature, instead the microwave was used at full power.

### 6.2.4 FAME Analysis

FAME was analyzed as per the procedure described in Section 4.2.4 (Chapter 4).

## 6.3 Results and Discussions

Operating variables studied for NaOH and CaO catalysts, for conventional heating and microwave irradiation, were (i) Methanol to triglyceride molar ratio, (ii) Catalyst concentration, and (iii) Residence time.

### 6.3.1 Effect of Methanol to triglyceride molar ratio

For the study using NaOH catalyst with conventional heating, methanol to oil molar ratio was varied as 6:1, 9:1, 12:1; feed residence time was kept constant at 6 min, catalyst concentration was 1mass% of NaOH, and water bath temperature was 60$^o$C (333K).

Highest FAME yield of 13.1% was obtained at 6:1 ratio. Yield decreased with the increase of methanol ratio, but the change was small. Yield at 12:1 ratio was 11.0%, a drop of only 2% from the highest value. When microwave irradiation was used, the oven was operated at full power. As in case of conventional heating, methanol to oil molar ratio was varied as 6:1, 9:1, 12:1; at a residence time of 6 min and 1 mass% NaOH. Yield at 6:1 ratio was 92.0%. Highest FAME yield of 96.2% was obtained at 9:1 methanol to oil ratio, and it decreased slightly when the ratio was raised to 12:1.

When CaO was used as a catalyst with conventional heating, residence time was kept constant at 6 min, CaO concentration was 1 mass% and water bath was at $60^{o}$C (333K), and methanol to oil molar ratio was varied as 6:1, 9:1, 12:1. Yields were in general low, with not much variation as the methanol ratio was increased from 6 to 12. Lowest FAME yield of 3.2% was obtained at 6:1 molar ratio while the highest yield of 4.9% was at 9:1 molar ratio. For a similar study using CaO catalyst and microwave irradiation, transesterification was carried out at a residence time of 6 min, catalyst CaO of 1 mass%, and microwave at full power. Methanol to oil ratio was varied as 6:1, 9:1 and 12:1. FAME yield increased from 16.3 to 19.5% when the methanol ratio was increased from 6 to 9. The yield dropped slightly to 18.3% when the methanol ratio was increased further to 12:1. Yield increases with increase in methanol ratio as it helps in driving the transesterification reaction in forward direction. However, high methanol also has disadvantages. At very high methanol ratio, as already mentioned under batch studies, the yield decreases as glycerol dissolves in excessive methanol and subsequently inhibits the forward reaction (Viriya-empikul *et al*., 2010). Other explanation for reducing yield is that catalyst concentration decreases with excess methanol (Liu *et al*., 2008; Bambase *et al*., 2007). Excess methanol affects the interphase area between alcohol and oil due to their immiscibility leading to a drop in yield (Babak *et al*., 2013).

Fig 6.3 gives the effect of methanol to oil ratio on yield for NaOH and CaO catalysts under conventional heating and microwave irradiation. Dotted lines are for microwave irradiation, and continuous line represents conventional heating.

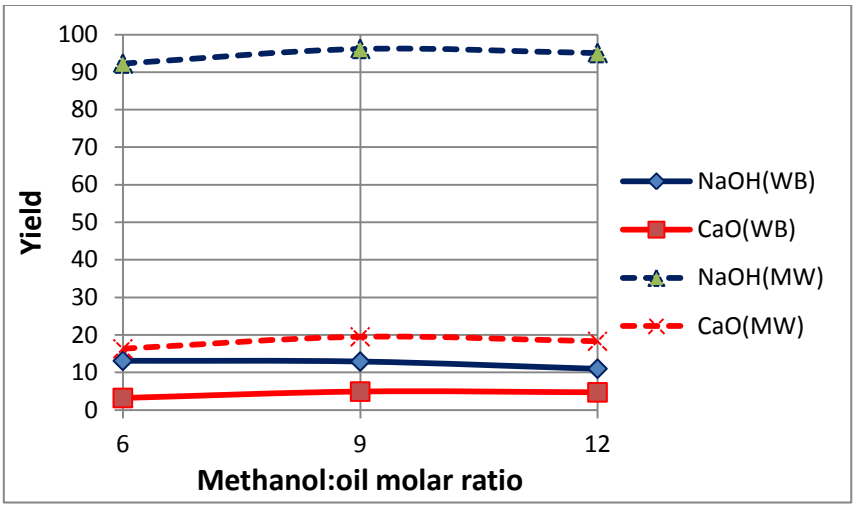


**Figure 6.3: Effect of Methanol:oil molar ratio on Yield for continuous transesterification**

### 6.3.2 Effect of Catalyst Concentration

Effect of concentration of NaOH and CaO catalysts on FAME yield was studied employing conventional water bath heating and microwave irradiation. During the study reactants residence time was 6 min, methanol to oil ratio was 9:1; and catalyst concentration varied as 0.5, 1.0, 1.5 mass% of oil. For conventional heating water bath was at 60$^{o}$C (333K), and for microwave irradiation the oven was at full power.

For NaOH catalyst with water bath, FAME yields at 0.5 and 1.0 mass% NaOH were almost similar being 12.9 and 12.3% respectively. As NaOH concentration was increased to 1.5%, yield slightly decreased to 10.3% of FAME.

For NaOH catalyst with microwave irradiation, yields were almost constant at around 96-97% as the NaOH concentration was raised from 0.5 to 1%. At higher concentration of 1.5% of NaOH, a slight drop in yield (93.1%) was noticed. The drop in yield at high NaOH concentrations has been attributed to soap formation.

When CaO and conventional heating was used, FAME yield increased with increase in catalyst concentration. The lowest yield was 3.7% of FAME at 0.5% of CaO and the highest being 5.2% of FAME at 1.5% of CaO.

When CaO catalyst and microwave irradiation was used, yield increased as CaO concentration was increased from 0.5 to 1%, from 12.9 to 19.5% of FAME. When the CaO concentration was further increased to 1.5%, the increase in yield was very small (0.6%) or rather negligible.

Fig 6.4 gives the effect of variation of NaOH and CaO catalysts on FAME yield for conventional heating and microwave irradiation.

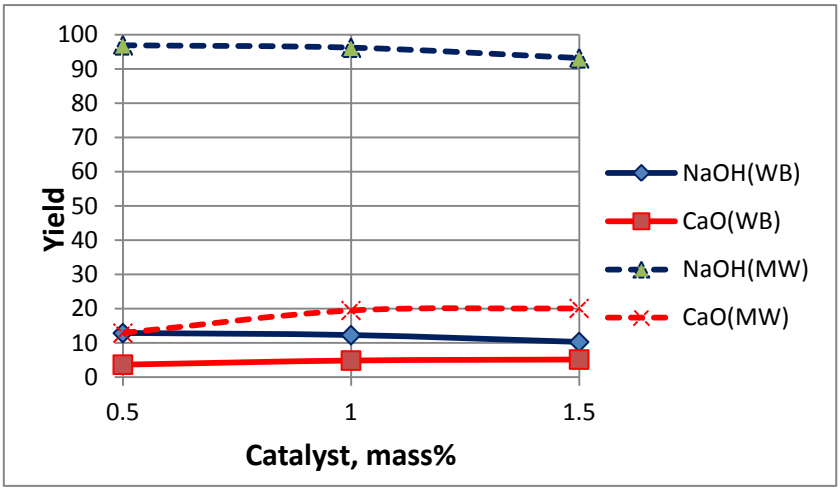


**Figure 6.4: Effect of Catalyst concentration on Yield for continuous transesterification**

### 6.3.3 Effect of Residence Time

Effect of reactor residence time was studied for NaOH and CaO catalysts, for conventional heating and microwave irradiation. During the study methanol to oil ratio was 9:1 and catalyst at 1 mass%, while residence time was varied as 3, 6 and 9 min. For conventional heating water bath was at 60$^{o}$C (333K), and for microwave irradiation the oven operated at full power.

When NaOH was used under conventional heating, highest FAME yield of 42.0% was obtained at 9 min, and the lowest yield of 7.1% was obtained at 3 min of residence time.

For NaOH under microwave irradiation, FAME yield increased as the residence time was increased from 3 to 6 min, from 94.2 to 96.2%. No substantive increase in yield was obtained when the time was further increased to 9 min, and yield was 96.5%.

When CaO was used under conventional heating, FAME yield at 3 min of time was just 1.2%, which increased to 4.9 and 7.9% for residence times of 6 and 9 min respectively.

For CaO under microwave irradiation, FAME yield increased from 14.3 to 19.5% as the time was increased from 3 to 6 min. When the residence time was increased further to 9 min no substantive increase was observed, and the yield was 19.9%.

Fig 6.5 gives the effect of Residence time on FAME yield for NaOH and CaO catalysts for conventional heating and microwave irradiation.

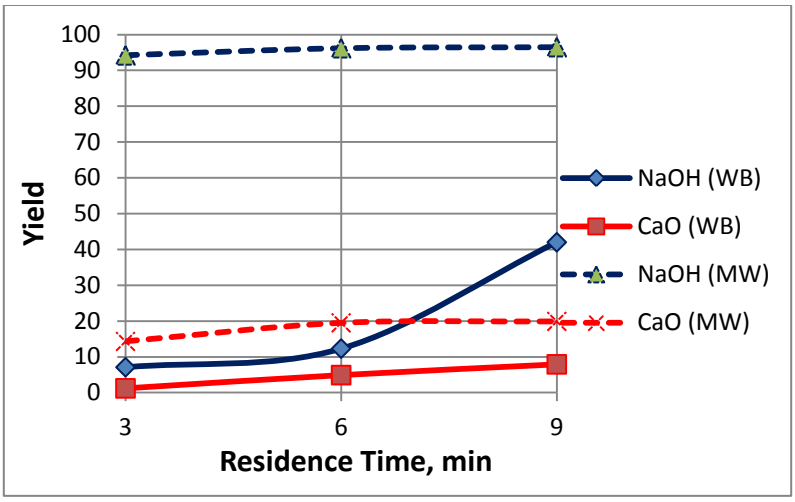


**Figure 6.5: Effect of Residence Time on Yield for continuous transesterification**

## 6.4 Summary

Transesterification of croton *megalocarpus* oil was successfully carried out in a continuous plug flow reactor. For studies using homogenous NaOH catalyst, microwave irradiation gave FAME yield exceeding 90% under all the operating conditions. Yields were low for NaOH catalyst using conventional water bath heating, ranging from 7 to 42% of FAME. High yields were obtained at 9 min of residence time, 0.5% of NaOH and for 6:1 methanol to oil ratio.

Yields were in general lower when heterogeneous CaO catalyst was used in the studies. In this case too, yields for microwave irradiation were higher as compared to conventional water bath heating. For microwave irradiation, yields ranged from 14 -20% of FAME; and for conventional heating from 1 – 8% of FAME.

# 7 FAME CHARACTERIZATION AND ENERGY NEEDS IN TRANSESTERIFICATION

## 7.1 Introduction

For biodiesel to be used as a fuel substitute for petrodiesel, the fuel must meet certain quality specifications. In the United States, biodiesel must meet the American Society for Testing and Materials (ASTM) requirements for biodiesel fuel in its D 6751 standard. The standard in Europe is defined by EN14214. A fuel not meeting the quality specifications may have adverse effect on the engine and the environment. Croton *megalocarpus* oil FAME was subjected to some tests to ascertain that it meets the requirements as a fuel. Rudimentary estimates for energy needed to produce FAME by conventional and microwave irradiation in laboratory conditions were made to compare the relative advantages of the two heating methods.

## 7.2 Materials and Methods

FAME density, viscosity, refractive index, acid value, sulphur content were obtained as given in Chapter 3. Water-and-sediment percentage was obtained by centrifuging (Centrifuge Hettich D-7200) 100 ml of FAME at high velocity for 10 min. Volume of water and sediment settled at the bottom of centrifuge tube was measured and reported as percentage of FAME sample. Iodine value was calculated based on GC analysis for fatty acid methyl esters (ISO/CD 3961, www.standardsproposals.bsigroup.com, accessed 29$^{th}$ April 2015). FAME composition was obtained by GC, as mentioned in Chapter 4. Calorific value was obtained by Bomb calorimeter (Gallenkamp Autobomb). Flash point was obtained by Cleveland Open cup apparatus. Distillation profile was obtained using standard procedures.

Calculations for energy requirements for conventional and microwave irradiation were made for yield data in Section 4.3.1.1.2 and Section 4.3.2.1.1 of Chapter 4. Wattage of water bath (Stuart RE 300B) was 1000 W, electric stirrer (Stuart SS10) and magnetic stirrer (Hanna HI80) were of 50W. Microwave oven (Shivaki, SMW-103) had an output rating of 1300W. Magnetron efficiency was take to be 60% (Barnard *et al*., 2007).

## 7.3 Results and Discussions

### 7.3.1 FAME Characterization

This section gives the physical appearance, some characteristic properties, composition, and distillation profile of Croton oil FAME.

**(i) Appearance:** FAME was clear liquid of light yellow colour, slightly lighter in shade compared to Croton oil. Fig 7.1a and 7.1b gives pictures of Croton oil and the FAME sample.


**Fig 7.1a: Croton oil**


**Fig 7.1b: Croton oil FAME**

**(ii) Properties**: Table 7.1 gives some of the characteristic properties for FAME sample.

**Table 7.1 Properties of Croton *megalocarpus* oil FAME**

| Property | Value | Standards: ASTM D6751 |
|---|---|---|
| Density at 20$^{o}$C (293K), kg m$^{-3}$ | 898.9 | not specified |
| Kinematic viscosity at 40$^{o}$C, mm$^{2}$ s$^{-1}$<br>Absolute viscosity at 40$^{o}$C, Pa.s | 2.66<br>2.397x10$^{-3}$ | 1.9 – 6.0 |
| Refractive index at 20$^{o}$C (293K) | 1.4673 | not specified |
| Acid value, mg KOH/g | 0.23 | 0.50 max |
| Water & Sediment | nil | 0.050 vol% max |
| Sulphur, mass% | 0.0012 | S 15 Grade 0.0015% max,<br>S 500 Grade 0.05% max |
| Iodine value | 143.6 | not specified |
| Flash point | 183$^{o}$ C | 130$^{o}$ C min |
| Distillation temperature (atmospheric equivalent) at 90% recovery by volume, $^{o}$C (from Table 13.2) | 341.6 | 360$^{o}$ C max |
| Calorific value, MJ kg$^{-1}$ | 41.3 | not specified |

**(iii) Composition**: GC analysis of FLAME for fatty acid methyl esters was carried out as given in Section 4.2.4 of Chapter 4. FAME was found to mostly consist of methyl esters of Myristic acid (Methyl tetradecanoate, C14:0), Palmitic acid (Methyl hexadecanoate, C16:0), Stearic acid (Methyl octadecanoate, C18:0), Oleic acid (Methyl cis-9-octadecenoate, C18:1), Linoleic acid (Methyl cis-9,cis-12-octadecadienoate, C18:2), Linolenic acid (Methyl octadecatrienoate, C18:3). Present in trace amount (< 0.1%) were Caprylic acid (Methyl octanoate, C8:0), Caproic acid (Methyl decanoate, C10:0), Lauric acid (Methyl dodecanoate, C12:0). Table 3.11 (Chapter 3) gives the mass fractions of fatty acids.

**(iv) Distillation profile:** Distillation profile gives the temperatures corresponding to volume fractions of fuel distilled off at atmospheric pressure, and it is characteristic of a particular fuel. As given in Table 7.1, distillation temperature at 90 vol% recovery should not exceed 360$^{o}$C. Distillation profile of Croton oil FAME (Test method ASTM D86-09e1/IP 123) is given in Table 7.2.

**Table 7.2: Distillation profile**

| Distillation recovery (volume%) | Temperature, $^{o}$C |
|---|---|
| Initial boiling point | 136.5 |
| 10% Recovered | 329.2 |
| 20% Recovered | 331.2 |
| 30% Recovered | 333.2 |
| 40% Recovered | 334.2 |
| 50% Recovered | 335.2 |
| 60% Recovered | 336.2 |
| 70% Recovered | 338.2 |
| 80% Recovered | 340.6 |
| 90% Recovered | 341.6 |
| 95% Recovered | 242.6 |
| End point | 343.6 |
| Recovery at 365$^{o}$C | > 90% volume |

Figure 7.2 is a plot of FAME and petro-diesel distillation profile. Petro-diesel had gradual rise in temperature whereas FAME profile was almost horizontal. This is due to very close

boiling range of fatty acid methyl esters. FAME mainly consisted of C18:1, C18:2 and C18:3, whose boiling temperatures (at 10 mm Hg) are 201, 200 and 202$^{o}$C respectively (Cermak *et al*., 2012).

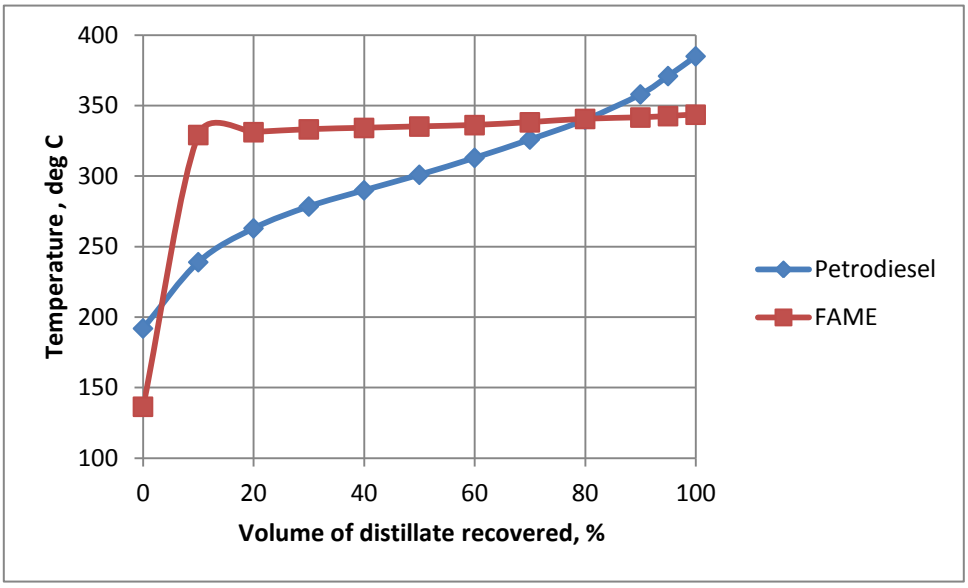


**Fig 7.2: Distillation profiles of FAME and petro-diesel**

### 7.3.2 Energy Needs in Transesterification

Molar masses of triglyceride and corresponding FAME are almost the same (For example, molar mass of Tristearin, a triglyceride of stearic acid = 891.5 and molar mass of Methyl ester of tristearin = 895.5). It shows that 1 kg of triglyceride would produce approximately 1 kg of FAME (at 100% yield).

For conventional heating 30 ml of croton oil gave a 97% FAME yield, at 6:1 methanol to oil molar ratio, 1% NaOH catalyst, in a time of 60 min. Table 7.3 gives the energy requirement for this reaction for conventional heating.

**Table 7.3: Conventional heating energy requirement**

| | |
|---|---|
| Water bath energy consumption (Power x Time) | 1000x1 = 1000 Wh |
| Stirrer energy consumption (Power x Time) | 50x1 = 50 Wh |
| Total energy consumption | 1050 Wh |
| Total energy consumption per litre of FAME | 1050/(30/1000) = 35 kWh |
| **Total energy consumption per kg of FAME** | 35/(0.8989) = **38.9 kWh** |

For microwave irradiation, 25 ml of croton oil gave a FAME yield of 96.5% at 9:1 methanol to oil ratio, 1% NaOH catalyst, in 1 min. For a microwave output of 1700 W, the power drawn = (Power output)/(magnetron efficiency) = 1700/0.6 = 2166.7 W. Table 7.4 gives the energy requirement for microwave irradiation.

**Table 7.4: Microwave irradiation energy requirement**

| | |
|---|---|
| Microwave energy consumption (Power x Time) | 2166.7x(1/60) = 36.1 Wh |
| Stirrer energy consumption (Power x Time) | 50x(1/60) = 0.8 Wh |
| Total energy consumption | 36.9 Wh |
| Total energy consumption per litre of FAME | 36.9/(25/1000) = 1.48 kWh |
| **Total energy consumption per kg of FAME** | 1.48/(0.8989) = **1.64 kWh** |

From Tables 7.3 and 7.4, Energy required by WB: Energy required by MW = 38.9: 1.64 = 23.7:1. The rudimentary calculations show that water bath required 24 times more energy as compared to microwave irradiation. This observation is in agreement with a similar analysis for *Camelina Sativa* oil FAME where a similar energy ratio for water bath: microwave was 23.4:1 (Patil *et al*., 2010b).

## 7.4 Summary

Characteristic properties as given in Table 7.1 conform to the requirements for Croton *megalocarpus* oil fatty acid methyl ester to be used as biodiesel fuel as per international standards. The energy required by conventional heating was found to be about 24 times larger when compared to microwave irradiation. This shows that microwave irradiation is a far more energy efficient mode of heat transfer.

# 8 CONCLUSIONS AND RECOMMENDATIONS

## 8.1 Introduction

The objective of the research was to study transesterification of *Croton megalocarpus* oil using homogenous NaOH and heterogeneous alkaline earth oxide catalysts. It was to include characterization of triglyceride and the solid catalysts, effect of operating variables on FAME yield leading to process optimization, and the reaction kinetics. Microwave irradiation was to be compared with conventional heating as an alternate mode for heat transfer. Transesterification in a continuous flow reactor was to be compared with batch process. The presented work covers all the aspects of research objectives as outlined in Section 1.3.1 (Chapter 1).

## 8.2 Characterization of alkaline earth oxides

Alkaline earth catalysts had varying surface area and porosity which were found to be in the following order: BeO > Nono MgO > Nano CaO > MgO > CaO > CaO RO > BaO > SrO. Special attention was given to calcium oxide catalysts due to their easy availability and non toxic nature. XRD showed that all the catalyst samples were of reasonable purity with exception of calcium oxide, which showed substantive presence of carbonate and hydroxide. Calcination at 800 - 900 $^{o}$C (1073– 1173 K) for 3 h was needed to get back to a pure calcium oxide form. Basicity as obtained by Hammett method puts the catalyst in almost reverse order as compared to their surface area and porosity. Catalysts arranged according to basicity were: BaO > SrO > Nano CaO > CaO RO > CaO > Nano MgO > MgO > BeO.

## 8.3 Transesterification studies

Studies using homogenous NaOH and the eight heterogeneous catalysts for transesterification reaction formed the major work. Selected reaction parameters were varied and FAME yields were obtained for both conventional heating and microwave irradiation. Catalysts can be classified as the ones giving high yield (> 60%), others giving moderate yield (20 – 60%), and lastly the ones giving poor yield (< 20%). For both conventional and microwave irradiation NaOH, BaO, SrO and Nano CaO gave high yields, CaO RO and CaO gave moderate yields, and BeO gave poor yield. Nano MgO and MgO gave moderate yields for conventional water bath heating and performed poorly for

microwave irradiation. Fig 8.1 is a bar chart giving the FAME yield for various catalysts for conventional heating and microwave irradiation.

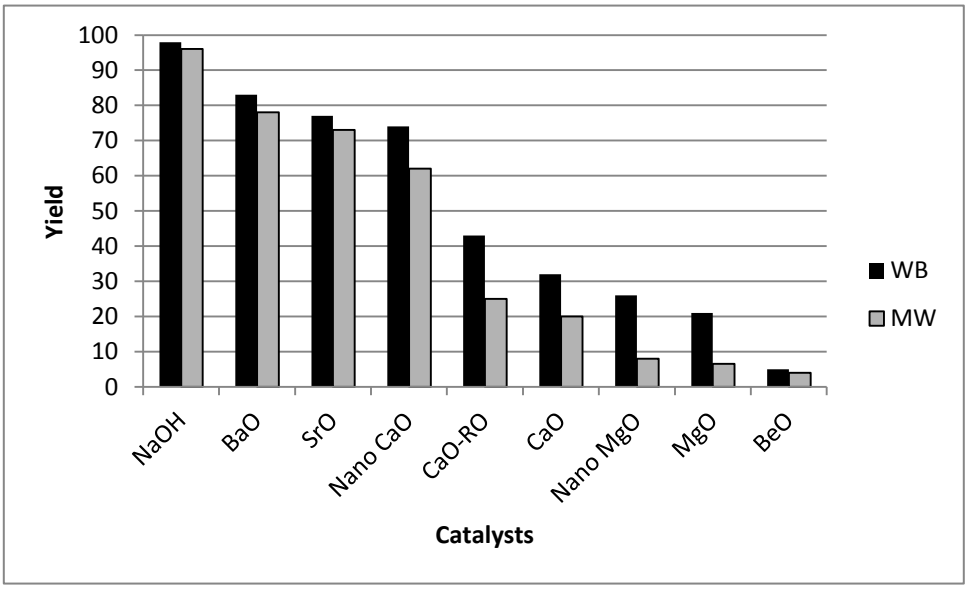


**Figure 8.1: FAME yield for catalysts for conventional heating (WB) and microwave irradiation (MW)**

Conditions for high FAME yield for conventional heating ranged: methanol to oil ratio 6 – 12:1, catalyst 1 – 2 mass%, reaction temperature close to methanol boiling point, and reaction time 1 – 2.5 h. High yield using microwave irradiation corresponded to: methanol to oil ratio 9 – 12:1, catalyst 0.5 – 2%, and reaction time of 1 – 5 min, at full microwave power. BeO was used for transesterification reaction for the first time, and the results were not very encouraging. Magnesium oxide performed poorly under microwave irradiation. For other catalysts yields under microwave irradiation were in general lower than those under conventional heating, but were comparable. Microwave irradiation also needed a slightly higher methanol:oil ratio and catalyst concentration as compared to conventional heating. Most remarkable difference was in the reaction time. For maximum yield, conventional heating needed time in hours whereas microwave irradiation required 1 – 5 min. This feature makes microwave irradiation a distinctly superior heat transfer mode. Variation in catalyst activity followed the trend in their basicity, and specific surface area had no effect. Beryllium oxide, for example, had the highest area and lowest basicity- and was the least active catalyst. When CaO was hydrated and calcined to obtain CaO RO, surface area of the new catalyst reduced while basicity increased, and a higher FAME yield

was obtained. For a given catalyst sample, a higher surface area resulted into a higher activity as Nano CaO was more active than CaO, and Nano MgO was more active than MgO. Mass transfer resistances were eliminated in transesterification studies and surface reaction prevailed.

The alkaline earth metal oxides can be arranged according to their activities as: BaO > SrO > CaO > MgO > BeO. The observed activities are also justified in terms of physical properties such as ionization energies, melting and boiling points of alkaline earth metals. Ionization energies, melting and boiling points follow the same order, being lowest for Ba and highest for Be.

## 8.4 Reaction Kinetics

Reaction kinetics data are needed for reactor design for process scale up. The overall reaction order was found to vary from 'first' to 'third' order. Table 8.1 summarizes the reaction order and rate constants for conventional water bath heating (WB) and microwave irradiation (MW) for all the catalysts.

**Table 8.1: Reaction order and rate constant**

| SN | Catalyst | Heating mode | Order w.r.t triglyceride | Order w.r.t Methanol | Overall order | Rate constant at 70$^{o}$ C | Units |
|---|---|---|---|---|---|---|---|
| **1** | NaOH | WB | 2 | 0 | 2 | 4.75E-01 | cm^3 mol^-1 min^-1 |
| | | MW | 1 | 0 | 1 | 2.45E+00 | min^-1 |
| **2** | BaO | WB | 2 | 1 | 3 | 1.27E-02 | cm^6 mol^-2 min^-1 |
| | | MW | 2 | 1 | 3 | 5.69E-01 | cm^6 mol^-2 min^-1 |
| **3** | SrO | WB | 2 | 1 | 3 | 6.19E-03 | cm^6 mol^-2 min^-1 |
| | | MW | 2 | 1 | 3 | 4.88E-01 | cm^6 mol^-2 min^-1 |
| **4** | Nano CaO | WB | 2 | 1 | 3 | 5.65E-03 | cm^6 mol^-2 min^-1 |
| | | MW | 2 | 1 | 3 | 2.68E-01 | cm^6 mol^-2 min^-1 |
| **5** | CaO-RO | WB | 2 | 1 | 3 | 1.59E-03 | cm^6 mol^-2 min^-1 |
| | | MW | 2 | 1 | 3 | 3.93E-02 | cm^6 mol^-2 min^-1 |
| **6** | CaO | WB | 2 | 1 | 3 | 9.80E-04 | cm^6 mol^-2 min^-1 |
| | | MW | 2 | 1 | 3 | 3.35E-02 | cm^6 mol^-2 min^-1 |
| **7** | Nano MgO | WB | 2 | 1 | 3 | 7.20E-04 | cm^6 mol^-2 min^-1 |
| | | MW | 0 | 1 | 1 | 1.62E-03 | min^-1 |
| **8** | MgO | WB | 2 | 1 | 3 | 5.41E-04 | cm^6 mol^-2 min^-1 |
| | | MW | 0 | 1 | 1 | 1.53E-03 | min^-1 |
| **9** | BeO | WB | 2 | 1 | 3 | 8.70E-05 | L^2 mol^-2 min^-1 |

| | | | | | | |
|---|---|---|---|---|---|---|
| | MW | 0 | 1 | 1 | 1.52E-03 | min^-1 |

Reaction rate constants for microwave irradiation were higher than those for conventional heating due to faster reaction rates under microwave irradiation. Reaction was of first order for microwave irradiation for NaOH, Nano MgO, MgO and BeO; and of second order for NaOH under conventional heating. For the remaining heterogeneous catalysts, overall reaction was of 3$^{rd}$ order, 2$^{nd}$ order with respect to triglyceride and 1$^{st}$ order with respect to methanol.

Arrhenius equation was used to obtain Activation energy and pre-exponential factor for all the reactions. Table 8.2 gives the Activation energy (*E*) and pre-exponential factor (*A*) for reactions in Table 14.1.

**Table 8.2:Activation energy, E and pre-exponential factor, A**

| SN | Catalyst | Heating mode | *E* (kJ/mol) | *A* *(units of k)* |
|---|---|---|---|---|
| **1** | NaOH | WB | 71.3 | 3.73E+10 |
| | | MW | 51.0 | 2.68E+06 |
| **2** | BaO | WB | 35.4 | 3.07E+03 |
| | | MW | 36.8 | 2.38E+05 |
| **3** | SrO | WB | 26.6 | 7.37E+01 |
| | | MW | 46.2 | 5.67E+06 |
| **4** | Nano CaO | WB | 33.7 | 8.80E+02 |
| | | MW | 36.6 | 1.79E+03 |
| **5** | CaO-RO | WB | 27.4 | 2.50E+01 |
| | | MW | 20.5 | 4.79E+01 |
| **6** | CaO | WB | 28.7 | 2.53E+01 |
| | | MW | 70.3 | 2.44E+07 |
| **7** | Nano MgO | WB | 24.5 | 4.18E+00 |
| | | MW | 35.6 | 7.46E+00 |
| **8** | MgO | WB | 34.3 | 1.03E+02 |
| | | MW | 34.7 | 2.99E+02 |
| **9** | BeO | WB | 32.1 | 7.17E+00 |
| | | MW | 42.3 | 7.86E+01 |

A catalyst lowers the activation energy of a reaction, but the magnitude of activation energy for a heterogeneously catalysed reaction is not automatically accepted to be a quantitative measure of the catalytic activity. The reason for not adopting this criterion is the widespread occurrence of compensation effects (Thomas and Thomas, 1967). For

heterogeneous catalysis compensation effect may occur when the overall reaction is a combination of a number of reactions which show the same mechanism and take place on different groups of active centres, each group showing different activation energy and pre-exponential factor (Marbán and Rio, 2013). Transesterification reaction consisting of three consecutive reactions falls under this category. Reaction velocity constant in this case is a sum of several reaction steps, and activation energy is termed 'apparent activation energy' ($E^{app}$) and pre-exponential factor is termed 'apparent pre-exponential factor', ($A_{app}$). In some reaction systems, it has been observed that the apparent activation energy varies under different reaction conditions. It is also found that the variation in apparent activation energy is accompanied by a change in $A_{app}$, i.e., a large apparent activation energy is accompanied by a large apparent pre-exponential factor and vice versa. In some cases, the changes in apparent pre-exponential factor and apparent activation energy display a linear dependency according to the Cremer-Constable relation (Andreasen *et al*., 2005):

$$\ln A_{app} = a E^{app} + b \qquad \ldots 8.1$$

Fig 8.2 is a Cremer-Constable scatter plot based on data in Table 8.2. The data broadly follow the relation and a compensation effect is apparent.

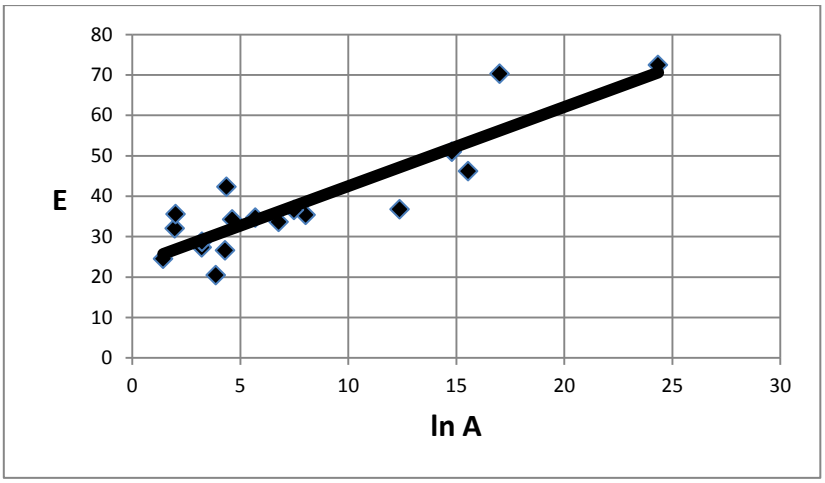


**Figure 8.2: Cremer Constable plot of $E^{app}$ and $A_{app}$ (Eqn 14.1)**

## 8.5 Process Optimization

A Box-Wilson Central Composite Design (CCD) was used to design experiments for process optimization. Experimental data were analyzed using design software and second order quadratic polynomials were obtained for FAME yield as a function of three reaction variables. Polynomial correlations met the statistical requirements for a satisfactory fit to

experimental data. Response surface and contour plots (RSM plots) gave the region of increasing yield and the reaction conditions for optimum yield. RSM plots were in agreement with experimental observations.

## 8.6 Continuous transesterification

Continuous transesterification was carried out in a plug flow reactor under conventional heating and microwave irradiation. Table 8.3 compares FAME yields for continuous transesterification (at residence time of 9 min), and batch processes (after 9 min), at 9:1 methanol to oil ratio and 1% catalyst (data for batch/conventional heating are approximate values estimated from Yield vs time plots). For NaOH and CaO catalysts, the yields were comparable with the corresponding studies with batch reactor for similar reaction times. Continuous transesterification is therefore a viable option to produce FAME from Croton *megalocarpus* oil.

**Table 8.3: Comparison of batch and continuous FAME yields**

| Catalyst | Conventional Heating | | Microwave irradiation | |
|---|---|---|---|---|
| | Batch | Continuous | Batch | Continuous |
| **NaOH** | 50 | 42 | 90* | 96.5 |
| **CaO** | 6 | 8 | 19** | 19.9 |

* for 3 min, ** for 5 min

## 8.7 Croton *megalocarpus* FAME as biofuel

Properties of *Croton megalocarpus* FAME as biofuel are characterized in Chapter 7. FAME satisfactorily meets the .requirements for a biodiesel.

## 8.8 Heat transfer mode

Microwave irradiation was found to be a more energy efficient mode of heat transfer for transesterification. Energy requirements for microwave irradiation were reduced by a factor of (1/24) when compared to conventional heating for a similar FAME yield, as shown in Chapter 7.

## 8.9 Recommendations for future work

Present work has demonstrated the relative activities of alkaline earth oxides as catalysts for Croton *megalocarpus* oil transesterification to produce biodiesel. Microwave irradiation has also been shown to be a better mode of heat transfer. However, a further study of the following is desired to add value to the work:

1. BaO and SrO have shown high activity but are toxic and expensive. Calcium oxide is the most promising catalyst due to its low cost, easy availability and ease in handling. Disadvantage is its poor activity. Nano CaO has shown good activity but is expensive. Activity of CaO may be increased by (i) calcination in inert atmosphere, (ii) reducing its particle size, (iii) hydrating and calcining as was done in the present work, (iv) by treating CaO with strong alkali before calcination (this should increase the basicity), (v) by depositing CaO over high surface supports like zeolite or alumina,(vi) metal oxides prepared with calcium show strong basic character, and have been tested for transesterification reaction. The calcium containing catalysts, $CaTiO_3$, $CaMnO_3$, $Ca_2Fe_2O_5$, $CaZrO_3$, and $CaO–CeO_2$, showed high activities and approximately 90% yields of FAME from rapeseed oil (Kawashima *et al*., 2008), and should be tested for croton *megalocarpus* oil.
2. Leaching of heterogeneous catalysts into biodiesel is related to its reusability and biodiesel quality. In theory, the catalysts can be recovered and reused indefinitely. However, the catalysts leach and also lose activity when recycled. A study is needed to study leaching and recyclability of CaO catalysts for Croton *megalocarpus* FAME.
3. Organic co-solvents have been used to reduce mass transfer resistances in the three phase transesterification reaction system with varying success. It would be interesting to see if a co-solvent can give a higher yield in the present study.
4. Studies with microwave irradiation have been limited to labs. An attempt to carry out such a process on pilot plant scale would expose the scale-up challenges.
5. Ultrasound irradiation coupled with microwave irradiation has been used to get very high FAME yields. It is a new area to be explored for Croton *megalocarpus* FAME (Martinez-Guerra and Gude, 2014; Hsiao *et al*. 2010 ).

## REFERENCES

Abreu, F.R., Alves, M.B., Macedo, C.C.S., Zara, L.F., Suarez, P.A.Z. 2005. New multi-phase catalytic system based on tin compounds active for vegetable oil transesterification reaction. *J. Mol. Cat. A: Chemical*, **227**, 263-267.

Abreu, F.R., Lima, D.G., Hamu, E.H., Wolf, G., Suarez, P.A.Z. 2004. Utilization of metal complex as catalysts in the transesterification of Brazilian vegetable oils with different alcohols. *J. Mol. Cat. A: Chem.*, **209**(1-2), 29-33.

Adams, C., Peters, J. F., Rand, M. C., Schroer, B. J., Ziemke, M.C. 1983. Investigation of soybean oil as a diesel fuel extender: Endurance tests. *JAOCS*, **60**, 1574-1579.

Aderemi. B.O., Hameed, B.H. 2009. Alum as a heterogeneous catalyst for the transesterification of palm oil. *Applied Catalysis A:General*, **370**, 54-58.

Adholeya, A., Dadhich, P.K. Production and technology of biodiesel, TERI Press, New Delhi, 2008.

Alberty, R.A. 1991. Physical Chemistry, 6th Edition, Wiley Eastern Ltd, New Delhi.

Albuquerque, M.C.G., Jiménez-Urbistondo, I., Santamaria-González, J., Mérida-Robles, J.M., Moreno-Tost, R., Rodriguez-Castellón, E., Jiménez-López, A., Azevedo, D.C.S., Cavalcante Jr., C.L., Maireles-Torres, P. 2008. CaO supported on mesoporous silicas as basic catalysts for transesterification reactions. *Applied Catalysis A: General*, **334**, 35-43.

Aliyu, B., Agnew, B., Douglas, S. 2010. Croton *megalocarpus* (Musine) seeds as a potential source of bio-diesel. *Biomass and Bioenergy*, **34**, 1495-1499.

Andreasen, A., Vegge, T., Pedersen, A.S. 2005. Compensation Effect in the Hydrogenation/Dehydrogenation Kinetics of Metal Hydrides. *J. Phys. Chem. B*, ***109***, 3340-3344.

Anon. 1982. Filtered used frying fat powers diesel fleet. JAOCS, **59**, 780A-781A.

Antunes, W.M., Veloso, C.D.O., Assumpc, C., Henriques, O. 2008. Transesterification of soybean oil with methanol catalyzed by basic solids. *Catalysis Today*, **133-135**, 548-554.

Arai, S., Nakashima, K., Tanino, T., Ogino, C., Kondo, A., Fukuda, H. 2010. Production of biodiesel fuel from soybean oil catalyzed by fungus whole-cell biocatalysts in ionic liquids. *Enzyme and Microbial Technology*, **46**, 51-55.

Arzamendi, G., Arguinarena, E., Campo, I., Zabala, S., Gandia, L.M. 2008. Alkaline and alkaline-earth metal compounds as catalysts for the methanolysis of sunflower oil. *Catalysis Today*, **133-135**, 305-313.

Au, C.T., Dai, H. 2012. Catalytic generation of biodiesel from vegetable oils. *SciTopics*. Available: http://www.scitopics.com/Catalytic_generation_of_biodiesel_ from_vegetable _oils.html, access 17 March 17, 2012.

Babak, S., Iman, H., Abdullah, A.Z. 2013. Alkaline earth metal oxide catalysts for biodiesel production from palm oil: Elucidation of process behaviours and modelling using response surface methodology. *Iran J. Chem. Chem. Eng*., **32**(1), 113-126.

Bacovsky, D., Körbitz, W., Mittelbach, M., Wörgetter, M. 2007. Biodiesel Production: Technologies and European Providers. *IEK Task 39, Report T39-B6*.

Bajaj, A., Lohan, P., Jha, P.N., Mehrotra, R. 2010. Biodiesel production through lipase catalyzed transesterification: an overview. *Journal of Molecular Catalysis B: Enzymatic*, **62**, 9-14.

Balasubramanian, R. K. 2010. Heterogeneous catalysis of plant derived oils. *DPhil Thesis*, National University of Singapore, Singapore.

Bambase, M.E. Jr., Nakamura, N., Tanaka, J., Matsumura, M. 2007. Kinetics of hydroxide-catalyzed methanolysis of crude sunflower oil for the production of fuel-grade methyl esters. *Journal of Chemical Technology and Biotechnology*., **82**, 273-280,

Barnard, M.T., Leadbeater, N.E., Boucher, M.B., Laurel, M.S. 2007. Continuous-flow preparation of biodiesel using microwave heating. *Energy Fuels*, **21**(3), 1777-1781.

Bejoy, N. 2001. Hydrotalcite. *Resonance*, **6**(2), 57-61.

Benjapornkulaphong, S., Ngamcharussrivichai, C., Bunyakiat, K. 2009. $Al_2O_3$-supportedalkali and alkali earth metal oxides for transesterification of palm kernel oil and coconut oil. *Chem Eng J*, vol. **145**(3), 468-474.

Biodiesel. 2013. http://www.biodiesel.org/what-is-biodiesel/biodiesel-basics, access date 17 Aug 2013.

Boey, P.-L., Maniam, G.P., Hamid, S.A. 2009. Biodiesel production via transesterification of palm olein using waste mud crab (Scylla serrata) shell as a heterogeneous catalyst. *Bioresource Technology*, **100**, 6362-6368.

Boey, P.-L., Maniam, G.P., Hamid, S.A., Ali, D.M.H. 2011. Crab and cockle shells as catalysts for the preparation of methyl estrs from low FFA chicken fat. J. Am. Oil. Chem. Soc., doi:10.1007/s11746-010-1660-4.

Bond, G.C. 1993. Strategy of research on supported metal catalysts. Problems of structure-sensitive reactions in the gas phase. *Acc. Chem. Res.*, **26**(9), 490–495.

Bota, R.M., Houthoofd, K., Grobet, P.J., Jacobs, P.A. 2010. Superbase catalysts from thermally decomposed sodium azide supported on mesoporous γ-alumina. *Catalysis Today*, **149**, 281-287.

Boz, N., Kara, M. 2009. Solid base catalyzed transesterification of canola oil. *Chem. Eng. Commun*., **196**, 80-92.

Brito, A., Borges, M.E., Otero, N. 2007. Zeolite Y as a heterogeneous catalyst in biodiesel fuel production from used vegetable oil. *Energy Fuels*, **21**(6), 3280-3283.

Bromberg, L., Fasoli, E., Alvarez, M., Hatton, T.A., Barletta, G.L. 2010. Biguanide-, imine-, and guanidine- based networks as catalysts for transesterification of vegetable oil. *React. Funct. Polym*., **70**(7), 433–441.

BRUKER Application Note CA-270358, Determination of Total FAME and Linoleic Acid Methyl Esters in Biodiesel According to EN-14103. http://www.aquilantscientific.com/assets/aquilantscientific/Products/applications/880135/CA-270358-biodiesel-FAME_01%5B1%5D.pdf (3rd Jan 2014)

Cao,F., Chen, Y., Zhai, F., Li, J., Wang, J., Wang, X. 2008. Biodiesel production from high acid value waste frying oil catalyzed by superacid heteropolyacid. *Biotechnol. Bioeng*., **101**, 93-100.

Cermak, S.C., Evangelista, R.L., Kenar, J.A. 2012. Distillation of Natural Fatty Acids & their Chemical Derivatives, *Advances from Modelling to Applications* (Dr Sina Zereshki, Ed.), ISBN 978-953-51-0428-5 (www.intechopen.com, accessed 29 April 2015).

Chand, P., Chintareddy, V.R., Verkade, J.G., Grewell, D. 2010. Enhancing biodiesel production from soybean oil using ultrasonics. *Energy Fuels*, **24**(3), 2010-2015.

Chang, H.M., Chen, Y.C., Shieh, J.C. 2008. Mg-Al Hydrotalcite as a Solid Catalysts for Biodiesel production from Soybean Oil. Available: http://www.taiwan921.lib.ntu.edu.tw/mypdf/myismab2008-d.pdf, access 17 March 12.

Chen, X., Du, W., Liu, D. 2008. Response surface optimization of biocatalytic biodiesel production with acid oils. *Biochemical Engineering Journal*, **40**, 423-429.

Chung, K.H., Park, B.G. 2009. Esterification of oleic acid in soybean oil on zeolite catalysts with different acidity. *J. Ind. Eng. Chem*., **15**, 388-392.

D'Cruz, A., Kulkarni, M.G., Meher, L.C., Dalai, A.K. 2007. Synthesis of biodiesel from canola oil using heterogeneous base catalyst. *J. Am. Oil. Chem. Soc*., **84**, 937-943.

Dalai, A.K., Kulkarni, M.G., Meher, L.C. 2008. Biodiesel production from vegetable oils using heterogeneous catalysts and their application as lubricity additives. *EIA Climate Change Tech., 2006 IEEE*, 1-8.

Danuthai, T., Jongpatiwut, S., Rirksomboon, T., Osuwan, S., Resasco, D.E. 2009. Conversion of methylesters to hydrocarbons over an H-ZSM5 zeolite catalyst. *Appl. Catal. A-Gen.*, **361**, 99-105.

Darnoko, D., Cheryan, M. 2000. Kinetics of palm oil transesterification in a batch reactor. *JAOCS*, **77**(12), 1263-1267.

Demirbas, A. 2002. Biodiesel from vegetable oils via transesterification in supercritical ethanol. *Energy Conversion Management*, **43**, 2349-2356.

Demirbas, A. 2003. Biodiesel fuels from vegetable oils via catalytic and non-catalytic supercritical alcohol transesterifications and other methods: a survey. *Energy Conversion and Management*, **44**, 2093-2109.

Demirbas, A. 2006. Biodiesel production via non-catalytic SFC method and biodiesel fuel characteristics. *Energy Conv. & Management*, **47**(15-16), 2271-2282.

Demirbas, A. 2007. Biodiesel from sunflower oil in supercritical methanol with calcium oxide *Energy Conv. & Management*, **48** , 937–941.

Demirbas, A. 2008. Biofuels sources, biofuel policy, biofuel economy and global biofuel projections. *Energy Conversion and Management*, **49**, 2106–2116.

Demirbas, A. 2009. Progress and recent trends in biodiesel fuels. *Energy Conversion and Management*, **50**, 14-34.

Ding, Y., Sun, H., Duan, J., Chen, P., Lou, H., Zheng, X. 2011. Mesoporous Li/ZrO2 as a solid base catalyst for biodiesel production from transesterification of soybean oil with methanol. *Cat. Commun.*, **12**, 606–610.

Dizge, N., Keskinler, B. 2008. Enzymatic production of biodiesel from canola oil using immobilized lipase. *Biomass and Bioenergy*, **32**, 1274-1278.

Dossin, T.F., Reyniers, M.F., Berger, R.J., Martin,G.B. 2006b. Simulation of heterogeneously MgO- catalyzed transesterification of fine-chemical and biodiesel industrial production. *Appl. Cat. B: Envir*, **61**, 136-148.

Dossin, T.F., Reyniers, M.F., Martin, G.B. 2006a. Kinetics of heterogeously MgO-catalyzed transesterification. *Appl. Cat. B: Envir*, **61**, 35-45.

Dunn, R.O. 2001. Alternative jet fuels from vegetable-oils. *Trans ASAE*, **44**, 1151-1757.

Ebiura,T., Echizen,T., Eshikawa, A., Murai, K., Baba,T. 2005. Selective transesterification of triolein with methanol to methyl oleate and glycerol using alumina loaded with alkali metal salt as a solid-base catalyst. *Applied Catalysis*, **283**(1-2), 111-116.

Eevera, T., Rajendran, K., Saradha, S. 2009. Biodiesel production process optimization and characterization to assess the suitability of the product for varied environmental conditions. *Renewable Energy*, **34**, 762-765.

Endalew, A.E., Kiros, Y., Zanzi, R. 2011. Inorganic heterogeneous catalysis for biodiesel production from vegetable oils. *Biomass & Bioenergy*, **35**, 3787-3809.

Engineering Statistics Handbook, Ch5, http://www.itl.nist.gov/div898/handbook/pri/section1/pri1.htm [5/1/2006 10:30:17 AM]

Farzaneh, F., Raashtizadeh, E. 2010. Transesterification of soybean oil to biodiesel using modifies zeolites (Y and clinoptilolite) as a solid base catalyst," *2nd Iran International Zeolite Conf*. Available: www.civilica.com/EnPaper-ZEOLITE02-ZEOLITE02_004.html, access 17th March 2012.

Ferella, F., Mazziotti Di Ceslo, G., De Michelis, I., Stanisci, V., Veglio, F. 2010. Optimization of the transesterification reaction in biodiesel production. *Fuel*, **89**, 36-42.

Freedman, B., Butterfield, R.O., Pryde, E.H. 1986. Transesterification kinetics of soybean oil. *J. Am.Oil Chem. Soc*., **63**(10),1375-1380.

Freedman, B., Pryde, E.H., Mounts, T.L. 1984. Variables affecting yield of fatty esters from transesterified vegetable oils. *JAOCS*, **61**, 1638-1643.

Froment G. F., Bischoff K. 1990. Chemical Reactor Analysis and Design, John Wiley & Sons, NY.

Frondel, M., Peters, J. 2007. Biodiesel: A new Oildorado. *Energy Policy*, **35**, 1675-1684.

Furuta, S., Matsuhashi, H., Arata, K. 2004. Biodiesel fuel production with solid superacid catalysis in fixed bed reactor under atmospheric pressure. *Catal. Commun*., **5**, 721-723.

Gao, L., Xu, B., Xiao, G., Lv, J. 2008. Transesterification of Palm Oil with Methanol to Biodiesel over a KF/Hydrotalcite Solid Catalyst. *Energy Fuels*, **22**(5), 3531–3535.

Gelbard, G., Vielfaure-Joly, F. 2001. Polynitrogen strong bases as immobilized Catalysts. *Reactive & Functional Polymers*, **48**, 65-74.

Gelbard, G., Vielfaure-Joly, F. 2000. Polynitrogen strong bases as immobilized catalysts for the transesterification of vegetable oils. *Comptes Rendus De L Academie Des Sciences Serie Ii Fascicule C-Chimie*, **3**, 563-567.

Georgogianni, K.G., Katsoulidis, A.P., Pomonis, P.J., Kontominas, M.G. 2009. Transesterification of soybean oil to biodiesel using heterogeneous catalysis. *Fuel Proc. Tech*., **90(**5), 671-676.

Gera, P., Puri, S.K., Jha, M.K. 2009. Use of Heterogeneous Catalysts for Biodiesel Production: A review. *New Frontiers in Biofuels*, Scitech Publications (India) Pvt Ltd, 370-379.

Gomes, J.F., Puna, J.F., Bordado, J.C., Correia, M.J.N. 2008. Development of heterogeneous catalysts for transesterification of triglycerides. *React. Kinet. Catal. Lett*., **96**(2), 273-279.

Granados, M.L., Poves, M.D.Z., Alonso, D.M., Mariscal, R., Galisteo, F.C., Moreno-Tost, R., Santamaria, J., Fierro, J.L.G. 2007. Biodiesel from sunflower oil by using activated calcium oxide. *Applied Catalysis B: Environmental*, **73**, 317-326.

Greve, A., Weidner, E., Umsicht, F.(n.d.). Biodiesel – Transesterification of Vegetable Oils with Guanidine Carbonate. Available: http://www.eurofedlipid.org/meetings/archive/gothenburg/5870/5870_0304.pdf-. access 17 March 2012.

Gryglewicz, G. 1999. Rapeseed oil methyl esters preparation using heterogeneous catalysts," *Biores Technol*., **70**, 249-253.

Gude, V.G., Patil, P., Martinez-Guerra, E., Deng, S., Nirmalakhandan, N. 2013. Microwave Energy potential for biodiesel production. *Sustainable Chemical Processes*, **1**:5, 1-31.

Gude, V.G., Patil, P.D., Deng, S., Nirmalakhandan. 2014. Microwave-enhanced methods for biodiesel production and other environmental applications. *Green Chemistry for Environmental Remediation* (Eds. Rashmi Singha and Vandana Singh), 209-250, Scrivener Publishing LLC.

Ha, S.H., Lan, M.N., Lee, S.H., Hwang, S.M., Koo, Y.M. 2007. Lipase-catalyzed biodiesel production from soybean oil in ionic liquids. *Enzyme and Microbial Technology*, **41**, 480-483.

Haber, J. 1991. Manual on catalyst characterization. *Pure & Appl. Chem*., **63** (9), 1227-1246.

Hameed, B.H., Lai, L.F., Chin, L.H. 2009. Production of biodiesel from palm oil (Elaeisguineensis) using heterogeneous catalyst: An optimized process. *Fuel Processing Technology*, **90**, 606-610.

Hattori, H. 2001. Solid base catalysis: generation of basic sites and application to organic synthesis. *Applied Catalysis A:Gen*, **222**, 247-259.

Hattori, H. 2004. Solid base catalysts: generation, characterization and catalytic behaviour of basic sites," *J. Jpn. Petrol. Inst.*, **47**(2).

Hawash, S., El Diwani, G., Kader, E.A. 2011. Optimization of biodiesel production from Jatropha oil by heterogeneous base catalyzed transesterification. *IJEST*, **3**(6).

Helwani, Z., Othman, M.R., Aziz, N., Fernando, W.J.N., Kim, J. 2009. Technologies for production of biodiesel focusing on green catalytic techniques: A review. *Fuel Processing Technology*, **90**, 1502-1514.

Hernández-Martin, E., Otero, C. 2008. Different enzyme requirements for the synthesis of biodiesel: Novozym® 435 and Lipozyme® TL IM. *Bioresource Technology*, **99**, 277-286.

Hew, K.L., Tamidi, A.M., Yusup, S., Lee, K.T., Ahmad, M.M. 2010. Catalytic cracking of bio-oil to organic liquid product (OLP). *Bioresource Technology*, **101**, 8855-8858.

Hsiao, M.C., Lin, C.C., Chang, Y.H., Chen, L.C. 2010. Ultrasonic mixing and closed microwave irradiation-assisted transesterification of soybean oil. *Fuel*, **89** , 3618-3622.

Hsiao, M.C., Lin, C.C., Chang, Y.H. 2011. Microwave irradiation assisted transesterification of soybean oil to biodiesel catalyzed by nanopowder calcium oxide. *Fuel*, **90**(5), 1963-1969.

Huang, K., Zhang, S., Xu, Q., Ren, Z., Yan, Y. 2009. Kinetics of transesterification crude soybean oil to biodiesel catalysed by magnesium methoxide. *Int. J. Global Energy Issues*, **31**(3-4), 251-261.

Ilgen, O., Dinc, I., Yidiz, M., Alptek, E., Boz, N., Anakc, M., Akin, A.N. 2007. Investigation of Biodiesel Production from Canola Oil using Mg-Al Hydrotalcite Catalysts. *Turk J. Chem*, **31**, 509 – 514.

International Energy Statistics. 2012, US Energy Information Administration- International energy statistics. Available: http://www.eia.gov/cfapps/ipdbproject /IEDIndex3. cfm?tid=5&pid=5&aid=2, access date 3 Mar 2012.

Islam, A., Taufiq-Yap, Y.H., Chu, C.-M., Chan, E.-S. 2013. Studies on design of heterogeneous catalysis for biodiesel production. *Process Safety and Environmental Protection*, **91**, 131-144.

Jain, S., Sharma, M.P. 2010. Kinetics of acid base catalyzed transesterification of *Jatropha curcas* oil. *Bioresource Technology*, **101**, 7701-7706.

Jain, S., Sharma, M.P., Rajvanshi, S. 2011. Acid base catalyzed transesterification kinetics of waste cooking oil. *Fuel Processing Technology*, **92**, 32-38.

Jerome, F., Kharchafi, G., Adam, I., Barrault, J. 2004. "One pot" selective synthesis of monoglycerides over homogeneous and heterogeneous guanidine catalysts. *Green Chemistry*, **6**, 72-74.

Jha, M.K., Gupta, A.K., Kumar, V. 2007. Kinetics of transesterification on Jatropha Curcas oil to biodiesel fuel. *Proceedings of the World Congress on Engineering and Computer Science 2007 WCECE 2007*, October 24-26, 2007, San Francisco, USA.

Jitputti, J., Kitiyanan, B., Rangsunvigit, P., Bunyakiat, K., Attanatho, L., Jenvanitpanjakul, P. 2006. Transesterification of crude palm kernel oil and crude coconut oil by different solid catalysts. *Chem. Eng. Journal*, **116**, 61-66.

Jothiramalingam, Viswanathan, B., Wang, M.K. 2011. Appraisal of heterogeneous solid acid-base catalysis for trans-esterification. *ChemInform*, **42**(3), 3-7.

Kafuku, G., Mbarawa, M. 2010. Biodiesel production from *Croton megalocarpus* oil and its process optimization. *Fuel*, **89**, 2556-2560.

Kafuku, G., Tan, K.T., Lee, K.T., Mbarawa, M. 2011. Noncatalytic biodiesel fuel production from *Croton megalocarpus* oil. Chemical Engineering Technology, 34 (11), 1827-1834.

Kaieda, M., Samukawa, T., Kondo, A., Fukuda, H. 2001. Effect of methanol and water contents on production of biodiesel fuel from plant oil catalyzed by various lipases in solvent-free system. *Journal of Bioscience and Bioengineering*, **91**, 12-15.

Kaneko, K. 1994. Determination of pore size and pore size distribution 1. Adsorbents and catalysis. *J of Membrane Science*, **96**, 50-89.

Kansedo, J., Lee, K.T., Bhatia, S. 2009. Biodiesel production from palm oil via heterogeneous transesterification. *Biomass and Bioenergy*, **33**, 271-276.

Kawashima, A., Matsubara, K., Honda, K. 2008. Development of heterogeneous base catalysts for biodiesel production. *Biores. Tech*., **99**(9), 3439-3443.

Kawashima, A., Matsubara, K., Honda, K. 2009. Acceleration of catalytic activity of calcium oxide for biodiesel production. *Biores. Tech*., **100**, 696-700.

Khemthong, P., Luadthong, C., Nualpaeng, W., Changsuwan, P., Tongprem, P. 2012. Industrial eggshell wastes as the heterogeneous catalysis for microwave- assisted biodiesel production. *Catalysis Today*, dio:10.1016/j.cattod.2011.12.024.

Kibazohi, O., Sangwan, R.S. 2011. Vegetable oil production from *Jatropha curcas, Croton megalocarpus, Aleurites moluccana, Moringa oleifera* and *Pachira glabra*: Assessment of renewable energy resources for bio-energy production in Africa, *Biomass and Bioenergy*, **25**(3), 1352-1356.

Kijeński, B., Zadrożny, R. 1979. A new method for poisoning surface active sites: Adsorption of Hammett indicators. *J. Res. Inst. Catalysis, Hokkaido Univ*., **27** (3), 145-156.

Kim, H.J., Kang, B. S., Kim, M. J., Park, Y.M., Kim, D.K., Lee, J.S., Lee, K.Y. 2004. Transesterification of vegetable oil to biodiesel using heterogeneous base catalyst. *Catalysis Today*, **93-95**, 315-320.

Kitakawa, N.S., Honda, H., Kuribayashi, H., Toda, T., Fukumura, T. 2007. Biodiesel production using anionic ion-exchange resin as heterogeneous catalyst. *Bioresource Tech*., **98**(2), 416-421.

Knothe, G., Sharp, C. A., Ryan, T. W. 2006. Exhaust emissions of biodiesel, petrodiesel, neat methyl esters, and alkanes in a new technology engine. *Energy Fuels*, **20**, 403-408.

Kolaczkowski, S.T., Asli, U.A., Davidson, M.G. 2009. A new heterogeneous ZnL2 catalyst on a structured support for biodiesel production. *Catalysis Today*, **147**, S220-S224.

KoohiKamali, S., Tan, C.P., Ling, T. C. 2012. Optimization of sunflower oil transesterification process using sodium methoxide. *The Scientific World Journal*, Article ID 475027, 8 pages, doi: 10.1100/2012/475027.

Kouzu, M., Kasuno, T., Tajika, M., Sugimoto, Y., Yamanaka, S., Hidaka, J. 2008a. Calcium oxide as a solid base catalyst for transesterification of soybean oil and its application to biodiesel production. *Fuel*, **87,** 2798–2806.

Kouzu, M., Kasuno, T., Tajika, M., Yamanaka, S., Hidaka, J. 2008b. Active phase of calcium oxide used as solid base catalyst for transesterification of soybean oil with refluxing methanol. *Applied Catalysis A: Gen*, **334**, 357-365.

Kouzu, M., Tsunomori, M., Yamanaka, S., Hidaka, J. 2010. Solid base catalysis of calcium oxide for a reaction to convert vegetable oil into biodiesel. *Advanced Powder Technology*, **21**, 488-494.

Kouzu, M., Yamanaka, S., Hidaka, J., Tsunomori, M. 2009. Heterogeneous catalysis of calcium oxide used for transesterification of soybean oil with refluxing methanol. *Applied Catalysis A: General*, **355**, 94–99.

Kumar V, Kumar, J. 2008. Kinetics of Jatropha curcas transesterification in batch reactor, *Proceedings of the World Congress on Engineering & Computer Science 2008*, USA, www.iaeng.org/publication/WCECS2008/WCECS2008_pp85-88.pdf, sighted 9-4-11.

Kumar, A., Namango, S.S., Kiriamiti, H. K. 2013. Study of Croton megalocarpus oil as a potential biodiesel feedstock for Kenya, its characterization and transesterification to produce fatty acid methyl ester. *MU 9th Annual International Conference*, *Eldoret*, Sept 2013.

Kumar, A., Some, D.K., Kiriamiti, K.H. 2014. Pretreatment of CaO Catalyst for Transesterification of Croton *Megalocarpus* Oil, *Journal of Sustainable Research in Engineering*, **1** (2), 57-62.

Kumar, A., Valoyi, R., Ochieng, A., Onyango, K. 2011. Acid –base transesterification of oil with high free fatty acid content. *Journal of Biofuels*, **1** (1), 7-14.

Labarta, J.A.R., Hernandez, R., Guillo, N., Valdes, F. 2009. Using hydrotalcite for biodiesel production. *8th Green Chemistry Conf., Spain*, 231-232.

Lam, M.K., Lee, K.T., Mohamed A.R. 2010. Homogenous, heterogeneous and enzymatic catalysts for transesterification of high free fatty acid oil (waste cooking oil) to biodiesel: A review. *Biotechnology Advances*, **28**, 500-518.

Leadbeater, N.E., Barnard, T.M., Stencel, L.M. 2008. Batch and continuous-flow preparation of biodiesel derived from butanol and facilitated by microwave heating. *Energy Fuels*, **22**(3), 2005-2008.

Lee, D.-W., Park,Y.-M., Lee, K.-Y. 2009. Heterogeneous base catalysis for transesterifcation in biodiesel synthesis. *Catal Surv Asia*, **13**, 63-67.

Leevijit, T., Wisutmethangoon, W., Prateepchaikul, G., Tongurai, C., Allen, M. A second order kinetics of palm oil transesterification. *The Joint Inernational Conference on "Sustainable Energy and Environment (SEE)"*, 1-3 December 2004, Hua Hin, Thailand, 277-281.

Leofanti, G., Tozzola, G., Padovan, M., Petrini, G., Bordiga, S., Zecchina, A. 1997. Chapter 4- Catalyst characterization: characterization techniques. *Catalysis Today*, **34**, 307-327.

Lertsathapornsuk, V., Ruangying, P., Pairintra, R., K Krisnangkura, K. Continuous transethylation of vegetable oils by microwave irradiation. *Proceedings of 1st conference*

*on energy network, 2005, Thailand*, RE11-1 – RE11-4, - e-nett.sut.ac.th/download/RE/RE11.pdf, access 10-4-2011.

Leung, D.Y.C., Wu, X., Leung, M.K.H. 2010. A review on biodiesel production using catalyzed transesterification. *Appl. Energy*, **87**, 1083-1095.

Leung, D.Y.C., Guo, Y. 2006. Transesterification of neat and used frying oil: optimization for biodiesel production. *Fuel Process Technol*, **87**, 883-890.

Levenspiel, O. 1972. Chemical Reaction Engineering. John Wiley & Sons, New York.

Li, H.T., Xie, W.L. 2006. Tranesterification of soybean oil to biodiesel witn Zn/I-2 catalyst. *Catalysis Letters*, **107**, 25-30.

Li, N.W., Zong, M.H., Wu, H. 2009. Highly efficient transformation of waste oil to biodiesel by immobilized lipase from *penicillum expansu*. *Process Biochem.*, **44**, 685-688.

Liang, X.Z., Gao, S., Wu, H.H., Yang, J.G. 2009. Highly efficient procedure for the synthesis of biodiesel from soybean oil. *Fuel Processing Technology*, **90**, 701-704.

Liu, X., He, H., Wang, Y., Zhu, S. 2007. Transesterification of soybean oil to biodiesel using SrO as a solid base catalyst. *Catalysis Communications,* **8**, 1107-1111.

Liu, X., He, H., Wang, Y., Zhu, S., Piao, X. 2008a. Transesterification of soybean oil to biodiesel using CaO as a solid base catalyst. *Fuel,* **87**, 216-221.

Liu, X., Piao, X., Wang, Y., Zhu, S., He, H. 2008b. Calcium methoxide as a solid base catalyst for the transesterification of soybean oil to biodiesel with methanol. *Fuel,* **87**, 1076-1082.

Liu, Y., Lotero, E., Goodwin, J.G., Mo, X. 2007. Transesterification of poultry fat with methanol using Mg–Al hydrotalcite derived catalysts. *Applied Catalysis A: General* , **331**, 138–148.

Lopez, D.E., Goodwin Jr, J.G., Bruce, D.A. 2007. Transesterification of triacetin with methanol on Nafion® acid resins. *J. of Catalysis,* **245** (2), 381-391.

Lopez, D.E., Goodwin Jr, J.G., Bruce, D.A., Lotero, E. 2005. Transesterification of triacetin with methanol on solid acid and base catalysts. *Applied Catalysis A: Gen.*, **295**, 97-105.

Lotero, E., Liu, Y., Lopez, D.E., Suwannakarn, K., Bruce, D.A., Goodwin Jr, J.G. 2005. Synthesis of biodiesel via acid catalysts. *Ind. Eng. Chem. Res.*, **44(**14), 5353-5363.

Lu, P.,Yuan,Z., Li, L., Wang, Z., Luo, W. 2010. Biodiesel from different oil using fixed-bed and plug flow reactors. *Renewable Energy*, **35**, 283-287.

Lujaji, F., A. Bereczky, A., Cs. Novak, Mbarawa, M. 2010. Cetane Number and Thermal Properties of Croton Oil, Biodiesel, 1-Butanol, and Diesel Blends. *Proceedings of the World Congress on Engineering 2010* Vol III WCE 2010, June 30 - July 2, 2010, London, U.K.

Lukic, I., Krstic, J., Jovanovic, D., Skala, D. 2009. Alumina/silica supported $K_2CO_3$ as a catalyst for biodiesel synthesis from sunflower oil. *Bioresour. Technol*., **100**, 4690-4696.

Ma, F., Hanna, M.A. 1999, Biodiesel production: a review. *Bioresource Technology*, **70**, 1-15.

Ma, F.R., Clements, L.D., Hanna, M.A. 1998. Biodiesel fuel from animal fat. Ancilliary studies on transesterification of beef tallow. *Industrial & Engineering Chemistry Research*, **37**, 3768-3771.

Macala, G.S., Robertson, A.W., Johnson, C.L., Day, Z.B., Lewis, R.S., White, M.G., Iretskii, A.V., Ford, P.C. 2008. Transesterification Catalysts from Iron Doped Hydrotalcite-like Precursors: Solid Bases for Biodiesel Production. *Catalysis Letters*, **122**(3-4), 205-209.

MacLeod, C.S., Harvey, A.P., Lee, A.F., Wilson, K. 2008. Evaluation of the activity and stability of alkali doped metal oxide catalysts for application to an intensified method of biodiesel production. *Chemical Engineering Journal*, **135**, 63-70.

Marbán, G., Rio, L.D. 2013. Tentative explanation for the kinetic compensation effect in doped catalysts. *Kinetics and Catalysis*, **54** (4), 463-468.

Marjanović, A.V., Stamenković, O.S., Todorović, Z.B., Lazić, M.L., Veljković, V.B. 2010. Kinetics of the base-catalyzed sunflower oil ethanolysis. *Fuel*, **89**, 665-671.

Martinez, S.L., Romeo, R., Lopez, J.C., Romero, A., Mandieta, V.S., Nativdad, R. 2011. Preparation and characterization of CaO nanoparticle/ NaX zeolite catalysts for the transesterification of sunflower oil. *Ind. Eng. Chem. Res.*, **50**(5), 2665-2670.

Martinez-Guerra, E., Gude, V.G. 2014. Synergistic effect of simultaneous microwave and ultrasound irradiations on transesterification of waste vegetable oil. *Fuel*, **137**, 100-108.

Matsuzaki, I., Masahiro, N. 1969. Application of Hammett indicators to estimating coverages of acid sites of silica-alumina by nitrogen, ethylene, water, ethyl alcohol, pyridine and n-butylamine. *J. Res. Inst. Catalysis, Hokkaido Univ*., **17** (1), 46-53.

McCabe, W.L., Smith, J.C., Hariott P, 1985, Unit Operations of Chemical Engineering, McGraw-Hill Book Co, New York.

Meher, L.C., Dharmagadda, V.S.S., Naik, S. N. 2006. Optimization of alkali-catalyzed transesterification of *Pongamia pinnata* oil for production of biodiesel. *Bioresource Technology*, **97**, 1392-7.

Micropore Analysis. www.atomikateknit.com/pdf/Mircopore Analysis.pdf, 6th May 2013.

Milch, L. (n.d.) Environmental comparisons of Croton Megalocarpus vs. other tropical feedstocks, Africa Biofuel with Emission Reduction (Tanzania) Ltd, www.africabiofuel.com/files/feedstocks.pdf , access 13-4-2011.

Mirie, S.N., Kioni, P.N., Thiong'o, G.T., Kariuki, P.N. 2012. Immobilized *Candida antarctica* lipase catalyzed transesterification of *Croton megalocarpus* seed oil for biodiesel production. *Journal of Energy Technologies and Policy*, **2**(5), 20-24.

Montgomery, D.C. 2013. Design and Analysis of Experiments, Ch 11, John Wiley & Sons, Inc. Singapore.

Muerbach, S.M., Carrado., C.A., Dutta, P.K., Eds. Handbook of zeolite science & technology, CRC Press, 2003.

Muniyappa, P.R., Brammer, S.C., Noureddini, H. 1996. Improved conversion of plant oils and animal fats into biodiesel and co-products. *Bioresource Technology*, **56**, 19-2.

Nakatani, N., Takamori, H., Takeda, K., Sakugawa, H. 2009. Transesterification of soybean oil using combusted oyster shell waste as a catalyst. *Bioresource Technology*, **100**, 1510-1513.

Narasimharao, K., Brown, D.R., Lee, A.F., Mewman, A.D., Siril, P.F., Tavener, S.J., Wilson, K. 2007a. Structure-activity relations in Cs- doped heteropolyacid catalysts for biodiesel production. *J. Catal*., **248**, 226-234.

Narasimharao, K., Lee, A., Wilson, K. 2007b. Catalysis in production of biodiesel. *J. Biobased Mat. Bioenergy*, **1**, 19-30.

NBS Monograph 25, Standard X-ray Powder Patterns. 1981. www.digicoll.manoa.hawaii.edu/techreports/PDF/NBS25- 9m.pdf. access 20 Oct 2013.

Ngamcharussrivichai, C., Totarat, P., Bunyakiat, K. 2009. K, Ca and Zn mixed oxide as a heterogeneous base catalyst for transesterification of palm kernel oil. *Appl Catal A*, **366**, 154-159.

Ngamcharussrivichai, C., Wiwatnimit, W., Wangnoi, S. 2007. Modified dolomites as catalysts for palm kernel oil transesterification. *Journal of Molecular Catalysis A: Chemical*, **276**, 24-33.

Nie, K., Xie, F., Wang, F., Tan, T. 2006. Lipase catalyzed methanolysis to produce biodiesel: Optimization of the biodiesel production. *Journal of Molecular Catalysis B: Enzymatic*, **43**, 142-147.

Nogueira, B.M., Corretoni, C., Cruz, R., Suely Freitas, Melo Jr, P.A., Costa-Felix, R., Pinto, J.C., Nele, M. 2010. Microwave activation of enzymatic catalysts for biodiesel production, *J of Molecular Catalysis B:Enzymatic*, **67**(1-2), 117-121.

Noiroj, K., Intarapong, P., Luengnaruemitchai, A., Jai-In, S. 2009. A comparative study of $KOH/Al_2O_3$ and KOH/NaY catalysts for biodiesel production via transesterification from palm oil. *Renewable Energy*, **34**(4), 1145-1150.

Noureddini, H., Zhu, D. 1997. Kinetics of transesterification of soybean oil. *JAOCS*, **74**(11), 1457-1463.

Ognjanovic, N., Bezbradica, D., Knezevic-Jugovic, Z. 2009. Enzymatic conversion of sunflower oil to biodiesel in a solvent-free system: Process optimization and the immobilized system stability. *Bioresource Technology*, **100**, 5146-5154.

Oliviera, C.F., Dezaneti, L.M., Garcia, F.A.C., de Macedo, J.L., Dias, J.A., Dias, S.C.L., Alvim, K.S.P. 2010. Esterification of oleic acid with ethanol by 12-tungstophosphoric acid supported on zirconia. *Appl. Catal. A-Gen*., **372**, 153-161.

Particle Analytical. 2013. www.particle.dk/methods-analytical-laboratory/surface-area-bet/surface-area-bet-theory/. Acess 13 October 2013.

Patil, P., Gude, V.G., Pinappu, S., Deng, S. 2011. Transesterification kinetics of *Camelina sativa* oil on metal oxide catalysts under convention and microwave heating conditions. *Chem. Eng. Journal*, **168**(3), 1296-1300.

Patil, P., Deng, S. 2009. Transesterification of *Camelina sativa* oil using heterogeneous metal catalysts. *Energy Fuels*, **23**, 4619-4624.

Patil, P., Gudu, V.G., Deng, S. 2009. Biodiesel production from *Jatropha curcas*, waste cooking, and *Camelina sativa* oils. *Ind. Eng. Chem. Res*., **48**, 10850-10856.

Patil, P.D., Gude, V.G., Camacho, L.M., Deng, S. 2010b. Microwave-assisted catalytic transesterification of *Camilina sativa* oil. *Energy Fuels*, **24**, 1298-1304.

Patil, P.D., Gude, V.G., Deng, S. 2010a. Transesterification of *Camelina sativa* oil using supercritical and subcritical methanol with cosolvents. *Energy Fuels*, **24**, 746-751.

Perin, G., Alvaro, G., Westphal, W., Viana, L.H., Jacob, R.G., Lenardao, E.J., D'Oca, M.G.M. 2008. Transesterification of castor oil assisted by microwave irradiation. *Fuel*, **87**, 2828-2841.

Perreux, L., Loupy, A. 2001. A tentative rationalization of microwave effects in organic synthesis according to the reaction medium, and mechanistic considerations. *Tetrahedron*, **57**, 9199-9223.

Peterson, C. L., Auld, D.L., Korus, R.A. 1983. Winter rape oil fuel for diesel engines: Recovery and utilization. *JAOCS*, **60**, 1579-1587.

Pinzi, S., Mata-Granados, J.M., Lopez-Gimenez, F.J., Luque de Castro, M.D., Dorado, M.P. 2011. Influence of vegetable oils fatty-acid composition on biodiesel optimization. *Bioresource Tehnology*, **102**, 1059-1065.

Pryde, E.H.1983. Vegetable oils as diesel fuels: overview. *JAOCS*, **60**, 1557.

Puna, J.F., Gomes, J.F., Correia, M.J.N., Soares Dias, A.P., Bordado, J.C. 2010. Advances on the development of novel heterogeneous catalysts for transesterification of triglycerides in biodiesel. *Fuel*, **89**, 3602-3606.

Ramadhas, A.S., Jayaraj, S., Muraleedharan, C. 2004. Use of vegetable oils as I.C. engine fuel- a review. *Renewable Energy*, **29**, 727-742.

Reddy, C.R.V., Oshel, R., Verkade, J.G. 2006. Room-temperature conversion of soybean oil and poultry fat to biodiesel catalyzed by nanocrystalline calcium oxides. *Energy Fuels*, **20** (3), 1310–1314.

Reefat, A.A., El Sheltawy, S.T. 2008. Time factor in microwave-enhanced biodiesel production, *WSEAS Transactions on Environment and Development*, **4**(4), 279-288.

Reefat, A.A., El Sheltawy, S.T., Sadek, K.U. 2008. Optimum reaction time, performance and exhaust emissions of biodiesel produced by microwave irradiation. *International Journal of Environmental Science & Technology*, **5**, 315-322.

Rubio-Caballero, J.M., Santamaria-Gonzalez, J., Merida-Robles, J., Moreno-Tost, R., Jimenez-Lopez, A., Maireles-Torres, P. 2009. Calcium zincate as precursor of active catalyst for biodiesel production under mild conditions. *Applied Catalysis B-Environmental*, **91**, 339-346.

Saka, S., Kusdiana, D. 2001. Biodiesel fuel from rapeseed oil as prepared in supercritical methanol. *Fuel*, **80**, 225-231.

Samart, C., Sreetongkittikul, R., Sookman, C. 2009. Heterogeneous catalysis of transesterification of soybean oil using KI/mesoporous silica. *Fuel Processing Technology*, **90**, 922-925.

Sarin,R., Arora, A.K., Puri, S.K., Praksah, S., Ranjan, R., Christopher, J., Tuli, D.K., Malhotra, R.K., Kumar, A. 2009. Novel catalyst composition for biodiesel production and

a process for producing biodiesel and product thereof. Patent applied (Appln. No. 13481N033).

Satyanarayanareddy, Y., Regupathi I. 2013. Mcrowave assisted batch and continuous transesterification of karanja oil: optimization of process parameters. *Biomass Conversion and Biorefinery*, **3** (4), 305-317.

Schuchardt, U., Sercheli, R., Vargas, R.M. 1998. Transesterification of vegetable oils: a review. *Journal of Brazilian Chemical Society*, **9**(1), 199-210.

Schuchardt, U., Vargas, R.M., Gelbard, G. 1996. Transesterfifcation of soybean oil catalyzed by alkylguanidines heterogenized on different substituted polystyrenes. *J. of Molecular Catalysis A: Chemical*, **109**, 37-44.

Semwal, S., Arora, A.K., Badoni, R.P., Tuli, D.K. 2011. Biodiesel production using heterogeneous catalysis. *Bioresource Technology*, **102**, 2151-2161.

Sharma, Y.C., Singh, B. 2011. Advancements in solid acid catalysts for ecofriendly and economically viable synthesis of biodiesel. *Biofuels, Bioprod. Bioref.*, **5**, 69-92.

Shay, E. G. 1993. Diesel fuel from vegetable oils: status and opportunities. *Biomass and Bioenergy* **4,** 227-242.

Sherrington, D.C., Kybette, A.P., Duncan, J.M., Mdoe, J.E.G., Brunel, D., Renard, G., Blanc, A. Guanidine catalysts supported on silica and micelle templated silicas, New basic catalysts for organic chemistry. *Supported Catalysts and their Applications*. Eds. Sherrington D.C. and Kybette A.P., Royal Society of Chemistry Publishing, 2001.

Shibasaki-Kitakawa, N., Honda, H., Kuribayashi, H., Toda, T., Fukumura, T., Yonemoto, T. 2007. Biodiesel production using aanionic ion-exchange resin as heterogeneous catalyst. *Bioresource Technology*, **88**, 103-106.

Shimada, Y., Watanabe, Y., Samukawa, T., Sugihara, A., Noda, H., Fukuda, H., Tominaga, Y. 1999. Conversion of vegetable oil to biodiesel using immobilized Candida Antarctica lipase. *JAOCS*, **76**, 789-793.

Sing, K. S. W. 1982. Reporting Physisorption data for gas/solid systems, *Pure & Appl. Chem*., **54**, 2201-2218.

Sing, K.S.W. 1985. Reporting physisorption data for gas/solid systems with special reference to the determination of surface area and porosity (Recommendations 1984). *Pure & Appl. Chem*., **57**(4), 603-619.

Singh, A.K., Fernando, S.D. 2007. Reaction kinetics of soybean oil transesterification using heterogeneous metal oxide catalysts. *Chem. Eng. Technol*., **30**(12), 1716-1720.

Singh, A.K., Fernando, S.D. 2008. Transesterification of soybean oil using heterogeneous catalysis. *Energy Fuels*, **22**, 2067-2069.

Sinnwell, S., Ritter, H. 2007. Recent advances in microwave-assisted polymer synthesis. *Australian Journal of Chemistry*, **60**, 729-743.

Sridharan, R., Mathai, I.M. 1974. Transesterification reactions. *J. Scient. Ind. Res*., **33**, 178-187.

Stamenkovic´, O.S., Lazic´, M.L., Todorovic´, Z.B., Veljkovic´, V.B., Skala, D.U. 2007. The effect of agitation intensity on alkali-catalyzed methanolysis of sunflower oil. *Bioresource Technology*, **98**, 2688-2699.

Suppes, G., Dasari, M.A., Doskocil, E.J., Mankidy, P., Goff, M.J. 2004. Transesterification of soybean oil with zeolite and metal catalysts. *Applied Catalysis A: Gen.*, **257**(2), 213-223.

Suwannakarn, K., Lotero, E., Ngaosuwan, K., Goodwin Jr, J.G. 2009. Simultaneous free fatty acid esterification and triglyceride transesterification using a solid acid catalyst with in situ removal of water and unreacted methanol. *Ind. Eng. Chem. Res.*, **48**, 2810-2818.

Tamunaidu, P., Bhatia, S. 2007. Catalytic cracking of palm oil for the production of biofuels: Optimization studies. *Bioresource Technology*, **98**, 3593-3601.

Tanabe, K., Yamaguchi, T. 1963. Basicity and acidity of solid surfaces, *Presented at the 13$^{th}$ Discussion Meeting on Catalysis, Sapporo*, September 24, 1963.

Tanabe**,** K.**,** Yoshii, N., Hattori, H. 1971. Catalytic activity and selectivity of evacuated calcium oxide for isomerization of but-1-ene. *J. Chem. Soc D: Chem. Commun*., **9**, 464-8.

Taufiqurrahmi, N. and Bhatia, S. 2011. Catalytic cracking of edible and non-edible oils for production of biofuels. *Energy & Environmental Science*, **4**, 1087-1112.

Taufiq-Yap, Y.H., Lee, H.V., Yunus, R., Juan, J.C. 2011. Transesterification of non-edible *Jatropha curcas* to biodiesel using binary Ca-Mg mixed oxide catalyst: Effect of stoichiometric composition. *Chemical Engineering Journal*, **178**, 342-347.

Tazerout, M., Ndayishimiye, P., Masimala, S. K. 2009. Performance and emission studies on a CI engine using methyl esters of palm oil and waste cooking oil mixture a fuel. *New Frontiers in Biofuels*, 154-161. Scitech Publications (India) Pvt Ltd.

Teng, A., Gao, L., Xiao, G., Liu, H. 2009. Transesterification of soybean oil to biodiesel over heterogeneous solid base catalyst. *Energy Fuels*, **23**, 4630-4634.

Thomas, J.M., Thomas, W.J. 1967. Introduction to the Principles of Heterogeneous Catalysis, 1st Edition, Academic Press, New York.

Todorovic´ , Z.B., Stamenkovic´,O.S., Stamenkovic´ ,I.S., Avramovic´ ,J.M., Velicˇkovic´ , A.V., Bankovic´ -Ilic´ ,I.B., Veljkovic´ V.B. 2012. The effects of cosolvents on homogeneously and heterogeneously base-catalyzed methanolysis of sunflower oil. *Fuel* (2012), http://dx.doi.org/10.1016/j.fuel.2012.11.049.

Turner, T. L. 2005. Modeling and Simulation of Reaction Kinetics for Biodiesel Production, MSc Thesis in Mechanical Engineering, Raleigh, NC.

Tyson, K.S. 2006. Biodiesel Handling and Use Guidelines (3rd Ed.), US Department of Energy, Energy Efficiency and Renewable Energy. USA.

Veljkovic, V.B., Stamenkovic, O.S., Todorovic, Z.B., Lazic, M.L., Skala, D.U. 2009. Kinetics of sunflower oil methanolysis by calcium oxide. *Fuel*, **88**, 1554-1562.

Vicente, G., Martinez, M., Aracil, J., Esteban, A. 2005. Kinetics of sunflower methanolysis. *Ind. Eng. Hem. Res*. **44**, 5447-5454.

Viriya-empikul, N., Krasae, P., Puttasawat, B., Yoosuk, B., Chollacoop, N., Faungnawakij, K. 2010. Waste shells of mollusk and egg as biodiesel production catalysts. *Bioresource Technology*, **101**,3765-3767.

Vyas, A.P., Subrahmanyam, N., Patel, P.A. 2009. Production of biodiesel through transesterification of Jatropha oil using KNO3/Al2O3 solid catalyst. *Fuel*, **88**, 625-628.

Wagutu, A.W., Chhabra, S.C., Thoruwa, C.L., Thoruwa, T.F., Mahunnah, R.L.A. 2009. Indigenous oil crops as a source for production of biodiesel in Kenya. *Bull. Chem. Soc. Ethiop*. **23**(3), 359-370.

Wan Isahak, W.N.R., Ismail, M., Mohd Jahim, J., Salimon, J., Yarmo, M.A. 2010. Transesterification of palm oil using Nano-Calcium oxide as a solid base catalyst. 2010. *World Applied Science Journal*, **9** (Special Issue Nanotechnology), 17-22.

Wang,L., Yang, J. 2007. Transesterification of soybean oil with nano-MgO or not in supercritical and subcritical methanol. *Fuel*, **86**, 328-333.

Wei, Z., Xu, C., Li, B. 2009. Application of waste eggshell as low-cost solid catalyst for biodiesel production. *Bioresource Technology*, **100**, 2883-2885.

Wu, D., Yu, H., Harvey, A., Roskilly, A.P. 2012. Mirco trigeneration system driven with preheated croton oil- A performance and particulate emission study. *The 4th International Conference on Applied Energy ICAE2012*, July 5-8, 2012, Suzhou, China.

Xie, W., Huang, X., Li, H. 2007. Soybean oil methyl esters preparation using NaX zeolites loaded with KOH as a heterogeneous catalyst. *Bioresource Technology*, **98**(4), 936-993.

Xie, W., Li, H. 2006. Alumina-supported potassium iodide as a heterogeneous catalyst for biodiesel production from soybean oil. *J. Mol. Catal. A: Chem*., **255**, 80-92.

Xie, W.L., Peng, H., Chen, L.G. 2006. Calcined Mg-Al hydrotalcites as solid base catalysts for methanolysis of soybean oil. *Journal of Molecular Catalysis A-Chemical*, **255**, 1-9.

Xu, B-Q., Wei, J-M., Wang, H-Y., Sun, K-Q., Zhu, Q-M. 2001. Nano-MgO novel preparation and application as support of Ni catalyst for $CO_2$ reforming of methane. *Catalysis Today*, **68**, 217-225.

Xu, L., Yang, X., Maynurkader, G.Y. 2008. Preparation of mesoporous polyxometalate-tantalum pentoxide composite catalyst for efficient esterification of fatty acid. *Catal. Commun*., **9**, 1607-1611.

Xue, W., Zhou, Y.C., Song, S.A., Shi, X., Wang, J., Yin, S.T., Hu, D.Y., Jin, L.H., Yang, S. 2009. Synthesis of biodiesel from Jatropha curcas L. seed oil using artificial zeolite loaded with $CH_3COOK$ as a heterogeneous catalyst. *Natural Science*, **1**, 55-62.

Yaacob, N.F., Farhah, N. 2010. Transesterification of castor oil to biodiesel by using Mg-Al hydrotalcites as a catalyst. Universiti Teknologi Petronas, Seri Iskandar ,Tronoh,Perak, 2010. Available: http://utpedia.utp.edu.my/1328/- . access 17 Mar 12.

Yadav, G.D., Nair, J.J. 1999. Sulfated zirconia and its modified versions as promising catalysts for industrial processes. *Microporous Mesoporous Mater*, **33**, 1-48.

Yancy-Caballero, D. M., Guirardello, R. 2013. Thermodynamic simulation of transesterification reaction by Gibbs energy minimization. *Fluid Phase Equilibria,* **341**, 12– 22.

Yang, F. 2004. Final Report: A novel acoustic biodiesel production from animal fats and waste grease. *US Environmental Protection Agency Report* EPD 04023.

Zabeti, M., Daud, W.M.A.W., Aroua, M.K. 2009a. Activity of solid catalysts for biodiesel production: A review. *Fuel Process. Tech*., **90**, 770-777.

Zabeti, M., Daud, W.M.A.W., Aroua, M.K. 2009b. Optimization of the activity of CaO/Al2O3 catalyst for biodiesel production using response surface methodology. *Appl.Catal. A: Gen*., **366**(1), 154-159.

Zhang, J., Zhao, Z., Qiao, Y., Lin, H., Pang, X., Bai, Q., Li, R. 2012. Thermodynamics analysis on preparation of methyl oleate via transesterification by group-contribution

method. CIESC Journal, 63(6), 1690-1690.

Zhang, S., Zu, Y.G., Fu, Y.J., Zhang, D.Y., Efferth, T. 2010. Rapid microwave assisted transesterification of yellow horn oil to biodiesel using a heterogeneous solid catalyst. *Bioresource Technol*., **101**, 931-836.

Zhang, Y., Dube, M.A., McLean, D.D., Kates, M. 2003. Biodiesel production from waste cooking oil: 2. Economic assessment and sensitivity analysis. *Bioresource Technology*, **90**, 229-240.

Zhao, L. 2010. Novel Solid Base Catalysts for the Production of Biodiesel from Lipids. PhD Thesis, University of Kansas.

Zhu, H., Wu, Z., Chen, Y., Zhang, P., Duan, S., Liu, X., Mao, Z. 2006. Preparation of biodiesel catalysts by solid super base of calcium oxide and its refining process. *Chinese J. of Catalysis*, **27**(5), 391-396.

# APPENDIX A
# RESPONSE SURFACE METHODOLOGY

## A.1 Introduction

Response surface methodology (RSM) is a collection of mathematical and statistical techniques useful in modeling and analysis of problems in which a response of interest is influenced by several variables and the objective is to optimize this response (Montgomery, 2013). RSM is used for design and collection of experimental data which allows fitting a general quadratic equation for data smoothing and prediction, regression analysis, and examination of fitted data which is usually done graphically through response surface plots.

## A.2 Experimental Design

### A.2.1 Box-Wilson Central Composite Design (CCD)

A Box-Wilson Central Composite Design, commonly called a 'Central Composite Design', contains an imbedded factorial or fractional factorial design with centre points that is augmented with a group of `star points' that allow estimation of curvature. If the distance from the center of the design space to a factorial point is ±1 unit for each factor, the distance from the center of the design space to a star point is ± α with | α | > 1. The precise value of α depends on certain properties desired for the design and on the number of factors involved. Similarly, the number of centrepoint runs the design is to contain also depends on certain properties required for the design. A central composite design always contains twice as many star points as there are factors in the design. The star points represent new extreme values (low and high) for each factor in the design. Figure A-1 shows a CCD for $k = 3$ factors. This design has $14 + n_C$ runs (usually $3 \leq n_C \leq 5$). Here $n_C$ is the number of replicates at the centre point.

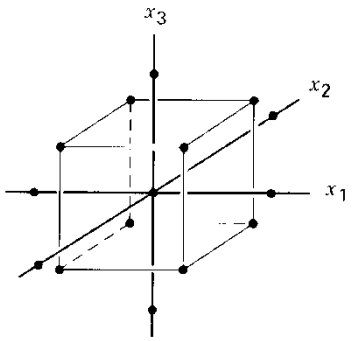


**Figure A-1: CCD for Three factors**

To maintain rotatability, the value of α depends on the number of experimental runs in the factorial portion of the central composite design: $\alpha = [\text{number of factorial runs}]^{1/4}$

If the factorial is a full factorial, then $\alpha = [\ 2^k]^{1/4}$ …A1

For a 3 factor design, $k = 3$, $\alpha = [\ 2^3]^{1/4} = 1.682$ (Engineering Statistics Handbook, 2006).

### A.2.2 Box-Behnken Designs

Box and Behnken have proposed some three-level designs for fitting response surfaces. These designs are formed by combining $2^k$ factorials with incomplete block designs. The resulting designs are usually very efficient in terms of the number of required runs, and they are either rotatable or nearly rotatable. Box-Behnken design is a spherical design, with all points lying on a sphere of radius $\sqrt{2}$ (Montgomery, 2013).

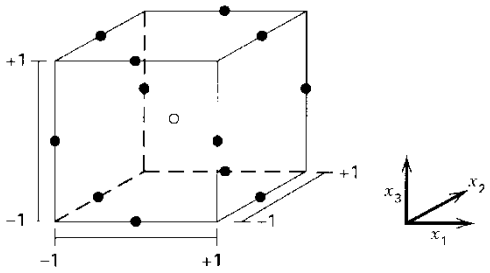


**Figure A-2: A Box-Behnken design for three factors**

## A.3 Analysis of Experimental Data

### A.3.1 Empirical Model

For response surface designs a complete description of the process behavior might require a quadratic or cubic model. A quadratic model for three independent variables is given by:

$$y = b_0 + b_1x_1 + b_2x_2 + b_3x_3 + b_{12}x_1x_2 + b_{13}x_1x_3 + b_{23}x_2x_3 + b_{11}x_1^2 + b_{22}x_2^2 + b_{33}x_3^2 \quad \ldots A2$$

And a cubic model is given by:

$$y = \text{quadratic model} + b_{123}x_1x_2x_3 + b_{112}x_1^2x_2 + b_{113}x_1^2x_3 + b_{122}x_1x_2^3 + b_{133}x_1x_3^3 + b_{223}x_2^2x_3 + b_{233}x_2x_3^3 + b_{111}x_1^3 + b_{222}x_2^3 + b_{333}x_3^3 \quad \ldots A3$$

In the above, y is the dependent variable and $x_1$, $x_2$ and $x_3$ are the independent variables. These are the full models, with all possible terms, rarely would all of the terms be needed in an application. If the experimenter has defined factor limits appropriately and/or taken advantage of all the tools available in multiple regression analysis, then finding an industrial process that requires a third-order model is highly unusual. Most of the response surface designs can be fitted by quadratic models.

### A.3.2 General linear model matrix

Fundamentals of regression analysis is explained in terms of a linear model. Any polynomial regression model are special cases of predictor variables making the response surface curvi-linear. Consider the following quadratic regression equation:

$$Y_i = \beta_0 + \beta_1 X_i + \beta_2 X_i^2 + \varepsilon_i \quad \ldots A4$$

In the above $\beta$ terms are constants and $\varepsilon$ represents random error.

Equation A4 can be expressed in a linear form by defining $X_{i1} = X_i$ and $X_{i2} = X_i^2$, to get:

$$Y_i = \beta_0 + \beta_1 X_{i1} + \beta_2 X_{i2} + \varepsilon_i \quad \ldots A5$$

Equation A5 is a linear expression for a quadratic equation. A general linear form for any polynomial can be written as:

$$Y_i = \beta_0 + \beta_1 X_{i1} + \beta_2 X_{i2} + \ldots + \beta_{p-1} X_{i,p-1} + \varepsilon_i \quad \ldots A6$$

Equation A6 in the matrix form is:

$$\boldsymbol{Y} = \boldsymbol{X}\boldsymbol{\beta} + \boldsymbol{\varepsilon} \quad \ldots A7$$

In equation A7, **Y** is a response vector (n x1), $\boldsymbol{\beta}$ is vector of constants (p x1), $\boldsymbol{X}$ is the matrix of parameters (n x p) and $\boldsymbol{\varepsilon}$ is a vector of random errors (n x 1). Number of observations is *n*, and number of parameters is *p*. Therefore:

$$Y = \begin{bmatrix} Y_1 \\ Y_2 \\ \vdots \\ \vdots \\ Y_n \end{bmatrix}, \quad \beta = \begin{bmatrix} \beta_0 \\ \beta_1 \\ \vdots \\ \vdots \\ \beta_{p-1} \end{bmatrix}, \quad X = \begin{bmatrix} 1 & X_{11} & X_{12} & \dots & X_{1,p-1} \\ 1 & X_{21} & X_{22} & \dots & X_{2,p-1} \\ \vdots & \vdots & \vdots & \ddots & \vdots \\ 1 & X_{n1} & X_{n2} & \dots & X_{n,p-1} \end{bmatrix}, \quad \varepsilon = \begin{bmatrix} \varepsilon_1 \\ \varepsilon_2 \\ \vdots \\ \vdots \\ \varepsilon_n \end{bmatrix} \qquad \ldots A8$$

### A.3.3 Estimation of regression coefficients

Regression coefficients are estimated by the use of least-square method. For a general regression model:

$$Q = \sum_{i=1}^{n} (Y_i - \beta_0 - \beta_1 X_{i1} - \ \ldots - \beta_{p-1} X_{i,p-1})^2 \qquad \ldots A9$$

The least square estimators are those values of $\beta_i$ that minimize Q, where the vector of the least square is estimated as regression coefficients $b_0$, $b_1$, …, $b_{p-1}$ as b such that:

$$b = \begin{bmatrix} b_0 \\ b_1 \\ \vdots \\ \vdots \\ b_{p-1} \end{bmatrix} \qquad \ldots A10$$

The least square normal equations for the general linear regression model are:

$$\boldsymbol{(X'X)b = (X'Y)} \qquad \ldots A11$$

And the least square estimators are:

$$\mathbf{b = (X'X)^{-1}(X'Y)} \qquad \ldots A12$$

### A3.4 Analysis of Variance (ANOVA)

If $Y_1$ is the experimental value and $\hat{Y}_i$ is the fitted value, a residual term $e_i$ is defined as:

$$e_i = Y_1 - \hat{Y}_i \qquad \ldots A13$$

In the above $\hat{Y}_i$ is a (n x1) vector containing $\hat{Y}_1, \hat{Y}_2, \ldots \hat{Y}_i$ terms. Similarly $e$ is a (n x1) vector containing $e_1, e_2, \ldots, e_n$ terms.

The fitted values are represented by, $\hat{Y} = Xb$ ; and residual terms are represented by,

$$e = Y - \hat{Y} \quad = Y - Xb \qquad \ldots A14$$

Table A1 gives ANOVA for general Linear Regression Model (Balasubramanian, 2010).

**Table A1: ANOVA for general Linear Regression Model**

| Source of variation | Sum of squares | DF | Mean Square |
|---|---|---|---|
| Regression | SSR= b'X'Y – (1/n)Y'JY | p-1 | MSR = SSR/(p-1) |
| Error | SSE = Y'Y – b'X'Y | n-p | MSE = SSE/(n-p) |
| Total | SSTO = Y'Y – (1/n)Y'JY | n-1 | |

In Table A1, J is an nxn matrix, SSR is Regression Sum of Squares, MSR is Regression Mean Square, SSE is Error Sum of Squares, MSE is Error Mean Square, and SSTO is Total Sum of Squares.

### A3.5 F-Test for regression model and Lack of Fit

A regression model exhibits lack-of-fit when it fails to adequately describe the functional relationship between the experimental factors and the response variable. Lack-of-fit may occur if important terms from the model, such as interactions or quadratic terms are not included. It may also occur if several large residuals result from fitting the model. The error sum square is decomposed into pure error and lack-of-fit components. The pure error sum of squares (SSPE) is obtained by calculating, for each replicate group, the sum of squared deviations of the Y observations around the group mean, where a replicate group has the same values for each of the X variables. The lack of fit sum of squares (SSLF) equals the difference between SSE and SSPE. The number of degrees of freedom associated with SSPE is n-c, whee c is the number of distinct levels of X variables. The number of degres of freedom ssociated with SSLF is (n–p) – (n–c) = c–p.

The test statistic $F^* = \frac{\left(\frac{SSLF}{c-p}\right)}{\left(\frac{SSPE}{n-c}\right)} = \frac{MSLF}{MSPE}$ …A15

If $F^* \leq (1-\alpha; c-p, n-c)$, conclude the lack of fit is insignificant

If $F^* > (1-\alpha; c-p, n-c)$, conclude the lack of fit is significant

### A3.6 Coefficient of Determination, $R^2$

The coefficient of determination, denoted by $R^2$, is defined as:

$$R^2 = \frac{SSR}{SSTO} = 1 - \frac{SSE}{SSTO} \quad \text{…A16}$$

$R^2$ measures the proportionate reduction of total variation Y associated with the use of the set of X variables. Even though $R^2$ is large, MSE may still be too large for inferences to be

useful when high precision is required. Another fact is that adding more X variables to the regression model can only increase $R^2$ and never reduce it, because SSE can never become larger with more variables and SSTO is always the same for a given set of responses.

The adjusted coefficient of multiple determination ($R^2_{adj}$) is used to adjust for the number of X variables in the model. It alters the $R^2$ by dividing each sum of squares by its associated degrees of freedom,

$$R^2_{adj} = 1 - \left(\frac{n-1}{n-p}\right)\frac{SSE}{SSTO} \quad \ldots A17$$

Predicted coefficient of determination, $R^2_{pred}$ , is calculated to indicate how well the model predicts responses for new observations. $R^2_{pred}$ can prevent over-fitting the model and can be more useful than $R^2_{adj}$ values for comparing models because it is calculated using observations not included in model simulation. Over-fitting refers to models that appear to explain the relationship between predictor and response variables for the data set used for model calculation but fail to provide valid predictions for new observations.

# APPENDIX B
# INTEGRATED FORM OF REACTION RATE EQUATIONS

Overall stoichiometry (Equation 2.1, Chapter 2) is written for a forward reaction, assuming negligible reverse reaction -

Overall reaction: $A + 3B \xrightarrow{k} 3R + S$ …(2.1)

Rate of reaction, written as rate of disappearance of triglyceride, *A* is:

$$-r_A = -\frac{d[A]}{dt} = k\,[A]^m\,[B]^n \quad ...(2.29)$$

Integrated form of the above equation in terms of triglyceride conversion ($x_A$), as obtained in Chapter 2, is:

$$\int \frac{dx_A}{(1-x_A)^m\,(\alpha_B - 3x_A)^n} = k\,[A]_o^{(m+n-1)} \int dt \quad (2.33)$$

where $[A]_o$ is the initial triglyceride concentration, and $\alpha_B = [B]_o / [A]_o$ ( molar ratio of methanol to triglyceride in the feed, a constant for a given reaction). Limits for the integral are: $x_A = 0$ at $t = 0$; and $x_A = x_A$ at $t$.

Integral has been evaluated for overall order varying from 0 to 3, for different combinations of *m* and *n*, and the integrated form of rate equation is given in Table 2.1 (Chapter 2). The detailed algebra for equations 2.34 – 2.43 is given below.

**Case 1**: Overall order – zero. $m = 0, n = 0$.

Equation 5.26 becomes: $\int dx_A = k\,[A]_o^{-1} \int dt$

Or, $x_A = k\,[A]_o^{-1}\,t + C$

For a fresh feed, $x_A = 0$ at $t = 0$; hence $C = 0$.

Therefore, $\boxed{[A]_o\,x_A = k\,t}$ …B1/ (2.34)

**Case 2**: Overall order – one. $m = 1, n = 0$

Equation 5.26 becomes: $\int dx_A = k \int (1 - x_A)\,dt$

Or, $\int_0^{x_A} \frac{dx_A}{(1-x_A)} = k \int_o^t dt$

Or, $\boxed{ln\left(\frac{1}{(1-x_A)}\right) = kt}$ …B2/(2.35)

**Case 3**: Overall order – one. $m = 0, n = 1$

Equation 5.26 becomes: $\int dx_A = k \int (\alpha_B - 3x_A)\, dt$

Or, $\int_0^{x_A} \frac{dx_A}{(\alpha_B - 3x_A)} = k \int_o^t dt$

Or,

$$\boxed{-\frac{1}{3} ln\left(\frac{\alpha_B - 3x_A}{\alpha_B}\right) = k\, t}$$ …B3/(2.36)

**Case 4**: Overall order – two. $m = 1, n = 1$

Equation 5.26 becomes: $\int \frac{dx_A}{(1-x_A)\ (\alpha_B - 3x_A)} = k\,[A]_o \int dt$

Or, $-\frac{1}{(\alpha_B - 3)} \int_o^{x_A} \frac{dx_A}{(1-x_A)} - \frac{3}{(\alpha_B - 3)} \int_o^{x_A} \frac{dx_A}{(\alpha_B - 3x_A)} = k\,[A]_o \int_o^t dt$

Or, $-\frac{1}{(\alpha_B - 3)} \ln(1 - x_A) + \frac{1}{(\alpha_B - 3)} ln \frac{(\alpha_B - 3x_A)}{\alpha_B} = k\,[A]_o\, t$

Or,

$$\boxed{\frac{1}{(\alpha_B - 3)} ln\left(\frac{\alpha_B - 3x_A}{(1 - x_A)\alpha_B}\right) = k\,[A]_o\, t}$$ .. …B4/(2.37)

**Case 5**: Overall order – two. $m = 2, n = 0$

Equation 5.26 becomes: $\int_o^{x_A} \frac{dx_A}{(1-x_A)^2} = k\,[A]_o \int_o^t dt$

Or,

$$\boxed{\left(\frac{x_A}{1 - x_A}\right) = k\,[A]_o\, t}$$ …B5/(2.38)

**Case 6**: Overall order – two. $m = 0, n = 2$

Equation 5.26 becomes: $\int_o^{x_A} \frac{dx_A}{(\alpha_B - 3x_A)^2} = k\,[A]_o \int_o^t dt$

Or, $\frac{1}{3}\left(\frac{1}{\alpha_B - 3x_A} - \frac{1}{\alpha_B}\right) = k\,[A]_o\, t$

Or,

$$\boxed{\frac{x_A}{(\alpha_B - 3x_A)\alpha_B} = k\,[A]_o\, t}$$ …B6/(2.39)

**Case 7**: Overall order – three. $m = 2, n = 1$

Equation 5.26 becomes: $\int \frac{dx_A}{(1-x_A)^2\ (\alpha_B - 3x_A)} = k\,[A]_o^2 \int dt$

Or, $-\frac{3}{(\alpha_B-3)^2}\int_0^{x_A}\frac{dx_A}{(1-x_A)}+\frac{1}{(\alpha_B-3)}\int_0^{x_A}\frac{dx_A}{(1-x_A)^2}+\frac{9}{(\alpha_B-3)^2}\int_0^{x_A}\frac{dx_A}{(\alpha_B-3x_A)}=\ k\ [A]_o^2\ t$

Or, $\frac{3}{(\alpha_B-3)^2}ln(1-x_A)+\frac{1}{(\alpha_B-3)}\left(\frac{x_A}{1-x_A}\right)-\frac{3}{(\alpha_B-3)^2}ln\left(\frac{\alpha_B-3x_A}{\alpha_B}\right)=\ k\ [A]_o^2\ t$

Or, $\boxed{\frac{1}{(\alpha_B-3)}\left(\frac{x_A}{1-x_A}-\frac{3}{\alpha_B-3}\right)ln\frac{(\alpha_B-\ 3x_A)}{(1-x_A)\alpha_B}=k\ [A]_o^2\ t}$ ..

B7/(2.40)

**Case 8**: Overall order – three. $m = 1, n = 2$

Equation 5.26 becomes: $\int\frac{dx_A}{(1-x_A)\ \ (\alpha_B-3x_A)^2}\ =\ k\ [A]_o^2\int dt$

Or, $\frac{1}{(\alpha_B-3)^2}\int_0^{x_A}\frac{dx_A}{(1-x_A)}-\frac{3}{(\alpha_B-3)^2}\int_0^{x_A}\frac{dx_A}{(\alpha_B-3x_A)}-\frac{3}{(\alpha_B-3)}\int_0^{x_A}\frac{dx_A}{(\alpha_B-3x_A)^2}=\ k\ [A]_o^2\ t$

Or, $-\frac{ln(1-x_A)}{(3-\alpha_B)^2}+\frac{1}{(3-\alpha_B)^2}ln\frac{\alpha_B-3x_A}{\alpha_B}+\frac{3}{(3-\alpha_B)}\frac{x_A}{\alpha_B(\alpha_B-3x_A)}=k\ [A]_o^2\ t$

Or, $\boxed{\frac{1}{(3-\alpha_B)}\left(\frac{3x_A}{(\alpha_B-3x_A)\alpha_B}-\frac{1}{3-\alpha_B}\right)ln\frac{(1-\ x_A)\alpha_B}{(\alpha_B-3x_A)}=k\ [A]_o^2\ t}$ ..

...B8/(2.41)

**Case 9**: Overall order – three. $m = 3, n = 0$

Equation 5.26 becomes: $\int_o^{x_A}\frac{dx_A}{(1-x_A)^3}\ =\ k\ [A]_o^2\int_o^t dt$

Or, $\frac{1}{2(1-x_A)^2}-\frac{1}{2}=k\ [A]_o^2\ t$

Or, $\boxed{\frac{(2-x_A)x_A}{(1-x_A)^2}=2\ k\ [A]_o^2\ t}$ …B9/(2.42)

**Case 10**: Overall order – three. $m = 0, n = 3$

Equation 5.26 becomes: $\int_0^{x_A}\frac{dx_A}{(\alpha_B-3x_A)^3}\ =\ k\ [A]_o^2\int_0^t dt$

Or, $\frac{1}{6}\left[\frac{1}{(\alpha_B-3x_A)^2}\right]_0^{x_A}\ =\ k\ [A]_o^2\ t$

Or, $\boxed{\frac{1}{(\alpha_B-3x_A)^2}-\frac{1}{{\alpha_B}^2}=6\ k\ [A]_o^2\ t}$ B10/(2.43)